frontiers | Research Topics

Cancer biomarkers: molecular insights into diagnosis, prognosis, and risk prediction, 2nd edition

Edited by
Matteo Becatti, Shaoquan Zheng and Giuseppe Bronte

Published in
Frontiers in Molecular Biosciences

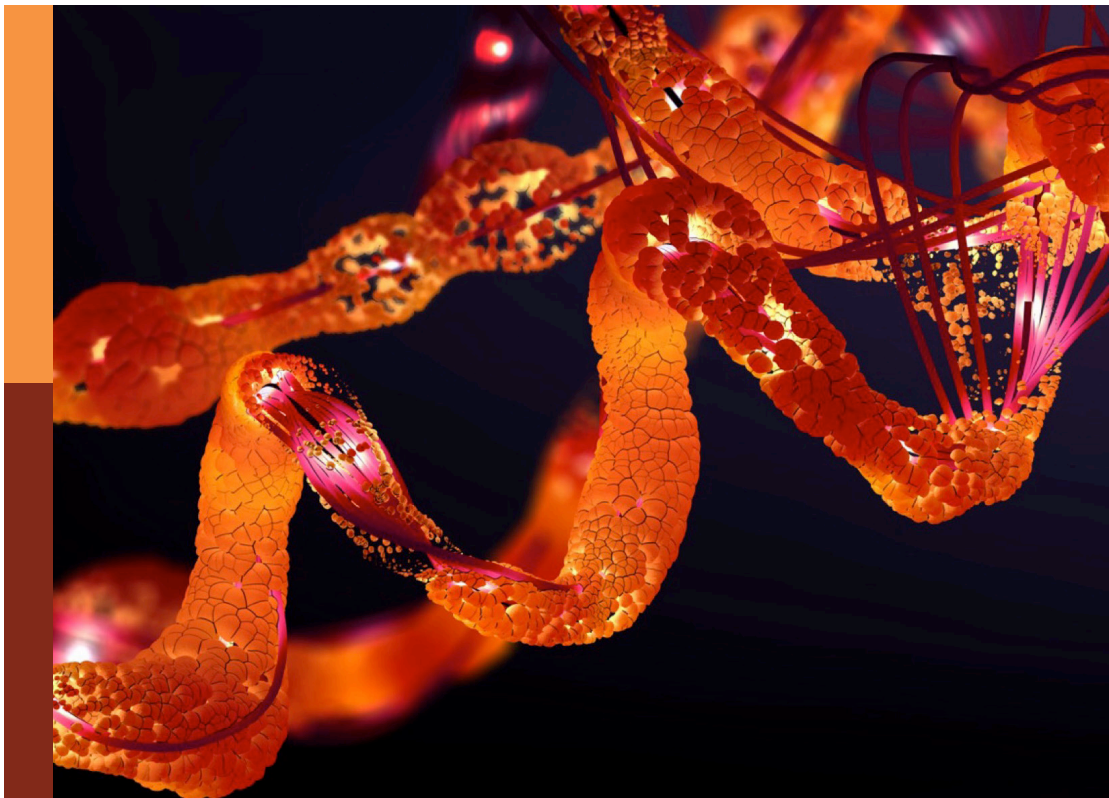

ISSN 1664-8714
ISBN 978-2-8325-7273-3
DOI 10.3389/978-2-8325-7273-3

Generative AI statement
Any alternative text (Alt text) provided alongside figures in the articles in this ebook has been generated by Frontiers with the support of artificial intelligence and reasonable efforts have been made to ensure accuracy, including review by the authors wherever possible. If you identify any issues, please contact us.

About Frontiers

Frontiers is more than just an open access publisher of scholarly articles: it is a pioneering approach to the world of academia, radically improving the way scholarly research is managed. The grand vision of Frontiers is a world where all people have an equal opportunity to seek, share and generate knowledge. Frontiers provides immediate and permanent online open access to all its publications, but this alone is not enough to realize our grand goals.

Frontiers journal series

The Frontiers journal series is a multi-tier and interdisciplinary set of open-access, online journals, promising a paradigm shift from the current review, selection and dissemination processes in academic publishing. All Frontiers journals are driven by researchers for researchers; therefore, they constitute a service to the scholarly community. At the same time, the *Frontiers journal series* operates on a revolutionary invention, the tiered publishing system, initially addressing specific communities of scholars, and gradually climbing up to broader public understanding, thus serving the interests of the lay society, too.

Dedication to quality

Each Frontiers article is a landmark of the highest quality, thanks to genuinely collaborative interactions between authors and review editors, who include some of the world's best academicians. Research must be certified by peers before entering a stream of knowledge that may eventually reach the public - and shape society; therefore, Frontiers only applies the most rigorous and unbiased reviews. Frontiers revolutionizes research publishing by freely delivering the most outstanding research, evaluated with no bias from both the academic and social point of view. By applying the most advanced information technologies, Frontiers is catapulting scholarly publishing into a new generation.

What are Frontiers Research Topics?

Frontiers Research Topics are very popular trademarks of the *Frontiers journals series*: they are collections of at least ten articles, all centered on a particular subject. With their unique mix of varied contributions from Original Research to Review Articles, Frontiers Research Topics unify the most influential researchers, the latest key findings and historical advances in a hot research area.

Find out more on how to host your own Frontiers Research Topic or contribute to one as an author by contacting the Frontiers editorial office: frontiersin.org/about/contact

Cancer biomarkers: molecular insights into diagnosis, prognosis, and risk prediction, 2nd edition

Topic editors

Matteo Becatti — University of Firenze, Italy

Shaoquan Zheng — The First Affiliated Hospital of Sun Yat-sen University, China

Giuseppe Bronte — University of Ferrara, Italy

Citation

Becatti, M., Zheng, S., Bronte, G., eds. (2025). *Cancer biomarkers: molecular insights into diagnosis, prognosis, and risk prediction, 2nd edition*. Lausanne: Frontiers Media SA. doi: 10.3389/978-2-8325-7273-3

Publisher's note: In this 2nd edition, the following article has been updated: [Li J, Zhang J, Zhang X, Cao C, Zhou T, Liu F, Hu L, Kwok HF and Zou H (2025) Prognostic model for lung adenocarcinoma based on experimental drug-resistant cell lines and clinical patients. *Front. Mol. Biosci*. 12:1654426. doi: 10.3389/fmolb.2025.1654426]

Table of contents

frontiers | Frontiers in Molecular Biosciences

TYPE Editorial
PUBLISHED 06 June 2025
DOI 10.3389/fmolb.2025.1636721

OPEN ACCESS

EDITED AND REVIEWED BY
Roberto Bei,
University of Rome Tor Vergata, Italy

*CORRESPONDENCE
Matteo Becatti,
matteo.becatti@unifi.it
Shaoquan Zheng,
zhengshq3@mail2.sysu.edu.cn

RECEIVED 28 May 2025
ACCEPTED 30 May 2025
PUBLISHED 06 June 2025

CITATION
Becatti M, Zheng S and Bronte G (2025) Editorial: Cancer biomarkers: molecular insights into diagnosis, prognosis, and risk prediction.
Front. Mol. Biosci. 12:1636721.
doi: 10.3389/fmolb.2025.1636721

Editorial: Cancer biomarkers: molecular insights into diagnosis, prognosis, and risk prediction

Matteo Becatti[1]*, Shaoquan Zheng[2]* and Giuseppe Bronte[3,4]

[1]Department of Experimental and Clinical Biomedical Sciences "Mario Serio", University of Firenze, Firenze, Italy, [2]Breast Disease Center, The First Affiliated Hospital, Sun Yat-sen University, Guangzhou, China, [3]Department of Translational Medicine, University of Ferrara, Ferrara, Italy, [4]Department of Oncology, University Hospital of Ferrara, Ferrara, Italy

KEYWORDS

cancer, biomarker, diagnosis, prognosis, risk prediction, tumor

Editorial on the Research Topic
Cancer biomarkers: molecular insights into diagnosis, prognosis, and risk prediction

Cancer biomarkers represent a critical frontier in precision oncology, enabling more refined stratification of patients, earlier detection, improved therapeutic targeting, and more accurate prognostic estimation. This Research Topic assembles a Research Topic of 14 diverse yet thematically converging articles that reflect the state-of-the-art and evolving paradigms in biomarker science across a variety of tumor types.

Several studies in this Research Topic identify gene expression drivers of tumor progression and therapy resistance, such as DAP3 in hepatocellular carcinoma, HJURP in gastric cancer, and ANTXR1 in bladder cancer. DAP3 was shown to promote tumor proliferation, invasion, and resistance to apoptosis, with a predictive model constructed based on its expression (Yuan et al.). HJURP was found to modulate chemoresistance via the MYC/TOP2A axis in gastric cancer, supporting its candidacy as a dual biomarker and therapeutic target (Liu et al.). ANTXR1 expression correlated with stromal scores and poor prognosis in bladder cancer, positioning it as both a prognostic marker and a candidate for targeted therapy (Franco et al.).

Other contributions focus on prognostic and predictive biomarker models. A meta-analysis of over 9,000 patients demonstrated that a high glucose-to-lymphocyte ratio (GLR) is a negative prognostic factor across various solid tumors, especially hepatocellular, breast, and pancreatic cancers (Li et al.). In esophageal squamous cell carcinoma, machine learning identified ATF2, ALOXE3, and SLC27A5 as predictive of response to chemoradiotherapy and overall survival, integrating gene expression, immune profiles, and drug sensitivity data (Cui et al.). Additionally, an epidemiological modeling study on lung cancer burden in BRICS nations revealed escalating trends in China and India, underscoring the importance of integrating biomarker strategies into public health policies (Wang et al.).

Innovations in diagnostic approaches also feature prominently. In colorectal cancer, immunolipid magnetic beads targeting EpCAM and vimentin enabled sensitive and

specific capture of circulating tumor cells (CTCs), with a high concordance to tissue-derived mutation profiles (Deng et al.). Plasma autoantibodies to COPT1 showed potential as early diagnostic biomarkers for non-small cell lung cancer (NSCLC), with combining IgG and IgM achieving an AUC of 0.784, further enhanced by CEA inclusion (Cao et al.). In rectal carcinoma, diffusion-weighted MRI and ADC mapping distinguished malignancy from radiation-induced proctitis and normal tissue with near-perfect sensitivity and specificity, though not linked to prognosis (Šarošković et al.).

The immune microenvironment and its modulation through intrinsic tumor pathways are also explored. One study evaluated cGAS/STING pathway activation across 15 checkpoint inhibitor-treated cohorts (Chen et al.). While STING activation correlated with improved survival in some datasets (e.g., melanoma and bladder cancer), it was paradoxically associated with poor outcomes in others (e.g., renal carcinoma), suggesting tumor-type-specific immune dynamics. This is echoed by work on circMIB1 in glioma, which functions as a competing endogenous RNA sponging miR-1290, thereby upregulating tumor suppressor genes involved in apoptosis and circadian rhythm regulation (Chen et al.). These insights contribute to our understanding of non-coding RNAs in modulating oncogenic pathways and immunogenicity.

Additional complexity is addressed in rare or diagnostically ambiguous tumors. A bioinformatic study identified overlapping gene signatures between acute myocardial infarction and non-small cell lung cancer (NSCLC). COL1A1 and PLAU were identified as key hub genes with diagnostic value. Repurposable drugs, such as zoledronic acid, emerged for connection with hub genes. These findings supported the usefulness of the protein-protein interaction network analysis to identify hub genes (Zheng et al.). A case report detailed the misdiagnosis of pulmonary Ewing sarcoma as NSCLC, corrected through molecular pathology revealing an EWSR1FLI1 fusion gene (Carter et al.). This led to a treatment shift to VDC + I.E., chemotherapy, surgery, and radiotherapy with excellent response, highlighting the vital role of molecular diagnostics and reference pathology centers. A comprehensive review article synthesized established and emerging biomarkers in colorectal cancer, including KRAS, BRAF, MSI, HER-2, RET, and ctDNA, providing a framework for integrating biomarkers into therapeutic algorithms and clinical trial design (Zhang et al.).

Taken together, these studies underscore the multifaceted role of biomarkers in guiding diagnosis, prognosis, and decision for personalized therapy. They also highlight persistent challenges, including biomarker standardization, cross-platform validation, and accessibility in clinical settings. Yet, the collective insights affirm that the integration of omics data, computational biology, and translational research is reshaping oncology toward a more precise and patient-centered practice. This Research Topic demonstrates that continued interdisciplinary collaboration is key to unlocking the full potential of biomarker-driven oncology.

Author contributions

MB: Writing – review and editing. SZ: Writing – review and editing. GB: Writing – review and editing.

Funding

The author(s) declare that no financial support was received for the research and/or publication of this article.

Conflict of interest

The authors declare that the research was conducted in the absence of any commercial or financial relationships that could be construed as a potential conflict of interest.

The author(s) declared that they were an editorial board member of Frontiers, at the time of submission. This had no impact on the peer review process and the final decision.

Generative AI statement

The author(s) declare that no Generative AI was used in the creation of this manuscript.

Publisher's note

frontiers | Frontiers in Oncology

TYPE Original Research
PUBLISHED 02 October 2024
DOI 10.3389/fonc.2024.1464183

OPEN ACCESS

EDITED BY
Matteo Becatti,
University of Firenze, Italy

REVIEWED BY
Mingzhu Wang,
Huazhong University of Science and Technology, China
Siqi Zhou,
Huazhong University of Science and Technology, China
Shengzhi Zhou,
Renmin Hospital of Wuhan University, China

*CORRESPONDENCE
Miloš Vuković
milos.vukovic@mf.uns.ac.rs

†These authors have contributed equally to this work and share first authorship

RECEIVED 13 July 2024
ACCEPTED 13 September 2024
PUBLISHED 02 October 2024

CITATION
Šarošković M, Vuković M, Stojanoski S, Zorić M, Prvulović Bunović N, Spirovski M and Nosek I (2024) Significance of apparent diffusion coefficient in diagnosis of rectal carcinoma. *Front. Oncol.* 14:1464183. doi: 10.3389/fonc.2024.1464183

Significance of apparent diffusion coefficient in diagnosis of rectal carcinoma

Milica Šarošković[1†], Miloš Vuković[1,2*†], Stefan Stojanoski[1,2], Milica Zorić[1], Nataša Prvulović Bunović[2,3], Milena Spirovski[2,4] and Igor Nosek[1,2]

[1]Department of Radiology, Faculty of Medicine Novi Sad, University of Novi Sad, Novi Sad, Serbia, [2]Department for Radiology diagnostics, Oncology Institute of Vojvodina, Sremska Kamenica, Serbia, [3]Department of Nuclear Medicine, Faculty of Medicine Novi Sad, University of Novi Sad, Novi Sad, Serbia, [4]Department of Oncology, Faculty of Medicine Novi Sad, University of Novi Sad, Novi Sad, Serbia

Introduction: The apparent diffusion coefficient (ADC) is a quantitative parameter that facilitates the detection and reliable differentiation of rectal cancer. MR differentiation between rectal carcinoma, post-radiation proctitis, and normal rectal wall with the ADC values and their comparison depending on the level of tumor markers and pathohistological characteristics of rectal carcinoma.

Methods: The retrospective study performed at the Oncology Institute of Vojvodina included 300 patients, 100 each with rectal cancer, post-radiation proctitis, and normal rectum. Mean ADC values were obtained by measuring the region of interest (ROI) of the rectal wall.

Results: Rectal cancer showed lower ADC values ($0.665 \pm 0.086 \times 10^{-3}mm^2/s$) compared to both post-radiation proctitis ($1.648 \pm 0.268 \times 10^{-3}mm^2/s$) and normal rectum ($1.180 \pm 0.110 \times 10^{-3}mm^2/s$) ($p<0.001$). No significant differences in ADC values were observed between different grades of rectal cancer ($p=0.874$; $p>0.05$), depending on the presence of metastases in the lymph nodes ($p=0.357$; $p>0.05$), different TN stage ($p=0.196$; $p>0.05$), local spread of the tumor ($p=0.312$; $p>0.05$), the presence of RAS mutation ($p=0.829$; $p>0.05$) and the value of tumor markers ($p=0.923$; $p>0.05$). ADC values below $1.013 \times 10^{-3}mm^2/s$ with 100% sensitivity and 96% specificity indicate the presence of rectal cancer in relation to normal wall, with a positive predictive value of 96.1% and a negative of 100%. ADC values below $1.255 \times 10^{-3}mm^2/s$ with 100% sensitivity and 95% specificity indicate rectal cancer in relation to post-radiation proctitis. ADC values above $1.339 \times 10^{-3}mm^2/s$ with 87% sensitivity and 89% specificity indicate post-radiation proctitis in relation to normal wall.

Discussion: The ADC is a useful marker in differentiating between rectal cancer, post-radiation proctitis, and normal rectal wall with high sensitivity and specificity, but it cannot be used to distinguish the histological grades of rectal cancer, nor other pathohistological parameters.

KEYWORDS

DWI, ADC, rectal cancer, post-radiation proctitis, TNM, lymph nodes

1 Introduction

Rectal cancer is the third most common malignancy and is currently one of the leading cause of cancer death in humans worldwide (1, 2). Despite advances in surgical techniques, chemotherapy regimens, and radiotherapy, which have led to reductions in recurrence and mortality rates, available treatment options still vary depending on tumor stage (2).

The prognosis of rectal cancer depends on several factors, among which are the pathohistological features of the tumor, the degree of differentiation, TNM classification, the level of tumor markers, the presence of molecular pathology and many others (3).

Diffusion-weighted imaging (DWI) with the apparent diffusion coefficient (ADC) gives us more precise data as a non-invasive functional MR technique sensitive to the movement of water molecules in tissues. It has high specificity in determining tissue cellularity, distinguishing recurrence after treatment or residual tumor tissue from fibrosis or necrosis (4).

With this research, we want to emphasize the importance of the apparent diffusion coefficient both in the diagnosis of rectal cancer and in differentiating tumoral thickening of the rectal wall from post-radiation proctitis, as well as its value in differentiating such findings from normal rectal wall. Also, the aim was to determine the difference in ADC values depending on the level of tumor markers and pathohistological characteristics of rectal carcinoma, with emphasis on tumor grade, local tumor status, infiltration of lymph nodes and the presence of RAS mutation. In order to find a valuable tool for differentiation between the conditions mentioned above, we calculated cut-off values.

2 Material and methods

2.1 Subject selection

This research was a retrospective study with a total of 300 patients, whose MR images are available in the database in the period from 2013 to 2023. Patients were divided into three groups:

1. The first group consisted of 100 patients with a pathohistologically confirmed diagnosis of rectal adenocarcinoma;

2. The second group consisted of 100 patients whose MR images showed thickening of the rectal wall from post-radiation proctitis, primarily as a result of irradiation of malignancy in other anatomical locations not including the rectum;

3. The third group consisted of 100 control subjects with normal findings of the rectum on MR images.

Inclusion criteria for patients in the first group were a pathohistologically confirmed diagnosis of rectal adenocarcinoma and the existence of the first diagnostic MRI scan of the pelvis done at the Oncology Institute of Vojvodina before any therapy (chemotherapy, irradiation or a combination of the above). Inclusion criteria for patients in the second group was the thickening of the rectal wall confirmed by MR imaging as a result of irradiation of other malignancies, excluding rectal malignancy (primarily of the uterus and prostate), while the only criterion for the control group was a normal finding of the rectum described on MR imaging. The inclusion criterion for all three groups was the existence of a DWI sequence with a corresponding ADC map as a standard part of the pelvic MR protocol.

The exclusion criteria for the first group were pelvic MRI scans not performed at the Oncology Institute of Vojvodina and the use of any type of therapy for rectal cancer before the MRI scan was performed. The exclusion criterion for the second group is inflammation of the rectal wall as a result of irradiation of primary rectal cancer, as well as inflammation of the wall as part of inflammatory bowel diseases (ulcerative colitis and Crohn's disease).

The study was approved by the institutional ethical review board and the informed consent was waived due to the retrospective manner of the study.

2.2 Patient data

As part of the research, the data taken from the information system of the Oncology Institute of Vojvodina were pathohistological type of tumor, values of tumor markers at the time of diagnosis, as well as the possible presence of molecular pathology findings, i.e. findings of RAS gene mutation.

2.3 Imaging analysis

Magnetic resonance examinations were performed on two devices: 1.5T (Siemens Aera, Erlagen, Germany) and 3T (Siemens Trio Tim, Erlagen, Germany). All patients underwent the following sequences: T1W, T2W, TIRM coronal tomograms, T1W parasagittal and T2W sagittal tomograms, T1W/T2W transverse tomograms, along with a DWI sequence with an ADC map in the transverse plane. The ADC values for all three groups were measured on the PACS system (5). The DWI sequence was analyzed to define the tumor, which was displayed as a high signal intensity corresponding to the location of the tumor mass. The ROI was manually placed on the corresponding ADC map while comparing other morphological MR sequences to ensure that the ROI was placed at the location of the primary tumor. All measurements were performed by two independent readers in consensus.

2.4 Statistical analysis

SPSS software version 27.0 (SPSS Inc, IBM, Armonk, NY) was used for statistical data processing. The confidence interval is 95% with a significance level of $p<0.05$.

The differences in the ADC values between the three groups were compared by the Kruskal-Wallis test, and between individual groups by the Mann-Whitney U test ($p=0.05$), because all data are continuous with an abnormal distribution that was tested by the

Kolmogorov-Smirnov test. The comparison between different degrees of tumor differentiation (grades) was performed with the ANOVA test, while the difference between the individual tumor grades was performed with the t-test. The Mann-Withney U test was used for analyzing differences in the values of the ADC depending on the presence of lymph node infiltration, while the t-test was used to examine the difference in the mean ADC values between groups with elevated and normal values of tumor markers, between groups depending on the presence of RAS gene mutation, as well as patients with locally confined (T1 and T2 stage) or locally advanced tumor (T3 and T4 stage). The ADC values were also analyzed in relation to different TN stage using the ANOVA test (M stage was generally not available). An analysis of the cut-off values for ADC between the examined groups (via the ROC curve) was performed, with the determination of its sensitivity, specificity, positive and negative predictive values ($p<0.001$).

3 Results

3.1 Demographic data

The research included 300 subjects, 100 patients with rectal cancer, 100 patients with post-radiation proctitis and 100 subjects with normal rectal wall. In the group of patients with rectal cancer, 73 men and 27 women were examined, among whom the mean age was 64.54 ± 10.74. The second group of patients with post-radiation proctitis included 27 men and 73 women, where the mean age was 62.52 ± 9.64. There were 26 men and 74 women in the group of subjects with normal wall, with the mean age of 59.47 ± 12.52 (Table 1).

3.2 Mean ADC values in relation to the study groups

By examining ADC values between the mentioned groups, it was determined that they differ significantly both in the whole sample and between individual groups ($p<0.001$) (Figure 1, Table 1). It was found that ADC values in patients with rectal cancer (Figures 2D–F, 3) were statistically significantly lower both in comparison to the group of patients with normal findings (Figures 2A–C) and in comparison to the group of patients with post-radiation proctitis (Figure 4). On the other hand, in the group of patients with post-radiation proctitis, it was determined that the ADC values were significantly higher compared to the group of patients with normal findings.

3.3 Determining the cut-off mean ADC values to differentiate between study groups

Table 2. presents the estimated cut-off values for each examined group, including their corresponding sensitivity (Sn), specificity (Sp), positive predictive value (PPV), and negative predictive value (NPV) ($p<0.001$). The primary objective was to enhance both the sensitivity and specificity of the diagnostic test, thereby maximizing its practical utility in routine radiological practice. To accomplish this, multiple cut-off values with varying sensitivity and specificity profiles were utilized, aiming to improve the differentiation between the study groups.

3.4 Clinical and histopathological characteristics of patients with rectal cancer

The characteristics of the patients with rectal cancer are listed in Table 3. Patients with a pathohistological diagnosis of adenocarcinoma were included in the study. Among them there were no T1 category patients, within the T2 category (Figures 2D–F) there were 26 patients, T3 (Figures 3A–C) 54 and T4 (Figures 3D–F) 20 patients. Lymph nodes were not infiltrated in 37 patients (N0 category), 1-3 lymph nodes were infiltrated in 31 patients (N1 category), and 4 or more lymph nodes were infiltrated in 32 patients (N2 category).

3.5 Mean ADC values in relation to the degree of differentiation of rectal cancer

In patients with rectal cancer, there were 5 patients with a well differentiated tumor (G1), 85 patients with a moderately differentiated tumor (G2) and 7 patients with a poorly differentiated tumor (G3), while data on tumor grade was not available for 3 patients. Examining the ADC values between the mentioned groups we did not reveal a statistically significant difference both in the whole sample ($p=0.874$; $p>0.05$) and between individual grades (Figure 5A). Statistical analysis showed that ADC values between G1 and G2 tumors do not differ significantly ($p=0.865$; $p>0.05$), nor between G1 and G3 tumors ($p=0.677$; $p>0.05$), nor between G2 and G3 tumors ($p=0.636$; $p>0.05$).

TABLE 1 Difference of mean ADC values between the study groups.

Groups	N	Age (mean ± SD)	ADC (mean ± SD) x 10^{-3} mm^2/s	p-value
				<0.001
Carcinoma	100	64.54 ± 10.74	0.665 ± 0.086	
Post-radiation proctitis	100	62.52 ± 9.64	1.648 ± 0.268	
Normal wall	100	59.47 ± 12.52	1.180 ± 0.110	

10.3389/fonc.2024.1464183

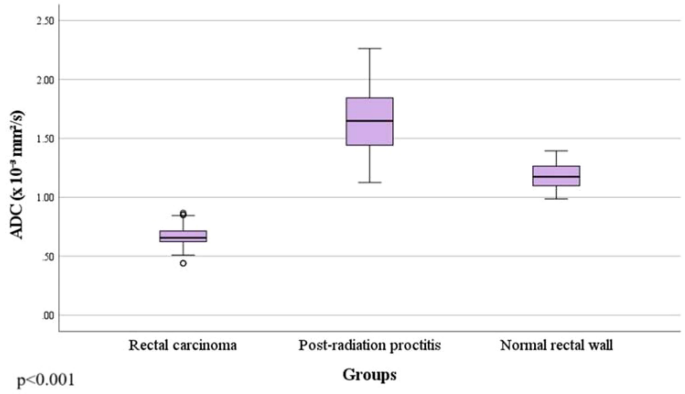

FIGURE 1
Comparison of mean ADC values between the study groups.

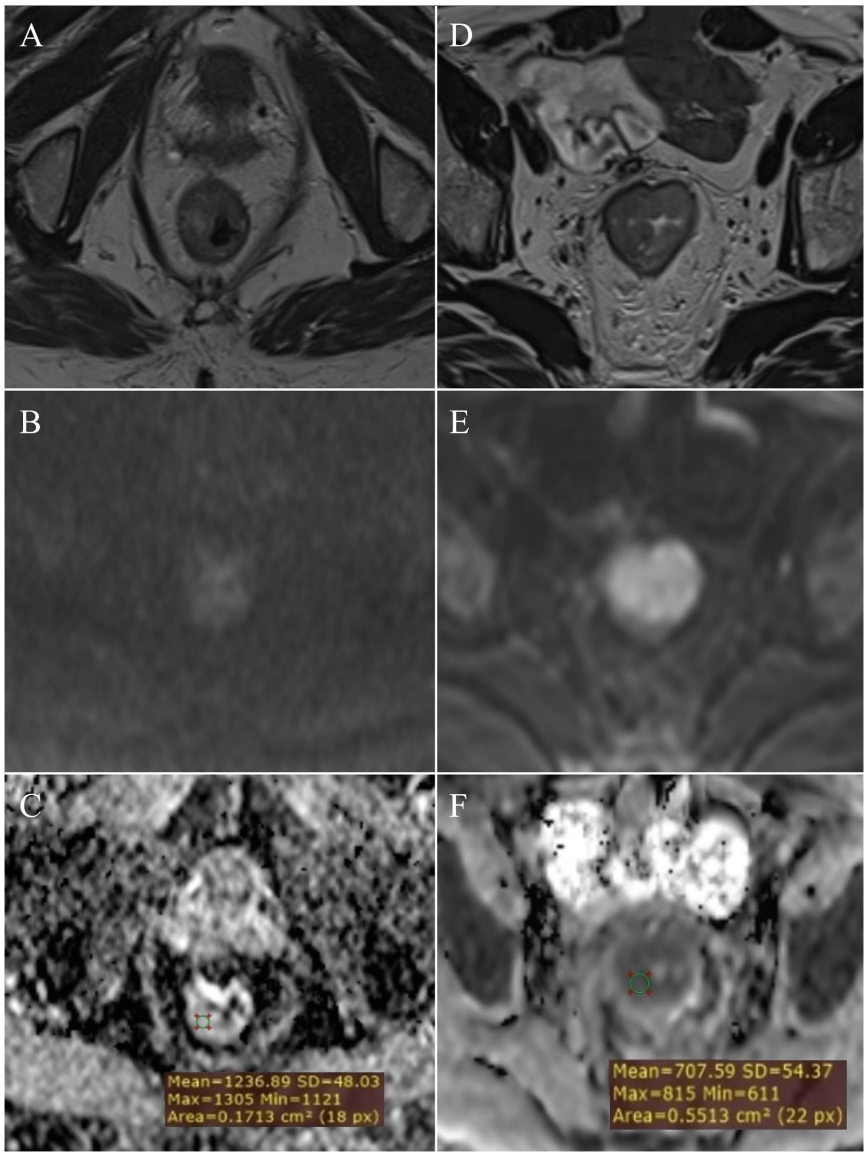

FIGURE 2
Measurement of ADC values: normal rectal wall – **(A)** (T2W), **(B)** (DWI), **(C)** (ADC map with ROI); T2 stage of rectal cancer - **(D)** (T2W), **(E)** (DWI), **(F)** (ADC map with ROI).

10.3389/fonc.2024.1464183

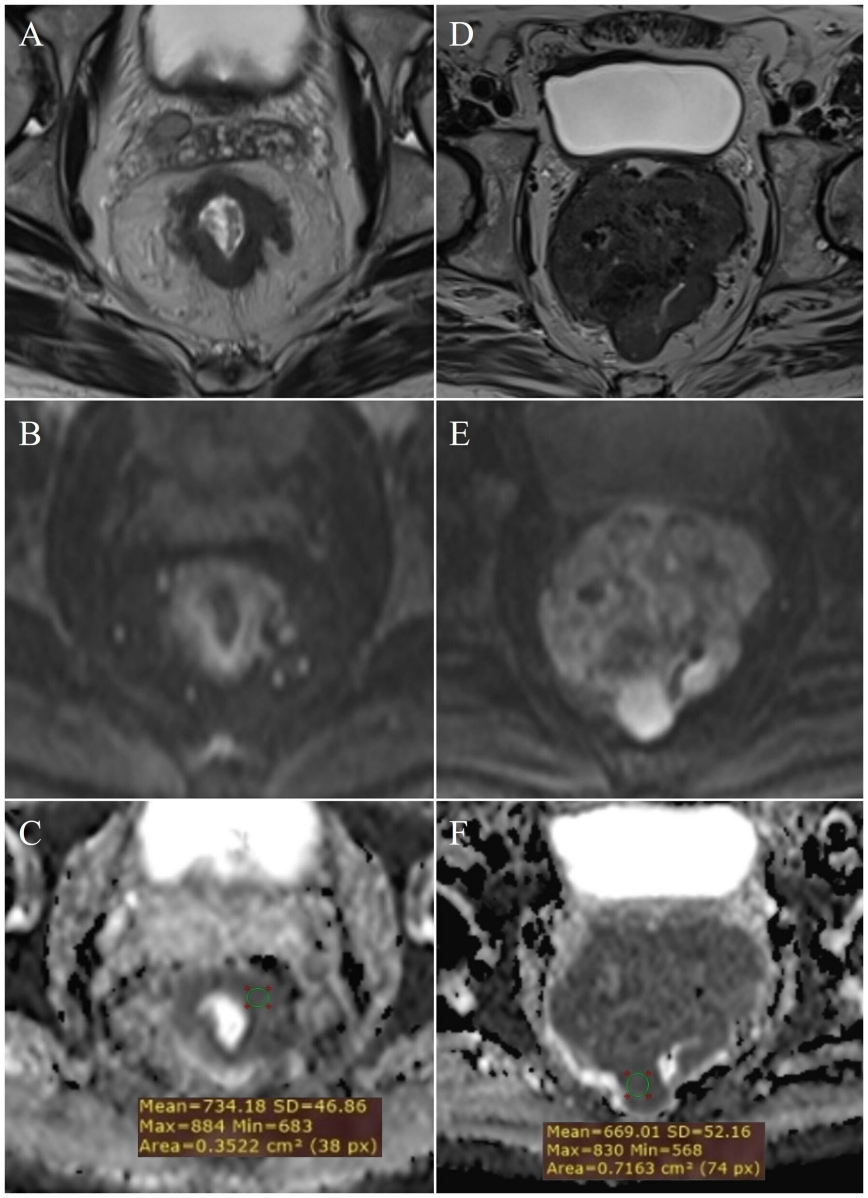

FIGURE 3
Measurement of ADC values: T3 stage of rectal cancer - **(A)** (T2W), **(B)** (DWI), **(C)** (ADC map with ROI); T4 stage - **(D)** (T2W), **(E)** (DWI), **(F)** (ADC map with ROI).

3.6 Mean ADC values in relation to the presence of metastases in regional lymph nodes

In patients with rectal cancer, the absence of metastatic infiltration of locoregional lymph nodes (negative nodes - N0) was found in 37 (37%) patients, while positive lymph nodes (N1 and N2) with present metastases were found in 63 (63%) of patients. The analysis of mean ADC values between the two mentioned subgroups did not reveal a statistically significant difference ($p=0.357$; $p>0.05$) (Figure 5B).

3.7 Mean ADC values in relation to TN stage

Based on data on local tumor extension and lymph node involvement (TN stage), patients were classified into the following stages: 19 patients with T2N0, 6 with T2N1, 1 with T2N2, 15 with T3N0, 17 with T3N1, 22 with T3N2, 3 with T4N0, 8 with T4N1 and 9 patients with T4N2. Analysis of the mean ADC values did not reveal a statistically significant difference depending on the different TN stage ($p=0.196$; $p>0.05$) (Figure 5C).

10.3389/fonc.2024.1464183

TABLE 2 Cut-off mean ADC values to differentiate between study groups.

Groups	Cut-off ADC x 10^{-3} mm^2/s	Sn* (%)	Sp* (%)	PPV* (%)	NPV* (%)	p-value
						<0.001
Carcinoma/normal wall (Figure 6A)	0.927	100	100			
	1.013	100	96	96.1	100	
Carcinoma/post-radiation proctitis (Figure 6A)	0.996	100	100			
	1.255	100	95	95.2	100	
Post-radiation proctitis/normal wall (Figure 6B)	1.339	87	89	87.9	87.2	

* Sn, sensitivity; Sp, specificity; PPV, positive predictive value; NPV, negative predictive value.

3.8 Mean ADC values in relation to local tumor status

Among patients with rectal cancer, the percentage of locally confined tumors (T1 and T2) was 26%, in contrast to locally advanced tumors (T3 and T4) which comprised 74%. Data processing did not reveal a statistically significant difference between ADC values in locally confined and locally advanced tumors (p=0.312; p>0.05) (Figure 5D).

3.9 Mean ADC values in relation to the presence of RAS mutation

Among patients with rectal cancer, molecular pathology for the presence of RAS mutation was performed in 19 patients, where the absence of RAS gene mutation was found in 9 patients, while 10 patients had a mutation of the mentioned gene. By comparing the mean ADC values between the mentioned subgroups, we did not find a statistically significant difference (p=0.829; p>0.05) (Figure 5E).

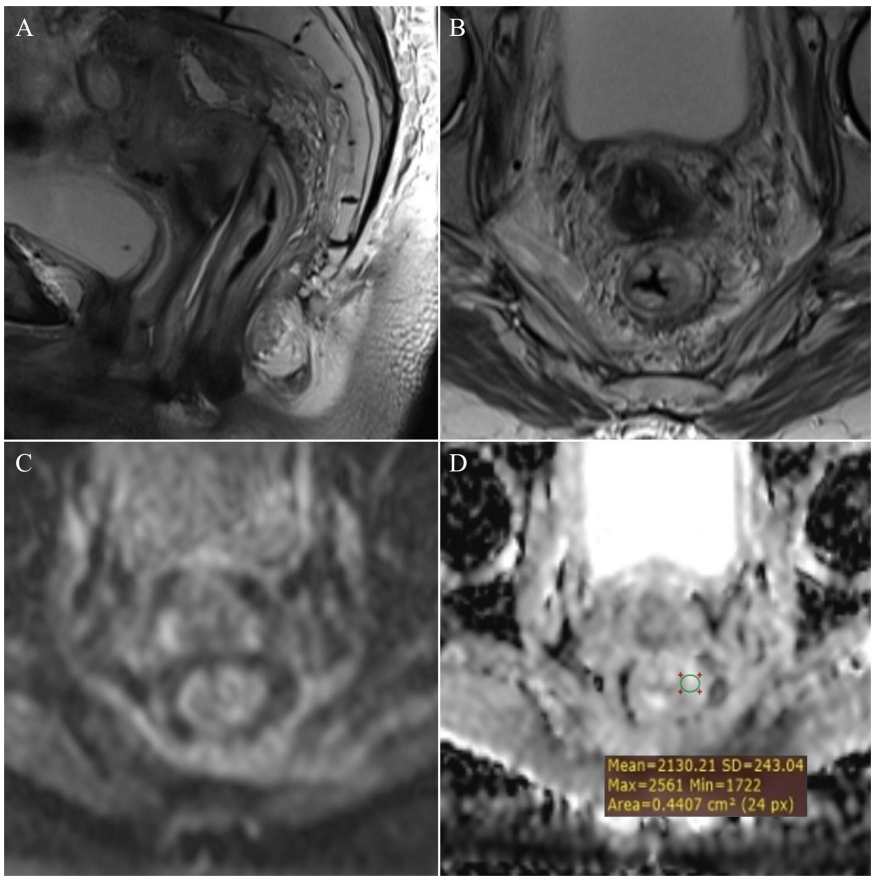

FIGURE 4
Measurement of ADC values: post-radiation proctitis - **(A)** (T2W sagittal plane), **(B)** (T2W axial plane), **(C)** (DWI) and **(D)** (ADC map with ROI).

10.3389/fonc.2024.1464183

TABLE 3 Correlation between histological, clinical parameters and ADC values of patients with rectal cancer.

Parameters	N (%)	ADC (mean ± SD) x 10^{-3} mm^2/s	p-value
Sex			0.332
Men	73 (73)	0.660 ± 0.083	
Women	27 (27)	0.680 ± 0.094	
Histological grade	97		0.874
Well differentiated (G1)	5 (5.1)	0.674 ± 0.059	
Moderately differentiated (G2)	85 (87.6)	0.667 ± 0.087	
Poorly differentiated (G3)	7 (7.2)	0.651 ± 0.110	
T category			0.552
T1	0 (0)		
T2	26 (26)	0.650 ± 0.072	
T3	54 (54)	0.667 ± 0.089	
T4	20 (20)	0.677 ± 0.097	
N category			0.590
N0	37 (37)	0.675 ± 0.081	
N1	31 (31)	0.653 ± 0.085	
N2	32 (32)	0.664 ± 0.094	
TN stage			0.196
T2N0	19 (19)	0.648 ± 0.069	
T2N1	6 (6)	0.632 ± 0.062	
T2N2	1 (1)	0.796 ± 0	
T3N0	15 (15)	0.713 ± 0.085	
T3N1	17 (17)	0.642 ± 0.077	
T3N2	22 (22)	0.656 ± 0.091	
T4N0	3 (3)	0.658 ± 0.079	
T4N1	8 (8)	0.694 ± 0.109	
T4N2	9 (9)	0.668 ± 0.099	
Local tumor status			0.312
Locally confined (T1 and T2)	26 (26)	0.650 ± 0.072	
Locally advanced (T3 and T4)	74 (74)	0.670 ± 0.091	
Lymph nodes			0.357
Negative (N0)	37 (37)	0.675 ± 0.081	
Positive (N1 and N2)	63 (63)	0.659 ± 0.089	
RAS status	19		0.829
Without mutation	9 (47.4)	0.647 ± 0.093	
With mutation	10 (52.6)	0.637 ± 0.098	
Tumor markers			0.923
CEA	42	0.653 ± 0.088	
<4.7 ng/ml	20 (47.6)	0.651 ± 0.072	

(Continued)

TABLE 3 Continued

Parameters	N (%)	ADC (mean ± SD) x 10^{-3} mm^2/s	p-value
Tumor markers			0.923
≥4.7 ng/ml	22 (52.4)	0.647 ± 0.108	
CA 19.9	40	0.648 ± 0.083	
<26.6 U/ml	25 (62.5)	0.641 ± 0.075	
≥26.6 U/ml	15 (37.5)	0.659 ± 0.096	

3.10 Mean ADC values in relation to the level of tumor markers

Twenty two patients had CEA tumor marker values above the reference range, while 22 patients had normal values of the mentioned oncomarker. An elevated concentration of the CA 19-9 tumor marker was found in 15 patients, while 25 patients had values of the mentioned tumor marker within the reference range. By analyzing the difference between patients with normal and elevated values of tumor markers, we did not find a statistically significant difference in the mean ADC values of rectal cancer (p=0.923; p>0.05) (Figure 5F).

4 Discussion

This study is the only one in the available literature that combined the entire spectrum of findings on the rectal wall, from normal findings to post-radiation proctitis to rectal cancer. The ADC values were observed in the mentioned conditions, all with the aim of more confident differentiation of rectal wall thickening in comparison to a normal wall.

Examining ADC values between the study groups, rectal cancer showed lower ADC values compared to both post-radiation proctitis and normal rectum. In comparison, post-radiation proctitis showed higher ADC values than normal rectum. At the same time, this is not the case with inflammation of the intestinal wall in inflammatory bowel diseases, where some authors show lower ADC values in relation to a normal intestinal wall (6). The explanation of this phenomenon lies in the fact that the free movement of water molecules is limited in hypercellular tumors (1), while in post-radiation proctitis there is damage to stem cells and atrophy of the mucosa with inflammation of the interstitium and edema (7), which facilitates the mentioned movement of water molecules and for this reason, the values in post-radiation proctitis are significantly different from the normal rectal wall, while lower ADC values in inflammation in inflammatory bowel diseases can be

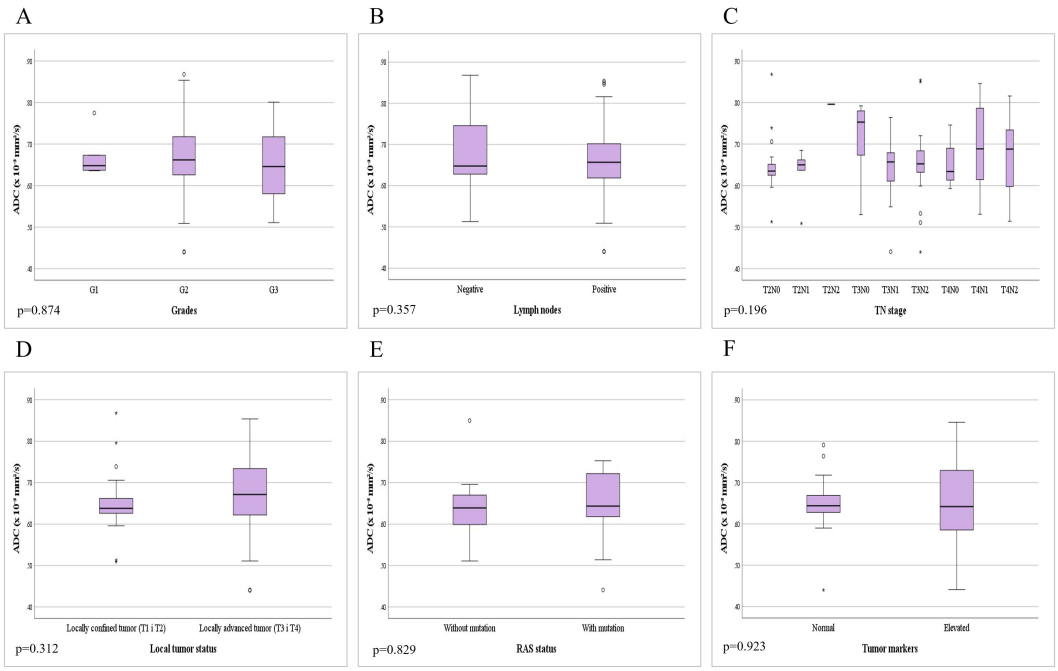

FIGURE 5
Comparison of mean ADC values depending on the: **(A)** different grades of rectal cancer; **(B)** presence of metastases in locoregional lymph nodes; **(C)** different TN stage; **(D)** local tumor status; **(E)** presence of RAS mutation; **(F)** level of tumor markers.

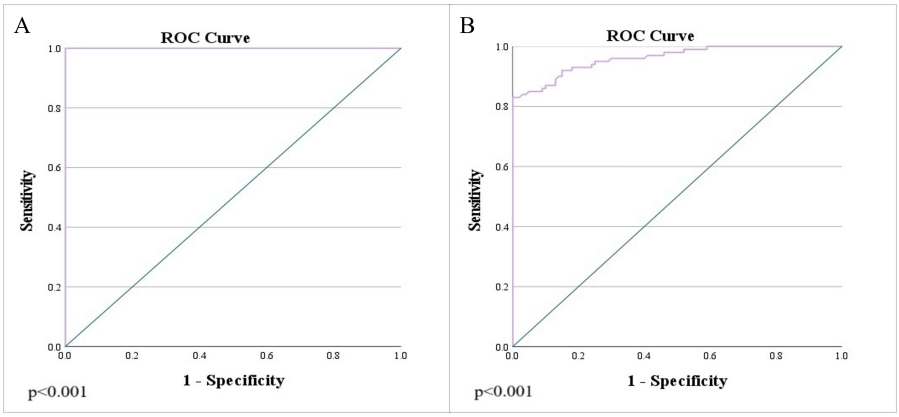

FIGURE 6
Analysis of the ROC curve of ADC values: **(A)** differentiation between rectal cancer and normal wall, as well as the differentiation of rectal cancer and post-radiation proctitis; **(B)** differentiation of post-radiation proctitis and normal wall.

explained by the increased density of inflammatory cells in the wall itself, which leads to restriction of the diffusion of water molecules. For this reason, post-radiation proctitis is a special type of inflammation that is pathophysiologically different from other types of intestinal inflammation.

During the last few years, there has been increasing interest in using quantitative DWI parameters, such as ADC values, as biomarkers to predict the outcome of rectal cancer in relation to TN-stage and pathohistological characteristics, such as the degree of tumor differentiation and the presence of lymph node metastases.

In our research, there was no difference in the mean ADC values between different degrees of differentiation of rectal cancer (Figure 5A), which is in agreement with the results of other researchers (8–10), while on the other hand, Sun et al. (11) report significantly lower ADC values in high-grade cancers of the rectum in relation to low-grade ones. A possible explanation for the different results could be the almost three times lower number of patients with G1 and G3 grades in our study, in contrast to the study by Sun et al. (11). Also, a study by Liu et al. (12) highlights the importance of tumor texture analysis in order to determine the prognostic assessment of ADC values. Additionally, heterogeneity is an important characteristic of malignant lesions that originates from variations in tumor cellularity, angiogenesis, extravascular and extracellular matrix, as well as areas of hemorrhage and necrosis within the tumor, which further implies that greater tumor heterogeneity can lead to significant variations in ADC values (12).

By analyzing the mean ADC values in relation to the presence of infiltration of locoregional lymph nodes, we did not find a statistically significant difference indicative of metastasis (Figure 5B), which is in agreement with the results of previous studies (8, 12). In addition to the nodal status (N stage), we examined the local tumor status according to the T stage (Figure 5D). We found no significant difference in ADC values between patients with locally confined tumors (T1 and T2) versus locally advanced tumors (T3 and T4), which correlates with the results of the study by Liu et al. (12). We additionally analyzed the presence of a difference in ADC values depending on the different TN stage, but we did not obtain statistically significant results (Figure 5C). All of the above tells us that ADC is not a good marker for distinguishing the local tumor status, but on the other hand, it facilitates the diagnosis because it shows clear signs of diffusion restriction from the early stages (T1 and T2) which are clearly present in locally advanced stages (T3 and T4).

To date, few studies have investigated the association of DWI parameters in rectal cancer with different RAS proto-oncogene mutation status. One such study, by Xu et al. (13), states that the ADC values are significantly lower in the "KRAS-mutant" group compared to the group with the "KRAS wild-type" gene. Therefore, lower ADC values in the mutated group may indirectly confirm the association between KRAS mutation and prognosis in rectal cancer. On the other hand, a meta-analysis by Surov et al. (14) did not prove a statistically significant difference in ADC values in relation to KRAS gene mutation, which is confirmed by the results of our research (Figure 5E).

The level of tumor markers is potentially an important factor affecting the prognosis of the disease. However, after the analysis, the mean ADC values in patients with normal tumor markers did not differ significantly from the values in patients with elevated markers (Figure 5F). Our results are in agreement with the study of Sun et al. (11), which had a similar number of patients in each of the subgroups.

The research has several limitations. One of the potential limitations is that the examinations were performed on two different MR machines, magnetic field strengths 1.5T and 3T, although a study by Caruso et al. (15) did not show a statistically significant difference in ADC values between MR machines of different field strengths. However, this study mentioned that a 3T MRI provides superior detection of potential tumor residue compared to a 1.5T MRI, as the latter may produce less reliable ADC values (15). Another important limitation of the study is the absence of a definitive pathohistological finding in patients with locally advanced tumors in whom there was no possibility of surgical treatment during the course of the disease, and the local stage (primarily T and N stage) was determined based on MR

examination. Additionally, the limitation of the study is the absence of ADC_{msi} and ADC_{min} values. These should be considered in future research, as some studies suggest that these values may be useful in assessing the aggressiveness of rectal cancer (16, 17). One of the most significant limitations of this study is the small sample size of certain subgroups, which may be why in several comparisons only a trend of increasing or decreasing values was observed, without statistically significant differences. Expanding the subgroups with smaller sample sizes in our study could reveal a statistically significant difference.

The advantage of this study is the unified presentation of the association of ADC values in relation to various pathohistological characteristics of rectal cancer and additional genetic and serological markers. Within this study, ADC values were examined in rectal adenocarcinoma, post-radiation proctitis and patients with normal rectum with a large sample, thus covering the spectrum of conditions that can be differential diagnostic problems. It is important to note that few studies looked at the ADC through the prism of RAS mutations and levels of tumor markers with a unique presentation of ADC values in patients with post-radiation proctitis and normal rectal wall. The ADC values can potentially help detect local recurrence following surgery or evaluate changes after chemoradiation therapy. These insights are crucial for clinicians, as they guide decisions on further diagnostic and therapeutic procedures, especially when evaluating suspicious thickening of the rectal wall, which is reflected in ADC values. Recent studies have identified various biomarkers that are useful in the diagnosis and prognosis of different carcinomas (18–21). Therefore, further research should aim to identify analogous radiological or other biomarkers and evaluate their impact on patient survival. Additionally, expanding the participant cohort and incorporating genetic parameters, as well as other biochemical markers associated with colorectal cancer, are crucial (22). Moreover, it is essential to investigate the potential of ADC as a prognostic biomarker and assess its impact on patient survival.

The ADC is a useful marker in differentiating between rectal cancer, post-radiation proctitis, and normal rectal wall with high sensitivity and specificity, but it cannot be used to distinguish the histological grades of rectal cancer, nor other pathohistological parameters like local tumor status, lymph nodes metastasis, TN stage and mutation of RAS gene, neither the level of tumor markers.

Data availability statement

The raw data supporting the conclusions of this article will be made available by the authors, without undue reservation.

Ethics statement

The studies involving humans were approved by Oncology Institute of Vojvodina. The studies were conducted in accordance with the local legislation and institutional requirements. The ethics committee/institutional review board waived the requirement of written informed consent for participation from the participants or the participants' legal guardians/next of kin because The informed consent was waived due to the retrospective manner of the study.

Author contributions

MŠ: Conceptualization, Formal analysis, Investigation, Writing – original draft, Writing – review & editing. MV: Conceptualization, Formal analysis, Investigation, Writing – original draft, Writing – review & editing. SS: Methodology, Writing – original draft, Writing – review & editing. MZ: Methodology, Writing – original draft, Writing – review & editing. NPB: Methodology, Writing – original draft, Writing – review & editing. MS: Supervision, Writing – original draft, Writing – review & editing. IN: Methodology, Supervision, Writing – original draft, Writing – review & editing.

Funding

The author(s) declare that no financial support was received for the research, authorship, and/or publication of this article.

Conflict of interest

The authors declare that the research was conducted in the absence of any commercial or financial relationships that could be construed as a potential conflict of interest.

Publisher's note

References

1. Zhao M, Zhao L, Yang H, Duan Y, Li G. Apparent diffusion coefficient for the prediction of tumor response to neoadjuvant chemo-radiotherapy in locally advanced rectal cancer. *Radiat Oncol.* (2021) 16:17. doi: 10.1186/s13014-020-01738-6

2. Babatürk A, Erden A, Geçim İE. Apparent diffusion coefficient histogram analysis for predicting neoadjuvant chemoradiotherapy response in patients with rectal cancer. *Diagn Interv Radiol.* (2022) 28:403–9. doi: 10.5152/dir.2022.201112

3. Lee YC, Hsieh CC, Chuang JP. Prognostic significance of partial tumor regression after preoperative chemoradiotherapy for rectal cancer: a meta-analysis. *Dis Colon Rectum.* (2013) 56:1093–101. doi: 10.1097/DCR.0b013e318298e36b

4. Yin JD, Song LR, Lu HC, Zheng X. Prediction of different stages of rectal cancer: Texture analysis based on diffusion-weighted images and apparent diffusion coefficient maps. *World J Gastroenterol.* (2020) 26:2082–96. doi: 10.3748/wjg.v26.i17.2082

5. El Kady RM, Choudhary AK, Tappouni R. Accuracy of apparent diffusion coefficient value measurement on PACS workstation: A comparative analysis. *AJR Am J Roentgenol*. (2011) 196:2804. doi: 10.1097/MD.0000000000005910

6. Stanescu-Siegmund N, Nimsch Y, Wunderlich AP, Wagner M, Meier R, Juchems MS, et al. Quantification of inflammatory activity in patients with Crohn's disease using diffusion weighted imaging (DWI) in MR enteroclysis and MR enterography. *Acta Radiol*. (2017) 58:264–71. doi: 10.1177/0284185116648503

7. Viswanathan C, Bhosale P, Ganeshan DM, Truong MT, Silverman P, Balachandran A. Imaging of complications of oncological therapy in the gastrointestinal system. *Cancer Imaging*. (2012) 12:163–72. doi: 10.1102/1470-7330.2012.0014

8. van Heeswijk MM, Lambregts DMJ, Maas M, Lahaye MJ, Ayas Z, Slenter JMGM, et al. Measuring the apparent diffusion coefficient in primary rectal tumors: is there a benefit in performing histogram analyses? *Abdom Radiol*. (2017) 42:1627–36. doi: 10.1007/s00261-017-1062-2

9. Sun Y, Tong T, Cai S, Bi R, Xin C, Gu Y. (ADC) value: A potential imaging biomarker that reflects the biological features of rectal cancer. *PloS One*. (2014) 9: e109371. doi: 10.1371/journal.pone.0109371

10. Yan C, Pan X, Chen G, Ge W, Liu S, Li M, et al. A pilot study on correlations between preoperative intravoxel incoherent motion MR imaging and postoperative histopathological features of rectal cancers. *Transl Cancer Res*. (2017) 6:1050–60. doi: 10.21037/tcr.2017.08.23

11. Sun H, Xu Y, Song A, Shi K, Wang W. Intravoxel incoherent motion MRI of rectal cancer: correlation of diffusion and perfusion characteristics with prognostic tumor markers. *AJR Am J Roentgenol*. (2018) 210:139–47. doi: 10.2214/AJR.17.18342

12. Liu L, Liu Y, Xu L, Li Z, Lv H, Dong N, et al. Application of texture analysis based on apparent diffusion coefficient maps in discriminating different stages of rectal cancer. *J Magn Reson Imaging*. (2017) 45:1798–808. doi: 10.1002/jmri.25460

13. Xu Y, Xu Q, Sun H, Liu T, Shi K, Wang W. Could IVIM and ADC help in predicting the KRAS status in patients with rectal cancer? *Eur Radiol*. (2018) 28:3059–65. doi: 10.1007/s00330-018-5329-y

14. Surov A, Pech M, Powerski M, Woidacki K, Wienke A. Pretreatment apparent diffusion coefficient cannot predict histopathological features and response to neoadjuvant radiochemotherapy in rectal cancer: A meta-analysis. *Dig Dis*. (2022) 40:33–49. doi: 10.1159/000515631

15. Caruso D, Zerunian M, De Santis D, Biondi T, Paolantonio P, Rengo M, et al. Magnetic resonance of rectal cancer response to therapy: An image quality comparison between 3.0 and 1.5 tesla. *BioMed Res Int*. (2020) 2020:1–8. doi: 10.1155/2020/9842732

16. Zheng X, Lu T, Tang Q, Yang M, Fan Y, Wen M. The clinical value of applying diffusion-weighted imaging combined with T2-weighted imaging to assess diagnostic performance of muscularis propria invasion in mid-to-high rectal cancer. *Abdom Radiol (NY)*. (2024). doi: 10.1007/s00261-024-04536-w

17. Liu J, Li Q, Tang L, Huang Z, Lin Q. Correlations of mean and mimimum apparent diffusion coefficient values with the clinicopathological features in rectal cancer. *Acad Radiol*. (2021) 28:S105–11. doi: 10.1016/j.acra.2020.10.018

18. Yu G, Yang L, Zhou J, Zhang L, Xia L. Abnormally expressed circular RNAs are promising biomarkers for diagnosis of hepatocellular carcinoma: A meta-analysis. *Clin Lab*. (2019) 65. doi: 10.7754/Clin.Lab.2019.190354

19. Zhou J, Zhang B, Zhang X, Wang C, Xu Y. Identification of a 3-miRNA signature associated with the prediction of prognosis in nasopharyngeal carcinoma. *Front Oncol*. (2022) 11:823603. doi: 10.3389/fonc.2021.823603

20. Ma Y, Liu Y, Meng H. Prognostic evaluation of oral squamous cell carcinoma based on pleiotrophin, urokinase plasminogen activator, and glycoprotein nonmetastatic melanoma protein B expression. *Med (Baltimore)*. (2023) 102:e35634. doi: 10.1097/MD.0000000000035634

21. Xu Q-L, Luo Z, Zhang B, Qin G-J, Zhang R-Y, Kong X-Y, et al. Methylation-associated silencing of miR-9-1 promotes nasopharyngeal carcinoma progression and glycolysis via HK2. *Cancer Sci*. (2021) 112:4127–38. doi: 10.1111/cas.15103

22. Jelski W, Mroczko B. Biochemical markers of colorectal cancer – present and future. *Cancer Manag Res*. (2020) 12:4789–97. doi: 10.2147/CMAR.S253369

frontiers | Frontiers in Oncology

TYPE Case Report
PUBLISHED 07 November 2024
DOI 10.3389/fonc.2024.1449119

OPEN ACCESS

EDITED BY
Matteo Becatti,
University of Firenze, Italy

REVIEWED BY
Panneerselvam Jayabal,
The University of Texas Health Science Center at San Antonio, United States
Oleg Tsodikov,
University of Kentucky, United States

*CORRESPONDENCE
Mary E. Carter
mary.carter@med.uni-tuebingen.de

RECEIVED 14 June 2024
ACCEPTED 11 October 2024
PUBLISHED 07 November 2024

CITATION
Carter ME, Benegiamo-Chilla A, Kloker LD, Paulsen N, Potkrajcic V, Paulsen F, Nemeth A, Steger V, Schulze M, Biskup S, Benzler K, Singer S, Lauer UM, Zender L and Deinzer CKW (2024) Case report: Pulmonary Ewing sarcoma disguised as non-small cell lung cancer.
Front. Oncol. 14:1449119.
doi: 10.3389/fonc.2024.1449119

Case report: Pulmonary Ewing sarcoma disguised as non-small cell lung cancer

Mary E. Carter[1]*, Alessia Benegiamo-Chilla[1], Linus D. Kloker[1], Nikolas Paulsen[1], Vlatko Potkrajcic[2], Frank Paulsen[2], Attila Nemeth[3], Volker Steger[3], Martin Schulze[4], Saskia Biskup[4,5], Katrin Benzler[1], Stephan Singer[6], Ulrich M. Lauer[1,7,8], Lars Zender[1,7,8] and Christoph K. W. Deinzer[1]

[1]Department of Medical Oncology and Pneumology, Medical University Hospital, Tübingen, Germany, [2]Department of Radiation Oncology, University Hospital, Tübingen, Germany, [3]Department of Thoracic and Cardiovascular Surgery, University Hospital, Tübingen, Germany, [4]Zentrum für Humangenetik Tübingen, Tübingen, Germany, [5]CeGaT GmbH, Center for Genomics and Transcriptomics, Tübingen, Germany, [6]Institute of Pathology and Neuropathology, University Hospital Tübingen, Tübingen, Germany, [7]University of Tübingen, iFIT Cluster of Excellence (EXC2180) "Image-Guided and Functionally Instructed Tumor Therapies", Tübingen, Germany, [8]German Cancer Research Consortium (DKTK), Partner Site Tübingen, German Cancer Research Center (DKFZ), Heidelberg, Germany

Ewing sarcoma is the second most common primary malignant bone cancer in children and adolescents. This rare type of cancer is characterized by its high malignancy and therefore high risk of metastases. Typically, Ewing sarcomas originate from bones. However, extraosseous Ewing sarcoma such as pulmonary Ewing sarcoma can also be found. In this case report, we present a 55-year old male patient who was initially diagnosed with non-small cell lung cancer at his local district hospital. However, the diagnosis was changed to one of pulmonary Ewing sarcoma after subsequent histopathological and molecular pathological analysis performed in a reference pathology laboratory. After patient referral to a certified (according to the German Cancer Society) high-volume sarcoma center, multimodal chemotherapy was initiated based on recently published clinical data as opposed to the more commonly used treatment regimen in Europe. The patient responded well to treatment and underwent a complete surgical tumor resection followed by radiotherapy. In summary, this case report highlights the importance of a rigorous and timely histopathological examination of biopsy samples by a specialized cancer center to enable a correct diagnosis of the cancer type. Additionally, molecular pathology plays a crucial part in this analysis and allows the necessary differentiation between cancer types. Up to now, there is no international treatment guideline available for the treatment of Ewing sarcoma. Patients should be referred to specialist centers to allow the best possible treatment of the cancer type in view of current published clinical data. In the case of Ewing sarcoma, and in accordance with the most recent research,

patients should be treated with vincristine, doxorubicin and cyclophosphamide plus ifosfamide and etoposide in combination with local treatment such as surgery and/or radiotherapy because this has been demonstrated to be the more effective therapy.

KEYWORDS

case report, Ewing sarcoma, pulmonary Ewing sarcoma, chemotherapy, molecular pathology, *EWSR1::FLI1*, tumor resection

1 Introduction

1.1 Ewing sarcoma

The Ewing's sarcoma family of tumors (ESFT) includes four main types of cancer: osseous Ewing sarcoma, primary neuroectodermal tumors, Askin tumor (Ewing sarcoma originating from the chest wall) and extraosseous Ewing sarcoma such as pulmonary Ewing sarcoma (1, 2).

Although the average annual incidence in the population is only 2.9 per million, Ewing sarcoma is, nevertheless, still the second most common primary malignant bone cancer in children and adolescents (2). Patients mostly present in their second to third decade of life (3, 4).

This rare type of cancer is characterized by its high malignancy and therefore high risk of metastases (3). Despite multimodal treatment, long-term survival in metastatic disease occurs in only 20–25% of patients. Metastases are predominantly present in the lungs (70–80%) and bone/bone marrow (40–45%) and are associated with a dismal prognosis. In addition, recurrent disease is observed in 30–40% of patients with primary non-metastatic disease, increasing to 60–80% for patients with metastatic disease at initial diagnosis (3).

An important part of the diagnostic workflow is histopathological characterization. Ewing sarcomas are characterized by a solid growth pattern with monomorphic small cells displaying round nuclei (5). Most Ewing sarcomas stain positive with immunohistochemical testing for cluster of differentiation (CD) 99 (5). However, this marker is not specific for Ewing sarcoma (3). A definitive diagnosis of Ewing sarcoma is only possible by molecular pathology. Ewing sarcoma is characterized by an aberrant gene fusion. The rearrangement often includes the *Ewing sarcoma breakpoint region 1* (*EWSR1*) which in most cases is joined with *Friend leukemia integration 1* (*FLI1*) (6). The onco-fusion gene *EWSR1::FLI1* can be detected by using a fluorescent *in-situ* hybridization (FISH)-based method and/or reverse transcriptase polymerase chain reaction (RT-PCR) detection (3, 7). In addition, the fusion gene can be detected with DNA or RNA sequencing. FISH-based detection is widely used for diagnostic purposes. However, in difficult cases RT-PCR is performed in addition for reliable diagnosis (8). In accordance with the World Health Organization the testing for molecular translocation is a requirement for diagnosis of Ewing sarcoma (9, 10).

Patients with pulmonary Ewing sarcoma often present with a few symptoms that mimic pneumonia with fever and dyspnea (11). As a consequence, further investigation is conducted with diagnostic imaging such as by computed tomography (CT). These scans of the chest often reveal a single well-defined mass with an inhomogeneous appearance. Calcifications and pleural effusions can also be seen. In some cases, the mass can extend to the chest wall and mediastinum with possible invasion of surrounding structures (11–13).

1.2 Therapeutic approaches

Therapeutic approaches for Ewing sarcoma combine chemotherapy, surgery and radiotherapy, while interdisciplinary sarcoma tumor boards help to facilitate decision making for optimal patient treatment (14). Importantly, there has been no successful introduction of new drugs for Ewing sarcoma in the last 40 years (3). A combination of surgery with neoadjuvant and adjuvant chemotherapy is the standard of care due to the high risk of metastases (3, 15). Radiotherapy (RT) is an important additional treatment pillar for the treatment of Ewing sarcoma as this cancer type has been found to be sensitive to RT (16). RT can be utilized in addition to surgery or as definitive treatment for local control of inoperable tumors.

The therapeutic approach to patients with Ewing sarcoma usually consists of a combination of different chemotherapeutic agents. Currently, there is no internationally standardized chemotherapeutic treatment for Ewing sarcoma. The regimen widely used in Europe according to the EURO-EWING 99 trial combines induction chemotherapy (vincristine, ifosfamide, doxorubicin und etoposide [VIDE] before local procedures) with consolidation chemotherapy according to risk (vincristine, actinomycin D, and ifosfamide or cyclophosphamide [VAI or VAC]). Alternatively, high-dose busulfan and melphalan can be used instead of consolidation chemotherapy for localized disease with preselected high-risk factors which leads to an improvement in event-free survival and overall survival (17).

The treatment regimen used mainly in the US is based on the Children's Oncology Group AEWS0031 trial (18). The induction therapy consists of alternating cycles of vincristine, doxorubicin and cyclophosphamide (VDC) with ifosfamide and etoposide (IE) once every two weeks. The subsequent consolidation therapy after surgery includes alternating cycles of IE and vincristine and cyclophosphamide (VC). The cycles during consolidation therapy have been shown to be more effective when administered once every 2 weeks (18).

A recent open-label randomized phase 3 trial (EE2012) directly compared the two therapeutic regimens mentioned above. The trial managed to recruit a total of 640 patients between the ages of 2 and 49 years and allocated 320 patients to each of two groups. Group 1 was treated with the European treatment regimen. Group 2 was treated according to the American protocol. The primary outcome measured was event-free survival. At 3 years, event-free survival was 67% for patients receiving VDC and IE as opposed to 61% for patients treated with VIDE (HR 0.71 [95% 0.55-0.92]). Overall, the results showed a higher effectivity, reduced toxicity and shorter duration of treatment. The trial concluded that the dose-intensive chemotherapy with VDC and IE is more beneficial for patients newly diagnosed with Ewing sarcoma and should therefore be used as the standard of care (15).

1.3 Case highlights

In this case report we describe a 55-year old male patient who was initially diagnosed with non-small cell lung cancer (NSCLC) at his local district hospital. However, the diagnosis was changed to one of pulmonary Ewing sarcoma after subsequent histopathological and molecular pathological analysis in a reference pathology laboratory. After patient referral to a certified (according to the German Cancer Society DKG) high-volume sarcoma center, multimodal chemotherapy was initiated based on recently published clinical data as opposed to the more commonly used treatment regimen in Europe. The patient responded well to treatment and underwent complete surgical tumor resection followed by radiotherapy to reduce the risk of tumor relapse.

2 Case report

2.1 Patient history

A 55-year-old man presented with coughing and dyspnea to his general practitioner. Two months after symptom onset the patient was referred to his local district hospital due to his worsening symptoms. A CT scan of the chest revealed a large pulmonary mass (14 cm x 9.5 cm) in the left upper lobe with infiltration of the thoracic wall, the left subclavian and vertebral artery (Figures 1A, B). The mass resulted in a shift of the mediastinum to the right. The patient had no previous relevant medical history or family history of cancer.

2.2 Diagnosis

A transthoracic biopsy of the mass in the left upper lobe led to an initial diagnosis of NSCLC by the institute of pathology of the district hospital. The initial primary tumor site and size (T), regional lymph node involvement (N) and possible distant metastatic spread (M), referred to as the TNM staging for NSCLC, was defined as cT4 cN2 cM1a (PLE), according to the Union for International Cancer Control (UICC) IV A. A pre-therapeutic PET-CT scan (Figures 1A, B) was performed externally.

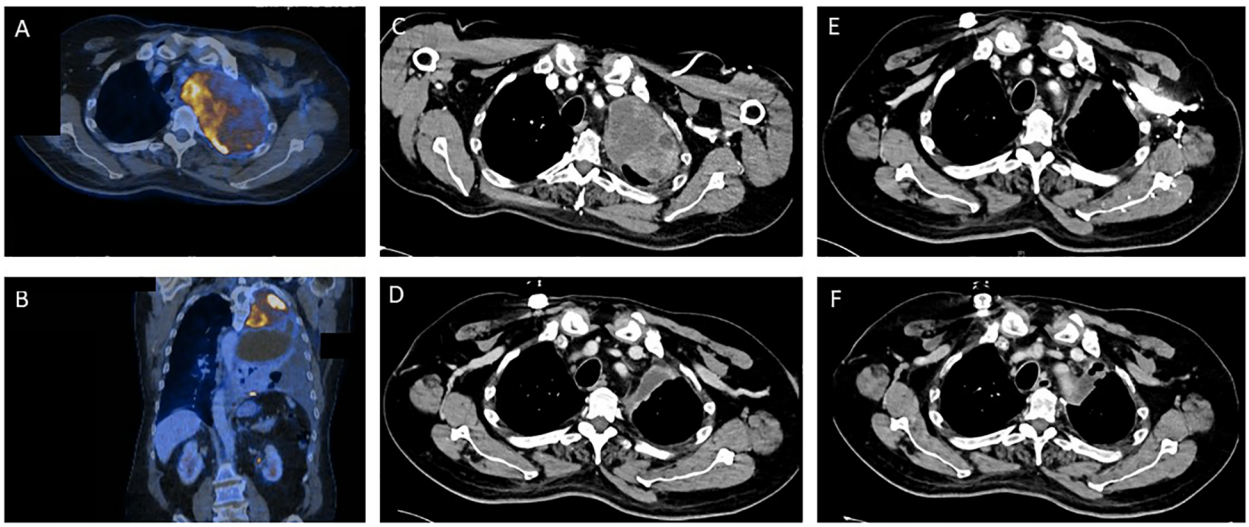

FIGURE 1
Tumor regression as depicted by sequential contrast enhanced computed tomography (CT) and positron emission tomography (PET) before and during the various stages of treatment for Ewing sarcoma. **(A, B)** Pre-therapeutic PET/CT imaging. **(C)** CT imaging prior to start of Ewing sarcoma chemotherapy. **(D)** CT Imaging after 2.5 cycles of induction chemotherapy. **(E)** CT Imaging after induction chemotherapy. **(F)** Post-operative CT imaging.

Reference pathology for molecular analysis of lung cancer was routinely sent from the district hospital to the institute of pathology at a university hospital. These results showed a small cell, solid growing tumor with immunohistochemical staining positive for CD56 as well as CD99. Additional immunostainings showed that the tumor was negative for AE1/3 cytokeratins, CK 7, BerEP4, CD34, CK5-14, p40, SOX 10, NUT, protein S100, chromogranin, synaptophysin and thyroid transcription factor (TTF-1). Nucleal expression of INI-1 was found to be intact.

Subsequent molecular pathological analysis was performed with next-generation sequencing (NGS) based on the Archer PanST V2 panel. The results clearly demonstrated a *EWSR1::FLI1* (E7F5) fusion with breaking points at an RNA level after *ESWR1* exon 7 and before FLI1 exon 5, thereby resulting in a diagnosis of a Ewing sarcoma (7).

After this diagnosis the patient was referred to the certified high-volume sarcoma center at the University Hospital Tübingen. Our interdisciplinary sarcoma tumor board recommended a complete CT body scan. This scan (Figure 1C) revealed a slight reduction in tumor mass when compared to the initial PET-CT performed in the local district hospital as mentioned above. However, the extent of the pulmonary mass was still large and metastases were present in the thoracic wall.

2.3 Treatment

Figure 2 offers an overview of the treatment described below.

The patient received chemotherapy based on the initial diagnosis of NSCLC according to German guidelines for the treatment of NSCLC. Treatment consisted of two cycles of carboplatin (AUC 5), paclitaxel (175 mg/m^2) and pembrolizumab (200 mg) due to the mediastinal shift and worsening dyspnea (19).

Shortly after the altered diagnosis and subsequent admission to the University Hospital Tübingen, our interdisciplinary sarcoma tumor board recommended initiation of a chemotherapeutic regimen according to the EWING 2012 trial (15). The patient was planned to receive 4.5 cycles of vincristine (1 day of 2 mg), doxorubicin (2 days of 37.5 mg/m^2) and cyclophosphamide (1 day of 1200 mg/m^2) followed by ifosfamide (5 days of 1800 mg/m^2) and etoposide (5 days of 100 mg/m^2). Figure 1D shows CT imaging after 2.5 cycles of induction chemotherapy.

After completion of 3 cycles of chemotherapy the patient underwent leukapheresis for a potentially necessary autologous blood stem-cell rescue.

The blood test showed a thrombocytopenia grade IV and a neutropenia grade IV. Consequently, the chemotherapeutic dose was reduced to 80% after 3.5 cycles. The patient completed the planned 4.5 cycles of chemotherapy. CT scans revealed a reduction in size of the pulmonary mass as well as no additional metastases (Figure 1E). Consequently, our interdisciplinary sarcoma tumor board recommended surgical tumor resection.

After completion of induction chemotherapy the patient underwent a left posterolateral thoracotomy with extended lobectomy of the left upper lobe with intrapericardial vessel resection. Additionally, a radical lymph node dissection was performed. The patient recovered well from surgery and there were no postoperative complications. The histopathological evaluation and molecular testing confirmed diagnosis of a *EWSR1::FLI1* fusion Ewing sarcoma and resulted in postoperative TNM classification of ypT2b, pN0 (0/4 LN), L0, V0, Pn0, R0. The vital residual tumor within the surgically removed tissue was described with 10%.

The pulmonary vital capacity increased during the preoperative chemotherapy from 1.06L to 1.60L. Due to initial exertional dyspnea, surgical resection was performed two months after completion of induction chemotherapy. After surgery the vital capacity further increased to 2.07L thereby resulting in increased cardiorespiratory exercise capacity for the patient. The postoperative CT scans revealed no pulmonary mass and no detection of metastases (Figure 1F). Additionally, no brain metastases could be detected in MRI scans and no bone marrow infiltration was found in bone marrow biopsy.

Postoperatively, the patient received 2.5 cycles of consolidation treatment with VC/IE. This treatment regimen included vincristine

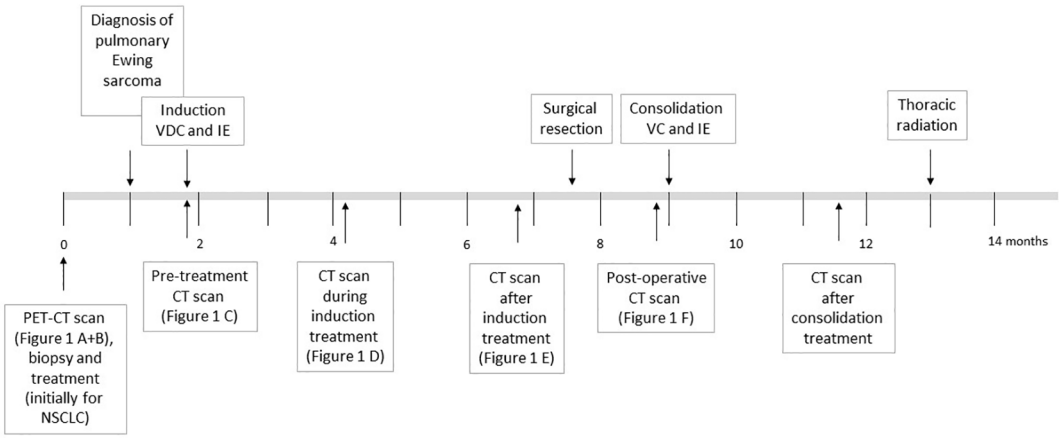

FIGURE 2
Overview of the chemotherapy treatment as described in the text for the patient diagnosed with Ewing sarcoma. The time in months since first hospital admission and diagnosis are shown.

(1 day of 2 mg) and cyclophosphamide (1 day of 1200 mg/m^2) followed by ifosfamide (5 days of 1800 mg/m^2 in 80%) and etoposide (5 days of 100 mg/m^2 in 80%). The post-therapeutic imaging revealed no residual tumor burden.

After surgery and postoperative consolidation chemotherapy, the patient will undergo radiotherapy of the operative field to reduce the risk of tumor relapse.

2.4 Molecular genetic analysis

The molecular genetic analysis was performed by the Center for Human Genetics in Tübingen. Tissue obtained from the initial biopsy of the lung and from surgically resected tissue was analyzed (Figures 3, 4). Supplementary Table 1 offers an overview of the full gene list and list of biomarkers routinely described in the panel.

The surgically resected tissue included sufficient tumor cells to allow reliable results. NGS of the DNA from the biopsy tissue detected a *EWSR1::FL1* fusion gene, which confirmed the initial diagnosis of Ewing sarcoma. In addition, an oncogenic mutation of the *human telomerase reverse transcriptase* (*TERT*) gene was found. The tumor displayed a low tumor mutational burden with 0.4 Var/Mb. Further analysis could not detect microsatellite instability or a deficit in homologous recombination.

A *ESWR1* fusion gene is typical for patients with Ewing sarcoma (20). The gene fusion consists of the N-terminus of an RNA-binding protein (ESWR1 = ES breakpoint region 1) and the carboxyl terminal DNA-binding domain of an erythroblast transformation specific (ETS) family transcription factor. In most cases the translocation t(11;22) (q24;q12) results in jointure of *ESWR1* from chromosome 22 with *FLI1* from chromosome 11 (Figure 4). The mechanism causing this chromosomal translocation is currently unknown. *EWSR1::FLI1* acts as a transcription factor to enable malignant transformation. Consequently, this influences the transcription of relevant downstream targets. In addition, it influences transcript degradation, alternative splicing and regulatory mechanisms for RNA abundance (6). The molecular mechanism by which the EWSR1::FLI1 fusion acts has not yet been fully characterized due to its complex nature. However, the fusion protein can act as both a transcriptional activator and a repressor. EWSR1::FLI1 can directly repress transcription by binding to wild-type ETS family binding sites in promoters and enhancers where it displaces normal transcription factors. Gene expression can also be negatively influenced indirectly by the activation of transcriptional repressors and by epigenetic mechanisms. Activation of gene expression by EWSR1::FLI1 occurs via the formation of new active gene enhancers at genomic GGAA microsatellite motifs. The recruitment of histone acetyl/methyltransferases increases chromatin accessibility and leads to the transcription of genes in previously epigenetically silenced regions of the genome (21). Although this fusion gene is tumor specific and seems to be a suitable drug target, there is no therapeutic agent approved by the Food and Drug Administration (FDA) or the European Medicines Agency (EMA) that addresses this specific defect. The complex structural features combined with the process of transcription are the main challenges for the development of small molecule inhibitors of *EWS/FLI1* (22).

In addition, a mutation of the *TERT* gene was detected with NGS. Typically, within an aging organism the telomers are shortened during the cell cycle. *TERT* allows lengthening of the telomers and thereby continuous cell division. During carcinogenesis mutations of *TERT* can be acquired that result in an infinite capacity for replication. The *TERT* activity has been found to be crucial for cell transformation. The telomerase activity is influenced by regulation at different stages including gene transcription and mRNA splicing (23). The mutation influencing *TERT* activity detected in this patient is located in the *TERT* promoter region (c.-124C>T). This alteration results in an enhanced *TERT* promotor activity by the generation of a binding site for erythroblast transformation specific (ETS) transcription factors. The *ESWR1:FLI1* fusion gene can potentially influence *TERT* activity via the binding site for ETS (24).

3 Discussion

This case report illustrates important aspects of the diagnosis and treatment of pulmonary Ewing sarcoma. The patient had no

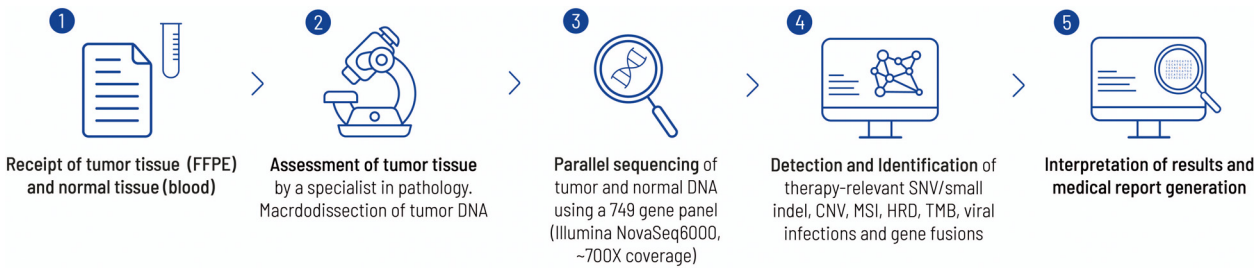

FIGURE 3
This figure highlights the work flow from sample receipt to the final medical report at the Centre for Human Genetics, Tübingen. Each FFPE block is examined by a pathology specialist before sequencing to verify the tumor entity and check for suitability with regard to tumor content. In the present case, a histological tumor content of 20% was determined. The bioinformatics pipeline has already been described elsewhere (26).

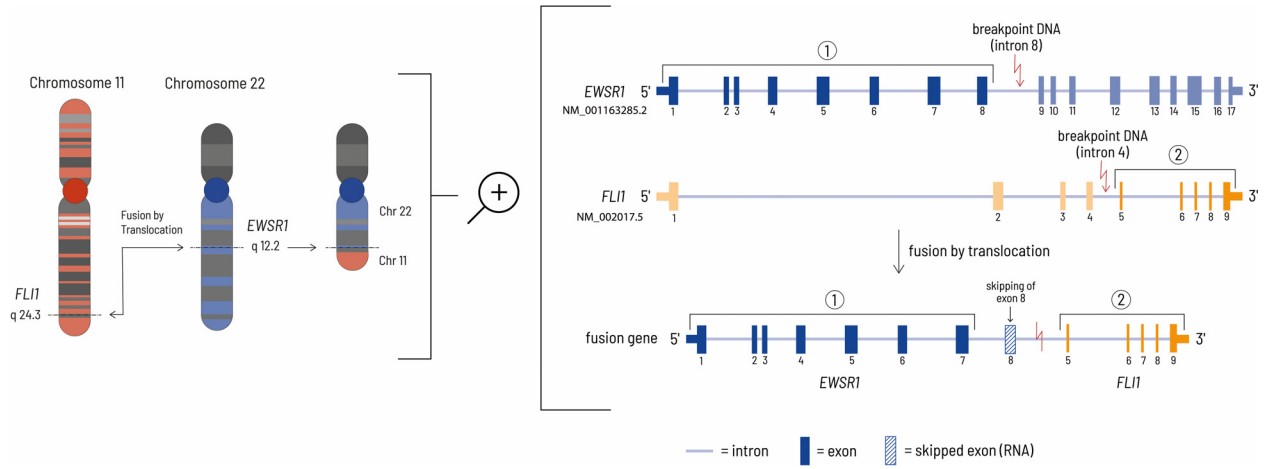

FIGURE 4
The left side of the figure shows the translocation event leading to the *EWSR1-FLI1* fusion gene at the chromosomal level. In this case, the genomic breakpoints are located at chr22:29685464 - chr11:128643985 (HG19 reference genome). The right side of the figure shows the details at the gene level. Although the genomic breakpoint in the EWSR1 gene is located after exon 8, the eighth exon of the *EWSR1* gene is removed during mRNA processing by HNRNPH1, thereby resulting in an inframe fusion protein consisting of the first 7 *EWSR1* exons and exons 5-9 of the *FLI1* gene (27, 28).

relevant medical history or family history of cancer. The initial symptoms leading to medical referral and diagnostic investigation were indistinct. The first histopathological examination of a transthoracic biopsy led to a diagnosis of lung cancer. Due to the severity of the symptoms and the size of the pulmonary mass chemotherapy was started before the results were obtained from the reference pathology laboratory. However, further examination of the tumor tissue in a certified reference pathology laboratory revealed a Ewing sarcoma. After diagnosis the patient was referred to our university hospital specialized and certified in sarcoma care.

The change of the initial diagnosis highlights the importance of ensuring the appropriate information is available in a timely manner for correct diagnosis and subsequent treatment. Indeed, molecular pathological confirmation, that is part of the diagnostic algorithm in specialized cancer centers, is indispensable for the confirmation of Ewing sarcoma. This further underlines the importance of such centers as molecular pathology is essential to differentiate tumors which can clinically present similarly and may need special knowledge to be correctly identified. In this case NGS allowed the identification of the *ESWR1::FLI1* gene fusion and thereby resulted in the diagnosis of a pulmonary Ewing sarcoma.

Up to now, there are no worldwide international guidelines available for the treatment of Ewing sarcomas. Nevertheless, in Europe a guideline does exist for the treatment of Ewing Sarcoma (25). Over the past decades, two main chemotherapeutic protocols have been established. In the US chemotherapy consists of an induction therapy with VDC and IE followed by consolidation therapy with alternating cycles of IE and VC (18). In Europe induction chemotherapy with VIDE is followed by consolidation chemotherapy according to risk (VAI or VAC) (17). A recent clinical trial (EE2012) found treatment with VDC and IE to be superior to VIDE and VAC/VAI. The results indicated a higher effectivity (for both event-free survival and overall survival) and reduced toxicity for VDC plus IE chemotherapy compared to VIDE and VAC/VAI (15). In accordance with these findings our patient underwent induction chemotherapy with VDC and IE. The patient displayed only mild side effects even though the patient was over 50 years of age. The resulting thrombocytopenia and leukopenia being the main side effects led to a reduction of the dose of chemotherapy used.

In some cases, chemotherapy can be followed by high-dose chemotherapy and autologous blood stem-cell rescue (17). Patients with low histological response at a localized stage may respond to this treatment. In a metastasized setting high-dose chemotherapy followed by autologous blood stem-cell rescue is not used as first-line treatment. However, in a relapsed situation this therapeutic approach is more widely used.

The EE2012 trial included patients aged 2-49 years with the median age being 15 years (15). Patients mostly present in their second to third decade of life (3, 4). The patient described in this case report was 55 years of age when admitted to our hospital for treatment of Ewing sarcoma. Thus, he was older than the average person diagnosed with Ewing sarcoma and older than any patient treated in the AEWS0031 and EE2012 trials. Nevertheless, it is important to note that the VDC plus IE chemotherapy was well tolerated and elicited a good clinical response in this older patient.

After completion of the thoracic radiotherapy the patient will be subject to regular after-care with CT scans in 3-month intervals. Ideally, these follow-up appointments should be performed at a certified sarcoma center which is crucial for early detection of tumor relapse.

4 Conclusion

In summary, this case report highlights the importance of a rigorous and timely histopathological examination of biopsy samples by a specialized cancer center to enable a correct diagnosis of the cancer type. Additionally, targeted NGS and RNA fusion panel sequencing plays a crucial part in this analysis and allows the necessary differentiation between cancer types, in this case between NSCLC and pulmonary Ewing sarcoma.

Currently, there is no worldwide international treatment guideline available for the treatment of Ewing sarcoma. Therefore, it is imperative to incorporate recently published international clinical data when choosing the best therapeutic approach for Ewing sarcoma. Patients should be referred to specialist centers to allow the best possible treatment of the cancer type. In the case of Ewing sarcoma and in accordance with the most recent research, patients should be treated with VDC plus IE because it has been demonstrated to be the most effective therapy. Moreover, the therapeutic regimen is well tolerated by both younger and older patients.

Data availability statement

The original contributions presented in the study are included in the article/Supplementary Material. Further inquiries can be directed to the corresponding author.

Ethics statement

The studies involving humans were approved by ethical commission of the Medical Faculty of the Karl Eberhard University and University Clinic in Tübingen (192/2024BO2). The studies were conducted in accordance with the local legislation and institutional requirements. The participants provided their written informed consent to participate in this study. Written informed consent was obtained from the individual(s) for the publication of any potentially identifiable images or data included in this article.

Author contributions

MC: Conceptualization, Data curation, Formal analysis, Investigation, Writing – original draft, Writing – review & editing. AB-C: Writing – review & editing. LK: Writing – review & editing. NP: Writing – review & editing. VP: Writing – review & editing. FP: Writing – review & editing. AN: Writing – review & editing. VS: Writing – review & editing. MS: Writing – review & editing. SB: Writing – review & editing. KB: Writing – review & editing. SS: Writing – review & editing. UL: Supervision, Writing – review & editing. LZ: Supervision, Writing – review & editing. CD: Conceptualization, Supervision, Writing – original draft, Writing – review & editing.

Funding

The author(s) declare financial support was received for the research, authorship, and/or publication of this article. MC received a stipend award (3033-0-0) from the intramural *fortüne* program of the Medical Faculty of The University of Tuebingen.

Acknowledgments

We would like to thank our patient for his support. We further acknowledge support by the Open Access Publishing Fund of the University of Tübingen.

Conflict of interest

CD is a consulting or advisory board member for Boehringer Ingelheim. He receives lecture honoraria from PharmaMar. In addition, he has accepted imbursement for travel, accommodation or congress registration expenses from Boehringer Ingelheim, Deciphera and Pierre Fabre.

VP is supported as a Clinician Scientist by the German Sarcoma Foundation. Author SB was employed by company CeGaT GmbH.

The remaining authors declare that the research was conducted in the absence of any commercial or financial relationships that could be construed as a potential conflict of interest.

Publisher's note

Supplementary material

The Supplementary Material for this article can be found online at: https://www.frontiersin.org/articles/10.3389/fonc.2024.1449119/full#supplementary-material

SUPPLEMENTARY TABLE 1
Provides a full gene list and list of biomarkers routinely analyzed and reported within the used NGS panel.

References

1. Takahashi D, Nagayama J, Nagatoshi Y, Inagaki J, Nishiyama K, Yokoyama R. Primary ewing's sarcoma family tumors of the lung – a case report and review of the literature. *Japanese J Clin Oncol*. (2007) 37:874–7. doi: 10.1093/jjco/hym108

2. Balamuth NJ, Womer RB. Ewing's sarcoma. *Lancet Oncol*. (2010) 11:184–92. doi: 10.1016/S1470-2045(09)70286-4

3. Zöllner SK, Amatruda JA, Bauer S, Collaud S, de Álava E, DuBois SG, et al. Ewing sarcoma—Diagnosis, treatment, clinical challenges and future perspectives. *J Clin Med*. (2021) 10:1685. doi: 10.3390/jcm10081685

4. Sohn AJ, Lang B, McCarroll M, Agarwa A. Primary pulmonary Ewing sarcoma/peripheral primitive neuroectodermal tumor. *Baylor Univ Med Center Proc*. (2020) 33:646–8. doi: 10.1080/08998280.2020.1798723

5. Marcilla D, Machado I, Grünewald TGP, Llombart-Bosch A, Álava E. (Immuno) histological analysis of ewing sarcoma. In: Cidre-Aranaz F, Grünewald TGP, editors. *Ewing Sarcoma: Methods and Protocols*. Springer US, New York, NY (2021). p. 49–64.

6. Yu L, Davis IJ, Liu P. Regulation of EWSR1-FLI1 function by post-transcriptional and post-translational modifications. *Cancers*. (2023) 15:382. doi: 10.3390/cancers15020382

7. Sorensen PHB, Liu XF, Delattre O, Rowland JM, Biggs CA, Thomas , et al. Reverse transcriptase PCR amplification of EWS/FLI-1 fusion transcripts as a diagnostic test for peripheral primitive neuroectodermal tumors of childhood. *Diagn Mol Pathol*. (1993) 2:147–57. doi: 10.1097/00019606-199303000-00022

8. Chen S, Deniz K, Sung Y-S, Zhang L, Dry S, Antonescu CR. Ewing sarcoma with ERG gene rearrangements: A molecular study focusing on the prevalence of FUS-ERG and common pitfalls in detecting EWSR1-ERG fusions by FISH. *Genes Chromosomes Cancer*. (2016) 55:340–9. doi: 10.1002/gcc.22336

9. Sbaraglia M, Bellan E, Dei Tos AP. The 2020 WHO Classification of Soft Tissue Tumours: news and perspectives. *Pathologica*. (2021) 113:70–84. doi: 10.32074/1591-951X-213

10. Moch H. Soft tissue and bone tumours WHO classification of tumours/volume 3. *WHO classification tumours*. Lyon: International Agency for Research on Cancer (2020) 3.

11. Akesh T, Obeidat N, Darweesh M. Thoracic ewing's sarcoma: A case report. *Cureus*. (2022) 14:e24150. doi: 10.7759/cureus.24150

12. Shet N, Stanescu L, Deutsch G. Primary extraosseous Ewing sarcoma of the lung: Case report and literature review. *Radiol Case Rep*. (2013) 8:832. doi: 10.2484/rcr.v8i2.832

13. Gladish GW, Sabloff BM, Munden RF, Truong MT, Erasmus JJ, Chasen MH. Primary thoracic sarcomas. *RadioGraphics*. (2002) 22:621–37. doi: 10.1148/radiographics.22.3.g02ma17621

14. Leitlinienprogramm Onkologie (Deutsche Krebsgesellschaft, Deutsche Krebshilfe, AWMF): S3-Leitlinie Adulte Weichgewebesarkome (2021). Available online at: https://www.leitlinienprogramm-onkologie.de/leitlinien/adulte-weichgewebesarkome/. (Accessed March 28, 2024)

15. Brennan B, Kirton L, Marec-Bérard P, Gaspar N, Laurence V, Javier Martín-Broto J. Comparison of two chemotherapy regimens in patients with newly diagnosed Ewing sarcoma (EE2012): an open-label, randomised, phase 3 trial. *Lancet*. (2022) 400:1513–21. doi: 10.1016/S0140-6736(22)01790-1

16. Ewing J. Diffuse endothelioma of bone. *CA: A Cancer J Clin*. (1972) 22:95–8. doi: 10.3322/canjclin.22.2.95

17. Whelan J, et al, Dirksen U, Le Teuff G, Brennan B, Gaspar N, Hawkins DS. High-dose chemotherapy and blood autologous stem-cell rescue compared with standard chemotherapy in localized high-risk ewing sarcoma: results of euro-E.W.I.N.G.99 and ewing-2008. *J Clin Oncol*. (2018) 36:Jco2018782516. doi: 10.1200/JCO.2018.78.2516

18. Womer RB, et al. Randomized controlled trial of interval-compressed chemotherapy for the treatment of localized Ewing sarcoma: a report from the Children's Oncology Group. *J Clin Oncol*. (2012) 30:4148–54. doi: 10.1200/JCO.2011.41.5703

19. Schütte W, Gütz S, Nehls W, Blum TG, Brückl W, Buttmann-Schweiger N, et al. Prävention, Diagnostik, Therapie und Nachsorge des Lungenkarzinoms. *Pneumologie* (2023) 77:671–813. doi: 10.1055/a-2029-0134

20. Delattre O, Zucman J, Plougastel B, Desmaze C, Melot T, Peter M, et al. Gene fusion with an ETS DNA-binding domain caused by chromosome translocation in human tumours. *Nature*. (1992) 359:162–5. doi: 10.1038/359162a0

21. Yasir M, Park J, Chun W. EWS/FLI1 characterization, activation, repression, target genes and therapeutic opportunities in ewing sarcoma. *Int J Mol Sci*. (2023) 24:15173. doi: 10.3390/ijms242015173

22. Flores G, Grohar PJ. One oncogene, several vulnerabilities: EWS/FLI targeted therapies for Ewing sarcoma. *J Bone Oncol*. (2021) 31:100404. doi: 10.1016/j.jbo.2021.100404

23. Heidenreich B, Rachakonda PS, Hemminki K, Kumar R. TERT promoter mutations in cancer development. *Curr Opin Genet Dev*. (2014) 24:30–7. doi: 10.1016/j.gde.2013.11.005

24. Vinagre J, Almeida A, Pópulo H, Batista R, Lyra J, Pinto V. Frequency of TERT promoter mutations in human cancers. *Nat Commun*. (2013) 4:2185. doi: 10.1038/ncomms3185

25. Strauss S, Frezza AM, Abecassis N, Bajpai J, Bauer S, Biagini R. Bone sarcomas: ESMO–EURACAN–GENTURIS–ERN PaedCan Clinical Practice Guideline for diagnosis, treatment and follow-up. *Ann Oncol*. (2021) 32:1520–36. doi: 10.1016/j.annonc.2021.08.1995

26. Forschner A, Weißgraeber S, Hadaschik D, Schulze M, Kopp M, Kelkenberg S, et al. Circulating tumor DNA correlates with outcome in metastatic melanoma treated by BRAF and MEK inhibitors - results of a prospective biomarker study. *Onco Targets Ther*. (2020) 13:5017–32. doi: 10.2147/OTT.S248237

27. Berger M, Dirksen U, Braeuninger A, Koehler G, Juergens H, Krumbholz M, et al. Genomic EWS-FLI1 fusion sequences in Ewing sarcoma resemble breakpoint characteristics of immature lymphoid Malignancies. *PloS One*. (2013) 8:e56408. doi: 10.1371/journal.pone.0056408

28. Grohar PJ, Kim S, Rivera Nirmalya Sen GOR N, Haddock S, Harlow ML, et al. Functional genomic screening reveals splicing of the EWS-FLI1 fusion transcript as a vulnerability in Ewing sarcoma. *Cell Rep*. (2016) 14:598–610. doi: 10.1016/j.celrep.2015.12.063

frontiers | Frontiers in Molecular Biosciences

TYPE Original Research
PUBLISHED 20 November 2024
DOI 10.3389/fmolb.2024.1512715

OPEN ACCESS

EDITED BY
Matteo Becatti,
University of Firenze, Italy

REVIEWED BY
Lucia Carmela Cosenza,
University of Ferrara, Italy
Jiaying Deng,
Fudan University, China

*CORRESPONDENCE
Changsen Leng,
lengcs@sysucc.org.cn
Jianhua Fu,
fujh@sysucc.org.cn

†These authors have contributed equally to this work

RECEIVED 17 October 2024
ACCEPTED 07 November 2024
PUBLISHED 20 November 2024

CITATION
Cui Y, Wen J, Fu J and Leng C (2024) Identification of key genes to predict response to chemoradiotherapy and prognosis in esophageal squamous cell carcinoma. *Front. Mol. Biosci.* 11:1512715. doi: 10.3389/fmolb.2024.1512715

Identification of key genes to predict response to chemoradiotherapy and prognosis in esophageal squamous cell carcinoma

Yingying Cui[1,2†], Jing Wen[1,3†], Jianhua Fu[1,3,4*] and Changsen Leng[1,3,4*]

[1]State Key Laboratory of Oncology in South China, Guangdong Provincial Clinical Research Center for Cancer, Sun Yat-sen University Cancer Center, Guangzhou, China, [2]Department of Hematologic Oncology, Sun Yat-sen University Cancer Center, Guangzhou, China, [3]Guangdong Esophageal Cancer Institute, Guangzhou, China, [4]Department of Thoracic Surgery, Sun Yat-sen University Cancer Center, Guangzhou, China

Background: Chemoradiotherapy is a crucial treatment modality for esophageal squamous cell carcinoma (ESCC). This study aimed to identify chemoradiotherapy sensitivity-related genes and analyze their prognostic value and potential associations with the tumor microenvironment in ESCC.

Methods: Utilizing the Gene Expression Omnibus database, we identified differentially expressed genes between ESCC patients who achieved complete and incomplete pathological responses following chemoradiotherapy. Prognostic genes were then screened, and key genes associated with chemoradiotherapy sensitivity were determined using random survival forest analysis. We examined the relationships between key genes, infiltrating immune cells, and immunoregulatory genes. Additionally, drug sensitivity and enrichment analyses were conducted to assess the impact of key genes on chemotherapy responses and signaling pathways. A prognostic nomogram for ESCC was developed incorporating key genes, and its effectiveness was evaluated. Genome-wide association study data were employed to investigate chromosomal pathogenic regions associated with key genes.

Results: Three key genes including *ATF2*, *SLC27A5*, and *ALOXE3* were identified. These genes can predict the sensitivity of ESCC patients to neoadjuvant chemoradiotherapy and hold significant clinical relevance in prognostication. These genes were also found to be significantly correlated with certain immune cells and immunoregulatory genes within the tumor microenvironment and were involved in critical tumor-related signaling pathways, including the epithelial-mesenchymal transition and P53 pathways. A nomogram was established to predict the prognosis of ESCC by integrating key genes with clinical stages, demonstrating favorable predictability and reliability.

Conclusion: This study identified three key genes that predict chemoradiotherapy sensitivity and prognosis and are involved in

multiple tumor-related biological processes in ESCC. These findings provide predictive biomarkers for chemoradiotherapy response and support the development of individualized treatment strategies for ESCC patients.

KEYWORDS

esophageal squamous cell carcinoma, chemoradiotherapy sensitivity, neoadjuvant chemoradiotherapy, pathological complete response, immune microenvironment

Introduction

Esophageal cancer ranks as the seventh most common malignant tumor globally, with approximately 604,100 new cases diagnosed annually (Sung et al., 2021). Histopathologically, it is primarily classified into esophageal squamous cell carcinoma (ESCC) and esophageal adenocarcinoma, each differing markedly in pathogenesis, biological behavior, treatment, and prognosis. ESCC, accounting for about 85% of esophageal cancers, is predominantly found in East Asia and Africa (He et al., 2021). This type is highly invasive, and symptoms such as dysphagia often manifest in the disease's late stages, leading to a dismal prognosis with a five-year survival rate between 15% and 25% (Shi et al., 2022).

At diagnosis, nearly 50% of patients exhibit tumor invasion beyond the primary lesion's local area, with 70%–80% presenting regional lymph node metastasis. Locally advanced ESCC is defined as stage T2-4 or N1-3 with M0 (Thakur et al., 2021; Puhr et al., 2023). The standard treatment for this stage is neoadjuvant chemoradiotherapy (NCRT) followed by surgical resection. In the CROSS trial, the NCRT group achieved a significantly higher R0 resection rate (92% vs. 69%), negative lymph node resection rates (31% vs. 75%), and improved overall survival (OS, 49.4 vs. 24 months) compared to the surgery-only group in treating locally advanced ESCC (van Hagen et al., 2012). The NEOCRTEC5010 study, involving 451 patients, demonstrated that NCRT significantly enhanced the five-year OS rate (from 49.1% to 59.9%) over surgery alone (Yang et al., 2021a). Chen et al. further validated the superiority of NCRT over neoadjuvant chemotherapy followed by surgery, showing higher pathological complete response (pCR) rates, negative lymph node resection rates, and reduced mortality due to tumor progression or recurrence in the NCRT group (Wang et al., 2021). Approximately 20%–40% of patients with locally advanced esophageal cancer achieve pCR following NCRT (van Hagen et al., 2012; Yang et al., 2021a; Wang et al., 2021). pCR is closely associated with extended OS and reduced rates of distant recurrence (Noordman et al., 2018; Hirata et al., 2021). For ESCC patients achieving pCR after NCRT, the need for esophagectomy and treatment strategies should be reassessed (Noordman et al., 2018). Furthermore, given the poor prognosis of advanced ESCC, predicting patient outcomes from chemoradiotherapy in advance can inform treatment planning (Hirata et al., 2021). Thus, identifying sensitive, specific, and accurate biomarkers to forecast ESCC patients' responses to chemoradiotherapy, especially their pCR status, is imperative. Previous studies suggested using clinical remission or imaging techniques to predict ESCC pCR post-NCRT (Squires et al., 2022; Liu et al., 2016). However, it remains unclear who benefits most from NCRT or chemoradiotherapy among ESCC patients.

In this study, we investigated the differentially expressed genes (DEGs) between patients who achieved pCR and did not achieve pCR (npCR) following NCRT, and screened key genes associated with the prognosis of ESCC. Subsequently, we assessed the relationships between these key genes and ESCC-related genes, infiltrating immune cells, and chemotherapy sensitivity. This analysis is intended to more accurately predict chemoradiotherapy sensitivity and prognosis, thereby enhancing treatment strategies for ESCC patients.

Methods

Data source and preprocessing

According to the 6th edition of the American Joint Committee on Cancer TNM staging system, the Guangzhou cohort included patients with ESCC staged IIb-III who underwent NCRT prior to surgery from September 2007 to March 2012. The RNA-seq data for these patients are accessible in the Gene Expression Omnibus (GEO) database under accession number GSE45670. We monitored these patients until July 2023, selecting those who survived over 3 months after treatment to assess their survival outcomes. Another cohort, the Beijing cohort (GSE53624), comprised tumor and adjacent normal tissues from 119 ESCC patients. The Series Matrix Files for GSE45670 and GSE53624 were based on annotation platforms GPL570 and GPL18109, respectively.

We retrospectively included the real-world patients with stage II-III ESCC from Sun Yat-sen University Cancer Center. Tissue samples and pathological results of these patients were obtained by endoscopic biopsy prior to treatment. After pathological diagnosis, they received NCRT combined with esophagectomy. This study was approved by the Ethics Committee of the Sun Yat-sen University Cancer Center and conducted in accordance with the local legislation and institutional requirements.

Identification of key chemoradiotherapy sensitivity-related genes

The "limma" package (Ritchie et al., 2015) was utilized to identify DEGs between pCR and npCR patients, while univariate Cox regression analysis determined genes associated with survival. We then identified genes that were highly expressed in pCR patients and suggested a favorable prognosis, and those underexpressed in pCR patients and indicated a poorer prognosis. The random survival forest algorithm executed using the "randomForestSRC" package, selected genes based on their prognostic importance. Genes with a

relative importance exceeding 0.7 were classified as key genes related to chemoradiotherapy sensitivity.

Analysis of immune cell infiltration in ESCC

Using the gene expression of each patient, the CIBERSORT deconvolution algorithm estimated the relative proportions of 22 immune cell types, including B cell subsets, T cell subsets, NK cells, and macrophages (Newman et al., 2015). We analyzed and compared the immune cell fractions in tumor and adjacent non-tumor tissues of ESCC patients employing the "CIBERSORT" and "ggpubr" R packages. Correlations between chemoradiotherapy sensitivity-related genes and immune cell fractions were examined using the "corrplot" R package.

Associations between key genes and immunoregulatory genes

To explore the associations between chemoradiotherapy sensitivity-related genes and immunoregulatory genes, we sourced gene encodings for immunomodulators from the TISIDB database (Ru et al., 2019), including 24 immunoinhibitors and 46 immunostimulators. After intersecting these with the ESCC gene expression profile, 60 genes encoding immunomodulators were retained. Pearson correlation analysis was conducted on the expression of immunoregulatory genes and chemoradiotherapy sensitivity-related genes. $P < 0.05$ was deemed statistically significant.

Drug sensitivity prediction

The Genomics of Drug Sensitivity in Cancer (GDSC) database records the responsiveness of cancer cells to drugs and molecular markers associated with drug response (Yang et al., 2013). Utilizing this pharmacogenomics database, the "oncoPredict" R package assessed the half-maximal inhibitory concentration (IC50) of chemotherapeutics for ESCC patients. We evaluated the impact of chemoradiotherapy sensitivity-related gene expression on chemotherapy sensitivity in these patients.

Expressions of key genes in pan-cancer

Employing the GEPIA database (http://gepia.cancer-pku.cn), we analyzed the differential expression of key chemoradiotherapy sensitivity-related genes in tumor samples and paired normal tissues across 32 cancer types, including ESCC.

Construction and assessment of nomogram

Cox regression analyses were performed on clinical factors to identify independent prognostic indicators. We constructed a nomogram incorporating these prognostic factors and chemoradiotherapy sensitivity-related genes using the "rms" R package, estimating the 1-, 3-, and 5-year survival probabilities for ESCC patients. The nomogram's consistency and accuracy were validated with a calibration curve.

Functional enrichment analysis

Using the "fgsea" and "enrichplot" R packages and the annotated gene set 'h.all.v2023.2.Hs.symbols.gmt' from the Molecular Signatures Database, we performed fast gene set enrichment analysis (fGSEA) to identify potential pathways and biological functions differing among chemoradiotherapy sensitivity-related gene expression groups. Based on the Net enrichment score (NES) and *P*-value, we identified significantly enriched hallmark pathways and explored the mechanisms through which key genes influence these pathways.

Genome-wide association study (GWAS)

Utilizing data from 452,264 individuals in the United Kingdom Biobank and documented in the Gene Atlas database (http://geneatlas.roslin.ed.ac.uk/), which links 778 traits to 30 million variants, we pinpointed pathogenic regions associated with key genes by analyzing GWAS data.

Statistical analysis

Statistical analyses were conducted using R software (version 4.3.1) (https://www.r-project.org). Survival analysis was performed using the Kaplan-Meier method and comparisons were made using the log-rank test. Pearson correlation tests evaluated relationships between variables. $P < 0.05$ was considered statistically significant.

Results

Identification of DEGs between pCR and npCR patients in ESCC

The Guangzhou cohort comprised 28 ESCC patients, including 39.3% (11/28) achieving pCR and 60.7% (17/28) exhibiting npCR. The clinicopathological features of these patients are summarized in Supplementary Table 1. Survival data for patients who underwent NRCT and surgical resection and survived at least 3 months after treatment was collected and performed Kaplan-Meier analysis to evaluate their survival probabilities in both groups. Patients who achieved pCR demonstrated a higher survival probability than those with npCR, particularly after 10 years (Figure 1A, n = 26). However, due to the limited sample size, the differences between the groups were not statistically significant. To identify key chemoradiotherapy sensitivity-related genes, we analyzed DEGs between pCR and npCR patients. We identified 1,726 DEGs, with 870 genes upregulated and 856 genes downregulated in npCR patients. The heatmap and volcano plot illustrating these DEGs are presented in Figures 1B, C.

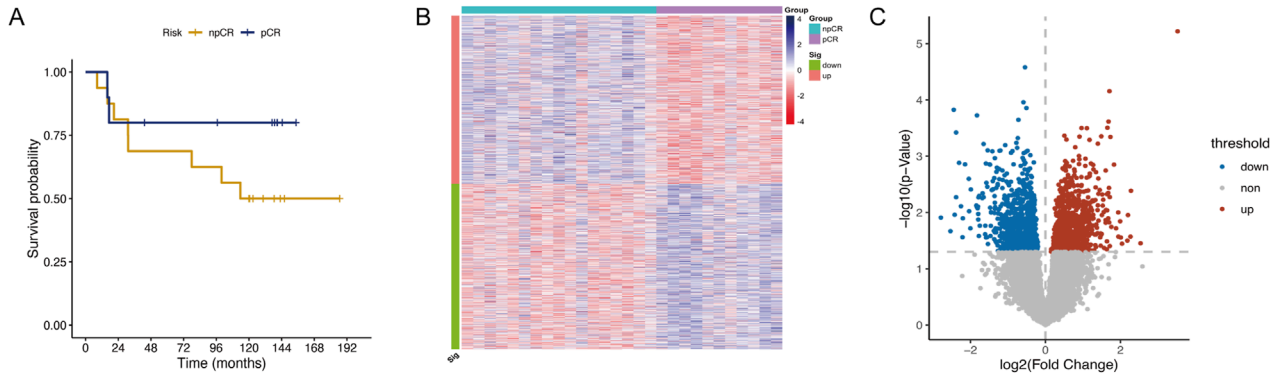

FIGURE 1
Identification of DEGs between pCR and npCR patients in ESCC. **(A)** Kaplan-Meier curve of pCR (n = 10) and npCR (n = 16) ESCC patients in the Guangzhou cohort. The heatmap **(B)** and volcano plot **(C)** of DEGs between pCR and npCR ESCC patients.

Identification of key genes in ESCC

To further identify key chemoradiotherapy sensitivity-related genes in ESCC, we conducted univariate Cox regression analysis using RNA-seq and prognostic data from the Beijing Cohort (Supplementary Table 1, n = 119). This analysis identified 126 prognosis-associated protein-encoding genes, comprising 52 associated with a good prognosis and 74 indicating a poor prognosis. After selecting genes highly expressed in pCR patients that indicate a good prognosis and genes lowly expressed in pCR patients indicating a poor prognosis, we identified 35 favorable and 40 unfavorable genes. Following random survival forest analysis, genes with a relative importance >0.7 were deemed key chemoradiotherapy sensitivity-related genes in ESCC. Ultimately, three genes, *ATF2*, *SLC27A5*, and *ALOXE3*, met the screening criteria and are illustrated in Figures 2A, B. Among these, *SLC27A5* and *ALOXE3* were not only highly expressed in pCR patients ($P < 0.01$ and $P = 0.01$, Figure 2C), but also significantly correlated with a favorable prognosis of ESCC ($P < 0.001$, Figures 2E, F). However, ATF2 was highly expressed in npCR patients ($P = 0.001$, Figure 2C) and was significantly associated with poor prognosis ($P = 0.001$, Figure 2D). By employing the X-tile software, the optimal expression level cut-off values of three genes were determined to be 12.5, 10.63 and 7.89, respectively.

By expanding the real-world sample (n = 50), we reanalyzed RNA-seq data from ESCC patients who underwent NCRT followed by surgery. Overall, their mean age was 58.2 years, 43 (86%) were male, 7 (14%) were female, 14 (28%) had stage II disease, and 36 (72%) had stage III disease. The expression of *ATF* in npCR patients was significantly upregulated compared with that in pCR patients, while the expression of *SLC27A5* and *ALOXE3* was significantly downregulated (Supplementary Figure 1A, B), which was consistent with our previous results.

Immune cell infiltration in ESCC

We analyzed immune cell infiltration between cancerous and normal tissues to assess immunological variations in ESCC. The proportions of infiltrating immune cells in each group were displayed in Figures 3A, B. Compared to normal tissue, cancerous tissue in ESCC showed increased infiltration of memory B cells, activated memory $CD4^+$ T cells, resting NK cells, M0 macrophages, M1 macrophages, resting dendritic cells, and activated dendritic cells and decreased infiltration of naive B cells, $CD8^+$ T cells, follicular helper T cells, regulatory T cells, activated NK cells, monocytes, activated mast cells, and eosinophils (Figure 3C). Correlations between infiltrating immune cells in ESCC were illustrated in Figure 3D. Further analysis of the associations between the expression of the three key genes and tumor immune cell infiltration revealed that *ATF2* negatively correlated with the infiltration of memory B cells, monocytes, and resting dendritic cells, among others. *SLC27A5* negatively correlated with the infiltration of memory B cells, resting memory $CD4^+$ T cells, and M0 macrophages, among others. *ALOXE3* negatively correlated with the infiltration of regulatory T cells, activated NK cells, and resting mast cells, among others (Figure 4A).

Associations between key genes and immunoregulatory genes

Considering that cancer patients often exhibit immune abnormalities related to tumor immune escape mechanisms, and the necessity to tailor immunotherapy targets and strategies based on individual immune characteristics (Sadun et al., 2007), we explored the associations between three key genes and immunoregulators, including 24 genes encoding immunoinhibitors and 46 genes encoding immunostimulators. Results indicated that *ATF2* was significantly positively correlated with *TNFRSF25*, *TNFRSF14*, and *ADORA2A*, and negatively correlated with *CD40*, *CD70*, *ENTPD1*, and *HAVCR2*. *SLC27A5* was significantly positively correlated with *CD274*, and negatively correlated with *TNFRSF9* and *TGFBR1*. *ALOXE3* was significantly positively correlated with *CD40* and *TNFSF14*, and negatively correlated with *CXCL12* (Figures 4B, C, all $p < 0.01$).

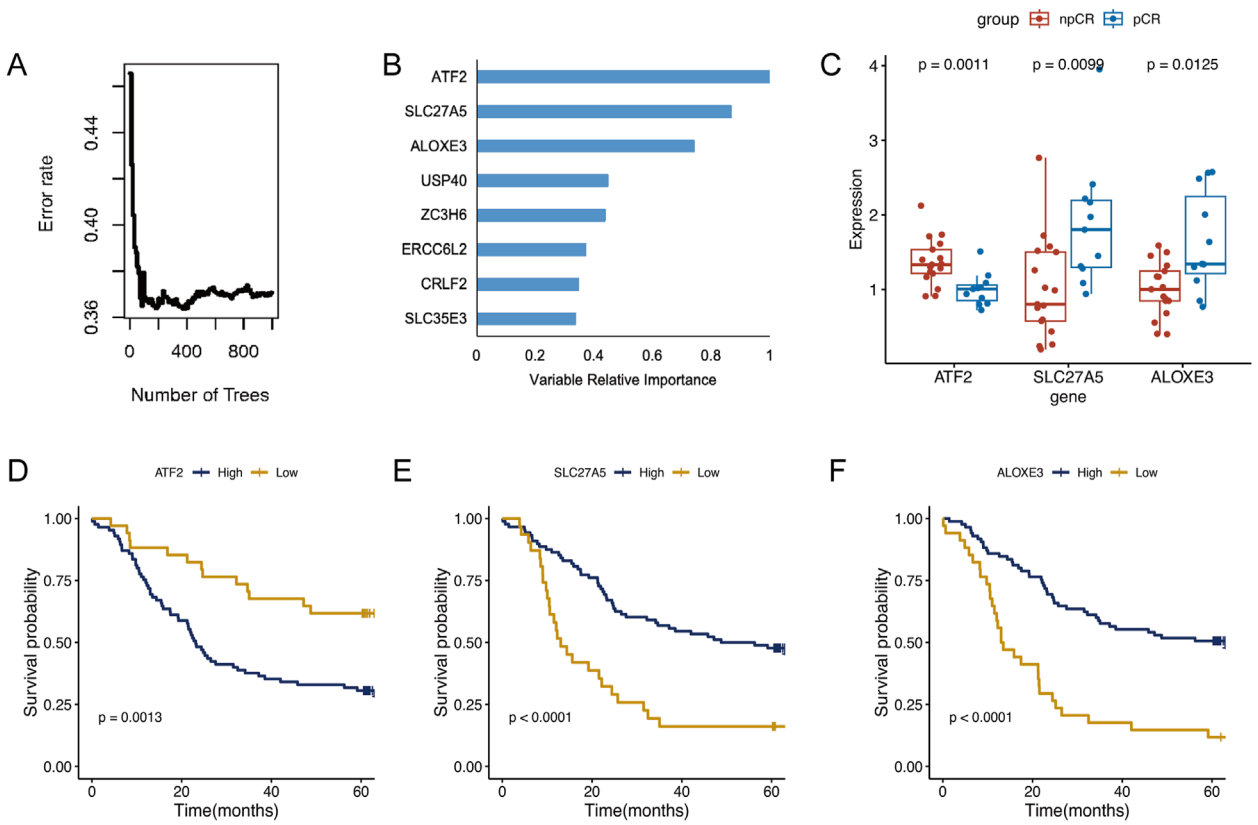

FIGURE 2
Identification of key genes in ESCC. **(A)** The random survival forest analysis of chemoradiotherapy sensitivity-related genes in ESCC. **(B)** The variable relative importance of three genes >0.7 were identified as key genes in ESCC. **(C)** Expression levels of *ATF2*, *SLC27A5*, and *ALOXE3* in pCR and npCR patients. **(D–F)** Kaplan-Meier survival analysis of ESCC patients with high- and low-expression of *ATF2*, *SLC27A5*, and *ALOXE3*.

Evaluation of drug-sensitivity prediction ability of key genes

The "pRRophetic" R package assessed the potential of key genes to predict drug sensitivity in ESCC patients. Compared with patients exhibiting higher expression of *ATF2* and lower expression of *SLC27A5* and *ALOXE3*, IC50 values for drugs including vinorelbine, paclitaxel, docetaxel, fluorouracil, cisplatin, oxaliplatin, erlotinib, gefitinib, and lapatinib, were lower in patients with decreased expression of *ATF2* and increased expression of *SLC27A5* and *ALOXE3*. Specifically, patients with higher *ATF2* expression were significantly less responsive to erlotinib and gefitinib, whereas those with increased *ALOXE3* expression were significantly more sensitive to vinorelbine, paclitaxel, docetaxel, fluorouracil, erlotinib, gefitinib, and lapatinib. Patients with higher *SLC27A5* expression were more sensitive to oxaliplatin (Figures 5A–I, $P < 0.05$). This further confirmed the clinical utility of these key genes in ESCC patients.

Expressions of key genes in pan-cancer

Using the GEPIA database (http://gepia.cancer-pku.cn), we analyzed the differential expression of key chemoradiotherapy sensitivity-related genes in tumor samples and paired normal tissues across 32 cancers, including ESCC. The results showed that *ATF2* is highly expressed in the tumor tissues of diffuse large B-cell lymphoma, esophageal carcinoma, pancreatic adenocarcinoma, stomach adenocarcinoma, and thymoma compared to normal tissues (Supplementary Figure 2A). However, the expressions of *SLC27A5* and *ALOXE3* were not significantly upregulated in esophageal cancer tissues compared to control tissues (Supplementary Figure 2B, C).

Construction and assessment of nomogram

We conducted Cox regression analyses on clinical factors to identify independent prognostic factors. Due to the limited number of TNM stage I cases (n = 6) in the Beijing cohort, we combined stages I and II for analysis. The nomogram was then constructed based on TNM staging and the expression levels of *ATF2*, *SLC27A5*, and *ALOXE3* to quantitatively predict 1-, 3-, and 5-year survival probabilities, providing a reference for clinical decision-making in ESCC patients. The results showed that all three chemoradiotherapy sensitivity-related genes had a greater impact on prognosis prediction than TNM staging, with *SLC27A5* contributing the most (Figure 6A). Calibration curves for 1-, 3- and 5-year OS demonstrated high consistency between the predictions and actual observations, underscoring the prognostic predictive power of these genes in ESCC (Figures 6B–D).

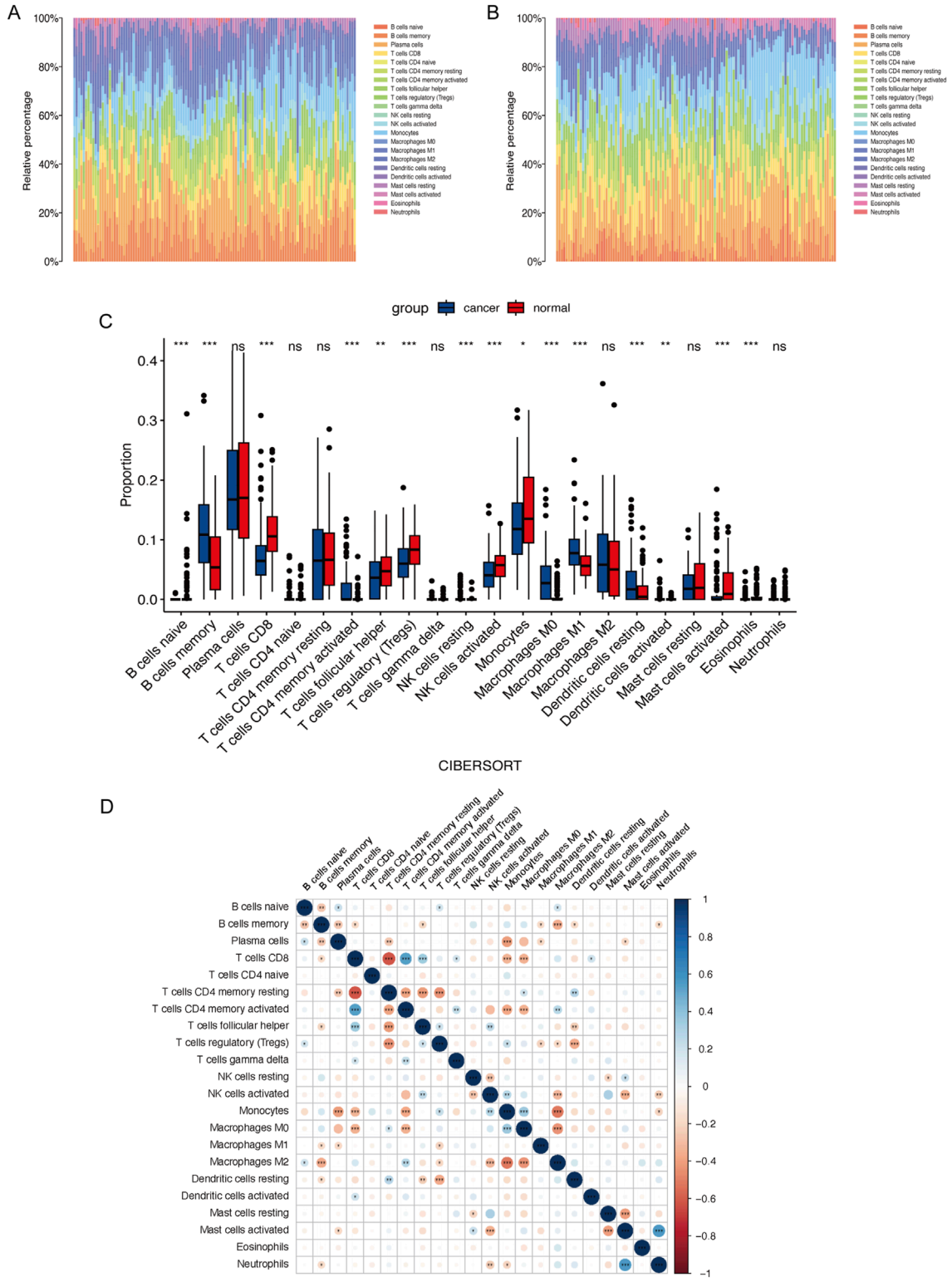

FIGURE 3
Immune cell infiltration in ESCC. Percentage of 22 types of immune cells infiltration in the cancer **(A)** and normal tissue **(B)** in ESCC patients. **(C)** Comparison of the immune cells proportion between cancer and normal tissue in ESCC patients. **(D)** Correlations between immune cells in ESCC.

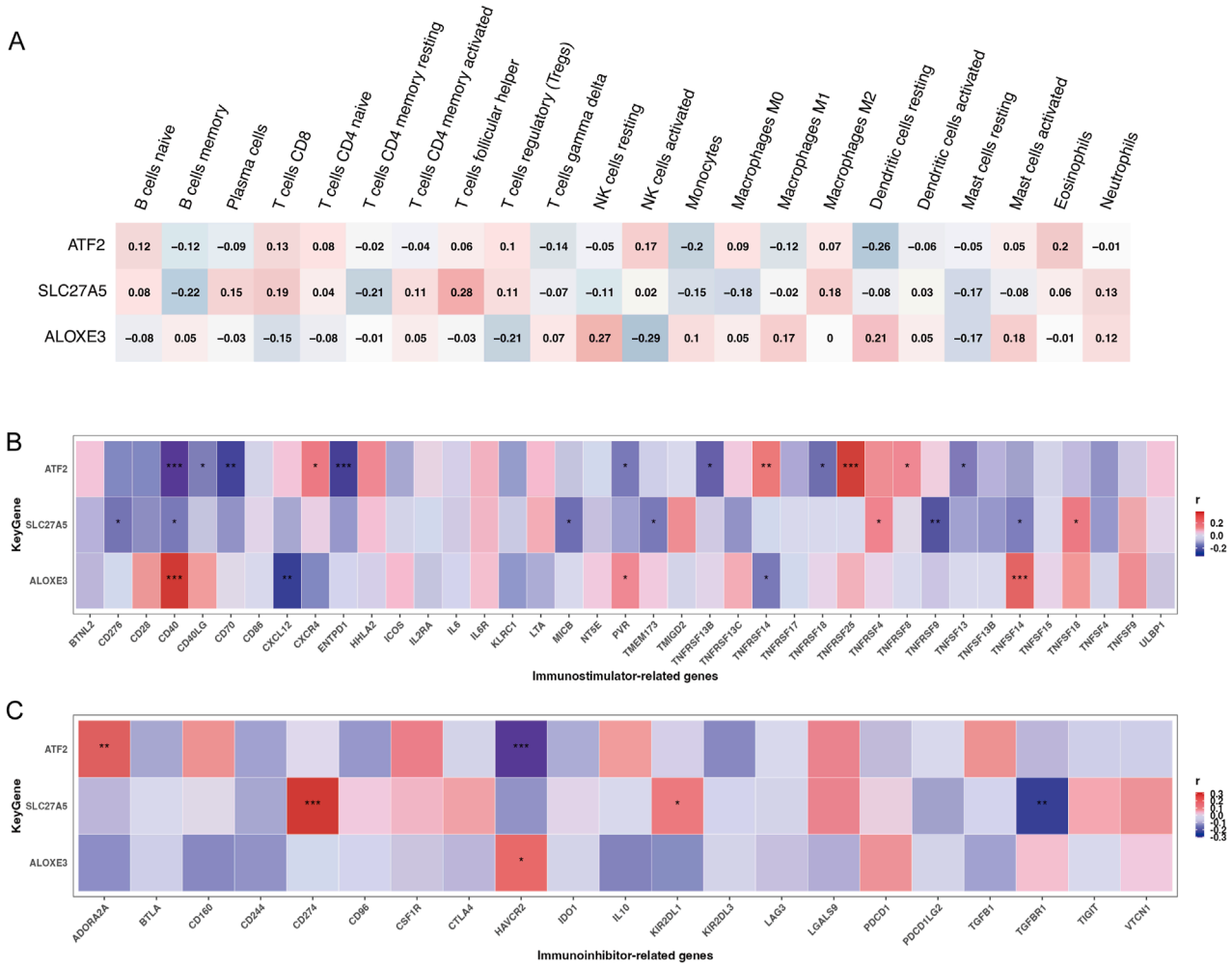

FIGURE 4
The relationship between key genes and immune cell infiltration and immunoregulators. The relationship of chemoradiotherapy sensitivity-related genes and infiltrating immune cells **(A)**, immunostimulators **(B)**, and immunoinhibitors **(C)** (*$P < 0.05$, **$P < 0.01$, ***$P < 0.001$; red color represented positive correlation, blue color represented negative correlation; darker colors indicated stronger correlations).

Gene set enrichment analysis (GSEA)

Utilizing hallmark gene sets from the Molecular Signatures Database, we conducted fast gene set enrichment analysis (fGSEA) to discern the differences in biological processes between high and low expressions of key genes. For the high-expression ATF2 group, the top three upregulated pathways were epithelial-mesenchymal transition (EMT), mitotic spindle, and myogenesis, while the top three downregulated pathways were oxidative phosphorylation, fatty acid metabolism, and KRAS signaling DN. Additionally, the p53 pathway was also downregulated (Supplementary Figure 3A, B). Conversely, the high-expression SLC27A5 group showed downregulation in the EMT pathway (Supplementary Figure 3C, D). Moreover, compared to the high-expression ATF2 group, the high-expression ALOXE3 group exhibited increased activity in the p53 pathway and the EMT pathway (Supplementary Figure 3E, F). These findings suggest that chemoradiotherapy sensitivity-related genes may influence ESCC progression by regulating the epithelial-mesenchymal transition and P53 pathways.

GWAS analysis

Using GWAS data, we identified the pathogenic regions of key genes in esophageal cancer (Supplementary Figure 4A, B). *ATF2*, *SLC27A5*, and *ALOXE3* were found in the pathogenic regions of chromosomes 2, 19, and 17, respectively (Supplementary Figure 4C–E).

Discussion

The high mortality rate of ESCC is associated with delayed diagnosis, tumor metastasis, treatment resistance, and recurrence (Sung et al., 2021; Thakur et al., 2021; Puhr et al., 2023). Owing to the advanced stage at diagnosis, nearly 50% of patients are not eligible for complete surgical resection. Evidence from several large clinical trials suggest that NCRT combined with esophagectomy is more effective than surgical resection alone (van Hagen et al., 2012; Yang et al., 2021a). However, due to tumor heterogeneity, therapeutic outcomes

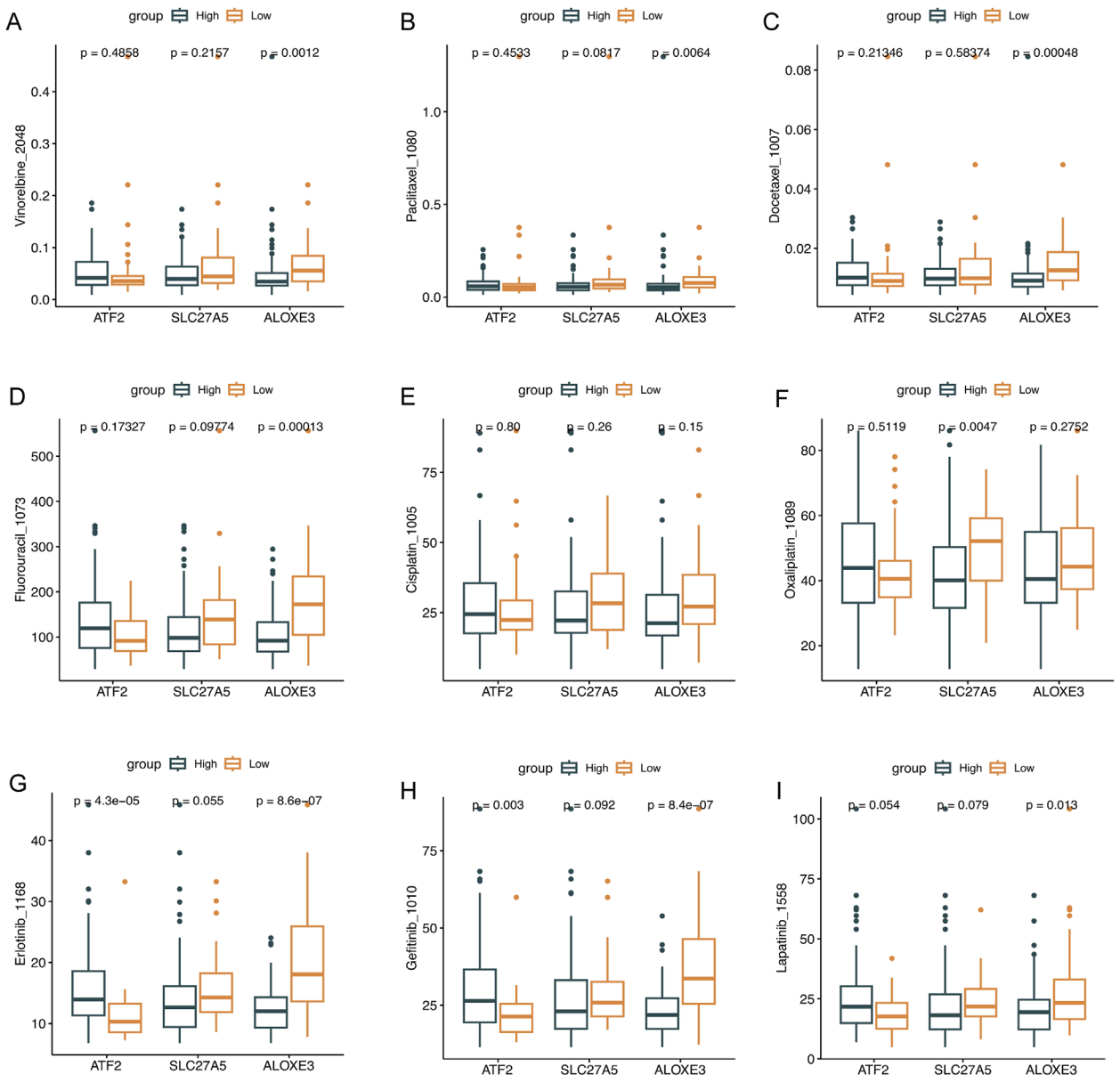

FIGURE 5
The evaluation of drug sensitivity. Drug sensitivity analysis of the low- and high-expression of *ATF2*, *SLC27A5*, and *ALOXE3* groups. **(A)** Vinorelbine, **(B)** Paclitaxel, **(C)** Docetaxel, **(D)** Fluorouracil, **(E)** Cisplatin, **(F)** Oxaliplatin, **(G)** Erlotinib, **(H)** Gefitinib, and **(I)** Lapatinib.

vary significantly among patients. Exploring the mechanisms of chemoradiotherapy sensitivity is crucial for improving ESCC prognosis. In this study, we investigated biomarkers and potential mechanisms of chemoradiotherapy sensitivity in ESCC patients. The findings could inform the development of precise treatment strategies for ESCC based on tumor molecular heterogeneity.

Our study revealed that *ATF2* is not only linked to chemoradiotherapy insensitivity in ESCC, but also indicative of poor prognosis. Located on chromosome 2q32 (Ozawa et al., 1991), *ATF2* has been shown in various cancer models to be overexpressed, phosphorylated, and mislocalized subcellularly. It interacts with oncogenic proteins such as JUN (Lopez-Bergami et al., 2010). Activation of the Rac1-P38-ATF2 signaling pathway in non-small cell lung cancer cells has been documented to upregulate the expressions of Cyclin A2, Cyclin D1, and MMP2 proteins, thus promoting tumor growth (Zhou et al., 2018). *ATF2* also binds to the promoter of miR-3913-5p, negatively regulating its expression, which targets CREB5 directly. Overexpression of *ATF2* enhances growth, migration, and invasion in colorectal cancer cells through this mechanism. The ATF2/miR-3913-5p/CREB5 axis is considered a potential therapeutic target for colorectal cancer (Dai et al., 2023). Furthermore, *ATF2* upregulation in gastric cancer correlates with a worse clinical prognosis, and silencing *ATF2* suppresses the malignant phenotype of gastric cancer cells. Notably, reducing *ATF2* expression significantly increases the sensitivity to sorafenib therapy (Xu et al., 2023a). Additionally, *ATF2* is implicated in platinum resistance in non-small cell lung cancer treatment and

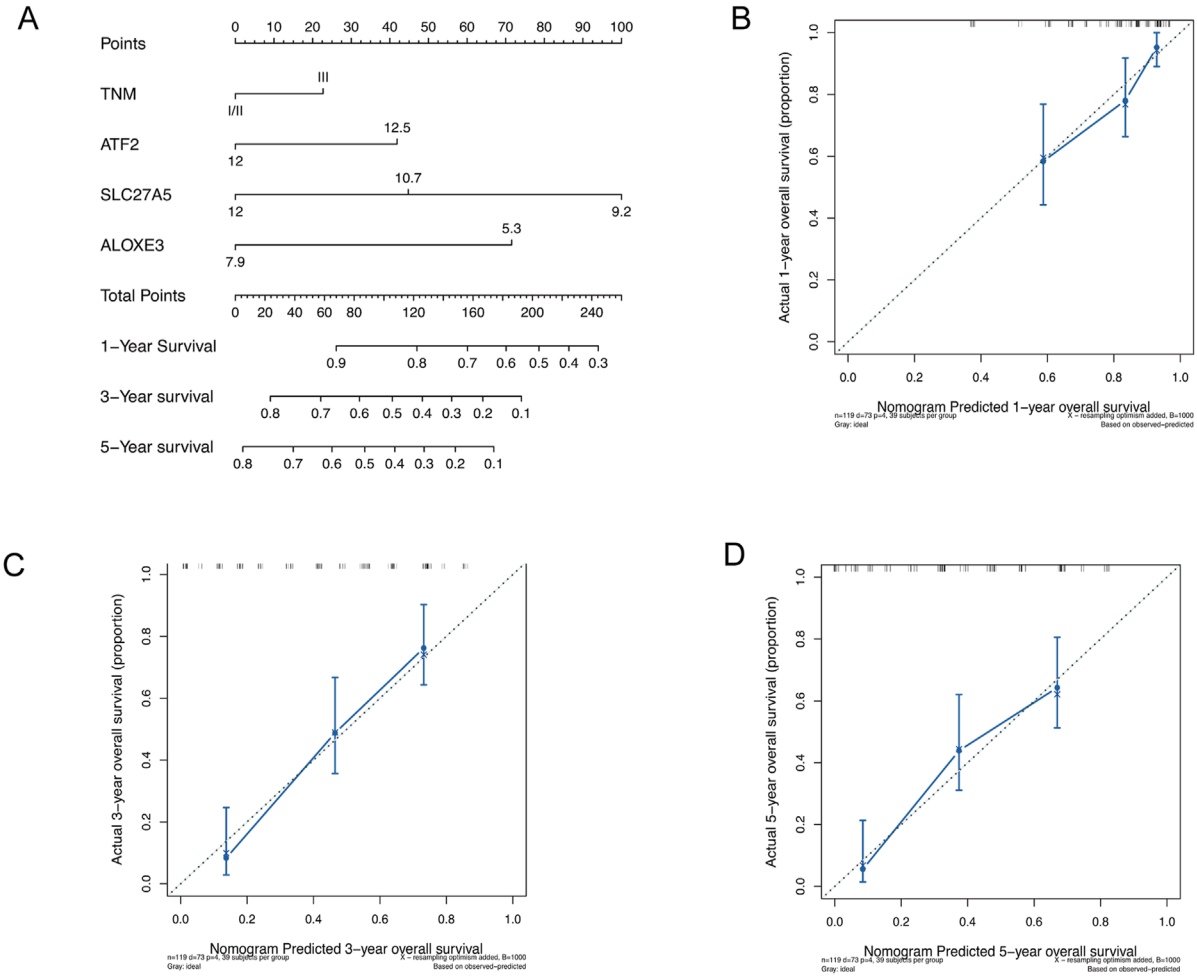

FIGURE 6
Construction and assessment of nomogram. **(A)** Construction of nomogram based on TNM staging and the expression of *ATF2*, *SLC27A5*, and *ALOXE3*. **(B–D)** Calibration curves of nomogram for OS prediction at 1-, 3- and 5- year in ESCC.

is targeted to restore chemotherapy sensitivity to platinum. Studies have confirmed that triptolide can enhance chemotherapy efficacy in drug-resistant cell lines by inhibiting the ATF2/cJUN function (Lo et al., 2015).

SLC27A5 encodes fatty acid transport protein 5. Reduced expression of *SLC27A5* is closely associated with poorer OS in ovarian cancer patients (Chen et al., 2021). Moreover, expression levels of *SLC27A5* are significantly lower in patients with hepatocellular carcinoma (Wang et al., 2022). *SLC27A5* suppresses proliferation and migration of hepatocellular carcinoma cells *in vitro*. This effect is likely due to *SLC27A5*'s role in promoting cuproptosis in hepatocellular carcinoma via upregulation of *FDX1*, making it a potential target for cuproptosis induction in this cancer type (Li et al., 2023). Critically, SLC27A5 enhances the therapeutic efficacy of sorafenib in hepatocellular carcinoma by promoting sorafenib-induced ferroptosis through inhibition of the NRF2/GSR pathway. A deficiency in SLC27A5 correlates with resistance to sorafenib in these cells (Xu et al., 2023b). Additionally, the overexpression of *SLC27A5* curtails the activation of KEAP1/NRF2 pathway and reduces TXNRD1 expression, which can augment the antitumor activity of sorafenib either genetically or pharmacologically by inhibiting the NRF2/TXNRD1 pathway (Gao et al., 2020).

ALOXE3 is a member of the mammalian lipoxygenase family, playing a role in lipid metabolism and acting as a regulator of ferroptosis (Yang et al., 2016; Yamamoto, 1992). In our study, high expression of *ALOXE3* was linked to improved prognosis in ESCC and increased sensitivity to chemoradiotherapy. Compared to normal human brain tissue, *ALOXE3* expression is significantly diminished in glioblastoma tissue. *ALOXE3* deficiency not only enhances the survival and migration of cancer cells but also supports glioblastoma growth in immunodeficient nude mice. It is crucial for p53-mediated ferroptosis, with miR-18a downregulating its expression by targeting ALOXE3 directly, thus contributing to resistance against p53-induced ferroptosis in glioblastoma cells (Yang et al., 2021b). Transcriptional upregulation of ALOXE3 by YAP promotes lipid peroxide accumulation and induces ferroptosis, making the YAP-ALOXE3 signaling pathway a potential biomarker for predicting ferroptosis-induced responses in hepatocellular carcinoma cells (Qin et al., 2021). In breast cancer, SBFI26, an inhibitor of FABP5, induces ferroptosis by elevating levels of ferrous ions and lipid peroxidation, increasing the expression of

ALOXE3, *ALOX5*, and *ALOX15*, thus driving ferroptosis in tumor cells (He et al., 2024). Furthermore, the novel ferroptosis inducer, talaroconvolutin A, has been shown to trigger ferroptosis and suppress colorectal cancer cell growth by modulating *ALOXE3* expression and other genes (Xia et al., 2020).

In a previous clinical study, triprilizumab combined with NCRT and surgical resection was used to treat locally advanced ESCC, achieving pCR rate of 50% and an R0 resection rate of 98% (Chen et al., 2023). EC-CRT-001, a prospective clinical trial, enrolled patients with unresectable ESCC and treated them with concurrent chemotherapy, radiotherapy, and triplizumab immunotherapy. Results showed that 62% of these patients achieved a complete response, with a median response duration exceeding 1 year, and a 1-year OS rate of 78.4%. The combination of immunotherapy with definitive chemoradiotherapy offers a promising treatment strategy for patients with unresectable, locally advanced ESCC (Zhu et al., 2023). However, the potential synergistic mechanism between immunotherapy and chemoradiotherapy remains unclear. Our results indicated that key genes associated with chemoradiotherapy sensitivity were significantly correlated with immune cells and immunomodulatory genes, suggesting a potential mechanism for their synergistic effect in ESCC.

In our study, the EMT pathway was the most significantly upregulated pathway in the high-expression *ATF2* group, and the most significantly down-regulated pathway in the high-expression *SLC27A5* group. EMT is recognized as a complex and coordinated process crucial for cancer initiation and progression (Dongre and Weinberg, 2019). ATF2 binds to the promoter region of GLUT3, enhancing EMT in colorectal cancer by inducing GLUT3 expression (Song et al., 2022). Through promoter binding, ATF2 and endoplasmic reticulum stress induce the expression of CAP2, promoting EMT in liver cancer cells (Yoon et al., 2021). In conjunction with TGF-beta1, ATF2 induces EMT in pancreatic cancer cell lines (Xu et al., 2012). Additionally, via the c-Met/BVR/ATF-2 pathway, lncRNA NR2F2-AS1 activates the EMT process and fosters the development of non-small cell lung cancer (Liu et al., 2021). EMT increases malignancy in non-small cell lung cancer cells and reduces chemosensitivity to cisplatin and paclitaxel. EMT marker expression is elevated in cells chronically exposed to these agents or radiation, linking EMT to chemoradiotherapy resistance (Shintani et al., 2011). Similarly, EGFR activation triggers EMT, reducing cellular responsiveness to radiation and cetuximab in head and neck cancer (Holz et al., 2011). Inhibitors of the EMT signaling pathway may enhance the sensitivity of cancer cells to chemoradiotherapy (Shintani et al., 2011). Downregulation of Delta-like Ligand 4 inhibits EMT in cervical cancer, thereby enhancing radiosensitivity (Yang et al., 2020). The EMT signaling pathway could provide a potential direction for further exploration into the mechanism of chemoradiotherapy sensitivity genes in ESCC.

In this study, we evaluated the role of chemoradiotherapy sensitivity-related genes in ESCC through survival analysis, drug sensitivity analysis, and the development and validation of a nomogram. While our results underscored the potential clinical relevance of three key genes in ESCC, there are notable limitations. This was a retrospective study that did not delve into the underlying mechanisms. Future studies should involve independent prospective cohorts and both *in vitro* and *in vivo* experiments to confirm these findings and further explore the mechanisms. Additionally, although these three key genes can predict the response of ESCC to NCRT and are significantly associated with certain immune cells and immunoregulatory genes in the tumor microenvironment, their efficacy in ESCC treated with combined immunotherapy and NCRT remains to be established.

Conclusion

In conclusion, we identified three pivotal genes that are crucial in predicting both the sensitivity of ESCC to radiochemotherapy and the prognosis of patients. We investigated the associations between these genes and infiltrating immune cells and immunoregulatory genes. Furthermore, we explored the signaling pathways influenced by these genes in ESCC and analyzed the chromosomal regions implicated in their pathogenesis. The identification of these key genes may facilitate the optimization of individual treatment strategies and improve prognosis management in ESCC.

Data availability statement

The datasets presented in this study can be found in online repositories. The names of the repository/repositories and accession number(s) can be found in the article/Supplementary Material.

Ethics statement

The studies involving humans were approved by the Ethics Committee of the Sun Yat-sen University Cancer Center (No. B2022-067-01). The studies were conducted in accordance with the local legislation and institutional requirements. The participants provided their written informed consent to participate in this study.

Author contributions

YC: Data curation, Formal Analysis, Funding acquisition, Investigation, Methodology, Software, Validation, Visualization, Writing–original draft. JW: Data curation, Formal analysis, Funding acquisition, Methodology, Project administration, Resources, Supervision, Validation, Visualization, Conceptualization, Investigation, Software, Writing–original draft, Writing–review and editing. JF: Data curation, Formal analysis, Funding acquisition, Methodology, Project administration, Resources, Supervision, Validation, Visualization, Conceptualization, Investigation, Software, Writing–original draft, Writing–review and editing. CL: Conceptualization, Project administration, Resources, Supervision, Writing–review and editing.

Funding

The author(s) declare that financial support was received for the research, authorship, and/or publication of this article. This

work was supported by the National Natural Science Foundation of China (Grant No. 82200565 and 82200566) and the Natural Science Foundation of Guangdong Province (Grant No. 2023A1515010356).

Conflict of interest

The authors declare that the research was conducted in the absence of any commercial or financial relationships that could be construed as a potential conflict of interest.

Generative AI statement

The author(s) declare that no Generative AI was used in the creation of this manuscript.

Publisher's note

Supplementary material

The Supplementary Material for this article can be found online at: https://www.frontiersin.org/articles/10.3389/fmolb.2024.1512715/full#supplementary-material

References

Chen, H., Han, T., Zhao, Y., and Feng, L. (2021). Identification of solute-carrier family 27A molecules (SCL27As) as a potential biomarker of ovarian cancer based on bioinformatics and experiments. *Ann. Transl. Med.* 9 (15), 1237. doi:10.21037/atm-21-3026

Chen, R., Liu, Q., Li, Q., Zhu, Y., Zhao, L., Liu, S., et al. (2023). A phase II clinical trial of toripalimab combined with neoadjuvant chemoradiotherapy in locally advanced esophageal squamous cell carcinoma (NEOCRTEC1901). *EClinicalMedicine* 62, 102118. doi:10.1016/j.eclinm.2023.102118

Dai, W., Hong, L., Xiao, W., Zhang, L., Sha, W., Yu, Z., et al. (2023). The ATF2/miR-3913-5p/CREB5 axis is involved in the cell proliferation and metastasis of colorectal cancer. *Commun. Biol.* 6 (1), 1026. doi:10.1038/s42003-023-05405-w

Dongre, A., and Weinberg, R. A. (2019). New insights into the mechanisms of epithelial-mesenchymal transition and implications for cancer. *Nat. Rev. Mol. Cell. Biol.* 20 (2), 69–84. doi:10.1038/s41580-018-0080-4

Gao, Q., Zhang, G., Zheng, Y., Yang, Y., Chen, C., Xia, J., et al. (2020). SLC27A5 deficiency activates NRF2/TXNRD1 pathway by increased lipid peroxidation in HCC. *Cell. Death Differ.* 27 (3), 1086–1104. doi:10.1038/s41418-019-0399-1

He, F., Wang, J., Liu, L., Qin, X., Wan, Z., Li, W., et al. (2021). Esophageal cancer: trends in incidence and mortality in China from 2005 to 2015. *Cancer Med.* 10 (5), 1839–1847. doi:10.1002/cam4.3647

He, G., Zhang, Y., Feng, Y., Chen, T., Liu, M., Zeng, Y., et al. (2024). SBFI26 induces triple-negative breast cancer cells ferroptosis via lipid peroxidation. *J. Cell. Mol. Med.* 28 (7), e18212. doi:10.1111/jcmm.18212

Hirata, H., Niida, A., Kakiuchi, N., Uchi, R., Sugimachi, K., Masuda, T., et al. (2021). The evolving genomic landscape of esophageal squamous cell carcinoma under chemoradiotherapy. *Cancer Res.* 81 (19), 4926–4938. doi:10.1158/0008-5472.CAN-21-0653

Holz, C., Niehr, F., Boyko, M., Hristozova, T., Distel, L., Budach, V., et al. (2011). Epithelial-mesenchymal-transition induced by EGFR activation interferes with cell migration and response to irradiation and cetuximab in head and neck cancer cells. *Radiother. Oncol.* 101 (1), 158–164. doi:10.1016/j.radonc.2011.05.042

Li, X., Wang, J., Guo, Z., Ma, Y., Xu, D., Fan, D., et al. (2023). Copper metabolism-related risk score identifies hepatocellular carcinoma subtypes and SLC27A5 as a potential regulator of cuproptosis. *Aging (Albany NY)* 15 (24), 15084–15113. doi:10.18632/aging.205334

Liu, C., Li, Q. G., Zhou, Y., Cao, Y. Y., Wei, Z. X., Jin, Y. H., et al. (2021). LncRNA NR2F2-AS1 induces epithelial-mesenchymal transition of non-small cell lung cancer by modulating BVR/ATF-2 pathway via regulating miR-545-5p/c-Met axis. *Am. J. Cancer Res.* 11 (10), 4844–4865.

Liu, S. L., Xi, M., Yang, H., Yang, Y. D., Wu, Y. J., Zhao, L., et al. (2016). Is there a correlation between clinical complete response and pathological complete response after neoadjuvant chemoradiotherapy for esophageal squamous cell cancer? *Ann. Surg. Oncol.* 23 (1), 273–281. doi:10.1245/s10434-015-4764-0

Lo, I. M., Monica, V., Vavala, T., Gisabella, M., Saviozzi, S., Bracco, E., et al. (2015). ATF2 contributes to cisplatin resistance in non-small cell lung cancer and celastrol induces cisplatin resensitization through inhibition of JNK/ATF2 pathway. *Int. J. Cancer* 136 (11), 2598–2609. doi:10.1002/ijc.29302

Lopez-Bergami, P., Lau, E., and Ronai, Z. (2010). Emerging roles of ATF2 and the dynamic AP1 network in cancer. *Nat. Rev. Cancer* 10 (1), 65–76. doi:10.1038/nrc2681

Newman, A. M., Liu, C. L., Green, M. R., Gentles, A. J., Feng, W., Xu, Y., et al. (2015). Robust enumeration of cell subsets from tissue expression profiles. *Nat. Methods* 12 (5), 453–457. doi:10.1038/nmeth.3337

Noordman, B. J., Wijnhoven, B. P. L., Lagarde, S. M., Boonstra, J. J., Coene, P., Dekker, J. W. T., et al. (2018). Neoadjuvant chemoradiotherapy plus surgery versus active surveillance for oesophageal cancer: a stepped-wedge cluster randomised trial. *BMC Cancer* 18 (1), 142. doi:10.1186/s12885-018-4034-1

Ozawa, K., Sudo, T., Soeda, E., Yoshida, M. C., and Ishii, S. (1991). Assignment of the human CREB2 (CRE-BP1) gene to 2q32. *Genomics* 10 (4), 1103–1104. doi:10.1016/0888-7543(91)90210-6

Puhr, H. C., Prager, G. W., and Ilhan-Mutlu, A. (2023). How we treat esophageal squamous cell carcinoma. *ESMO Open* 8 (1), 100789. doi:10.1016/j.esmoop.2023.100789

Qin, Y., Pei, Z., Feng, Z., Lin, P., Wang, S., Li, Y., et al. (2021). Oncogenic activation of YAP signaling sensitizes ferroptosis of hepatocellular carcinoma via ALOXE3-mediated lipid peroxidation accumulation. *Front. Cell. Dev. Biol.* 9, 751593. doi:10.3389/fcell.2021.751593

Ritchie, M. E., Phipson, B., Wu, D., Hu, Y., Law, C. W., Shi, W., et al. (2015). Limma powers differential expression analyses for RNA-sequencing and microarray studies. *Nucleic Acids Res.* 43 (7), e47. doi:10.1093/nar/gkv007

Ru, B., Wong, C. N., Tong, Y., Zhong, J. Y., Zhong, S. S. W., Wu, W. C., et al. (2019). TISIDB: an integrated repository portal for tumor-immune system interactions. *Bioinformatics* 35 (20), 4200–4202. doi:10.1093/bioinformatics/btz210

Sadun, R. E., Sachsman, S. M., Chen, X., Christenson, K. W., Morris, W. Z., Hu, P., et al. (2007). Immune signatures of murine and human cancers reveal unique mechanisms of tumor escape and new targets for cancer immunotherapy. *Clin. Cancer Res.* 13 (13), 4016–4025. doi:10.1158/1078-0432.CCR-07-0016

Shi, Z., Zhu, X., Ruan, C., Wei, G., Li, J., Qiu, H., et al. (2022). Evaluation of concurrent chemoradiotherapy for survival outcomes in patients with synchronous oligometastatic esophageal squamous cell carcinoma. *JAMA Netw. Open* 5 (12), e2244619. doi:10.1001/jamanetworkopen.2022.44619

Shintani, Y., Okimura, A., Sato, K., Nakagiri, T., Kadota, Y., Inoue, M., et al. (2011). Epithelial to mesenchymal transition is a determinant of sensitivity to chemoradiotherapy in non-small cell lung cancer. *Ann. Thorac. Surg.* 92 (5), 1794–1804. ; discussion 804. doi:10.1016/j.athoracsur.2011.07.032

Song, M. Y., Lee, D. Y., Yun, S. M., and Kim, E. H. (2022). GLUT3 promotes epithelial-mesenchymal transition via TGF-β/JNK/ATF2 signaling pathway in colorectal cancer cells. *Biomedicines* 10 (8), 1837. doi:10.3390/biomedicines10081837

Squires, M. H., Gower, N., Benbow, J. H., Donahue, E. E., Bohl, C. E., Prabhu, R. S., et al. (2022). PET imaging and rate of pathologic complete response in esophageal squamous cell carcinoma. *Ann. Surg. Oncol.* 29 (2), 1327–1333. doi:10.1245/s10434-021-10644-4

Sung, H., Ferlay, J., Siegel, R. L., Laversanne, M., Soerjomataram, I., Jemal, A., et al. (2021). Global cancer statistics 2020: GLOBOCAN estimates of incidence and mortality worldwide for 36 cancers in 185 countries. *CA Cancer J. Clin.* 71 (3), 209–249. doi:10.3322/caac.21660

Thakur, B., Devkota, M., and Chaudhary, M. (2021). Management of locally advanced esophageal cancer. *JNMA J. Nepal Med. Assoc.* 59 (236), 409–416. doi:10.31729/jnma.4299

van Hagen, P., Hulshof, M. C., van Lanschot, J. J., Steyerberg, E. W., van Berge Henegouwen, M. I., Wijnhoven, B. P., et al. (2012). Preoperative chemoradiotherapy for esophageal or junctional cancer. *N. Engl. J. Med.* 366 (22), 2074–2084. doi:10.1056/NEJMoa1112088

Wang, H., Tang, H., Fang, Y., Tan, L., Yin, J., Shen, Y., et al. (2021). Morbidity and mortality of patients who underwent minimally invasive esophagectomy after neoadjuvant chemoradiotherapy vs neoadjuvant chemotherapy for locally advanced esophageal squamous cell carcinoma: a randomized clinical trial. *JAMA Surg.* 156 (5), 444–451. doi:10.1001/jamasurg.2021.0133

Wang, J., Qiao, Y., Sun, H., Chang, H., Zhao, H., Zhang, S., et al. (2022). Decreased SLC27A5 suppresses lipid synthesis and tyrosine metabolism to activate the cell cycle in hepatocellular carcinoma. *Biomedicines* 10 (2), 234. doi:10.3390/biomedicines10020234

Xia, Y., Liu, S., Li, C., Ai, Z., Shen, W., Ren, W., et al. (2020). Discovery of a novel ferroptosis inducer-talaroconvolutin A-killing colorectal cancer cells *in vitro* and *in vivo*. *Cell. Death Dis.* 11 (11), 988. doi:10.1038/s41419-020-03194-2

Xu, F. L., Wu, X. H., Chen, C., Wang, K., Huang, L. Y., Xia, J., et al. (2023b). SLC27A5 promotes sorafenib-induced ferroptosis in hepatocellular carcinoma by downregulating glutathione reductase. *Cell. Death Dis.* 14 (1), 22. doi:10.1038/s41419-023-05558-w

Xu, X., Li, Y., Wu, Y., Wang, M., Lu, Y., Fang, Z., et al. (2023a). Increased ATF2 expression predicts poor prognosis and inhibits sorafenib-induced ferroptosis in gastric cancer. *Redox Biol.* 59, 102564. doi:10.1016/j.redox.2022.102564

Xu, Y., Liu, Z., and Guo, K. (2012). The effect of JDP2 and ATF2 on the epithelial-mesenchymal transition of human pancreatic cancer cell lines. *Pathol. Oncol. Res.* 18 (3), 571–577. doi:10.1007/s12253-011-9476-6

Yamamoto, S. (1992). Mammalian lipoxygenases: molecular structures and functions. *Biochim. Biophys. Acta* 1128 (2-3), 117–131. doi:10.1016/0005-2760(92)90297-9

Yang, H., Liu, H., Chen, Y., Zhu, C., Fang, W., Yu, Z., et al. (2021a). Long-term efficacy of neoadjuvant chemoradiotherapy plus surgery for the treatment of locally advanced esophageal squamous cell carcinoma: the NEOCRTEC5010 randomized clinical trial. *JAMA Surg.* 156 (8), 721–729. doi:10.1001/jamasurg.2021.2373

Yang, S. S., Yu, D. Y., Du, Y. T., Wang, L., Gu, L., Zhang, Y. Y., et al. (2020). Inhibition of Delta-like Ligand 4 enhances the radiosensitivity and inhibits migration in cervical cancer via the reversion of epithelial-mesenchymal transition. *Cancer Cell. Int.* 20, 344. doi:10.1186/s12935-020-01434-1

Yang, W., Soares, J., Greninger, P., Edelman, E. J., Lightfoot, H., Forbes, S., et al. (2013). Genomics of Drug Sensitivity in Cancer (GDSC): a resource for therapeutic biomarker discovery in cancer cells. *Nucleic Acids Res.* 41 (Database issue), D955–D961. doi:10.1093/nar/gks1111

Yang, W. S., Kim, K. J., Gaschler, M. M., Patel, M., Shchepinov, M. S., and Stockwell, B. R. (2016). Peroxidation of polyunsaturated fatty acids by lipoxygenases drives ferroptosis. *Proc. Natl. Acad. Sci. U. S. A.* 113 (34), E4966–E4975. doi:10.1073/pnas.1603244113

Yang, X., Liu, J., Wang, C., Cheng, K. K., Xu, H., Li, Q., et al. (2021b). miR-18a promotes glioblastoma development by down-regulating ALOXE3-mediated ferroptotic and anti-migration activities. *Oncogenesis* 10 (2), 15. doi:10.1038/s41389-021-00304-3

Yoon, S., Shin, B., and Woo, H. G. (2021). Endoplasmic reticulum stress induces CAP2 expression promoting epithelial-mesenchymal transition in liver cancer cells. *Mol. Cells* 44 (8), 569–579. doi:10.14348/molcells.2021.0031

Zhou, H., Cai, L., Zhang, X., Li, A., Miao, Y., Li, Q., et al. (2018). ARHGEF39 promotes tumor progression via activation of Rac1/P38 MAPK/ATF2 signaling and predicts poor prognosis in non-small cell lung cancer patients. *Lab. Invest.* 98 (5), 670–681. doi:10.1038/s41374-018-0022-y

Zhu, Y., Wen, J., Li, Q., Chen, B., Zhao, L., Liu, S., et al. (2023). Toripalimab combined with definitive chemoradiotherapy in locally advanced oesophageal squamous cell carcinoma (EC-CRT-001): a single-arm, phase 2 trial. *Lancet Oncol.* 24 (4), 371–382. doi:10.1016/S1470-2045(23)00060-8

frontiers | Frontiers in Molecular Biosciences

TYPE Original Research
PUBLISHED 04 December 2024
DOI 10.3389/fmolb.2024.1513919

OPEN ACCESS

EDITED BY
Giuseppe Bronte,
University of Ferrara, Italy

REVIEWED BY
Ozlem Ay,
Faculty of Medicine, Mersin University, Türkiye
Lucia Carmela Cosenza,
University of Ferrara, Italy

*CORRESPONDENCE
Zuping Zhang,
zhangzuping@csu.edu.cn

†These authors have contributed equally to this work

RECEIVED 19 October 2024
ACCEPTED 13 November 2024
PUBLISHED 04 December 2024

CITATION
Chen S, Li L, Xu W, Xie N, Xu H, Zhou Y, Zou Y, Yi K and Zhang Z (2024) CircMIB1 inhibits glioma development and progression through a competing endogenous RNA interaction network.
Front. Mol. Biosci. 11:1513919.
doi: 10.3389/fmolb.2024.1513919

CircMIB1 inhibits glioma development and progression through a competing endogenous RNA interaction network

Simin Chen[1†], Longping Li[1†], Wei Xu[1], Nanjiao Xie[1], Huiting Xu[1], Yongjun Zhou[1], Ying Zou[1], Kai Yi[1] and Zuping Zhang[2*]

[1]Department of Clinical Laboratory, Yiyang Central Hospital, Yiyang, Hunan, China, [2]School of Xiangya Basic Medical Science, Central South University, Changsha, Hunan, China

Introduction: The critical role of circular RNAs as non-coding RNAs in glioma has been extensively investigated. Therefore, we aimed to explore the role and potential molecular mechanisms of circRNA-mind bomb homolog 1 (circMIB1) in gliomas.

Methods: RNA sequencing was used to analyze the expression profiles of circRNAs in glioma tissues and normal brain tissues. Quantitative real-time polymerase chain reaction was implemented to examine the levels of circMIB1 in glioma cells and tissues. The circMIB1 was identified as a cyclic RNA molecule by DNA nucleic acid electrophoresis and ribonuclease R assay. The relationship between circMIB1 expression and the prognosis of glioma patients and its potential as a biomarker were analysed using Kaplan-Meier, Receiver operating characteristic curves, and Principal component analysis. Bioinformatics analysis predicted the miRNAs that bind to circMIB1 and their downstream targets, and analysed the functions of these genes.

Results: Firstly, a novel circRNA molecule termed circMIB1 was identified and validated by RNA sequencing. The expression of circMIB1 was significantly downregulated in glioma cells and tissues, and was closely associated with the tumor grade and survival prognosis of patients with glioma. Hence, it may be useful as a biomarker for glioma. Secondly, it was predicted that circMIB1 binds to hsa-miR-1290 based on bioinformatics analysis, which was significantly upregulated in glioma cells and tissues, and correlated with the tumor grade and overall survival of patients. Thirdly, through a series of bioinformatics analyses identified six genes downstream of hsa-miR-1290 that were significantly associated with glioma expression and prognosis, these genes are associated with cell cycle, cell necrosis and cell circadian rhythms.

Discussion: CircMIB1 may play a role in inhibiting glioma development through the hsa-miR-1290 competitive endogenous RNA interaction network, these findings provide new ideas and directions for the diagnosis and treatment of glioma.

KEYWORDS

CircMIB1, glioma, MiR-1290, ceRNA, prognostic, biomarker

Introduction

Gliomas are among the most common primary brain tumors, accounting for approximately 30% of all brain and central nervous system malignancies. Gliomas are highly aggressive and are linked to a high mortality rate, thus, these tumors have become a serious threat to human health (Chew et al., 2018). Although some progress has been made in the treatment of this disease, there is currently a lack of effective and noninvasive diagnostic methods (Cheng et al., 2020; Stupp et al., 2005). Consequently, gliomas represent a major source of both health-related challenges and economic burden due to their aggressive nature and the costs of ongoing treatment (Hervey-Jumper and Berger, 2014). In addition, complete removal of high-grade glioma (HGG) through surgery is typically difficult. Moreover, glioma stem cells exhibit enhanced self-renewal, division, and proliferation, and are often resistant to conventional therapies, such as chemotherapy and radiotherapy, contributing to tumor recurrence and poor prognosis (Ostrom et al., 2015). Therefore, elucidating the molecular regulatory mechanisms during glioma development and identifying molecular markers can further advance the genetic diagnosis of clinical glioma and improve therapeutic efficacy.

Circular RNA (circRNA) is a new type of non-coding RNA with a covalently closed circular structure (Acunzo et al., 2015). CircRNAs are resistant to ribonuclease R (RNase R) degradation due to their covalently closed circular structure, which enhances their stability in biological fluids such as blood compared to linear RNAs. Therefore, circRNAs have great application value in the field of noninvasive diagnostics, and have emerged as a new class of potential tumor markers (Zhang et al., 2016). Tang et al. found that gastric cancer tissue-derived circKIAA1244 could be used as a new circulating biomarker for gastric cancer (Tang et al., 2018). Moreover, Li et al. demonstrated that hsa_circ_002059 may be a novel and stable biomarker for the diagnosis of gastric cancer from patient tissue and plasma samples (Li et al., 2015). In recent years, numerous studies reported that the expression of circRNAs in gliomas differs significantly. The expression of certain circRNAs varies depending on the degree of malignancy (Lu et al., 2019), and these circRNAs play a crucial role in glioma development by regulating both oncogenes and tumor suppressor genes. This process affects the invasion and metastasis of tumors, as well as the staging and grading of tumors (Sun et al., 2020). Studies have shown that some circRNAs correlate with the pathological grading of glioma, as well as the survival rate of patients with glioma. For example, circCDK14 expression correlates with the World Health Organization pathological grading of glioma (Chen et al., 2022), and hsa_circ_0001649 may be an independent prognostic indicator for patients with glioma after surgery (Wang et al., 2018). In addition, some circRNAs in gliomas act as miRNA sponges, sequestering the activity of miRNAs and indirectly regulating the expression of target genes (Lei et al., 2019; Shi et al., 2019), others behave as RNA-binding proteins and regulate protein interactions (Lou et al., 2020; Du et al., 2016), and still others have been reported to be translatable (Yang et al., 2018; Zhang et al., 2018). Currently, the exact functions and molecular mechanisms of most circRNAs in glioma are unknown. There is also a need to determine the expression and mechanism of action of circRNAs involved in the pathogenesis of glioma. Further studies are warranted to confirm whether circRNAs can be used as therapeutic targets or diagnostic and prognostic markers for glioma.

The circRNA-miRNA-mRNA pathway plays an important role in the development and progression of glioma, though the full extent of its involvement and mechanisms remains under investigation. Most circRNAs can be used as sponges of miRNA to regulate gene expression; this is key to clarifying the molecular mechanism of circRNA (Zhong et al., 2018). Studies have shown that circHIPK3 can also promote glioma progression by acting on its downstream target miR-654 and further regulating the circHIPK3/miR-654/IGF2BP3 network pathway (Jin et al., 2018). Another study also showed that deletion of circ_0074026 promotes apoptosis by regulating miR-1304 to block cell growth, migration, and invasion, providing a new therapeutic target for patients with gliomas (Chen et al., 2020). However, there may be other circRNAs regulated by the competing endogenous RNA (ceRNA) network in gliomagenesis and progression that have not yet been identified.

This study was performed to further investigate the influence of differentially expressed circRNAs on the occurrence, development, and prognosis of glioma. Firstly, the differential expression of circRNAs in glioma tissues and normal brain tissues was screened using circRNA high-throughput sequencing technology. Secondly, the study of unreported low-expression circRNAs in gliomas (circMIB1) was planned. Thirdly, we sought to examine their correlation with clinicopathological features of patients with glioma and reveal the mechanism by which they inhibit gliomagenesis through the ceRNA regulatory network. The objective was to provide new directions and ideas for the diagnosis, prognosis prediction, and molecular-targeted therapy of glioma.

Materials and methods

Tissues specimens and cell lines

In this study, 76 primary glioma samples were collected from glioma patients, and 17 nontumor brain tissues were obtained from patients with brain trauma or epilepsy. These samples were obtained from the Department of Neurosurgery of Yiyang Central Hospital (Yiyang, China). Following surgical resection, all specimens were frozen in liquid nitrogen and stored at −80°C. All participants or their guardians provided written informed consent for their participation. This study was approved by the Ethics Committee of Yiyang Central Hospital (Ethics approval reference number: V2.02024JJ9575).

The normal human glial cell line HEB was acquired from the Cell Bank of the Type Culture Collection of the Chinese Academy of Sciences (Shanghai, China). Human glioma cell lines SF126 (a glioblastoma cell line), U251, and U87 (glioma cell lines) were obtained from the American Type Culture Collection (ATCC, Manassas, VA, USA). The cell lines were grown in Dulbecco's modified Eagle's medium supplemented with 10% fetal bovine serum (Gibco, USA) at 37°C and 5% CO_2.

RNA sequencing and bioinformatic analyses

Five glioma samples and four non-tumor brain tissues were processed and RNA sequenced by Lc-Bio Technologies (Hangzhou, China). A larger sample size would be ideal to ensure statistical significance and biological reproducibility in future studies. Results were screened for significant differences in the expression of circRNAs using the edgeR software package (https://www.Bioconductor.org/) to identify differences with $|\log_2$fold-change $(\log_2 FC)| \geq 1$ and p-values < 0.05. The results showed significant differences in circRNA expression levels between glioblastoma (GBM) and non-tumor brain tissues.

Quantitative real-time polymerase chain reaction (qRT-PCR)

Total RNA isolation was performed using TRIzol reagent (Takara, Japan) according to the instructions provided by the manufacturer. Individual RNA samples (1 μg per sample) were converted to complementary DNA (cDNA) using the Prime Script RT kit (Takara) and the cDNA conversion step used a DNase (Takara) treatment to eliminate residual genomic DNA, and a RT-free control to check for genomic DNA contamination was used. While cDNA detected on an ABI Prism 7,500 Sequence Detection System (Applied Biosystems, USA) using the Hieff® qPCR SYBR Green Master Mix (Yeasen, China). Of note, glyceraldehyde-3-phosphate dehydrogenase (GAPDH) was used as an endogenous control. The qRT-PCR was performed using primers obtained from Bioengineering Biologicals (Changsha, China). The relative quantitative expression levels of circRNAs, miRNAs, and mRNAs were compared with those of the endogenous reference and analyzed using the $2^{-\Delta\Delta CT}$ method. Divergent primers were used to detect post-splicing junctions of circRNAs, and convergent primers were used to detect linear mRNAs. The primer sequences used are described in Supplementary Table S1.

Nucleic acid electrophoresis

The cDNA and genomic DNA amplification products were separated by 2% agarose gel electrophoresis in tris-acetic acid-ethylenediaminetetraacetic acid buffer, the DNA was separated by electrophoresis at 120 V for 25 min, and the DNA sizes were compared with those of Marker L (50–5,000 bp) (Sangon Biotech, China). Ultraviolet light was used to detect the bands.

RNase R assay

Original RNA (2 μg) was added to 2U RNase R (GeneSeed, Guangzhou, China), and a large amount of linear RNA could be digested by incubation at 37°C for 30 min. The reverse-transcription reaction was carried out by inactivating RNase R at 70°C for 10 min. The other untreated group was tested for circMIB1 and MIB1 levels by qRT-PCR using an internal control (i.e., GAPDH) as the calculation standard.

miRNA binding site prediction

The miRNA bindig sites were predicted using Circular RNA Interactome (https://circinteractome.nia.nih.gov/), and data from the GEO database (GSE90603, https://www.ncbi.nlm.nih.gov/gds/). The screening criteria were |log2FC|≥1 and p-values < 0.05, totaling yielding 59 differential miRNAs.

Bioinformatic analyses of mRNA

The Cancer Genome Atlas (TCGA, https://portal.gdc.ancer.gov/) includes a total of 393 cases of GBM and 508 cases of low-grade glioma (LGG). RNA expression data of normal brain tissue from the Genotype-Tissue Expression (GTEx) were downloaded from the UCSC Xena database (https://xenabrowser.net/datapages/). RNA transcriptomes of glioma specimens were obtained from The Cancer Genome Atlas (TCGA; https://portal.gdc.cancer.gov/). Subsequently, the RNA-sequencing data were $\log_2$ transformed and normalized for transcription per kilobase (TPM) values, and RNA-sequencing data (RSEM values) to make the gene expression profiles of the different platforms comparable. The R "limma" package was used to analyze the differential mRNA expression in the glioma tissues and normal brain tissues.

We also used GEPIA2 (Gene Expression Profiling Interactive Analysis, version 2) (http://gepia2.cancer-pku.cn/#index) to perform survival analysis and disease-free status analysis of differentially expressed genes in glioma. The Chinese Glioma Genome Atlas (CGGA, http://www.cgga.org.cn/) was also utilized for validation. Furthermore, we performed Gene Ontology (GO) enrichment analysis and pathway analysis. Finally, using the R package ggplot2 (https://www.r-proje ct.org/) in R version 4.2.2, dot plots were plotted to visualize valid terms and significant pathways for the GO enrichment analysis ($p < 0.05$).

Statistical analysis

Data were analyzed using unpaired Student's t-test or one-way analysis of variance (ANOVA) after confirming normal distribution of the data with the Shapiro-Wilk test, using GraphPad Prism eight software (GraphPad Software Inc, San Diego, CA, USA). All experiments were performed at least in triplicates. Pearson's correlation coefficient was employed to examine correlations. Data are presented as the mean ± standard deviation. The p-values < 0.05 indicate statistically significant differences.

Results

High-throughput sequencing to screen differentially expressed circRNAs

We performed circRNA high-throughput sequencing on four normal brain tissues and five glioma tissues. A total of 1,248 differentially expressed circRNA molecules were identified, of which 158 were upregulated and 1,090 were downregulated in

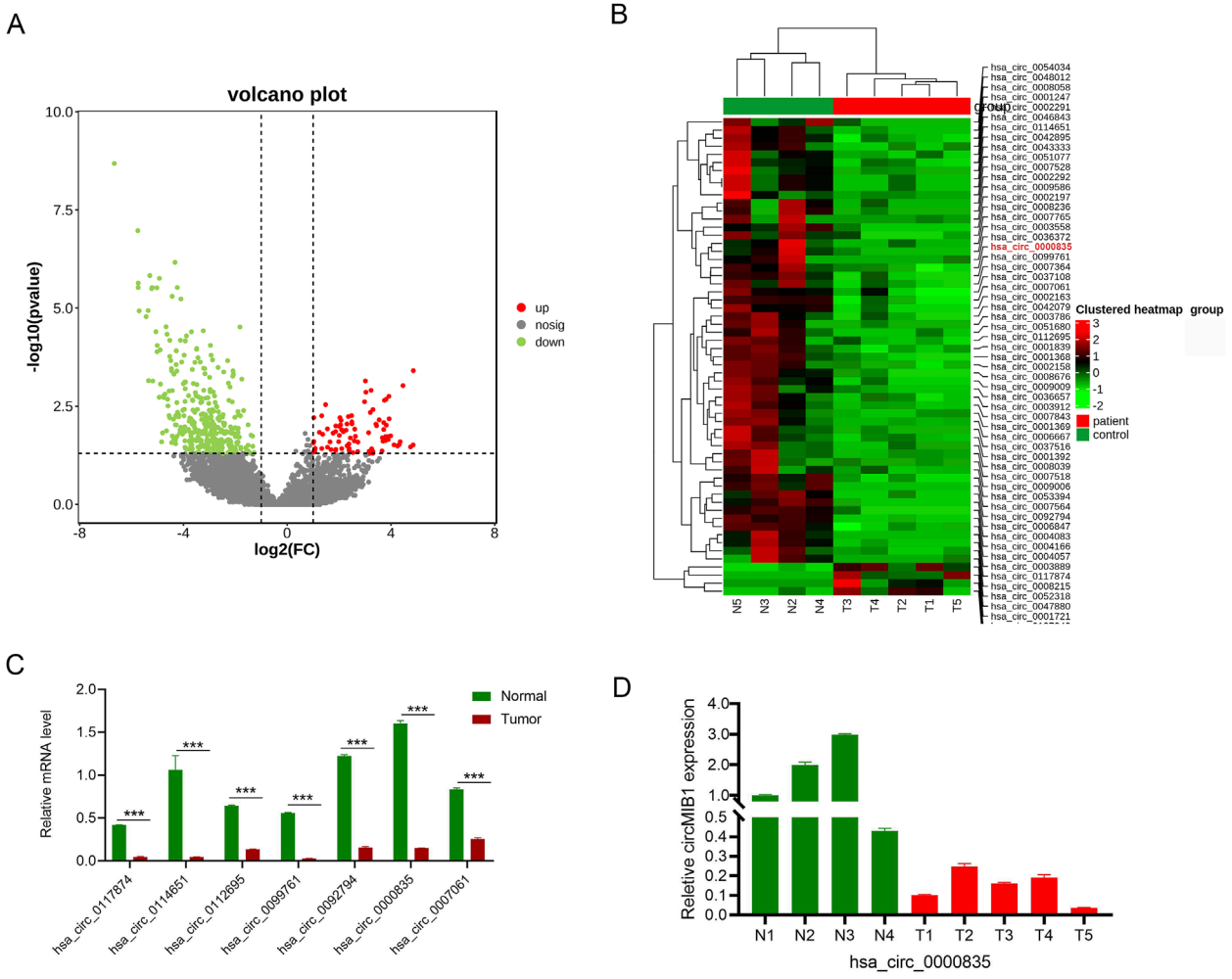

FIGURE 1
High-throughput sequencing to screen differentially expressed circRNAs. **(A)** Volcano plot of diferentially expressed circRNAs. The green dots represent downregulated circRNAs, whereas the red dots represent upregulated circRNAs in glioma compared with non-tumor tissue. **(B)** Clustered heatmap of circRNAs exhibiting significant differential expression in glioma tissues and non-tumor brain tissues (|log2 fold-change| ≥2, $p < 0.05$). Red and green indicate upregulated and downregulated circRNAs, respectively; hsa_circ_0000835 is labeled in red. **(C)** Downregulated circRNAs in glioma tissue. **(D)** Expression of circMIB1 in four and five samples of non-tumor and tumor tissues, respectively. Data are presented as the mean ± SD.*$p < 0.05$;**$p < 0.01$;***$p < 0.001$;****$p < 0.0001$.

glioma. The 652 differentially expressed circRNA molecules were recognized based on set criteria (|log2FC| ≥2 and p-values < 0.05), including 67 genes with upregulated expression and 585 genes with downregulated expression (Figure 1A). Sixty differentially expressed circRNA molecules were subsequently selected for cluster analysis based on statistical significance (|log2FC| ≥2 and p-values < 0.01), there was an overall decrease in circRNA expression abundance in cancer tissues compared to normal tissues. Consequently, we focused on circRNA molecules with downregulated expression and identified a significantly downregulated circRNA molecule, namely, hsa_circ_0000835 (circMIB1) (Figure 1B). Seven circRNA molecules with downregulated expression were randomly selected for RT-PCR validation. The validation results were consistent with the sequencing results, thereby confirming the findings (Figure 1C). Among all the validated genes, circMIB1 demonstrated the most significant expression difference in four normal brain tissues and five glioma tissues, and it has not been studied thus far in glioma (Figure 1D). Therefore, it was selected as the final target circRNA for further analysis.

Low expression of circMIB1 in glioma cells and tissues

We identified circMIB1 (hsa_circ_0000835) through the circBase database as being formed by reverse splicing of its parental gene MIB1 localized in exons 2–6 on chromosome 18 at positions 19,345,732–19,359,646, with a length of 679 bp (Figure 2A). MIB1 is an E3 ubiquitin ligase, which is widely expressed in adult brains and plays an important role in the morphogenesis of neurons. It interacts with certain proteins to form a network hub (Yoon et al., 2012), which plays a broad and powerful control role in the development of cells, tissues and organs (Mertz et al., 2015). However, the function of circRNAs derived from MIB1 in glioma remains unknown. The

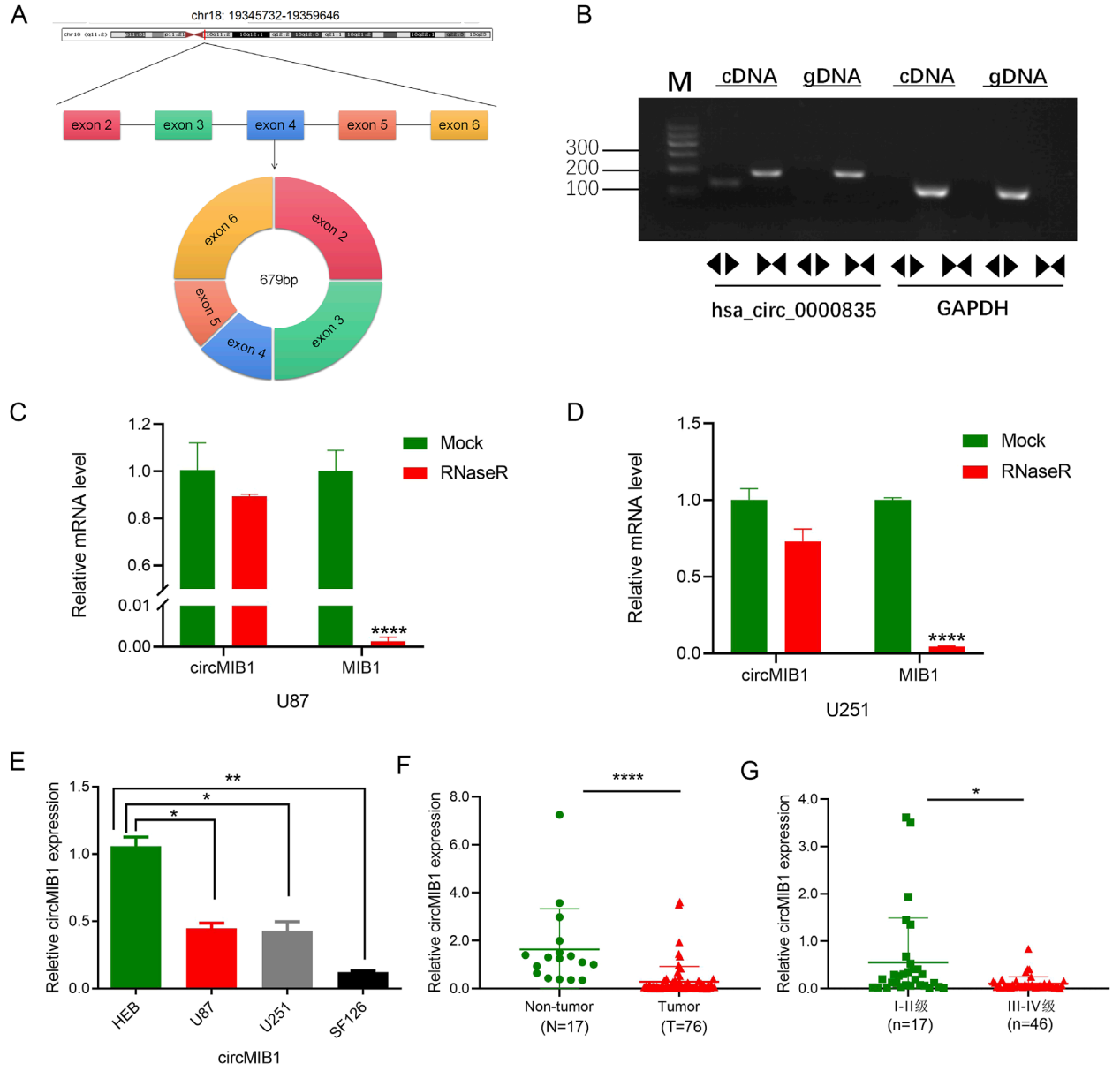

FIGURE 2
Low expression of circMIB1 in glioma cells and tissues. **(A)** Schematic showing the circMIB1 derived from exons 2–6 circularization of MIB1. **(B)** PCR was performed to analyze the circular RNA characterization of the circMIB1 (hsa_circ_0000835) using the divergent and convergent primers for amplification from the cDNA and genomic DNA (gDNA) of U251 cells, respectively. **(C, D)** RT-PCR analysis of circMIB1 and linear MIB1 mRNA, in presence or absence of RNaseR treatment for 30 min. **(E)** The expression level of circMIB1 in glioma cell lines (U87, U251 and SF126) and normal brain glial cells (HEB) was quantified by qRT-PCR. **(F, G)** CircMIB1 levels in 76 glioma and 17 non-tumor brain tissues, and in 30 patients with I-II grade glioma and 46 patients with III-IV grade glioma. Data are presented as mean ± SD.$^{*}p < 0.05$;$^{**}p < 0.01$;$^{***}p < 0.001$;$^{****}p < 0.0001$.

divergent and convergent primers were designed based on the characteristics of circMIB1. Using PCR analysis, we found that the divergent primers successfully amplified circMIB1 from cDNA of U251 cells, whereas genomic DNA (gDNA) did not. In contrast, the linear transcript MIB1 was amplified with the convergent primers. Agarose gel electrophoresis was used to verify that circMIB1 is indeed a circRNA molecule (Figure 2B).

Following treatment of cDNA with ribonuclease R (RNase R), circMIB1 was found to be resistant to RNase R by qRT-PCR; however, its linear MIB1 was disrupted by RNase R in U87 and U251 cells, suggesting that circMIB1 is unaffected by RNase R and has a circular structure (Figures 2C,D). The expression of circMIB1 in normal brain astrocyte cell line HEB and malignant glioma cell lines U251, U87, and SF126 was evaluated. The expression of circMIB1 was significantly lower in malignant glioma cell lines *versus* normal brain astrocyte cells (Figure 2E). The downregulated expression of circMIB1 in glioma tissues was further investigated in a larger sample size using RT-PCR. The analysis showed that the expression levels of circMIB1 were significantly lower in 76 GBM tissues compared with 17 normal brain tissues. Among 76 glioma

tissues of different grades, circMIB1 expression had significantly lower expression in high-grade tissues *versus* low-grade tissues ($p < 0.05$) (Figures 2F, G). These data indicated that circMIB1 has a circRNA profile and is lowly expressed in glioma.

CircMIB1 expression correlates with patient clinical characteristics and haspotential as a diagnostic marker for gliomas

To investigate whether circMIB1 levels were associated with clinical features of gliomas, patients with glioma were grouped according to age, sex, and clinical stage; and 76 patients with gliomas were divided into two groups based on the median circMIB1 levels. We found that circMIB1 expression was not statistically correlated with the age and sex of patients with glioma and was strongly associated with the clinical stage ($p < 0.005$). Higher clinical stages were linked to lower expression levels of hsa_circ_circMIB1 (Table 1). According to the log-rank test statistic for survival curves, the survival rate of 76 glioma patients with high expression of circMIB1 was 81.6%, whereas the survival rate of patients with low expression was 47.4%. Thus, the survival rate of glioma patients with high circMIB1 expression was significantly longer than that of patients with low circMIB1 expression. This observation suggested a positive correlation between circMIB1 expression and the overall survival time of patients with glioma (95% confidence interval: 0.6326–0.9543, $p < 0.0001$) (Figure 3A). Similarly, the Kaplan–Meier curve analysis showed that patients with low circMIB1 expression were associated with a higher recurrence rate and shorter time to recurrence (95% confidence interval: 0.8213–0.9511, $p < 0.0001$) (Figure 3B). The same receiver operating characteristic (ROC) curve without adjustment (e.g., age, gender, or tumour type) for other factors showed that circMIB1 could differentiate between non-glioma patients and glioma patients with an area under the curve (AUC) of 0.928 (95% confidence interval:0.855-0.9871; $p < 0.0001$) (Figure 3C). Similarly, CircMIB1 has a relatively low ability to distinguish between LGG patients and HGG patients, with AUC of 0.7028 (95% confidence interval: 0.5571–0.8395; $p < 0.01$) (Figure 3D). Principal component analysis of circMIB1 expression levels was performed to validate the above results, and the results showed that circMIB1 expression levels could effectively differentiate between non-glioma patients and those with glioma (Figure 3E), as well as between patients with LGG and those with HGG (Figure 3F). These results indicate that circMIB1 has potential value as a biomarker for glioma, which needs to be further investigated.

Downstream miRNA prediction of circMIB1 in glioma

CircMIB1 may be involved in the development of glioma through miRNA sponging, thus preventing the inhibitory effect of miRNA on its target genes. To explore the downstream target genes of circMIB1, we first analyzed differentially expressed miRNAs in glioma using GSE90603 RNA-sequencing data from the GEO database (https://www.ncbi.nlm.nih.gov/gds/), and identified 59 differentially expressed miRNA ($p < 0.05$, $|\log2FC| \geq 2$) using R language analysis. Subsequently, we predicted downstream miRNAs of circMIB1 by searching a bioinformatics database (Circular RNA Interactome), and performed Venn analysis of these target miRNAs with differential miRNAs in the GEO database. This led to the identification of two miRNAs (hsa-miR-1290 and hsa-miR-330-5p) (Figure 4A). Notably, hsa-miR-1290 was upregulated, whereas hsa-miR-330-5p was downregulated. Of note, hsa-miR-330 inhibits the growth of gliomas, this is not consistent with the normal logic of regulation. Consequently, hsa-miR-1290 was selected for subsequent analysis in this study (Figure 4B). Differential analysis and survival analysis using CGGA (http://www.cgga.org.cn/) prediction combined with miRNAs. Differential and survival analyses were conducted using the CGGA (http://www.cgga.org.cn/) prediction combined with miRNAs. The results showed that hsa-miR-1290 exhibited significant differential expression in different grades of glioma, and the expression levels of hsa-miR-1290 increased with the grade of tumor ($p < 0.01$) (Figure 4C). Nonetheless, there was no significant difference in expression in patients depending on sex and age (Figures 4D, F). Kaplan–Meier curve analysis revealed that the survival of patients with glioma was significantly lower in those with high hsa-miR-1290 expression *versus* those with low hsa-miR-1290 expression. These findings suggested a negative correlation between hsa-miR-1290 levels and the overall survival time of patients with glioma ($p < 0.05$) (Figure 4E).

CircMIB1 target genes and their expression and survival prognostic value

We further investigated the potential prognostic value of the ceRNA network in glioma, through miRTarBasesearch (https://mirtarbase.cuhk.edu.cn/), TargetScan8.0 (https://www.targetscan.org/), and the miRWalk (http://mirwalk.umm.uni-heidelberg.de/) to predict the target genes of miR-1290. A total of 25 differentially expressed target genes were identified by the Venn analysis (Figure 5A). We initially analyzed the expression levels of these target genes in normal and tumor tissues using the R "limma" package, which showed that 11 genes were downregulated in glioma tissues (Figure 5B). We further performed survival analysis and disease-free status analysis of differentially expressed genes in glioma using the GEPIA2 to explore the prognostic value of these target genes. The findings revealed that patients with glioma with high expression of adducin 2 (ADD2), CST telomere replication complex component 1 (CTC1), SRC kinase signaling inhibitor 1 (SRCIN1), RAR related orphan receptor A (RORA), vacuolar protein sorting four homolog A (VPS4A), and unc-51 like autophagy activating kinase 2 (ULK2) had a longer survival than those with low expression (Figures 5C–H). Moreover, high expression of ataxin 1 (ATXN1), collagen type XXVII alpha one chain (COL27A1), interphotoreceptor matrix proteoglycan 1 (IMPG1), N-myc downstream regulated 1 (NDRG1), and THAP domain containing 6 (THAP6) offered some advantages in terms of survival (Supplementary Figure S1). Similarly, disease-free survival was found to be longer in patients with glioma with high expression of ADD2, CTC1, SRCIN1, RORA, VPS4A, and ULK2 than in those with low expression (Figures 5C–H). These results suggest that

TABLE 1 Correlation of circMIB1 expression levels with clinicopathological parameters in glioma patients.

Characteristic	Case	CircMIB1 expression		χ2	*p*-Value
		High	low		
All cases	76	38	38		
Age (years)				0.210	0.646
>50	37	16	21		
≤50	39	22	17		
Gender				1.317	0.251
Male	38	18	20		
Female	38	20	18		
Grade				7.930	**0.005**
I-II	30	21	9		
III-IV	46	17	29		

downstream target genes that bind to miR-1290 are associated with survival and prognosis in glioma patients.

Functional analysis of six downstream target genes of circMIB1

To further investigate the function of circMIB1 downstream target genes, we used the CGGA (http://www.cgga.org.cn/) to validate the expression and prognostic analyses associated with six such genes. We found significant differences in the expression levels of ADD2, CTC1, SRCIN1, RORA, and ULK2 genes in gliomas of different grades, excluding VPS4A (Figures 6A–F). In addition, these genes were generally expressed at higher levels in isocitrate dehydrogenase-mutant (IDH-mutant) gliomas relative to IDH-wild-type gliomas, and were also generally expressed at higher levels in gliomas with chromosome 1p19q deletion than in gliomas without chromosome 1p19q deletion. This evidence implied that the expression of these genes correlates with both the grade of glioma, glioma IDH mutation, and chromosome 1p19q deletion (Supplementary Figure S2).

Furthermore, survival analysis revealed that patients with glioma with high expression of ADD2, CTC1, SRCIN1, VPS4A, ULK2, excluding RORA, had a longer overall survival than those with low expression (Figures 6A–F). Subsequently, we performed GO and Kyoto Encyclopedia of Genes and Genomes (KEGG) enrichment analyses of these genes. Based on the GO enrichment analysis of the dataset, the functions of these genes were mainly related to the cell cycle, and were highly correlated with glioma (Figure 6G). In addition, the KEGG analysis showed that these genes were mainly closely related to the circadian rhythm and apoptotic necrosis (Figure 6H). This provided an alternative explanation for the mechanism underlying the inhibition of glioma by circMIB1. The above results indicate that circMIB1 is involved in the progression of glioma by potentially targeting downstream mRNAs through miR-1290. These data provide suggestions for further investigation of the biological mechanism of circMIB1 involved in the development of glioma.

Discussion

Gliomas are the most common malignant brain tumors, pathologically characterized by a high degree of morphological and genetic complexity and heterogeneity (Chen et al., 2017). Patients with glioma are linked to a high rate of recurrence, a low survival rate, and a dismal prognosis (Xu et al., 2020; Tom et al., 2019). Therefore, in-depth study of the pathogenesis of glioma and identification of biomarkers and new therapeutic targets are necessary. In recent years, it has been found that circRNA is significantly differentially expressed in glioma (Lu et al., 2019; Sun et al., 2020). Such molecules affect tumor invasion and metastasis, as well as staging and typing, and plays a crucial role in the development of glioma (Liu et al., 2022). In this study, we found that circMIB1 is lowly expressed in glioma tissues and cells, and demonstrated that it correlates with survival prognosis of patients with glioma and has some potential as a biomarker. Moreover, we revealed the molecular mechanism underlying the regulation of the ceRNA network by circMIB1. Furthermore, we emphasized that circMIB1 is closely related to the cell cycle, cellular necrosis, and circadian rhythms, and that it may be a target for the treatment of glioma.

Accumulating evidence suggests that the development of glioma is closely related to the differential expression of circRNAs. Yuan et al. found that 2,038 circRNAs were abnormally expressed between GBM and matched normal brain tissue (Yuan et al., 2018). We similarly found 1,248 differentially expressed circRNA molecules in glioma tissues by high-throughput sequencing, with >87% (n =

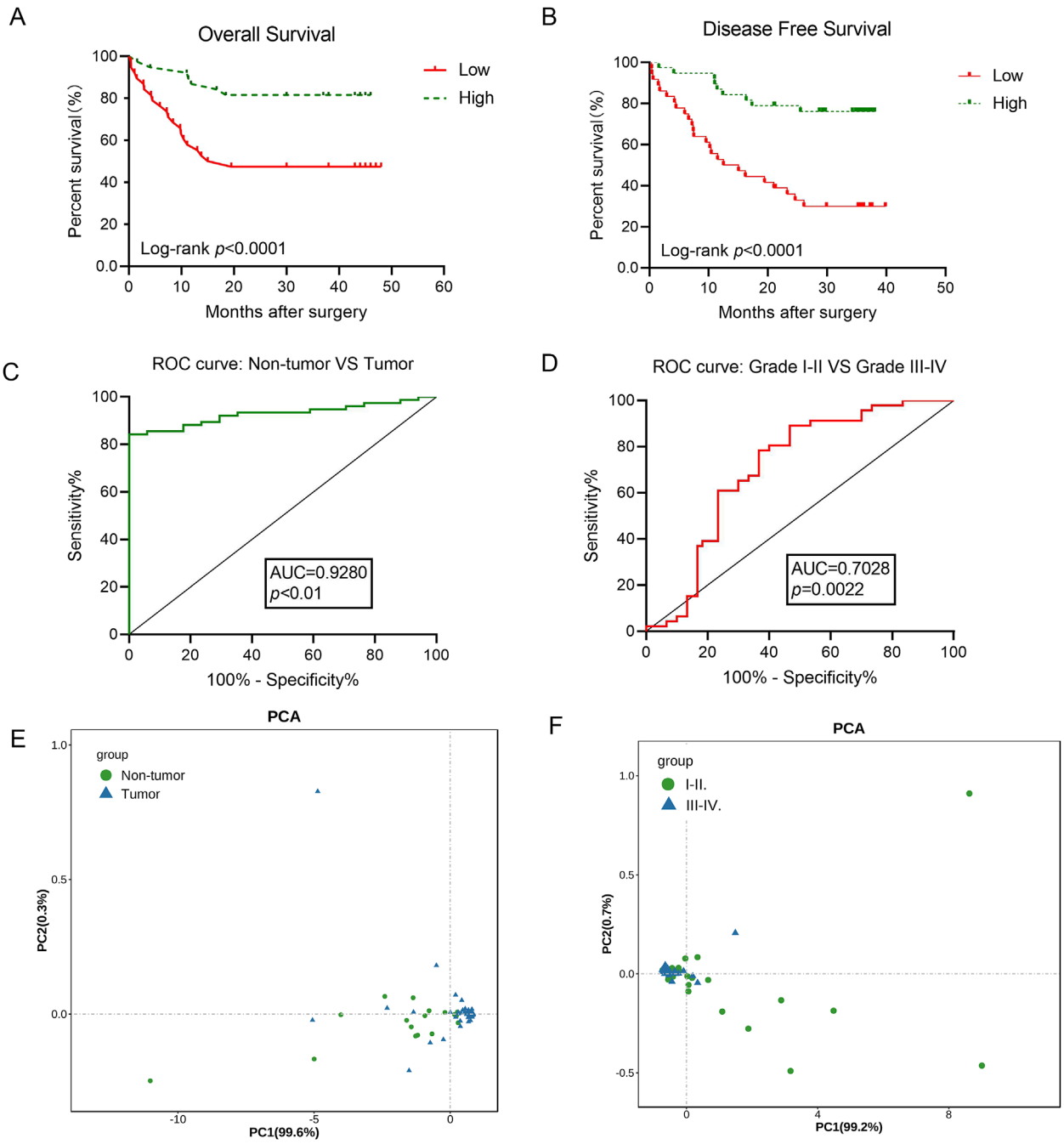

FIGURE 3
CircMIB1 expression correlates with patient clinical characteristics and has potential as a diagnostic marker for gliomas. **(A)** Overall survival curve, based on the circMIB1 levels, plotted with the Kaplan–Meier method and analyzed using the rank test. **(B)** Disease-free survival curve, based on the circMIB1 levels, plotted with the Kaplan–Meier method and analyzed using the rank test. **(C)** ROC curve of glioma tissue and non-tumor tissue. **(D)** ROC curve of grade I-II tumor from grade III-IV tumor. **(E)** PCA plot consisting of the circMIB1 levels in glioma tissue and non-tumor tissue. **(F)** PCA plot consisting of the circMIB1 levels in grade I–II tumor from grade III–IV tumor. Data are presented as the mean ± SD.*$p < 0.05$;**$p < 0.01$;***$p < 0.001$;****$p < 0.0001$.

1,090) of the circRNAs significantly downregulated. In addition, it was shown that the majority of circRNAs were negatively correlated with tumor proliferation and more opportunistically involved in glioma progression (Bachmayr-Heyda et al., 2015). Therefore, this study focused on circRNAs with downregulated expression. Next, we observed that circMIB1 expression was downregulated and most significantly differentially expressed in glioma cells and tissues by RNA sequencing. CircMIB1 is an emerging molecule that has not been studied and reported in gliomas and other diseases, but its parental protein, MIB1, is an E3 ubiquitin ligase required for the activation of the Notch pathway, and dysregulation of Notch signalling has been associated with cell transformation and tumourigenesis in various types of cancer (Li et al., 2018). Moreover, it has been demonstrated that MIB1 plays an important role in

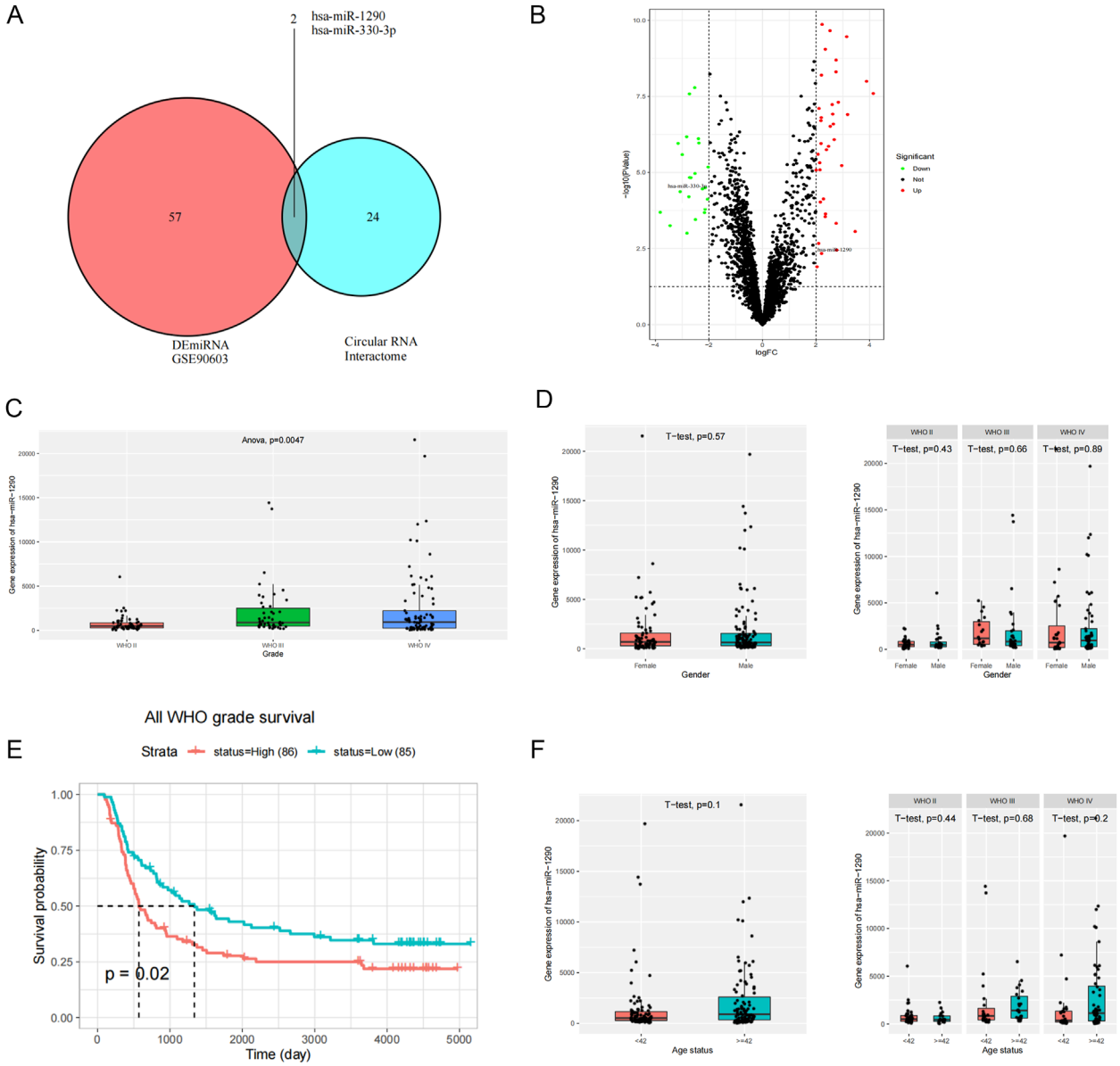

FIGURE 4
Downstream miRNA prediction of circMIB1 in glioma. **(A)** Predicted target miRNA of circMIB1 based on data obtained from the Circular RNA Interactome and GEO databases. **(B)** Volcano plot of differentially expressed miRNAs predicted to interact with circMIB1. **(C)** Differential analysis of miR-1290 expression in different grades of gliomas. **(D)** Analysis of miR-1290 expression differences between glioma patients of different genders. **(E)** Total survival curve of miR-1290 level. **(F)** Analysis of miR-1290 expression differences between glioma patients of different ages.

the development of a variety of tumors. For example, in lung cancer, MIB1 is involved in epithelial–mesenchymal transition, cell migration and cell survival (Wang et al., 2022), MIB1 aslo can be used as a marker for the proliferation and prognosis of LGG in children (Gorodezki et al., 2024). Therefore, we predicted that circMBI1 might be involved in the development of gliomas, which was subsequently validated by expanding the sample size by RT-qPCR, and found that circMBI1 expression levels in glioma tissues were significantly downregulated compared with those in normal brain tissues. Therefore, we conjecture that it is important to investigate the mechanism of circMIB1 involvement in glioma development and to determine its role in disease progression and prognosis.

The potential influence of circRNAs on the pathological grading and prognosis of glioma has attracted extensive attention in cancer biology (Sun et al., 2020). The expression levels of hsa_circ_0001649, Circ-ITCH and circNALCN are correlated with the WHO pathological grading of gliomas, and may be an independent prognostic indicator for postoperative patients with glioma (Wang et al., 2018; Liu et al., 2021; Chen et al., 2021). Similarly, our findings showed that circMIB1 was not statistically correlated with age and gender of glioma patients, but was

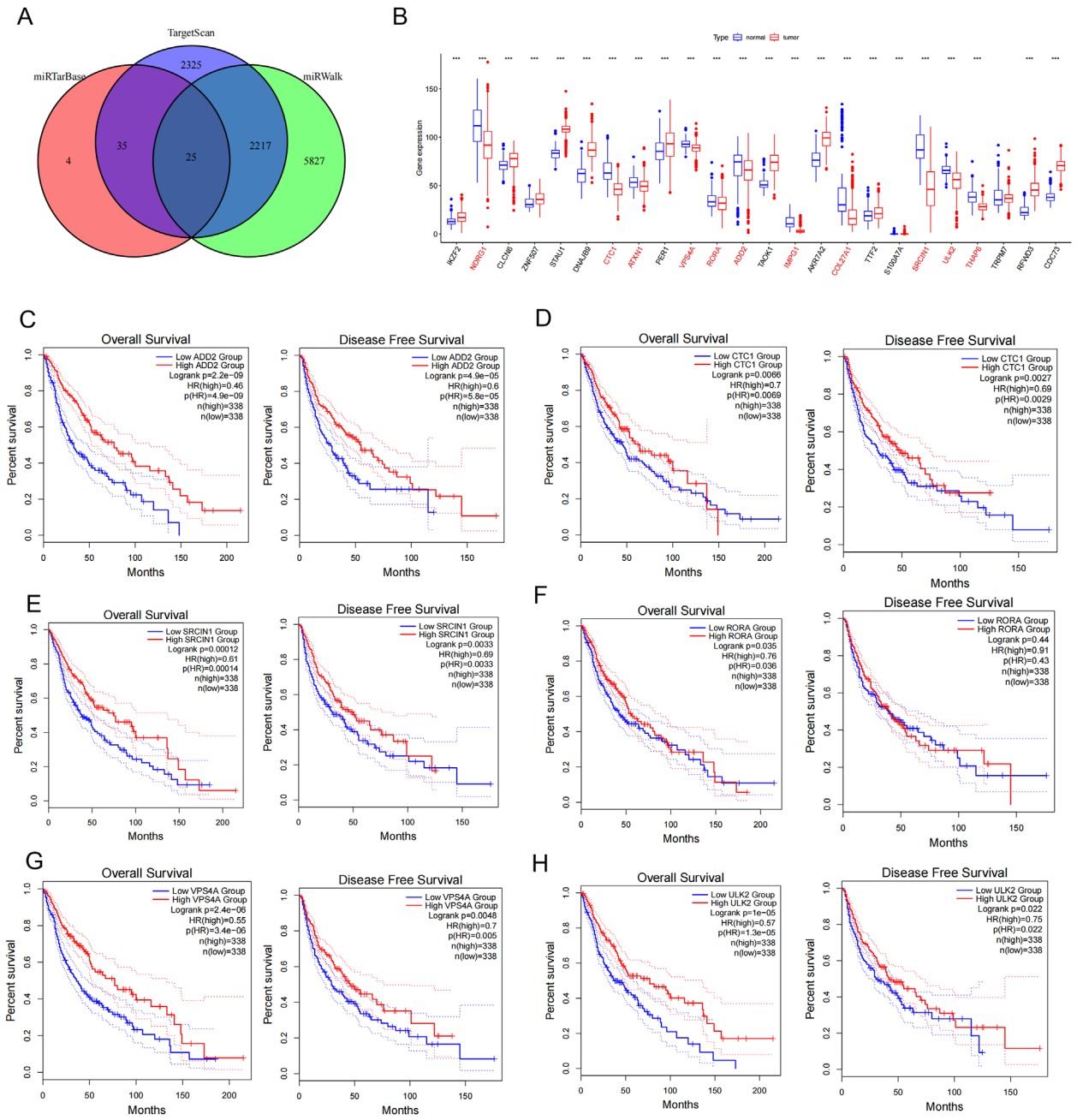

FIGURE 5
Exploring CircMIB1 downstream genes and their expression and survival prognosis analysis. **(A)** Predicted target mRNA of miR-1290 using data obtained from the miRTarBasesearch, miRWalk, and TargetScan 8.0 databases. **(B)** Differential mRNA expression in glioma tissue and normal brain tissue. **(C)** Overall survival and disease-free survival in ADD2. **(D)** Overall survival and disease-free survival in CTC1. **(E)** Overall survival and disease-free survival in SRCIN1. **(F)** Overall survival and disease-free survival in RORA. **(G)** Overall survival and disease-free survival in VPS4A. **(H)** Overall survival and disease-free survival in ULK2.

strongly associated with the clinical stage of patients. Notably, these molecules, including circMIB1, will likely be able to assist in diagnosing the clinical staging of gliomas in the future. Additionally, Kaplan-Meier curve analysis, without considering the influence of other factors, showed that glioma patients with high circMIB1 expression had significantly longer survival and lower recurrence rates than those with low expression. These results suggest that circMIB1 expression reflects the degree of malignancy of the tumour and correlates with the survival and prognosis of glioma patients. Hence, this evidence may provide a basis for the clinical treatment of glioma. Recent studies have increasingly focused on the use of circRNAs as cancer diagnostic biomarkers due to their high tolerance to ribonuclease R and high cellular stability (Zou et al., 2020), Zhou et al. found that hsa_circ_0004214 has diagnostic value and may be a promising biomarker for glioma (Zhou et al., 2023). We further verified that circMIB1 may be a suitable molecule to be used

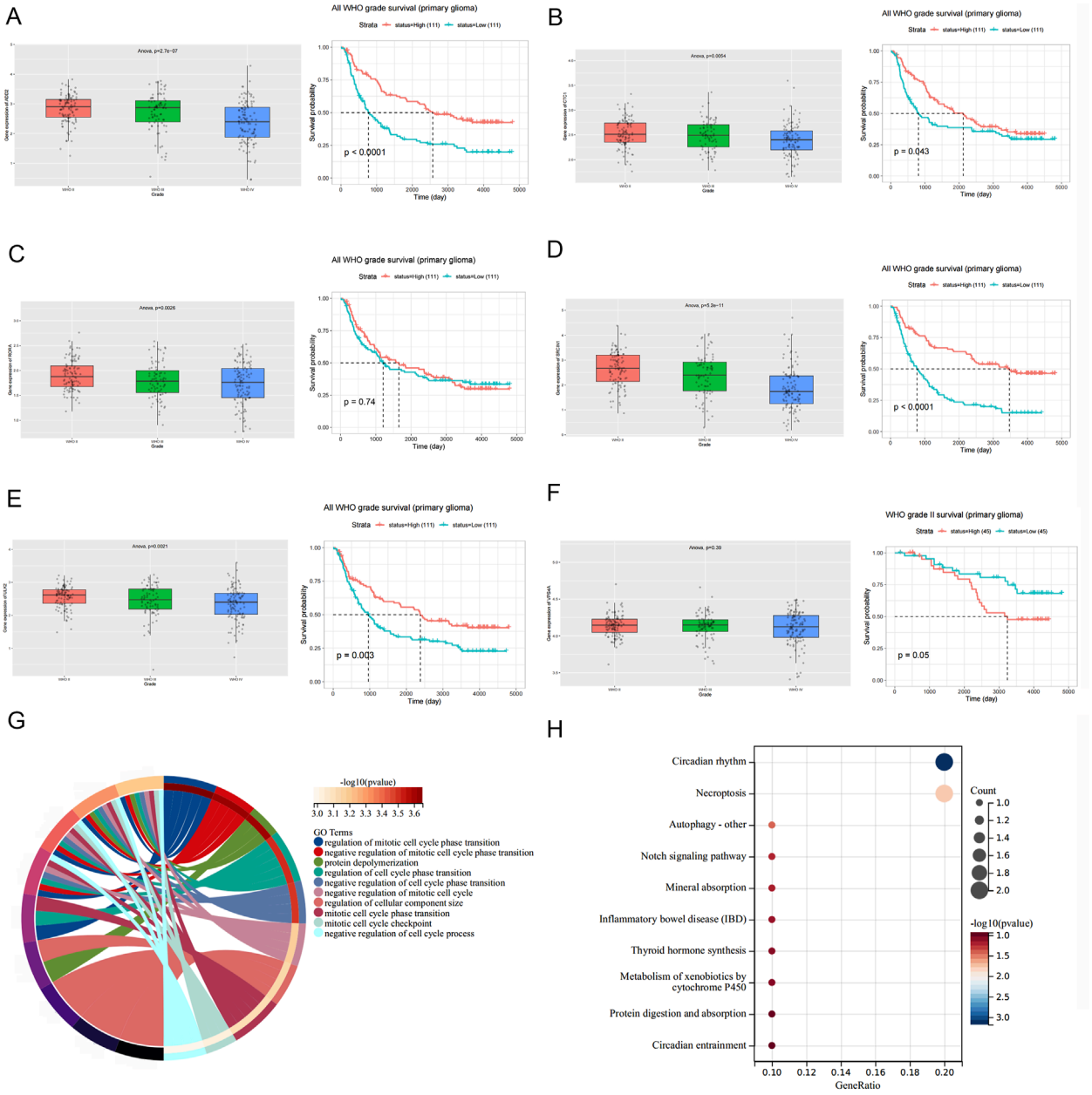

FIGURE 6
Functional analysis of six downstream target genes of circMIB1. **(A)** Expression and survival analysis of CDD2 in glioma tissues of different grades. **(B)** Expression and survival analysis of CTC1 in glioma tissues of different grades. **(C)** Expression and survival analysis of RORA in glioma tissues of different grades. **(D)** Expression and survival analysis of SRCIN1 in glioma tissues of different grades. **(E)** Expression and survival analysis of ULK2 in glioma tissues of different grades. **(F)** Expression and survival analysis of VPS4A in glioma tissues of different grades. **(G)** GO functional analysis of six downstream target genes. **(H)** KEGG functional analysis of six downstream target genes.

as a diagnostic biomarker for glioma based on the results of ROC curves and principal component analysis, but the magnitude of its potential remains to be investigated by us further.

Interestingly, circRNAs function as mRNA 'sponges', and negatively regulate miRNAs by absorbing and specifically binding to them, thereby increasing the expression of miRNA-associated target genes (Wang et al., 2020; Liu et al., 2022). A study suggested that overexpression of circHIPK3 promotes the proliferation and invasive ability of glioma cells through sponge miR- 124-3p upregulation of signal transducer and activator of STAT3 levels (Hu and Zhang, 2019). Another study also showed that circPTN promotes glioma growth and stemness by sponging miR-145-5p and miR-330-5p, this results in increased expression of NES, CD133, SOX9 and SOX2, which promotes self-renewal of glioma stem cells and regulates gliomagenesis (Chen et al., 2019). Previous studies reported that hsa-miR-1290 is significantly upregulated in glioma cells and tissues and is strongly associated with patient survival and tumor grade (Zhao et al., 2022). Thus, we consider hsa-miR-1290 a

downstream regulatory molecule of circMIB1, which in turn inhibits glioma cell growth and affects patient prognosis.

In particular, circRNAs also regulate miRNA sponges and downstream RNA-binding proteins, which participate in and influence the circulatory pathways of glioma progression (Qu et al., 2015). However, the potential function of circRNAs as a ceRNA network and their involvement in glioma warrant further investigation. Hence, we constructed a circRNA-miRNA-mRNA network by bioinformatics analysis, and identified six genes as the central downstream genes in the circMIB1 regulatory axis (i.e., ADD2, CTC1, SRCIN1, VPS4A, ULK2, and RORA). These downstream target genes were differentially expressed in different grades of glioma, exhibited good tumor suppression, and were significantly associated with survival and recurrence rates in patients with glioma. Among these predicted targets, SRCIN1 possesses tumor-suppressive properties in breast cancer and lung cancer inhibiting cell migration and proliferation (Dong et al., 2020; Guo et al., 2019). VPS4A acts as a tumor suppressor by regulating the secretion and uptake of extracellular miRNAs in human hepatocellular carcinoma cells (Wei et al., 2015). ULK1/2 inhibits the actin assembly and hinders breast cancer cell contraction and migration (Liang et al., 2023), Selective splicing of genes in the intronic protein family, including ADD2, leads to alterations in cellular function during pathogenesis are associated with cancer (Kiang and Leung, 2018).

In addition, it has been suggested in the literature that differentially expressed circRNAs are drivers of brain tumors or neurological disorders and are enriched in a variety of cancer-associated signaling pathways (Yuan et al., 2018). Thus, we further explored the functions of the six key genes downstream of circMIB1 and the affected signaling pathways. Results of the GO analysis showed that these six target genes may be associated with the cell cycle, and that disruption of cell cycle regulation is a major mechanism for glioma development and progression (Mason and Cairncross, 2008). Hence, these six genes may be involved in the regulation of the cell cycle, thereby inhibiting tumor development and progression. In addition, KEGG analysis revealed that target genes are mainly involved in pathological processes, such as circadian rhythms and apoptotic necrosis. Studies have found that GBM has a problem with cellular rhythms, and that the circadian gene CSNK1E is a potent target for the treatment of GBM. The growth of GBM can be effectively inhibited by using a CSNK1E inhibitor, which leads to massive death of GBM cells (Varghese et al., 2018). These findings reveal that downstream target genes are closely associated with cancer development and may be involved in different network mechanisms during glioma formation, potentially involving the regulation of circMIB1.

Collectively, our data illustrate that circMIB1 may play an inhibitory role in glioma pathogenesis. Importantly, circMIB1 has the potential to serve as a biomarker for glioma and may play a regulatory role through the ceRNA network. Nevertheless, this study had some limitations. Firstly, the sample size of our cohort study was relatively small and not comprehensive, hence, subsequent studies involving larger sample sizes are warranted. Secondly, functional tests of circMIB1 have not yet been performed *in vitro* and *in vivo*, circMIB1 inhibits glioma growth by participating in the cell cycle, apoptosis, or other pathways, and these functional validation studies would make the findings more reliable. Thus, the present findings only provide a direction to further explore the regulatory pathways underlying the effects of circMIB1 on gliomas. Therefore, in-depth study of the role and exact mechanism of circMIB1 in glioma is our research focus in the future.

In conclusion, we demonstrated that circMIB1 is lowly expressed in glioma tissues and cells, and that its expression is closely related to the survival prognosis of patients. Thus, circMIB1 may be able to serve as a target for glioma diagnosis and treatment. In addition, circMIB1 may also regulate the differential expression of downstream hsa-miR-1290 and related target genes, which are further involved in glioma progression. Further understanding of the specific role of circMIB1 in tumour grading and treatment through ceRNA networks will provide new perspectives and approaches for early diagnosis and treatment of gliomas.

Data availability statement

The datasets presented in this study can be found in online repositories. The names of the repository/repositories and accession number(s) can be found in the article/Supplementary Material.

Ethics statement

The studies involving humans were approved by the Ethics Committee of Yiyang Central Hospital (Yiyang, China). The studies were conducted in accordance with the local legislation and institutional requirements. The participants provided their written informed consent to participate in this study.

Author contributions

SC: Funding acquisition, Conceptualization, Data curation, Formal Analysis, Investigation, Methodology, Supervision, Visualization, Writing – original draft, Writing – review and editing. LL: Resources, Formal Analysis, Methodology, Visualization, Writing – original draft, Writing – review and editing. WX: Software, Investigation, Methodology, Writing – original draft. NX: Software, Investigation, Writing – original draft. HX: Software, Investigation, Writing – review and editing. YoZ: Investigation, Writing – review and editing. YiZ: Software, Writing – review and editing. KY: Software, Writing – review and editing. ZZ: Resources, Investigation, Funding acquisition, Supervision, Conceptualization, Writing – review and editing.

Funding

The author(s) declare that financial support was received for the research and/or publication of this article. Our research was

supported by Hunan Provincial Natural Science Foundation of China (No. 2024JJ9575).

Conflict of interest

The authors declare that the research was conducted in the absence of any commercial or financial relationships that could be construed as a potential conflict of interest.

Generative AI statement

The author(s) declare that no Generative AI was used in the creation of this manuscript.

Publisher's note

Supplementary material

The Supplementary Material for this article can be found online at: https://www.frontiersin.org/articles/10.3389/fmolb.2024.1513919/full#supplementary-material

References

Acunzo, M., Romano, G., Wernicke, D., and Croce, C. M. (2015). MicroRNA and cancer–a brief overview. *Adv. Biol. Regul.* 57, 1–9. doi:10.1016/j.jbior.2014.09.013

Bachmayr-Heyda, A., Reiner, A. T., Auer, K., Sukhbaatar, N., Aust, S., Bachleitner-Hofmann, T., et al. (2015). Correlation of circular RNA abundance with proliferation–exemplified with colorectal and ovarian cancer, idiopathic lung fibrosis, and normal human tissues. *Sci. Rep.* 5, 8057. doi:10.1038/srep08057

Chen, J., Chen, T., Zhu, Y., Li, Y., Zhang, Y., Wang, Y., et al. (2019). circPTN sponges miR-145-5p/miR-330-5p to promote proliferation and stemness in glioma. *J. Exp. Clin. Cancer Res.* 38 (1), 398. doi:10.1186/s13046-019-1376-8

Chen, M., Liu, X., Xie, P., Wang, P., Liu, M., Zhan, Y., et al. (2020). Circular RNA circ_0074026 indicates unfavorable prognosis for patients with glioma and facilitates oncogenesis of tumor cells by targeting miR-1304 to modulate ERBB4 expression. *J. Cell Physiol.* 235 (5), 4688–4697. doi:10.1002/jcp.29347

Chen, R., Smith-Cohn, M., Cohen, A. L., and Colman, H. (2017). Glioma subclassifications and their clinical significance. *Neurotherapeutics* 14 (2), 284–297. doi:10.1007/s13311-017-0519-x

Chen, S., Zhang, Z., Zhang, B., Huang, Q., Liu, Y., Qiu, Y., et al. (2022). CircCDK14 promotes tumor progression and resists ferroptosis in glioma by regulating PDGFRA. *Int. J. Biol. Sci.* 18 (2), 841–857. doi:10.7150/ijbs.66114

Chen, W., Wu, M., Cui, S. T., Zheng, Y., Liu, Z., and Luo, L. S. (2021). CircRNA circ-ITCH inhibits the proliferation and invasion of glioma cells through targeting the miR-106a-5p/SASH1 Axis. *Cell Transpl.* 30, 963689720983785. doi:10.1177/0963689720983785

Cheng, J., Meng, J., Zhu, L., and Peng, Y. (2020). Exosomal noncoding RNAs in Glioma: biological functions and potential clinical applications. *Mol. Cancer* 19 (1), 66. doi:10.1186/s12943-020-01189-3

Chew, C. L., Conos, S. A., Unal, B., and Tergaonkar, V. (2018). Noncoding RNAs: master regulators of inflammatory signaling. *Trends Mol. Med.* 24 (1), 66–84. doi:10.1016/j.molmed.2017.11.003

Dong, J., Li, B., Lin, D., Lu, D., Liu, C., Lu, X., et al. (2020). LincRNA00494 suppresses non-small cell lung cancer cell proliferation by regulating SRCIN1 expression as a ceRNA. *Front. Oncol.* 10, 79. doi:10.3389/fonc.2020.00079

Du, W. W., Yang, W., Liu, E., Yang, Z., Dhaliwal, P., and Yang, B. B. (2016). Foxo3 circular RNA retards cell cycle progression via forming ternary complexes with p21 and CDK2. *Nucleic Acids Res.* 44 (6), 2846–2858. doi:10.1093/nar/gkw027

Gorodezki, D., Zipfel, J., Bevot, A., Nägele, T., Ebinger, M., Schuhmann, M. U., et al. (2024). Prognostic utility and characteristics of MIB-1 labeling index as a proliferative activity marker in childhood low-grade glioma: a retrospective observational study. *J. Cancer Res. Clin. Oncol.* 150 (4), 178. doi:10.1007/s00432-024-05701-w

Guo, L., Zhu, Y., Li, L., Zhou, S., Yin, G., Yu, G., et al. (2019). Breast cancer cell-derived exosomal miR-20a-5p promotes the proliferation and differentiation of osteoclasts by targeting SRCIN1. *Cancer Med.* 8 (12), 5687–5701. doi:10.1002/cam4.2454

Hervey-Jumper, S. L., and Berger, M. S. (2014). Reoperation for recurrent high-grade glioma: a current perspective of the literature. *Neurosurgery* 75 (5), 491–499. ; discussion 498-9. doi:10.1227/neu.0000000000000486

Hu, D., and Zhang, Y. (2019). Circular RNA HIPK3 promotes glioma progression by binding to miR-124-3p. *Gene* 690, 81–89. doi:10.1016/j.gene.2018.11.073

Jin, P., Huang, Y., Zhu, P., Zou, Y., Shao, T., and Wang, O. (2018). CircRNA circHIPK3 serves as a prognostic marker to promote glioma progression by regulating miR-654/IGF2BP3 signaling. *Biochem. Biophys. Res. Commun.* 503 (3), 1570–1574. doi:10.1016/j.bbrc.2018.07.081

Kiang, K. M., and Leung, G. K. (2018). A review on adducin from functional to pathological mechanisms: future direction in cancer. *Biomed. Res. Int.* 2018, 3465929. doi:10.1155/2018/3465929

Lei, B., Huang, Y., Zhou, Z., Zhao, Y., Thapa, A. J., Li, W., et al. (2019). Circular RNA hsa_circ_0076248 promotes oncogenesis of glioma by sponging miR-181a to modulate SIRT1 expression. *J. Cell Biochem.* 120 (4), 6698–6708. doi:10.1002/jcb.27966

Li, B., Yu, L., Liu, D., Yang, X., Zheng, Y., Gui, Y., et al. (2018). MIB1 mutations reduce Notch signaling activation and contribute to congenital heart disease. *Clin. Sci. (Lond)* 132 (23), 2483–2491. doi:10.1042/cs20180732

Li, P., Chen, S., Chen, H., Mo, X., Li, T., Shao, Y., et al. (2015). Using circular RNA as a novel type of biomarker in the screening of gastric cancer. *Clin. Chim. Acta* 444, 132–136. doi:10.1016/j.cca.2015.02.018

Liang, P., Zhang, J., Wu, Y., Zheng, S., Xu, Z., Yang, S., et al. (2023). An ULK1/2-PXN mechanotransduction pathway suppresses breast cancer cell migration. *EMBO Rep.* 24 (11), e56850. doi:10.15252/embr.202356850

Liu, X., Zhang, Y., Zhou, S., Dain, L., Mei, L., and Zhu, G. (2022). Circular RNA: an emerging frontier in RNA therapeutic targets, RNA therapeutics, and mRNA vaccines. *J. Control Release* 348, 84–94. doi:10.1016/j.jconrel.2022.05.043

Liu, Y., Chen, S., Peng, G., Liao, Y., Fan, X., Zhang, Z., et al. (2021). CircRNA NALCN acts as an miR-493-3p sponge to regulate PTEN expression and inhibit glioma progression. *Cancer Cell Int.* 21 (1), 307. doi:10.1186/s12935-021-02001-y

Lou, J., Hao, Y., Lin, K., Lyu, Y., Chen, M., Wang, H., et al. (2020). Circular RNA CDR1as disrupts the p53/MDM2 complex to inhibit Gliomagenesis. *Mol. Cancer* 19 (1), 138. doi:10.1186/s12943-020-01253-y

Lu, Y., Deng, X., Xiao, G., Zheng, X., Ma, L., and Huang, W. (2019). circ_0001730 promotes proliferation and invasion via the miR-326/Wnt7B axis in glioma cells. *Epigenomics* 11 (11), 1335–1352. doi:10.2217/epi-2019-0121

Mason, W. P., and Cairncross, J. G. (2008). Invited article: the expanding impact of molecular biology on the diagnosis and treatment of gliomas. *Neurology* 71 (5), 365–373. doi:10.1212/01.wnl.0000319721.98502.1b

Mertz, J., Tan, H., Pagala, V., Bai, B., Chen, P. C., Li, Y., et al. (2015). Sequential elution interactome analysis of the mind bomb 1 ubiquitin ligase reveals a novel role in dendritic spine outgrowth. *Mol. Cell Proteomics* 14 (7), 1898–1910. doi:10.1074/mcp.M114.045898

Ostrom, Q. T., de Blank, P. M., Kruchko, C., Petersen, C. M., Liao, P., Finlay, J. L., et al. (2015). Alex's lemonade stand foundation infant and childhood primary brain and central nervous system tumors diagnosed in the United States in 2007-2011. *Neuro Oncol.* 16, x1–x36. doi:10.1093/neuonc/nou327

Qu, S., Yang, X., Li, X., Wang, J., Gao, Y., Shang, R., et al. (2015). Circular RNA: a new star of noncoding RNAs. *Cancer Lett.* 365 (2), 141–148. doi:10.1016/j.canlet.2015.06.003

Shi, F., Shi, Z., Zhao, Y., and Tian, J. (2019). CircRNA hsa-circ-0014359 promotes glioma progression by regulating miR-153/PI3K signaling. *Biochem. Biophys. Res. Commun.* 510 (4), 614–620. doi:10.1016/j.bbrc.2019.02.019

Stupp, R., Mason, W. P., van den Bent, M. J., Weller, M., Fisher, B., Taphoorn, M. J., et al. (2005). Radiotherapy plus concomitant and adjuvant temozolomide for glioblastoma. *N. Engl. J. Med.* 352 (10), 987–996. doi:10.1056/NEJMoa043330

Sun, J., Li, B., Shu, C., Ma, Q., and Wang, J. (2020). Functions and clinical significance of circular RNAs in glioma. *Mol. Cancer* 19 (1), 34. doi:10.1186/s12943-019-1121-0

Tang, W., Fu, K., Sun, H., Rong, D., Wang, H., and Cao, H. (2018). CircRNA microarray profiling identifies a novel circulating biomarker for detection of gastric cancer. *Mol. Cancer* 17 (1), 137. doi:10.1186/s12943-018-0888-8

Tom, M. C., Cahill, D. P., Buckner, J. C., Dietrich, J., Parsons, M. W., and Yu, J. S. (2019). Management for different glioma subtypes: are all low-grade gliomas created equal? *Am. Soc. Clin. Oncol. Educ. Book* 39, 133–145. doi:10.1200/edbk_238353

Varghese, R. T., Young, S., Pham, L., Liang, Y., Pridham, K. J., Guo, S., et al. (2018). Casein kinase 1 epsilon regulates glioblastoma cell survival. *Sci. Rep.* 8 (1), 13621. doi:10.1038/s41598-018-31864-x

Wang, H., Huang, Q., Xia, J., Cheng, S., Pei, D., Zhang, X., et al. (2022). The E3 ligase MIB1 promotes proteasomal degradation of NRF2 and sensitizes lung cancer cells to ferroptosis. *Mol. Cancer Res.* 20 (2), 253–264. doi:10.1158/1541-7786.Mcr-21-0342

Wang, J., Zhao, X., Wang, Y., Ren, F., Sun, D., Yan, Y., et al. (2020). circRNA-002178 act as a ceRNA to promote PDL1/PD1 expression in lung adenocarcinoma. *Cell Death Dis.* 11 (1), 32. doi:10.1038/s41419-020-2230-9

Wang, Y., Sui, X., Zhao, H., Cong, L., Li, Y., Xin, T., et al. (2018). Decreased circular RNA hsa_circ_0001649 predicts unfavorable prognosis in glioma and exerts oncogenic properties *in vitro* and *in vivo*. *Gene* 676, 117–122. doi:10.1016/j.gene.2018.07.037

Wei, J. X., Lv, L. H., Wan, Y. L., Cao, Y., Li, G. L., Lin, H. M., et al. (2015). Vps4A functions as a tumor suppressor by regulating the secretion and uptake of exosomal microRNAs in human hepatoma cells. *Hepatology* 61 (4), 1284–1294. doi:10.1002/hep.27660

Xu, S., Tang, L., Li, X., Fan, F., and Liu, Z. (2020). Immunotherapy for glioma: current management and future application. *Cancer Lett.* 476, 1–12. doi:10.1016/j.canlet.2020.02.002

Yang, Y., Gao, X., Zhang, M., Yan, S., Sun, C., Xiao, F., et al. (2018). Novel role of FBXW7 circular RNA in repressing glioma tumorigenesis. *J. Natl. Cancer Inst.* 110 (3), 304–315. doi:10.1093/jnci/djx166

Yoon, K. J., Lee, H. R., Jo, Y. S., An, K., Jung, S. Y., Jeong, M. W., et al. (2012). Mind bomb-1 is an essential modulator of long-term memory and synaptic plasticity via the Notch signaling pathway. *Mol. Brain* 5, 40. doi:10.1186/1756-6606-5-40

Yuan, Y., Jiaoming, L., Xiang, W., Yanhui, L., Shu, J., Maling, G., et al. (2018). Analyzing the interactions of mRNAs, miRNAs, lncRNAs and circRNAs to predict competing endogenous RNA networks in glioblastoma. *J. Neurooncol* 137 (3), 493–502. doi:10.1007/s11060-018-2757-0

Zhang, M., Zhao, K., Xu, X., Yang, Y., Yan, S., Wei, P., et al. (2018). A peptide encoded by circular form of LINC-PINT suppresses oncogenic transcriptional elongation in glioblastoma. *Nat. Commun.* 9 (1), 4475. doi:10.1038/s41467-018-06862-2

Zhang, X. O., Dong, R., Zhang, Y., Zhang, J. L., Luo, Z., Zhang, J., et al. (2016). Diverse alternative back-splicing and alternative splicing landscape of circular RNAs. *Genome Res.* 26 (9), 1277–1287. doi:10.1101/gr.202895.115

Zhao, L., Zhang, P., Nan, Y., Ren, B., Ma, H., Xie, J., et al. (2022). Bioinformatics analysis of potential glioblastoma circular RNA sponge network. *Transl. Cancer Res.* 11 (5), 1017–1032. doi:10.21037/tcr-21-2597

Zhong, Y., Du, Y., Yang, X., Mo, Y., Fan, C., Xiong, F., et al. (2018). Circular RNAs function as ceRNAs to regulate and control human cancer progression. *Mol. Cancer* 17 (1), 79. doi:10.1186/s12943-018-0827-8

Zhou, Y., Zhang, Y., Tian, J., Miao, Z., Lv, S., and Zhao, X. (2023). A meaningful strategy for glioma diagnosis via independent determination of hsa_circ_0004214. *Brain Sci.* 13 (2), 193. doi:10.3390/brainsci13020193

Zou, Y., Zheng, S., Deng, X., Yang, A., Kong, Y., Kohansal, M., et al. (2020). Diagnostic and prognostic value of circular RNA CDR1as/ciRS-7 for solid tumours: a systematic review and meta-analysis. *J. Cell Mol. Med.* 24 (17), 9507–9517. doi:10.1111/jcmm.15619

frontiers | Frontiers in Molecular Biosciences

TYPE Correction
PUBLISHED 16 April 2025
DOI 10.3389/fmolb.2025.1599157

OPEN ACCESS

APPROVED BY
Frontiers Editorial Office,
Frontiers Media SA, Switzerland

*CORRESPONDENCE
Zuping Zhang,
zhangzuping@csu.edu.cn

†These authors have contributed equally to this work

RECEIVED 31 March 2025
ACCEPTED 31 March 2025
PUBLISHED 16 April 2025

CITATION
Chen S, Li L, Xu W, Xie N, Xu H, Zhou Y, Zou Y, Yi K and Zhang Z (2025) Corrigendum: CircMIB1 inhibits glioma development and progression through a competing endogenous RNA interaction network. *Front. Mol. Biosci.* 12:1599157. doi: 10.3389/fmolb.2025.1599157

Corrigendum: CircMIB1 inhibits glioma development and progression through a competing endogenous RNA interaction network

Simin Chen[1†], Longping Li[1†], Wei Xu[1], Nanjiao Xie[1], Huiting Xu[1], Yongjun Zhou[1], Ying Zou[1], Kai Yi[1] and Zuping Zhang[2*]

[1]Department of Clinical Laboratory, Yiyang Central Hospital, Yiyang, Hunan, China, [2]School of Xiangya Basic Medical Science, Central South University, Changsha, Hunan, China

KEYWORDS

CircMIB1, glioma, MiR-1290, ceRNA, prognostic, biomarker

A Corrigendum on
CircMIB1 inhibits glioma development and progression through a competing endogenous RNA interaction network

by Chen S, Li L, Xu W, Xie N, Xu H, Zhou Y, Zou Y, Yi K and Zhang Z (2024). Front. Mol. Biosci. 11:1513919. doi: 10.3389/fmolb.2024.1513919

In the published article, there was an error in the **Author list**. Corresponding author Zuping Zhang was erroneously excluded and author Yi Liu was erroneously included. The corrected **Author list** appears below. The correspondence section has been updated accordingly.

Simin Chen[1†], Longping Li[1†], Wei Xu[1], Nanjiao Xie[1], Huiting Xu[1], Yongjun Zhou[1], Ying Zou[1], Kai Yi[1], Zuping Zhang[2*]

In the published article, there was an error in **Affiliation 2**. Instead of "Department of Emergency Medicine and Laboratory of Emergency Medicine, West China Hospital, West China School of Medicine, Sichuan University Chengdu, Chengdu, China", it should be "School of Xiangya Basic Medical Science, Central South University, Changsha, Hunan, China".

In the published article, there was an error in the **Author contributions**. The updated statement appears below:

AUTHOR CONTRIBUTIONS

SC: Funding acquisition, Conceptualization, Data curation, Formal Analysis, Investigation, Methodology, Supervision, Visualization, Writing – original draft, Writing – review and editing. LL: Resources, Formal Analysis, Methodology, Visualization, Writing – original draft, Writing – review and editing. WX: Software, Investigation, Methodology, Writing – original draft. NX: Software, Investigation, Writing – original draft. HX: Software, Investigation, Writing – review and editing. YoZ: Investigation, Writing – review and editing. YiZ: Software, Writing – review and editing. KY: Software, Writing – review and editing. ZZ: Resources, Investigation, Funding acquisition, Supervision, Conceptualization, Writing – review and editing.

In the published article, there was an error in the **Funding**statement. Due to an oversight on the part of the first author, the name of funder does not correspond to the official one. The correct **Funding**statement appears below.

FUNDING

The author(s) declare that financial support was received for the research and/or publication of this article. Our research was supported by Hunan Provincial Natural Science Foundation of China (No. 2024JJ9575).

The authors apologize for these errors and state that these do not change the scientific conclusions of the article in any way. The original article has been updated.

Publisher's note

frontiers | Frontiers in Molecular Biosciences

TYPE Original Research
PUBLISHED 06 December 2024
DOI 10.3389/fmolb.2024.1502509

OPEN ACCESS

EDITED BY
Giuseppe Bronte,
University of Ferrara, Italy

REVIEWED BY
Laura Duran-Lozano,
Vall d'Hebron Institute of Oncology (VHIO), Spain
Florentina Duica,
Carol Davila University of Medicine and Pharmacy, Romania

*CORRESPONDENCE
Luxi Wang,
wangluxi@wmu.edu.cn

†These authors have contributed equally to this work

RECEIVED 27 September 2024
ACCEPTED 19 November 2024
PUBLISHED 06 December 2024

CITATION
Zheng H, Wang J, Zheng Y, Hong X and Wang L (2024) Identification of genetic associations between acute myocardial infarction and non-small cell lung cancer. *Front. Mol. Biosci.* 11:1502509. doi: 10.3389/fmolb.2024.1502509

Identification of genetic associations between acute myocardial infarction and non-small cell lung cancer

Hao Zheng[1†], Jie Wang[2,3†], Yijia Zheng[1], Xiaofan Hong[1] and Luxi Wang[4*]

[1]First School of Clinical Medicine, Wenzhou Medical University, Wenzhou, China, [2]Wenzhou Medical University, Wenzhou, China, [3]Department of Psychiatry, Wenzhou Seventh People's Hospital, Wenzhou, China, [4]Department of Neurology, The First Affiliated Hospital of Wenzhou Medical University, Wenzhou, China

Introduction: A growing body of evidence suggests a potential connection between myocardial infarction (MI) and lung cancer (LC). However, the underlying pathogenesis and molecular mechanisms remain unclear. This research aims to identify common genes and pathways between MI and LC through bioinformatics analysis.

Methods: Two public datasets (GSE166780 and GSE8569) were analyzed to identify differentially expressed genes (DEGs). Common DEGs were enriched using Gene Ontology (GO) and the Kyoto Encyclopedia of Genes and Genomes (KEGG). Hub genes were identified and their diagnostic performance was evaluated. Gene co-expression networks, as well as regulatory networks involving miRNA-hub genes and TF-hub genes, were also constructed. Finally, candidate drugs were predicted.

Results: Among the datasets, 34 common trend DEGs were identified. Enrichment analysis linked these DEGs to key biological processes, cellular components, and molecular functions. Eight hub genes (*CEBPA*, *TGFBR2*, *EZH2*, *JUNB*, *JUN*, *FOS*, *PLAU*, *COL1A1*) were identified, demonstrating promising diagnostic accuracy. Key transcription factors associated with these hub genes include *SP1*, *ESR1*, *CREB1*, *ETS1*, *NFKB1*, and *RELA*, while key miRNAs include hsa-mir-101-3p, hsa-mir-124-3p, hsa-mir-29c-3p, hsa-mir-93-5p, and hsa-mir-155-5p. Additionally, potential therapeutic drugs were identified, with zoledronic acid anhydrous showing potential value in reducing the co-occurrence of the two diseases.

Discussion: This study identified eight common signature genes shared between NSCLC and AMI. Validation datasets confirmed the diagnostic value of key hub genes *COL1A1* and *PLAU*. These findings suggest that shared hub genes may serve as novel therapeutic targets for patients with both diseases. Ten candidate drugs were predicted, with zoledronic acid showing potential for targeting dual hub genes, offering a promising therapeutic approach for the comorbidity of lung cancer and myocardial infarction.

KEYWORDS

non-small cell lung cancer (NSCLC), acute myocardial infarction (AMI), differentially expressed genes (DEGs), hub genes, bioinformatics analysis

1 Introduction

Lung cancer (LC), a leading cause of cancer-related death globally (Shtivelman et al., 2014), encompasses small cell lung cancer (SCLC) as well as non-small cell lung cancer (NSCLC), which includes lung adenocarcinoma (LUAD), lung squamous cell carcinoma (LSCC), and large cell carcinoma (Sahu et al., 2023). NSCLC accounts for approximately 85% of all LC diagnoses (Stolz et al., 2022). Though studies in epidemiology have clearly demonstrated that cigarette smoke (CS) exposure contributes to the risk of NSCLC (Hecht, 1999), and many studies have focused on identifying specific targets for NSCLC, such as *PIK3CA* (Yamamoto et al., 2008), *PDGFRA* (Ramos et al., 2009), *EPHA2* (Psilopatis et al., 2022), etc., the precise etiology and pathogenesis remain elusive.

Myocardial infarction (MI) is a form of cardiac injury caused by inadequate blood supply and oxygen deprivation (Murphy and Goldberg, 2022), usually associated with the ongoing development of arterial plaque over time. The main pathological characteristic is the impairment of endothelial function (Zhang et al., 2024). Acute myocardial infarction (AMI) is the main factor contributing to deaths among cardiovascular diseases, with increasing incidence and fatality rates (Huang et al., 2024). Studies have revealed associations between MI and processes such as pyroptosis, apoptosis, and PAN apoptosis (Chang et al., 2024).

There are certain associations between MI and LC. Firstly, these two diseases share common risk factors such as smoking (Ambrose and Barua, 2004) and personality type (Nagano et al., 2001). In terms of epidemiology, patients with lung malignancies show an increased incidence of cardiovascular (CV) events (Mitchell et al., 2023). Additionally, recent studies have shown that the heart, especially myocardial mesenchymal stromal cells, releases extracellular vesicles with tumor characteristics after MI, and their tumor-promoting effects have a greater impact on LC (Caller et al., 2024). This provides further evidence for the link between MI and LC. The side effects of NSCLC treatment also have a certain impact. Platinum is associated with the occurrence of AMI, and tyrosine kinase inhibitors have shown certain cardiotoxicity (Chang et al., 2023). It is reported that the incidence of vascular events in patients with NSCLC treated with immune checkpoint inhibitors cannot be ignored (Giustozzi et al., 2021). It is worth noting that NSCLC and AMI share some common pathogenesis. As for the inflammatory response, the occurrence and development of AMI is closely related to abnormal inflammatory cells (Sun et al., 2024) and persistent inflammation will increase the risk of lung cancer (Elsayed, 2024). In addition, oxidative stress (Di Carlo and Sorrentino, 2024; Guo et al., 2024), vascular remodeling and endothelial dysfunction (Li et al., 2023; Meng et al., 2021) are involved in the pathogenesis of both diseases. However, the specific pathogenesis and molecular mechanisms underlying the association between MI and LC have not yet been fully understood.

Microarray technology and network-based analysis provide valuable insights into gene expression profiles across various cancers. In this research, we performed a bioinformatics analysis to detect shared molecular mechanism-based biomarkers (*CEBPA*, *TGFBR2*, *EZH2*, *JUNB*, *JUN*, *FOS*, *PLAU*, *COL1A1*) between NSCLC and AMI, validating their correlation and identifying candidate drugs targeting hub genes. These hub genes may be involved in the onset and progression of AMI and NSCLC through inflammatory response, oxidative stress, apoptosis, and related signaling pathways. In NSCLC and AMI, *COL1A1* is involved through EMT and arterial dissection, while *PLAU* contributes through tumor invasiveness and macrophage function, each separately. Notably, *COL1A1* and *PLAU* are dual targets of zoledronic acid anhydrous, a drug proven in previous experiments to reduce cancer mortality and the incidence of cardiovascular events. Our study suggests that zoledronic acid anhydrous has promising potential in the combined treatment of AMI and NSCLC. This study offers insights into the formulation of dual-purpose preventative and therapeutic approaches. The research process is illustrated in Figure 1.

2 Materials and methods

2.1 Data collection

The Gene Expression Omnibus (GEO) is the largest and most comprehensive public gene expression data resource (https://www.ncbi.nlm.nih.gov/geo/). We used the keywords "lung cancer" and "myocardial infarction" to identify datasets related to NSCLC and MI. The selected datasets were based on the following criteria: they must cover both cases and controls, samples must be from human subjects, and they must provide original information for subsequent analysis. Finally, we chose the NSCLC-related dataset GSE8569 and the AMI-related dataset GSE166780 for subsequent research. Furthermore, we included the NSCLC-related dataset GSE75037 and the AMI-related dataset GSE34198 for validation. Detailed information on these datasets is provided in Table 1.

2.2 Identification of differentially expressed genes (DEGs)

The online analysis tool GEO2R was utilized to identify DEGs, using screening criteria of $|\log2(FC)| > 1$ and $p < 0.05$. DEGs specific to NSCLC and AMI were obtained by comparing gene expression profiles between NSCLC cancer cells and normal cells, as well as between peripheral blood samples from AMI patients and normal peripheral blood samples. The Venn diagram tool of the Xiantao Academic Platform (https://www.xiantaozi.com) was used to find the common DEGs of the two diseases. The results were visualized using volcano plots, box plots, and Venn diagrams.

2.3 Enrichment analysis of DEGs

First, the common DEGs were converted to gene IDs, followed by gene enrichment analysis. Gene Ontology (GO) analysis, encompassing biological processes (BP), molecular function (MF), and cellular component (CC), is a widely used gene annotation bioinformatics tool. Kyoto Encyclopedia of Genes and Genomes (KEGG) provides comprehensive information on genomes, biological pathways, diseases, and chemicals. Using the clusterProfiler package in RStudio, we conducted GO functional enrichment and KEGG pathway analyses on the common DEGs. The ggplot2 package was used to visualize the data. The filtering condition was set at $p < 0.05$.

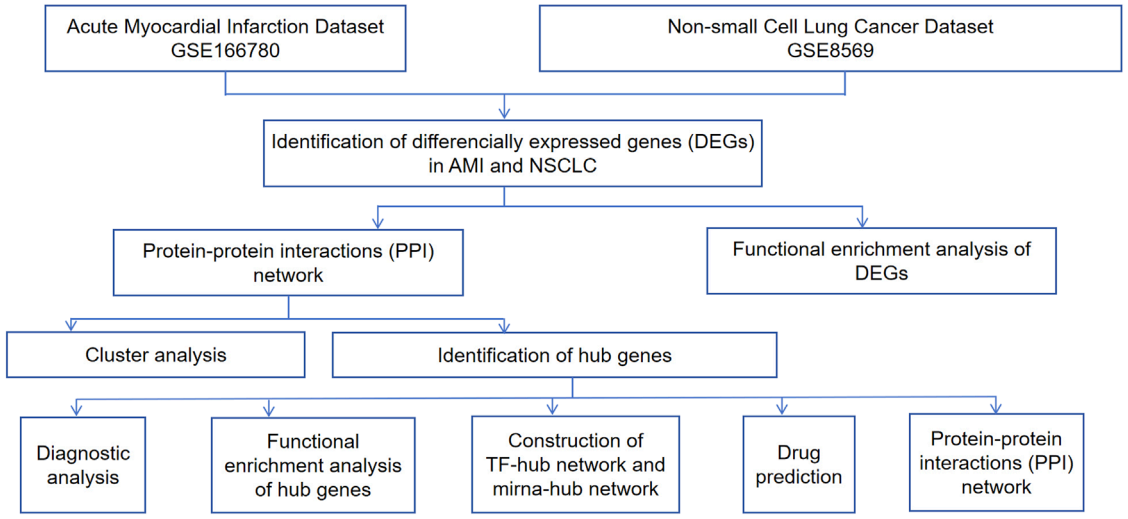

FIGURE 1
Flowchart of the study.

TABLE 1 Clinical characteristics.

	GSE166780			GSE8569			GSE75037[a]			GSE34198		
	N	AMI	P	LC	N	P	N	LC	P	N	AMI	P
Sample Count	8	8		69	6		83	83		48	45	
Age[b] (years)	59.75 ± 8.71	63.25 ± 8.29	0.424	NA	NA	NA	68.11 ± 9.74	68.11 ± 9.74	1.000	65.69 ± 9.30	63.62 ± 9.24	0.286
Female (%)	38	25	1.000	14	NA	NA	71	71	1.000	33	31	0.819
Ancestry (%)			NA			NA			1.000			NA
Asian	NA	NA		NA	NA		30	30		NA	NA	
European	NA	NA		NA	NA		67	67		NA	NA	
American Indian or Alaska Native	NA	NA		NA	NA		1	1		NA	NA	
Source Name	Peripheral Blood Monocyte			Lung			Lung			Peripheral Whole Blood		

[a]Tumor tissue and normal tissue are from the same patient.
[b]Data are presented as mean ± standard deviation.
Abbreviations: N, normal; AMI, acute myocardial infarction; P, *p*-value; LC, lung cancer; NA, not available.

2.4 Protein-protein interaction (PPI) network construction

We used the STRING database (https://cn.string-db.org/) to construct a PPI network for the co-expressed DEGs in NSCLC and AMI. The minimum interaction score was set to 0.400 and the FDR stringency for filtering was set to 0.500 to identify interactions among protein-coding genes. Then, we processed the data using Cytoscape 3.10.2, clustered the gene network using the "MCODE" plug-in, identified key subnetwork modules, and performed cluster analysis. Hub genes were determined using the cytohubba method (Degree, EPC, MCC, and MNC). We constructed a hub gene expression network using the GeneMANIA database (http://www.genemania.org/).

2.5 Diagnostic significance of hub genes

We further investigated the importance of key genes as potential biomarkers. The receiver operating characteristic (ROC) curve was employed to assess the sensitivity and specificity of our selected target genes. The area under the ROC curve (AUC) was used to evaluate the results.

2.6 Construction of miRNA-hub gene network and TF-hub gene network

The online database NetworkAnalyst 3.0 (https://www.networkanalyst.ca/) was used to construct the miRNA-hub and TF-hub networks of hub genes to describe the associations between hub genes, miRNA, and TF. The selected TF-gene interaction database was ENCODE, using criteria of peak intensity signal <500 and the predicted regulatory potential score <1. The miRNA-gene interaction data were collected from miRTarBase.

2.7 Drug prediction based on hub genes

We searched DGIdb (https://dgidb.genome.wustl.edu), a database for exploring known and potential drug-gene interactions, to identify candidate drugs associated with the hub genes.

2.8 Statistical analyses

Statistical analyses were performed using SPSS version 27. Clinical characteristics were compared using Student's t-test, Pearson Chi-Square test or Fisher's exact test, as appropriate. A two-sided *p*-value of less than 0.05 was considered statistically significant.

3 Results

3.1 Identification of DEGs

The AMI-related dataset GSE166780 contains 8 normal and 8 AMI samples, while the NSCLC-related dataset GSE8569 includes 69 NSCLC and 6 normal samples. We compared the gene expression of AMI and normal samples in GSE166780 and identified 3060 AMI DEGs, including 1,498 upregulated genes and 1,223 downregulated genes (Figures 2A, C). Similarly, we compared the gene expression of normal and NSCLC samples in GSE8569 and identified 678 NSCLC DEGs, including 182 upregulated genes and 359 downregulated genes (Figures 2B, D). Through the Venn diagram, 13 co-upregulated DEGs and 21 co-downregulated DEGs were filtered out (Figures 2E, F). The co-expressed genes and their corresponding *p*-values are listed in Table 2.

3.2 Functional annotation analysis of DEGs

GO and KEGG analysis were conducted on 34 co-expressed DEGs in NSCLC and AMI, and the outcomes are depicted in Figure 3. Concerning the BP, DEGs were significantly concentrated in "response to oxidative stress" and "response to reactive oxygen species." In terms of CC, DEGs were enriched in "RNA polymerase II transcription regulator complex," "focal adhesion," and "cell-substrate junction." For MF, DEGs are enriched in "DNA-binding transcription activator activity, RNA polymerase II-specific," and "DNA-binding transcription activator activity." KEGG analysis revealed that DEGs were enriched in "Human T-cell leukemia virus 1 infection" and "Relaxin signaling pathway."

3.3 PPI network analysis, cluster analysis, and identification of hub genes

We analyzed 34 shared DEGs using the STRING online database (Figure 4) and imported the data into Cytoscape for visualization. After removing isolated points, the PPI of the shared DEGs is illustrated in Figure 5A, with 27 nodes and 53 edges. Additionally, we employed the MCODE plug-in to identify crucial gene cluster modules and discovered 2 clusters. Cluster 1 contains 6 nodes and 14 edges with a score of 5.6. Cluster 2 includes 3 nodes and 3 edges with a score of 3 (Figures 5B, C). To identify hub genes, we used the CytoHubba plug-in. By taking the intersection of the four algorithms, we identified 8 hub proteins: *CEBPA*, *TGFBR2*, *EZH2*, *JUNB*, *JUN*, *FOS*, *PLAU* and *COL1A1* (Figure 6). In the NSCLC and AMI datasets, *EZH2*, *COL1A1* and *PLAU* were upregulated, and *CEBPA*, *TGFBR2*, *JUN*, *JUNB* and *FOS* were downregulated.

3.4 Enrichment analysis of hub genes

GO and KEGG analyses were conducted (Figure 7). The hub genes were mainly related to "integrated stress response signaling," "cellular response to salt," "cellular response to metal iron," "response to reactive oxygen species" "cellular response to inorganic substance," "myeloid leukocyte differentiation," "cellular response to transforming growth factor beta" in BP terms. In CC terms, they were predominantly associated with the "RNA polymerase II transcription regulator complex." In MF terms, they were mainly related to "DNA-binding transcription activator activity, RNA polymerase II-specific," "DNA-binding transcription activator activity," "SMAD binding," "RNA polymerase II-specific DNA-binding transcription factor binding," and "DNA-binding transcription factor binding." In KEGG analysis, they were enriched in "Relaxin signaling pathway," and "Osteoclast differentiation."

3.5 PPI analysis of hub genes

Based on GeneMANIA, PPI analysis was performed on 8 hub genes and 20 cross genes (Figure 8). Among them, predicted accounted for 32.57%, physical Interactions for 28.18%, co-expression for 28.02%, shared protein domains for 10.32%, co-localization for 0.73% and genetic interactionsfor 0.18%. The primary biological roles of this network

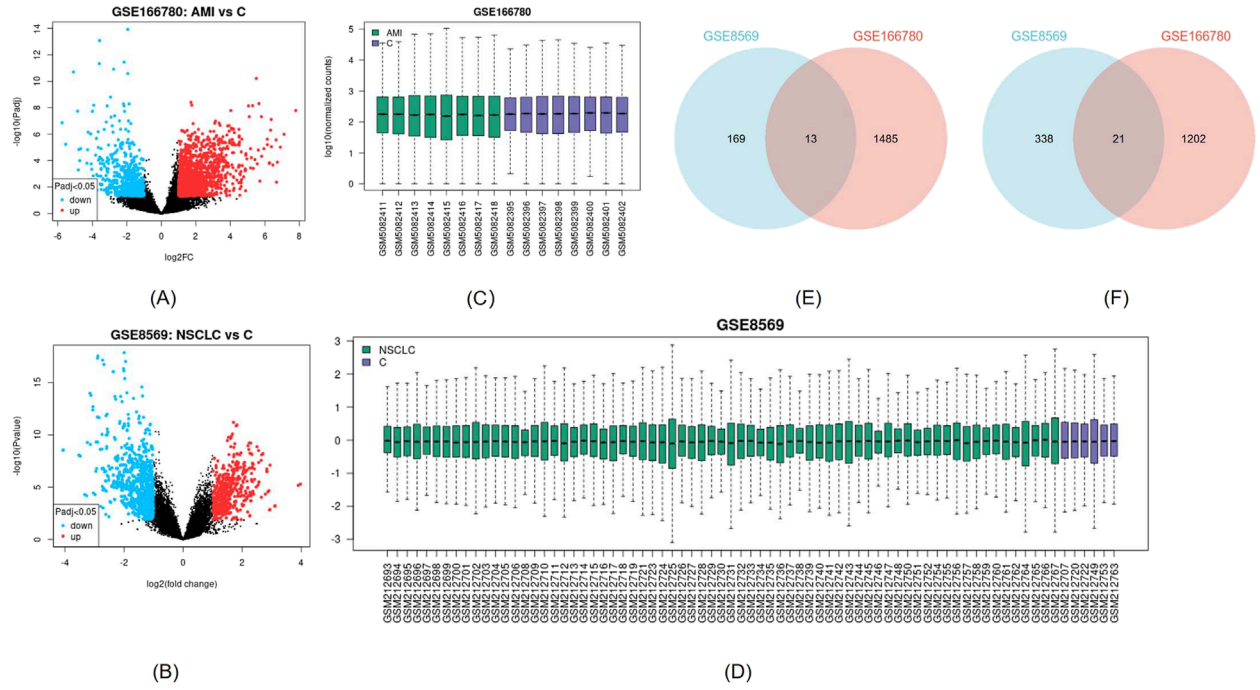

FIGURE 2
(A, B) Visualization of DEGs of GSE166780 and GSE8569 using volcano plots, blue represents downregulation, red represents upregulation (|log2(FC)|>1, $p < 0.05$) **(C, D)** Visualization of GSE166780 and GSE8569 using box plots **(E)** Co-expressed upregulated differentially expressed genes (DEGs) of GSE166780 and GSE8569 (|log2(FC)|>1, $p < 0.05$) **(F)** Co-expressed downregulated DEGs of GSE166780 and GSE8569 (|log2(FC)|>1, $p < 0.05$).

pertain to the myeloid dendritic cell activation, response to cadmium ion, dendritic cell differentiation, regulation of DNA binding, RNA polymerase II transcription regulator complex, response to reactive oxygen species and transcription regulator complex.

3.6 Diagnostic significance of hub genes

According to the ROC curve developed by the eight candidate hub genes, we evaluated the specificity and sensitivity of each gene for diagnosis (Figure 9). We calculated the AUC of each item, among which the AUCs of *COL1A1*, *JUN*, *EZH2*, *FOS*, *PLAU*, *CEBPA*, *TGFBR2*, and *JUNB* in the NSCLC-related dataset were 0.925, 0.879, 0.937, 0.935, 0.906, 0.853, 0.957, and 0.957, respectively. The AUCs of *COL1A1*, *JUN*, *EZH2*, *FOS*, *PLAU*, *CEBPA*, *TGFBR2*, and *JUNB* in the AMI-related dataset were 0.625, 0.922, 0.922, 0.859, 0.859, 1.000, 0.984, and 0.859, respectively. These genes have high diagnostic value for both NSCLC and AMI. Among them, the AUC of *EZH2* and *TGFBR2* were greater than 0.9 in both diseases, showing high diagnostic efficacy. In the validation dataset of NSCLC, the AUCs of *COL1A1*, *CEBPA*, *PLAU*, *JUNB*, *JUN*, *TGFBR2*, *FOS*, and *EZH2* were 0.946, 0.794, 0.725, 0.836, 0.859, 0.985, 0.862, and 0.905, respectively. In the validation dataset of AMI, the AUCs of *COL1A1*, *CEBPA*, *PLAU*, *JUNB*, *JUN*, *TGFBR2*, *FOS*, and *EZH2* were 0.739, 0.570, 0.860, 0.671, 0.716, 0.679, 0.592, and 0.642, respectively. In both validation datasets, *COL1A1*, *PLAU*, *JUNB*, *JUN*, *TGFBR2*, and *EZH2* maintained high diagnostic efficacy.

3.7 Construction of TF-hub gene network and miRNA-hub gene network

We used NetworkAnalyst 3.0 software to construct the TF-Hub genes and miRNA-Hub genes regulatory networks. The TF-Hub network consists of 100 nodes and 121 edges, and the miRNA-Hub network has 358 nodes and 407 edges. We found that in the TF-Hub network, *SP1* interacts with *TGFBR2*, *FOS*, *PLAU*, and *COL1A1*. *ESR1* regulates *FOS*, *JUN*, and *JUNB*. *CREB1* regulates *PLAU*, *JUN*, and *FOS*. *ETS1* interacts with *COL1A1*, *TGFBR2*, and *PLAU*. Notably, *NFKB1* and *RELA* simultaneously regulate *COL1A1*, *JUNB* and *PLAU* (Figure 10A). In the miRNA-Hub network, hsa-mir-101-3p interacts with 4 genes, including *JUN*, *EZH2*, *TGFBR2* and *FOS*. Hsa-mir-124-3p targets *EZH2*, *COL1A1*, and *CEBPA*. Hsa-mir-29c-3p targets *JUN*, *FOS*, and *COL1A1*. Hsa-mir-93-5p targets *JUN*, *TGFBR2*, and *EZH2*. Hsa-mir-155-5p targets *JUN*, *JUNB*, and *FOS* (Figure 10B).

3.8 Identification of drug candidates

To investigate gene-drug interactions, 8 validated hub genes were submitted to the DGIdb database, and the results were visualized in Cytoscape (Figure 11). A total of 145 drugs were identified, and the top ten were CGP-37157, OICR-9429, EPZ005687, EPZ011989, HESPERETIN, PROTEIN KINASE A INHIBITOR, JQEZ5, SKLB-03220, EBI-2511, CPI-1205 (Table 3). It is worth noting that zoledronic acid anhydrous and antibiotic are connected with two hub genes.

10.3389/fmolb.2024.1502509

TABLE 2 Differential expression genes.

DEG	AMI		NSCLC		DEG	AMI		NSCLC	
	P	L2FC	P	L2FC		P	L2FC	P	L2FC
PRC1	0.0105	1.76	0.0003	1.69	*MMP14*	0.0015	3.08	0.0389	1.09
PSME4	0.0030	1.57	<0.0001	1.02	*HYAL2*	0.0256	−1.84	<0.0001	−1.85
PTTG1	0.0124	1.86	0.0007	1.51	*MAP3K11*	0.0241	−1.35	<0.0001	−2.01
MCM6	0.0024	1.69	0.0001	1.31	*JUNB*	0.0408	−1.57	<0.0001	−1.99
EZH2	<0.0001	2.99	0.0008	1.31	*DAPK2*	0.036	−1.37	0.0001	−1.08
PPIF	0.0020	1.81	0.0056	1.07	*FLI1*	0.0314	−1.17	<0.0001	−1.53
COL1A1	0.0137	2.59	0.0005	2.87	*FOS*	0.037	−1.20	<0.0001	−2.70
HMGA1	0.047	1.36	0.0009	1.59	*GNAI2*	0.0296	−1.34	<0.0001	−1.10
TNFRSF21	0.0103	1.76	0.0045	1.23	*TGFBR2*	0.0078	−1.01	<0.0001	−1.22
CFB	<0.0001	6.90	0.0074	1.06	*PINK1*	0.0004	−1.59	<0.0001	−1.03
PLAU	<0.0001	6.15	0.0147	1.36	*RHOB*	0.0019	−2.17	0.0001	−1.07
MAFG	0.0002	2.74	0.0060	−1.24	*CSF3R*	0.0246	−1.13	0.0002	−1.17
PAQR8	0.0107	−2.24	0.0002	−1.21	*CITED2*	0.026	−1.69	0.0030	−1.32
FKBP8	0.0168	−1.30	0.0005	−1.07	*GIMAP6*	0.0363	−1.51	0.0041	−1.31
JUN	0.0382	−1.20	0.0011	−1.18	*ZYX*	0.0412	−1.21	0.0063	−1.05
IMPDH1	0.0335	−1.24	0.0011	−1.30	*CEBPA*	<0.0001	−3.40	0.0165	−1.32
TLN1	0.0083	−1.24	0.0016	−1.20	*HLA-G*	0.0142	−1.43	0.0178	−1.47

Abbreviations: P, *p*-value; L2FC, log2(FC).

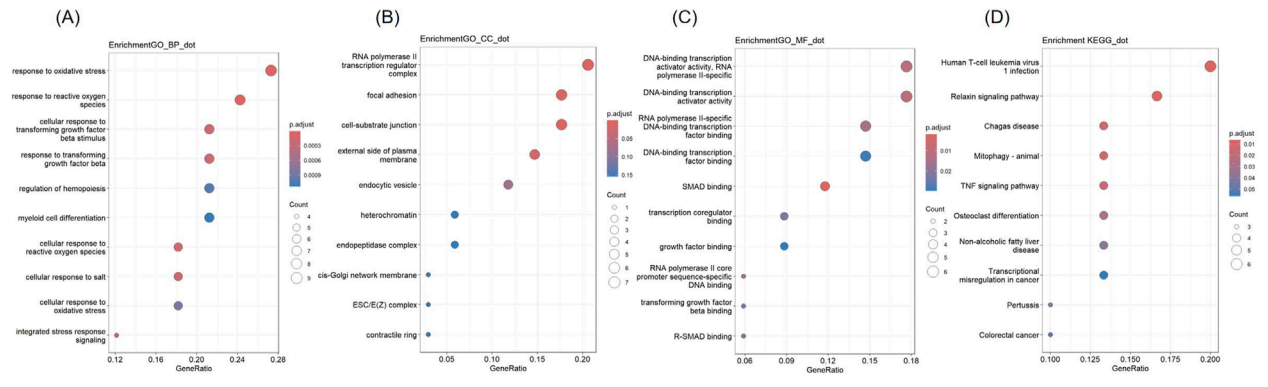

FIGURE 3
Gene Ontology (GO) and Kyoto Encyclopedia of Genes and Genomes (KEGG) analysis of DEGs **(A)** Biological Processes **(B)** Cellular Component **(C)** Molecular Function **(D)** KEGG.

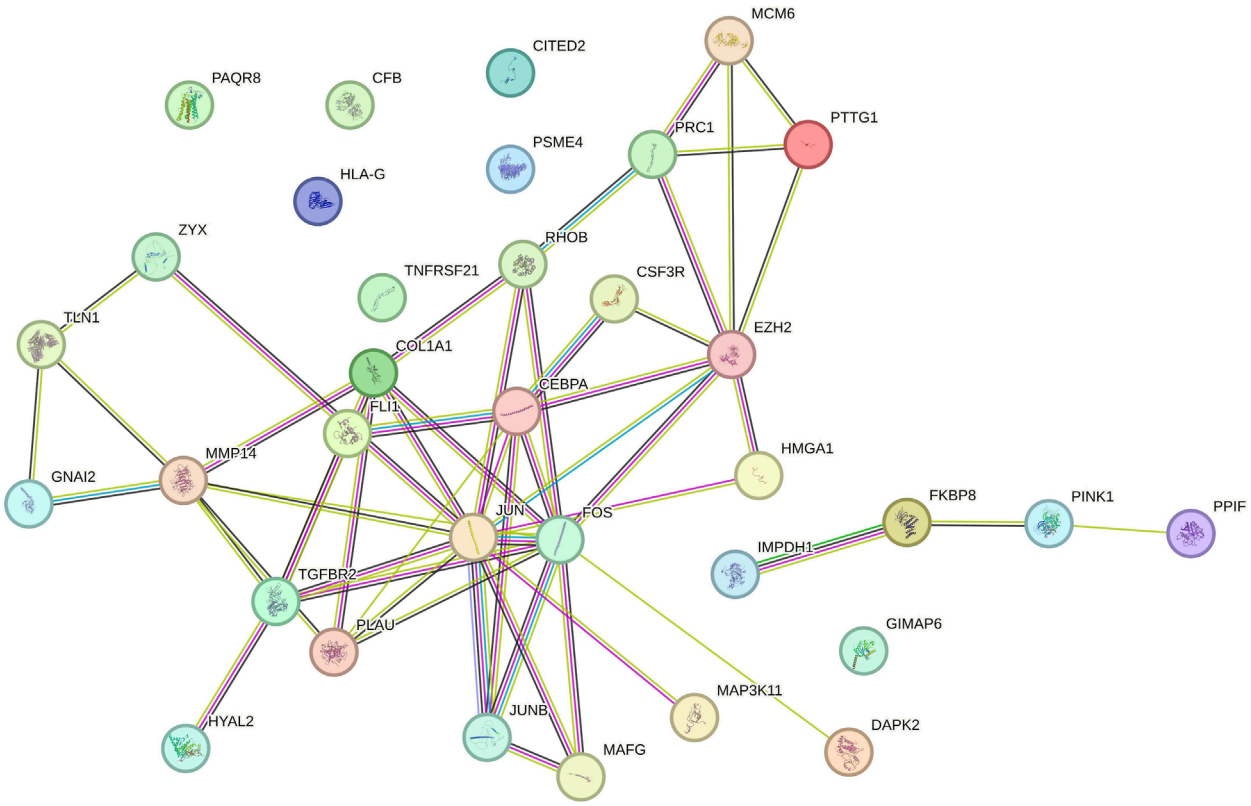

FIGURE 4
Protein-protein interaction (PPI) network of common DEGs.

4 Discussion

Previous studies have demonstrated an inverse relationship between cardiovascular disease and cancer. The mechanism behind this relationship is not fully understood. Still, it may be associated with circulating microRNAs, extracellular vesicles, cardiac-derived mediators, along with pathways associated with inflammatory responses, clonal hematopoiesis, and oxygen deprivation (Aboumsallem et al., 2020). Several studies have indicated an increased risk of cancer in patients with MI (Hasin et al., 2016; Rinde et al., 2017). Research into the common mechanisms between MI and cancer has gained attention recently (Yuan et al., 2023; Meijers et al., 2018). However, limited studies have explored the shared genetic underpinnings between NSCLC and AMI at the genetic level. Our study has examined the molecular biological roles and common pathways of NSCLC and AMI, offering insights for the development of dual-purpose prevention and therapy strategies.

In this study, we utilized bioinformatics tools to identify 34 common DEGs between an NSCLC dataset and an AMI dataset. GO analysis of these DEGs revealed their association with "response to reactive oxygen species," "response to oxidative stress," "RNA polymerase II transcription regulator complex," "focal adhesion," "cell-substrate junction," "RNA polymerase II-specific DNA binding transcription factor binding," "DNA-binding transcription activator activity, RNA polymerase II-specific." KEGG analysis revealed that these DEGs were linked to pathways involving "Human T-cell leukemia virus 1 infection," and "Relaxin signaling pathway."

We developed a PPI network of DEGs and detected 8 hub genes, namely, *CEBPA*, *TGFBR2*, *EZH2*, *JUNB*, *JUN*, *FOS*, *PLAU* and *COL1A1*. In both datasets, *EZH2*, *COL1A1* and *PLAU* were upregulated, while *CEBPA*, *TGFBR2*, *JUN*, *JUNB* and *FOS* were downregulated.

COL1A1 encodes the pro-α1 chain of type I collagen, a fibrillogenic collagen found abundantly in bone, cornea, dermis, and tendon. It has been recognized as a predictive biomarker for LUAD, and its increased expression has been observed in LC tissue samples, consistent with our findings (Dong et al., 2023). EMT and fibroblast-myofibroblast-myofibroblast transition (FMT) are involved in the initiation and progression of cancer (Ribatti et al., 2020), and studies have demonstrated that fibroblasts with high levels of *COL1A1* are related to EMT (Wang et al., 2022). This means that highly expressed *COL1A1* may participate in the onset and progression of LC by participating in the EMT process. Spontaneous coronary artery dissection (SCAD) constitutes a non-atherosclerotic etiology for AMI (Saw et al., 2017). Studies have linked *COL1A1* to the formation of arterial dissection (Zekavat et al., 2022), which may explain the association between AMI and *COL1A1*. Some studies have also pointed out that type I collagen's effective deposition is crucial for the healing process after MI (Nong et al., 2011). More research is still needed to elucidate the underlying mechanism.

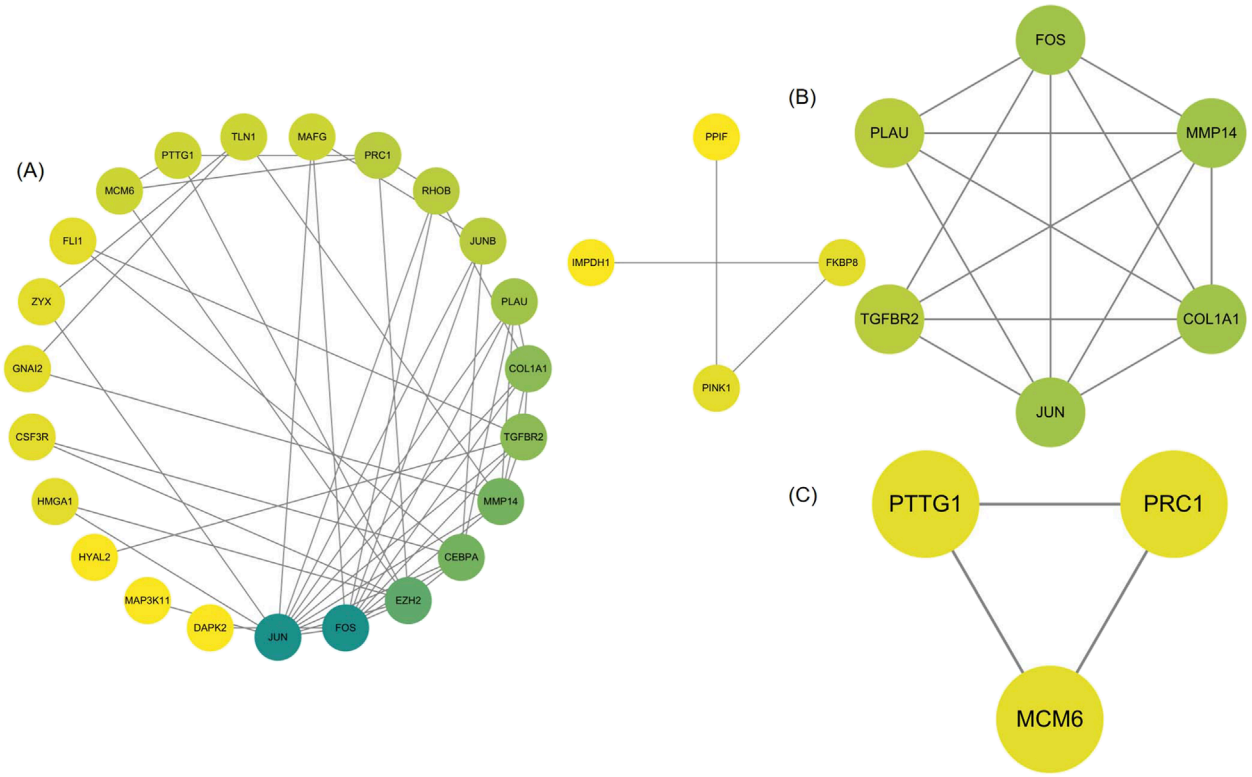

FIGURE 5
(A) PPI network of common DEGs visualized using Cytoscape **(B, C)** MCODE plugin shows that cluster 1 contains 6 nodes and 14 edges with a score of 5.6. Cluster 2 contains 3 nodes and 3 edges with a score of 3.

CEBPA contributes to the development, expansion, metabolic functions, and immune responses (Newman and Keating, 2003). It has been reported to be downregulated in various solid tumors, including liver, breast cancer, and LC (Lourenco and Coffer, 2017), similar to our findings. *CEBPα* is reported to act as a key factor in preserving the stability of the epithelial cell layer by suppressing the transcription of vital mesenchymal markers, which in turn stops the initiation of tumors driven by the EMT process (Lourenco et al., 2020). Studies have shown that therapeutic upregulation of *CEBPA* leads to inactivation of immunosuppressive myeloid cells and has effective anti-tumor responses in different tumor models and cancer patients (Hashimoto et al., 2021). Furthermore, some scholars have demonstrated that JAM-A activates *CEBPα* and induces the transcription of the claudin-5 gene, which plays a key role in maintaining the vascular barrier (Kakogiannos et al., 2020). However, there are a few reports that deviate from this trend (Zhu et al., 2024), and it is reported that *CEBPA* can promote *LOXL2* and *LOXL3* transcription and stabilize *BCL-2*, thereby enhancing the proliferation and metastasis of LC cells *in vitro* (Fan et al., 2024). In short, the function of *CEBPA* in the genesis and progression of tumors still needs further confirmation. In cardiac research, studies have revealed that the C/EBP family's transcription factors (TFs) are activated in the epicardium upon receiving developmental prompts and injury indicators. They collaborate with *HOX*, *MEIS*, and Grainyhead TFs to clarify the genomic program directing embryonic gene transcription in the epicardium (Huang et al., 2012). However, the relationship between *CEBPA* and AMI has not been fully elucidated.

FOS is a member of the *FOS* gene family. The protein encoded by *FOS* can form the TF complex AP-1 with the *Jun* family proteins through the leucine zipper and is vital in signal transduction, cell proliferation, and differentiation (Li et al., 2024). A study has shown that the levels of *c-fos* and *c-jun* in tumor tissues of NSCLC cases are lower than those in adjacent normal tissues (Levin et al., 1994). It is reported that *FOS* is downregulated in cases of heart failure (HF) after MI as well (Hu et al., 2023). Our results similarly found that *FOS* was downregulated in both diseases. However, some reports show the opposite. As a target for miR-101A, overexpression of *FOS* can lead to aggravated myocardial fibrosis after MI (Pan et al., 2012), and inhibition of Fos/AP-1 can reduce inflammatory response and cardiac dysfunction (Zhuang et al., 2022). At the same time, miR-29b-3p mitigates cardiac fibrosis following infarction by directly targeting *FOS* (Xue et al., 2020). Studies have also found that focusing on *c-fos* may be a supplementary treatment approach to hinder and diminish metastasis in LUAD patients carrying SNP BRMS1v2 A273V/A273V (Liu et al., 2022). Therefore, the association between the *FOS* gene and the two diseases requires further study.

JUN is a potential oncogene of avian sarcoma virus 17. Dysregulation of the mitogen-activated protein kinase (MAPK) signaling pathway is critical in the progression of LC and several other cancer types (Braicu et al., 2019). The c-Jun N-terminal kinase (JNK) pathway, one of the MAPK pathways, is involved in various cellular functions in tumor development, including proliferation, differentiation, survival, and apoptosis (Johnson and Lapadat, 2002). Mesothelin (MSLN) promotes the level and

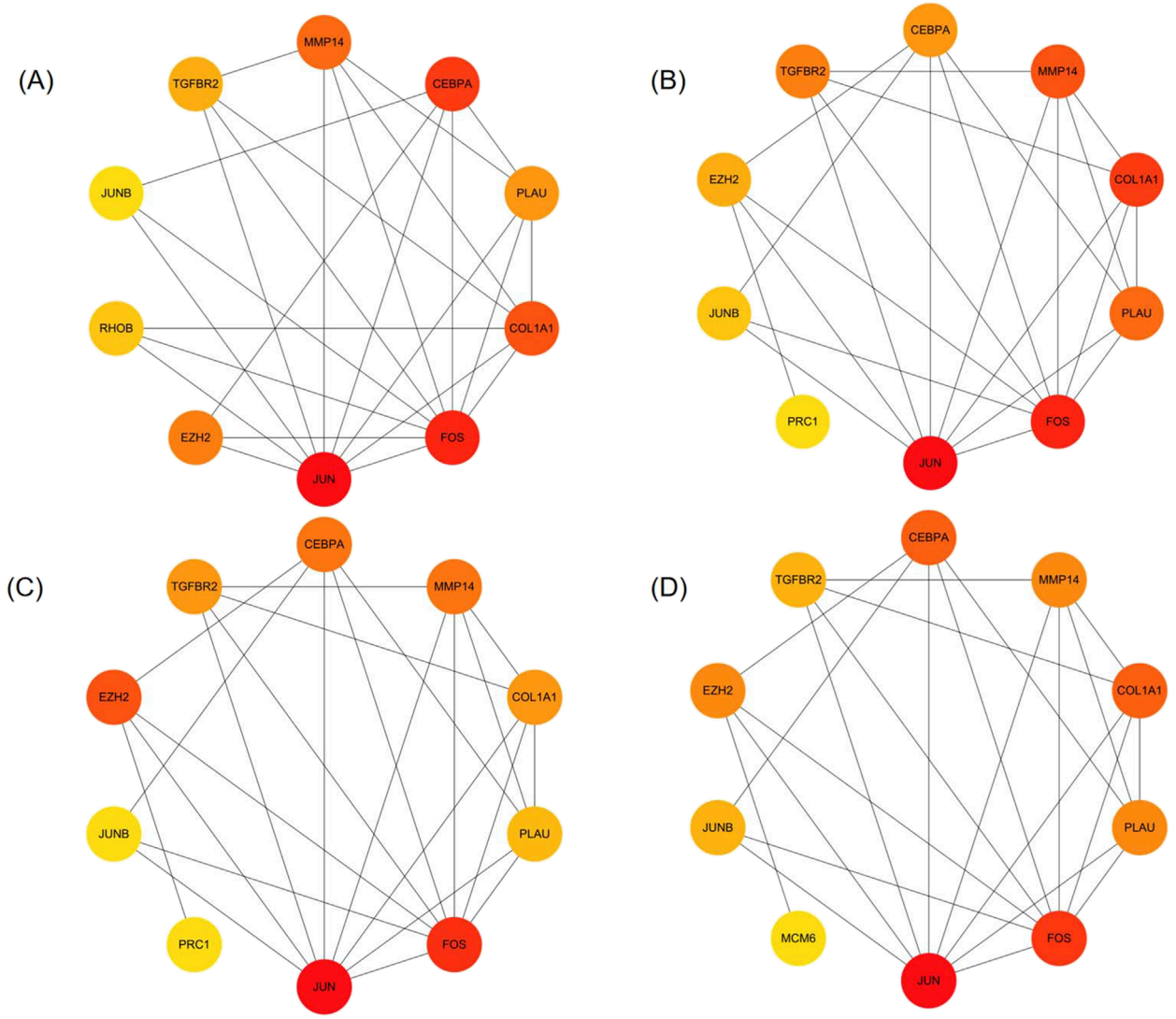

FIGURE 6
Identification of hub genes **(A–D)** The top 10 genes in the PPI network were sorted by Degree, MCC, EPC, and MNC respectively. The 8 hub genes identified are *CEBPA, TGFBR2, EZH2, JUNB, JUN, FOS, PLAU, COL1A1*.

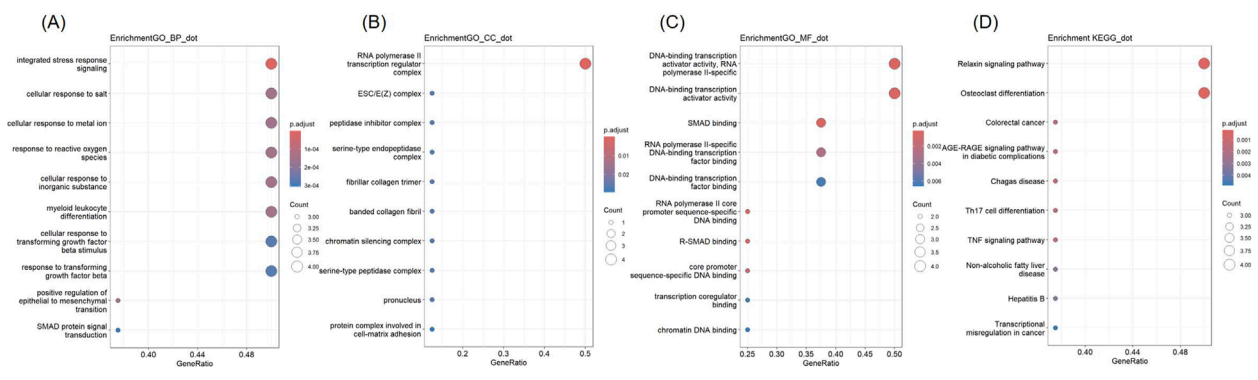

FIGURE 7
GO and KEGG analysis of Hub genes **(A)** Biological Processes **(B)** Cellular Component **(C)** Molecular Function **(D)** KEGG.

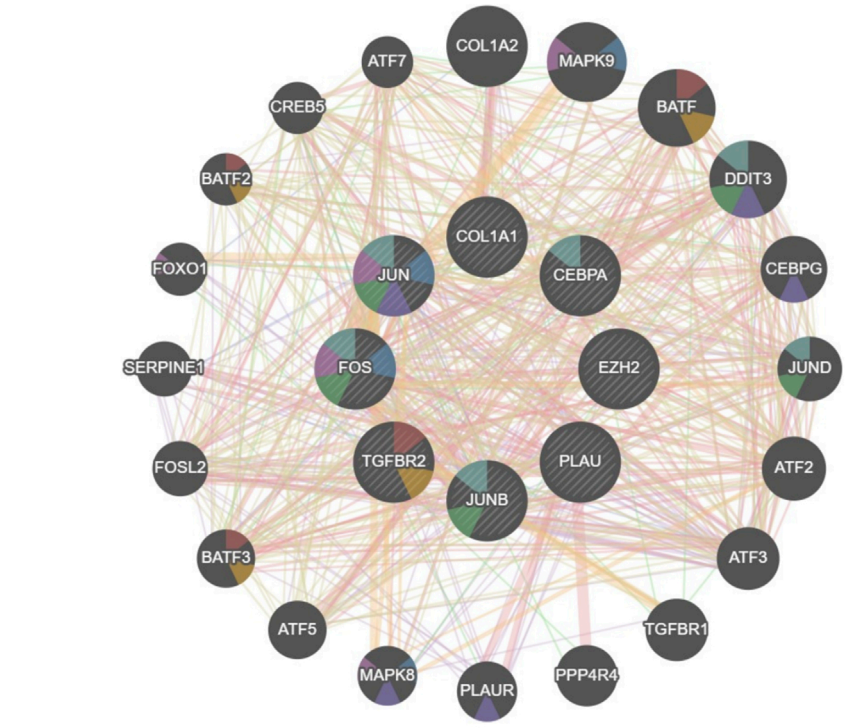

FIGURE 8
PPI analysis of hub genes using GeneMANIA.

activation of MET through the JNK signaling pathway, enabling cancer cells to disrupt tight junctions and the integrity of the blood-brain barrier (BBB), thus penetrating the barrier (Xia et al., 2024). Studies have also demonstrated that c-Jun is essential for coordinating the developmental processes of cardiac cells during their early stages (Su et al., 2023). Activation of JNK has been linked to myocardial injury, left ventricular remodeling (LVR), and HF after MI (Plotnikov et al., 2023). In our study, *JUN* was downregulated in both AMI and NSCLC, which may be related to these mechanisms and thus supporting these findings to a certain extent.

EZH2 is an important catalytic protein and is part of the polycomb repressive complex 2 (PRC2) family. In our study, *EZH2* was upregulated in both diseases. Previous studies have demonstrated that *EZH2* is elevated in ischemic hearts (Zhao et al., 2021). In the context of MI, inhibition of *EZH2*-induced cardiac recruitment and enhanced activity of non-classical monocytes accelerates the resolution of inflammation and reduces infarct scar expansion, thereby contributing to decreased cardiac remodeling and dysfunction after MI (Rondeaux et al., 2023). Exosomal miR-25-3p from mesenchymal stem cells reduces MI by inhibiting *EZH2* (Peng et al., 2020). *EZH2* is a target of *SETD1A*, which maintains cancer stem cell properties by triggering Wnt/β-catenin pathway activity (Wang R. et al., 2021). It has been proposed that inhibition of *EZH2* combined with inhibition of *PI3K* is a possible combination therapy against LC with *PIK3CA* alteration or overexpression (Chen et al., 2022). Previous studies have shown that BMSC-exo-miR-30b-5 can regulate the development of NSCLC by targeting *EZH2* (Wu et al., 2023).

PLAU is a urokinase plasminogen activator known for its role in cancer invasiveness, positioning it as a central figure in cancer metastasis and related invasion processes, including attachment, movement, and infiltration (Han et al., 2005; Sliva, 2008). Our results showed that *PLAU* was upregulated in both diseases. *PLAU* is closely associated with mutations in the tumor suppressor gene *TP53*, which prevents the occurrence of anoikis (Barta et al., 2020). *PLAU* has been associated with a wide range of biological and pathological mechanisms, covering chemotaxis, adhesion processes, migration and growth (Chavakis et al., 2002). Overexpression of *PLAU* positively regulates the growth and colony formation of NSCLC cells (Zheng et al., 2024). Elevated *PLAU* levels in

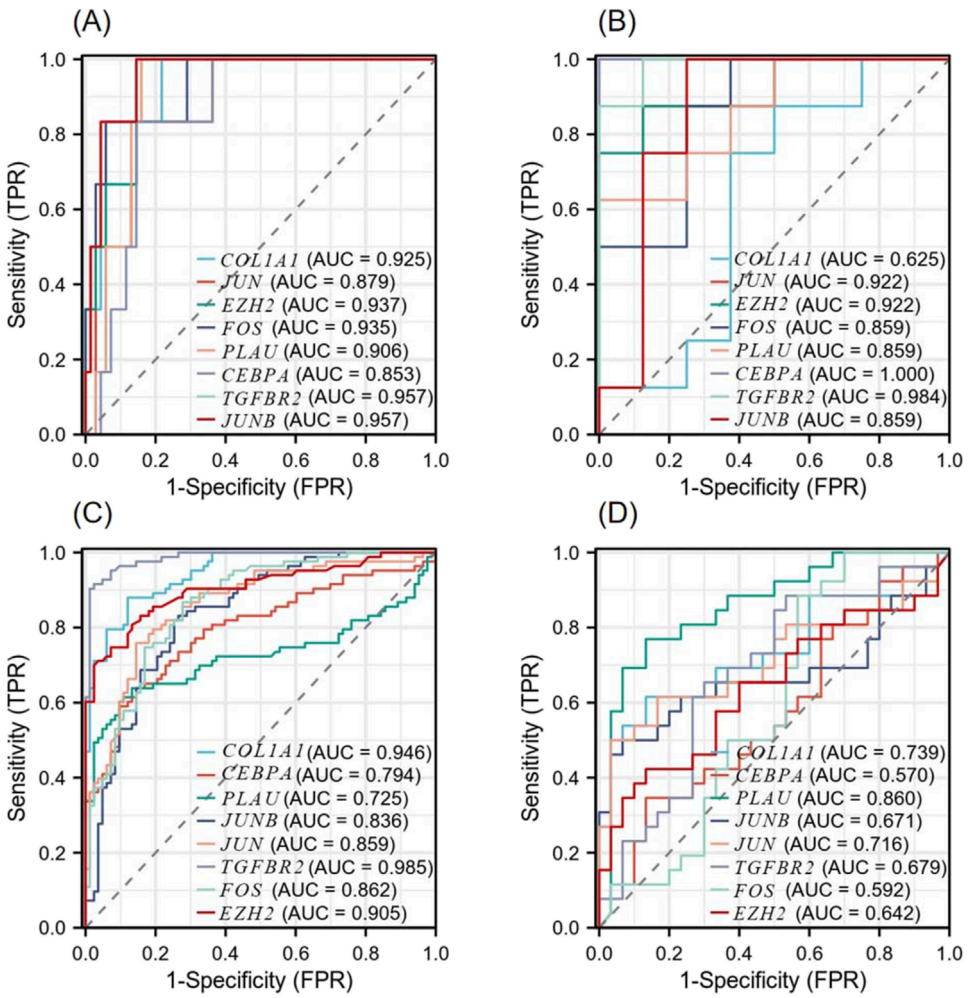

FIGURE 9
Diagnostic Receiver operating characteristic (ROC) curves of 8 co-expressed hub genes **(A)** ROC curve of the hub gene in the GSE8569 dataset. **(B)** ROC curve of the hub gene in the GSE166780 dataset. **(C)** ROC curve of the hub gene in the GSE75037 dataset. **(D)** ROC curve of the hub gene in the GSE34198 dataset.

macrophages accelerate atherosclerosis and blockage of the coronary arteries (Cozen et al., 2004).

TGFBR2, a central component of the TGF-β pathway, is often deleted during carcinogenesis in numerous cancer types, including NSCLC (Wang et al., 2007), and functions as an effective tumor suppressor in NSCLC (Lo Sardo et al., 2021). We found that *TGFBR2* was downregulated in NSCLC and AMI. Masaki Ikeuchi et al. revealed that activation of TGF-β provides protective benefits against early ischemic heart damage. However, if its expression persists, the beneficial effects may be compromised, leading to LVR and failure after MI (Ikeuchi et al., 2004). Conversely, a study has demonstrated the potential benefits of targeting *TGFBR2* in alleviating MI-like symptoms *in vivo* and *in vitro* (Wang X. et al., 2021).

JUNB belongs to the family of activator protein-1 (AP-1) TFs and binds to specific sequences in the cis-regulatory domains of target genes, regulating multiple biological mechanisms encompassing cell division, cell growth, and programmed cell death. It has been reported that *JUNB* exhibited a substantial decrease in its mRNA and protein levels in cardiac tissues of HF mice (Yan et al., 2018). However, another study demonstrated that during early myocardial ischemia (EMI), *JUNB* increases in the nuclei of cardiomyocytes in both *in vivo* models and in human myocardium (Aljakna et al., 2018). The andrographolide can inhibit tumor growth and invasion of NSCLC by upregulating *HLJ1*, a novel tumor suppressor, through activation of *JUNB* (Lai et al., 2013). In this study, *JUNB* was downregulated in both diseases. In conclusion, research on the relationship between JUNB and these two diseases is limited, and more follow-up studies are needed.

GeneMANIA-based PPI analysis indicated that the primary biological functions of the hub genes and their interconnected genes are related to the myeloid dendritic cell activation, response to cadmium ion, dendritic cell differentiation, regulation of DNA binding, RNA polymerase II transcription regulator complex, response to reactive oxygen species and transcription regulator complex. Reactive oxygen species (ROS)-induced cardiomyocyte injury is critical for the pathogenesis of various heart diseases and involves multiple genes, TFs, and oxidation-sensitive signaling

10.3389/fmolb.2024.1502509

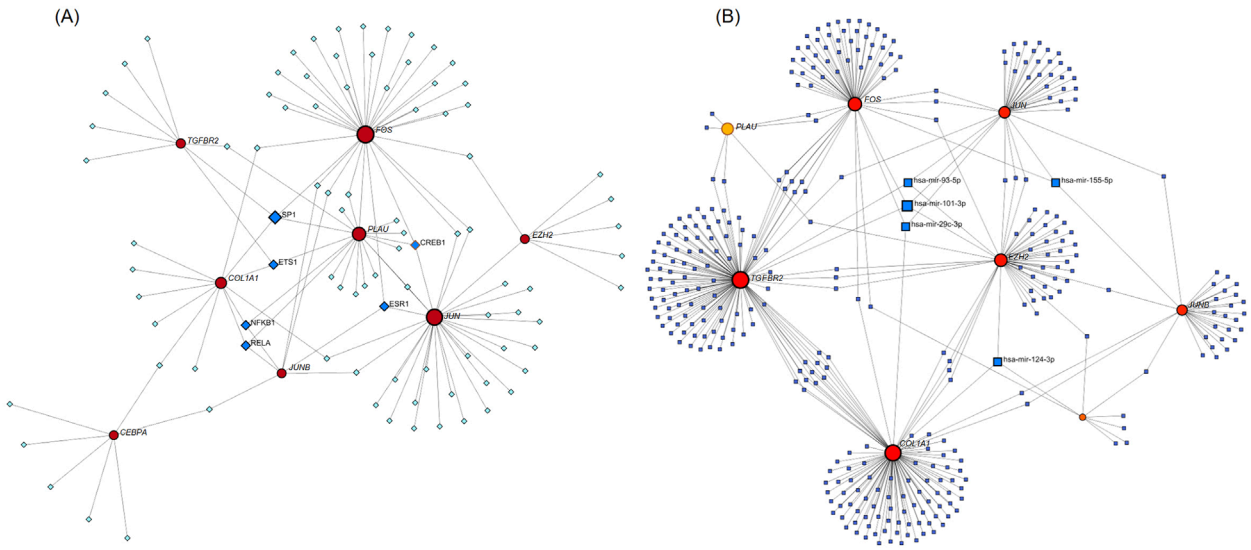

FIGURE 10
(A) TF-Hub genes network, circles are hub genes, and squares are TFs. **(B)** miRNA-Hub genes network, circles are hub genes, and squares are miRNAs.

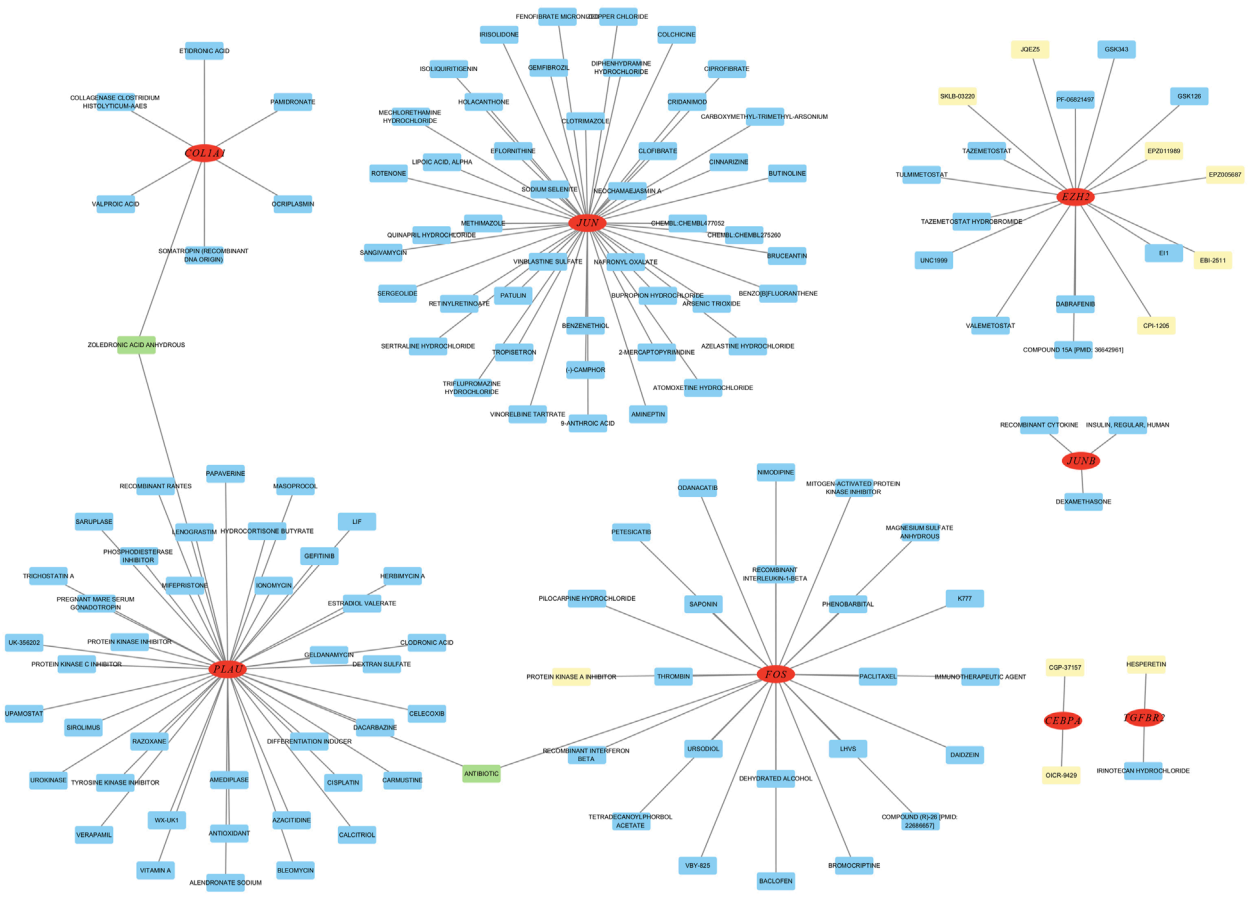

FIGURE 11
Analysis of hub genes on DGibd, a sum of 145 drugs were discovered. Red indicates hub genes, yellow indicates the top ten drugs, green indicates drugs connected with two genes, and blue indicates other potential drugs.

TABLE 3 The top ten drugs selected by DGIdb according to the score ranking.

Drug	Interaction type and directionality	Interaction score	Target gene
CGP-37157	inhibitor (INHIBITORY)	26.25	*CEBPA*
OICR-9429	n/a	13.12	*CEBPA*
EPZ005687	inhibitor (INHIBITORY)	11.66	*EZH2*
EPZ011989	inhibitor (INHIBITORY)	5.83	*EZH2*
HESPERETIN	n/a	5.83	*TGFBR2*
PROTEIN KINASE A INHIBITOR	n/a	4.2	*FOS*
JQEZ5	inhibitor (INHIBITORY)	2.91	*EZH2*
SKLB-03220	inhibitor (INHIBITORY)	2.91	*EZH2*
EBI-2511	inhibitor (INHIBITORY)	2.91	*EZH2*
CPI-1205	inhibitor (INHIBITORY)	2.91	*EZH2*

pathways (Li et al., 2013). MI and LC are both associated with oxidative stress. The cross-linking of cysteine residues 1,078 and 2,991 is essential for the redox control of the cardiac ryanodine receptor (RyR) (Nikolaienko et al., 2023). NOP56 and mTOR cooperate to maintain homeostasis in response to oxidative stress and significantly enhance cell death in KRAS mutant tumor cells (Yang et al., 2022).

ROC curve analysis was employed to assess the diagnostic efficacy of key genes, revealing their high diagnostic value for both NSCLC and AMI. Among these, *EZH2* and *TGFBR2* exhibited AUCs greater than 0.9 in both diseases. These findings underscore the significant roles of *COL1A1*, *JUN*, *EZH2*, *FOS*, *PLAU*, *CEBPA*, *TGFBR2*, and *JUNB* in the development of NSCLC and AMI. Subsequently, we used validation datasets to verify the diagnostic efficacy of hub genes and *COL1A1*, *PLAU*, *JUNB*, *JUN*, *TGFBR2* as well as *EZH2* maintaining high diagnostic efficacy. This further screened out genes with greater diagnostic value.

NetworkAnalyst was used to construct related miRNA-hub networks and TF-hub networks. The five most active miRNAs interacting with hub genes are hsa-mir-101-3p, hsa-mir-124-3p, hsa-mir-29c-3p, hsa-mir-93-5p, and hsa-mir-155-5p. The 6 TFs that predominantly interact with hub genes are *SP1*, *ESR1*, *CREB1*, *ETS1*, *NFKB1*, and *RELA*. These miRNAs and TFs could be correlated with the initiation and progression of NSCLC and AMI.

Previous studies have linked many of these miRNAs to the development of LC and AMI. For instance, miR-101-3p downregulation in cancer-associated fibroblasts (CAFs) increases vascular endothelial growth factor A (VEGFA) secretion, promoting LC metastasis via the Akt/eNOS pathway (Guo et al., 2021). Conversely, overexpression of miR-101a-3p can enhance cardiac function after MI (Li et al., 2019). In NSCLC, miR-124-3p markedly suppresses metastasis via exosomal transport and intracellular PI3K/AKT signaling (Zhu et al., 2023). Inhibition of miR-124-3p may activate the FGF21/CREB/PGC1α pathway, reducing cardiomyocyte apoptosis and improving oxidative stress and inflammatory responses (Wei et al., 2021). miR-29c-3p suppresses the activity of Mitochondrial fission regulator 1 (MTFR1), thereby inhibiting the progression of lung adenocarcinoma via the AMPK/mTOR signaling pathway (Li et al., 2021). miR-93-5p is often overexpressed in NSCLC and acts as an oncogene by inhibiting the tumor suppressor activities of PTEN and RB1 (Yang et al., 2018). The suppression of miR-155-5p rejuvenates senescent mesenchymal stem cells, thereby augmenting their cardioprotective effects post-myocardial infarction (Hong et al., 2020). Also, it can mediate the inhibition of radiotherapy in NSCLC (Zhu et al., 2019). In conclusion, these miRNAs are closely associated with both NSCLC and AMI.

There are also studies proving that predicted TFs are related to NSCLC and AMI. For example, HIF1α-SP1 interaction can promote the development of NSCLC (Wu et al., 2022). KN-93 enhances fatty acid oxidation in MI via the HDAC4-SP1 axis (Zhao et al., 2024). ESR1 expression serves as an independent prognostic indicator in metastatic NSCLC (Atmaca et al., 2014). ESR1 encodes the nuclear receptor ERα, which leads to a reduction in infarct size, inflammatory response, and oxidative stress in animal models (Puzianowska-Kuznicka, 2012). Inactivation of CREB1 may confer cisplatin resistance in metastatic NSCLC (Kim et al., 2019). *ETS1* mediates the initiation of gene expression patterns that result from the RAS/MAPK signaling pathway (Plotnik and Hollenhorst, 2017). The rs28362491 ins/del variation of the *NFKB1* gene is linked to a higher likelihood of MI and increased severity of coronary artery disease (Luo et al., 2020). *MUC3A* interacts with *RELA* to activate the NFκB pathway (Sun et al., 2021). In summary, these TFs could contribute to the onset and progression of the two diseases.

We used DGibd to predict dual-use drugs for AMI and NSCLC. A total of 145 candidate drugs were retrieved, of which the top ten scores were CGP-37157, OICR-9429, EPZ005687, EPZ011989, HESPERETIN, PROTEIN KINASE A INHIBITOR, JQEZ5, SKLB-03220, EBI-2511, and CPI-1205. Notably, zoledronic acid anhydrous and antibiotic target two hub genes. Zoledronic acid anhydrous targets *PLAU* and *COL1A1*, which are the two genes with the

highest diagnostic value identified in our study. This offers a new perspective on the dual-use treatment of the two diseases. Some studies proved that zoledronic acid anhydrous may affect *COL1A1* expression. Specifically, treatment with bisphosphonates, including zoledronic acid anhydrous, inhibits expression levels of the *COL1A1* chains of type-I collagen in oral fibroblasts (Ravosa et al., 2011). A study indicates that women who received zoledronic acid treatment experienced fewer vascular events, lower cancer rates, and a tendency towards reduced mortality (Reid et al., 2020). This greatly confirms our view that zoledronic acid can be used in a dual-use treatment strategy for NSCLC and AMI. Zoledronic acid has also been reported to boost the effectiveness of immunotherapy in NSCLC (Zheng et al., 2022). This is a significant finding, as it suggests that zoledronic acid anhydrous could be a valuable adjunct to current immunotherapeutic approaches, potentially improving patient outcomes. Additionally, some antibiotics have been shown to affect *COL1A1* expression. The transgenes integrated at the *COL1A1* locus have demonstrated strong transgenerational inheritance of epigenetic alterations caused by fetal exposure to doxycycline (Wan et al., 2013), which is a tetracycline antibiotic. Scholars also found that the expression of *COL1A1* was significantly reduced in the rabbit model of benign tracheal stenosis treated with penicillin (Enyuan et al., 2018). However, it is reported that antibiotics can decrease the efficacy of immune checkpoint inhibitors in NSCLC treatment (Qiu et al., 2022). Therefore, the role of antibiotics in NSCLC remains to be determined. Evidence also suggests that among the top ten ranked drugs, some possess the potential for application in the treatment of both diseases. Some scholars have discovered that hesperetin regulates the inflammatory response caused by AMI in mouse models (Meng et al., 2018). Protein kinase A (PKA) inhibition enhances susceptibility to ferroptosis in NSCLC cells and could improve the efficacy of ferroptosis inhibitors in the treatment of NSCLC patients (Shan et al., 2023). The effects of these drugs on the two diseases warrant further investigation. Our results provide further ideas for drug therapy of the two diseases.

In summary, we comprehensively analyzed public databases and gene expression microarray data from NSCLC and AMI patients and healthy controls. We identified eight common signature genes (*CEBPA*, *TGFBR2*, *EZH2*, *JUNB*, *JUN*, *FOS*, *PLAU*, *COL1A1*) and their co-regulated pathways between NSCLC and AMI. All eight common signature genes have high diagnostic value, among which *EZH2* and *TGFBR2* perform well. In the validation datasets, *COL1A1*, *PLAU*, *JUNB*, *JUN*, *TGFBR2*, and *EZH2* retain their high diagnostic effect. Undoubtedly, detecting shared hub genes and pathways in NSCLC and AMI provides new insights into potential therapeutic targets for patients with both diseases and this finding may facilitate the diagnosis of LC-related MI. Among these genes, *COL1A1* may be involved in the occurrence and progression of the two diseases by participating in the EMT process and the formation of arterial dissection separately. Meanwhile, the association of *PLAU* with these two diseases may be related to tumor invasiveness and macrophage activity, respectively. We also constructed miRNA-hub and TF-hub networks, in which five miRNAs and 6 TFs were found to be active in the network. These miRNAs and TFs are implicated in various cellular processes, including cell proliferation, differentiation, apoptosis, and immune responses, which are critical to the development and progression of both NSCLC and AMI. Furthermore, we predicted potential drugs based on common targets and obtained ten candidate drugs, providing more treatment options for related diseases. It is worth emphasizing that zoledronic acid targets two hub genes simultaneously and has shown in past experiments that it can reduce the risk of both cancer and cardiovascular disease. Therefore, our research suggests that zoledronic acid anhydrous may have great therapeutic prospects as a treatment for the comorbidity of lung cancer and myocardial infarction.

However, this study's limitations involve the need for further experimental validation of the shared hub genes and pathways identified in AMI and NSCLC. There is no specific relationship among the selected datasets. If patients with AMI who also have NSCLC were included as the research subjects, the results might be more representative. Additionally, the diagnosis of NSCLC and AMI should not rely solely on these signature genes and pathways but also needs to consider clinical symptoms and laboratory tests. Also, the availability of extensive and valuable public datasets for AMI and NSCLC is somewhat limited, highlighting the need for additional data in future studies to substantiate our findings.

Data availability statement

Publicly available datasets were analyzed in this study. This data can be found here: https://www.ncbi.nlm.nih.gov/geo/query/acc.cgi?acc=gse166780 https://www.ncbi.nlm.nih.gov/geo/query/acc.cgi?acc=GSE8569.

Author contributions

HZ: Data curation, Formal Analysis, Investigation, Methodology, Project administration, Software, Validation, Visualization, Writing–original draft. JW: Resources, Software, Writing–review and editing. YZ: Methodology, Writing–review and editing. XH: Data curation, Validation, Writing–review and editing. LW: Conceptualization, Data curation, Formal Analysis, Investigation, Methodology, Project administration, Resources, Supervision, Validation, Visualization, Writing–original draft, Writing–review and editing.

Funding

The author(s) declare that no financial support was received for the research, authorship, and/or publication of this article.

Conflict of interest

The authors declare that the research was conducted in the absence of any commercial or financial relationships that could be construed as a potential conflict of interest.

Generative AI statement

The author(s) declare that no Generative AI was used in the creation of this manuscript.

Publisher's note

References

Aboumsallem, J. P., Moslehi, J., and de Boer, R. A. (2020). Reverse cardio-oncology: cancer development in patients with cardiovascular disease. *J. Am. Heart Assoc.* 9 (2), e013754. doi:10.1161/JAHA.119.013754

Aljakna, A., Fracasso, T., and Sabatasso, S. (2018). Molecular tissue changes in early myocardial ischemia: from pathophysiology to the identification of new diagnostic markers. *Int. J. Leg. Med.* 132 (2), 425–438. doi:10.1007/s00414-017-1750-z

Ambrose, J. A., and Barua, R. S. (2004). The pathophysiology of cigarette smoking and cardiovascular disease: an update. *J. Am. Coll. Cardiol.* 43 (10), 1731–1737. doi:10.1016/j.jacc.2003.12.047

Atmaca, A., Al-Batran, S. E., Wirtz, R. M., Werner, D., Zirlik, S., Wiest, G., et al. (2014). The validation of estrogen receptor 1 mRNA expression as a predictor of outcome in patients with metastatic non-small cell lung cancer. *Int. J. Cancer* 134 (10), 2314–2321. doi:10.1002/ijc.28571

Barta, J. A., Pauley, K., Kossenkov, A. V., and McMahon, S. B. (2020). The lung-enriched p53 mutants V157F and R158L/P regulate a gain of function transcriptome in lung cancer. *Carcinogenesis* 41 (1), 67–77. doi:10.1093/carcin/bgz087

Braicu, C., Buse, M., Busuioc, C., Drula, R., Gulei, D., Raduly, L., et al. (2019). A comprehensive review on MAPK: a promising therapeutic target in cancer. *Cancers (Basel)* 11 (10), 1618. doi:10.3390/cancers11101618

Caller, T., Rotem, I., Shaihov-Teper, O., Lendengolts, D., Schary, Y., Shai, R., et al. (2024). Small extracellular vesicles from infarcted and failing heart accelerate tumor growth. *Circulation* 149 (22), 1729–1748. doi:10.1161/CIRCULATIONAHA.123.066911

Chang, W. T., Lin, H. W., Chang, T. C., Lin, S. H., and Li, Y. H. (2023). Assessment of tyrosine kinase inhibitors and survival and cardiovascular outcomes of patients with non-small cell lung cancer in taiwan. *JAMA Netw. Open* 6 (5), e2313824. doi:10.1001/jamanetworkopen.2023.13824

Chang, X., Wang, B., Zhao, Y., Deng, B., Liu, P., and Wang, Y. (2024). The role of IFI16 in regulating PANoptosis and implication in heart diseases. *Cell Death Discov.* 10 (1), 204. doi:10.1038/s41420-024-01978-5

Chauhan, S. J., Thyagarajan, A., Chen, Y., Travers, J. B., and Sahu, R. P. (2020). Platelet-Activating factor-receptor signaling mediates targeted therapies-induced microvesicle particles release in lung cancer cells. *Int. J. Mol. Sci.* 21 (22), 8517. doi:10.3390/ijms21228517

Chavakis, T., Kanse, S. M., May, A. E., and Preissner, K. T. (2002). Haemostatic factors occupy new territory: the role of the urokinase receptor system and kininogen in inflammation. *Biochem. Soc. Trans.* 30 (2), 168–173. doi:10.1042/0300-5127:0300168

Chen, F., Liu, J., Song, X., DuCote, T. J., Byrd, A. L., Wang, C., et al. (2022). EZH2 inhibition confers PIK3CA-driven lung tumors enhanced sensitivity to PI3K inhibition. *Cancer Lett.* 524, 151–160. doi:10.1016/j.canlet.2021.10.010

Cozen, A. E., Moriwaki, H., Kremen, M., DeYoung, M. B., Dichek, H. L., Slezicki, K. I., et al. (2004). Macrophage-targeted overexpression of urokinase causes accelerated atherosclerosis, coronary artery occlusions, and premature death. *Circulation* 109 (17), 2129–2135. doi:10.1161/01.CIR.0000127369.24127.03

Di Carlo, E., and Sorrentino, C. (2024). Oxidative stress and age-related tumors. *Antioxidants (Basel)* 13 (9), 1109. doi:10.3390/antiox13091109

Dong, L., Fu, L., Zhu, T., Wu, Y., Li, Z., Ding, J., et al. (2023). A five-collagen-based risk model in lung adenocarcinoma: prognostic significance and immune landscape. *Front. Oncol.* 13, 1180723. doi:10.3389/fonc.2023.1180723

Elsayed, N. (2024). Selective imaging, gene, and therapeutic delivery using PEGylated and pH-Sensitive nanoparticles for enhanced lung disorder treatment. *Int. J. Pharm.* 666, 124819. doi:10.1016/j.ijpharm.2024.124819

Enyuan, Q., Mingpeng, X., Luoman, G., Jinghua, G., Yu, L., Wentao, L., et al. (2018). Erythromycin combined with corticosteroid reduced inflammation and modified trauma-induced tracheal stenosis in a rabbit model. *Ther. Adv. Respir. Dis.* 12, 1753466618773707. doi:10.1177/1753466618773707

Fan, L., Jiang, W., Chen, C., Gao, H., Shi, J., and Wang, D. (2024). CEBPA facilitates LOXL2 and LOXL3 transcription to promote BCL-2 stability and thus enhances the growth and metastasis of lung carcinoma cells *in vitro*. *Exp. Cell Res.* 435 (2), 113937. doi:10.1016/j.yexcr.2024.113937

Giustozzi, M., Becattini, C., Roila, F., Agnelli, G., and Mandala, M. (2021). Vascular events with immune checkpoint inhibitors in melanoma or non-small cell lung cancer: a systematic review and meta-analysis. *Cancer Treat. Rev.* 100, 102280. doi:10.1016/j.ctrv.2021.102280

Guo, X., Chen, M., Cao, L., Hu, Y., Li, X., Zhang, Q., et al. (2021). Cancer-associated fibroblasts promote migration and invasion of non-small cell lung cancer cells via miR-101-3p mediated VEGFA secretion and AKT/eNOS pathway. *Front. Cell Dev. Biol.* 9, 764151. doi:10.3389/fcell.2021.764151

Guo, Z., Tian, Y., Liu, N., Chen, Y., Chen, X., Yuan, G., et al. (2024). Mitochondrial stress as a central player in the pathogenesis of hypoxia-related myocardial dysfunction: new insights. *Int. J. Med. Sci.* 21 (13), 2502–2509. doi:10.7150/ijms.99359

Han, B., Nakamura, M., Mori, I., Nakamura, Y., and Kakudo, K. (2005). Urokinase-type plasminogen activator system and breast cancer (Review). *Oncol. Rep.* 14 (1), 105–112. doi:10.3892/or.14.1.105

Hashimoto, A., Sarker, D., Reebye, V., Jarvis, S., Sodergren, M. H., Kossenkov, A., et al. (2021). Upregulation of C/EBPα inhibits suppressive activity of myeloid cells and potentiates antitumor response in mice and patients with cancer. *Clin. Cancer Res.* 27 (21), 5961–5978. doi:10.1158/1078-0432.CCR-21-0986

Hasin, T., Gerber, Y., Weston, S. A., Jiang, R., Killian, J. M., Manemann, S. M., et al. (2016). Heart failure after myocardial infarction is associated with increased risk of cancer. *J. Am. Coll. Cardiol.* 68 (3), 265–271. doi:10.1016/j.jacc.2016.04.053

Hecht, S. S. (1999). Tobacco smoke carcinogens and lung cancer. *J. Natl. Cancer Inst.* 91 (14), 1194–1210. doi:10.1093/jnci/91.14.1194

Hong, Y., He, H., Jiang, G., Zhang, H., Tao, W., Ding, Y., et al. (2020). miR-155-5p inhibition rejuvenates aged mesenchymal stem cells and enhances cardioprotection following infarction. *Aging Cell* 19 (4), e13128. doi:10.1111/acel.13128

Hu, Y., Chen, X., Mei, X., Luo, Z., Wu, H., Zhang, H., et al. (2023). Identification of diagnostic immune-related gene biomarkers for predicting heart failure after acute myocardial infarction. *Open Med. (Wars)* 18 (1), 20230878. doi:10.1515/med-2023-0878

Huang, G. N., Thatcher, J. E., McAnally, J., Kong, Y., Qi, X., Tan, W., et al. (2012). C/EBP transcription factors mediate epicardial activation during heart development and injury. *Science* 338 (6114), 1599–1603. doi:10.1126/science.1229765

Huang, X., Bai, S., and Luo, Y. (2024). Advances in research on biomarkers associated with acute myocardial infarction: a review. *Med. Baltim.* 103 (15), e37793. doi:10.1097/MD.0000000000037793

Ikeuchi, M., Tsutsui, H., Shiomi, T., Matsusaka, H., Matsushima, S., Wen, J., et al. (2004). Inhibition of TGF-beta signaling exacerbates early cardiac dysfunction but prevents late remodeling after infarction. *Cardiovasc Res.* 64 (3), 526–535. doi:10.1016/j.cardiores.2004.07.017

Johnson, G. L., and Lapadat, R. (2002). Mitogen-activated protein kinase pathways mediated by ERK, JNK, and p38 protein kinases. *Science* 298 (5600), 1911–1912. doi:10.1126/science.1072682

Kakogiannos, N., Ferrari, L., Giampietro, C., Scalise, A. A., Maderna, C., Rava, M., et al. (2020). JAM-A acts via C/EBP-α to promote claudin-5 expression and enhance endothelial barrier function. *Circ. Res.* 127 (8), 1056–1073. doi:10.1161/CIRCRESAHA.120.316742

Kim, I. K., McCutcheon, J. N., Rao, G., Liu, S. V., Pommier, Y., Skrzypski, M., et al. (2019). Acquired SETD2 mutation and impaired CREB1 activation confer cisplatin resistance in metastatic non-small cell lung cancer. *Oncogene* 38 (2), 180–193. doi:10.1038/s41388-018-0429-3

Lai, Y. H., Yu, S. L., Chen, H. Y., Wang, C. C., Chen, H. W., and Chen, J. J. (2013). The HLJ1-targeting drug screening identified Chinese herb andrographolide that can suppress tumour growth and invasion in non-small-cell lung cancer. *Carcinogenesis* 34 (5), 1069–1080. doi:10.1093/carcin/bgt005

Levin, W. J., Casey, G., Ramos, J. C., Arboleda, M. J., Reissmann, P. T., and Slamon, D. J. (1994). Tumor suppressor and immediate early transcription factor genes in non-small cell lung cancer. *Chest* 106 (6 Suppl. l), 372S–6S. doi:10.1378/chest.106.6.372s

Li, B., Li, Y., Chen, S., Wang, Y., and Zheng, Y. (2023). VEGF mimetic peptide-conjugated nanoparticles for magnetic resonance imaging and therapy of myocardial infarction. *J. Control Release* 360, 44–56. doi:10.1016/j.jconrel.2023.06.017

Li, X., Kong, M., Jiang, D., Qian, J., Duan, Q., and Dong, A. (2013). MicroRNA-150 aggravates H2O2-induced cardiac myocyte injury by down-regulating c-myb gene. *Acta Biochim. Biophys. Sin. (Shanghai)* 45 (9), 734–741. doi:10.1093/abbs/gmt067

Li, X., Wu, W., He, H., Guan, L., Chen, G., Lin, Z., et al. (2024). Analysis and validation of hub genes in neutrophil extracellular traps for the long-term prognosis of myocardial infarction. *Gene* 914, 148369. doi:10.1016/j.gene.2024.148369

Li, X., Zhang, S., Wa, M., Liu, Z., and Hu, S. (2019). MicroRNA-101 protects against cardiac remodeling following myocardial infarction via downregulation of runt-related transcription factor 1. *J. Am. Heart Assoc.* 8 (23), e013112. doi:10.1161/JAHA.119.013112

Li, Y., Liu, Y., Jin, K., Dong, R., Gao, C., Si, L., et al. (2021). Negatively regulated by miR-29c-3p, MTFR1 promotes the progression and glycolysis in lung adenocarcinoma via the AMPK/mTOR signalling pathway. *Front. Cell Dev. Biol.* 9, 771824. doi:10.3389/fcell.2021.771824

Liu, Y., Chudgar, N., Mastrogiacomo, B., He, D., Lankadasari, M. B., Bapat, S., et al. (2022). A germline SNP in BRMS1 predisposes patients with lung adenocarcinoma to metastasis and can be ameliorated by targeting c-fos. *Sci. Transl. Med.* 14 (665), eabo1050. doi:10.1126/scitranslmed.abo1050

Lo Sardo, F., Pulito, C., Sacconi, A., Korita, E., Sudol, M., Strano, S., et al. (2021). YAP/TAZ and EZH2 synergize to impair tumor suppressor activity of TGFBR2 in non-small cell lung cancer. *Cancer Lett.* 500, 51–63. doi:10.1016/j.canlet.2020.11.037

Lourenco, A. R., and Coffer, P. J. (2017). A tumor suppressor role for C/EBPα in solid tumors: more than fat and blood. *Oncogene* 36 (37), 5221–5230. doi:10.1038/onc.2017.151

Lourenco, A. R., Roukens, M. G., Seinstra, D., Frederiks, C. L., Pals, C. E., Vervoort, S. J., et al. (2020). C/EBPα is crucial determinant of epithelial maintenance by preventing epithelial-to-mesenchymal transition. *Nat. Commun.* 11 (1), 785. doi:10.1038/s41467-020-14556-x

Luo, J. Y., Li, Y. H., Fang, B. B., Tian, T., Liu, F., Li, X. M., et al. (2020). NFKB1 gene rs28362491 ins/del variation is associated with higher susceptibility to myocardial infarction in a Chinese Han population. *Sci. Rep.* 10 (1), 19518. doi:10.1038/s41598-020-72877-9

Meijers, W. C., Maglione, M., Bakker, S. J. L., Oberhuber, R., Kieneker, L. M., de Jong, S., et al. (2018). Heart failure stimulates tumor growth by circulating factors. *Circulation* 138 (7), 678–691. doi:10.1161/CIRCULATIONAHA.117.030816

Meng, C., Guo, Z., Li, D., Li, H., He, J., Wen, D., et al. (2018). Preventive effect of hesperidin modulates inflammatory responses and antioxidant status following acute myocardial infarction through the expression of PPAR-gamma and Bcl-2 in model mice. *Mol. Med. Rep.* 17 (1), 1261–1268. doi:10.3892/mmr.2017.7981

Meng, Y. M., Jiang, X., Zhao, X., Meng, Q., Wu, S., Chen, Y., et al. (2021). Hexokinase 2-driven glycolysis in pericytes activates their contractility leading to tumor blood vessel abnormalities. *Nat. Commun.* 12 (1), 6011. doi:10.1038/s41467-021-26259-y

Mitchell, J. D., Laurie, M., Xia, Q., Dreyfus, B., Jain, N., Jain, A., et al. (2023). Risk profiles and incidence of cardiovascular events across different cancer types. *ESMO Open* 8 (6), 101830. doi:10.1016/j.esmoop.2023.101830

Murphy, A., and Goldberg, S. (2022). Mechanical complications of myocardial infarction. *Am. J. Med.* 135 (12), 1401–1409. doi:10.1016/j.amjmed.2022.08.017

Nagano, J., Sudo, N., Kubo, C., and Kono, S. (2001). Lung cancer, myocardial infarction, and the Grossarth-Maticek personality types: a case-control study in Fukuoka, Japan. *J. Epidemiol.* 11 (6), 281–287. doi:10.2188/jea.11.281

Newman, J. R., and Keating, A. E. (2003). Comprehensive identification of human bZIP interactions with coiled-coil arrays. *Science* 300 (5628), 2097–2101. doi:10.1126/science.1084648

Nikolaienko, R., Bovo, E., Kahn, D., Gracia, R., Jamrozik, T., and Zima, A. V. (2023). Cysteines 1078 and 2991 cross-linking plays a critical role in redox regulation of cardiac ryanodine receptor (RyR). *Nat. Commun.* 14 (1), 4498. doi:10.1038/s41467-023-40268-z

Nong, Z., O'Neil, C., Lei, M., Gros, R., Watson, A., Rizkalla, A., et al. (2011). Type I collagen cleavage is essential for effective fibrotic repair after myocardial infarction. *Am. J. Pathol.* 179 (5), 2189–2198. doi:10.1016/j.ajpath.2011.07.017

Pan, Z., Sun, X., Shan, H., Wang, N., Wang, J., Ren, J., et al. (2012). MicroRNA-101 inhibited postinfarct cardiac fibrosis and improved left ventricular compliance via the FBJ osteosarcoma oncogene/transforming growth factor-β1 pathway. *Circulation* 126 (7), 840–850. doi:10.1161/CIRCULATIONAHA.112.094524

Peng, Y., Zhao, J. L., Peng, Z. Y., Xu, W. F., and Yu, G. L. (2020). Exosomal miR-25-3p from mesenchymal stem cells alleviates myocardial infarction by targeting pro-apoptotic proteins and EZH2. *Cell Death Dis.* 11 (5), 317. doi:10.1038/s41419-020-2545-6

Plotnik, J. P., and Hollenhorst, P. C. (2017). Interaction with ZMYND11 mediates opposing roles of Ras-responsive transcription factors ETS1 and ETS2. *Nucleic Acids Res.* 45 (8), 4452–4462. doi:10.1093/nar/gkx039

Plotnikov, M. B., Chernysheva, G. A., Smol'yakova, V. I., Aliev, O. I., Fomina, T. I., Sandrikina, L. A., et al. (2023). Cardioprotective effects of a selective c-jun N-terminal kinase inhibitor in a rat model of myocardial infarction. *Biomedicines* 11 (3), 714. doi:10.3390/biomedicines11030714

Psilopatis, I., Karniadakis, I., Danos, K. S., Vrettou, K., Michaelidou, K., Mavridis, K., et al. (2022). May EPH/ephrin targeting revolutionize lung cancer treatment? *Int. J. Mol. Sci.* 24 (1), 93. doi:10.3390/ijms24010093

Puzianowska-Kuznicka, M. (2012). ESR1 in myocardial infarction. *Clin. Chim. Acta* 413 (1-2), 81–87. doi:10.1016/j.cca.2011.10.028

Qiu, H., Ma, Q. G., Chen, X. T., Wen, X., Zhang, N., Liu, W. M., et al. (2022). Different classes of antibiotics exhibit disparate negative impacts on the therapeutic efficacy of immune checkpoint inhibitors in advanced non-small cell lung cancer patients. *Am. J. Cancer Res.* 12 (7), 3175–3184.

Ramos, A. H., Dutt, A., Mermel, C., Perner, S., Cho, J., Lafargue, C. J., et al. (2009). Amplification of chromosomal segment 4q12 in non-small cell lung cancer. *Cancer Biol. Ther.* 8 (21), 2042–2050. doi:10.4161/cbt.8.21.9764

Ravosa, M. J., Ning, J., Liu, Y., and Stack, M. S. (2011). Bisphosphonate effects on the behaviour of oral epithelial cells and oral fibroblasts. *Arch. Oral Biol.* 56 (5), 491–498. doi:10.1016/j.archoralbio.2010.11.003

Reid, I. R., Horne, A. M., Mihov, B., Stewart, A., Garratt, E., Bastin, S., et al. (2020). Effects of zoledronate on cancer, cardiac events, and mortality in osteopenic older women. *J. Bone Min. Res.* 35 (1), 20–27. doi:10.1002/jbmr.3860

Ribatti, D., Tamma, R., and Annese, T. (2020). Epithelial-mesenchymal transition in cancer: a historical overview. *Transl. Oncol.* 13 (6), 100773. doi:10.1016/j.tranon.2020.100773

Rinde, L. B., Smabrekke, B., Hald, E. M., Brodin, E. E., Njolstad, I., Mathiesen, E. B., et al. (2017). Myocardial infarction and future risk of cancer in the general population-the Tromso Study. *Eur. J. Epidemiol.* 32 (3), 193–201. doi:10.1007/s10654-017-0231-5

Rondeaux, J., Groussard, D., Renet, S., Tardif, V., Dumesnil, A., Chu, A., et al. (2023). Ezh2 emerges as an epigenetic checkpoint regulator during monocyte differentiation limiting cardiac dysfunction post-MI. *Nat. Commun.* 14 (1), 4461. doi:10.1038/s41467-023-40186-0

Sahu, P., Donovan, C., Paudel, K. R., Pickles, S., Chimankar, V., Kim, R. Y., et al. (2023). Pre-clinical lung squamous cell carcinoma mouse models to identify novel biomarkers and therapeutic interventions. *Front. Oncol.* 13, 1260411. doi:10.3389/fonc.2023.1260411

Saw, J., Humphries, K., Aymong, E., Sedlak, T., Prakash, R., Starovoytov, A., et al. (2017). Spontaneous coronary artery dissection: clinical outcomes and risk of recurrence. *J. Am. Coll. Cardiol.* 70 (9), 1148–1158. doi:10.1016/j.jacc.2017.06.053

Shan, G., Bi, G., Zhao, G., Liang, J., Bian, Y., Zhang, H., et al. (2023). Inhibition of PKA/CREB1 pathway confers sensitivity to ferroptosis in non-small cell lung cancer. *Respir. Res.* 24 (1), 277. doi:10.1186/s12931-023-02567-3

Shtivelman, E., Hensing, T., Simon, G. R., Dennis, P. A., Otterson, G. A., Bueno, R., et al. (2014). Molecular pathways and therapeutic targets in lung cancer. *Oncotarget* 5 (6), 1392–1433. doi:10.18632/oncotarget.1891

Sliva, D. (2008). Suppression of cancer invasiveness by dietary compounds. *Mini Rev. Med. Chem.* 8 (7), 677–688. doi:10.2174/138955708784567412

Stolz, D., Mkorombindo, T., Schumann, D. M., Agusti, A., Ash, S. Y., Bafadhel, M., et al. (2022). Towards the elimination of chronic obstructive pulmonary disease: a Lancet Commission. *Lancet* 400 (10356), 921–972. doi:10.1016/S0140-6736(22)01273-9

Su, L., Zhang, G., Jiang, L., Chi, C., Bai, B., and Kang, K. (2023). The role of c-Jun for beating cardiomycyte formation in prepared embryonic body. *Stem Cell Res. Ther.* 14 (1), 371. doi:10.1186/s13287-023-03544-9

Sun, H., Liu, H., Li, J., Kou, J., and Yang, C. (2024). Analysis of the clinical predictive value of the novel inflammatory indices SII, SIRI, MHR and NHR in patients with acute myocardial infarction and their extent of coronary artery disease. *J. Inflamm. Res.* 17, 7325–7338. doi:10.2147/JIR.S479253

Sun, Y., Sun, X., You, C., Ma, S., Luo, Y., Peng, S., et al. (2021). MUC3A promotes non-small cell lung cancer progression via activating the NFκB pathway and attenuates radiosensitivity. *Int. J. Biol. Sci.* 17 (10), 2523–2536. doi:10.7150/ijbs.59430

Wan, M., Gu, H., Wang, J., Huang, H., Zhao, J., Kaundal, R. K., et al. (2013). Inducible mouse models illuminate parameters influencing epigenetic inheritance. *Development* 140 (4), 843–852. doi:10.1242/dev.088229

Wang, J., Zhang, L., Luo, L., He, P., Xiong, A., Jiang, M., et al. (2022). Characterizing cellular heterogeneity in fibrotic hypersensitivity pneumonitis by single-cell transcriptional analysis. *Cell Death Discov.* 8 (1), 38. doi:10.1038/s41420-022-00831-x

Wang, J. C., Su, C. C., Xu, J. B., Chen, L. Z., Hu, X. H., Wang, G. Y., et al. (2007). Novel microdeletion in the transforming growth factor beta type II receptor gene is associated with giant and large cell variants of nonsmall cell lung carcinoma. *Genes Chromosom. Cancer* 46 (2), 192–201. doi:10.1002/gcc.20400

Wang, R., Liu, J., Li, K., Yang, G., Chen, S., Wu, J., et al. (2021a). An SETD1A/Wnt/β-catenin feedback loop promotes NSCLC development. *J. Exp. Clin. Cancer Res.* 40 (1), 318. doi:10.1186/s13046-021-02119-x

Wang, X., Zhu, Y., Wu, C., Liu, W., He, Y., and Yang, Q. (2021b). Adipose-derived mesenchymal stem cells-derived exosomes carry MicroRNA-671 to alleviate myocardial infarction through inactivating the TGFBR2/smad2 Axis. *Inflammation* 44 (5), 1815–1830. doi:10.1007/s10753-021-01460-9

Wei, Y. J., Wang, J. F., Cheng, F., Xu, H. J., Chen, J. J., Xiong, J., et al. (2021). miR-124-3p targeted SIRT1 to regulate cell apoptosis, inflammatory response, and oxidative stress in acute myocardial infarction in rats via modulation of the FGF21/CREB/PGC1α pathway. *J. Physiol. Biochem.* 77 (4), 577–587. doi:10.1007/s13105-021-00822-z

Wu, D., Chen, T., Zhao, X., Huang, D., Huang, J., Huang, Y., et al. (2022). HIF1α-SP1 interaction disrupts the circ-0001875/miR-31-5p/SP1 regulatory loop under a hypoxic microenvironment and promotes non-small cell lung cancer progression. *J. Exp. Clin. Cancer Res.* 41 (1), 156. doi:10.1186/s13046-022-02336-y

Wu, T., Tian, Q., Liu, R., Xu, K., Shi, S., Zhang, X., et al. (2023). Inhibitory role of bone marrow mesenchymal stem cells-derived exosome in non-small-cell lung cancer: microRNA-30b-5p, EZH2 and PI3K/AKT pathway. *J. Cell Mol. Med.* 27 (22), 3526–3538. doi:10.1111/jcmm.17933

Xia, S., Duan, W., Xu, M., Li, M., Tang, M., Wei, S., et al. (2024). Mesothelin promotes brain metastasis of non-small cell lung cancer by activating MET. *J. Exp. Clin. Cancer Res.* 43 (1), 103. doi:10.1186/s13046-024-03015-w

Xue, Y., Fan, X., Yang, R., Jiao, Y., and Li, Y. (2020). miR-29b-3p inhibits post-infarct cardiac fibrosis by targeting FOS. *Biosci. Rep.* 40 (9). doi:10.1042/BSR20201227

Yamamoto, H., Shigematsu, H., Nomura, M., Lockwood, W. W., Sato, M., Okumura, N., et al. (2008). PIK3CA mutations and copy number gains in human lung cancers. *Cancer Res.* 68 (17), 6913–6921. doi:10.1158/0008-5472.CAN-07-5084

Yan, M., Yang, S., Meng, F., Zhao, Z., Tian, Z., and Yang, P. (2018). MicroRNA 199a-5p induces apoptosis by targeting JunB. *Sci. Rep.* 8 (1), 6699. doi:10.1038/s41598-018-24932-9

Yang, W., Bai, J., Liu, D., Wang, S., Zhao, N., Che, R., et al. (2018). MiR-93-5p up-regulation is involved in non-small cell lung cancer cells proliferation and migration and poor prognosis. *Gene* 647, 13–20. doi:10.1016/j.gene.2018.01.024

Yang, Z., Liang, S. Q., Zhao, L., Yang, H., Marti, T. M., Hegedus, B., et al. (2022). Metabolic synthetic lethality by targeting NOP56 and mTOR in KRAS-mutant lung cancer. *J. Exp. Clin. Cancer Res.* 41 (1), 25. doi:10.1186/s13046-022-02240-5

Yuan, Y., Mei, Z., Qu, Z., Li, G., Yu, S., Liu, Y., et al. (2023). Exosomes secreted from cardiomyocytes suppress the sensitivity of tumor ferroptosis in ischemic heart failure. *Signal Transduct. Target Ther.* 8 (1), 121. doi:10.1038/s41392-023-01336-4

Zekavat, S. M., Chou, E. L., Zekavat, M., Pampana, A., Paruchuri, K., Lino Cardenas, C. L., et al. (2022). Fibrillar collagen variants in spontaneous coronary artery dissection. *JAMA Cardiol.* 7 (4), 396–406. doi:10.1001/jamacardio.2022.0001

Zhang, Y., Yu, W., Zhang, L., and Li, P. (2024). Nanozyme-based visual diagnosis and therapeutics for myocardial infarction: the application and strategy. *J. Adv. Res.* doi:10.1016/j.jare.2024.04.019

Zhao, J., Li, L., Wang, X., and Shen, J. (2024). KN-93 promotes HDAC4 nucleus translocation to promote fatty acid oxidation in myocardial infarction. *Exp. Cell Res.* 438 (2), 114050. doi:10.1016/j.yexcr.2024.114050

Zhao, L., You, T., Lu, Y., Lin, S., Li, F., and Xu, H. (2021). Elevated EZH2 in ischemic heart disease epigenetically mediates suppression of Na(V)1.5 expression. *J. Mol. Cell Cardiol.* 153, 95–103. doi:10.1016/j.yjmcc.2020.12.012

Zheng, Y., Wang, P. P., Fu, Y., Chen, Y. Y., and Ding, Z. Y. (2022). Zoledronic acid enhances the efficacy of immunotherapy in non-small cell lung cancer. *Int. Immunopharmacol.* 110, 109030. doi:10.1016/j.intimp.2022.109030

Zheng, Y., Zhang, L., Zhang, K., Wu, S., Wang, C., Huang, R., et al. (2024). PLAU promotes growth and attenuates cisplatin chemosensitivity in ARID1A-depleted non-small cell lung cancer through interaction with TM4SF1. *Biol. Direct* 19 (1), 7. doi:10.1186/s13062-024-00452-7

Zhu, J., Zhu, X., Shi, C., Li, Q., Jiang, Y., Chen, X., et al. (2024). Integrative analysis of aging-related genes reveals CEBPA as a novel therapeutic target in non-small cell lung cancer. *Cancer Cell Int.* 24 (1), 267. doi:10.1186/s12935-024-03457-4

Zhu, L., Xue, F., Cui, Y., Liu, S., Li, G., Li, J., et al. (2019). miR-155-5p and miR-760 mediate radiation therapy suppressed malignancy of non-small cell lung cancer cells. *Biofactors* 45 (3), 393–400. doi:10.1002/biof.1500

Zhu, Q., Zhang, Y., Li, M., Zhang, Y., Zhang, H., Chen, J., et al. (2023). MiR-124-3p impedes the metastasis of non-small cell lung cancer via extracellular exosome transport and intracellular PI3K/AKT signaling. *Biomark. Res.* 11 (1), 1. doi:10.1186/s40364-022-00441-w

Zhuang, L., Wang, Y., Chen, Z., Li, Z., Wang, Z., Jia, K., et al. (2022). Global characteristics and dynamics of single immune cells after myocardial infarction. *J. Am. Heart Assoc.* 11 (24), e027228. doi:10.1161/JAHA.122.027228

frontiers | Frontiers in Immunology

TYPE Systematic Review
PUBLISHED 06 December 2024
DOI 10.3389/fimmu.2024.1454393

OPEN ACCESS

EDITED BY
Giuseppe Bronte,
University of Ferrara, Italy

REVIEWED BY
Mansoor-Ali Vaali-Mohammed,
King Saud University, Saudi Arabia
Hester Doyle,
Yale University, United States

*CORRESPONDENCE
Weixing Wang
wangwx@whu.edu.cn
Chen Chen
appreciation@whu.edu.cn

†These authors have contributed equally to this work

RECEIVED 03 September 2024
ACCEPTED 22 November 2024
PUBLISHED 06 December 2024

CITATION
Liu R, Shen Y, Cui J, Ma W, Wang J, Chen C and Wang W (2024) Association between glucose to lymphocyte ratio and prognosis in patients with solid tumors. *Front. Immunol.* 15:1454393. doi: 10.3389/fimmu.2024.1454393

Association between glucose to lymphocyte ratio and prognosis in patients with solid tumors

Rongqiang Liu[1†], Yankun Shen[1,2†], Jiahui Cui[3†], Wangbin Ma[1], Jianguo Wang[1], Chen Chen[1*] and Weixing Wang[1*]

[1]Department of Hepatobiliary Surgery, Renmin Hospital of Wuhan University, Wuhan, Hubei, China, [2]Department of General Surgery, Zhongshan Hospital, Fudan University, Shanghai, China, [3]Department of Anesthesiology, Renmin Hospital of Wuhan University, Wuhan, Hubei, China

Background: Glucose-to-lymphocyte ratio (GLR) plays an important role in the prognosis of various tumors. The aim of this study was to comprehensively evaluate the prognostic value of GLR in solid tumors through the meta-analysis.

Methods: A comprehensive search of eligible studies was performed by scrutinizing the Pubmed, Embase and Web of science databases until May 30, 2024. The pooled hazard ratios (HRs) with 95% confidence intervals (CIs) were calculated to evaluate overall survival (OS), disease-free survival (DFS) and recurrence free survival (RFS).

Results: A total of 22 studies from 14 articles involving 9472 patients were included in the study. The pooled analysis showed that cancer patients with high GLR was significantly associated with unfavorable OS (HR:1.48,95% CI:1.34-1.63) and DFS/RFS (HR:2.20,95% CI:1.66-2.92). Subgroup analysis further showed that high GLR had better predictive value in liver cancer (HR:2.66, 95%CI:1.80-3.93), breast cancer (HR:2.13, 95%CI:1.10-4.13) and pancreatic cancer (HR:1.92, 95% CI:1.30-2.84).

Conclusions: GLR can be used as an effective prognostic marker in patients with solid tumors.

KEYWORDS

glucose-to-lymphocyte ratio, tumor, prognosis, meta-analysis, survival

Introduction

According to the World Health Organization, cancers have become the leading cause of human death (1). In China, colorectal, stomach, esophagus and liver cancers are also commonly diagnosed as the leading causes of cancer deaths (2). Despite tremendous progress in the prevention and treatment of cancer, the incidence and mortality of cancers

continue to rise (3). Many cancer patients are diagnosed at advanced stages and miss the best time for treatment. Many effective prognostic markers have been used for cancers, but their clinical application is not satisfactory. Therefore, there is an urgent need to identify new and more effective prognostic markers for cancers.

Inflammatory, immune and nutritional status influence tumor biological behavior (4–6). Multiple immunoinflammatory or nutritional indicators have been used to assess the prognosis of patients with tumors (7–9). However, these indicators only reflect inflammation, immune and nutritional status, and do not embody the body's metabolic status. Tumor prognosis is not only related to inflammation, immunity and nutritional status, but also closely associated with glucose metabolism (10). Therefore, a new prognostic marker that can indicate both inflammatory immune status and metabolic status is needed.

Glucose-to-lymphocyte ratio(GLR) composed of glucose and lymphocyte as a new prognostic marker, is believed that it can effectively reflect the body's glucose metabolism and inflammatory immune status (11). GLR was found to play an important role in tumor prognosis. Navarro et al. suggested that preoperative GLR was an independent predictor of overall survival(OS) and disease-free survival (DFS) in gallbladder cancer (12). Yang et al. showed that GLR can independently predict the prognosis of patients with colorectal cancer (13). Yılmaz et al. found that GLR was a new prognostic biomarker in advanced hepatocellular carcinoma (14). Hannarici et al. revealed that GLR was found to be independently prognostic factor for both recurrence free survival (RFS) and OS in metastatic gastric cancer (15). Park et al. reported that elevated preoperative GLR was associated with aggressive tumor characteristics and was an independent predictor of poor OS in patients with pancreatic cancer (16). Ni et al. displayed that high GLR represented adverse prognosis in renal cell carcinoma patients (17). Yang et al. disclosed that GLR was independent prognostic factors for patients with non-small cell lung cancer (18). Zhang et al. proved that GLR had predictive value for the survival of patients with breast cancer (19). Liu et al. demonstrated that elevated preoperative GLR was remarkably associated with poorer prognosis in patients with esophageal cancer and melanoma (20). However, due to the limited number of patients in a single study, the reliability of the conclusions was insufficient. Therefore, we conducted a meta-analysis to synthesize and clarify the applicability of GLR as a prognostic marker in solid tumors.

Material and methods

Search strategy

Articles in electronic databases (Pubmed, Embase and Web of science) were retrieved until May 30, 2024. We used the following keywords: "glucose to lymphocyte ratio" OR "glucose-to-lymphocyte ratio". Language restriction was not set. The titles, abstracts, full texts, and the possible references were screened to identify qualified studies.

Inclusion and exclusion criteria

Three researchers independently conducted the literature search. The inclusion criteria were as follows: (1) investigated the relationship between GLR and survival outcomes in solid tumors. (2) provided sufficient data to calculate the hazard ratios (HRs) and 95% confidence intervals (CIs). The exclusion criteria were as follows: (1) insufficient data to calculate the 95% CIs and HRs; (2) abstracts, case reports, reviews and letters.

Data extraction and quality assessment

The relevant information was extracted, such as the name of the first author, year of publication, country, cancer type, sample size, treatment methods, analysis types and survival outcomes. We assessed the quality of each study according to the Newcastle–Ottawa Quality Assessment Scale (NOS) (21). The multivariate analysis was preferred because it considered the confounding factors.

Statistical analysis

All data analysis was performed using the STATA version 12.0 software (Stata Corporation, College Station, TX, USA). HRs and their corresponding 95% CIs were used to analyze the pooled data. A fixed effects model was used when I (2) was <50%. A random effects model was used when I (2) was >50% (22). The subgroup analysis was performed to further explore the prognostic value of GLR in solid tumors. Meta-regression was used to explore the sources of heterogeneity. Sensitivity analysis was used to test the stability of the results. Begg's test, Egger's test and trim-and-fill method were used to assess publication bias (23, 24). $P<0.05$ denoted statistical significance.

Results

Search results

Through a systematic literature search, we primarily identified a total of 80 articles. After removal of 62 duplicate publications, 18 articles remained. We further excluded 4 articles by browsing the titles and abstracts. Finally, we identified 22 studies from 14 articles published between 2019 and 2024 (9, 12–20, 25–28). The flow diagram of the literature search was shown in Figure 1.

Study characteristics

The total number of patients in the included articles was 9472 (range: 110–1772 patients).18 studies were produced in China, 2 study were conducted in Korea and 2 study were from Turkey. 22 studies reported overall survival data, 1 study displayed disease-free survival data, and 3 studies covered recurrence free survival data. 10 different tumors were included, such as gastric cancer, gallbladder cancer, renal

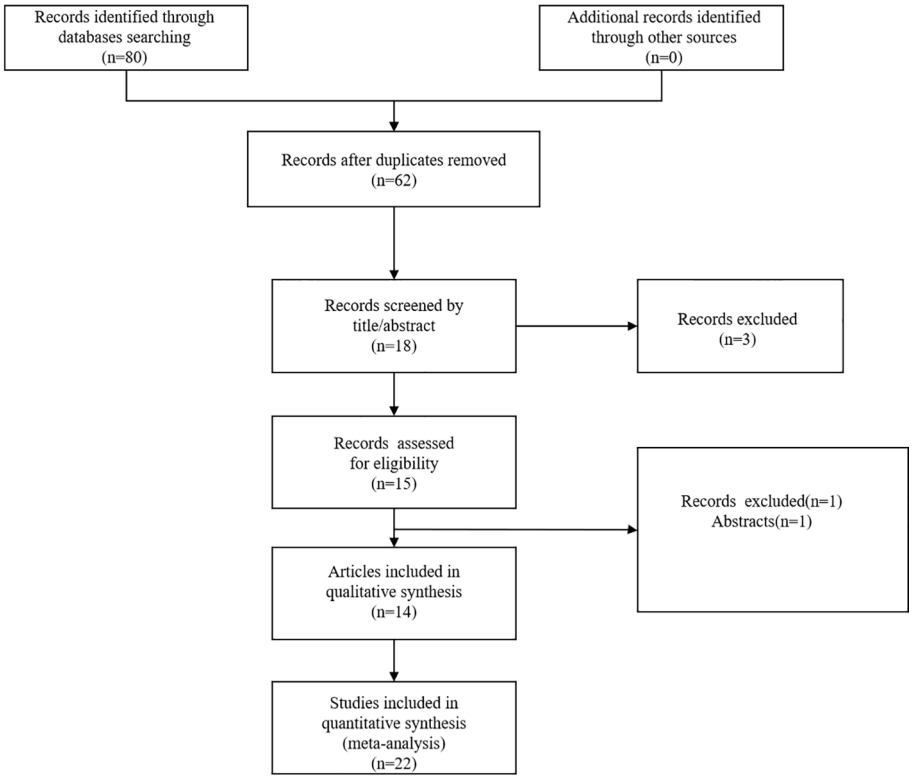

FIGURE 1
Flow diagram of the literature search.

cancer, lung cancer, colorectal cancer, liver cancer, breast cancer, pancreatic cancer, esophageal cancer and melanoma. The NOS scores of the included studies ranged from 6 to 8 (mean: 6.5). The basic information was shown in (Table 1).

Association between high GLR and OS

22 studies from 14 articles explored the association between GLR and prognosis using OS. We used a random effects model to calculate the pooled HRs due to moderate heterogeneity (I^2 = 86.3%). The results of the meta-analysis revealed that high GLR was significantly related to poor OS (HR:1.48,95% CI:1.34-1.63) (Figure 2).

Subgroup analysis and meta-regression for OS

We further conducted subgroup analysis based on cancer type, sample size, treatment method and country. The results were shown in (Table 2). We found that high GLR was an unfavorable prognostic marker in liver cancer (HR:2.66, 95%CI:1.80-3.93), breast cancer (HR:2.13, 95%CI:1.10-4.13) and pancreatic cancer (HR:1.92, 95%CI:1.30-2.84). Moreover, we also found that high GLR was associated with poor OS for the China group (HR: 1.37; 95% CI:1.25–1.51) and Turkey group (HR:2.18; 95% CI: 1.50–3.19). Regardless of the surgical or non-surgical group, high GLR indicated adverse prognosis. Meta-regression showed that sample size was the main source of heterogeneity.

Association between high GLR and DFS/PFS

4 studies involving 616 patients documented the association between high GLR and prognosis using DFS/PFS. A fixed-effect model was used because of the obvious heterogeneity (I^2 = 12.1%). The results showed that high GLR was correlated with adverse DFS/PFS (HR:2.20,95% CI:1.66-2.92) (Figure 3).

Sensitivity analysis

Sensitivity analysis was implemented by removing one study. The results were consistent with the comprehensive analysis, confirming that the outcomes of the combined OS and DFS/PFS were stable (Figures 4A, B).

Publication bias

Begg's test and Egger's test were used to evaluate the publication bias. P value of Begg's test and Egger's test for OS was 0.028 and 0.01 (Figure 5A), respectively. There was a degree of publication bias.

TABLE 1 Basic information of the included articles.

Study	Year	Country	Design	Cancer type	Sample size	Analysis type	Survival analysis	Treatment methods	NOS score
Hannarici	2023	Turkey	R	Gastric cancer	159	Multivariate analysis	OS,PFS	Non-surgery	7
Navarro	2019	Korea	R	Gallbladder Cancer	197	Multivariate analysis	OS,DFS	Surgery	7
Ni	2022	China	R	Renal cancer	420	Multivariate analysis	OS	Surgery	7
Song	2022	China	R	Lung cancer	1772	Multivariate analysis	OS	Non-surgery	8
Yang	2022	China	R	Lung cancer	862	Multivariate analysis	OS	Surgery	7
Yang	2022	China	R	Colorectal cancer	1448	Multivariate analysis	OS	Surgery	7
Yilmaz	2021	China	R	Liver cancer	150	Multivariate analysis	OS,PFS	Non-surgery	7
Yilmaz	2022	China	R	Breast cancer	110	Multivariate analysis	OS,PFS	Non-surgery	7
Zhang	2021A	China	R	Pancreatic cancer	130	Multivariate analysis	OS	Surgery	6
Zhang	2021B	China	R	Pancreatic cancer	129	Multivariate analysis	OS	Surgery	6
Zhong	2020	China	R	Pancreatic cancer	238	Multivariate analysis	OS	Non-surgery	6
Liu	2024A	China	R	Lung cancer	240	Multivariate analysis	OS	Surgery	6
Liu	2024B	China	R	Colorectal cancer	378	Multivariate analysis	OS	Surgery	6
Liu	2024C	China	R	Breast cancer	221	Multivariate analysis	OS	Surgery	6
Liu	2024D	China	R	Gastric cancer	335	Multivariate analysis	OS	Surgery	6
Liu	2024E	China	R	Liver cancer	270	Multivariate analysis	OS	Surgery	6
Liu	2024F	China	R	Esophageal Cancer	233	Multivariate analysis	OS	Surgery	6
Liu	2024H	China	R	Renal Cancer	295	Multivariate analysis	OS	Surgery	6
Liu	2024G	China	R	Melanoma	200	Multivariate analysis	OS	Surgery	6
Zhang	2023	China	R	Breast cancer	1125	Multivariate analysis	OS	Non-surgery	8
Aydin	2024	Turkey	R	Colorectal cancer	222	Multivariate analysis	OS	Surgery	6
Park	2024	Korea	R	Pancreatic cancer	338	Multivariate analysis	OS	Surgery	6

R, retrospective; OS, overall survival; DFS, disease-free survival; PFS, progression-free survival; NOS score, Newcastle-Ottawa Scale score.

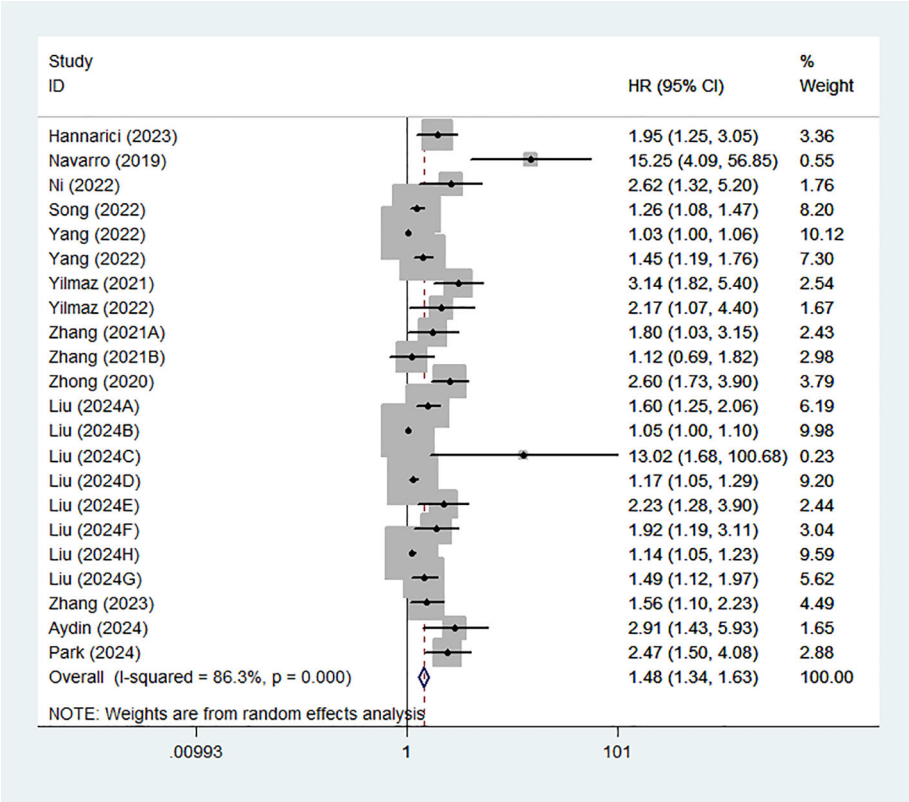

FIGURE 2
Forest plot assessing the relationship between GLR and OS.

TABLE 2 Subgroup analysis for OS.

Factors	Studies	HR(95%)	P	Heterogeneity		Meta-regression		
				I^2	P	Tau^2	Adj R^2(%)	P
Country						0.0889	20.13	0.93
China	18	1.37(1.25-1.51)	<0.001	84.9	<0.001			
Korea	2	5.525 (0.94-32.43)	0.058	84.4	0.011			
Turkey	2	2.18(1.50-3.19)	<0.001	0	0.352			
Treatment method						0.1032	7.32	0.383
Non-surgery	6	1.93(1.40-2.66)	<0.001	76.6	0.001			
Surgery	16	1.35(1.22-1.49)	<0.001	85.1	<0.001			
Sample size						0.059	46.5	0.025
<250	12	2.08(1.64-2.63)	<0.001	62.2	0.002			
>250	10	1.21(1.11-1.32)	<0.001	83.9	<0.001			
Cancer type								
Gastric cancer	2	1.44(0.88-2.36)	0.148	79.1	0.029	0.092	17.01	0.139
Renal cancer	2	1.61(0.72-3.59)	0.248	82.2	0.018			

(Continued)

TABLE 2 Continued

Factors	Studies	HR(95%)	P	Heterogeneity		Meta-regression		
				I^2	P	Tau^2	Adj R^2(%)	P
Cancer type								
Lung cancer	3	1.24(0.98-1.57)	0.072	88.8	<0.001			
Colorectal cancer	3	1.21(0.98-2.01)	0.63	88.3	<0.001			
Liver cancer	2	2.66(1.80-3.93)	<0.001	0	0.393			
Breast cancer	4	2.13(1.10-4.13)	0.025	55.1	0.106			
Pancreatic cancer	4	1.92(1.30-2.84)	0.001	61.7	0.05			
Gallbladder Cancer	1	15.25(4.1-56.85)						
Esophageal Cancer	1	1.925(1.19-3.11)						
Melanoma	1	1.486(1.12-1.97)						

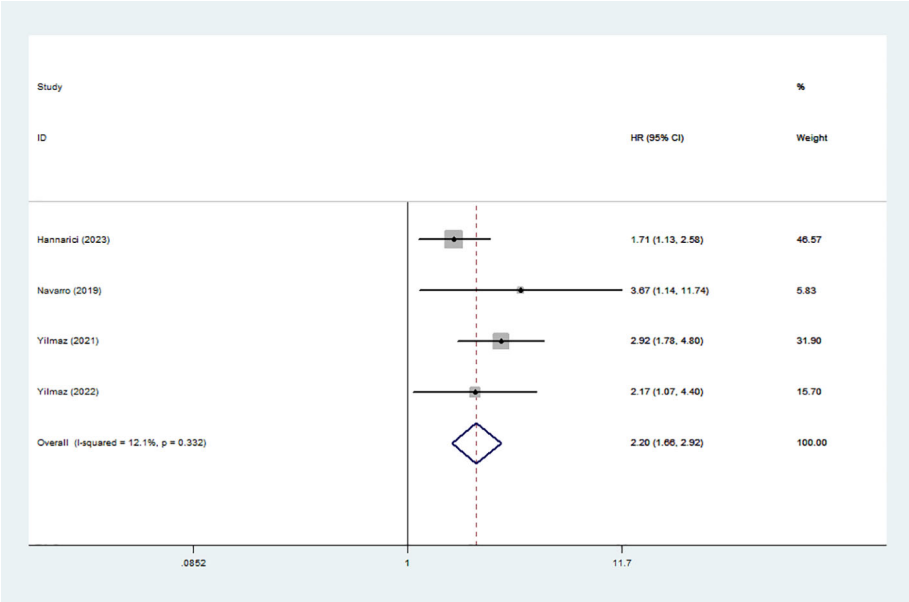

FIGURE 3
Forest plot accessing the relationship between GLR and DFS/PFS.

However, we found that the comprehensive results were not affected through the trim-and-fill method (HR:1.258,95%CI:1.140-1.388) (Figure 5B). P values of Begg's and Egger's tests for DFS/PFS were 0.734 and 0.411, respectively (Figure 5C). P was more than 0.05 and no significant bias was observed.

Discussion

To our knowledge, this study was the first meta-analysis to comprehensively assess the prognostic value of GLR in solid tumors. Our results suggested that high GLR was significantly associated with unfavorable OS and DFS/PFS in solid tumors. Subgroup analysis further showed that high GLR had better predictive value in liver cancer, breast cancer and pancreatic cancer.

GLR was firstly established as an effective prognostic indicator for gallbladder cancer (12). Subsequently, its prognostic value was confirmed in other cancers. In non-neoplastic diseases such as acute pancreatitis, myocardial infarction and acute respiratory distress syndrome, GLR also was shown to play an important role (29–31). Blood glucose was thought to be involved in the development of inflammation (32). The disturbance of glucose metabolism or

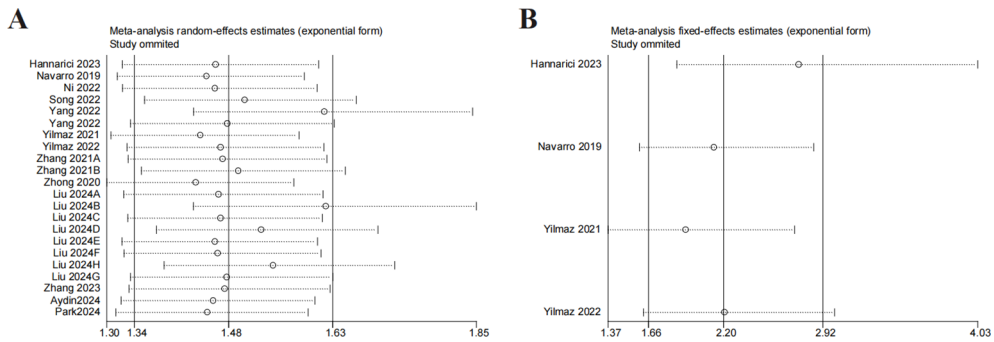

FIGURE 4
Sensitivity analysis. **(A)** sensitivity analysis for OS. **(B)** sensitivity analysis for DFS/PFS.

hyperglycemia was found to promote the proliferation of tumor cells and increase the risk of death in patients (33). As one of immune cells, lymphocyte played a vital role in anti-tumor immune defense. Lymphocytopenia in tumor patients predicted poor prognosis (34). By combining blood glucose level and lymphocytes, GLR overcame the limitations of using blood glucose level or lymphocytes alone, and can more effectively reflect the metabolic, inflammatory and immune status of tumor patients.

GLR had significant advantages in predicting the prognosis of tumor patients by evaluating the metabolic, inflammatory and immune status of tumor patients. However, the specific mechanism that GLR affected the prognosis of tumor patients remained unclear. We tried to explain the phenomenon by the composition of GLR.

Blood glucose is an important component of human plasma, and is a good indicator of the body's metabolic and endocrine functions. The survival of cancer cells is dependent on glucose. Hyperglycemia can promote the proliferation, invasion and migration of tumor cells, and enhance drug resistance of tumor cells (35). Hyperglycemia is conducive to the metabolic adaptation of tumor microenvironment and the maintenance of local immunosuppression (36). Hyperglycemia accelerates cancer progression by increasing reactive oxygen species levels (37). Elevated blood glucose levels produce many free radicals, leading

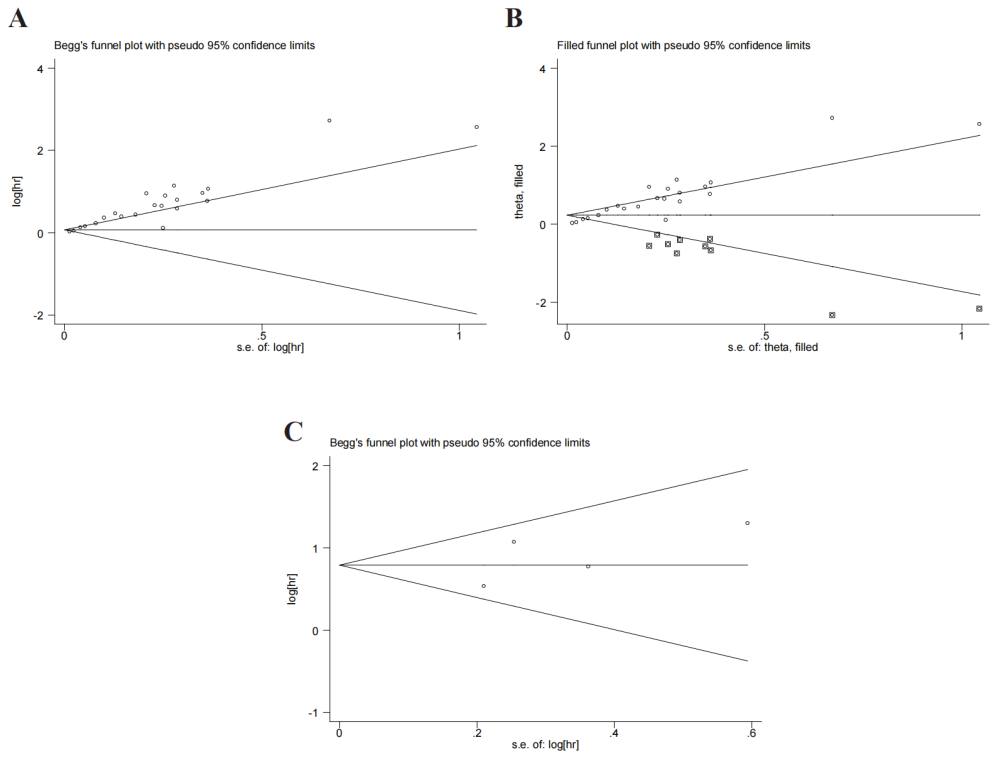

FIGURE 5
Publication bias. **(A)** publication bias for OS. **(B)** trim-and-fill method for OS. **(C)** publication bias for DFS/PFS.

to inflammation and metabolic disorders (38). Inflammation can accelerate cancer progression and lead to adverse survival (39). Evidence suggests that high blood glucose levels are associated with poor survival outcomes in a variety of tumors (40).

Lymphocyte as the important part of immune system plays an indispensable role in anti-tumor immune defense. Lymphocytes can inhibit tumor progression by directly inhibiting tumor cell proliferation (41). In addition, lymphocytes can activate cell-mediated immune responses and stimulate cytokines to promote tumor lysis (42). The data shows that T cells are more effective in suppressing anti-tumor immune response under hypoglycemic conditions (43). Accumulating evidences suggest that lymphocytes can reflect the nutritional status of patients (44). Studies have shown that high lymphocyte levels in the blood benefit the prognosis of patients with tumors, while lymphocytopenia may predict poorer survival outcomes (45, 46).

A high GLR indicated high glucose levels and a low lymphocyte count. The high GLR reflected more obvious the inflammation of tumor patients and the worse immune function of tumor patients. Therefore, it was not difficult to understand that high GLR was associated with a poor prognosis in patients with solid tumors.

There were some limitations in the study. Firstly, all articles had small sample sizes. Secondly, the included articles were retrospective studies. Thirdly, all studies included in the meta-analysis were conducted in Asia. More studies from other regions were warranted. Fourthly, publication bias for OS existed in the study. Finally, due to the lack of data, we were unable to assess the relationship between GLR and some pathological features.

Although there were some defects, the study also had some strengths. Firstly, we firstly demonstrated the prognostic value of GLR in solid tumors by meta-analysis. Secondly, the combined results were stable through sensitivity analysis. Thirdly, the trim-and-fill method found that the results for OS were unaffected by the publication bias. Finally, as a convenient serum marker, GLR can dynamically monitor the prognosis and therapeutic effect of patients with solid tumors.

In conclusions, we demonstrated that high GLR was associated with unfavorable survival outcome in solid tumors. GLR can serve as an effective prognostic indicator for patients with solid tumors, especially for liver, breast and pancreatic cancers. It can help doctors better identify high-risk patients so they can treat them more effectively. However, due to the shortcomings, more prospective studies were needed to confirm our findings.

Data availability statement

The original contributions presented in the study are included in the article/Supplementary Material. Further inquiries can be directed to the corresponding authors.

Author contributions

RL: Data curation, Formal analysis, Methodology, Writing – original draft. YS: Data curation, Methodology, Project administration, Writing – original draft. JC: Data curation, Formal analysis, Methodology, Writing – original draft. WM: Supervision, Validation, Writing – original draft. JW: Supervision, Validation, Writing – original draft. CC: Conceptualization, Project administration, Writing – review & editing. WW: Conceptualization, Project administration, Writing – review & editing.

Funding

The author(s) declare that no financial support was received for the research, authorship, and/or publication of this article.

Conflict of interest

The authors declare that the research was conducted in the absence of any commercial or financial relationships that could be construed as a potential conflict of interest.

Publisher's note

Supplementary material

The Supplementary Material for this article can be found online at: https://www.frontiersin.org/articles/10.3389/fimmu.2024.1454393/full#supplementary-material

References

1. Sung H, Ferlay J, Siegel RL, Laversanne M, Soerjomataram I, Jemal A, et al. Global cancer statistics 2020: GLOBOCAN estimates of incidence and mortality worldwide for 36 cancers in 185 countries. *CA Cancer J Clin*. (2021) 71:209–49. doi: 10.3322/caac.21660

2. Maomao C, He L, Dianqin S, Siyi H, Xinxin Y, Fan Y, et al. Current cancer burden in China: epidemiology, etiology, and prevention. *Cancer Biol Med*. (2022) 19:1121–38. doi: 10.20892/j.issn.2095-3941.2022.0231

3. Bray F, Laversanne M, Sung H, Ferlay J, Siegel RL, Soerjomataram I, et al. Global cancer statistics 2022: GLOBOCAN estimates of incidence and mortality worldwide for 36 cancers in 185 countries. *CA Cancer J Clin*. (2024) 74:229–63. doi: 10.3322/caac.21834

4. Greten FR, Grivennikov SI. Inflammation and cancer: triggers, mechanisms, and consequences. *Immunity*. (2019) 51:27–41. doi: 10.1016/j.immuni.2019.06.025

5. Mellman I, Chen DS, Powles T, Turley SJ. The cancer-immunity cycle: Indication, genotype, and immunotype. *Immunity*. (2023) 56:2188–205. doi: 10.1016/j.immuni.2023.09.011

6. Schab M, Skoczen S. Nutritional status, body composition and diet quality in children with cancer. *Front Oncol*. (2024) 14:1389657. doi: 10.3389/fonc.2024.1389657

7. Peng P, Chen L, Shen Q, Xu Z, Ding X. Prognostic Nutritional Index (PNI) and Controlling Nutritional Status (CONUT) score for predicting outcomes of breast cancer: A systematic review and meta-analysis. *Pak J Med Sci*. (2023) 39:1535–41. doi: 10.12669/pjms.39.5.7781

8. Guven DC, Sahin TK, Erul E, Kilickap S, Gambichler T, Aksoy S. The association between the pan-immune-inflammation value and cancer prognosis: A systematic review and meta-analysis. *Cancers (Basel)*. (2022) 14:2675. doi: 10.3390/cancers14112675

9. Song M, Zhang Q, Song C, Liu T, Zhang X, Ruan G, et al. The advanced lung cancer inflammation index is the optimal inflammatory biomarker of overall survival in patients with lung cancer. *J Cachexia Sarcopenia Muscle*. (2022) 13:2504–14. doi: 10.1002/jcsm.13032

10. Bose S, Le A. Glucose metabolism in cancer. *Adv Exp Med Biol*. (2018) 1063:3–12. doi: 10.1007/978-3-319-77736-8_1

11. Li L, Zou G, Liu J. Preoperative glucose-to-lymphocyte ratio is an independent predictor for acute kidney injury after cardiac surgery in patients in intensive care unit. *Int J Gen Med*. (2021) 14:6529–37. doi: 10.2147/IJGM.S335896

12. Navarro J, Kang I, Hwang HK, Yoon DS, Lee WJ, Kang CM. Glucose to lymphocyte ratio as a prognostic marker in patients with resected pT2 gallbladder cancer. *J Surg Res*. (2019) 240:17–29. doi: 10.1016/j.jss.2019.02.043

13. Yang M, Zhang Q, Ge Y, Tang M, Zhang X, Song M, et al. Glucose to lymphocyte ratio predicts prognoses in patients with colorectal cancer. *Asia Pac J Clin Oncol*. (2023) 19:542–8. doi: 10.1111/ajco.13904

14. Yılmaz A, Şimşek M, Hannarici Z, Büyükbayram ME, Bilici M, Tekin SB. The importance of the glucose-to-lymphocyte ratio in patients with hepatocellular carcinoma treated with sorafenib. *Future Oncol*. (2021) 17:4545–59. doi: 10.2217/fon-2021-0457

15. Hannarici Z, Yılmaz A, Buyukbayram ME, Turhan A, Çağlar AA, Bilici M, et al. The value of pretreatment glucose-to-lymphocyte ratio for predicting survival of metastatic gastric cancer. *Future Oncol*. (2023) 19:315–25. doi: 10.2217/fon-2022-0579

16. Park SH, Kang IC, Hong SS, Kim HY, Hwang HK, Kang CM. Glucose-to-lymphocyte ratio (GLR) as an independent prognostic factor in patients with resected pancreatic ductal adenocarcinoma-cohort study. *Cancers (Basel)*. (2024) 16:1844. doi: 10.3390/cancers16101844

17. Ni J, Li Z, Song W, Zhang H, Wang Y, Zhang Y, et al. Prognostic value of glucose to lymphocyte ratio for patients with renal cell carcinoma undergoing laparoscopic nephrectomy: A multi-institutional, propensity score matching cohort study. *Front Surg*. (2022) 9:911411. doi: 10.3389/fsurg.2022.911411

18. Yang M, Zhang Q, Ge YZ, Tang M, Hu CL, Wang ZW, et al. Prognostic roles of glucose to lymphocyte ratio and modified glasgow prognosis score in patients with non-small cell lung cancer. *Front Nutr*. (2022) 9:871301. doi: 10.3389/fnut.2022.871301

19. Zhang XW, Ge YZ, Song MM, Ruan GT, Xie HL, Hu CL, et al. Prognostic power of nutrition-inflammation indicators in patients with breast cancer. *Clin Breast Cancer*. (2023) 23:e312–21. doi: 10.1016/j.clbc.2023.04.009

20. Liu L, Zhang BB, Li YZ, Huang WJ, Niu Y, Jia QC, et al. Preoperative glucose-to-lymphocyte ratio predicts survival in cancer. *Front Endocrinol (Lausanne)*. (2024) 15:1284152. doi: 10.3389/fendo.2024.1284152

21. Stang A. Critical evaluation of the Newcastle-Ottawa scale for the assessment of the quality of nonrandomized studies in meta-analyses. *Eur J Epidemiol*. (2010) 25:603–5. doi: 10.1007/s10654-010-9491-z

22. Huedo-Medina TB, Sánchez-Meca J, Marín-Martínez F, Botella J. Assessing heterogeneity in meta-analysis: Q statistic or I2 index? *Psychol Methods*. (2006) 11:193–206. doi: 10.1037/1082-989X.11.2.193

23. Zeng YF, Wei XY, Guo QH, Chen SY, Deng S, Liu ZZ, et al. The efficacy and safety of anti-PD-1/PD-L1 in treatment of glioma: a single-arm meta-analysis. *Front Immunol*. (2023) 14:1168244. doi: 10.3389/fimmu.2023.1168244

24. Duval S, Tweedie R. Trim and fill: A simple funnel-plot-based method of testing and adjusting for publication bias in meta-analysis. *Biometric*. (2000) 56:455–63. doi: 10.1111/j.0006-341X.2000.00455.x

25. Aydin İC, Subasi IE, Sunar AO, Ademoglu S, Gulmez S, Dincer M, et al. GLR in colorectal cancers: an easily accessible prognostic marker. *Int J Gen Med*. (2024) 17:2361–9. doi: 10.2147/IJGM.S463769

26. Yilmaz H, Nigdelioglu B, Aytac A, Turan M, Oktay E, Yersal O, et al. The prognostic importance of glucose-to-lymphocyte ratio and uric acid in metastatic breast cancer patients treated with Cdk 4/6 inhibitors. *Future Oncol*. (2022) 18:3043–53. doi: 10.2217/fon-2022-0464

27. Zhang Y, Xu Y, Wang D, Kuang T, Wu W, Xu X, et al. Prognostic value of preoperative glucose to lymphocyte ratio in patients with resected pancreatic cancer. *Int J Clin Oncol*. (2021) 26:135–44. doi: 10.1007/s10147-020-01782-y

28. Zhong A, Cheng CS, Kai J, Lu R, Guo L. Clinical significance of glucose to lymphocyte ratio (GLR) as a prognostic marker for patients with pancreatic cancer. *Front Oncol*. (2020) 10:520330. doi: 10.3389/fonc.2020.520330

29. Liu J, Hu X. Association between glucose-to-lymphocyte ratio and in-hospital mortality in acute myocardial infarction patients. *PloS One*. (2023) 18:e0295602. doi: 10.1371/journal.pone.0295602

30. Zhang Y, Zhang S. Prognostic value of glucose-to-lymphocyte ratio in critically ill patients with acute respiratory distress syndrome: A retrospective cohort study. *J Clin Lab Anal*. (2022) 36:e24397. doi: 10.1002/jcla.24397

31. Chen Y, Tang S, Wang Y. Prognostic value of glucose-to-lymphocyte ratio in critically ill patients with acute pancreatitis. *Int J Gen Med*. (2021) 14:5449–60. doi: 10.2147/IJGM.S327123

32. Hotamisligil GS. Inflammation, metaflammation and immunometabolic disorders. *Nature*. (2017) 542:177–85. doi: 10.1038/nature21363

33. Hirakawa Y, Ninomiya T, Mukai N, Doi Y, Hata J, Fukuhara M, et al. Association between glucose tolerance level and cancer death in a general Japanese population: the Hisayama Study. *Am J Epidemiol*. (2012) 176:856–64. doi: 10.1093/aje/kws178

34. Wild AT, Ye X, Ellsworth SG, Smith JA, Narang AK, Garg T, et al. The association between chemoradiation-related lymphopenia and clinical outcomes in patients with locally advanced pancreatic adenocarcinoma. *Am J Clin Oncol*. (2015) 38:259–65. doi: 10.1097/COC.0b013e3182940ff9

35. Li W, Zhang X, Sang H, Zhou Y, Shang C, Wang Y, et al. Effects of hyperglycemia on the progression of tumor diseases. *J Exp Clin Cancer Res*. (2019) 38:327. doi: 10.1186/s13046-019-1309-6

36. Rice CM, Davies LC, Subleski JJ, Maio N, Gonzalez-Cotto M, Andrews C, et al. Tumour-elicited neutrophils engage mitochondrial metabolism to circumvent nutrient limitations and maintain immune suppression. *Nat Commun*. (2018) 9:5099. doi: 10.1038/s41467-018-07505-2

37. Li W, Liu H, Qian W, Cheng L, Yan B, Han L, et al. Hyperglycemia aggravates microenvironment hypoxia and promotes the metastatic ability of pancreatic cancer. *Comput Struct Biotechnol J*. (2018) 16:479–87. doi: 10.1016/j.csbj.2018.10.006

38. Wang B, Smyl C, Chen CY, Li XY, Huang W, Zhang HM, et al. Suppression of postprandial blood glucose fluctuations by a low-carbohydrate, high-protein, and high-omega-3 diet via inhibition of gluconeogenesis. *Int J Mol Sci*. (2018) 19:1823. doi: 10.3390/ijms19071823

39. Coussens LM, Werb Z. Inflammation and cancer. *Nature*. (2002) 420:860–7. doi: 10.1038/nature01322

40. Zhao H, Wu K. Effect of hyperglycemia on the occurrence and prognosis of colorectal cancer. *Am J Transl Res*. (2024) 16:2070–81. doi: 10.62347/NYHH3132

41. Zou Z, Li J, Ji X, Wang T, Chen Q, Liu Z, et al. Naples prognostic score as an independent predictor of survival outcomes for resected locally advanced non-small cell lung cancer patients after neoadjuvant treatment. *J Inflammation Res*. (2023) 16:793–807. doi: 10.2147/JIR.S401446

42. Koliaraki V, Prados A, Armaka M, Kollias G. The mesenchymal context in inflammation, immunity and cancer. *Nat Immunol*. (2020) 21:974–82. doi: 10.1038/s41590-020-0741-2

43. Kishton RJ, Sukumar M, Restifo NP. Metabolic regulation of T cell longevity and function in tumor immunotherapy. *Cell Metab*. (2017) 26:94–109. doi: 10.1016/j.cmet.2017.06.016

44. McMillan DC. Systemic inflammation, nutritional status and survival in patients with cancer. *Curr Opin Clin Nutr Metab Care*. (2009) 12:223–6. doi: 10.1097/MCO.0b013e32832a7902

45. Clark EJ, Connor S, Taylor MA, Madhavan KK, Garden OJ, Parks RW. Preoperative lymphocyte count as a prognostic factor in resected pancreatic ductal adenocarcinoma. *HPB (Oxford)*. (2007) 9:456–60. doi: 10.1080/13651820701774891

46. Lee YJ, Chung YS, Lee JY, Nam EJ, Kim SW, Kim S, et al. Pretreatment lymphocytopenia is an adverse prognostic biomarker in advanced-stage ovarian cancer. *Cancer Med*. (2019) 8:564–71. doi: 10.1002/cam4.2019.8.issue-2

frontiers | Frontiers in Oncology

TYPE Original Research
PUBLISHED 03 January 2025
DOI 10.3389/fonc.2024.1511530

OPEN ACCESS

EDITED BY
Matteo Becatti,
University of Firenze, Italy

REVIEWED BY
Raziye Özdemir,
Karabük University, Türkiye
Pengpeng Ye,
Chinese Center For Disease Control and Prevention, China

*CORRESPONDENCE
Jihong Zhou
1103244278@qq.com

RECEIVED 17 October 2024
ACCEPTED 10 December 2024
PUBLISHED 03 January 2025

CITATION
Wang Y, Zhu J, Wang S and Zhou J (2025) The trends of lung cancer burden in BRICS from 1990 to 2021 and its projection to 2035. *Front. Oncol.* 14:1511530. doi: 10.3389/fonc.2024.1511530

The trends of lung cancer burden in BRICS from 1990 to 2021 and its projection to 2035

Yifan Wang[1], Jingwen Zhu[2], Shaoqiang Wang[3] and Jihong Zhou[1]*

[1]The Seventh Clinical College of Guangzhou University of Chinese Medicine, Shenzhen, China, [2]The Fourth Clinical College of Guangzhou University of Chinese Medicine, Shenzhen, China, [3]The Information and Control Engineering College of Qingdao University of Technology, Qingdao, China

Background: Lung cancer has become the malignant tumor with the highest morbidity and mortality in the world. This study aims to analyze the burden of lung cancer and risk factors associated with lung cancer in the BRICS from 1990-2021 and to project the burden of lung cancer in the BRICS from 2021-2035.

Methods: The Global Burden of Disease (GBD) 2021 database was searched to collect the incidence, prevalence, mortality, disability-adjusted life years (DALYs), and risk factors of lung cancer in the BRICS. Trends in lung cancer burden from 1990-2021 were analyzed using Joinpoint 4.9.1.0, and Bayesian age-period-cohort (BAPC) analyses were performed using R4.4.1 to project the disease burden of lung cancer from 2021-2035.

Results: AAPC(average annual percentage change) and EAPC(estimated average percentage change) of ASIR(age-standardized incidence), ASPR(age-standardized prevalence), ASMR(age-standardized mortality), and ASDR(age-standardized disability-adjusted life year) for lung cancer in Brazil, Russia, and Ethiopia 1990-2021 were less than 0. Egypt's AAPC and EAPC for ASIR, ASPR, ASMR, and ASDR were all greater than 0 for 1990-2021, and China's ASIR, ASPR, ASMR, and ASDR were all at the top of the BRICS in 2021. According to BAPC projection Brazil, Iran, Russia, and South Africa will have a decreasing trend in ASIR, ASPR, ASMR, and ASDR from 2021-2035. Egypt will have an increasing trend in ASIR, ASPR, ASMR, and ASDR from 2021-2035. With the exception of Ethiopia, the top tier level 1 and level 2 risk factors in the rest of the BRICS were behavioral factors and smoking factors, respectively.

Conclusion: The BRICS still have a heavy burden of lung cancer, and there are significant differences in the burden of lung cancer among the BRICS. At the same time, many BRICS lung cancer prevention and control measures are worth learning from other developing countries.

KEYWORDS

lung cancer, GBD database, burden of disease, risk factors, BRICS

1 Introduction

Lung cancer, also known as primary bronchopulmonary cancer, refers to malignant tumors originating from the bronchial mucosa or glands that originate in the lungs (1). According to the global cancer statistics report released by the World Health Organization (WHO), in 2022, there were 2.5 million new cases of lung cancer globally, accounting for about one-eighth of all new malignant tumors, and 1.82 million deaths, accounting for about one-fifth of all malignant tumor deaths. Lung cancer has become the malignant tumor with the highest global morbidity and mortality and is the leading cause of cancer morbidity and mortality in men and the 2nd leading cause of cancer morbidity and mortality in females worldwide (1).

BRICS is an international cooperation organization comprising emerging markets and developing countries that aims to promote economic, political, and social cooperation among member countries and to advance the reform of the global governance system. BRICS initially consisted of five countries, Brazil, Russia, India, China, and South Africa. On January 1, 2024, with Saudi Arabia, Egypt, the United Arab Emirates, Iran, and Ethiopia becoming full members of BRICS, the number of BRICS member countries increased from five to ten, and BRICS achieved a historic expansion. Data show that after the expansion of the BRICS accounted for nearly half of the world's population, nearly 30% of the world's total economic output, and nearly 40% of the world's total industrial value (2). The BRICS are facing many problems such as population aging, environmental pollution, imbalance of health resources, high smoking rates, and industrial pollution along with rapid economic and social development, which may lead to an increase in the incidence, prevalence, mortality, and DALYs of lung cancer. Therefore, an in-depth understanding of the burden of lung cancer and the main risk factors behind it in the BRICS, which can be used to optimize public health policies, rationalize the allocation of health resources, and evaluate the effectiveness of interventions, is of great significance in reducing the burden of lung cancer and improving public health.

GBD database covers the incidence rate, morbidity, mortality, and DALYs of lung cancer (3). Therefore, this study quantifies the overall burden of lung cancer in the BRICS based on the GBD database, provides focus and direction for lung cancer prevention and treatment in the relevant countries, and provides data support for health policy decision-makers to accurately and efficiently allocate healthcare resources, identify high-risk populations, and formulate prevention strategies.

2 Materials and methods

2.1 Data sources

The data of this study were based on the GBD 2021 database published by the Institute for Health Metrics and Evaluation at the University of Washington in the United States of America (4).

2.2 Research method

In this study, "tracheal, bronchial and lung cancers" (International Classification of Diseases (ICD) 10 codes: C33-C34.9, D02.1-D02.3, D14.2-D14.3, and D38.1) were selected as the classification criteria for lung cancer. ASIR, ASPR, ASMR, ASDR, and 95% uncertainty intervals (95% UI) for the BRICS (Brazil, Russia, India, China, South Africa, Saudi Arabia, Egypt, UAE, Iran, and Ethiopia) for the years 1990-2021 were extracted from the GBD database (5). And calculate the AAPC, EAPC, and 95% UI of the ASIR, ASPR, ASMR, and ASDR of the BRICS from 1990 to 2021. Simultaneously using BAPC to predict the ASIR, ASPR, ASMR, and ASDR of lung cancer from 2021 to 2035. The GBD2021 database categorizes disease risk factors at four levels, with level 1 covering three major categories of risk factors, including environmental/occupational risks, behavior risks, and metabolic risks, and the subsequent levels continue to be subdivided on this basis (6). In this study, we calculated the proportion of lung cancer deaths attributable to the corresponding risk factors to the total number of lung cancer deaths, the proportion of lung cancer DALYs attributable to the corresponding risk factors to the total lung cancer DALYs, and the change of both from 1990 to 2021, respectively.

2.3 Statistical methods

Use Excel 2023 and the tidyverse and reshape2 packages in R 4.4.1 for data organization. The joinpoint regression model is a collection of linear statistical models that were used to evaluate the trends in disease burdens attributable to lung cancer across time. This model's calculating approach is to estimate the changing rule of illness rates using the least square method, avoiding the non-objectivity of typical trend analyses based on linear trends (7). In this study, Joinpoint 4.9.1.0 was used for AAPC analysis to describe the overall trend of disease burden. The EAPC value is calculated by a linear regression model and is widely used in the field of public health. Its role is to summarize the age-standardized rate trend in a specific time interval (8). This study used the GBDR package in R 4.4.1 for EAPC analysis.The BAPC model is based on the age period cohort analysis (APC) model. However, there is a linear relationship between the three factors in the APC model, which makes parameter estimation difficult. Therefore, a Bayesian model is added on the basis of the APC model. Bayesian model can estimate the prior information of unknown parameters and sample information to obtain the posterior distribution and infer the unknown parameters according to the posterior distribution. The model estimates the posterior edge distribution directly using the integrated nested Laplace approximation (INLA) algorithm. Because the expected effects of time adjacency may be similar, the second-order random walk (RW2) model is used to study the influence of age, period, and cohort, and estimate the number of cases, age-specific incidence, and standardized incidence (9). The BAPC package and INLA package in r.4.4.1 were used for BAPC analysis in this study (10).

3 Result

3.1 Burden of disease

The country with the highest lung cancer incidence among the BRICS in 2021 was China, with an ASIR of 44.0/100,000 (95% UI: 35.45, 53.35), which ranked 7th out of 204 countries and territories in the world in terms of ASIR, and the lowest was India, with an ASIR of 5.99 per 100,000 (95% UI: 4.92, 6.92), as shown in Figure 1. The ASIR for lung cancer in China, Egypt, India, and South Africa all showed an increasing trend (EAPC>0) compared to 1990. The largest increase was in Egypt, with an EAPC of 3.99 (95% CI: 3.42, 4.56), as shown in Figure 2, Table 1. The ASIR for lung cancer in the rest of the BRICS except China in 2021 was below the global average of 26.43/100,000 (95% UI: 23.90, 29.07).

The highest lung cancer prevalence in BRICS in 2021 was in China, with an ASPR of 57.95/100,000 (95% UI: 46.20, 70.78), which ranked 18th out of 204 countries and territories in terms of lung cancer ASPR, and the lowest was in India, with an ASPR of 6.32/100,000 (95% UI: 5.19, 7.30), as shown in Figure 1B. The ASPR of lung cancer in China, Egypt, India, and Iran showed an increasing trend (EAPC>0) compared with 1990. The largest increase was in Egypt, with an EAPC of 3.68 (95% CI: 3.17, 4.19), as shown in Figure 3, Table 2. The ASPR for lung cancer in 2021 in all BRICS except China was below the global average of 37.28/100,000 (95% UI: 33.76, 40.77).

The highest lung cancer mortality in BRICS in 2021 was in China with an ASMR of 38.98/100,000 (95% UI: 31.40, 47.06), which ranked 9th out of 204 countries and territories, and the lowest was in India with an ASMR of 6.23/100,000 (95% UI: 5.12, 7.19), as shown in Figure 1C. The ASMR of lung cancer in China, Egypt, India, and Iran showed an increasing trend (EAPC>0) compared with 1990. The largest increase was in Egypt, with an EAPC of 4.09 (95% CI: 3.51, 4.68), as shown in Figure 4, Table 3. The ASMR for lung cancer in the rest of the BRICS except China in 2021 was below the global average of 23.50/100,000 (95% UI: 21.22, 25.85).

The highest lung cancer DALYs in BRICS in 2021 was in China with an ASDR of 878.24/100,000 (95% UI: 703.53, 1068.71), which ranked 12th out of 204 countries and territories, and the lowest was in Saudi Arabia with an ASDR of 158.31/100,000 (95% UI: 124.44, 199.60), as shown in Figure 1D. Compared with 1990, Egypt and India ASDR showed an increasing trend (EAPC>0). The largest increase was in Egypt with an EAPC of 6.22 (95% UI:5.98, 6.46), as shown in Figure 5, Table 4. In 2021 The ASMR for lung cancer in the rest of the BRICS except China in 2021 was below the global average of 533.00/100,000 (480.13, 586.36).

In terms of gender, ASIR, ASPR, ASMR, and ASDR for lung cancer were higher in males than females in all BRICS except UAE, where ASIR, ASPR, ASMR, and ASDR for lung cancer were higher in female than male lung cancer patients after 2014.

3.2 Risk factors

The different levels of lung cancer risk factors obtained in this study are as follows: Level 1 includes metabolic, environmental/occupational, and behavioral risks; level 2 includes tobacco (cigarette smoking, secondhand smoke), dietary risks (low-fruit diet), air pollution (ambient particulate matter pollution, indoor air pollution due to solid fuels), other environmental risks (indoor radon contamination), occupational risks (occupational exposure to asbestos, chromium, arsenic, beryllium, nickel, cadmium, diesel engine exhaust, polycyclic aromatic hydrocarbons, and silica), and high fasting blood glucose levels.

In 2021, among the level 1 risk factors, the ratio of lung cancer deaths attributable to behavioral risks to all lung cancer deaths was highest in all BRICS except Ethiopia, and the ratio of DALYs attributable to behavioral risks to total DALYs was highest in all BRICS except Ethiopia. In 2021, the number of lung cancer deaths attributed to behavioral risks in Russia accounted for 67.77% (95% CI: 63.46, 71.94) of all lung cancer deaths in the country, making it the country with the highest proportion of behavioral risks among BRICS. In 2021, the number of lung cancer deaths attributed to environmental/

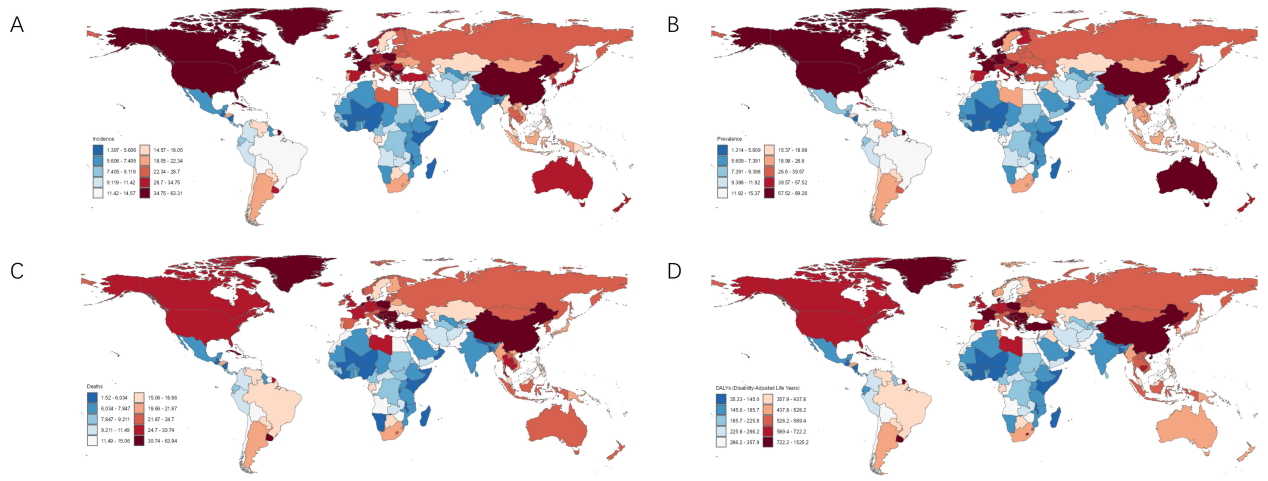

FIGURE 1
Burden of disease for lung cancer in 204 countries and territories in 2021. **(A)** ASIR; **(B)** ASPR; **(C)** ASMR; **(D)** ASDR.

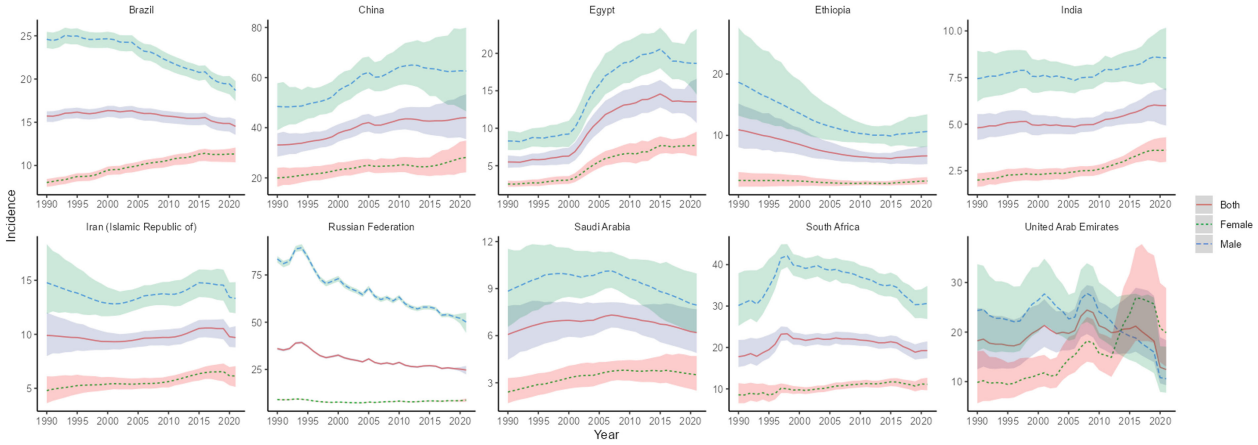

FIGURE 2
Time trend of ASIR in lung cancer in BRICS from 1990 to 2021. The blue line and its surrounding area represent the projection curves and uncertainty intervals for males; The green line and its surrounding area represent the projection curves and uncertainty intervals for females; The red line and its surrounding area represent the projection curves and uncertainty intervals for both sexes in total.

occupational risks in Ethiopia accounted for 47.88% (95% CI: 35.06, 59.27) of all lung cancer deaths in the country, making it the country with the highest proportion of environmental/occupational risks among BRICS, as shown in Figure 6A. DALYs attributable to behavioral risks accounted for 70.47% (95% CI:66.39, 74.63) of total DALYs in 2021 in Russia, the highest percentage of behavioral risks among BRICS. DALYs attributable to environmental/occupational risks accounted for 47.25% (95% CI: 38.92, 55.27) of total DALYs in Ethiopia in 2021, the highest proportion of environmental/occupational risks among BRICS, as shown in Figure 6B.

In 2021, among the level 2 risk factors, all BRICS except Ethiopia had the highest proportion of lung cancer deaths attributable to the risk of smoking as a percentage of all lung cancer deaths, and all BRICS except Ethiopia had the highest proportion of DALYs attributable to the risk of smoking as a percentage of total DALYs. The number of lung cancer deaths attributable to the risk of smoking accounted for 66.54% (95% CI: 62.20, 70.97) of all lung cancer deaths in Russia in 2021, making it the BRICS with the highest proportion of smoking risk. In 2021, the number of lung cancer deaths attributed to air pollution in Ethiopia accounted for 41.23% (95% CI: 28.30, 52.80) of all lung cancer deaths, making it the country with the highest proportion of air pollution risk among BRICS, as shown in Figure 7A. In 2021, DALYs attributed to smoking risks accounted for 69.34% (95% CI: 65.11, 73.55) of the total DALYs in Russia, making it the country with the highest proportion of smoking risks among BRICS. In 2021, DALYs attributed to air pollution accounted for 41.06% (95% CI: 28.16, 52.61) of the total DALYs in Ethiopia, making it the country with the highest proportion of air pollution risks among BRICS, as shown in Figure 7B.

TABLE 1 ASIR and tends of lung cancer in BRICS.

Country	Age-standardized incidence per 100,000 population (95% UI)		EAPC (95% CI)	AAPC (95% CI)
	1990	2021		
Brazil	15.72(15.05, 16.27)	14.53(13.54, 15.34)	-0.24(-0.32, -0.16)	-0.03(-0.04, -0.03)
China	33.11(28.47, 37.79)	44.01(35.45, 53.35)	1.03(0.88, 1.17)	0.34(0.32, 0.37)
Egypt	5.50(4.72, 6.37)	13.53(10.69, 16.61)	3.99(3.42, 4.56)	0.26(0.25, 0.26)
Ethiopia	10.91(8.07, 15.19)	6.66(5.33, 8.25)	-1.89(-2.15, -1.63)	-0.14(-0.14, -0.14)
India	4.80(4.15, 5.54)	5.99(4.92, 6.92)	0.63(0.47, 0.79)	0.04(0.04, 0.05)
Iran (Islamic Republic of)	9.90(7.98, 12.02)	9.70(8.79, 10.75)	0.24(0.11, 0.37)	-0.01(-0.01, -0.00)
Russian Federation	36.01(35.27, 36.63)	24.69(22.35, 26.86)	-1.35(-1.51, -1.19)	-0.33(-0.37, -0.29)
Saudi Arabia	6.08(4.46, 7.89)	6.19(4.90, 7.69)	0.02(-0.18, 0.22)	0.00(-0.00, 0.01)
South Africa	17.78(15.28, 21.82)	19.24(17.39, 21.47)	0.14(-0.17, 0.45)	0.03(0.00, 0.05)
United Arab Emirates	18.25(12.48, 24.84)	12.43(9.28, 18.37)	-0.04(-0.60, 0.52)	-0.23(-0.31, -0.14)
Gobal	28.54(27.06, 29.91)	26.43(23.90, 29.07)	-0.24(-0.31, -0.17)	-0.07(-0.08, -0.06)

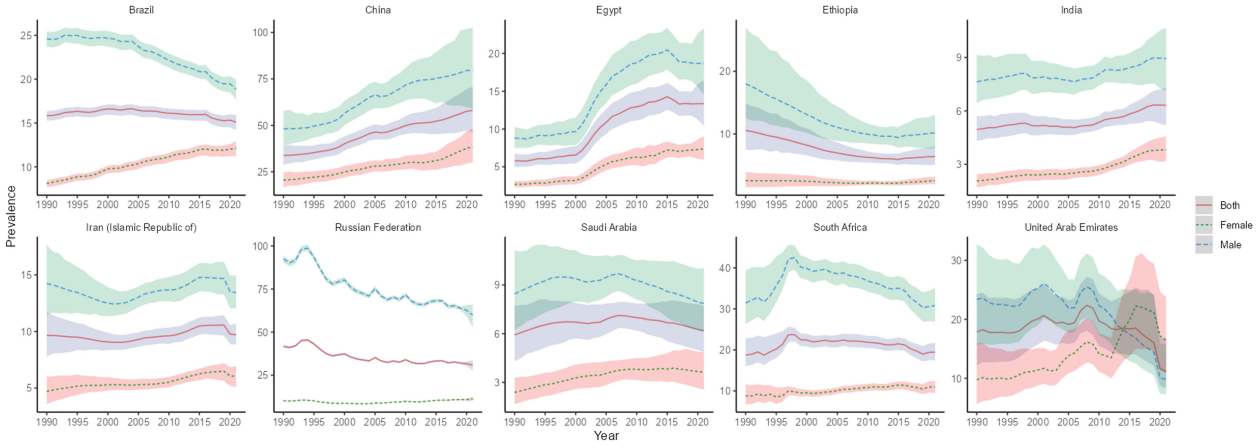

FIGURE 3
Time trend of ASPR in lung cancer in BRICS from 1990 to 2021. The blue line and its surrounding area represent the projection curves and uncertainty intervals for males; The green line and its surrounding area represent the projection curves and uncertainty intervals for females; The red line and its its surrounding area represent the projection curves and uncertainty intervals for both sexes in total.

3.3 Projection of disease burden trends

According to BAPC projection Brazil, Iran, Russia, and South Africa will have a decreasing trend in ASIR, ASPR, ASMR, and ASDR from 2021-2035. Egypt will have an increasing trend in ASIR, ASPR, ASMR, and ASDR from 2021-2035. By 2035, China's lung cancer ASIR [50.96/100,000 (95% UI:28.90, 73.02)], ASPR [63.61/100,000 (95% UI:56.55, 70.68)], ASMR [36.53/100,000 (95% UI:32.38, 40.69)] and ASDR [916.28/100,000 (95% UI:500.19, 1332.37)] will be the highest in the BRICS. China's lung cancer ASIR, ASPR, and ASDR will be in an upward trend during 2021-2035, but China's lung cancer ASMR will be in an upward trend during 2021-2032 and then in a downward trend during 2022-2035, as shown in Figure 8A. By 2035, Ethiopia's lung cancer ASIR [4.87/100000 (95% UI: 3.70, 6.04)], ASPR [4.89/100000 (95% UI: 3.77, 6.01)], ASMR [5.27/100000 (95% UI: 4.02, 6.53)], and ASDR [132.4/100000 (95% UI: 105.13159.66)] will all be the lowest among BRICS, as shown in Figure 8B.

4 Discussion

As an emerging global multilateral cooperation mechanism and the most rapidly developing economic cooperation organization today, BRICS has gradually become an important force in global governance, but due to factors such as the continuous advancement of population aging, the frequent occurrence of epidemics, the problem of accessibility to medicines, the acceleration of the urbanization process, the changes in lifestyle brought about by economic development, and the relatively weak public health

TABLE 2 ASPR and trends of lung cancer in BRICS.

Country	Age-standardized prevalence per 100,000 population (95% UI)		EAPC (95% CI)	AAPC (95% CI)
	1990	2021		
Brazil	15.85(15.28, 16.35)	15.09(14.23, 15.89)	-0.16(-0.24, -0.08)	-0.02(-0.03, -0.02)
China	33.74(28.90, 38.65)	57.95(46.20, 70.78)	1.91(1.80, 2.02)	0.77(0.74, 0.80)
Egypt	5.80(4.99, 6.74)	13.35(10.44, 16.42)	3.68(3.17, 4.19)	0.24(0.23, 0.25)
Ethiopia	10.55(7.56, 14.85)	6.41(5.10, 8.02)	-1.93(-2.19, -1.66)	-0.13(-0.14, -0.13)
India	4.96(4.31, 5.71)	6.32(5.19, 7.30)	0.71(0.55, 0.87)	0.04(0.04, 0.05)
Iran (Islamic Republic of)	9.65(7.77, 11.69)	9.71(8.82, 10.68)	0.33(0.18, 0.48)	-0.00(-0.01, 0.00)
Russian Federation	41.76(40.94, 42.43)	30.78(27.76, 33.62)	-1.06(-1.27, -0.85)	-0.32(-0.41, -0.23)
Saudi Arabia	5.92(4.29, 7.73)	6.19(4.86, 7.73)	0.13(-0.05, 0.31)	0.01(0.00, 0.01)
South Africa	18.71(16.07, 22.90)	19.46(17.50, 21.74)	0.00(-0.27, 0.27)	-0.00(-0.03, 0.03)
United Arab Emirates	17.89(12.21, 24.27)	11.16(8.34, 16.53)	-0.56(-1.09, -0.04)	-0.21(-0.26, -0.17)
Gobal	34.25(32.66, 35.69)	37.28(33.76, 40.77)	0.40(0.27, 0.53)	0.09(0.08, 0.10)

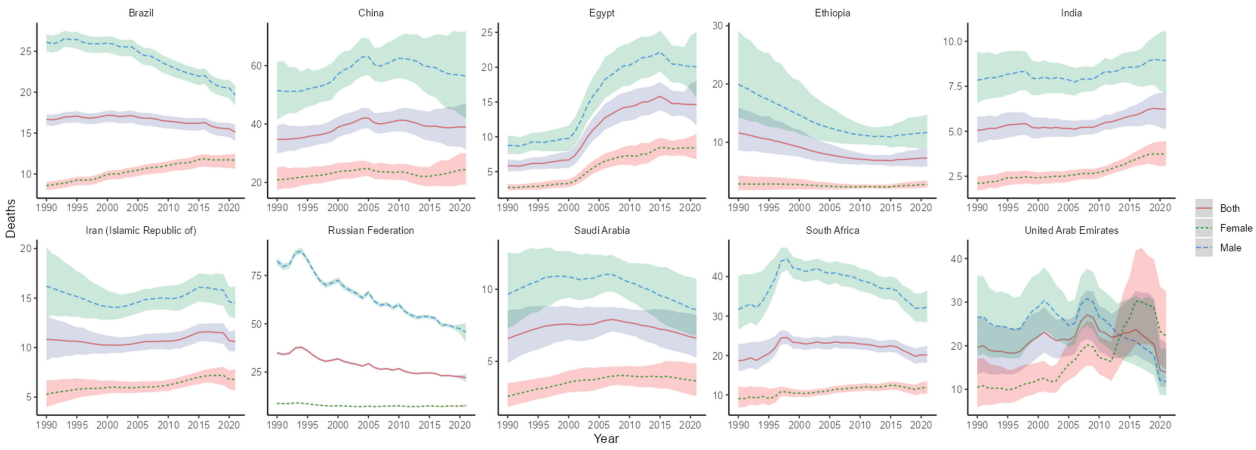

FIGURE 4
Time trend of ASMR in lung cancer in BRICS from 1990 to 2021. The blue line and its surrounding area represent the projection curves and confidence intervals for males; The green line and its surrounding area represent the projection curves and uncertainty intervals for females; The red line and its surrounding area represent the projection curves and uncertainty intervals for both sexes in total.

capacity building in developing countries, BRICS are also facing common public health security challenges (11, 12). In 2021, BRICS accounted for approximately 50.16%, 45.69%, 49.72%, and 51.83% of global lung cancer deaths, prevalence, incidence, and DALYs, respectively. There are also large differences in the burden of lung cancer, predicted trends, and risk factors among BRICS.

Brazil is the largest and most populous country in Latin America, and the largest emerging economy in Latin America. The AAPC and EAPC of ASIR, ASPR, ASMR, and ASDR of lung cancer in Brazil were all less than 0 in 1990-2021, and according to the BAPC projection, from 2021 to 2035, ASIR, ASPR, ASMR, and ASDR will all be in a decreasing trend. This may be related to the smoking ban and environmental protection measures in Brazil. Since 1990, the Brazilian government has formulated a number of powerful anti-smoking measures, such as banning smoking in public places, raising the tax rate of tobacco products, and setting health warning labels on cigarette packages (13). In 2006, the smoking population in Brazil accounted for 15,7% of the national population, while by 2018, the smoking population accounted for only 9,3% of the national population, a decrease of nearly 40% (14). In terms of environmental governance, Brazil's Air Pollution Control Program for Motor Vehicles was established in 1987 to reduce vehicle air pollution. Brazil also established a National Programme for Control of Air Quality in 1989 which established strategies for setting national standards for air quality and emissions at source (15). Although the burden of lung cancer in Brazilian males was in a decreasing trend between 1990 and 2021, the ASIR, ASPR, ASMR, and ASDR of lung cancer in Brazilian females were in an increasing trend between 1990 and 2021. Although there were fewer female smokers compared to males, the reduction in the number of smokers in females was also lower compared to males (16). According to the findings, females are 31% less likely to quit

TABLE 3 ASMR and trends in lung cancer in BRICS.

Country	Age-standardized rate (per 100000)		EAPC (95% CI)	AAPC (95% CI)
	1990	2021		
Brazil	16.66(15.91, 17.26)	15.12(14.04, 15.98)	-0.28(-0.36, -0.21)	-0.05(-0.06, -0.04)
China	34.74(29.96, 39.52)	38.98(31.40, 47.06)	0.42(0.24, 0.60)	0.15(0.11, 0.18)
Egypt	5.83(4.99, 6.74)	14.63(11.55, 17.96)	4.09(3.51, 4.68)	0.28(0.27, 0.29)
Ethiopia	11.59(8.63, 15.98)	7.27(5.85, 8.98)	-1.79(-2.04, -1.54)	-0.14(-0.14, -0.14)
India	5.05(4.37, 5.83)	6.23(5.12, 7.19)	0.59(0.44, 0.75)	0.04(0.04, 0.05)
Iran (Islamic Republic of)	10.83(8.71, 13.16)	10.61(9.59, 11.76)	0.23(0.10, 0.36)	-0.01(-0.01, -0.00)
Russian Federation	35.00(34.29, 35.64)	22.14(20.09, 24.09)	-1.66(-1.79, -1.52)	-0.39(-0.47, -0.30)
Saudi Arabia	6.58(4.88, 8.54)	6.62(5.26, 8.19)	-0.03(-0.24, 0.18)	0.00(-0.00, 0.00)
South Africa	18.63(16.04, 22.89)	20.14(18.17, 22.44)	0.14(-0.18, 0.45)	0.02(-0.00, 0.05)
United Arab Emirates	19.65(13.51, 26.47)	13.85(10.43, 20.65)	0.15(-0.43, 0.72)	-0.22(-0.32, -0.13)
Gobal	27.58(26.09, 28.99)	23.50(21.22, 25.85)	-0.54(-0.60, -0.47)	-0.14(-0.15, -0.13)

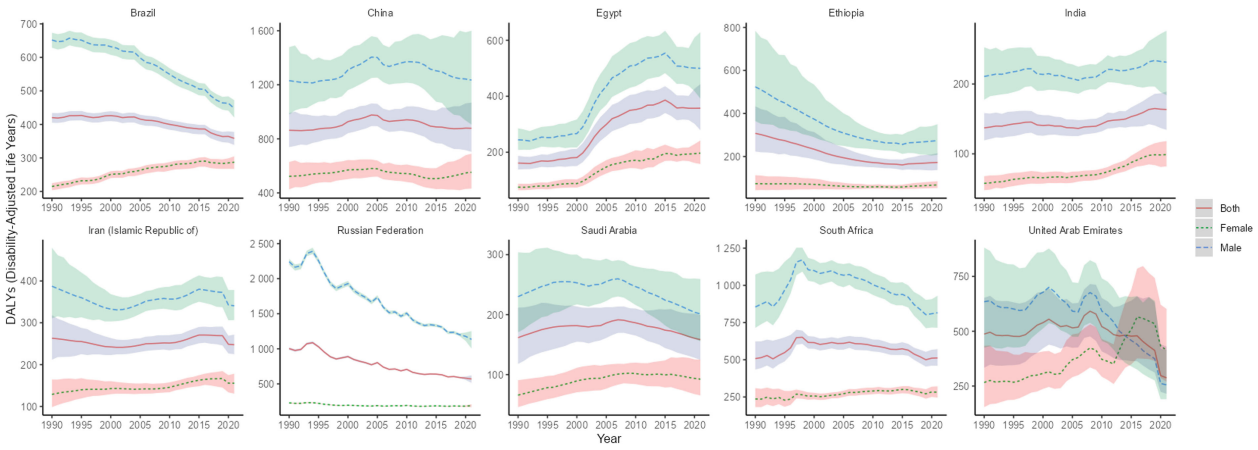

FIGURE 5
Time trend of ASDR in lung cancer in BRICS from 1990 to 2021. The blue line and its surrounding area represent the projection curves and confidence intervals for males; The green line and its surrounding area represent the projection curves and uncertainty intervals for females; The red line and its surrounding area represent the projection curves and uncertainty intervals for both sexes in total.

smoking than men, and the percentage of females who succeed in quitting smoking is also lower compared to men (17). Moreover, the type of lung cancer with high incidence in females is lung adenocarcinoma, and the type of lung cancer with high incidence in males is lung squamous cell carcinoma. Compared with lung squamous cell carcinoma, the relationship between lung adenocarcinoma and smoking is relatively low. Therefore, after the decline in the proportion of smokers, the decline in the burden of lung cancer in women is less significant than that in men (18). Based on the above, the Brazilian government should pay more attention to females' lung cancer burden in the future of lung cancer prevention and control.

China is one of the permanent members of the United Nations Security Council, the third largest country in the world in terms of land area and the second largest economy in the world. In 2022, the number of female lung cancer cases accounted for 17.5% of female malignant tumors in China, surpassing that of breast cancer (15.6%), and in China lung cancer ranked first in terms of morbidity and mortality among malignant tumors for both males and females (19, 20). China's ASIR, ASPR, ASMR, and ASDR of lung cancer were the first in BRICS, and the AAPC and EAPC of China's lung cancer ASIR, ASPR, and ASMR were greater than 0 from 1990 to 2021, the EAPC95% UI of ASDR passed through 0, and the AAPC of ASDR was greater than 0. The projection of BAPC showed that from 2021-2035 China's lung cancer ASIR, ASPR, and ASDR will be in an upward trend. Studies have shown that the prevalence of smoking among Chinese males is as high as 60% (21), and the prevalence of smoking among Chinese females and adolescents is rapidly increasing (22). The willingness of Chinese smokers to quit is low, only 16.1% of smokers plan to or consider

TABLE 4 ASDR and trends in lung cancer in BRICS.

Country	Age-standardized DALYs per 100,000 population (95% UI)		EAPC (95% CI)	AAPC (95% CI)
	1990	2021		
Brazil	420.31(405.09, 434.13)	358.46(338.55, 377.47)	-0.52(-0.61, -0.43)	-1.99(-2.16, -1.83)
China	863.54(738.86, 991.39)	878.24(703.53, 1068.71)	0.07(-0.09, 0.22)	0.66(0.04, 1.29)
Egypt	161.37(138.44, 187.31)	357.30(278.46, 443.28)	3.54(3.03, 4.06)	6.22(5.98, 6.46)
Ethiopia	307.74(223.09, 433.51)	172.44(137.47, 215.52)	-2.20(-2.47, -1.94)	-4.37(-4.45, -4.30)
India	137.23(119.37, 158.43)	163.58(134.43, 189.13)	0.49(0.34, 0.64)	0.85(0.76, 0.94)
Iran (Islamic Republic of)	263.05(211.58, 318.24)	247.42(224.91, 271.78)	0.12(-0.02, 0.26)	-0.60(-0.75, -0.45)
Russian Federation	1003.29(984.26, 1020.47)	569.75(513.85, 621.48)	-2.06(-2.21, -1.90)	-12.88(-14.10, -11.66)
Saudi Arabia	161.60(117.77, 211.66)	158.31(124.44, 199.60)	-0.07(-0.28, 0.13)	-0.12(-0.24, -0.00)
South Africa	507.87(434.31, 623.40)	512.22(459.74, 571.46)	-0.10(-0.41, 0.21)	0.35(-0.63, 1.34)
United Arab Emirates	487.00(333.49, 652.53)	287.29(214.77, 429.88)	-0.75(-1.29, -0.21)	-6.93(-8.69, -5.17)
Gobal	690.86(654.39, 725.97)	533.00(480.13, 586.36)	-0.87(-0.93, -0.81)	-5.20(-5.34, -5.06)

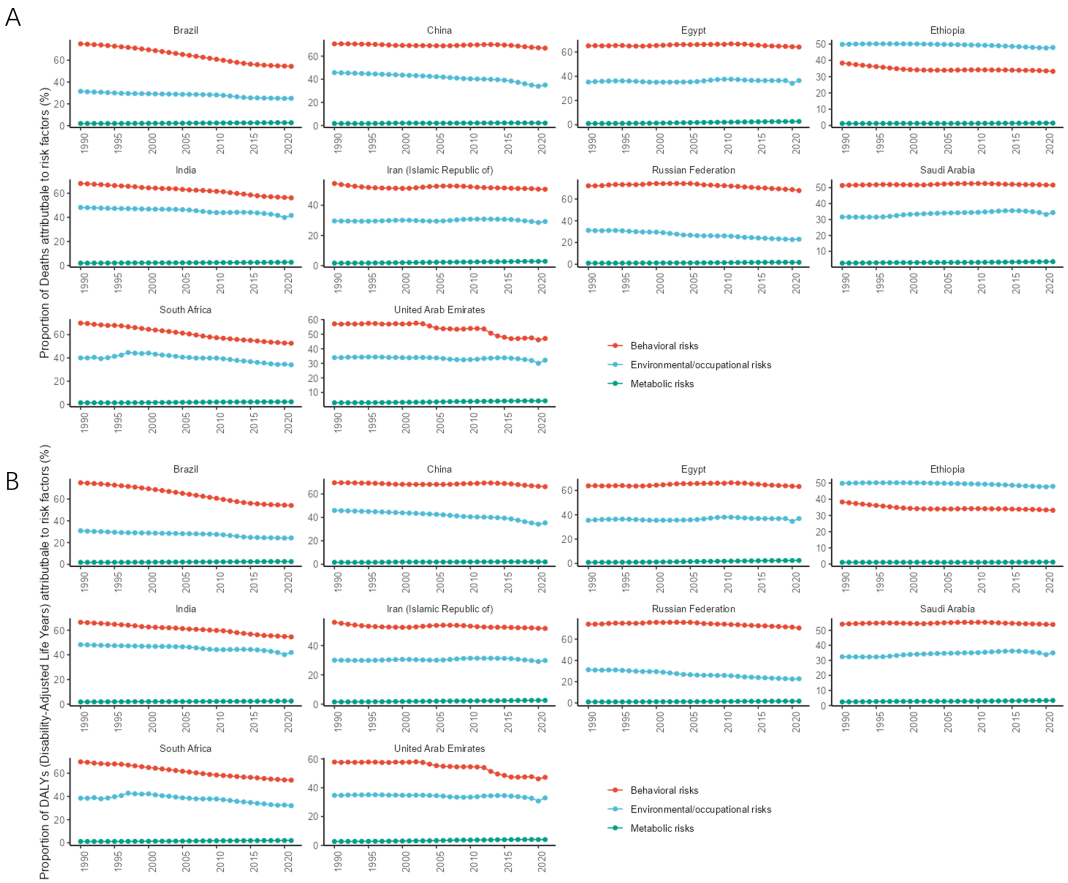

FIGURE 6
Time trend of the proportion of level 1 risk factors for lung cancer in BRICS from 1990 to 2021. **(A)** Proportion of deaths; **(B)** Proportion of DALYs.

quitting (21). Meanwhile, with the rapid development of industrialization and transportation in China, especially the extensive use of coal and petroleum, several hazardous substances have been emitted into the atmosphere, exacerbating the high lung cancer disease burden in China (23). Previous studies have shown that there is a dose-response relationship between lung cancer risk and exposure to cooking fumes and that Chinese cooking is typically more likely to result in the evaporation of fumes compared to its regional cooking methods (24). Not only that, China has one of the highest levels of population aging in the world, but also the highest level of population aging among the BRICS (25), and the increase in the proportion of the older adult population has exacerbated the disease burden of lung cancer. Although China's economic development and medical level have significantly improved after the reform and opening up, there is still a huge gap in the level of medical security between urban and rural areas. According to data from the National Bureau of Statistics of China, the per capita medical and health expenditure of urban residents in 2023 (2850 yuan) was 1.49 times that of rural residents (1916 yuan). At the same time, in 2023, the per capita financing of employee medical insurance (6182 yuan) was 5.63 times that of urban and rural residents' medical insurance (1098 yuan). The above data all indicate an extreme imbalance in the allocation of medical resources between urban and rural areas in China, which exacerbates the burden of lung cancer disease on rural areas and farmers in China (26). However, according to predictions, the ASMR of lung cancer in China is expected to decrease in 2032-2035, which may be due to the popularization of clean energy, the improvement of healthcare and education levels, and the decrease in smoking rates among adolescents (27). The gender difference in lung cancer disease burden in China was very obvious, with ASIR, ASPR, ASMR, and DALYs for lung cancer in males being more than twice as high as those in females. The smoking rate of Chinese males is much higher than that of females, which may be one of the reasons for the significant gender differences in lung cancer burden in China (28). Another possible reason is that men and women have different sensitivities to tobacco carcinogens. However, studies have shown that the risk of lung cancer in Chinese male nonsmokers is also higher than that in female nonsmokers, while in Western populations, the risk of lung cancer in male nonsmokers is very low and not higher than that in women (29, 30). To sum up, China's rapid economic growth has also caused environmental problems. The aggravation of environmental problems has increased the burden of lung cancer. Coordinating the contradiction between economic development and the environment, promoting the upgrading of industrial structure, dealing with the problem of uneven distribution of medical resources, slowing down the aging process of the population, and promoting stricter tobacco control

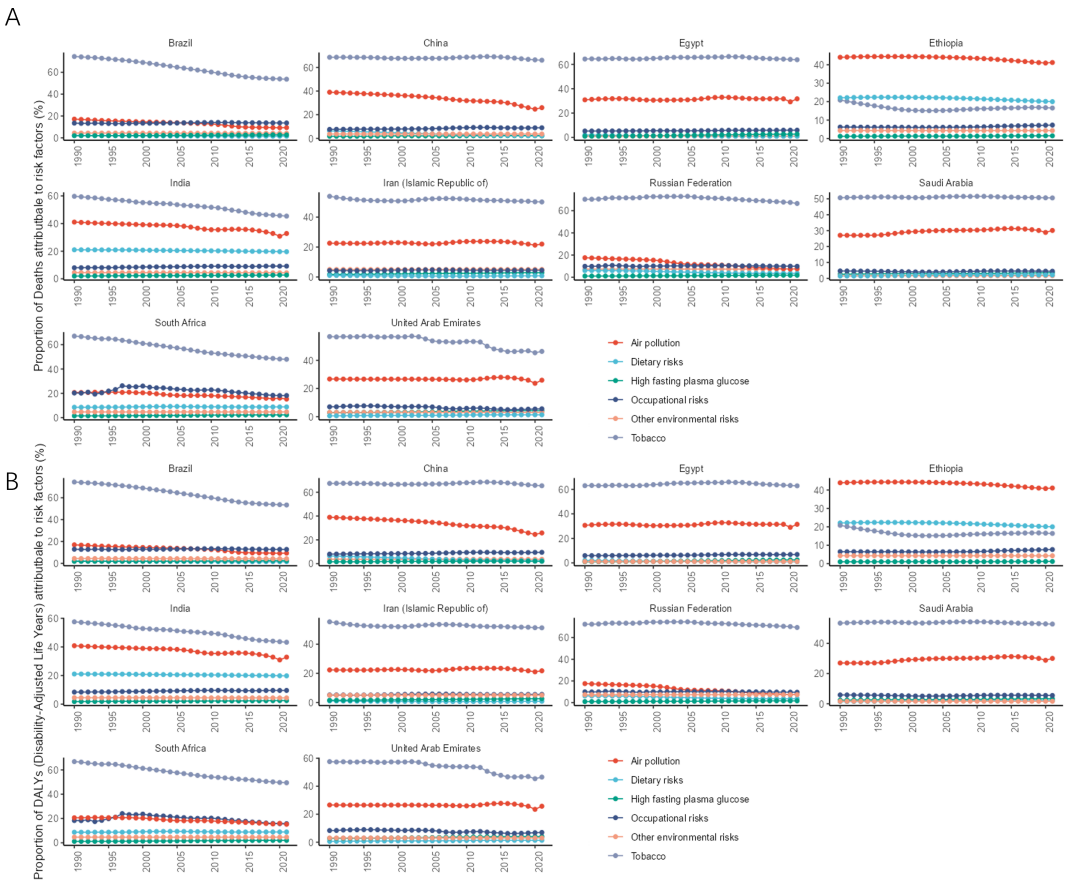

FIGURE 7
Time trend of the proportion of level 1 risk factors for lung cancer in BRICS from 1990 to 2021. **(A)** Proportion of deaths; **(B)** Proportions of DALYs.

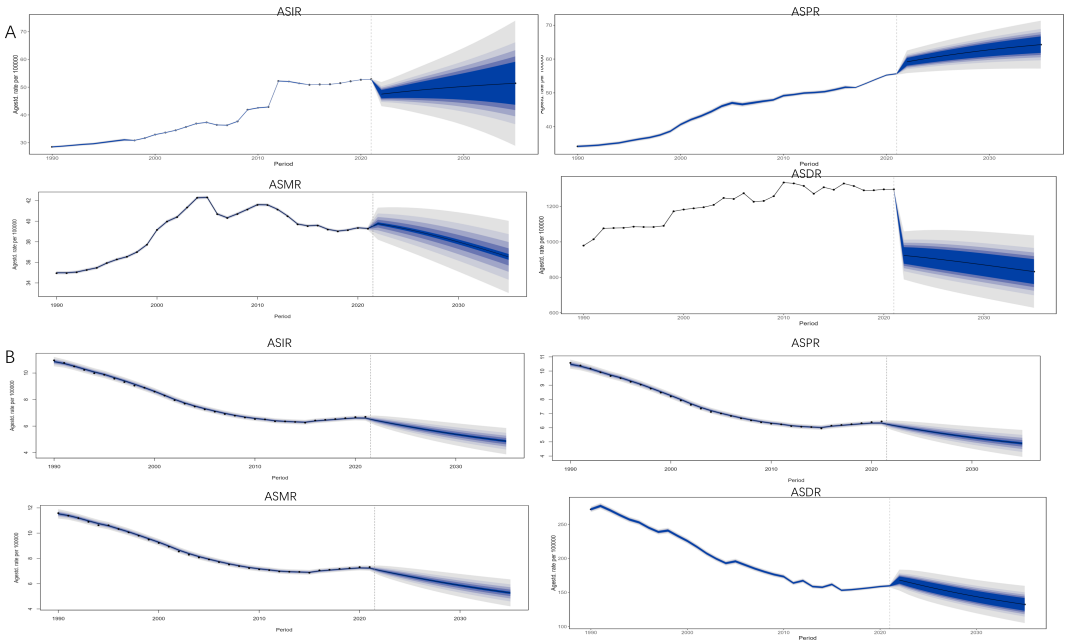

FIGURE 8
Projection of lung cancer ASIR, ASMR, ASMR, and ASDR trends in BRICS from 2021 to 2035. The blue area represents 95% UI. **(A)** China; **(B)** Ethiopia.

policies are the key and difficult points for the Chinese government's disease prevention and control in the future.

Egypt is one of the initiators of the Arab League and plays an important role in Arab, African, and international affairs. It is the third largest economy in Africa. The AAPC and EAPC of ASIR, ASPR, ASMR, and ASDR of lung cancer in Egypt were greater than 0 in 1990-2021, and according to the BAPC, it was predicted that ASIR, ASPR, ASMR, and ASDR of lung cancer in Egypt would be in an upward trend in the period of 2021-2035, which may be closely related to the turbulent political situation in Egypt. Egypt faced serious political divisions and social unrest after the Arab Spring, and the political turmoil caused by the Arab Spring led to frequent changes in government disrupted the continuity of health policies, and affected the implementation of public health programs (31). In terms of risk factors, according to WHO statistics, about 22% of the Egyptian population are smokers(without counting hookah), Egypt consumes about 20 billion cigarettes per year, and the prevalence of smoking among Egyptian adolescents is increasing (32). Under the dual influence of politics and lifestyle (smoking), the burden of lung cancer in Egypt is not optimistic. Reducing the smoking rate and maintaining social stability are important ways to reduce the burden of lung cancer in Egypt.

Ethiopia is the fifth largest economy and second largest population country in Africa, and a member of the African Union. The headquarters of the African Union and the United Nations Economic Commission for Africa are both located in Ethiopia. The AAPC and EAPC of ASIR, ASPR, ASMR and ASDR of lung cancer in Ethiopia were less than 0 in 1990-2021, and based on BAPC, it was predicted that ASIR, ASPR, and ASMR of lung cancer in Ethiopia would be in a decreasing trend in the period of 2021-2035 and that the DALYs of lung cancer in Ethiopia will be on the rise in the period of 2021-2022 after which 2022-2035 will be in decreasing trend. Although Ethiopia's total and per capita GDP is at the bottom of the BRICS, Ethiopia's GDP maintained a high average annual growth rate of 10% between 2000 and 2010, and between 1990 and 2023, Ethiopia's total GPP increased 5.12 times, and per capita GDP increased 4.96 times, making it one of the fastest growing economies. Ethiopia's economic development has led to investment in public health infrastructure and increased capacity for early screening and treatment of lung cancer (33). In terms of risk factors, Ethiopia is the only BRICS country where environmental/occupational risks rank first in level 1 risk factors and air pollution risks rank first in level 2 risk factors. First of all, Ethiopia's rapid economic development has caused environmental damage (34). Secondly, in Ethiopia, especially in rural areas, due to the lack of clean energy and modern energy facilities, many households rely on biomass fuels (such as wood, crop residues, and animal manure) for cooking and heating. These fuels will produce a large number of harmful air pollutants during combustion, leading to indoor air quality problems. In terms of behavioral risk, Ethiopia's degree of industrialization and urbanization is lower than that of other BRICS, while the high industrialization and urbanization of other BRICS bring higher living standards and also lead to an increase in behavioral risks such as smoking. Therefore, Ethiopia's behavioral risk has a lower impact on lung cancer than other BRICS.

India is the largest country in the South Asian subcontinent, the most populous country in the world, and the fifth largest economy in the world. The AAPC and EAPC of ASIR, ASPR, ASMR, and ASDR of lung cancer in India for the period 1990-2021 were greater than 0. Meanwhile, according to BAPC projection, India's ASIR, ASMR, and ASDR will be in an upward trend in 2021-2022 after declining in 2022-2035 and India's ASPR will be in an upward trend during 2021-2035. India is the world's second-largest consumer of tobacco after China, and smoking prevalence among males in India nearly tripled between 1998 and 2010, with a particularly marked increase among younger age groups (35, 36). Rapid economic development, industrialization, and urbanization in India have increased energy consumption and industrial waste emissions, leading to a growing air pollution problem in India. In numerous parts of India, where air pollution levels far exceed the safety standards set by WHO (24-hour ambient PM2.5 standard of 15 $\mu g/m^3$, not to be exceeded more than 3 to 4 times per year), such as Delhi, the capital of India, has an average PM2.5 of up to 100 $\mu g/m^3$ in 2021. Burning celebrations during festivals and burning of crop residues in India can even elevate PM2.5 to 700-1000 $\mu g/m^3$ (37). Although the Indian constitution stipulates that all citizens can enjoy free healthcare, the government's investment in healthcare is very limited. According to WHO data, in 2021, India's healthcare expenditure accounted for 3.28% of GDP, which is only slightly higher than Ethiopia's (3.21%) among BRICS (38). Therefore, under the multiple influences of insufficient medical expenditure, lifestyle (smoking), and environmental issues, the burden of lung cancer disease in India is increasing.

Iran is located in the heart of West Asia, known as the "Eurasian land bridge" and "East-West air corridor", and is the world's largest Shiite Islamic country with rich oil and gas resources. ASIR, ASMR, ASPR, and ASDR of lung cancer in Iran 1990-2021 showed large fluctuations, especially during 2019-2021. The EAPC of ASIR, ASMR, and ASPR for lung cancer in Iran between 1990-2021 was greater than 0, and the 95% uncertainty interval of the EAPC of ASDR passed through 0. The EAPC of ASIR, ASMR, and ASPR for lung cancer between 1990-2021 was less than 0, and the 95% uncertainty interval of the AAPC of ASPR passed through 0. According to BACPs projection, ASIR, ASPR, ASMR, and ASDR of lung cancer in Iran will be in a decreasing trend between 2021-2035. The reason for this phenomenon may be due to the fact that Iran was affected by the COVID-19 outbreak leading to the distortion of the data, which in turn led to huge fluctuations in the data related to lung cancer in 2019-2021. In Iran, lung cancer ranks 4th and 5th in the order of incidence and mortality of malignant tumors in males and females, respectively (39). According to the National Cancer Registration Program (NCRP) of Iran, the incidence of lung cancer in Iran increased by an average of 6.8% per year in males and 7.7% per year in females during the period from 2000 to 2016 (39). The increased burden of lung cancer in Iran may be closely related to influences such as high smoking prevalence (39), environmental pollution (40), economic sanctions (41), and gas warfare during the Iran-Iraq war (42).

Russia is one of the permanent members of the United Nations Security Council and the largest country in the world. AAPC and EAPC of ASIR, ASPR, ASMR, and ASDR for Lung Cancer in Russia

from 1990 to 2021 were less than 0. According to BACPs projection, lung cancer ASIR, ASPR, ASMR & ASDR in RUS will be on a downward trend between 2021-2035. The reason for the improvement in the burden of lung cancer in Russia may be related to a series of tobacco control measures taken by the Russian government (43), such as the signing of the WHO Framework Convention on Tobacco Control in 2008 and subsequent measures. From 2009 to 2016, the smoking rate in Russia decreased by 21.5% (44). Although the ASIR, ASPR, ASMR, and ASDR of lung cancer in Russia have a downward trend, and the burden of lung cancer in Russian females is low in BRICS, the ASIR, ASPR, ASMR, and ASDR of lung cancer in Russian males are still at a high level. First of all, this may be related to the low smoking rate of Russian females (45). Secondly, industry plays an important role in the Russian economy, especially the energy industry and heavy industry. The work related to it may involve occupational exposure related to lung cancer, such as asbestos, cadmium, and silicon (46). The proportion of males in these jobs is often high. Hence, the burden of lung cancer on males in Russia is still worthy of attention.

Saudi Arabia has the second largest sand oil reserves in the world, is one of the major members of the Organization of Petroleum Exporting Countries (OPEC), has the second largest total GDP in the Middle East, is the world's largest Sunni Islamist country, and has a pivotal political and economic influence in the Middle East. The 95% uncertainty intervals for the EAPC of ASIR, ASPR, ASMR, and ASDR for lung cancer in Saudi Arabia 1990-2021 passed through 0. The 95% uncertainty intervals for the AAPC of ASIR and ASMR all passed through 0. The AAPC of ASPR was greater than 0, and the AAPC of ASDR was less than 0. According to BACP projection, ASIR for lung cancer in Saudi Arabia will be declining in 2021-2031 and will be in an upward trend in 2031-2035, ASPR will be in an upward trend in 2021-2035, ASMR will be in a downward trend in 2021-2035, ASDR will be in a downward trend in 2021-2023, and in an upward trend in 2024-2035 will be on an upward trend. It is worth noting that ASIR, ASPR, ASMR, and ASDR of lung cancer in Saudi Arabia were in a continuous downward trend from 2007 to 2021, and in 2021 Saudi Arabia's ASIR, ASPR, ASMR of lung cancer was only higher than India's among the BRICS and in 2021 Saudi Arabia's ASDR was ranked the lowest among the BRICS. This may be related to Saudi Arabia's strict Islamic doctrine, which banned smoking until the 1960s. Although smoking is now legal, it is still considered a condemned behavior at the religious level in Saudi Arabia. Saudi Arabia passed the WHO Framework Convention on Tobacco Control in 2015 and began imposing heavy taxes on cigarettes after 2017 (47). However, although the Ministry of Commerce and Investment of the Kingdom of Saudi Arabia formally implemented the ban on the sale of electronic cigarettes in September 2015, in August 2019, the Saudi Food and Drug Administration began to implement the technical regulation SFDA FD.60 for tobacco products, which opened the way for the opening and compliance of the electronic cigarette market in Saudi Arabia, and the regulation does not restrict the Internet sales of electronic cigarettes. Therefore, electronic cigarette products in Saudi Arabia are allowed to be sold through online channels at present (48). In addition, with the implementation of Saudi Arabia's "Vision 2030" policy and the advancement of secularization, Saudi Arabia will still face challenges such as environmental pollution and changes in lifestyle habits.

Located at the southernmost tip of the African continent, South Africa is the second largest economy in Africa and the most economically developed and industrialized country in Africa. The 95% uncertainty intervals for the EAPC of ASIR, ASPR, ASMR, and ASDR for lung cancer from 1990-2021 passed through 0. The 95% uncertainty intervals for the AAPC of ASPR, ASMR, and ASDR passed through 0, and the AAPC of ASIR was greater than 0. According to BACP projection, lung cancer ASIR, ASPR, ASMR, and ASDR in South Africa will be on a declining trend between 2021-2035. South Africa has implemented strict tobacco control policies such as restricting smoking in public places and increasing excise taxes on cigarettes since 1993 (49). The per capita cigarette consumption in South Africa decreased by 54% from 1999 to 2011 (50). However, on the other hand, South Africa has a huge gap between the rich and the poor. According to Statistics South Africa, the Gini coefficient of South Africa is 0.67, which belongs to the high-income inequality countries. At the same time, South Africa's health care system is divided into the public (83%) and the private (17%) sectors, the public health care system suffers from understaffing and a lack of resources, in contrast to the private system which has sufficient resources staffing and advanced and modern treatments. As a result, early screening and effective treatment of lung cancer are often difficult to access for low-income groups in South Africa (51). In the future, the huge gap between the rich and the poor and the imbalance in the distribution of healthcare resources may be a problem to be faced in the future of lung cancer prevention and control in South Africa. In terms of regulating electronic cigarettes, South Africa proposed the Control of Tobacco Products and Electronic Delivery Systems Bill in 2018, which aims to regulate electronic cigarette products as tobacco products rather than as drugs or consumer goods. However, due to strong opposition from the electronic cigarette industry and lobbying activities, the bill has not yet been officially enacted into law (52). In the future, how to reduce the wealth gap and alleviate the imbalance in the allocation of medical resources, as well as how to strengthen the regulation of electronic cigarette products, will be the problems that South Africa's lung cancer prevention and control will face.

The United Arab Emirates is located at the southeastern end of the Arabian Peninsula, facing Iran across the sea. It is a maritime transportation hub that controls the Persian Gulf and enters the Indian Ocean, with abundant oil and gas resources. At the same time, the United Arab Emirates is also the country with the highest per capita GDP in the Middle East and an important hub for East-West trade. The AAPC and EAPC of ASIR, ASPR, and ASDR for lung cancer in the UAE 1990-2021 were less than 0, the AAPC of ASMR was less than 0, and the 95% uncertainty interval of the EAPC of ASMR passed through 0. According to BACP projection, lung cancer ASIR, ASPR, and ASMR in the UAE will be in a declining trend between 2021-2035, ASDR will rise in 2021-2022 and be in a declining trend in 2023-2035. It is worth noting that the ASIR, ASPR, ASMR, and ASDR for lung cancer in UAE females exceeded those of males after 2014, and the UAE is the only BRICS country to have a higher lung cancer burden indicator for females than for males. The UAE 2023 census data shows that the gender ratio in the UAE shows a large disparity,

with males comprising 68.58% of the country's population and females comprising 31.42% (53). The oil boom changed the economic landscape of the Gulf region and driven by the oil industry, Gulf countries such as the UAE entered an era of large-scale importation of foreign labor in the 1970s, with the number of expatriates in the UAE exceeding the number of locals. According to 2017 data, the UAE has the highest percentage of expatriate working population among the BRICS and Gulf countries, and the expatriate working population is mainly concentrated in young males (54), with a relatively low incidence of lung cancer, which may have led to an imbalance in the male-to-female ratio in the UAE and a lower burden of lung cancer in males than in females after age standardization after 2014. The other reason may be due to the increasing popularity of smoking behavior with the advancement of secularization in the UAE, especially hookah is becoming more popular among females (55). Meanwhile, studies have shown that higher levels of estrogen in females have a promoting effect on lung cancer (56), making them more sensitive to tobacco carcinogens and more susceptible to lung cancer than males under the same exposure conditions (57). The above reasons may have contributed to the higher indicators of lung cancer burden among females than males in the UAE. Therefore, for the UAE, protecting the medical rights and interests of migrant workers and reducing the female smoking rate will be the focus of lung cancer prevention and control in the future.

There are some limitations in this study, firstly, the fact that all BRICS members are developing countries, which may not be able to provide comprehensive and accurate disease and health data due to resource and infrastructure limitations. Secondly, there are significant regional and urban-rural differences within developing countries represented by China, India, Russia, etc., but the data in the GBD database cannot fully reflect these differences. Moreover, the economic growth and health data of developing countries represented by Iran, Egypt, and Russia are extremely vulnerable to external economic and political factors, which may lead to bias in BAPC prediction. At the same time, the policy adjustments of electronic cigarettes in different countries in the future may also bias the BAPC prediction of diseases. Thirdly, according to the WHO report in August 2020, since the outbreak of COVID-19, 90% of the world's key medical services have been affected, while cancer diagnosis and treatment have been affected as much as 55% (58). In addition, studies have shown that during the initial peak period of the COVID-19 epidemic, many countries have reported a significant decline in lung cancer cases, which suggests that the epidemic has an important impact on cancer diagnosis, and the mortality of lung cancer patients with COVID-19 is as high as 30% ~50% (59). Therefore, the epidemic of COVID-19 may have a certain impact on the statistics of incidence rate and mortality of lung cancer, thus causing data bias.

5 Conclusion

In general, although BRICS are all developing countries, due to the influence of living habits, national policies, economic development level, population aging, politics, religion, war, and other factors, there are also great differences in the burden of lung cancer among countries. Understanding these differences can enable BRICS to make more accurate decisions in future public health construction, and to realize the rational allocation of resources. At the same time, although BRICS still have a heavy burden of lung cancer, the strict tobacco control policies of Brazil, Russia, South Africa, and Saudi Arabia, the environmental protection policies and energy structure adjustment policies of China and Brazil, and Ethiopia's increased investment in medical construction have all played a positive role in reducing the burden of lung cancer. These policies also provide ideas for the prevention and control of lung cancer in other developing countries.

Data availability statement

The original contributions presented in the study are included in the article/supplementary material. Further inquiries can be directed to the corresponding author.

Author contributions

YW: Writing – original draft, Writing – review & editing, Methodology, Resources. JZhu: Formal analysis, Software, Writing – review & editing. SW: Software, Writing – review & editing. JZho: Conceptualization, Writing – review & editing.

Funding

The author(s) declare that no financial support was received for the research, authorship, and/or publication of this article.

Conflict of interest

The authors declare that the research was conducted in the absence of any commercial or financial relationships that could be constructed as a potential conflict of interest.

Generative AI statement

The author(s) declare that no Generative AI was used in the creation of this manuscript.

Publisher's note

References

1. Leong TL, Steinfort DP. Contemporary concise review 2023: advances in lung cancer and interventional pulmonology. *Respirology*. (2024) 29:665–73. doi: 10.1111/resp.14789

2. Xin HS. (2024). Available online at: https://www.gov.cn/yaowen/liebiao/202405/content_6949027.htm (Accessed September 21, 2024).

3. Zhang M, Jin W, Tian Y, Zhu H, Zou N, Jia Y, et al. Cancer burden variations and convergences in globalization: a comparative study on the tracheal, bronchus, and lung (tbl) and liver cancer burdens among who regions from 1990 to 2019. *J Epidemiol Glob Health*. (2023) 13:696–724. doi: 10.1007/s44197-023-00144-x

4. Collaborators GNSD. Global, regional, and national burden of disorders affecting the nervous system, 1990-2021: a systematic analysis for the global burden of disease study 2021. *Lancet Neurol*. (2024) 23:344–81. doi: 10.1016/S1474-4422(24)00038-3

5. Collaborators GF. Burden of disease scenarios for 204 countries and territories, 2022-2050: a forecasting analysis for the global burden of disease study 2021. *Lancet*. (2024) 403:2204–56. doi: 10.1016/S0140-6736(24)00685-8

6. Steiner TJ, Husøy A, Stovner LJ. Gbd2021: headache disorders and global lost health - a focus on children, and a view forward. *J Headache Pain*. (2024) 25:91. doi: 10.1186/s10194-024-01795-2

7. Zhang Y, Liu J, Han X, Jiang H, Zhang L, Hu J, et al. Long-term trends in the burden of inflammatory bowel disease in China over three decades: a joinpoint regression and age-period-cohort analysis based on gbd 2019. *Front Public Health*. (2022) 10:994619. doi: 10.3389/fpubh.2022.994619

8. Fan YX, Zhang W, Li W, Ma YJ, Zhang HQ. Global, regional, and national impact of air pollution on stroke burden: changing landscape from 1990 to 2021. *BMC Public Health*. (2024) 24:2786. doi: 10.1186/s12889-024-20230-4

9. Shanshan L, Zhihua Z, Chengcheng L, Huijing C, Shangcheng Z. Diabetes in China: burden analysis between 1990 and 2019 and incidence prediction between 2020 and 2030. *Chin Gen Practice*. (2023) 26:2013–9. doi: 10.12114/j.issn.1007-9572.2023.0009

10. rdrr.io. Bapc: projection of cancer incidence and mortality data using bayesian apc models fitted with inla(2022). Available online at: https://rdrr.io/rforge/BAPC/ (Accessed December 3, 2024).

11. Jiyong J, Kai H. The motivation, path, and challenges of BRICS countries' Participation in global health governance. *Int Review*. (2019), 120–41.

12. Zou Z, Cini K, Dong B, Ma Y, Ma J, Burgner DP, et al. Time trends in cardiovascular disease mortality across the brics: an age-period-cohort analysis of key nations with emerging economies using the global burden of disease study 2017. *Circulation*. (2020) 141:790–9. doi: 10.1161/CIRCULATIONAHA.119.042864

13. Campos MR, Rodrigues JM, Marques AP, Faria LV, Valerio TS, Silva M, et al. Smoking, mortality, access to diagnosis, and treatment of lung cancer in Brazil. *Rev Saude Publica*. (2024) 58:18. doi: 10.11606/s1518-8787.2024058005704

14. Mathias C, Prado GF, Mascarenhas E, Ugalde PA, Zimmer GA, Carvalho ES, et al. Lung cancer in Brazil. *J Thorac Oncol*. (2020) 15:170–5. doi: 10.1016/j.jtho.2019.07.028

15. The Climate And Clean Coalition. Brazilian environmental protection policy (2023). Available online at: https://www.ccacoalition.org/partners/Brazil (Accessed December 3, 2024).

16. Cabral JF, Caló R, Evangelista FM, Reis JB, Oliveira J, Lima F, et al. Trend analysis of lung cancer incidence and mortality in grande cuiabá, mato grosso, Brazil, 2000 to 2016. *Rev Bras Epidemiol*. (2022) 25:e220014. doi: 10.1590/1980-549720220014.supl.1

17. Smith PH, Kasza KA, Hyland A, Fong GT, Borland R, Brady K, et al. Gender differences in medication use and cigarette smoking cessation: results from the international tobacco control four country survey. *Nicotine Tob Res*. (2015) 17:463–72. doi: 10.1093/ntr/ntu212

18. Hao S, Wenzhao Z. Higher lung cancer incidence in young women than young men in the United States. *J Evidence-Based Med*. (2018) 18:216–8. doi: 10.12019/j.issn.1671-5144.2018.04.005

19. Rongshou Z, Ru C, Bingfeng H, Shaoming W, Li L, Kexin S, et al. Analysis of the epidemic situation of Malignant tumors in China in 2022. *Chin J Oncol*. (2024) 46:221–31. doi: 10.3760/cma.j.cn112152-20240119-00035

20. Bray F, Laversanne M, Sung H, Ferlay J, Siegel RL, Soerjomataram I, et al. Global cancer statistics 2022: globocan estimates of incidence and mortality worldwide for 36 cancers in 185 countries. *CA Cancer J Clin*. (2024) 74:229–63. doi: 10.3322/caac.21834

21. Hoffman SJ, Mammone J, Rogers VKS, Sritharan L, Tran M, Al-Khateeb S, et al. Cigarette consumption estimates for 71 countries from 1970 to 2015: systematic collection of comparable data to facilitate quasi-experimental evaluations of national and global tobacco control interventions. *BMJ*. (2019) 365:l2231. doi: 10.1136/bmj.l2231

22. Yang JJ, Yu D, Wen W, Shu XO, Saito E, Rahman S, et al. Tobacco smoking and mortality in asia: a pooled meta-analysis. *JAMA Netw Open*. (2019) 2:e191474. doi: 10.1001/jamanetworkopen.2019.1474

23. Yang D, Liu Y, Bai C, Wang X, Powell CA. Epidemiology of lung cancer and lung cancer screening programs in China and the United States. *Cancer Lett*. (2020) 468:82–7. doi: 10.1016/j.canlet.2019.10.009

24. Li C, Lei S, Ding L, Xu Y, Wu X, Wang H, et al. Global burden and trends of lung cancer incidence and mortality. *Chin Med J (Engl)*. (2023) 136:1583–90. doi: 10.1097/CM9.0000000000002529

25. Wang MY, Sung HC, Liu JY. Population aging and its impact on human wellbeing in China. *Front Public Health*. (2022) 10:883566. doi: 10.3389/fpubh.2022.883566

26. National Bureau of Statistics of China. Statistical bulletin on national economic and social development of the people's republic of China in 2023 (2024). Available online at: https://www.stats.gov.cn/sj/zxfb/202402/t20240228_1947915.html (Accessed December 2, 2024).

27. Fan Y, Jiang Y, Li X, Li X, Li Y, Wu H, et al. Burden of lung cancer attributable to occupational carcinogens from 1990 to 2019 and projections until 2044 in China. *Cancers (Basel)*. (2022) 14:3883. doi: 10.3390/cancers14163883

28. Stapelfeld C, Dammann C, Maser E. Sex-specificity in lung cancer risk. *Int J Cancer*. (2020) 146:2376–82. doi: 10.1002/ijc.32716

29. He B, Zhao X, Pu Y, Sun R, Gao X, Liu W. Trends and projection of burden on lung cancer and risk factors in China from 1990 to 2060. *Thorac Cancer*. (2024) 15:1688–704. doi: 10.1111/1759-7714.15332

30. Wu Z, Tan F, Yang Z, Wang F, Cao W, Qin C, et al. Sex disparity of lung cancer risk in non-smokers: a multicenter population-based prospective study based on China national lung cancer screening program. *Chin Med J (Engl)*. (2022) 135:1331–9. doi: 10.1097/CM9.0000000000002161

31. Wenlin T. *Decay and Turmoil: Reflections on the 10th Anniversary of the Arab Spring* Vol. 23. Beijing: International Forum (2021) p. 3–17. doi: 10.13549/j.cnki.cn11-3959/d.2021.03.001

32. Jazieh AR, Algwaiz G, Errihani H, Elghissassi I, Mula-Hussain L, Bawazir AA, et al. Lung cancer in the middle east and north africa region. *J Thorac Oncol*. (2019) 14:1884–91. doi: 10.1016/j.jtho.2019.02.016

33. Awedew AF, Asefa Z, Belay WB. National burden and trend of cancer in Ethiopia, 2010-2019: a systemic analysis for global burden of disease study. *Sci Rep*. (2022) 12:12736. doi: 10.1038/s41598-022-17128-9

34. Gebremariam TH, Haisch DA, Fernandes H, Huluka DK, Binegdie AB, Woldegeorgis MA, et al. Clinical characteristics and molecular profiles of lung cancer in Ethiopia. *JTO Clin Res Rep*. (2021) 2:100196. doi: 10.1016/j.jtocrr.2021.100196

35. Mishra S, Joseph RA, Gupta PC, Pezzack B, Ram F, Sinha DN, et al. Trends in bidi and cigarette smoking in India from 1998 to 2015, by age, gender and education. *BMJ Glob Health*. (2016) 1:e5. doi: 10.1136/bmjgh-2015-000005

36. Roy MP. Factors associated with mortality from lung cancer in India. *Curr Probl Cancer*. (2020) 44:100512. doi: 10.1016/j.currproblcancer.2019.100512

37. de Bont J, Krishna B, Stafoggia M, Banerjee T, Dholakia H, Garg A, et al. Ambient air pollution and daily mortality in ten cities of India: a causal modelling study. *Lancet Planet Health*. (2024) 8:e433–40. doi: 10.1016/S2542-5196(24)00114-1

38. World Health Organization. Current health expenditure (che) as percentage of gross domestic product (gdp) (%)(2024). Available online at: https://apps.who.int/gho/data/node.main.GHEDCHEGDPSHA2011?lang=en (Accessed December 2, 2024).

39. Mirahmadizadeh A, Hassanzadeh J, Moradi AM, Gheibi Z, Heiran A. Projection of the prevalence of tracheal, bronchus, and lung cancer incidence using cigarette smoking prevalence in Iran from 1990 to 2018: a comparison of latent period-based models with standard forecasting models. *BMC Public Health*. (2024) 24:1896. doi: 10.1186/s12889-024-19407-8

40. Khorrami Z, Pourkhosravani M, Rezapour M, Etemad K, Taghavi-Shahri SM, Künzli N, et al. Multiple air pollutant exposure and lung cancer in tehran, Iran. *Sci Rep*. (2021) 11:9239. doi: 10.1038/s41598-021-88643-4

41. Sajadi HS, Majdzadeh R. Health system to response to economic sanctions: global evidence and lesson learned from Iran. *Global Health*. (2022) 18:107. doi: 10.1186/s12992-022-00901-w

42. Salehiniya H, Bahadori M, Ghanizadeh G, Raei M. Epidemiological study of lung cancer in Iran: a systematic review. *Iran J Public Health*. (2022) 51:306–17. doi: 10.18502/ijph.v51i2.8683

43. Shkolnikov VM, Churilova E, Jdanov DA, Shalnova SA, Nilssen O, Kudryavtsev A, et al. Time trends in smoking in Russia in the light of recent tobacco control measures: synthesis of evidence from multiple sources. *BMC Public Health*. (2020) 20:378. doi: 10.1186/s12889-020-08464-4

44. Bai R, Dong W, Chu M, Liu B, Li Y. Trends in mortality due to tracheal, bronchial, and lung cancer across the brics: an age-period-cohort analysis based on the global burden of disease study 1990-2019. *Chin Med J (Engl)*. (2024) 137:2860-2867. doi: 10.1097/CM9.0000000000002977

45. Carioli G, Malvezzi M, Bertuccio P, Levi F, Boffetta P, Negri E, et al. Cancer mortality and predictions for 2018 in selected australasian countries and Russia. *Ann Oncol*. (2019) 30:132–42. doi: 10.1093/annonc/mdy489

46. Schüz J, Kovalevskiy E, Olsson A, Moissonnier M, Ostroumova E, Ferro G, et al. Cancer mortality in chrysotile miners and millers, Russian federation: main results

(asbest chrysotile cohort-study). *J Natl Cancer Inst*. (2024) 116:866–75. doi: 10.1093/jnci/djad262

47. Jazieh AR, Algwaiz G, Alshehri SM, Alkattan K. Lung cancer in Saudi Arabia. *J Thorac Oncol*. (2019) 14:957–62. doi: 10.1016/j.jtho.2019.01.023

48. Saudi Food and Drug Authority. Saudi food & drug authority standard on plain packaging of tobacco products(2018). Available online at: https://www.tobaccocontrollaws.org/laws/plain-pkg-standard-saudi-arabia (Accessed December 2, 2024).

49. Zatoński MZ, Egbe CO, Robertson L, Gilmore A. Framing the policy debate over tobacco control legislation and tobacco taxation in South Africa. *Tob Control*. (2023) 32:450–7. doi: 10.1136/tobaccocontrol-2021-056675

50. Bello B, Fadahun O, Kielkowski D, Nelson G. Trends in lung cancer mortality in South Africa: 1995-2006. *BMC Public Health*. (2011) 11:209. doi: 10.1186/1471-2458-11-209

51. van Eeden R, Tunmer M, Geldenhuys A, Nayler S, Rapoport BL. Lung cancer in South Africa. *J Thorac Oncol*. (2020) 15:22–8. doi: 10.1016/j.jtho.2019.06.032

52. Ayo-Yusuf O, Nkosi L, Agaku I. E-cigarette use and regulation in South Africa: a synthesis of evidence in response to industry efforts to undermine product regulation. *Curr Addict Rep*. (2022) 9:363–72. doi: 10.1007/s40429-022-00451-6

53. Ceicdata. United Arab Emirates Economic Indicators 1950-2024 (2024). Available online at: https://www.ceicdata.com.cn/zh-hans/indicator/united-arab-emirates/population (Accessed September 27, 2024).

54. Jie C, Jieying Z. The problem of marginal people and its governance in GCC countries. *Arab World Stud*. (2021), 57–75. doi: 10.3969/j.issn.1673-5161.2021.05.004

55. Al-Zalabani AH. Cancer incidence attributable to tobacco smoking in gcc countries in 2018. *Tob Induc Dis*. (2020) 18:18. doi: 10.18332/tid/118722

56. Henschke CI, Yip R, Miettinen OS. Women's susceptibility to tobacco carcinogens and survival after diagnosis of lung cancer. *JAMA*. (2006) 296:180–4. doi: 10.1001/jama.296.2.180

57. Tse LA, Mang OW, Yu IT, Wu F, Au JS, Law SC. Cigarette smoking and changing trends of lung cancer incidence by histological subtype among chinese male population. *Lung Cancer*. (2009) 66:22–7. doi: 10.1016/j.lungcan.2008.12.023

58. World Health Organization. Medical services in 90% of the world's countries are disrupted by the covid-19 (2020). Available online at: https://news.un.org/zh/story/2020/08/1065742 (Accessed December 4, 2024).

59. Lovlekar SK, Wang Y. Impact of the covid-19 pandemic on lung cancer treatment and research. *Genes Dis*. (2023) 10:1217–9. doi: 10.1016/j.gendis.2023.01.028

frontiers | Frontiers in Molecular Biosciences

TYPE Original Research
PUBLISHED 23 January 2025
DOI 10.3389/fmolb.2024.1520223

OPEN ACCESS

EDITED BY
Giuseppe Bronte,
University of Ferrara, Italy

REVIEWED BY
Rishi Kumar Jaiswal,
University of Arkansas for Medical Sciences, United States
Donald Rao,
Gradalis, Inc., United States

*CORRESPONDENCE
P. L. Hallenbeck,
phallenbeck@senecatherapeutics.com

RECEIVED 31 October 2024
ACCEPTED 27 December 2024
PUBLISHED 23 January 2025

CITATION
Franco LS, Arunachalam S, Chauhan A, Kareff SA and Hallenbeck PL (2025) Elevated expression of *ANTXR1* gene in tumors is a poor prognostic biomarker for patients with bladder cancer.
Front. Mol. Biosci. 11:1520223.
doi: 10.3389/fmolb.2024.1520223

Elevated expression of *ANTXR1* gene in tumors is a poor prognostic biomarker for patients with bladder cancer

L. S. Franco[1], S. Arunachalam[1], A. Chauhan[2], S. A. Kareff[3] and P. L. Hallenbeck[1]*

[1]Seneca Therapeutics, Inc., Blue Bell, PA, United States, [2]Sylvester Comprehensive Cancer Center, University of Miami Health System, Miami, FL, United States, [3]Lynn Cancer Institute, Boca Raton Regional Hospital, Boca Raton, FL, United States

The TEM8 protein coded by the *ANTXR1* gene represents an emerging biomarker in solid tumors. In addition to the various roles TEM8 plays in oncogenesis, including angiogenesis, epithelial-to-mesenchymal transition, and cell migration, it has also been shown that the overexpression of the *ANTXR1* gene in solid tumors correlates with poor prognostic indicators in several solid tumor histologies. As such, TEM8 has been identified as the target of novel oncologic therapies. It is especially attractive given its selective expression on the surface of solid tumor cells and associated stromal cells, such as cancer stem cells, invasive cancer cells, and immune cells, such as macrophages, angiogenic endothelial cells, pericytes, and cancer-associated fibroblasts. Furthermore, TEM8 plays this unique role as a mostly non-mutated gene in solid cancers. Here, we demonstrate that elevated expression of ANTXR1 in bladder cancer showed a statistical difference not only in overall survival (OS) but in progression-free survival (PFS), confirming the prognostic biomarker power of *ANTXR1* expression.

KEYWORDS

TEM8, prognostic biomarker, bladder cancer, downstream pathway, survival

Introduction

The tumor endothelial marker 8 (TEM8) or anthrax receptor 1 (ANTXR1) is a protein that is encoded by the *ANTXR1* gene and is part of the receptors that are involved in the facilitation of the entry of anthrax into the cell (Alcalá et al., 2019). It is homologous to the protein capillary morphogenesis protein 2 (CMG2 or ANTXR2), that the anthrax toxin binds to. However, the severity of pathology from the toxin is very different. CMG2 is the major receptor involved in the lethality of the anthrax toxin *in vivo* (Fu, et al., 2010). TEM8, on the other hand, is expressed during angiogenesis, as well as in some somatic tissues and human tumors (Friebe et al., 2015). It was thought that higher expression of TEM8 in tumors was mainly due to angiogenesis within the tumor, however, high TEM8 expression has also been observed in stroma cells like cancer associated fibroblasts (CAFs) and pericytes (Hsu et al., 2022; Kareff et al., 2023) and cancer cells themselves (Hoye, et al., 2018).

TEM8 has been shown to activate different pathways in tumors like that of PI3K/Akt/mTOR in gastric cancer (Cai, et al., 2020) and glioblastoma (Kundu, et al., 2024). It has also been linked with the activation of the Wnt/beta catenin pathway in lung

adenocarcinoma (Ding, et al., 2021) and in recurrent glioblastomas (Kundu, et al., 2024). The TGF-beta pathway, one of the most common pathways involved in cancer, is also activated in gastric cancer and is correlated with high expression of *ANTXR1* (Huang et al., 2020). Lastly, it is known that TEM8 is involved in the collagen pathway by facilitating the uptake of collagen VI in cancer stroma, which is key for cancer survival (Hsu, et al., 2022), and in breast cancer, in which Chen, et al. demonstrated that it was involved in collagen trafficking (Chen et al., 2013).

TEM8 has been targeted before due to its correlation with the pathways that are involved in tumor progression, invasion and aggressiveness. There have been several reports involving monoclonal antibodies that are bound to TEM8 and showed slowed tumor growth in animal models (Chaudhary et al., 2012).

Seneca Valley Virus (SVV) is a naturally occurring swine picornavirus that is spread throughout the world that does not infect humans (Venkataraman, et al., 2008). SVV does, however, infect solid cancer cells. The initial isolate called SVV-001 has been studied in three prior clinical trials when systemically delivered to patients with solid cancers and demonstrated promising signals of efficacy and safety (Rudin, et al., 2011). The receptor of SVV was identified to be TEM8 (Evans, et al., 2018; Corbett et al., 2022). It has also been demonstrated that SVV-001 infection in solid tumors can induce an influx of immune cells by turning the tumor microenvironment from "cold" (low immunogenicity) to a "hot" tumor (high immunogenicity), thus enabling synergistic checkpoint inhibitor function. SVV has high specificity for TEM8 expressing tumors, making SVV a promising candidate for difficult to treat solid cancers that express TEM8.

More ways to possibly predict the outcome of a patient are being investigated. Currently, many cancer types rely on the TNM classification, but this system does not take into account the tumor microenvironment, which plays a key role in tumor progression (Wang, et al., 2023; Luo et al., 2021). An alternative way that has been explored to predict outcome is the Estimation of STromal and Immune cells in MAlignant Tumors using Expression (ESTIMATE) data' that uses tumoral gene expression signatures to determine the number of stromal cells and infiltration of immune cells in the tumor (Yoshihara, et al., 2013). In gastric cancer, the stromal score was demonstrated to be related to immune gene signature and macrophage infiltration (Wei et al., 2020). Similarly, in colorectal cancer the combination of the TNM staging system in combination with the stromal and immune score gives a better accuracy than the TNM alone (Luo et al., 2021). Other prognostic biomarkers are needed to predict with a higher accuracy a patient's outcome in different types of cancer.

In previous studies, TEM8 has been described as a potential biomarker for different types of cancer including colorectal cancer, where TEM8 expression was significantly correlated with TMN stage and high TEM8 expression in serum was correlated with worse overall survival than those with lower TEM8 expression (Pietrzyk et al., 2021). Similarly, TEM8 was described as a new biomarker in pancreatic cancer (Alcalá et al., 2019) and for gastric cancer, in which it was suggested as a prognostic biomarker due to its relationship with the immune and stromal scores as well as correlation between high expression with clinicopathological parameters (Huang et al., 2020; Cai, et al., 2020). In lung cancer, higher TEM8 expression was associated with lower OS (Sun, et al., 2021).

Bladder cancer is the most common urogenital cancer (10th most prevalent), affecting more than 1.6 million people worldwide (Castaneda et al., 2023; Flores Monar et al., 2023). This cancer is one of the most onerous cancers, necessitating personal healthcare costs. In 2015 in the U.S., bladder cancer incurred a cost of $7.93 billion and is expected to ~ double by 2030 (Flores Monar et al., 2023). More biomarkers (predictive and/or prognostic) are needed to manage patients with this cancer. Currently, there are only six biomarker tests approved by the FDA for surveillance for bladder cancer, but many of them still present high false-positive rates (Flores Monar et al., 2023). Some of the molecular biomarkers seem promising in early development, however they have yet to successfully transition to the bedside (Castaneda et al., 2023). Here, we studied the effect of *ANTXR1* gene expression in different types of cancers and chose bladder cancer to understand the implications of high expression of *ANTXR1* as a poor prognostic marker. We also investigated the pathways that are enriched in tumors downstream of the *ANTXR1* gene to complement the effect of this gene in the tumor metabolism.

Materials and methods

Overall survival and progression-free survival

The Cancer Genome Atlas was used to study the expression of *ANTXR1* and its prognosis. The clinical, RNA expression data are downloaded from cbioportal (https://www.cbioportal.org).

Multiple cancer types were analyzed. The upper quartile of TEM8 fragments per kilobase per million mapped reads (FPKM) was labeled as high expression, and the rest of quartiles are labeled as low expression of *ANTXR1*. The Kaplan-Meier method was used to estimate overall survival as a function of time. Survival statistical differences were assessed by Log-rank test with a threshold of p value ≤ 0.05. The Kaplan-Meier analysis is done using KaplanMeierFitter.

For bladder cancer specifically, TCGA data had 133 patients from which 86 patients were treated with chemotherapy, 18 patients were treated with radiotherapy, 16 patients were treated with a combination of chemotherapy and radiotherapy, and 13 patients were treated with other treatments (Supplementary File S1).

For melanoma, the TCGA data obtained was from the Pan cancer atlas data (448 samples). Other data for the calculation of the immune score of melanomas was obtained from immunogenic studies made in DFCI (metastatic melanoma, 110 samples) and UCLA (metastatic melanoma, 38 samples). A graphical description of the workflow of the study is represented in Supplementary Figure S1.

Stromal score and immune score

Stromal and immune score were calculated using algorithms like ESTIMATE (Estimation of STromal and Immune cells in MAlignant Tumor tissues using Expression data) which analyze gene expression profiles to determine the relative proportion of these cell types within a tumor. For the stromal score, 141 genes were analyzed

using ssGSEA as a stromal signature in tumors and for the immune score, 141 genes were analyzed using ssGSEA as a immune signature, as described elsewhere without modifications (Yoshihara, et al., 2013). Statistical differences in the high and low expressing *ANTXR1* populations were assessed using the Wilcoxon-test, using a threshold of p value ≤ 0.05.

Validation of membrane bound biomarkers in bladder cancer

We identified 28 previously published survival associated individual genes (*HRAS, SPP1, VEGFA, TGFB1, CDKN2A, FGF3, KRT38, FABP1, GUCA1C, PYGM, CLEC3B, KCNB1, FBXL22, CFD, HLF, FLT1, KDR, CXCR7, FGFR3, TACSTD2, ABCB1, ERBB2, ITGB8, MACC1, SPON2, RHOA, CXCR4, CXCL12*). Each of these biomarker candidates were investigated using TCGA cancer patients for prognosis (overall survival and progression-free survival) and compared with *ANTXR1* expression levels and patient prognosis. The number of patients analyzed for the *CXCR7* was 406 for OS and 174 for PFS. The number of patients analyzed for the *SPON2* was 406 for OS and 174 for PFS.

Deseq2 and GSEA: Differential expression analysis (DEA) with TCGA RNA data was done using PyDESeq2 (https://pydeseq2.readthedocs.io/en/latest/index.html) version DESeq2 (v1.34.0) (For more details: https://github.com/owkin/PyDESeq2?tab=readme-ov-file#documentation). Gene set enrichment analysis (GSEA) was done using GSEAPY package (https://gseapy.readthedocs.io/en/latest/introduction.html). Gene ontology, Kyoto Encyclopedia of Genes and Genomes analysis, Hallmark and Reactome pathway analysis were performed to identify possible enrichment of genes with specific biological themes. The thresholds for statistical significance were analyzed by the following criteria: log(fold change) > 1 corresponds to upregulated pathway analysis; and log(fold change) < − 1 corresponds to a downregulated pathway analysis. And adjusted p value < 0.05.

Results

Stromal score is correlated to *ANTXR1* expression in tumors

Stromal score represents the presence of stromal tissue, and more precisely the number of cells in the tumor microenvironment of a tumor. In this particular study, stromal score was determined by using the stromal signature of 141 genes using single-sample gene set-enrichment analysis (ssGSEA) as described before (Yoshihara, et al., 2013).

We analyzed eleven different types of cancer for differences of stromal score when there is high or low expression of *ANTXR1* in tumors (basal breast cancer, melanoma, lung squamous cancer, lung adenocarcinoma, colorectal adenocarcinoma, head and neck squamous cell carcinoma, cervical squamous cell carcinoma, bladder urothelial carcinoma, kidney renal clear cell carcinoma, glioblastoma, and metastatic melanoma). Six out of the eleven types of cancer analyzed showed a statistically significant difference of the stromal score when comparing high or low expression levels of *ANTXR1* in each group (Figure 1). The other types of cancer did not show a statistically significant difference (not shown). This figure shows that *ANTXR1* expression has a direct correlation to stromal scores, meaning the higher the expression of *ANTXR1,* the more directly correlated it is to higher stromal scores. This is expected due to the potential expression of *ANTXR1* in different types of stroma cells.

Immune score may not be correlated to *ANTXR1* expression in tumors

Immune score represents the infiltration of immune cells into the tumor. In this particular study, it was determined by using the immune signature of 141 genes using ssGSEA, as we did with the stromal score (Yoshihara et al., 2013).

We analyzed eleven different types of cancer for differences of immune score in varying rates of expression of *ANTXR1* in tumors (same types of cancer as the stromal score). Only two (bladder urothelial cancer and colorectal adenocarcinoma) out of the eleven types of cancer analyzed showed a statistically significant difference of the immune score with different levels of expression of *ANTXR1* (Figure 2). The other types of cancer did not show a statistically significant difference between the high and low *ANTXR1* expression groups (not shown). This figure shows that, paradoxically, a higher immune score (more infiltration of immune cells) is correlated to higher levels of *ANTXR1,* suggesting that for some cancers the infiltration of immune cells may not be a definitive factor when treating cancer. Supporting this suggestion, we also found that in the presence of higher levels of *ANTXR1* in melanoma, a difficult cancer to treat, correlated with poor prognosis in terms of overall survival in patients when treated with immunotherapy.

To investigate the impact of high or low expression of *ANTXR1* in different types of cancer, the probability of survival (overall survival and progression-free survival) was determined for the eleven types of cancer described above as well as small cell lung cancer, for a total of twelve types of cancer.

In Figure 3 we demonstrate that the probability of overall survival (OS) for bladder cancer and cervical squamous cell carcinoma is correlated with the tumor expression of *ANTXR1* gene. High *ANTXR1* expression correlates with lower probability of survival *versus* when there is a low expression of *ANTXR1*. Thus, *ANTXR1* expression is a statistically significant biomarker for prognosis in bladder cancer and cervical squamous cell carcinoma.

OS may vary depending on the treatment that the patient received, therefore we analyzed the probability of survival of bladder cancer patients according to the treatments received. Figure 4A shows that patients that are treated with chemotherapy have a higher probability of survival for a longer time (~0.55) than patients treated with radiotherapy or a combination of both. To understand if *ANTXR1* expression would have any impact on the probability of survival depending on the treatment of the patient, the probability of survival was analyzed according to these parameters. Figure 4B shows that when patients are treated with chemotherapy and have low expression of *ANTXR1,* they have a higher survival probability (~0.6) for more than 150 months than patients expressing high levels of *ANTXR1* (probability of survival ~0.5 for 90 months).

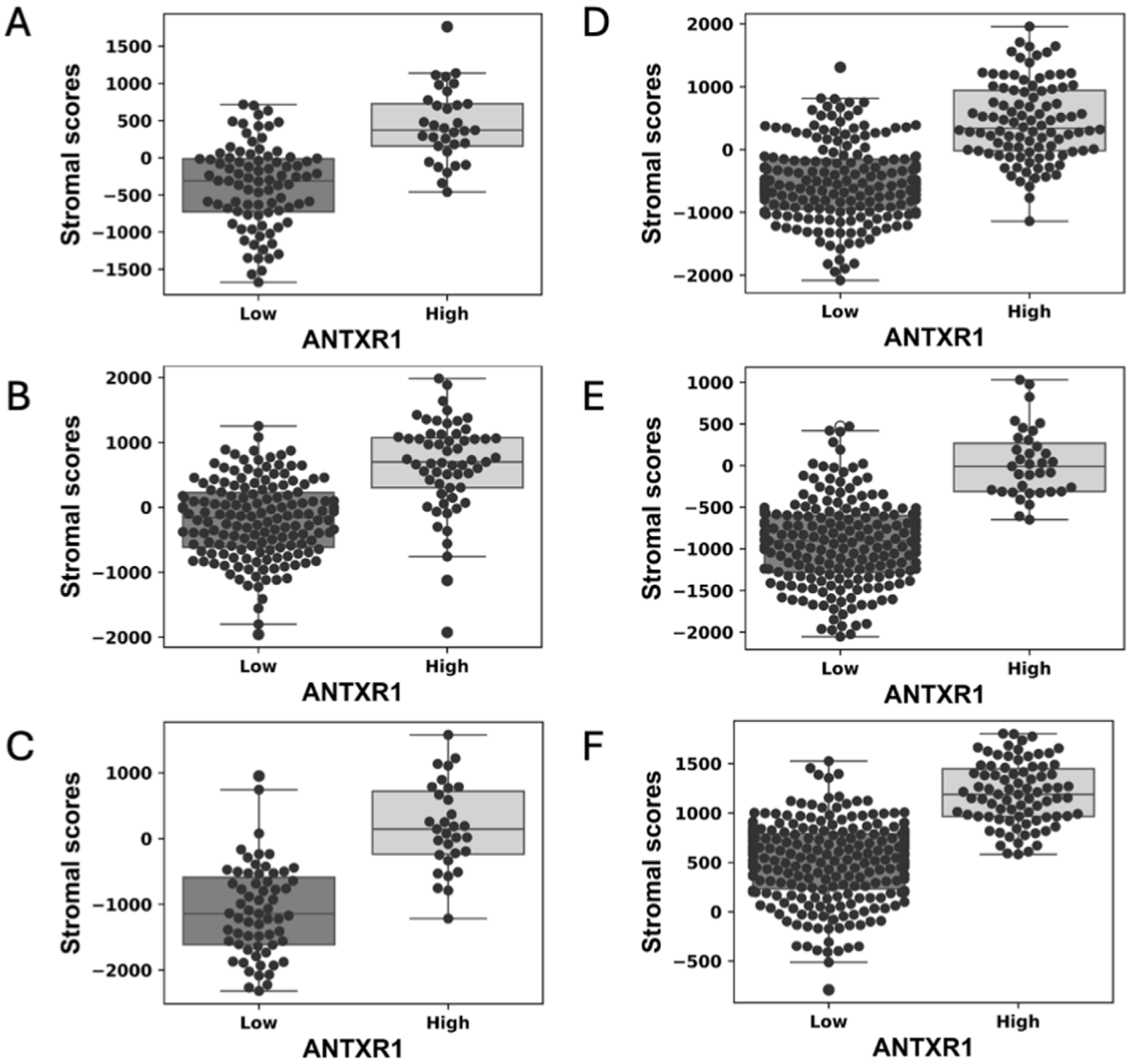

FIGURE 1
High expression of ANTXR1 in tumor is correlated with high stromal score in different types of cancer. Box plot of stromal score in **(A)** Lung squamous cell carcinoma, **(B)** Lung adenocarcinoma **(C)** Bladder urothelial carcinoma **(D)** Head and neck squamous carcinoma **(E)** Colorectal adenocarcinoma and **(F)** Kidney renal clear cell carcinoma, analyzed by high or low expression of ANTXR1 in tumor. The line in the middle represents the median of the stromal score; top and bottom of the box represent the 75% quartile and 25% quartile of the patients, respectively.

This trend is similar in patients treated with radiotherapy and the combination of radiotherapy with chemotherapy. This indicates the impact of *ANTXR1* expression independent of the treatment received by the patient.

While OS refers to the time from treatment initiation until death, other measurements like progression-free survival (PFS) and disease-free survival (DFS) can be related in some, but not all types of cancer. PFS is the time from treatment initiation until disease progression and DFS refers to the time from treatment until recurrence of disease. To further investigate the relationship between different types of survival, more specifically PFS and DFS, and expression of *ANTXR1* in bladder cancer patients, we analyzed the probability of survival for bladder cancer patients according to these parameters. Figures 4C, D show the PFS of bladder cancer patients and DFS in cancer patients, respectively. PFS shows congruency between the overall survival and PFS showing a p value less than 0.05. This demonstrates a statistically significant difference between a patient that expresses high levels of *ANTXR1* expression vs low levels of *ANTXR1* expression in bladder cancer. However, the *ANTXR1* expression levels suggest having no impact in the DFS. In conclusion, high expression of *ANTXR1* in bladder cancer is a predictor of bad prognosis even when the patient is using different cancer treatments, and it can be observed in both overall and progression free survival rates.

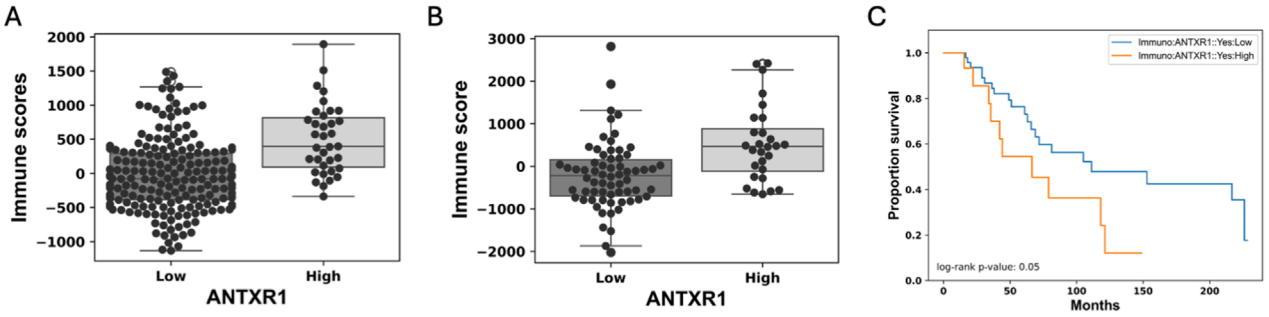

FIGURE 2
Low expression of ANTXR1 in tumor seems to be correlated with immune response. Box plot of the immune score representing the infiltration of immune cells in **(A)** Colorectal adenocarcinoma, and **(B)** Bladder urothelial carcinoma. The line in the middle represents the median of the immune score; top and bottom of the box represent the 75% quartile and 25% quartile of the patients, respectively. **(C)** Survival curve of patients with Melanoma treated with immunotherapy when there is high (orange) or low expression of ANTXR1 (blue) showing a statistical difference between the two populations.

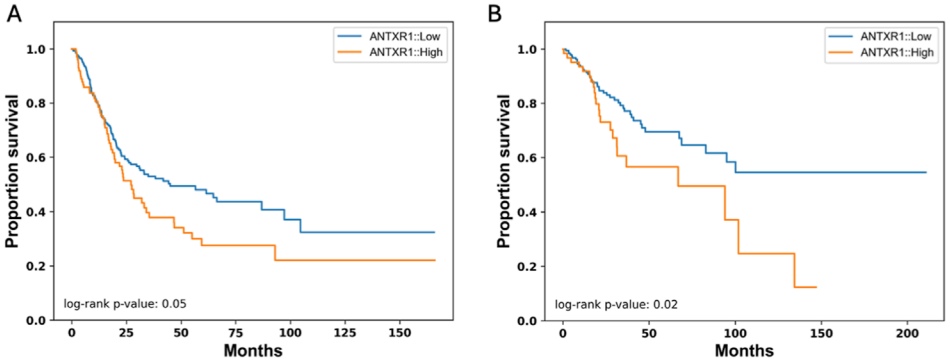

FIGURE 3
High expression of ANTXR1 is correlated to low overall survival. Kaplan-Meier survival curve for overall survival in **(A)** Bladder cancer and **(B)** Cervical squamous cell carcinoma and endocervical adenocarcinoma when there is high (orange) or low expression of ANTXR1 (blue) showing a statistical difference between the two populations in both types of cancers.

ANTXR1 expression as a unique gene to predict prognosis in bladder cancer

In previous studies TEM8, the protein expressed from *ANTXR1*, has been associated with lipid rafts, which are known to have clusters of membrane proteins (Ju et al., 2010). To understand the uniqueness of TEM8 as a membrane protein predictor of good or poor prognosis, we analyzed for low and high expression of 28 different membrane protein encoding genes and examined the probability of survival. Of the twenty-eight genes, only two genes showed a statistically significant difference between high and low expression in terms of overall survival and PFS. These genes correspond to *CXCR7* and *SPON2* (Figure 5). Figures 5A, B show that when there is low expression of *CRCR7* the probability of survival increases in both overall survival and PFS, respectively. The p value in both comparisons show the high impact of *CXCR7* expression in prognosis of bladder cancer patients. For *SPON2*, there is a significant difference in both overall survival and PFS (Figures 5C, D, respectively) when there is low expression vs. high expression of this gene. However, the impact of *SPON2* is lower than the impact of *CXCR7*. In conclusion, after analyzing ~30 membrane protein genes for their role in survival, only *ANTXR1*, *CXCR7*, and *SPON2* demonstrated a statistically significant impact. Future studies will investigate potential associations involving these proteins. This demonstrates the uniqueness of *ANTXR1* as a prognosis predictor in bladder cancer.

Pathways associated with high *ANTXR1* expression in bladder cancer

After understanding the impact of *ANTXR1* expression in tumors and its impact on tumor prognosis, we wanted to further investigate the possible mechanisms and/or pathways that were impacted by the expression of *ANTXR1* that might lead to poor prognosis. To understand this, Gene Set Enrichment Analysis (GSEA) was performed on bladder cancer patients with high *ANTXR1* expression (Figure 6). On the volcano plot (Figure 6A) we discerned between the genes that

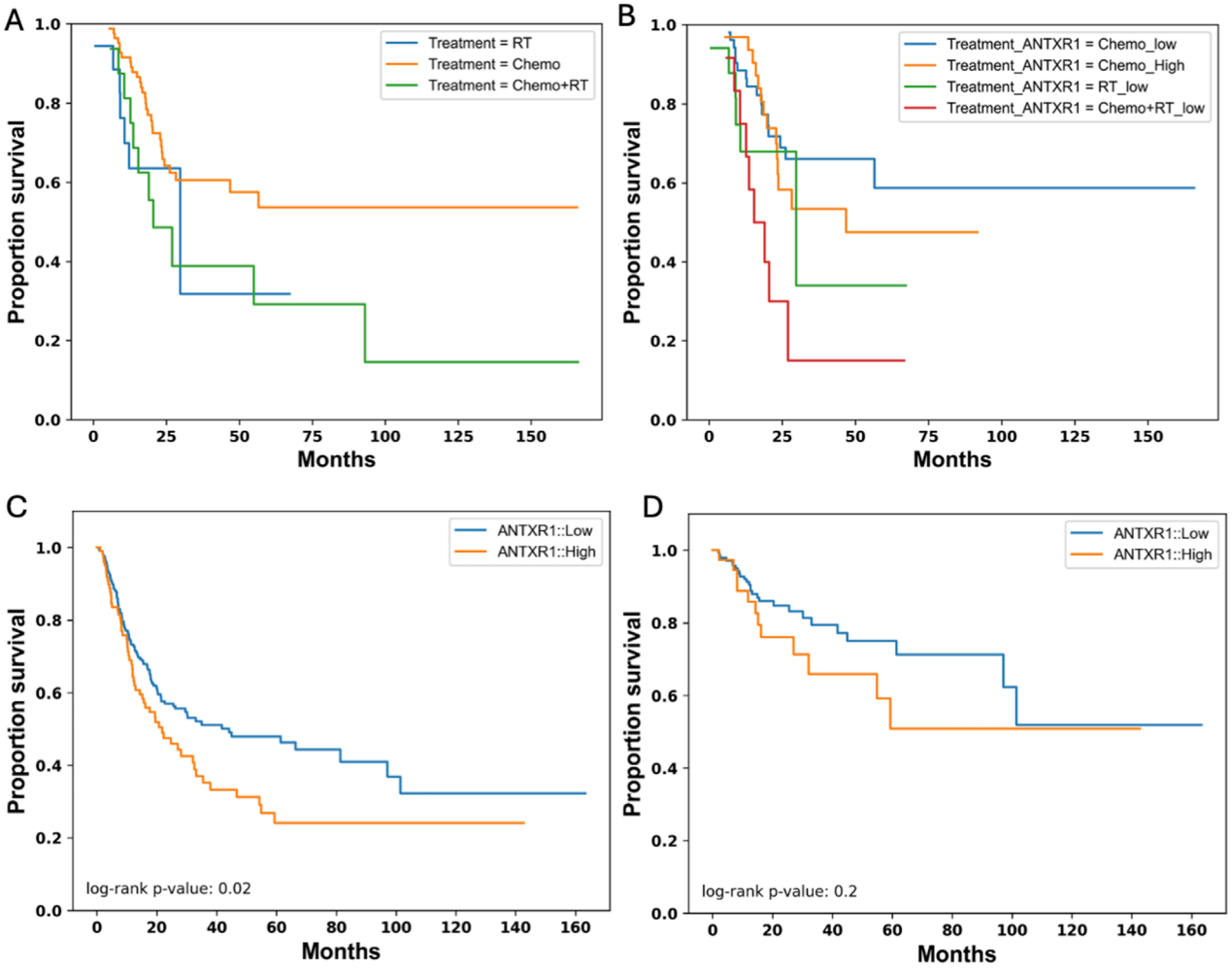

FIGURE 4
Survival in bladder cancer patients expressing different levels of ANTXR1. Kaplan-Meier survival curve for overall survival in bladder cancer patients separated by **(A)** different treatments (RT: Radiotherapy (blue); Chemo: chemotherapy (orange); Chemo + RT: chemotherapy and radiotherapy (green)); and separated by **(B)** treatments and high or low expression of ANTXR1 in tumor (Chemo_High: chemotherapy with high expression of ANTXR1 (orange); Chemo_low: chemotherapy with low expression of ANTXR1 (blue); RT_low: Radiotherapy with low expression of ANTXR1 (green); Chemo + RT_low: chemotherapy and radiotherapy with low expression of ANTXR1 (red)). Kaplan-Meier survival curve for **(C)** Progression Free survival when there is high (orange) or low expression of ANTXR1 (blue). Kaplan-Meier survival curve for **(D)** Disease-free survival with when there is high (orange) or low expression of ANTXR1 (blue) in tumor.

were overexpressed (activated) when *ANTXR1* was highly expressed. These genes were then divided into the pathways in which they were involved (Figure 6B) using KEGG pathway analysis.

The GSEA revealed that among the top 20 KEGG pathways associated with *ANTXR1* expression, the PI3K-Akt signaling pathway, MAPK signaling pathway, and TGF-beta signaling pathway were prominent. These pathways are well-known for their roles in cancer activation and the aggressiveness of the disease. This KEGG analysis was also congruent with MSigDB hallmark pathways (Supplementary Table S1), where TGF-beta signaling is within the top 20 pathways associated among other signaling pathways related to aggressiveness of the tumor such as KRAS, TNFalpha signaling pathways and inflammatory responses (IL-6/STAT3, IL-2/STAT5 and IFNgamma pathways).

Discussion

TEM8 is part of the tumor endothelial family of proteins and is part of the anthrax receptors, in addition to the capillary morphogenesis gene 2 (CMG2). Although these proteins are homologous, in reality they have quite different roles in terms of disease. Here, we have focused on the role of TEM8, its expression in different types of cancer, and its potential impact in cancer patients.

First, the stromal score was analyzed for different types of cancer evaluated when there was high or low expression of *ANTXR1*. Stromal cells are thought to have important roles in tumor growth, disease progression and drug resistance (Yoshihara, et al., 2013), and tumor related stroma has a role in progression, metastasis of tumor and response to chemotherapy (Stein et al., 2019). The tumor microenvironment (TME) has been demonstrated to play a key role in solid cancers and therefore, the stromal score could be a good indicator

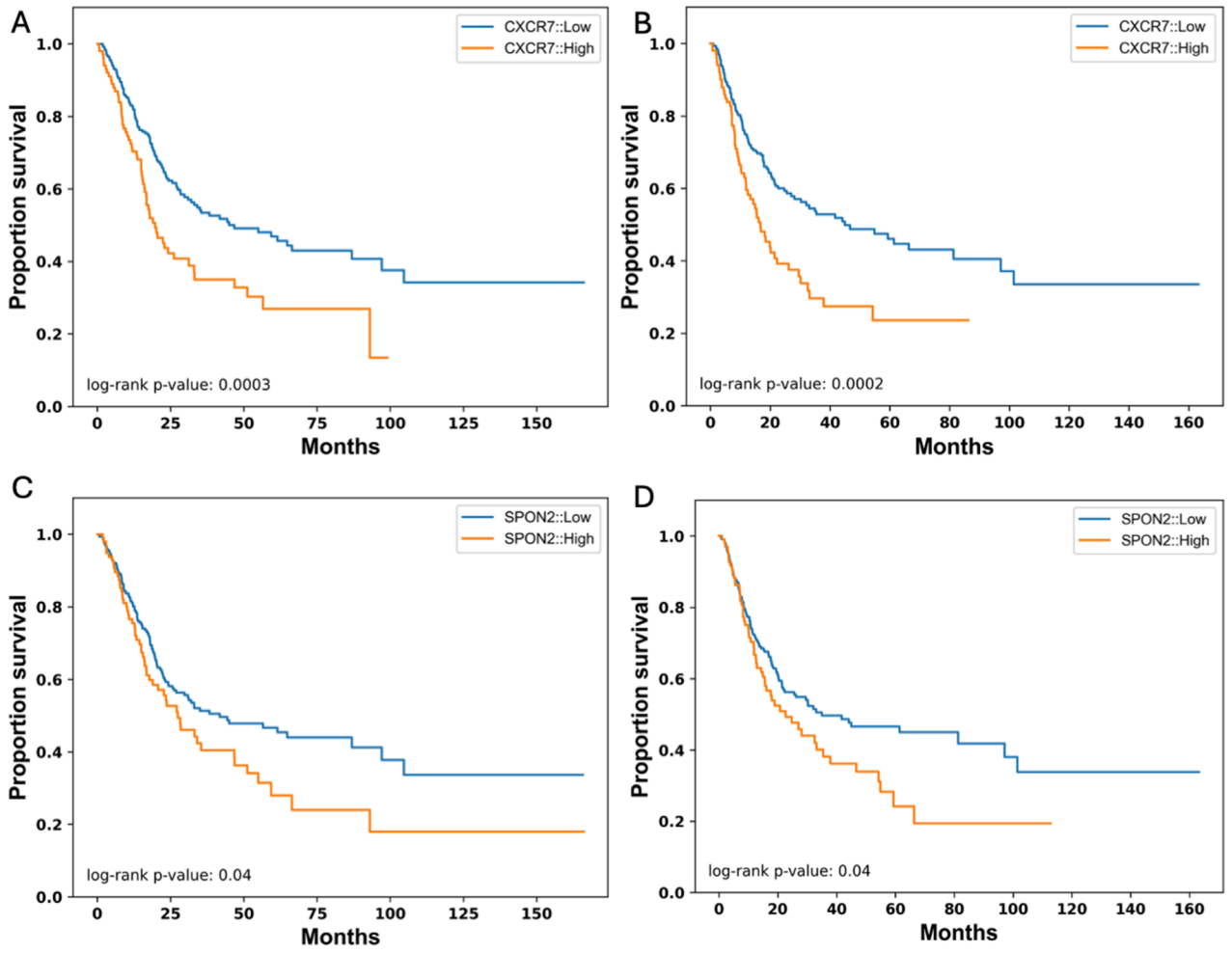

FIGURE 5
Other Cancer-Associated Membrane Protein genes that their expression affect survival in bladder cancer. Expression of CXCR7 in tumor (high in orange vs. low in blue) affects overall survival **(A)** and progression free survival **(B)** represented by a Kaplan-Meier survival curve. Similarly, expression of SPON2 in tumor (high in orange vs. low in blue) affects overall survival **(C)** and progression free survival **(D)** represented by a Kaplan-Meier survival curve.

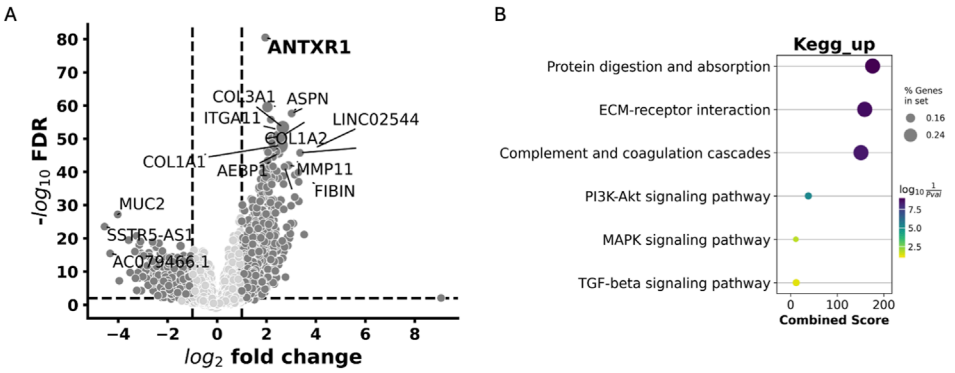

FIGURE 6
Pathways associated with high expression of ANTXR1 in bladder cancer. **(A)** Volcano plot of Differentially expressed genes impacted by ANTXR1 high expression. **(B)** Gene set enrichment analysis shows KEGG pathways upregulated in ANTXR1 high expression patients. Darker and wider dots represent more genes differentially expressed within the same pathway; lighter and smaller dots represent less genes differentially expressed within the same pathway.

of prognosis in solid cancers. This statement has also been tested before to find complementary ways to the long known TMN stage score (Xu et al., 2023). Here, the stromal score in six out of eleven cancer types analyzed, had a significant difference between low and high expression of *ANTXR1*. This implies a reciprocal relationship between *ANTXR1* expression level and stromal score, suggesting that *ANTXR1* could be a potential prognostic indicator. That there is more *ANTXR1* expressed with a greater amount of stroma cells is congruent with the fact that *ANTXR1* expression has been found in some stromal cells including cancer stem cells (Szot et al., 2018).

Another way to predict prognosis in patients with cancer is the immune score, and sometimes this prediction can mirror the stromal score. The immune score corresponds to the expression of key markers of immune cells found in the tumor which represent the immune cells infiltrated with potentially better outcomes. Here, we observed that two of the cancer types analyzed had a significant difference when analyzing immune score in terms of high or low expression of *ANTXR1*. This indicates that, for the majority of the cancer types studied, high stromal scores are correlated with high expression of *ANTXR1 -but* not necessarily the immune score. This finding is similar to those of renal cancer cells, where high levels of $CD8^+$ infiltration do not correlate with a favorable prognosis (Xu et al., 2023). Furthermore, this paradox is also present in patients with melanoma in whom the immune score did not reflect any significant difference between high or low expression of *ANTXR1*. However, patients had a longer survival probability (Figure 2C) when patients with low expression of *ANTXR1* were treated with immunotherapy. However, in previous studies high *ANTXR1* expression has been correlated with tumor associated macrophage differentiation and immunosuppression factor in the TME (Huang et al., 2020) suggesting that the immune score might be low. The relationship between immune score and prognosis prediction still needs to be further investigated, as well as its potential relationship with *ANTXR1* expression.

TEM8 has been found in different studies to be a poor prognostic marker especially for a native mostly unmutated gene. Here, we analyzed different types of cancer in terms of probability of OS and expression of *ANTXR1* and found that bladder cancer and cervical squamous cell carcinoma showed significant statistical difference, but there were some cancers (small cell lung cancer OS ($p = 0.06$) and breast cancer PFS ($p = 0.07$)) that approached statistical significance. More clinical data analyzed within each cancer type can further clarify the impact of *ANTXR1* expression in these cases. This also translates into the analysis of PFS or DFS, which give another perspective of the prognosis of the patients for different cancers. For bladder cancer, the impact of *ANTXR1* expression showed a statistical difference not only in OS but in PFS, confirming the prognostic biomarker power of *ANTXR1* expression. Similarly, in gastric cancer high ANTXR1 expression was correlated with poor OS and PFS (Huang et al., 2020). It is important to highlight that, to compare between bioinformatic studies of *ANTXR1* expression, it is necessary to understand how the data was analyzed differently in each study, for instance, varying parameters for gene expression.

ANTXR1 expression is generally associated with tumor metastasis, aggressiveness and tumor invasion in different types of tumors (Hoye et al., 2018). To fully understand the impact of high *ANTXR1* expression, it is key to determine the downstream pathways affected that could potentially lead to tumor progression and aggressiveness. In bladder cancer, the clinical data analyzed via gene set enrichment analysis (GSEA) showed that the extracellular matrix (ECM)- receptor interaction pathway was upregulated, as well as other cancer associated pathways such as PI3K-Akt, MAPK, and TGF-beta signaling pathways (KEGG pathways). These upregulated pathways were also confirmed using the MSigDB Hallmark pathways, including the KRAS Hallmark pathway that is partially in the PI3K-Akt KEGG pathway. One of the key genes in the ECM-receptor interaction pathway is collagen, which has been previously described as a key protein for cancer cell survival mediated by TEM8 in tumor-associated stroma (Hsu et al., 2022) and TEM8 association with the PI3K-Akt signaling pathway in glioblastoma (Kundu et al., 2024) and gastric cancer (Cai et al., 2020). TGF-beta signaling pathway has also been found to be enriched in gastric cancer (Huang et al., 2020), and it is involved with the telomerase (hTERT) enzyme in upregulating the urokinase-type plasminogen activator (uPA) for endothelial-mesenchymal transition (EMT) (Jaiswal and Yadava, 2020; Jaiswal and Yadava, 2019). EMT is one of the principal mechanisms responsible for changes in the ECM and metastasis, indicating poor prognosis in patients (Jaiswal and Yadava, 2020). Since TEM8 also serves as a receptor for uPA via EGFR phosphorylation (Zhang et al., 2018) it should be further investigated the relation between TEM8 and EMT pathways, as this will confirm its role as a prognosis indicator. Regarding the MAPK signaling KEGG pathway, more specifically the p38 MAPK pathway, contains the *NLK* gene that is a precursor for the Wnt pathway, which has been previously demonstrated to be key for metastasis and tumor proliferation in lung adenocarcinoma (Ding et al., 2021). Our findings confirm the unique role of high *ANTXR1* expression in bladder cancer as a precursor for key signaling pathways that induce tumor aggressiveness, metastasis and invasion, indicating a poor prognosis. Future studies need to investigate the role of *ANTXR1* expression in other pathways like EGFR, the complement and coagulation cascades, as well as metastatic pathways including the potential role of TEM8 in the EMT process (with uPA and transgelin), and its importance in tumor biology.

ANTXR1 expression has been linked to different proteins that may be interacting with TEM8 in the membrane, but to understand its role of tumor prognosis we analyzed the expression level of different membrane proteins and how it was impacting OS and PFS. Of more than 25 membrane proteins, only *CXCR7*, *SPON2* and *ANTXR1* had a significant difference in probability of survival in bladder cancer patients (only ~10%). *CXCR7* expression has been linked with aggressiveness or metastasis, progression of the tumor and poor overall survival across multiple cancer types (Al-toub et al., 2019). Similarly, high expression of *SPON2* in laryngeal squamous cell carcinoma was associated with metastasis and higher pathological grade (Zhang et al., 2024). These findings and the above confirm the uniqueness of *ANTXR1* as a membrane protein with prognostic biomarker significance.

Although we described a bioinformatic study analyzing clinical data from patients with different types of cancers, further investigations must address not only the *ANTXR1* expression at the RNA, but at the protein level (TEM8). TEM8 has five isoforms that differ mainly in the membrane and intracellular domain and occur after alternative splicing (Vargas et al., 2012). It is still unknown the tropism of expression of these isoforms (cancer or angiogenic cells), or when the isoforms are expressed. There are two indications that the isoforms could play a different role in cancer cells *versus* in somatic cells. First, it was previously found that alpha-smooth muscle actin and transgelin are two intracellular factors that alter the form of TEM8 extracellularly

(Yang et al., 2011). As the isoforms have different intracellular lengths, this also may alter the surface form of TEM8, and also potentially affect the downstream pathways that are upregulated in angiogenic and cancer cells. Second, in previous studies it was demonstrated that some post-translational modifications like N-glycosylation of extracellular domain of TEM8 are key for Seneca Valley Virus (SVV) binding to TEM8 in solid cancer cells (Jayawardena et al., 2018); and it is known that this oncolytic virus only infects solid cancer cells (Venkataraman et al., 2008; Rudin et al., 2011). Further studies will explore the role of the isoform in cancer metabolism, as well as the impact that these might have in the downstream pathways from *ANTXR1*.

As TEM8 becomes a more important target for cancer cell killing targeting due to its important role in carcinogenesis as well as selective high expression in solid cancer cells and associated stromal cells, a need to find a specific therapeutic agent to TEM8 has grown over time. Direct pathway inhibitors, RNA targeting, DNA-based vaccines, antibodies, antibody-like molecules, antibody-drug conjugates, CAR-T cells and oncolytic viruses have been used before in pre-clinical stages (Kareff et al., 2023). Most of these approaches are still in the pre-clinical phase. Antibodies and antibody-drug conjugates (ADCs) have demonstrated some success in clinical trials like the monoclonal antibodies SB5 and AF334; a tri-specific killer engager (TriKe) that lead to anti-angiogenic and anti-stroma effects; an ADC with MMAE with high tumor killing and anti-stroma effects; and CAR-T cells that blocked neo-vascularization in breast cancer (Kareff et al., 2023). However, no other therapeutic agent against TEM8 has shown any promising efficacy clinical trials except SVV. This oncolytic RNA virus uses TEM8 to infect TEM8 positive solid cancer cells with high specificity and delivers durable anti-tumor responses by turning "cold" non-immunogenic tumor into a "hot" immunogenic tumor. Further, it has been shown that the treatment of solid cancers in difficult to treat solid tumor animal models with of SVV and immune checkpoint inhibitors can eradicate primary tumors and block secondary tumors from developing indicating that an anti-tumor immune response developed (Corbett et al., 2022).

The role of *ANTXR1* as a prognostic biomarker has been demonstrated not only in this study for bladder cancer, but for other types of cancer. The impact of *ANTXR1* expression may also contribute to the prediction of some therapies' success such as immune checkpoint inhibitors, TEM8 targeted therapies, or even oncolytic virotherapy. However, this needs to be further investigated as the role of TEM8 in cancer progression is still been elucidated, as well as its effects in other well-known pathways such as TGF-beta, EGFR, MAPK and Wnt-beta catenin. A starting step could be to analyze more real-world data, such as the publicly available in TCGA database, but other available sources could have contributed more valuable information and confirmed our hypothesis in this study. More available data from different sources for these types of studies could speed the advances of the field and specifically for the discovery of the role of TEM8. Nevertheless, future experimental studies would be needed to confirm the bioinformatic analysis done in this study.

In conclusion, in this paper we demonstrated that *ANTXR1* expression has a unique role as a prognostic biomarker not only for bladder cancer, but also for other types of cancer. The downstream activated pathways found in solid cancers with high expression of *ANTXR1* confirmed what has been found in previous studies in other types of cancer., i.e., to be linked with cancer aggressiveness, invasion and metastasis. SVV is the only therapeutic agent with promising efficacy in clinical trials against TEM8 expressing tumors with high specificity. Further studies will address the impact of the *ANTXR1* expression at the protein level, as it could give more information or the role in cancer cells vs. somatic cells.

Data availability statement

Publicly available datasets were analyzed in this study. This data can be found here: https://www.cbioportal.org and in the Supplementary Material.

Author contributions

LF: Writing–review and editing, Conceptualization, Supervision, Writing–original draft. SA: Data curation, Formal Analysis, Visualization, Writing–review and editing. AC: Writing–review and editing. SK: Writing–review and editing. PH: Writing–review and editing, Conceptualization, Supervision, Visualization.

Funding

The author(s) declare that no financial support was received for the research, authorship, and/or publication of this article.

Conflict of interest

Authors LF, SA, and PH were employed by Seneca Therapeutics, Inc.

The remaining authors declare that the research was conducted in the absence of any commercial or financial relationships that could be construed as a potential conflict of interest.

Generative AI statement

The author(s) declare that no Generative AI was used in the creation of this manuscript.

Publisher's note

Supplementary material

The Supplementary Material for this article can be found online at: https://www.frontiersin.org/articles/10.3389/fmolb.2024.1520223/full#supplementary-material

References

Alcalá, S., Martinelli, P., Hermann, P. C., Heeschen, C., and Sainz, Jr.B. (2019). The anthrax toxin receptor 1 (ANTXR1) is enriched in pancreatic cancer stem cells derived from primary tumor cultures. *Stem Cells* 2019, 1378639. doi:10.1155/2019/1378639

Al-toub, M., Almohawes, M., Alajez, N. M., Vishnubalaji, R., Alfayez, M., Aldahmash, A., et al. (2019). CXCR7 signaling promotes breast cancer survival in response to mesenchymal stromal stem cell-derived factors. *Cell Death Discov.* 5 (87), 87. doi:10.1038/s41420-019-0169-3

Cai, C., Dung, W., Liu, S., Huang, L., Li, Y., Li, G., et al. (2020). Anthrax toxin receptor 1/Tumor endothelial marker 8 promotes gastric cancer progression through activation of the P13K/AKT/mTOR signaling pathway. *Cancer Sci.* doi:10.1111/cas.14326

Castaneda, P. R., Theodorescu, D., Rosser, C. J., and Ahdoor, M. (2023). Identifying novel biomarkers associated with bladder cancer treatment outcomes. *Front. Oncol.* 13, 1114203. doi:10.3389/fonc.2023.1114203

Chaudhary, S. C., Siddiqui, M. S., Athar, M., and Alam, M. S. (2012). D-Limonene modulates inflammation, oxidative stress and Ras-ERK pathway to inhibit murine skin tumorigenesis. *Hum. Exp. Toxicol.* 31 (8), 798–811. doi:10.1177/0960327111434948

Chen, D., Bhat-Nakshatri, P., Goswami, C., Badve, S., and Nakshatri, H. (2013). ANTRXi, a stem cell enriched functional biomarker, conncets collagen signaling to cancer stem-like cells and metastasis in breast cancer. *Pub Med.* doi:10.1158/0008-5472.CAN-13-1080

Corbett, V., Hallenbeck, P., Rychahou, P., and Chauhan, A. (2022). Evolving role of seneca valley virus and its biomarker TEM8/ANTXR1 in cancer therapeutics. *Front. Mol. Biosci.* 9, 930207. doi:10.3389/fmolb.2022.930207

Ding, C., Liu, J., Zhang, J., Wan, Y., Hu, L., Charwudzi, A., et al. (2021). Tumor endothelial marker 8 promotes proliferation and metastasis *via* the wnt/β-catenin signaling pathway in lung adenocarcinoma. *Front. Oncol.* 11, 712371. doi:10.3389/fonc.2021.712371

Evans, D. J., Wasinger, A. M., Brey, R. N., Dunleavey, J. M., St. Croix, B., and Bann, J. G. (2018). Seneca Valley virus exploits TEM8, a collagen receptor implicated in tumor growth. *Front. Oncol.* 8, 506. doi:10.3389/fonc.2018.00506

Flores Monar, G. V., Reynolds, T., Gordon, M., Moon, D., and Moon, C. (2023). Molecular markers for bladder cancer screening: an insight into bladder cancer and FDA-approved biomarkers. *Int. J. Mol. Sci.* 24, 14374. doi:10.3390/ijms241814374

Friebe, S., Deuquet, J., and van der Goot, F. G. (2015). Differential dependence on N-glycosylation of anthrax toxin receptors CMG2 and TEM8. *PLoS One* 10, e0119864. doi:10.1371/journal.pone.0119864

Fu, S., Tong, X., Cai, C., Zhao, Y., Wu, Y., Li, Y., et al. (2010). The structure of tumor endothelial marker 8 (TEM8) extracellular DOmain and implications for its receptor function for recognizing anthrax toxin. *PLoS One* 5, e11203. doi:10.1371/journal.pone.0011203

Hoye, A. M., Tolstrup, S. D., Horton, E. R., Nicolau, M., Frost, H., Woo, J. H., et al. (2018). Tumor endothelial marker 8 promotes cancer progression and metastasis. *Oncotarget* 9 (53), 30173–30188. doi:10.18632/oncotarget.25734

Hsu, K.-S., Dunleavey, J. M., Szot, C., Yang, L., Hilton, M., Morris, K., et al. (2022). Cancer cell survival depends on collagen uptake into tumor-associated stroma. *Nat. Commun.* 13, 7078. doi:10.1038/s41467-022-34643-5

Huang, X., Zhang, J., and Zheng, Y. (2020). ANTXR1 is a prognostic biomarker and correlates with stromal and immune cell infiltration in gastric cancer. *Front. Mol. Biosci.* 7, 598221. doi:10.3389/fmolb.2020.598221

Jaiswal, R. K., and Yadava, P. K. (2019). TGF-β-mediated regulation of plasminogen activators is human telomerase reverse transcriptase dependent in cancer cells. *BioFactors* 45 (5), 803–817. doi:10.1002/biof.1543

Jaiswal, R. K., and Yadava, P. K. (2020). Assessment of telomerase as drug target in breast cancer. *J. Biosci.* 45, 72. doi:10.1007/s12038-020-00045-2

Jayawardena, N., Burga, L. N., Easingwood, R. A., Takizawa, Y., Wolf, M., and Bostina, M. (2018). Structural basis for anthrax toxin receptor 1 recognition by Seneca Valley Virus. *Proc. Natl. Acad. Sci. U. S. A.* 115 (46), E10934-E10940. doi:10.1073/pnas.1810664115

Ju, J., Faundez, V., and Werner, E. (2010). Endosomal recycling regulates anthrax toxin receptor 1/tumor endothelial marker 8-dependent cell spreading. *Exp. Cell Res.* 12 (316), 1946–1957. doi:10.1016/j.yexcr.2010.03.026

Kareff, S. A., Corbett, V., Hallenbeck, P., and Chauhan, A. (2023). TEM8 in oncogenesis: protein biology, pre-clinical agents, and clinical rationale. *Cells* 12, 2623. doi:10.3390/cells12222623

Kundu, P., Jain, R., Kanuri, N. N., Arimappamagan, A., Santosh, V., and Kondaiah, P. (2024). DNA methylation in recurrent glioblastomas: increased TEM8 expression activates the src/PI3K/AKT/GSK-3β/B-catenin pathway. *Cancer Genomics and Proteomics* 21, 485–501. doi:10.21873/cgp.20466

Luo, Q., He, F., and Cao, J. (2021). A stromal and immune cell infiltration based score model predicts prognosis and chemotherapy effect in colorectal cancer. *Int. Immunopharmacol.* 99, 107940. doi:10.1016/j.intimp.2021.107940

Pietrzyk, L., Korolezuk, A., Matysek, M., Arciszewski, M. B., and Torres, K. (2021). Clinical value of detecting tumor endothelial marker 8 (ANTXR1) as a biomarker in the diagnosis and prognosis of colorectal cancer. *Cancer Manag. Res.* 13, 3113–3122. doi:10.2147/CMAR.S298165

Rudin, C. M., Poirier, J. T., Senzer, N. N., Stephenson, Jr, J., Loesch, D., Burroughs, K. D., et al. (2011). Phase I clinical study of Seneca Valley Virus (SVV-001), a replication-competent picornavirus, in advanced solid tumors with neuroendocrine features. *Clin. Cancer Res.* 17 (4), 888–895. doi:10.1158/1078-0432.CCR-10-1706

Stein, Y., Aloni-Grinstein, R., and Rotter, V. (2019). Mutant p53 - a potential player in shaping the tumor-stroma crosstalk. *J. Mol. Cell Biol.* 11 (7), 600–604. doi:10.1093/jmcb/mjz071

Sun, M., Li, H., Liu, J., Ning, L., Zhao, D., and Liu, S. (2021). The relationship between TEM8 and early diagnosis and prognosis of lung cancer. *Minerva Medica* 112 (3), 359–364. doi:10.23736/S0026-4806.20.06444-7

Szot, C., Dimitrov, D. S., and St. Croix, B. (2018). Tumor stroma–targeted antibody-drug conjugate triggers localized anticancer drug release. *J. Clin. Investgation* 128 (7), 2927–2943. doi:10.1172/JCI120481

Vargas, M., Karamsetty, R., Leppla, S. H., and Chaudry, G. J. (2012). Broad expression analysis of human ANTXR1/TEM8 transcripts reveals differential expression and novel splizce variants. *PLoS One* 7, e43174. doi:10.1371/journal.pone.0043174

Venkataraman, S., Reddy, S. P., Loo, J., Idamakanti, N., Hallenbeck, P. L., and Reddy, V. S. (2008). Structure of Seneca Valley Virus-001: an oncolytic picornavirus representing a new genus. *NIH Public Access* 16 (10), 1555–1561. doi:10.1016/j.str.2008.07.013

Wang, Q., Shao, X., Zhang, Y., Zhu, M., Wang, F. X., Mu, J., et al. (2023). Role of tumor microenvironment in cancer progression and therapeutic strategy. *Cancer Med.* 12, 11149–11165. doi:10.1002/cam4.5698

Wei, S., Lu, J., Lou, J., Shi, C., Mo, S., Shao, Y., et al. (2020). Gastric cancer tumor microenvironment characterization reveals stromal-related gene signatures associated with macrophage infiltration. *Front. Genet.* 11, 663. doi:10.3389/fgene.2020.00663

Xu, X., Xu, Y., Hu, W., Hong, W., Wang, Y., Zhang, X., et al. (2023). Stromal score is a promising index in tumor patients' outcome determination. *Heliyon* 9, e22432. doi:10.1016/j.heliyon.2023.e22432

Yang, M. Y., Chaudhary, A., Seaman, S., Dunty, J., Stevens, J., Elzarrad, M. K., et al. (2011). The cell surface structure of tumor endothelial marker 8 (TEM8) is regulated by the actin cytoskeleton. *Biochim. Biophys. Acta* 1813 (1), 39–49. doi:10.1016/j.bbamcr.2010.11.013

Yoshihara, K., Shahmoradgoli, M., Martínez, E., Vegesna, R., Kim, H., Torres-Garcia, W., et al. (2013). Inferring tumour purity and stromal and immune cell admixture from expression data. *Nat. Commun.* 4, 2612. doi:10.1038/ncomms3612

Zhang, J., Liu, G., Liu, Y., Yang, P., Xie, J., and Wei, X. (2024). The biological functions and related signaling pathways of SPON2. *Front. Oncol.* 13, 1323744. doi:10.3389/fonc.2023.1323744

Zhang, L.-C., Shao, Y., Gao, L.-H., Liu, J., Xi, Y.-Y., Xu, Y., et al. (2018). TEM8 functions as a receptor for uPA and mediates uPA-stimulated EGFR phosphorylation. *Cell Commun. Signal* 16 (1), 62. doi:10.1186/s12964-018-0272-8

frontiers | Frontiers in Oncology

TYPE Original Research
PUBLISHED 24 January 2025
DOI 10.3389/fonc.2024.1531972

OPEN ACCESS

EDITED BY
Matteo Becatti,
University of Firenze, Italy

REVIEWED BY
Pasquale Pisapia,
University of Naples Federico II, Italy
Zhifang Zhang,
City of Hope National Medical Center, United States
Julie Pannequin,
Centre National de la Recherche Scientifique (CNRS), France
Lianming Liao,
Fujian Medical University Union Hospital, China

*CORRESPONDENCE
Yao Wang
tongjimc12@126.com

†These authors have contributed equally to this work and share first authorship

RECEIVED 21 November 2024
ACCEPTED 31 December 2024
PUBLISHED 24 January 2025

CITATION
Deng Q, Li W, Huang Y, Wang H, Zhou X, Guan Z, Cheng B and Wang Y (2025) Immunolipid magnetic bead-based circulating tumor cell sorting: a novel approach for pathological staging of colorectal cancer.
Front. Oncol. 14:1531972.
doi: 10.3389/fonc.2024.1531972

Immunolipid magnetic bead-based circulating tumor cell sorting: a novel approach for pathological staging of colorectal cancer

Qingyan Deng†, Weidong Li†, Yueming Huang, Haitao Wang, Xinhao Zhou, Zhifen Guan, Bohao Cheng and Yao Wang*

Department of Gastrointestinal Surgery, Zhongshan People's Hospital, Zhongshan, Guangdong, China

Objective: This study aimed to assess whether circulating tumor cells (CTCs) from colorectal cancer (CRC) could be used as an alternative to tissue samples for genetic mutation testing, overcoming the challenge of difficult tumor tissue acquisition.

Methods: We developed an immunolipid magnetic bead (IMB) system modified with antibodies against epithelial cell adhesion molecule (EpCAM) and vimentin to efficiently separate CTCs. We prepared EpCAM-modified IMBs (Ep-IMBs) and vimentin-modified IMBs (Vi-IMBs). The separation efficiency of the system was evaluated via *in vitro* experiments and by capturing and counting CTCs in blood samples from 23 CRC patients and 20 healthy controls. Hotspot mutations in patient tissue samples were identified via next-generation sequencing (NGS), whereas mutations in blood CTCs were detected via Sanger sequencing. The concordance between hotspot mutations in tumor tissue and blood CTCs was analyzed.

Results: The CTC sorting system exhibited good dispersion, stability, and low cytotoxicity, with a specificity of 90.54% and a sensitivity of 89.07%. CRC patients had an average of 8.39 CTCs per 7.5 mL of blood, whereas healthy controls had 0.09 per 7.5 mL of blood. The consistency of gene mutations was as follows: *TP53* (91.31%), *PIK3CA* (76.00%), *KRAS* (85.36%), *BRAF* (51.00%), *APC* (65.67%), and *EGFR* (74.00%), with an overall gene mutation consistency of 85.06%.

Conclusion: Our CTC sorting system, which is based on Ep-IMBs and Vi-IMBs, effectively captures CTCs in the peripheral blood of CRC patients and enables clinical hotspot gene mutation testing via these enriched CTCs. This system partially solves the problem of difficult tumor tissue sample collection and provides a reference for gene mutation testing in early diagnosis, therapeutic efficacy evaluation, prognosis assessment, and minimal metastasis detection in CRC patients, showing significant potential for clinical application, especially in targeted therapy gene testing for CRC.

KEYWORDS

colorectal cancer, NGS sequencing, immunolipid magnetic bead, circulating tumor cells, mutations in tumor tissue

Introduction

Colorectal Cancer, which includes both colon and rectal malignancies, is a common malignancy of the digestive tract. It is the third most common cancer worldwide, following lung and breast cancer, and is also the second leading cause of cancer-related deaths worldwide (1). Given the severity of CRC, early prevention, diagnosis, and treatment have become focal points of research (Buccafusca et al., 2019; Mauri et al., 2019) (2, 3). With the advancement of molecular biology techniques, there has been a deeper understanding of genetic alterations during CRC carcinogenesis. CRC is widely believed to be a complex disease involving multiple steps, stages, genes, and molecular regulations (4–6).

More than 90% of cancer-related deaths are attributed to distant metastases (7). As a critical link in the distant metastasis of malignant tumors, the presence and number of CTCs in a patient's bloodstream not only reflects the ability of the primary tumor to invade blood vessels but also indicates the potential to form metastatic foci in distant organs (8). Therefore, the detection and quantification of CTCs is of significant prognostic value in assessing the risk of malignancy and metastasis of tumors. In addition, CTCs, as an integral part of liquid biopsy, can compensate for the inadequacy of traditional methods in the dynamic monitoring of tumor tissue and provide more precise personalized treatment guidance through real-time molecular and functional typing (9). However, traditional serological, imaging, and pathological testing methods struggle to detect CTCs, as only 1 CTC can be found per 10 billion normal blood cells, requiring an extremely sensitive detection method (10). Immunochemical magnetic nanoparticles can efficiently and selectively recognize and capture CTCs in whole blood (11). Currently, the only approved method for CTC detection is the CellSearch system, which uses EpCAM-coated to enrich CTCs and anti-CK antibodies for identification; however, this system has limitations, such as its inability to capture CTCs that have undergone epithelial –mesenchymal transition (EMT) (12, 13). Therefore, magnetic beads modified with other specific protein antibodies are required to achieve efficient enrichment of CTCs. A substantial body of research indicates that vimentin is highly expressed in various tumor cells, especially in tumor cells undergoing EMT (14, 15). Thus, vimentin may serve as a potential target for CTC capture in CRC.

High-throughput sequencing, also known as "next-generation" sequencing technology (NGS), is characterized by its ability to perform sequence determination of hundreds of thousands to millions of DNA molecules simultaneously, albeit with relatively short read lengths (16, 17). NGS methods fall into two main categories: mutational genomic panel sequencing of solid tumors and liquid biopsy of peripheral blood and urine (18, 19). Solid tumor NGS panels reflect only the status of the tumor at one point in time, which is very timely and necessary to guide the treatment of newly diagnosed patients. However, for patients who need to track the progression of tumor drug resistance throughout the process, the status of the tumor in the body will change over time (20, 21). In addition, for cancer patients who have already metastasized at the time of detection, taking a sample from only a certain part of the cancer tissue may not reflect the overall condition of the patient; for patients who have undergone surgery to reduce the tumor burden, rebiopsy of the tissue may be difficult. Therefore, there is a strong clinical need and scientific research value for NGS-based CTC liquid biopsy-targeted gene detection.

Molecular cytopathology, a growing specialty, offers insights into personalized therapy responses and prognoses from cytological neoplasm samples. Liquid biopsies, monitoring biomarkers like CTCs and ctDNA in blood and body fluids, are non-invasive and can be repeated, even in patients with comorbidities. Despite challenges posed by low biomarker concentrations, sensitive molecular techniques can detect them, necessitating validation and integration with tissue-based assessments (22).

This study aims to develop an efficient and specific CTC sorting system for CRC based on multifunctional targeted IMBs to achieve efficient, rapid, and accurate separation and enrichment of peripheral blood CTCs. By using NGS to detect hot mutation genes in patient tissues and Sanger sequencing to detect hot mutation genes in CTCs, we aimed to understand the consistency and differences between the tissue and peripheral blood levels of CRC and the trends of these differences. The aim of this study is to solve the clinical problem of difficult tumor tissue sampling and provide a reference for gene mutation detection in early diagnosis, efficacy evaluation, prognosis assessment, and micrometastasis detection in tumor patients.

Materials and methods

Sample collection and processing

The study included a total of 23 CRC patients treated at our hospital from January 2023 to July 2023. Patient selection was based on the availability of high-quality CTC samples and aimed to represent a diverse range of disease stages and characteristics. The 23 patients included in this study were carefully chosen to ensure that the sample population was representative of the broader patient cohort. Despite the relatively small sample size, the rigorous study design, including the use of validated markers and standardized CTC isolation and enumeration procedures, ensures the reliability and validity of the results obtained. A control group of 20 healthy volunteers was also recruited, and 7.5 mL of blood was collected from each volunteer. The inclusion criteria were as follows: (I) aged between 18 and 90 years; (II) had histologically confirmed CRC (AJCC stages I - IV); and (III) signed written informed consent before participation. The exclusion criteria were as follows: (I) unresectable primary or metastatic tumors; (II) any treatment received prior to surgery (including chemotherapy, radiotherapy and targeted therapy); and (III) other concurrent malignancies.

Abbreviations: CTCs, circulating tumor cells; CRC, colorectal cancer; IMB, immunolipid magnetic bead; EpCAM, epithelial cell adhesion molecule; NGS, next-generation sequencing; EMT, epithelial–mesenchymal transition; AFM, atomic force microscopy.

Peripheral blood samples of 15 mL were collected from CRC patients via medical blood collection tubes containing EDTA/K2 as an anticoagulant. The samples were stored at 4°C and protected from freezing during storage, processing and transport to ensure sample quality. All samples were assayed within 72 hours. This study's adoption of a 72-hour timeframe is supported by several rationales: pre-experiments established the stability of CTC biomarkers and genetic material within this period, ensuring the impact on detection outcomes is negligible. Considering geographical disparities in sample collection and laboratory operational schedules, a 72-hour window is a feasible timeframe to process samples under optimal conditions. Rigorous quality control measures, such as the use of anticoagulant tubes and 4°C refrigeration, were employed to maintain sample integrity. Comparative analysis with samples processed within 24 hours verified the high consistency of results processed within 72 hours, validating our chosen protocol. The detection indicators included (1) counting CTCs in the peripheral blood of CRC patients via the magnetic separation immunofluorescence identification method; (2) analyzing hotspot mutated genes in the patient's tumor tissue via next-generation sequencing (NGS); and (3) genetic testing of CRC CTCs.

Experimental materials and instruments

In this study, we used the CRC cell lines CT26, HCT-8, SW480 and LS174T from the ATCC cell bank for our experiments. The cell culture conditions were strictly controlled in RPMI 1640 medium containing 10% neonatal calf serum, which was maintained at 37°C and 5% CO2 in an incubator. The key reagents and consumables used in the experiments were purchased from reputable biotechnology companies, including Solarbio's Prussian blue staining kit, Gibco's culture medium and serum, Abcam's antibodies, Sigma's DAPI staining solution, and eBioscience's CD45-PE, among others. In addition, Huzhou Lie Yuan Medical Laboratory Co., Ltd. provided EpCAM antibody derivatives and magnetic nanoparticles, whereas Avanti supplied DSPC-APC. The high-end instruments and equipment used in the experiments included a BI-90Plus laser particle size analyzer/zeta potential analyzer from Bruker-Haven of America, an XL-30 environmental scanning electron microscope from Philips of the Netherlands, an LDJ9600-1 VSM magnetic property tester from Digital Instruments of America, an OLYMPUS B×61 fluorescence microscope from Olympus of Japan, and an XD-52AA rotary evaporator from Shanghai Banno Biotechnology Co., Ltd.

Preparation of the IMB system

In this study, we innovatively employed the reverse evaporation method to prepare immunomagnetic beads (IMBs), marking a novel improvement upon existing techniques aimed at enhancing the efficiency and specificity of circulating tumor cell (CTC) separation. Our methodological contribution lies in the development of a new preparation technique for IMBs, which, to our knowledge, has not been previously reported. This advancement offers a new tool for the detection and analysis of CTCs. The experimental steps were as follows: First, 5 mg of 1,2-dioleoyl-sn-glycero-3-phosphocholine (DOPC) and 5 mg of cholesterol (Chol) were accurately weighed and added separately to two 50 mL three-necked flasks. A total of 1.0 mL of Fe3O4-HMN solution was measured, the ethanol was removed, the solution was dissolved in 3.0 mL of dichloromethane (CH2Cl2), and the mixture was transferred to the abovementioned three-necked flasks. The mixture was emulsified in an ice bath for 6 minutes via an ultrasonic probe processor. During this time, 2 mg of the EpCAM antibody 1,2-distearoyl-sn-glycero-3-phosphoethanolamine-N-[7-(dimethylamino)-4-trifluoromethyl]coumarin (GHDC) was dissolved in 6 mL of double-distilled water (ddH2O) and slowly injected into the three-necked flask. At the end of the ultrasonic treatment, the remaining CH2Cl2 was removed via a rotary evaporator. Finally, Ep-IMB was isolated via magnetic separation and triple-washed for purity. Vi-IMB was also synthesized successfully via the same method.

Characterization testing of IMB systems

In this study, we used a BI-90Plus laser particle size analyzer/zeta potential analyzer to accurately measure the particle size and zeta potential of the IMBs. In addition, the microscopic morphology of the IMBs under different modification conditions was observed via atomic force microscopy (AFM). UV absorption spectroscopy was performed on the IMB solution via a UV−Vis spectrophotometer to analyze its spectral characteristics. We also used a Bio-Rad FTS3000 Fourier transform infrared (FTIR) spectrometer to observe and analyze the functional groups on the surface of the microspheres or modified materials. Finally, to verify the cell capture ability of the IMBs, we stained CT26 cells captured by the IMBs via a Prussian blue staining kit.

Testing the cytotoxicity of the IMB system in CRC cell lines

In this study, we used standard cell culture techniques to culture CRC cell lines (including CT26, HCT-8, SW480 and LS174T). Specifically, the cells were cultured in complete RPMI 1640 medium supplemented with 10% fetal bovine serum (FBS) and 1% penicillin −streptomycin at 37°C and 5% CO2 in a humidified environment. To prepare a single-cell suspension, we digested the CRC cells with trypsin and then added the cell suspension to serum-containing medium to neutralize the trypsin. By diluting the cells and using a cell counting chamber, we accurately determined the cell concentration. The cells were then plated in a 96-well plate with 1000 cells per well, and 200 μL of culture medium was added to each well. After overnight incubation at 37°C, different concentrations of IMB were added to each well to yield final concentrations of 0, 10, 50, 100 and 200 μg/mL. The cells were then incubated for an additional 24 hours at 37°C, after which 10 μL of 5 mg/mL MTT reagent was added to each well, after which the mixture was returned to the incubator for 3 hours. After incubation, the medium was removed, and 200 μL of dimethyl sulfoxide (DMSO) was added to each

well. Finally, a Spectra Max M5/M5e multifunctional microplate reader (Molecular Devices) was used to read the absorbance at a wavelength of 560 nm, which was used to analyze and process the experimental data.

Measuring the cell capture efficiency of the IMB system

In this study, we first prepared a single-cell suspension of the CT26 cell line and accurately adjusted the cell concentration to 100 cells/7.5 mL to simulate the suspension state of CTCs. This simulated CTC suspension was subsequently divided equally into four experimental groups: the Ep-IMB group, the Vi-IMB group, the Ep/Vi-IMB group and the Ep+Vi-IMB group. In the Ep-IMB and Vi-IMB groups, immunomagnetic beads were added in volumes of 9, 15, 21, and 27 μL, respectively. In the Ep/Vi-IMB group, the two types of immunomagnetic beads were mixed at a 1:1 volume ratio, and 9, 15, 21, and 27 μL of the mixed immunomagnetic beads were added. In the Ep-IMB + Vi-IMB group, 6, 10, 14, or 18 μL of Ep-IMB or Vi-IMB immunomagnetic beads were added sequentially, with triplicate samples for each group. By comparing the capture efficiencies of each group, we aimed to determine the optimal capture scheme. After determining the best capture scheme, we applied it to capture experiments with CRC cells such as CT26, HCT-8, SW480, and LS174T cells. In the experiment, we added 10, 50, 100, 200, 500, and 1000 cells to 2 mL of phosphate buffer solution (PBS) and calculated the sensitivity of the capture scheme. To evaluate the specificity of the capture scheme, we also performed cell capture experiments using blood instead of PBS. In addition, we optimized the ratio of magnetic beads to antibodies in the immunomagnetic beads. In the experiment, we added 7 μL of IMBs containing 0, 10, 20, 30, 40, 50, 60, 70, or 80 μg of antibody and captured different numbers of CT26 cells, ultimately determining the best bead-to-antibody ratio according to the cell capture efficiency.

Capture, characterization and enumeration of CTCs in blood samples from patients with CRC

In this study, we collected 7.5 mL peripheral blood samples from patients with CRC and stored them in anticoagulation tubes containing EDTA. The serum and plasma layers were then separated via centrifugation at 2500 rpm for 10 minutes and transferred to EP tubes. An equal amount of PBS was added to the EP tubes and mixed well. Next, 7 μL of Ep-IMB or Vi-IMB immunomagnetic beads were added sequentially to the tubes, which were subsequently incubated for 20 minutes at room temperature and mixed every 5 minutes. After incubation, the tubes were placed on a magnetic separation rack for 15 minutes, after which the waste solution was aspirated. To fix the cells, 10 μL of 4% paraformaldehyde solution was added, and the cells were fixed for 10 minutes. The cells were then washed three times with PBS. For immunofluorescence staining, 30 μL of DAPI staining solution, 10 μL of CK19-FITC staining solution and 10 μL of CD45-PE staining solution were added, mixed well and stained for 15 minutes under light-free conditions. After staining, the cells were washed three times with PBS. Finally, 15 μL of deionized water was added to the EP tubes to resuspend the cells, and then the cells were evenly spread on the anti-stick slides. After drying, the droplets were observed and counted under a fluorescence microscope.

Tumor tissue and CTC nucleic acid extraction and mutation detection

In this study, we used the TIANamp Genomic DNA Kit to extract total DNA from tumor tissue and CTCs, ensuring that the total amount of tissue DNA exceeded 100 ng and that the total amount of CTC DNA exceeded 10 ng. The tumor tissue DNA samples were then sent to Huzhou Lie Yuan Medical Laboratory for high-throughput sequencing (NGS) via the Illumina NovaSeq 6000 platform to perform a comprehensive scan of 18 genes (including *KRAS*, *NRAS*, *BRAF*, *Tp53*, *APC*, *DPYD*, *NTRK*, *HER-2*, *UGT1A*, *PIK3CA*, *PTEN*, *POLD1*, *B2M*, *STK11*, *EGFR*, *MDM2*, *MDM4*, and *DNMT3A*). For CTC DNA, we followed the PCR procedures and systems described in Supplementary Table S1 and Supplementary Table S2 for amplification, using primers synthesized by Shanghai Bio-Engineering Co., Ltd., with specific sequence information provided in Supplementary Table S3. The amplified DNA fragments were then sent to Shanghai Bio-Engineering for sequencing to identify the gene mutation status.

High-throughput sequencing (NGS) and Sanger sequencing were utilized for their respective strengths in detecting genetic mutations. NGS's high-throughput capability allows for the simultaneous sequencing of hundreds of thousands to millions of DNA molecules, making it ideal for analyzing multiple gene statuses and changes in tumor tissues. This comprehensive approach is vital for guiding treatment in newly diagnosed patients and tracking tumor evolution over time. Sanger sequencing, known for its precision, is employed for validating specific mutation genes in CTCs, which complements NGS by offering a detailed verification of suspected mutations. This combination leverages the strengths of both methods for a more accurate genetic analysis and personalized treatment guidance (Jennings, L. J., & Kirschmann, D. 2016, Schmid, K,eg al 2022) (23, 24).

Statistical analysis

In this study, data analysis was performed via SPSS 21.0 statistical software. The experimental data are expressed as the means ± standard deviations (x ± s). One-way analysis of variance (ANOVA) was used for within-group comparisons. Statistical significance was determined according to the following criteria: when $P < 0.05$, the difference between the two groups was considered statistically significant and marked with an asterisk (*); when $P < 0.01$ or $P < 0.001$, the difference was considered highly significant and marked with two asterisks (**) and three asterisks (***), respectively.

Results

Preparation of immunoliposomal magnetic beads and CTC detection of CRC

The IMBs were composed of five key components: (I) antibody derivatives designed for specific recognition of antigens on the surface of cancer cells; (II) iron oxide (Fe3O4) nanoparticles, which serve as the core of the beads to provide magnetic properties; (III) cholesterol, which enhances membrane stability; (IV) 1,2-dioleoyl-sn-glycero-3-phosphocholine (DOPC), a major component of the lipid bilayer; and (V) 1,2-dioleoyl-sn-glycero-3-phosphoethanolamine-N-[7-(diethylamino)-4-trifluoromethyl]coumarin (GHDC), which enhances fluorescent labeling. The integration of specific antibodies into the IMBs enabled highly selective capture of CRC CTCs. After capture, the CTCs were separated according to the magnetic properties of the superparamagnetic Fe3O4 nanoparticles and subsequently identified via immunofluorescence techniques. A schematic representation of multitarget immunomagnetic bead CTC detection is shown in Figure 1.

Characterization and analysis of nanomagnetic beads

To further confirm that the manufactured magnetic beads had a small particle size and favorable stability, we analyzed the particle size and zeta potential of Ep-IMB and Vi-IMB. The average particle size of Ep-IMB was determined to be 116.2 nm (Figure 2A), with a zeta potential of +23.6 mV (Figure 2B). For Vi-IMB, the average particle size was measured to be 120.4 nm (Figure 2C), and the zeta potential was +21.6 mV (Figure 2D).

Infrared spectroscopy analysis (Figure 2E) revealed characteristic absorption peaks for Ep-IMB and Vi-IMB at 1725 cm^{-1} for the ester carbonyl (C=O) stretching vibration, 1186 cm^{-1} for the ether (C-O-C) stretching vibration, 1650 cm^{-1} for the amide carbonyl (C=O) stretching vibration, and 3500 cm^{-1} for the amine (C-N) stretching vibration. These characteristic peaks confirmed the successful synthesis of the IMBs.

Ultraviolet spectroscopy (Figure 2F) revealed a broad absorption peak at approximately 279 nm for both types of antibody-modified magnetic beads, indicating that EpCAM and vimentin were successfully conjugated to the surface of the beads.

The AFM images (Figures 2G, H) revealed that both types of immunomagnetic microspheres were spherical in shape, varied in size, and did not aggregate, indicating their good stability and regular morphology. The size ranged from 100 to 150 nm, showing characteristics of liposome-like vesicles.

IML cytotoxicity and capture efficiency

The Prussian blue staining results shown in Figure 3A clearly demonstrated robust cell growth, with cells exhibiting a typical regular morphology. The IMBs were randomly distributed around the cells, whereas Ep-IMB and Vi-IMB were uniformly attached to the cell surface, indicating the immune recognition properties of Ep-IMB and Vi-IMB. These findings were consistent with the results of

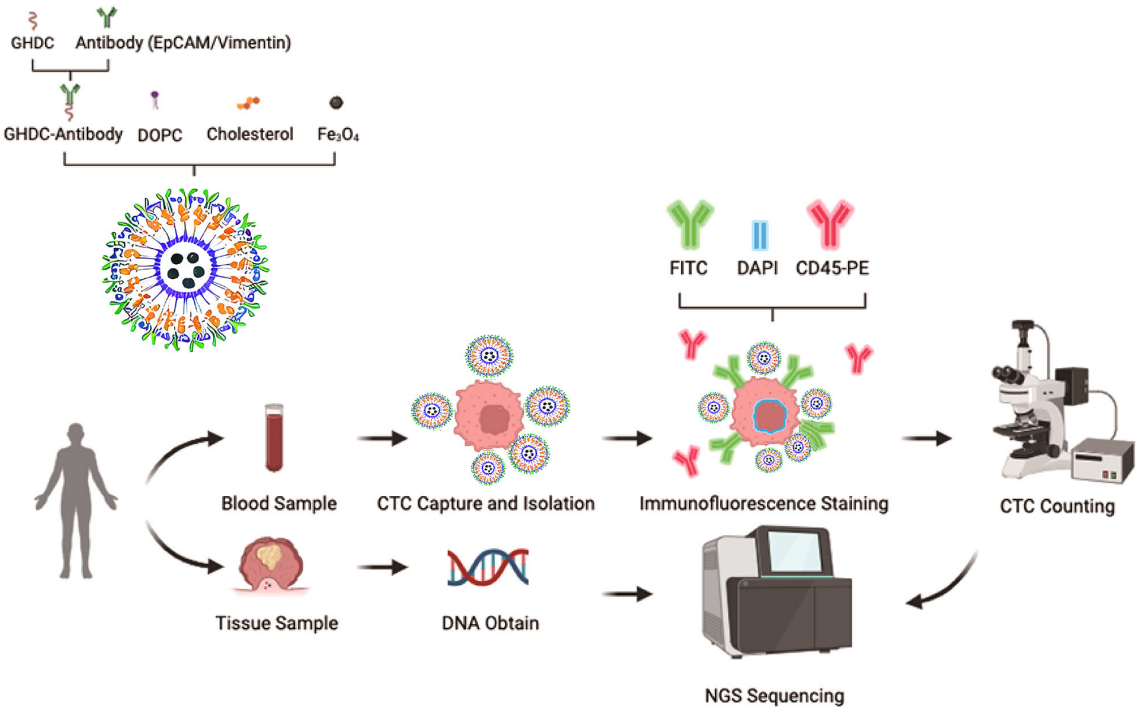

FIGURE 1
Flowchart of immunolipid magnetic ball (IMB) model preparation and CTC capture.

the UV assays and did not adversely affect cell morphology. A closer examination of the data in Figures 3B, C revealed that Ep-IMB and Vi-IMB at a concentration of 50 μg/mL exhibited low toxicity toward various cancer cell lines, with cell viability rates above 90%. As the concentration of magnetic beads increased, the cell viability rate gradually decreased, indicating that high concentrations of beads have some inhibitory effect on cell growth. Even at a relatively high concentration of 200 μg/mL, the viability of the cell lines remained above 60%, suggesting that although Ep-IMB and Vi-IMB have a certain degree of cytotoxicity toward the cell lines, the overall level of toxicity was relatively low.

To further validate the effects of different capture schemes and magnetic bead dosages on the efficiency of CRC cell capture, an experiment was conducted. The results showed that within the PBS system, the sequential introduction of Ep-IMB and Vi-IMB resulted in the highest capture efficiency when the magnetic bead dosage was held constant (Figure 4A). Notably, the capture efficiency peaked when 7 μL of Ep/Vi-IMB was added, and further increases in the magnetic bead

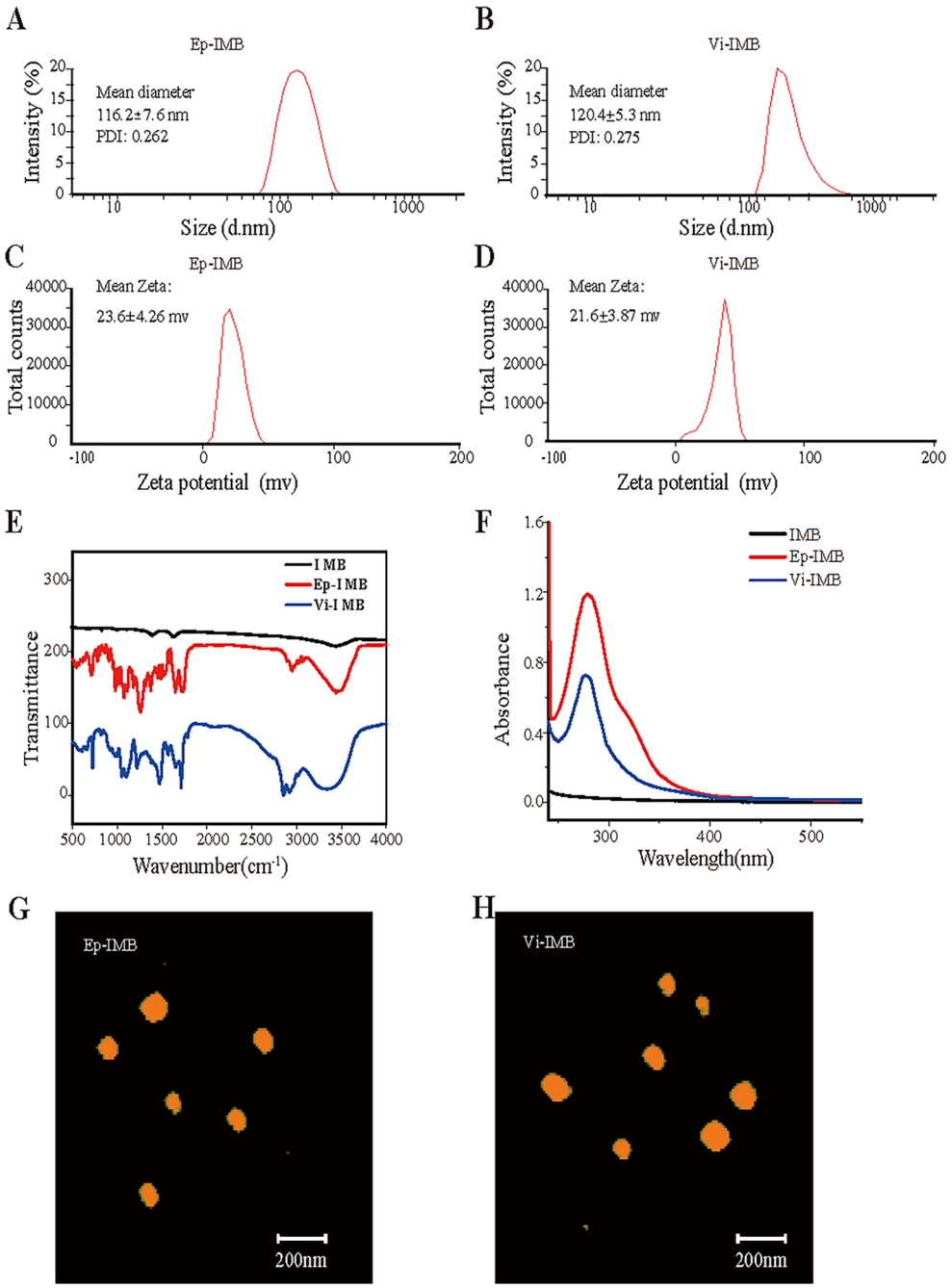

FIGURE 2
Characterization of the IMB models. **(A)** Ep-IMB particle size test plot; **(B)** Vi-IMB particle size test plot; **(C)** Ep-IMB potential test plot; **(D)** Vi-IMB potential test plot; **(E)** Immunolipid magnetic sphere infrared spectra; **(F)** Immunolipid magnetic sphere ultraviolet absorption spectra; **(G)** Ep-IMB AFM observation plot; **(H)** Vi-IMB AFM observation plot.

dosage stabilized the capture efficiency. On the basis of these results, the sequential capture method with the addition of 7 μL of Ep/Vi-IMB was identified as the optimal strategy, which was subsequently verified in a simulated blood system (Figure 4B). In the PBS system, the average capture efficiency was evaluated across different cell lines and with a gradient of cell numbers, and the results demonstrated that the specificity of the capture system reached 90.54% (Figure 4C). In addition, the average capture efficiency tested in the simulated blood system indicated that the sensitivity of the separation system was 89.07% (Figure 4D). Furthermore, the cell capture efficiency was optimized by adjusting the ratio of magnetic beads to antibodies, with magnetic bead preparation being most effective at an antibody concentration of 50 μg (Figure 4E).

Statistics on the sorting effect of various magnetic balls on CRC cells

A total of 23 patients with CRC were enrolled in this study, with a mean age of 62.7 years and a standard deviation of 16.5 years. There

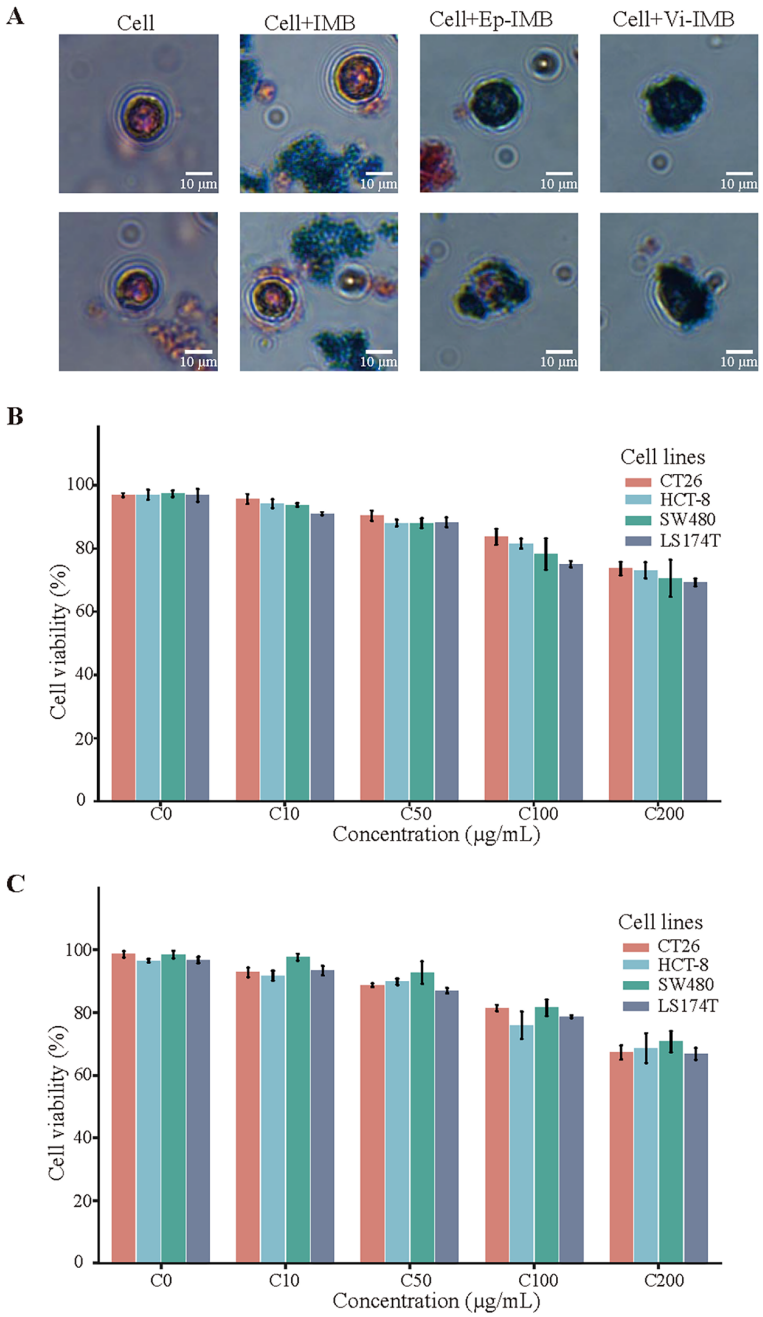

FIGURE 3
Cytotoxicity assay of the IMB models. **(A)** Prussian staining results; **(B)** Cellular activity assay of Ep-IMB in cell lines (CT26, HCT-8, SW480, and LS174T); **(C)** Cellular activity assay of Vi-IMB in cell lines (CT26, HCT-8, SW480, and LS174T).

were 7 male patients, accounting for 30.4% of the total. The distribution of pathological stages from I to IV was relatively uniform, with proportions of 8.7%, 21.7%, 34.8%, and 34.8%, respectively. The main tumor sites were the left colon (21.7%) and the right colon (43.5%), with 4 cases in the rectum, 3 in the sigmoid colon and 1 in the transverse colon. Moderate differentiation was the predominant type, accounting for 65.2% of the cases. In terms of metastatic status, 8 patients had distant metastases, representing 34.8% of the total patients. More detailed information can be found in Table 1.

In the present study, we identified and quantified CTCs via immunofluorescence analysis. Under white light, the cellular morphology was clearly visible, with CK19-FITC fluorescence showing a strong positive signal in green and DAPI fluorescence showing a strong positive signal in blue, while CD45 staining was negative. These characteristics facilitated the accurate detection of CTCs (Figure 5A). Using these criteria, we performed CTC enumeration and statistical analysis on blood samples from 20 healthy individuals and 23 patients with CRC (Figure 5B).

The results showed that in patients with CRC, the average number of CTCs captured by Ep-IMB was 5.61 per 7.5 mL; the average number captured by Vi-IMB was 2.78 per 7.5 mL; and with the Ep/Vi-IMB system, we achieved an average CTC capture yield

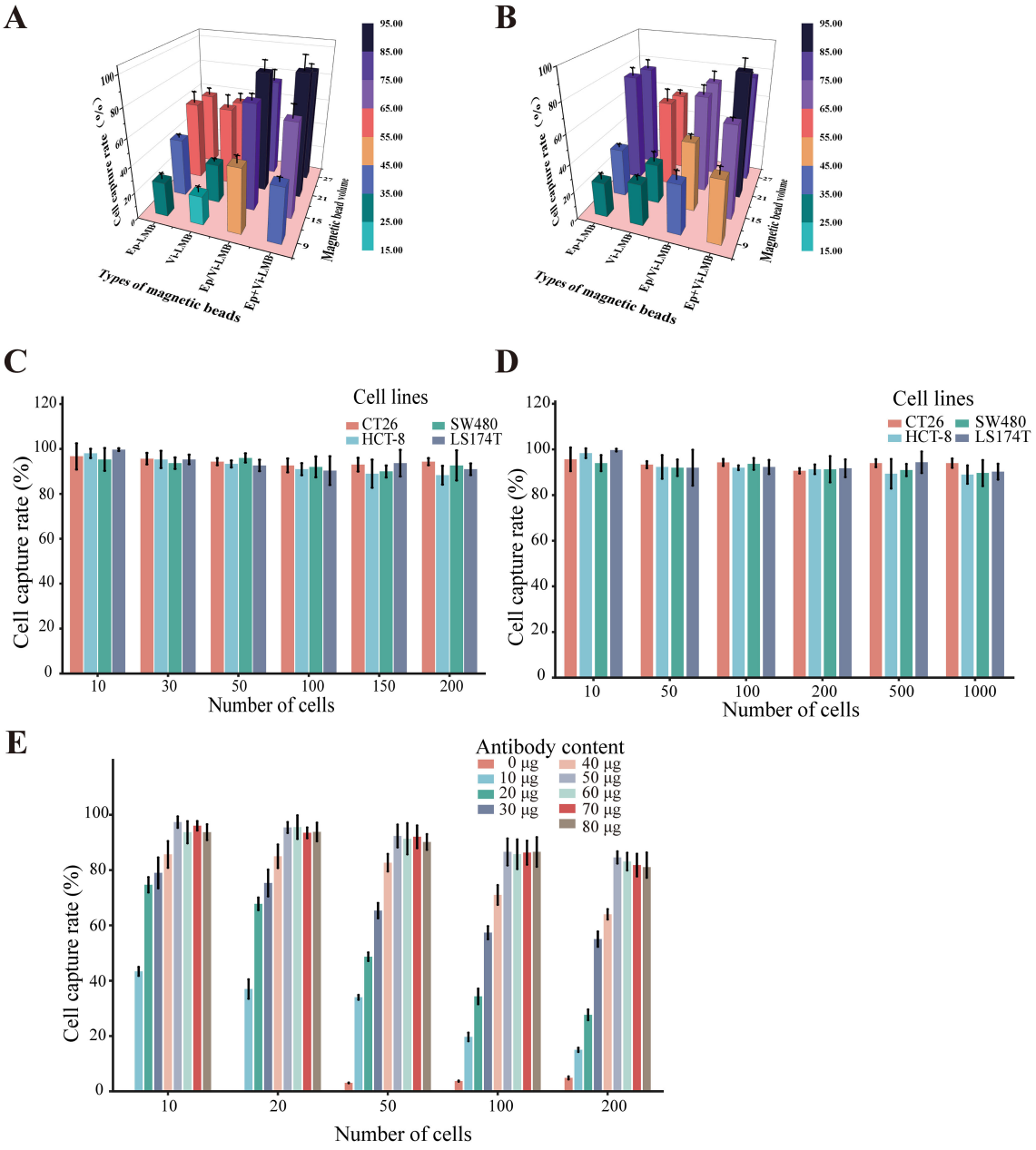

FIGURE 4
Cell capture efficiency of the IMB model. **(A)** Capture efficiency of CT26 cells by different inputs of the IMB model in PBS; **(B)** capture efficiency of CT26 cells by different inputs of the IMB model in the blood simulation system; **(C)** verification of the specificity of the IMB model in the PBS system; **(D)** verification of the sensitivity of the IMB model in the simulated blood system; **(E)** capture efficiency of CT26 cells by magnetic spheres prepared with different antibody contents in prepared magnetic spheres on the capture efficiency of CT26 cells. (Error lines represent the standard deviation).

TABLE 1 Characteristics of the enrolled CRC patients.

Characterization	Number (%)
Age	62.7±16.5
Sex	
Female	16 (69.6)
Male	7 (30.4)
Pathological staging	
I	2 (8.7)
II	5 (21.7)
III	8 (34.8)
IV	8 (34.8)
Tumor site	
Left hemicolon	5 (21.7)
Right hemicolon	10 (43.5)
Rectum	4 (17.4)
Sigmoid colon	3 (13.0)
Transverse colon	1 (4.3)
Degree of differentiation	
Moderately differentiated	15 (65.2)
Moderately to poorly differentiated	4 (17.4)
Poorly differentiated	4 (17.4)
Distant metastatic site	
M0	15 (65.2)
M1	8 (34.8)

of 8.39 per 7.5 mL. In the blood samples from healthy individuals, a low number of CTCs was detected, with an average of 0.09 per 7.5 mL, and the CTC counts from all three capture systems were significantly lower than those from patients with CRC ($P < 0.001$).

Furthermore, we observed that the number of captured epithelial or mesenchymal CTCs gradually increased with increasing tumor stage, and the CTC counts from all three capture systems significantly differed across stages (Figure 5C). In addition, the number of CTCs captured by Ep-IMB and Vi-IMB differed significantly between stages II, III and IV ($P < 0.05$) (Supplementary Figure S1).

Comparative analysis of genomic heterogeneity in CRC tissue and CTCs

According to the heatmap, the *Tp53* gene mutation frequency in CRC tissue samples was the highest at 65.22%, followed by the *PIK3CA* (39.13%), KRAS (30.43%), *BRAF* (17.39%), *APC* (26.09%) and *EGFR* (34.78%) genes (Figure 6A). Subsequent testing of CTC samples by Sanger sequencing revealed that the Tp53 gene mutation showed the highest concordance (91.31%) compared with the hotspot gene mutations identified in tissue samples, whereas mutations in *PIK3CA* (76.00%), *KRAS* (85.36%), *BRAF* (51.00%), *APC* (65.67%) and *EGFR* (74.00%) also showed good concordance. Overall, the two detection methods achieved a concordance rate of 85.06% in terms of genetic mutation (Figure 6B).

Discussion

Liquid biopsy has emerged as a burgeoning focal point within the realm of oncological research, demonstrating substantial potential across various stages of cancer screening and therapeutics. In asymptomatic populations, this noninvasive approach can identify individuals harboring cancer, thereby increasing early detection rates and facilitating more efficacious intervention strategies. Moreover, it provides dynamic insights into the progression of CRC and assesses the sensitivity of the disease to therapeutic interventions (25). CTCs have played a critical role in the advancement of precision medicine. Compared with traditional invasive tissue biopsies and cytology, CTC detection offers several distinct advantages, including a straightforward sample collection process and the ability to perform multiple repeated assessments (26). As intact neoplastic cells, CTCs provide a wealth of information on the genomic, transcriptomic, proteomic and metabolomic profiles of tumors (27). In addition, CTCs can be analyzed ex vivo, making it easier to study tumor cells (28).

In 2010, the American Joint Committee on Cancer (AJCC) included CTCs in the TNM cancer staging system for the first time (29). The study of CTC dynamics throughout tumor progression offers potential predictive information for cancer screening, prognostic assessment, disease monitoring and therapeutic response. Currently, CTCs have been extensively used in the prognostic evaluation of various malignancies, including lung, head and neck, esophageal, gastric and breast cancer (30–33). Given the low five-year survival rate for patients with advanced colorectal cancer, early detection and treatment are critical for improving survival. Yang et al. (34) used an immunoaffinity negative enrichment method to detect CTCs in benign colorectal disease patients (such as polyps) and nonmetastatic CRC patients preoperatively and reported that the CTC count in CRC patients was significantly greater than that in patients with colorectal polyps (3.47 ± 0.32 cells/3.2 mL vs. 1.49 ± 0.2 cells/3.2 mL, $P < 0.001$). Tsai et al. (35)also demonstrated a close correlation between CTC counts and disease progression ($P < 0.0001$), with high specificity (86%) and sensitivity (79%) in 95% of CRC stages and 79% of adenomatous lesions. Sastre et al. (36) used the CellSearch system to detect peripheral blood CTCs in 1202 CRC patients and reported that a CTC count of ≥3 cells/7.5 mL was associated with adverse prognostic factors. The CellSearch system was once an option on the domestic market, it was discontinued in 2016 because of its low detection rate. Although Parsortix device from Angle Company has been FDA-approved to enumerate and sort CTCs, providing an alternative technology in this field, Recently. In this study, a novel CTC sorting system was developed on the basis of the CellSearch system, which sequentially enriches CTCs with Ep/Vi-IMB and demonstrates good dispersion, stability and low cytotoxicity, with a specificity of 90.54% and a sensitivity of 89.07%. Therefore, our research retains its uniqueness and value. Our IMB system, by combining EpCAM and vimentin dual markers, effectively captures CTCs, including those undergone EMT, demonstrating higher specificity and sensitivity

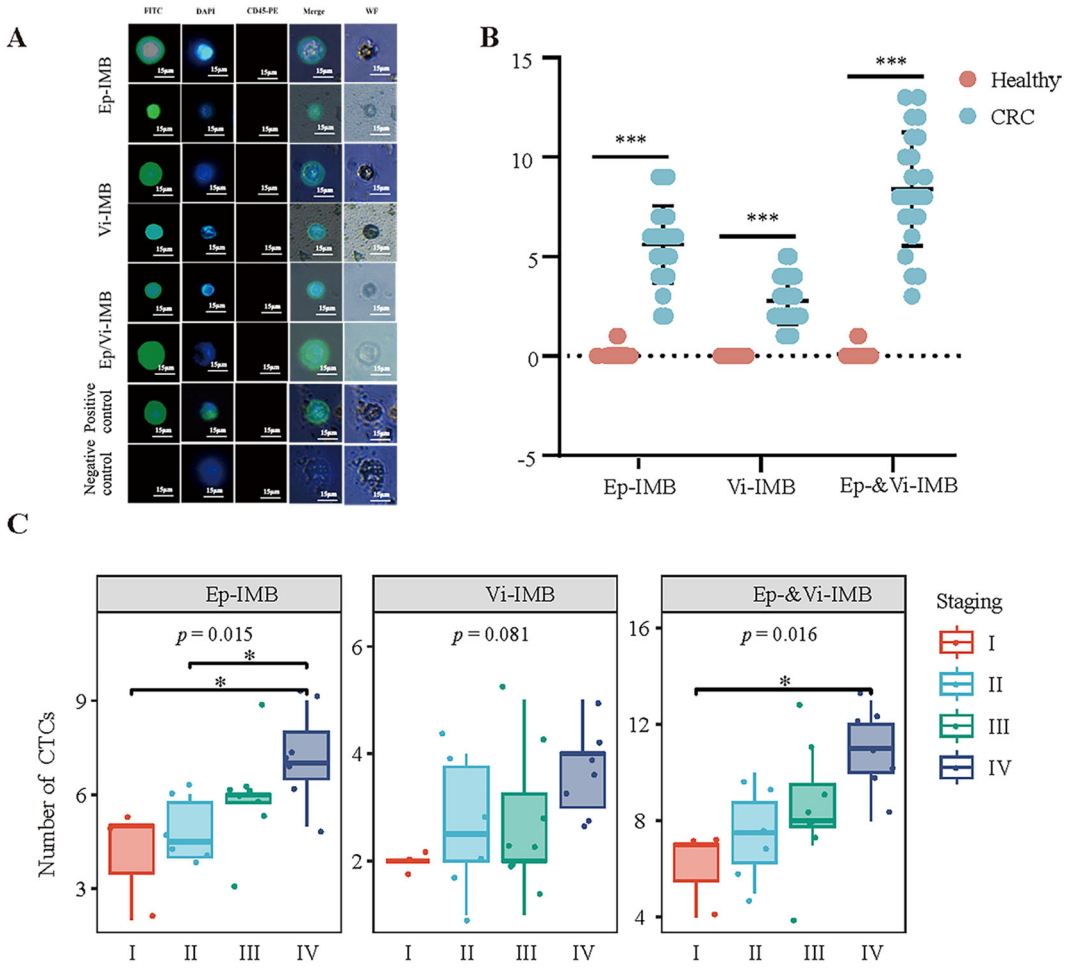

FIGURE 5
Immunofluorescence identification and counting of CTCs in blood samples from CRC patients. **(A)** Immunofluorescence identification of captured CTCs. **(B)** Comparison of the ability of the Ep-IMB, Vi-IMB and EP/Vi-IMB models to capture CTCs in the blood of CRC patients with the blood of the normal population. **(C)** The number of CTCs captured by the Ep-IMB, Vi-IMB and EP/Vi-IMB models in the blood of CRC patients with different pathological stages.

compared to the CellSearch system. To address the potential for false positives associated with vimentin as a marker, we implemented a dual-marker approach using both EpCAM and vimentin-modified immunomagnetic beads (Ep-IMBs and Vi-IMBs) for the capture of CTCs. This strategy ensures that only cells co-expressing both markers are classified as CTCs, thereby increasing specificity. We also utilized highly specific vimentin antibodies to reduce non-specific binding, which was optimized through preliminary experiments and competitive assays. The inclusion of additional unique tumor-associated antigens in our detection system further enhances specificity by capitalizing on the distinctive features of CTCs. Finally, stringent data analysis, including the exclusion of non-tumor cells by negating common leukocyte markers such as CD45, was performed to minimize false positives. Compared to microfluidic and nanoparticle-based technologies, the IMB system offers advantages in cost-effectiveness and ease of operation while maintaining low cytotoxicity, which is crucial for clinical applications (37, 38). Nevertheless, the preparation process of the IMB system is relatively complex, and future studies should focus on further optimization to enhance its practicality and clinical feasibility. The average detection volume of CTCs in the blood of CRC patients was 8.39 cells/7.5 mL. Notably, the detection rate of CTCs increased with the TNM stage of the patients, indicating a close relationship between the number of CTCs and the progression of primary malignancies and suggesting its potential as an adjunct indicator for CRC TNM staging. However, the relationships between the number and type of CTCs and specific pathological histological characteristics and actual degree of tissue metastasis require further in-depth research.

Precision medicine has achieved significant success in the treatment of CRC, with the key being the detection of specific mutated genes to select the most appropriate targeted therapeutic agents. Compared with traditional detection methods, next-generation sequencing (NGS) technology can analyze the status and alterations of multiple genes in the body in a single high-throughput test, greatly enriching the clinical applications for CRC patients in diagnosis, treatment, and disease prognosis monitoring. In an NGS study of 526 CRC tumor samples, mutations in the *TP53* and *KRAS* genes were found to be frequent, whereas mutations in *PIK3CA* often coexisted with *KRAS*, *NRAS*, or *BRAF* mutations (39). The *TP53* gene encodes the p53 protein, an important tumor suppressor, and any mutation that inactivates this protein can lead

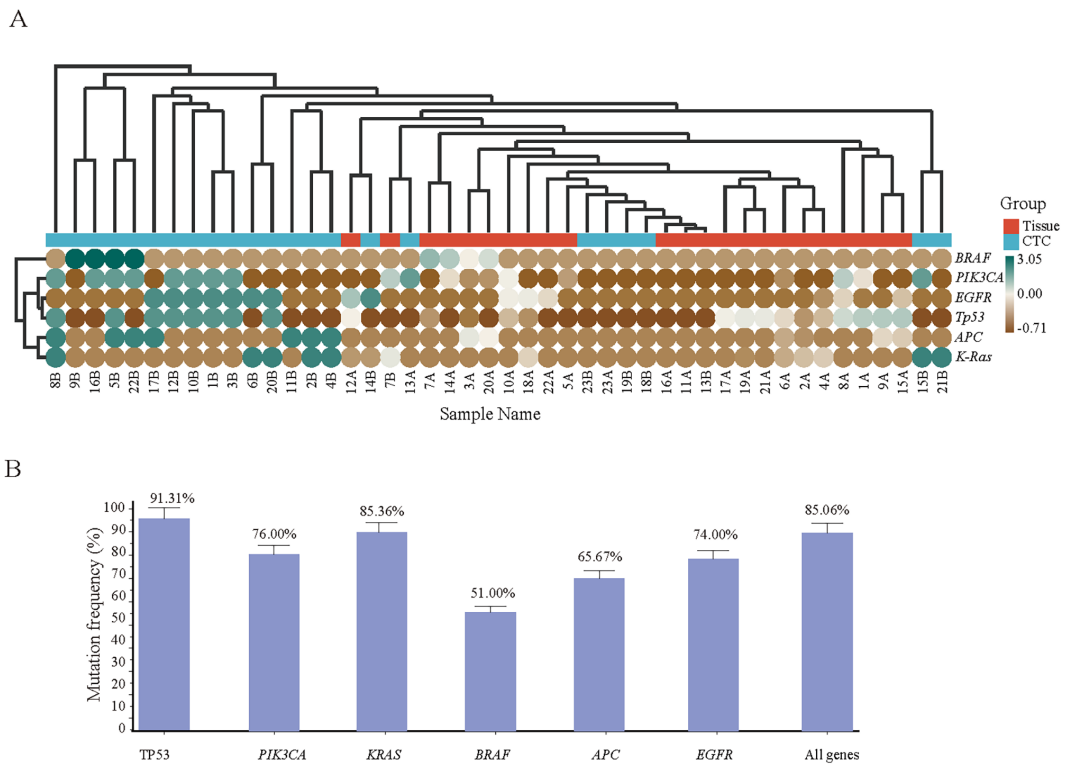

FIGURE 6
(A) onsistency validation of the tissue and corresponding CTC gene mutation results of 23 CRC patients. Hotspot gene mutation results of tissue and blood CTC samples from 23 CRC patients; **(B)** Consistency rate statistics of tissue and blood CTC gene mutations.

to tumorigenesis (40, 41). Mutation of the *KRAS* gene, a member of the RAS family, can lead to continued activation of the RAS protein, thereby causing abnormal cell growth and proliferation and promoting tumor development (42, 43). This study uses next-generation sequencing (NGS) technology to analyze colorectal tumor tissue and reveals high mutation frequencies in the *Tp53*, *PIK3CA*, *EGFR*, and *KRAS* genes. Subsequently, when patient-isolated CTCs were used as templates, hotspot mutation genes were verified via Sanger sequencing, and the mutation rate and its consistency with tissue sample mutations were calculated. The study showed high consistency for mutations in *Tp53* (91.31%), *PIK3CA* (76.00%), *KRAS* (85.36%), *BRAF* (51.00%), *APC* (65.67%), and *EGFR* (74.00%), with an overall gene mutation consistency rate of 85.06%. This finding indicates that there is a high degree of concordance between the tumor-related hotspot mutation genes detected by NGS technology in CRC tissue samples and those detected by Sanger sequencing in CTC samples. Therefore, in cases where it is difficult to obtain tumor tissue samples, enriched CTCs may serve as a suitable alternative for clinically targeted drug gene mutation detection, effectively overcoming the challenge of tumor tissue sampling.

Limitations of the study

This study focused on several key hotspot mutated genes, but given the complexity of the tumor genome, future studies will need to use advanced means such as whole-genome sequencing to achieve a more comprehensive analysis of genetic variants. In addition, although this study proposed an individualized treatment strategy based on CTCs, its applicability and efficacy in different patient groups still need to be validated in large-scale clinical trials. Moreover, this study lacked data on long-term patient tracking and follow-up, which limited the in-depth understanding of CTCs as indicators for prognosis and efficacy assessment. Therefore, future studies should include long-term clinical follow-up to assess the role of CTCs in cancer treatment more comprehensively.

Conclusion

The analysis of CTCs offers us a crucial tool for comprehending and capitalizing on tumor heterogeneity, which facilitates a more profound understanding of the biological properties of tumors and guides the development of personalized therapeutic strategies. Future studies will delve deeper into the role of CTCs in tumor heterogeneity, using this knowledge to refine treatment plans and potentially increase patient survival rates.

Building on previous studies that enhanced the capture efficiency of circulating tumor cells (CTCs) using immunolipid magnetic bead (IMB) systems modified with specific antibodies (44, 45), our research has achieved significant technological advancements: Firstly, we employed a reverse evaporation method for IMB preparation and optimized the ratio of EpCAM to

Vimentin antibodies, thereby enhancing the uniformity and stability of CTC capture. Secondly, we validated the IMB system in a larger cohort of 23 colorectal cancer (CRC) patients, yielding more compelling data on clinical relevance. Additionally, we analyzed gene mutations in CTCs using next-generation sequencing (NGS) and Sanger sequencing, finding a high degree of concordance with mutations in tumor tissues. Lastly, we addressed the heterogeneity of CTCs by employing a dual-marker strategy with EpCAM and Vimentin, allowing for a comprehensive assessment of CTC biology. In summary, we have successfully developed a CTC sorting system based on Ep-IMB and Vi-IMB technology that efficiently captures CTCs from the peripheral blood of CRC patients and detects clinically relevant genetic mutations, effectively overcoming the challenge of obtaining tumor tissue samples. This system not only offers a novel approach for early diagnosis, therapeutic efficacy evaluation, prognostic assessment, and minimal residual disease detection but also holds significant potential for clinical application in the field of targeted therapy gene testing for CRC.

Data availability statement

The original contributions presented in the study are includedin the article/Supplementary Material. Further inquiries can be directed to the corresponding author/s.

Ethics statement

The study was approved by the Clinical Research and Experimental Animal Ethics Committee of Zhongshan People's Hospital (Approval No: 2024–041). The studies were conducted in accordance with the local legislation and institutional requirements. Written informed consent for participation in this study was provided by the participants' legal guardians/next of kin.

Author contributions

QD: Conceptualization, Data curation, Formal Analysis, Funding acquisition, Investigation, Methodology, Project administration, Resources, Software, Supervision, Validation, Visualization, Writing – original draft, Writing – review & editing. WL: Conceptualization, Data curation, Formal analysis, Funding acquisition, Investigation, Methodology, Project administration, Resources, Software, Supervision, Validation, Visualization, Writing – original draft, Writing – review & editing. YH: Conceptualization, Data curation, Formal analysis, Funding acquisition, Investigation, Methodology, Project administration, Resources, Software, Supervision, Validation, Visualization, Writing – original draft, Writing – review & editing. HW: Conceptualization, Data curation, Formal analysis, Funding acquisition, Investigation, Methodology, Project administration, Resources, Software, Supervision, Validation, Visualization, Writing – original draft, Writing – review & editing. XZ: Conceptualization, Data curation, Formal analysis, Funding acquisition, Investigation, Methodology, Project administration, Resources, Software, Supervision, Validation, Visualization, Writing – original draft, Writing – review & editing. ZG: Conceptualization, Data curation, Formal analysis, Funding acquisition, Investigation, Methodology, Project administration, Resources, Software, Supervision, Validation, Visualization, Writing – original draft, Writing – review & editing. BC: Conceptualization, Data curation, Formal analysis, Funding acquisition, Investigation, Methodology, Project administration, Resources, Software, Supervision, Validation, Visualization, Writing – original draft, Writing – review & editing. YW: Conceptualization, Data curation, Formal analysis, Funding acquisition, Investigation, Methodology, Project administration, Resources, Software, Supervision, Validation, Visualization, Writing – original draft, Writing – review & editing.

Funding

The author(s) declare that no financial support was received for the research, authorship, and/or publication of this article.

Conflict of interest

The authors declare that the research was conducted in the absence of any commercial or financial relationships that could be construed as a potential conflict of interest.

Generative AI statement

The author(s) declare that no Generative AI was used in the creation of this manuscript.

Publisher's note

Supplementary material

The Supplementary Material for this article can be found online at: https://www.frontiersin.org/articles/10.3389/fonc.2024.1531972/full#supplementary-material

SUPPLEMENTARY FIGURE 1
Differences in the number of CTCs captured by Ep-IMB and Vi-IMB among different pathological stages.

References

1. Xi Y, Xu P. Global colorectal cancer burden in 2020 and projections to 2040. *Transl Oncol*. (2021) 14:101174. doi: 10.1016/j.tranon.2021.101174

2. Mauri G, Sartore-Bianchi A, Russo AG, Marsoni S, Bardelli A, Siena S. Early-onset colorectal cancer in young individuals. *Mol Oncol*. (2019) 13:109–31. doi: 10.1002/mol2.2019.13.issue-2

3. Buccafusca G, Proserpio I, Tralongo AC, Rametta Giuliano S, Tralongo P. Early colorectal cancer: diagnosis, treatment and survivorship care. *Crit Rev Oncol Hematol*. (2019) 136:20–30. doi: 10.1016/j.critrevonc.2019.01.023

4. Yang M, Liu Q, Dai M, Peng R, Li X, Zuo W, et al. FOXQ1-mediated SIRT1 upregulation enhances stemness and radio-resistance of colorectal cancer cells and restores intestinal microbiota function by promoting β-catenin nuclear translocation. *J Exp Clin Cancer Res*. (2022) 41:70. doi: 10.1186/s13046-021-02239-4

5. Ghafouri-Fard S, Hussen BM, Badrlou E, Abak A, Taheri M. MicroRNAs as important contributors in the pathogenesis of colorectal cancer[J. *BioMed Pharmacother*. (2021) 140:111759. doi: 10.1016/j.biopha.2021.111759

6. Huang D, Sun W, Zhou Y, Li P, Chen F, Chen H, et al. Mutations of key driver genes in colorectal cancer progression and metastasis. *Cancer Metastasis Rev*. (2018) 37:173–87. doi: 10.1007/s10555-017-9726-5

7. Ganesh K, Massagué J. Targeting metastatic cancer. *Nat Med*. (2021) 27:34–44. doi: 10.1038/s41591-020-01195-4

8. Ring A, Nguyen-Sträuli BD, Wicki A, Aceto N. Biology, vulnerabilities and clinical applications of circulating tumoour cells. *Nat Rev Cancer*. (2023) 23:95–111. doi: 10.1038/s41568-022-00536-4

9. Nikanjam M, Kato S, Kurzrock R. Liquid biopsy: current technology and clinical applications. *J Hematol Oncol*. (2022) 15:131. doi: 10.1186/s13045-022-01351-y

10. Bailey PC, Martin SS. Insights on CTC biology and clinical impact emerging from advances in capture technology. *Cells*. (2019) 8(6):553. doi: 10.20944/preprints201905.0226.v1

11. Zhao H, Huang C, Lin M, Zhou M, Huang C. Dynamic detection of HER2 of circulating tumor cells in patients with gastric carcinoma and its clinical application. *Mol Med Rep*. (2022) 25(5):187. doi: 10.3892/mmr.2022.12703

12. Andree KC, Van Dalum G, Terstappen LW. Challenges in circulating tumor cell detection by the CellSearch system. *Mol Oncol*. (2016) 10:395–407. doi: 10.1016/j.molonc.2015.12.002

13. Adams DL, Stefansson S, Haudenschild C, Martin SS, Charpentier M, Chumsri S, et al. Cytometric characterization of circulating tumor cells captured by microfiltration and their correlation to the CellSearch(®) CTC test. *Cytometry A*. (2015) 87:137–44. doi: 10.1002/cyto.a.22613

14. Satelli A, Li S. Vimentin in cancer and its potential as a molecular target for cancer therapy. *Cell Mol Life Sci*. (2011) 68:3033–46. doi: 10.1007/s00018-011-0735-1

15. Usman S, Waseem NH, Nguyen TKN, Mohsin S, Jamal A, Teh MT, et al. Vimentin is at the heart of epithelial mesenchymal transition (EMT) mediated metastasis. *Cancers (Basel)*. (2021) 13(19):4985. doi: 10.3390/cancers13194985

16. Sabour L, Sabour M, Ghorbian S. Clinical applications of next-generation sequencing in cancer diagnosis. *Pathol Oncol Res*. (2017) 23:225–34. doi: 10.1007/s12253-016-0124-z

17. Hussen BM, Abdullah ST, Salihi A, Sabir DK, Sidiq KR, Rasul MF, et al. The emerging roles of NGS in clinical oncology and personalized medicine. *Pathol Res Pract*. (2022) 230:153760. doi: 10.1016/j.prp.2022.153760

18. Jennings LJ, Arcila ME, Corless C, Kamel-Reid S, Lubin IM, Pfeifer J, et al. Guidelines for validation of next-generation sequencing-based oncology panels: a joint consensus recommendation of the association for molecular pathology and college of american pathologists. *J Mol Diagn*. (2017) 19:341–65. doi: 10.1016/j.jmoldx.2017.01.011

19. Cirillo M, Craig AFM, Borchmann S, Kurtz DM. Liquid biopsy in lymphoma: Molecular methods and clinical applications. *Cancer Treat Rev*. (2020) 91:102106. doi: 10.1016/j.ctrv.2020.102106

20. Jiang L, Lin X, Chen F, Qin X, Yan Y, Ren L, et al. Current research status of tumor cell biomarker detection. *Microsyst Nanoeng*. (2023) 9:123. doi: 10.1038/s41378-023-00581-5

21. Abbosh C, Birkbak NJ, Wilson GA, Jamal-Hanjani M, Constantin T, Salari R, et al. Phylogenetic ctDNA analysis depicts early-stage lung cancer evolution. *Nature*. (2017) 545:446–51. doi: 10.1038/nature22364

22. Pallante P, Pisapia P, Bellevicine C, Malapelle U, Troncone G. Circulating tumour cells in predictive molecular pathology: focus on drug-sensitive assays and 3D culture. *Acta Cytologica*. (2019) 63:171–81. doi: 10.1159/000496213

23. Jennings LJ, Kirschmann D. Genetic testing requires NGS and sanger methodologies. *Pediatr Neurol Briefs*. (2016) 30:36. doi: 10.15844/pedneurbriefs-30-9-1

24. Schmid K, Dohmen H, Ritschel N, Selignow C, Zohner J, Sehring J, et al. Sequence analysis SangeR: the high-throughput Sanger sequencing analysis pipeline. *Bioinf Adv*. (2022) 2022:1–2. doi: 10.1093/bioadv/vbac009

25. Chen M, Zhao H. Next-generation sequencing in liquid biopsy: cancer screening and early detection. *Hum Genomics*. (2019) 13:34. doi: 10.1186/s40246-019-0220-8

26. Pereira-Veiga T, Schneegans S, Pantel K, Wikman H. Circulating tumor cell-blood cell crosstalk: Biology and clinical relevance. *Cell Rep*. (2022) 40:111298. doi: 10.1016/j.celrep.2022.111298

27. Visal TH, Den Hollander P, Cristofanilli M, Mani SA. Circulating tumoour cells in the -omics era: how far are we from achieving the 'singularity'? *Br J Cancer*. (2022) 127:173–84. doi: 10.1038/s41416-022-01768-9

28. Siravegna G, Marsoni S, Siena S, Bardelli A. Integrating liquid biopsies into the management of cancer. *Nat Rev Clin Oncol*. (2017) 14:531–48. doi: 10.1038/nrclinonc.2017.14

29. Amin MB, Greene FL, Edge SB, Compton CC, Gershenwald JE, Brookland RK, et al. The Eighth Edition AJCC Cancer Staging Manual: Continuing to build a bridge from a population-based to a more "personalized" approach to cancer staging. *CA Cancer J Clin*. (2017) 67:93–9. doi: 10.3322/caac.21388

30. He W, Hou M, Zhang H, Zeng C, He S, Chen X, et al. Clinical significance of circulating tumor cells in predicting disease progression and chemotherapy resistance in patients with gestational choriocarcinoma. *Int J Cancer*. (2019) 144:1421–31. doi: 10.1002/ijc.v144.6

31. Yang L, Yan X, Chen J, Zhan Q, Hua Y, Xu S, et al. Hexokinase 2 discerns a novel circulating tumor cell population associated with poor prognosis in lung cancer patients. *Proc Natl Acad Sci U.S.A*. (2021) 118 (11):e2012228118. doi: 10.1073/pnas.2012228118

32. Radovich M, Jiang G, Hancock BA, Chitambar C, Nanda R, Falkson C, et al. Association of circulating tumor dna and circulating tumor cells after neoadjuvant chemotherapy with disease recurrence in patients with triple-negative breast cancer: preplanned secondary analysis of the BRE12-158 randomized clinical trial. *JAMA Oncol*. (2020) 6:1410–5. doi: 10.1001/jamaoncol.2020.2295

33. Zhou J, Ma X, Bi F, Liu M. Clinical significance of circulating tumor cells in gastric cancer patients. *Oncotarget*. (2017) 8:25713–20. doi: 10.18632/oncotarget.14879

34. Yang C, Zhuang W, Hu Y, Zhu L. Clinical significance of peripheral circulating tumor cell counts in colorectal polyps and nonnon-metastatic colorectal cancer. *World J Surg Oncol*. (2018) 16:13. doi: 10.1186/s12957-017-1305-2

35. Tsai WS, You JF, Hung HY, Hsieh PS, Hsieh B, Lenz HJ, et al. Novel circulating tumor cell assay for detection of colorectal adenomas and cancer. *Clin Transl Gastroenterol*. (2019) 10:e00088. doi: 10.14309/ctg.0000000000000088

36. Sastre J, Orden V, Martínez A, Bando I, Balbín M, Bellosillo B, et al. Association between baseline circulating tumor cells, molecular tumor profiling, and clinical characteristics in a large cohort of chemo-naïve metastatic colorectal cancer patients prospectively collected. *Clin Colorectal Cancer*. (2020) 19:e110–6. doi: 10.1016/j.clcc.2020.02.014

37. Descamps L, Le Roy D, Deman A-L. Microfluidic-based technologies for CTC isolation: A review of 10 years of intense efforts towards liquid biopsy. *Int J Mol Sci*. (2022) 23:1981. doi: 10.3390/ijms23041981

38. Pipatwatcharadate C, Iyer PR, Pissuwan D. Recent update roles of magnetic nanoparticles in circulating tumor cell (CTC)/non-CTC separation. *Pharmaceutics*. (2023) 15:2482. doi: 10.3390/pharmaceutics15102482

39. Li W, Qiu T, Guo L, Ying J, Zhou A. NGS-based oncogenic mutations analysis in advanced colorectal cancer patients improves targeted therapy prediction. *Pathol Res Pract*. (2019) 215:483–9. doi: 10.1016/j.prp.2018.12.037

40. Voskarides K, Giannopoulou N. The role of TP53 in adaptation and evolution. *Cells*. (2023) 12(3):512. doi: 10.3390/cells12030512

41. Giacomelli An AO, Yang X, Lintner RE, McFarland JM, Duby M, Kim J, et al. Mutational processes shape the landscape of TP53 mutations in human cancer. *Nat Genet*. (2018) 50:1381–7. doi: 10.1038/s41588-018-0204-y

42. Godwin I, Anto NP, Bava SV, Babu MS, Jinesh GG. Targeting K-Ras and apoptosis-driven cellular transformation in cancer. *Cell Death Discovery*. (2021) 7:80. doi: 10.1038/s41420-021-00457-5

43. Luo J. KRAS mutation in pancreatic cancer. *Semin Oncol*. (2021) 48:10–8. doi: 10.1053/j.seminoncol.2021.02.003

44. Wang Y, Xia L, Wu M, Huang C. Prognostic evaluation of a multi-target magnetic bead-enriched circulating tumor cell-enriched identification system for colorectal cancer. *J Gastrointest Oncol*. (2024) 15:134–46. doi: 10.21037/jgo-23-735

45. Liu Y, Li Q, Chen T, Shen T, Zhang X, Song P, et al. Clinical verification of vimentin/EpCAM immunolipid magnetic sorting system in monitoring CTCs in arterial and venous blood of advanced tumor. *J Nanobiotechnol*. (2021) 19:185. doi: 10.1186/s12951-021-00929-x

frontiers | Frontiers in Immunology

TYPE Original Research
PUBLISHED 20 February 2025
DOI 10.3389/fimmu.2025.1528853

OPEN ACCESS

EDITED BY
Matteo Becatti,
University of Firenze, Italy

REVIEWED BY
Sven Dennerlein,
University Medical Center Göttingen, Germany
Da Sun,
Wenzhou University, China

*CORRESPONDENCE
Lin Chen
xiaobei227@sina.com
Feng Xiao
xfeng_1981@163.com

†These authors share first authorship

RECEIVED 15 November 2024
ACCEPTED 03 February 2025
PUBLISHED 20 February 2025

CITATION
Yuan L-X, Yue Z-Q, Ma Q-R, Zhang P, Xiao F and Chen L (2025) Identification of DAP3 as candidate prognosis marker and potential therapeutic target for hepatocellular carcinoma.
Front. Immunol. 16:1528853.
doi: 10.3389/fimmu.2025.1528853

Identification of DAP3 as candidate prognosis marker and potential therapeutic target for hepatocellular carcinoma

Liu-Xia Yuan[1†], Zhi-Qiang Yue[2†], Qin-Rong Ma[3], Peng Zhang[2], Feng Xiao[3*] and Lin Chen[1*]

[1]Institute of Liver Diseases, Nantong Third People's Hospital, Affiliated Nantong Hospital 3 of Nantong University, Nantong, Jiangsu, China, [2]Department of Hepatobiliary Surgery, Nantong Third People's Hospital, Affiliated Nantong Hospital 3 of Nantong University, Nantong, Jiangsu, China, [3]Department of Pathology, Nantong Third People's Hospital, Affiliated Nantong Hospital 3 of Nantong University, Nantong, Jiangsu, China

Background: Among malignant tumors, hepatocellular carcinoma (HCC) is both prevalent and highly lethal. Most patients with advanced-stage liver cancer have a poor prognosis. Death-associated protein 3 (DAP3) is reportedly related to tumors and may hold great promise for the future.

Methods: DAP3 transcriptome data along with related clinical information were obtained from The Cancer Genome Atlas (TCGA), GEO, and ICGC databases. We assessed its prognostic value, clinical relevance, associated pathways, immune infiltration, gene mutations, and sensitivity to chemotherapeutics. A prognostic risk model was subsequently developed and evaluated using receiver operating characteristic (ROC) curves and Kaplan-Meier (KM) plots. Additionally, a nomogram was created and validated through calibration and decision curve analysis (DCA). Furthermore, quantitative real-time PCR (qRT-PCR), Western blot, and immunohistochemical (IHC) staining were performed to examine the expression of DAP3 in HCC. Finally, gene knockdown and overexpression experiments, along with cell counting kit-8 (CCK-8) assays, colony formation assays, and tests for cell apoptosis, migration, and invasion, were conducted to investigate the role of DAP3 in HCC.

Results: The study discovered that DAP3 expression was linked to HCC subtypes, and its high expression was linked to a poor prognosis. There were significant differences in immune infiltration level, mutation level, prognostic value and chemotherapeutic efficacy. Subsequently, we constructed a prognostic model and demonstrated that high risk score was significantly related to a poor survival rate. A predictive nomogram demonstrated that the nomogram model was effective prediction tool that can accurately predict the survival rate of patients with different clinical characteristics. Additionally, DAP3 expression significantly increased in both tissue samples and cell lines. Elevated levels of DAP3 were correlated with larger tumor size and higher alpha-fetoprotein (AFP) levels, and Cox analysis confirmed that DAP3 was a clinically independent prognostic marker. Finally, cell assays revealed that the knockdown of DAP3 significantly impeded cell proliferation and metabolic activity and induced apoptosis. Conversely, the overexpression of DAP3 had opposite effects on these cellular processes.

Conclusions: Our study on DAP3 can provide a reference for HCC diagnosis, treatment and prognosis assessment.

KEYWORDS

hepatocellular carcinoma, DAP3, prognostic model, bioinformatics, biomarker

Introduction

Liver cancer is recognized as the leading malignancy in the digestive system, characterized by a notably high mortality rate (1). The genetic, metabolic, and inflammatory heterogeneity of liver cancer presents significant challenges in the development of effective therapies. While chemotherapy is utilized, it typically results in only modest increases in overall survival and limited improvements in quality of life (2, 3). Hepatocellular carcinoma (HCC) is the most frequent subtype of primary liver cancer and one of the leading causes of cancer-related death worldwide (4). Despite the widespread clinical application of associated biomarkers, such as α-fetoprotein (AFP), for the diagnosis of hepatocellular carcinoma (HCC), their use remains controversial and constrained by limitations (5). Thus, it is essential to clarify the underlying mechanisms of hepatocellular carcinoma (HCC) to discover novel biomarkers for early detection, prognosis, and treatment.

Mitochondria are crucial in regulating cellular life and death processes, influencing the initiation of apoptosis as well as survival, proliferation, and metabolism (6). The human mitochondrial ribosome is one of the most protein-rich ribosomes, as reported, MRP genes were significantly upregulated in HCC tumor samples and showed promising diagnostic value (7, 8). DAP3 is the only GTP-binding protein component of the small subunit of mammalian and yeast mitochondrial ribosomes and plays an important role in tumor progression (9–11).DAP3 has been shown to have dual roles in tumorigenesis, functioning either as a tumor suppressor or promoter, depending on the particular cell type and tumor context. These findings suggest that DAP3 may have distinct biological functions across various cancers. For example, DAP3 is overexpressed in several cancer types, including human pancreatic cancer, invasive glioblastoma multiforme, and human thyroid tumors (12–15). Conversely, decreased expression of DAP3 has been observed in gastric cancer and colorectal cancer (CRC) (16, 17). Furthermore, DAP3 expression is correlated with tumor stage and clinical outcomes in breast cancer patients (18). Notably, downregulation of DAP3 has been shown to reduce mitochondrial respiration in HeLa cells, underscoring the essential role of DAP3 in mammalian cells (11). In conclusion, the potential roles of DAP3 in carcinogenesis and cancer development warrant further investigation. Although previous studies have reported on DAP3 expression and its basic functions in liver cancer (19), this study provides new insights from the perspective of the immune microenvironment and prognostic modeling, thereby expanding the functional understanding of DAP3 within the tumor microenvironment. These phenotypic data will further enhance our understanding of the potential biological roles of DAP3.

In this study, we systematically investigated the functions of DAP3 by integrating bioinformatics analyses with experimental approaches. Using public datasets, we performed survival analysis, Gene Set Enrichment Analysis (GSEA), Kyoto Encyclopedia of Genes and Genomes (KEGG) analysis, immune infiltration analysis, single-cell sequencing analysis, mutation analysis, and chemotherapeutic efficacy analysis. From these studies, we constructed a risk score prognostic model and a nomogram for prediction. *In vitro* findings confirmed the overexpression of DAP3, and further investigations demonstrated that DAP3 regulates cell proliferation, apoptosis, cell cycle dynamics, and metastasis. Thus, DAP3 may hold significant promise for cancer prognosis and treatment.

Materials and methods

Clinical samples

HCC tissues were obtained from Nantong Third Hospital Affiliated with Nantong University. This study received approval from the ethics committees of Nantong Third Hospital Affiliated with Nantong University, and written consent was obtained from all patients or their guardians. None of the patients had undergone radiotherapy or chemotherapy prior to surgery.

Data acquisition and analysis

We downloaded expression profile data and clinical phenotype data for liver hepatocellular carcinoma (LIHC) from the TCGA database (https://www.cancer.gov/tcga). Additionally, we obtained single-cell sequencing data (CSE000000) from the CNGBdb database (https://db.cngb.org/). The GSE14520 dataset was acquired from the GEO database (https://www.ncbi.nlm.nih.gov/), while the LIRI-JP sequencing data were sourced from the ICGC database (https://dcc.icgc.org/). Furthermore, we downloaded sequencing data for 33 types of pan-cancer along with the corresponding survival information from UCSC Xena (https://xena.ucsc.edu/).

Enrichment analysis

In the TCGA cohort, we conducted differential analysis on tumor and adjacent normal tissues, as well as on groups stratified by DAP3 expression levels. We identified consistently upregulated and downregulated genes as characteristic markers for the DAP3-stratified groups. Next, we conducted Gene Ontology (GO) and Kyoto Encyclopedia of Genes and Genomes (KEGG) analyses on the candidate genes using the clusterProfiler R package. Additionally, we downloaded gene sets related to the hall v2023.1.Hs.symbols pathways from the GSEA website and conducted Gene Set Enrichment Analysis (GSEA) to identify significantly different biological processes between the low-expression and high-expression groups by ranking the changes in gene expression.

Genomic alterations and mutation profiles

To explore the relationship between mutations and DAP3 expression levels, we downloaded somatic SNP data for liver cancer from TCGA via UCSC Xena. We analyzed mutation differences between groups using the maftools package and conducted statistical tests on the calculated tumor mutational burden. Additionally, we calculated the frequency of copy number variations (CNVs) and performed online analysis using GISTIC2.

Immune infiltration analysis

We estimated immune scores using the TIMER, CIBERSORT, and MCPcounter algorithms and predicted potential responses to immune checkpoint inhibitors in HCC using the Tumor Immune Dysfunction and Exclusion (TIDE) method. The proportion of responders among different sample types was illustrated using the ggplot2 package. Additionally, we generated box plots and incorporated immune checkpoint-related genes and utilized the Wilcoxon test to assess the significance of differences between different groups.

Construction of a prognostic risk score model for HCC

We used GSE144269, GSE14520, LIRI_JP, and OEP000321 as validation sets, with TCGA as the training set. We identified 73 prognostic genes through univariate Cox regression ($p < 0.05$) in the DAP3-stratified groups and validated 33 genes that appeared more than 500 times through 80% resampling. Using the Bioinformatics Soup database, we applied these 33 genes in the LIHC cohort to create a machine learning model with leave-one-out cross-validation (LOOCV) and calculated the C-index for each model. HCC patients were categorized into high-risk and low-risk groups according to the median risk score, and the predictive ability was assessed using the area under the time-dependent receiver operating characteristic curve (AUROC). Risk curves were plotted to assess survival differences between groups.

Construction and validation of predictive models for clinical trials

We performed univariate and multivariate analyses using TCGA data. We also conducted decision curve analysis (DCA) to assess the net benefit at different risk thresholds, evaluating the clinical applicability of the risk score model. Next, we constructed a nomogram that integrated clinical characteristics using the 'regplot' package for survival prediction. Calibration and ROC curves were plotted to evaluate the predictive accuracy of the nomogram.

Chemotherapy drug sensitivity analysis

Based on CTRP (Cancer Therapeutics Response Portal, https://portals.broadinstitute.org/ctrp) and PRISM (Profiling Relative Inhibition Simultaneously in Mixtures, https://depmap.org/portal/prism/) datasets, we conducted a drug sensitivity assay, analyzed the differences in AUC values for each chemotherapy drug among the high- and low-risk score groups and performed correlation analysis.

Cell lines and cell culture

LO2 and five HCC cell lines (PLC/PRF/5, HCCLM3, SMMC-7721, SK-Hep-1, and Li-7) were obtained from the Cell Culture Facility (Shanghai, China). PLC/PRF/5 and SK-Hep-1 cells were cultured in MEM (Gibco, USA) supplemented with 10% fetal bovine serum (Gibco, USA). LO2 and SMMC-7721 cells were cultured in RPMI-1640 medium (Gibco, USA) supplemented with 10% FBS, and HCCLM3 cells were cultured in DMEM (Gibco, USA) supplemented with 10% FBS at 37°C with 5% CO2.

Construction of plasmids and siRNAs

The siRNAs targeting the negative controls si-NC, si-1, and si-3 were purchased from Gene Pharma (Suzhou, China). The pcDNA3.1-DAP3 for the overexpression of DAP3 and the empty plasmid (pc-DNA3.1-NC) were purchased from Gene Pharma (Suzhou, China). We used Lipofectamine3000 (Invitrogen, USA) for transfection and overexpression according to the manufacturer's instructions.

si-1 sense: 5'-GGAUGGAAUCAAUGCUCUUTT-3';
antisense: 5'-AAGAGCAUUGAUUCCAUCCTT-3'
si-3 sense: 5' -CCCUAAGUCUUUGCCAUGUTT-3';
antisense: 5'-ACAUGGCAAAGACUUAGGGTT -3'

IHC staining

Dewaxing and rehydration were performed in graded ethanol, followed by citrate antigen retrieval. The tissues were sealed at room temperature and incubated overnight at 4°C with an anti-DAP3 antibody (Santa Cruz, 1:200). The sections were then incubated with a horseradish peroxidase-conjugated secondary antibody at room temperature for 30 minutes. Staining was performed using 3,3′-diaminobenzidine (DAB), followed by washing and counterstaining with hematoxylin. Immunohistochemical scoring was based on the product of the staining intensity and extent scores. Staining intensity: 0 (no staining), 1 (weak staining), 2 (moderate staining), and 3 (strong staining); staining extent scoring: 0 (≤10%), 1 (10%-25%), 2 (25%-50%), 3 (50%-75%), or 4 (75%).

RNA preparation and RT-qPCR

Total RNA was isolated with TRIzol reagent (Invitrogen, USA), reverse transcribed into cDNA with a Revert Aid First Strand cDNA Synthesis Kit (Thermo Fisher Scientific, USA), and finally, SYBR reagent (Bio-Rad, China) and specific primers (Generay, China) were used for quantification. After normalization to GAPDH, the relative expression was calculated. The RT–qPCR sequences of primers used were as follows:

GAPDH forward: 5'-GGACCTGACCTGCCGTCTAG-3',
GAPDH reverse: 5'-GTAGCCCAGGATGCCCTTGA-3';
DAP3 forward: 5'-TCCAGCTACAACAAACAGCG-3',
DAP3 reverse: 5'-CTCACCCGTGTTATGCCCTG-3'.

Western blot

Total protein was extracted in RIPA buffer with 1% PMSF (Beyotime, China). The samples were separated using 4–12% SDS-PAGE gels and subsequently transferred to polyvinylidene fluoride (PVDF) membranes (Millipore, USA). After blocking, the membranes were incubated with primary and secondary antibodies, and protein expression was detected using an enhanced chemiluminescence (ECL) kit (Tanon, China). The antibodies used for Western blot were as follows: anti-GAPDH antibody (1:20000, Proteintech, China), anti-DAP3 antibody (1:200, Santa Cruz, China), HRP-conjugated-β-actin antibody (1:5000, Proteintech, China) and HRP-conjugated goat anti-mouse IgG antibody (1:1000, Beyotime, China).

Flow cytometry

The transfected cells were harvested for apoptosis analysis, and an Annexin V/7-AAD kit (BD Biosciences, USA) was used to detect the apoptotic rate under the constructions, with analysis performed using FlowJo.

CCK-8 assay

A total of 3,000 transfected cells were seeded in 96-well plates and incubated overnight. The cells were subsequently incubated with CCK-8 solution (MCE, USA) for 2 hours, and the optical density (OD) value was subsequently measured at 450 nm using a plate reader (Thermo, USA) every 24 hours.

Colony formation assay

A total of 2000 transfected cells were seeded in a six-well plate. After 2 weeks, the cells were fixed with 4% formaldehyde (Beyotime, China) and stained with 0.1% crystal violet (Sigma, USA). Cell colonies were counted and analyzed using GraphPad Prism 8.0.

Transwell assay

Transwell assays were conducted using the concentration difference of serum. The chamber (Costar, USA) and Matrigel (BD, USA) were used for invasion assays, whereas migration assays were performed with no gel. After 48 hours, the cells were fixed with 4% paraformaldehyde (Beyotime, China), stained with 0.1% crystal violet (Sigma, USA), and photographed under a microscope (Olympus, Japan). The cells in random fields were counted and analyzed using GraphPad Prism 8.0.

Co expression analysis

LinkedOmics (http://www.linkedomics.org/login.php) platform include Linkfinder and LinkInterpreter section. Linkfinder was used to obtain co-expressed proteins associated with DAP3 in HCC.

Statistics analyses

The data are presented as the means ± standard deviations (SDs). A t test was used for comparisons between two groups, whereas one-way analysis of variance (ANOVA) was used for comparisons involving more than two groups. Statistical significance was calculated using GraphPad Prism 8.0 and SPSS 17.0. All experiments were repeated independently at least twice. A p value of less than 0.05 was considered statistically significant.

Results

DAP3 expression was related to poor prognosis in public datasets

We analyzed DAP3 expression using datasets from TCGA, ICGC, and GSE14520. Our results revealed significant upregulation of DAP3 expression in tumor samples (Figure 1A). Further

assessment of the prognostic value of DAP3 in TCGA and ICGC cohorts revealed that higher DAP3 expression was significantly associated with shorter overall survival (Figures 1B, C). Univariate Cox regression analysis identified DAP3 as a risk factor for poor prognosis, yielding a hazard ratio (HR) of 1.62 (Figure 1D). Multivariate analysis confirmed that DAP3 served as an independent prognostic factor (Figure 1E). Additionally, DAP3 was found to be broadly overexpressed across various cancers, and linked to the severity of HCC lesions (Figures 1F, G). High expression was significantly correlated with poor prognosis in multiple cancer types,

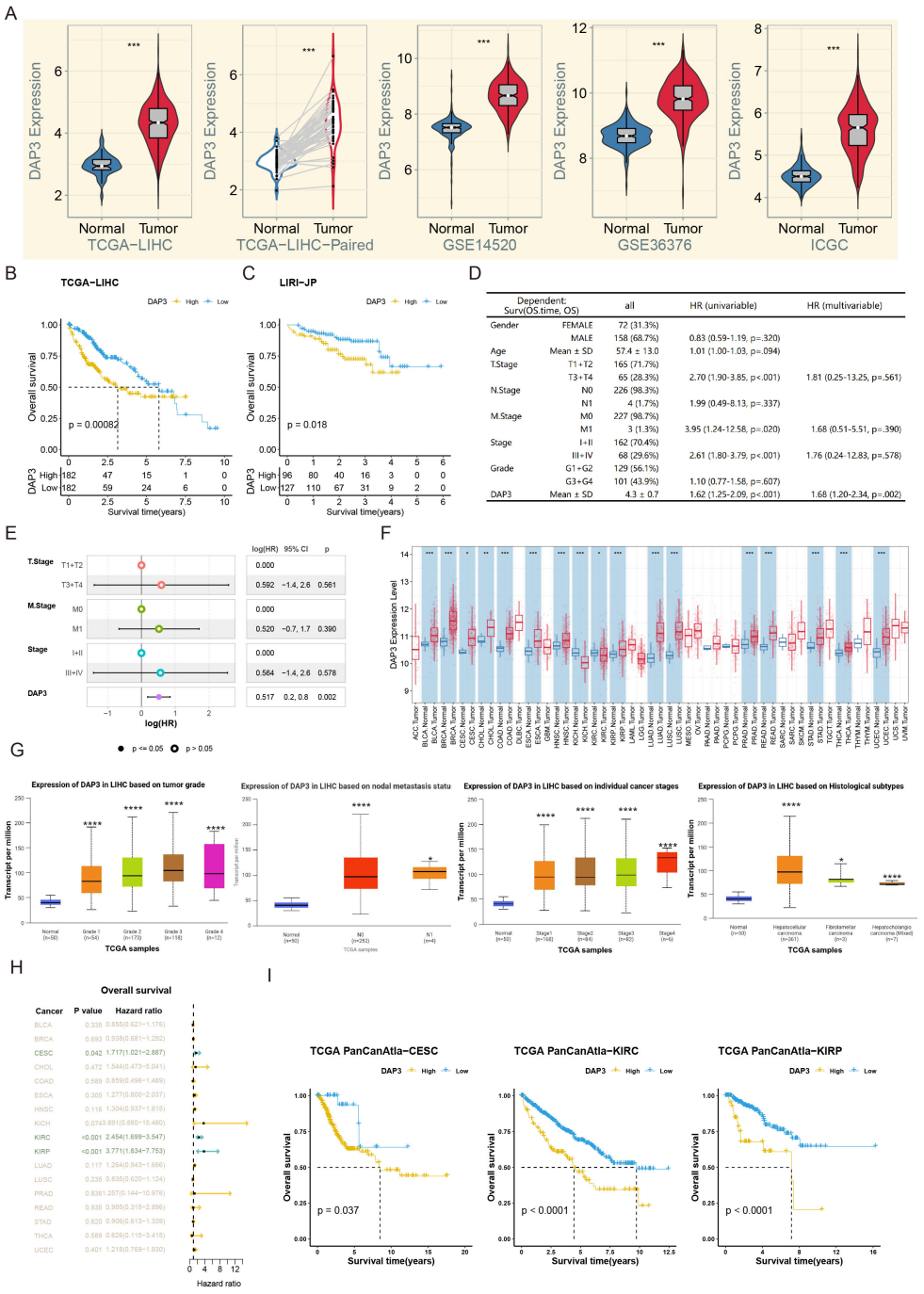

FIGURE 1
DAP3 expression was related with poor prognosis in public datasets: **(A)** Relative DAP3 expression levels across TCGA, GEO, and ICGC datasets. **(B)** Survival curves derived from TCGA datasets. **(C)** Survival curves based on ICGC datasets. **(D)** Univariate Cox regression analysis for overall survival in HCC. **(E)** Multivariate Cox regression analysis related to overall survival in HCC. **(F)** DAP3 expression in various pan-cancers using TIMER2.0 datasets. **(G)** DAP3 expression in various HCC subtypes using UALCAN datasets. **(H)** Overall survival analysis across pan-cancers. **(I)** Survival curves in CESC, KIRC, and KIRP. *P<0.05, **P<0.01, ***P<0.001, ****P < 0.0001.

such as cervical squamous cell carcinoma (CESC), kidney renal clear cell carcinoma (KIRC), and kidney renal papillary cell carcinoma (KIRP) (Figures 1H, I).

Kyoto encyclopedia of genes and genomes analysis and GSEA

In the TCGA cohort, we conducted differential analysis between the tumor-adjacent group and the high-low-expression group, followed by the generation of a volcano plot to visualize the results (Figures 2A, B). A Venn diagram illustrated the extensive overlap of differentially expressed genes between the two groups (Figure 2C). Next, we performed KEGG enrichment analysis, which revealed distinct pathways enriched in the high-DAP3 group versus the low-DAP3 group, such as those related to cell metabolism, transcription, drug metabolism, and the immune environment, providing new avenues for future research. (Figures 2D, E). GSEA revealed that several cancer-related pathways, including the Wnt, apoptosis, TGF-beta, epithelial-mesenchymal transition, and PI3K pathways, were enriched in the high-DAP3 group (Figure 2F). These findings indicate that DAP3 may play a major role in regulating cell proliferation and migration.

Correlation between DAP3 and immune-related functions in HCC

First, we calculated the scores of six immune cell types using the TIMER, CIBERSORT, and MCP counter algorithms. The results

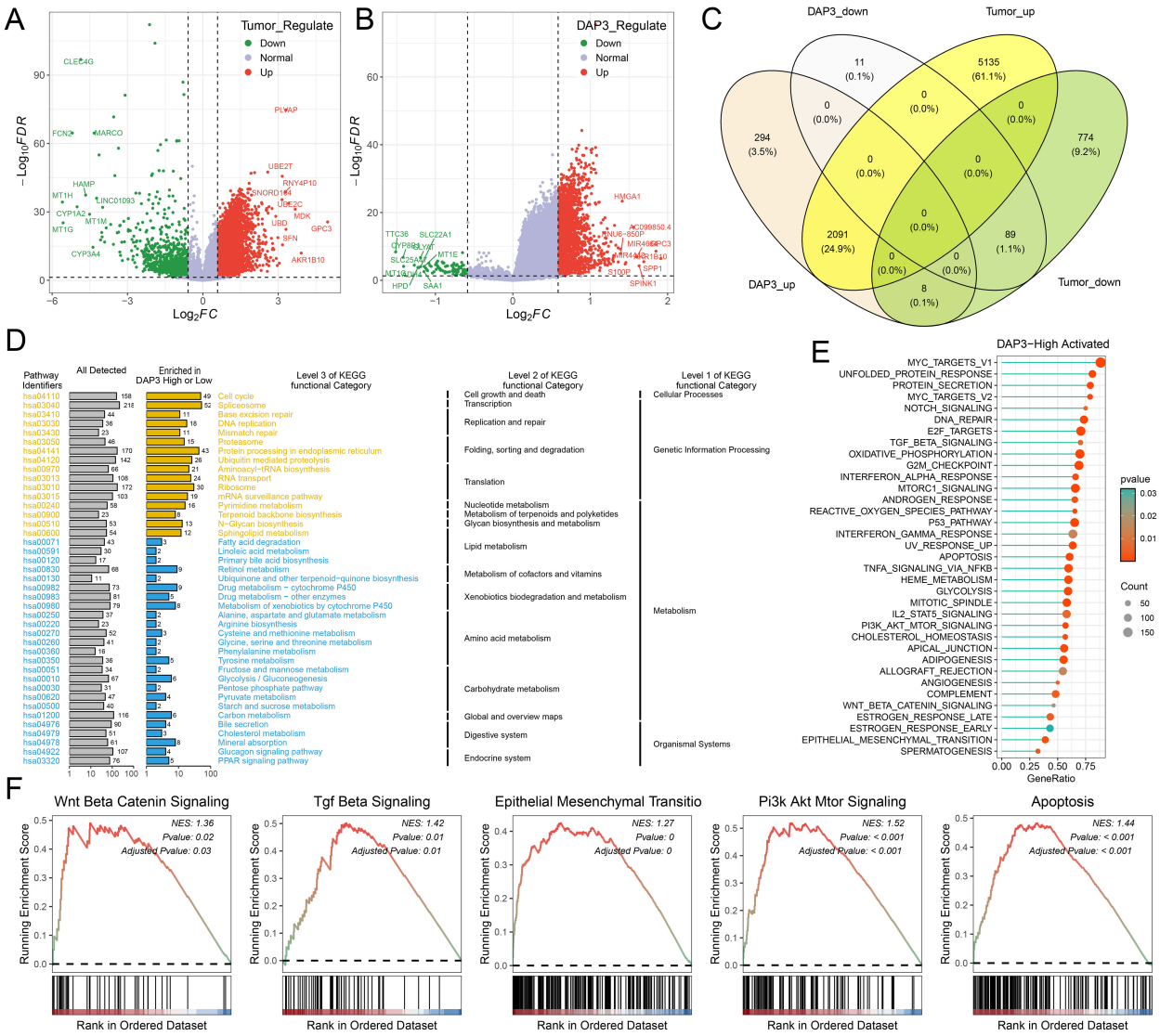

FIGURE 2
Kyoto Encyclopedia of Genes and Genomes (KEGG) and GSEA analysis: **(A)** A volcano plot illustrating differential gene expression between tumor-adjacent groups. **(B)** A volcano plot depicting differential gene expression between high and low expression groups. **(C)** A Venn diagram showcasing the overlap of differentially expressed genes between the two comparisons. **(D, E)** KEGG analysis highlighting enriched pathways in the high expression groups. **(F)** GSEA analysis demonstrating enriched signaling pathways.

indicated that patients in the high DAP3 expression group had higher immune cell scores across most immune cell types (Figures 3A–C). To evaluate patient responsiveness to immunotherapy, we utilized TIDE data for prediction, which revealed that patients with high DAP3 expression had greater potential for immune evasion (Figure 3D). Additionally, we found that the high DAP3 expression group showed a significantly higher response to Sorafenib treatment compared to the low DAP3 expression group, with a statistically significant difference (Supplementary Figure 1A). The ROC curve further validated the

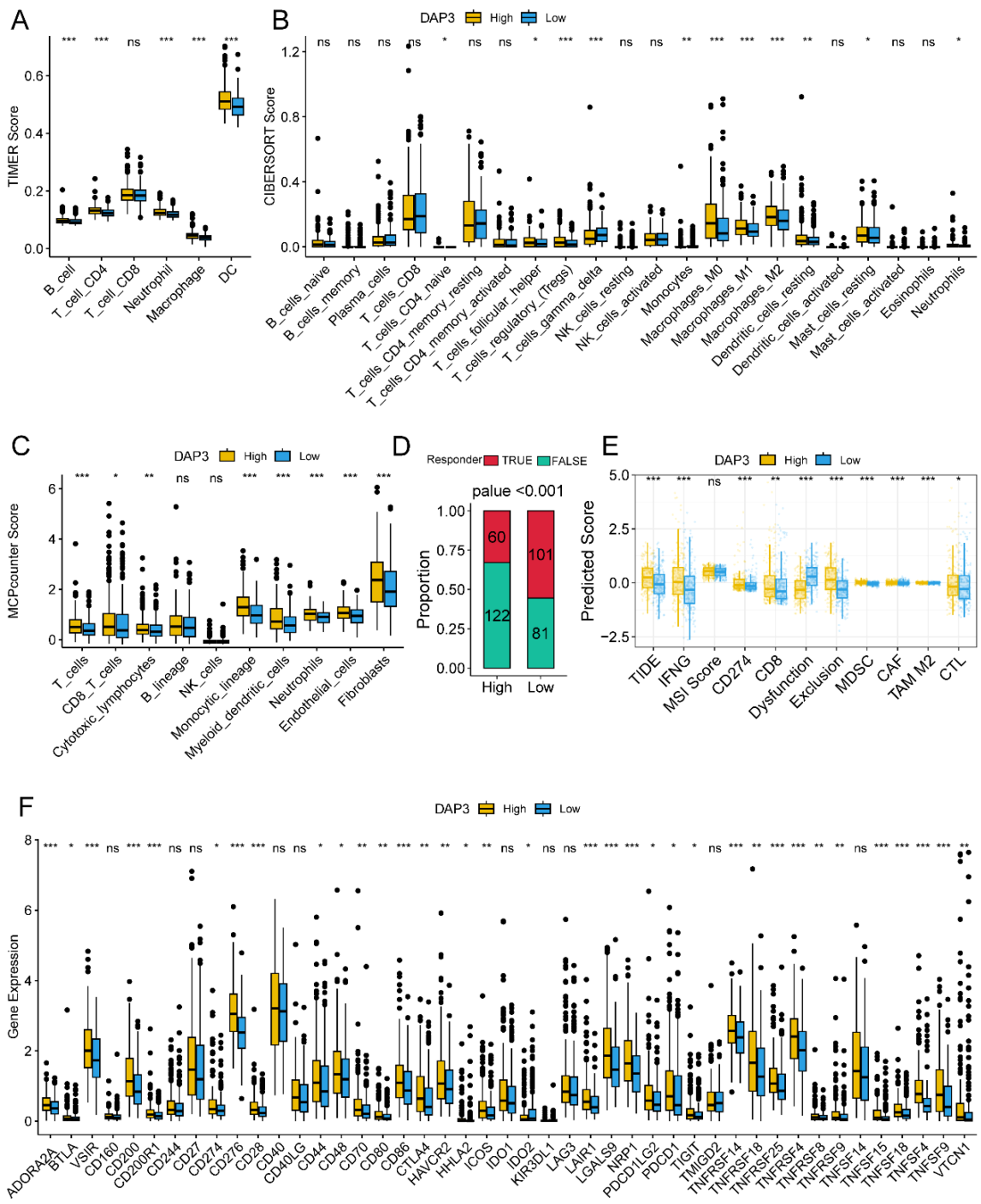

FIGURE 3
Correlation between DAP3 and immune-related functions in HCC: **(A)** Immune cell infiltration in low and high DAP3 expression groups based on TIMER scores. **(B)** Immune cell infiltration in low and high DAP3 expression groups based on CIBERSORT scores. **(C)** Immune cell infiltration in low and high DAP3 expression groups based on MCP-counter scores. **(D)** Proportional plot illustrating the relationship between DAP3 expression and responder numbers based on TIDE scores. **(E)** Predicted immune response and tumor microenvironment characteristics in low and high DAP3 expression groups. **(F)** Expression levels of immune checkpoint genes in low and high-risk groups. *P<0.05,**P<0.01,***P<0.001.

sensitivity and specificity of DAP3 in predicting treatment response (Supplementary Figure 1B). Moreover, we observed significant differences in the predicted scores for features such as TIDE, dysfunction, exclusion, and myeloid-derived suppressor cells (MDSCs) based on DAP3 expression levels (Figure 3E). Furthermore, analysis of immune checkpoint genes (20) identified in previous studies revealed higher expression levels of these genes in the high DAP3 group (Figure 3F). These findings showed that DAP3 could influence the tumor microenvironment and may be an important biomarker for immunotherapy.

Potential role of DAP3 in HCC genomic alterations

To investigate the relationship between mutations and DAP3 expression levels, we downloaded somatic SNP data for HCC from the TCGA database via UCSC Xena. Our analysis revealed that the predominant mutation type was missense mutation, with single nucleotide polymorphisms (SNPs) being the primary variant type in hepatocellular carcinoma (Figure 4A). We subsequently examined the distribution of gene mutations in samples with high DAP3

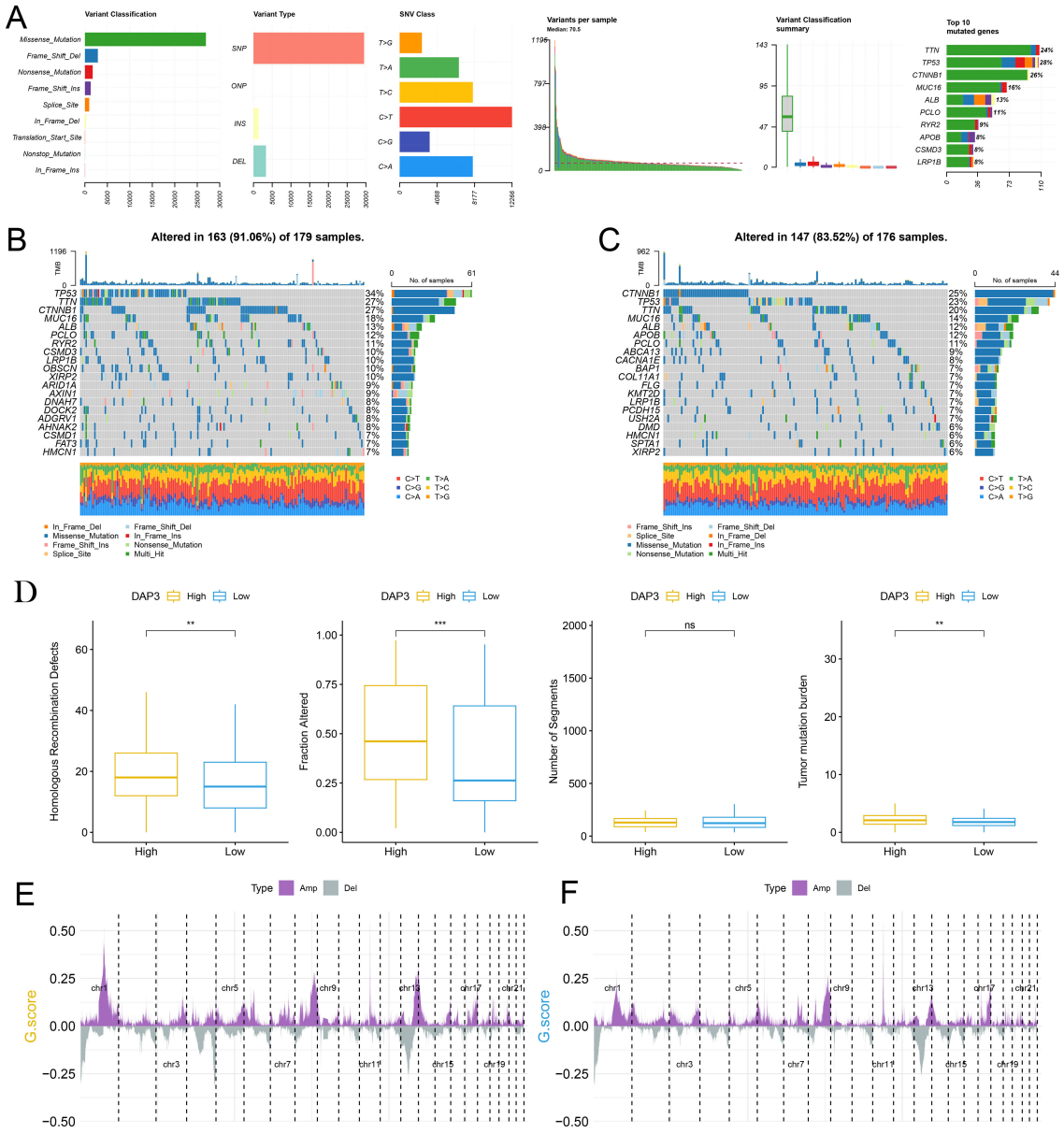

FIGURE 4
The potential role of DAP3 in HCC genomic alterations: **(A)** Classification and frequency of gene mutations. **(B)** Waterfall plot depicting gene mutations in the high-DAP3 expression group. **(C)** Waterfall plot illustrating gene mutations in the low-DAP3 expression group. **(D)** DAP3 expression levels and genomic alterations in low versus high DAP3 expression groups. **(E)** Distribution of copy number variations (CNVs) across different chromosomal regions in the high-DAP3 expression group. **(F)** Distribution of CNVs across different chromosomal regions in the low-DAP3 expression group. **P<0.01, ***P<0.001.

expression (Figure 4B) compared with those with low DAP3 expression (Figure 4C). The box plots indicated that the high DAP3 expression group exhibited significantly more homologous recombination defects and fusion genes than the low DAP3 expression group. Additionally, there was a notable difference in tumor mutation burden, suggesting that DAP3 expression levels may be associated with genomic instability and mutation rates (Figure 4D). Furthermore, gene amplifications and deletions were widespread across various chromosomes (Figures 4E, F). These findings showed that high DAP3 expression may be linked to increased mutation rates, homologous recombination defects, and copy number variations, indicating a potential role for DAP3 in tumor genomic alterations.

A single-cell expression atlas and identification of DAP3 in HCC by scRNA-seq

Stemness scores (CytoTRACE2) were significantly higher in the high DAP3 expression group (DAP3+) compared to the low expression group (DAP3−) (Supplementary Figure 2A), and a clear positive correlation was observed between DAP3 expression levels and CytoTRACE2 scores (Supplementary Figure 2B).The UMAP distribution further revealed heterogeneity in stemness levels across different cell populations (Supplementary Figure 2C), suggesting a potential role for DAP3 in regulating cellular stemness. To further investigate the distribution characteristics of DAP3 in the tumor microenvironment, we analyzed the relationships and gene characteristics among distinct cell populations through the integration of single-cell transcriptome data. Using a combination of classical markers, we identified seven major cell groups (Figure 5A). We compared the distribution of cells between adjacent and tumor samples, revealing significant differences in cell distribution between tumor tissue and adjacent normal liver tissue (Figure 5B). Next, we identified the top five most significant marker genes for each subcluster (Figure 5C). DAP3 was widely expressed in tumor cells, plasmacytoid dendritic cells (pDCs), and endothelial cells, with higher expression levels in tumor samples than in adjacent samples (Figures 5D–F). Differential analysis between tumor and adjacent samples revealed that DAP3 was upregulated in pDCs (Figure 5G). Furthermore, differential analysis between primary and recurrent samples indicated significant upregulation of DAP3 in myeloid cells, suggesting that DAP3 may influence tumor development and progression (Figure 5H). Finally, we conducted differential gene expression and functional enrichment analyses, which revealed that the differentially expressed genes in the DAP3+ group were significantly enriched in lipid metabolism, glycolysis, and the PPAR signaling pathway (Supplementary Figures 2D, E). Metabolic heatmap analysis further demonstrated substantial activation of lipid metabolism, glycolysis, and oxidative phosphorylation in the DAP3+ group, particularly in recurrent tumor samples (Supplementary Figure 2F). These findings suggest that DAP3 may drive metabolic reprogramming, thereby promoting rapid tumor cell proliferation and invasion.

Construction and evaluation of prognostic risk-score model

Through a leave-one-out cross-validation (LOOCV) framework, we fitted 101 predictive models and calculated the concordance index (c-index) for each model across all the validation datasets. The optimal model, a combination of Cox Boost and Super PC, achieved the highest average c-index in the test set (Figure 6A). Additionally, we identified 10 key genes (TRIP13, NDC80, CSTF2, UBE2S, NCL, CDC20, NUSAP1, CEP55, SSB, and KIF2C), as illustrated in the forest plot (Figure 6B). The risk scores for both the training and validation sets indicated that patients in the high-risk group had poorer prognoses, whereas those in the low-risk group exhibited better prognoses across all cohorts (Figures 6C–G). Furthermore, time-dependent ROC curve analysis was used to assess the predictive efficacy of the prognostic signature based on both training and validation datasets (Supplementary Figure 3). The risk score demonstrated strong predictive ability across different liver cancer datasets, with higher risk scores significantly associated with poorer survival outcomes.

Integration of the risk score with clinicopathological features

Next, we conducted univariate and multivariate Cox regression analyses incorporating risk scores and clinical characteristics, revealing that the risk score was the most significant prognostic factor (Figures 7A, B). To quantify patients' risk assessments and survival probabilities, we developed a nomogram that integrated the risk score with other clinicopathological features. The results demonstrated that the risk score had the most significant impact on survival prediction (Figure 7C). We further evaluated the predictive accuracy of the model using calibration curves. The calibration curves at 1, 3, and 5 years closely aligned with the standard curve, indicating that the nomogram demonstrated good predictive performance (Figure 7D). Additionally, we employed DCA to assess the model's reliability, which revealed that both the risk score and the nomogram provided significantly greater net benefits than the extreme curves (Figure 7E). Time-dependent AUC analysis illustrated the predictive ability of the different models over time, with the nomogram and risk score performing well at multiple time points (Figure 7F). Thus, the risk score and nomogram model serve as effective predictive tools that, in conjunction with clinical characteristics, can accurately predict patient survival.

Identification of potential therapeutic agents for high-risk HCC patients

The CTRP and PRISM drug databases were utilized to identify potential therapeutic agents. Differential drug response analysis between the high-risk and low-risk score groups was performed, identifying drugs with lower predicted AUC values in the high-risk score group. Subsequently, Spearman correlation analysis between

the AUC values and risk scores was conducted to select drugs with a negative correlation coefficient (Figures 8A, B). All drugs exhibited lower estimated AUC values in the high-risk score group than in the low-risk score group, indicating increased drug sensitivity (Figures 8C, D). The mechanisms of potential drugs were searched from Selleck websites (Figure 8E).

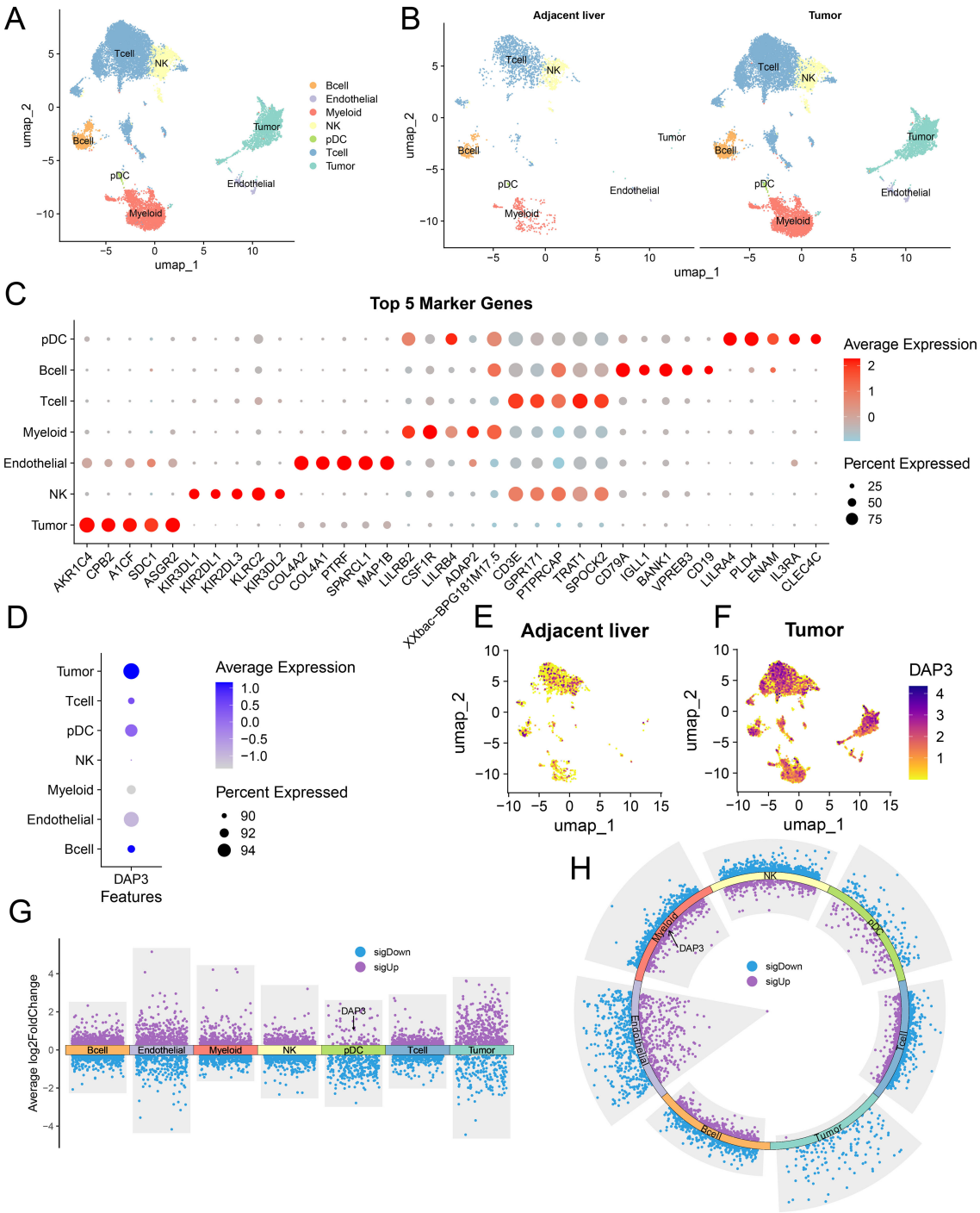

FIGURE 5
A single-cell expression atlas and the identification of DAP3 in HCC by scRNA-seq: **(A)** Distribution of various cell types in hepatocellular carcinoma (HCC). **(B)** Comparison of cell type distribution in adjacent liver and tumor tissues. **(C)** Top five marker genes for different cell types. **(D)** Expression levels of DAP3 across various cell types. **(E)** Expression and distribution of DAP3 in adjacent liver tissues. **(F)** Expression and distribution of DAP3 in tumor tissues. **(G)** Comparison of gene expression levels in different cell types within tumor tissues versus adjacent tissues. **(H)** Gene expression levels in different cell types during recurrence compared to non-recurrence conditions.

Increased DAP3 expression was related to poor prognosis in HCC patients

Based on expression patterns from various datasets, we collected tumor and paired adjacent tissues from Nantong Third People's Hospital. We found that DAP3 expression was significantly higher in HCC tissues than in the adjacent tissues using RT-qPCR and Western blot analyses (Figures 9A–C), which was also confirmed by IHC analysis (Figure 9D). ROC analysis revealed that the AUC of DAP3 was 0.802 (95% CI: 0.67–0.92, p<0.05), and the area of AFP was 0.726 (95% CI: 0.608–0.845, p<0.05) (Figure 9E). Kaplan-Meier survival analysis revealed that patients with higher DAP3 expression had shorter overall survival (Figure 9F). Elevated DAP3 levels were correlated with increased AFP levels (P=0.044) and larger tumor size (P=0.024) (Table 1). Univariate Cox regression revealed that DAP3 expression (p=0.047) and TNM stage (p=0.044) were risk factors for HCC. Multivariable analysis confirmed that DAP3 expression (p=0.040) was an independent prognostic indicator for overall survival (OS) in HCC patients (Table 2). Thus, DAP3 is a promising independent prognostic marker for overall survival.

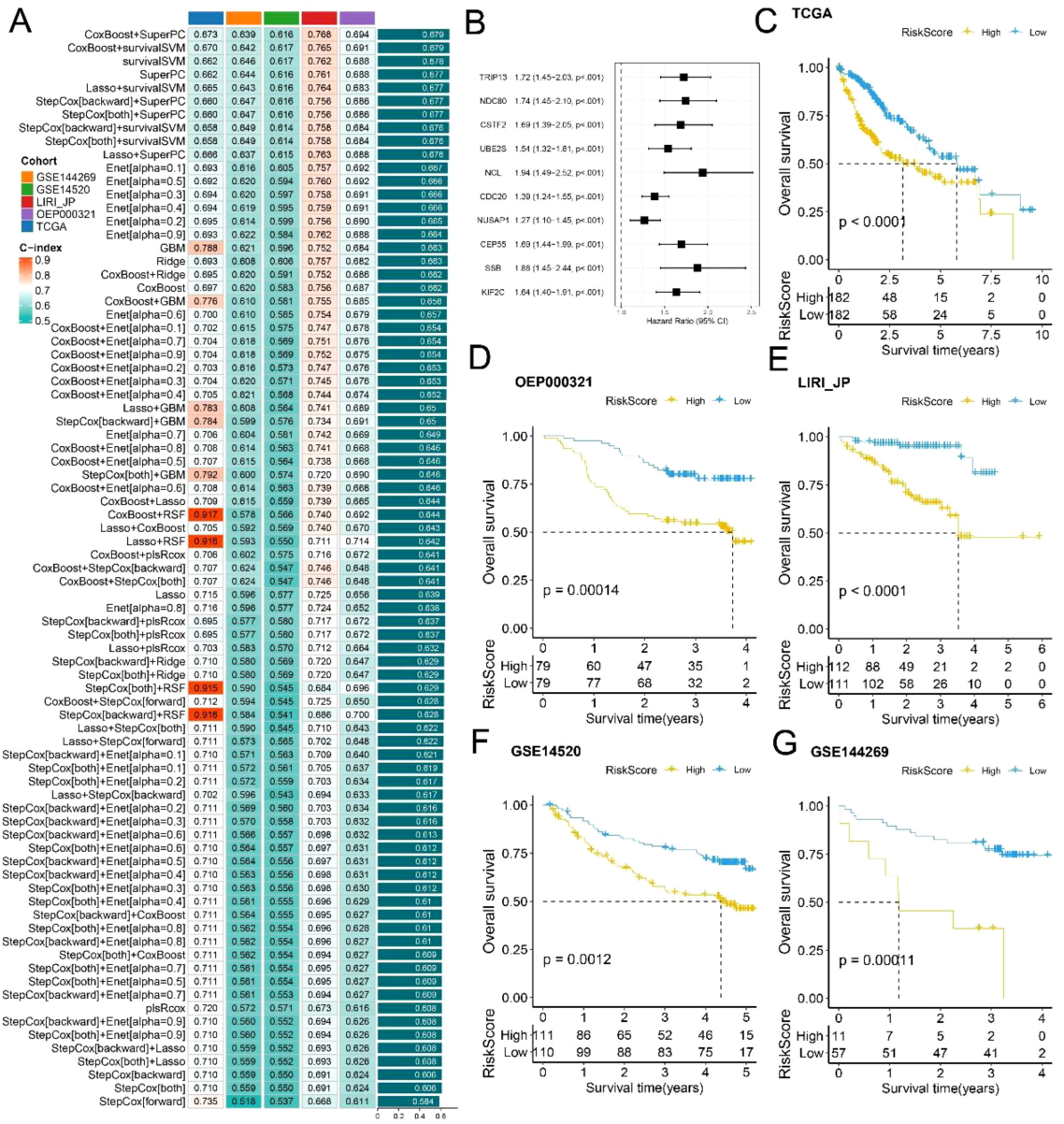

FIGURE 6
Construction and Evaluation of Prognostic Risk-Score Model: **(A)** Performance comparison of survival prediction models across different cohorts, assessed using C-index. **(B)** Forest plot highlighting 10 key genes. **(C-G)** Survival curves comparing low- and high-risk score groups based on the TCGA, OEP000321, LIRI_JP, GSE14520, and GSE144269 datasets.

Knockdown of DAP3 inhibited the progression of HCC cells

DAP3 was highly expressed in HCC cell lines (Figure 10A). To investigate the functional role of DAP3, we transfected HCCLM3 cells with DAP3 siRNAs. RT-qPCR confirmed effective knockdown (Figure 10B), and Western blot analyses validated this finding (Figure 10C). For cell proliferation studies, CCK-8 and colony formation assays revealed that reduced DAP3 expression decreased HCCLM3 cell viability (Figure 10D) and significantly reduced colony numbers (Figures 10E, F). In transwell assays, DAP3 knockdown led to a notable decrease in the migratory and invasive capabilities of HCCLM3 cells (Figures 10G, H). Additionally, flow cytometric analysis revealed that DAP3 downregulation promoted apoptosis in these cells (Figures 10I, J).

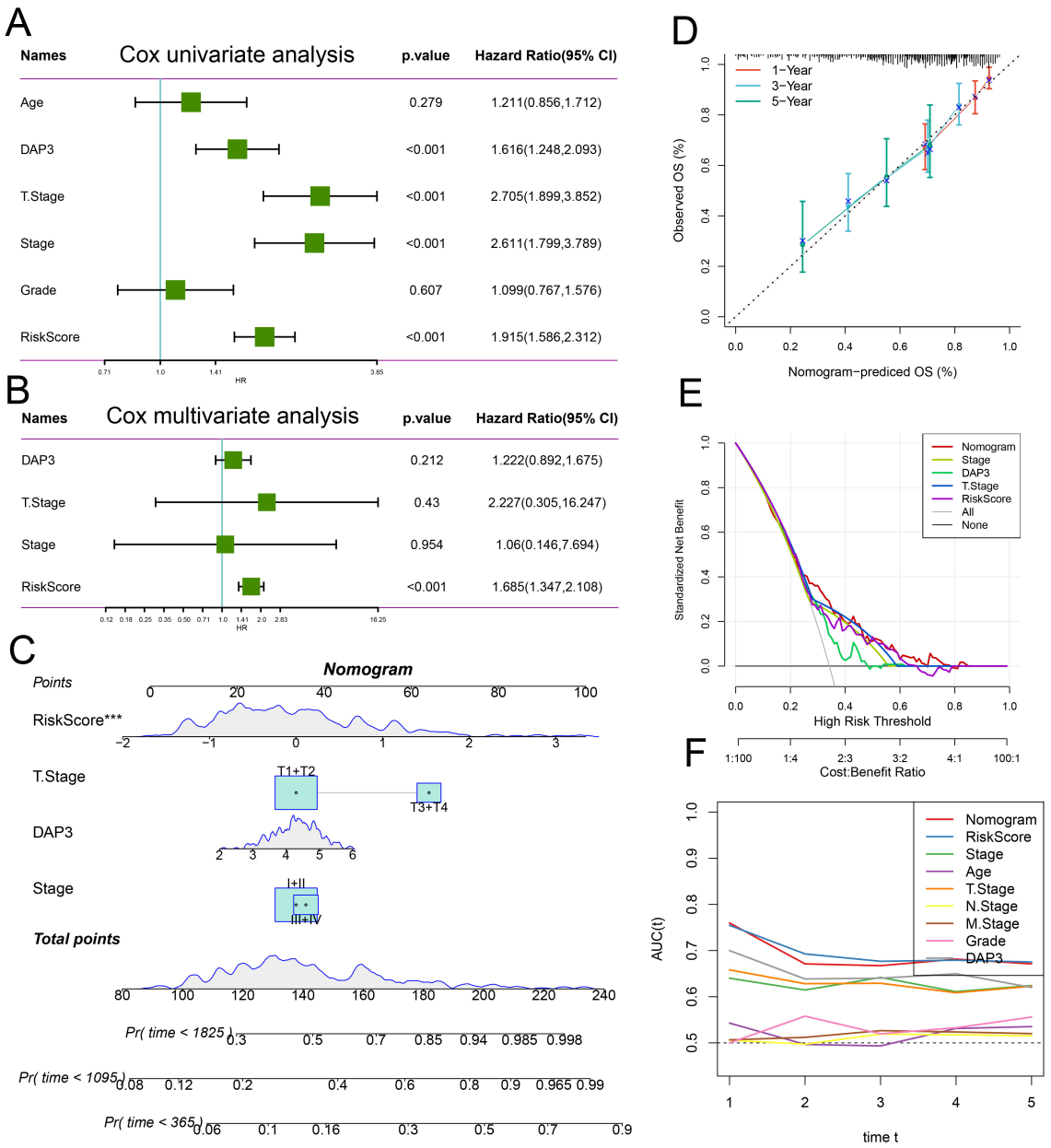

FIGURE 7
Integration of risk score with clinicopathological features: **(A)** Univariate Cox regression analysis of the risk score alongside other clinical features. **(B)** Multivariate Cox regression analysis incorporating the risk score and additional clinical characteristics. **(C)** Nomogram designed to predict patients' survival probabilities at various time intervals. **(D)** Calibration curves illustrating the predictions of the established nomogram for 1-, 3-, and 5-year overall survival. **(E)** Decision curve analysis for 5-year overall survival in the TCGA-LIHC dataset. **(F)** Time-dependent ROC curve analysis to assess the predictive efficacy of the prognostic signature.

Overexpression of DAP3 promoted the progression of HCC cells

To investigate the functional role of DAP3 in HCC cells, we constructed a DAP3 overexpression plasmid and transfected it into SK-Hep1 cells. Both RT-qPCR and Western blot analyses confirmed the efficient overexpression of DAP3 (Figures 11A, B). Subsequently, CCK-8 assays demonstrated that increased DAP3 expression significantly enhanced the viability of SK-Hep1 cells (Figure 11C). Furthermore, DAP3 overexpression notably increased the number of colonies formed by SK-Hep1 cells (Figures 11D, E). Additionally, the overexpression of DAP3 promoted both cell migration and invasion (Figures 11F, G). Flow cytometric analysis revealed that upregulation of DAP3 inhibited apoptosis in SK-Hep1 cells (Figures 11H, I). To investigate the potential function and mechanism in HCC, we constructed a co-expression network of DAP3 in HCC through the linkedomics platform. A volcano plot showing the proteins positively and negatively associated with DAP3 was constructed (Figure 11J), showing 5685 genes negatively correlated with DAP3 and 3292 genes exhibiting positive correlation with HCC. Correlation analysis was conducted by GEPIA datasets which revealed that mitochondrial-related genes (FLAD1, HAX1 and NDUFS2) were positively correlated with DAP3 (Figure 11K), suggesting that DAP3 plays an important role in OXPHOS. However, additional work on identifying the DAP3 regulatory network needs to be performed in the future.

Discussion

Currently, cancer is widely recognized as a metabolic disorder (21). Hepatocellular carcinoma (HCC) is one of the most prevalent forms of primary liver cancer worldwide (22). HCC can be classified based on various criteria, including histological characteristics, molecular features, tumor growth patterns, etiological background, and degree of differentiation, which could help us to better understand the heterogeneity of HCC and provide guidance for precision medicine (23–25). KEGG analysis and GSEA revealed that higher DAP3 expression is linked to various biological processes, including cell metabolism, transcription, drug metabolism, and the immune environment, thereby opening new avenues for future research.

Mitochondria provide energy for eukaryotic cells by oxidizing fats and sugars to produce ATP, and oxidative phosphorylation (OXPHOS) is one of the core metabolic pathways in this process (26). As reported, DAP3 can increase mitochondrial complex I activity in HCC cells by regulating the translation and expression of MT-ND5 (19). In our study, HAX1, FLAD1 and NDUFS2, which were positively correlated with DAP3, were reported to play a crucial in mitochondria which could regulate the progression in numerous cancers (27–29), indicating that DAP3 may be an important role in OXPHOS, which could affect HCC progression. In public datasets, we concluded that DAP3 expression was linked to the subtypes of HCC, and that its high expression was linked to a poor prognosis, its elevated expression correlated with poor

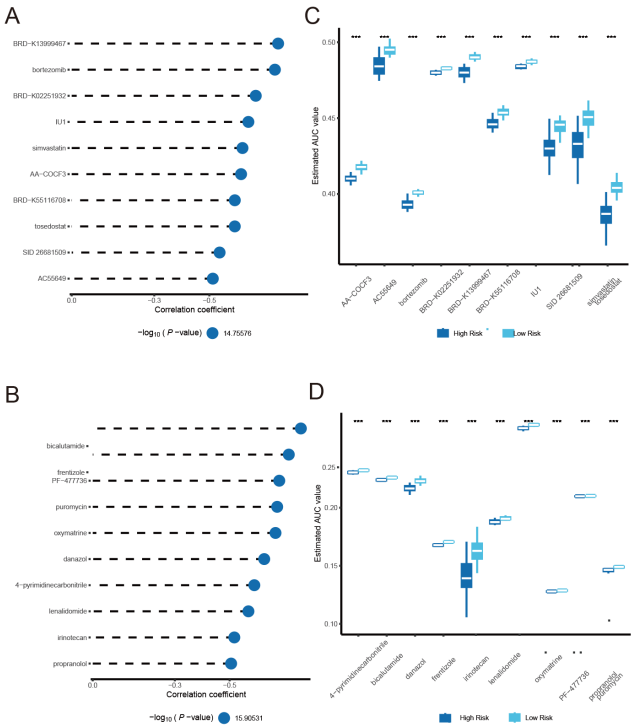

E

Drug Name	Mechanism	Category
Bortezomib	Inhibits proteasome activity, blocking tumor growth.	Anti-cancer drug
Simvastatin	Inhibits HMG-CoA reductase, potential anti-cancer effect.	Anti-cancer drug
Tosedostat	Inhibits amino acid metabolism in tumor cells.	Anti-cancer drug
Ac66694	Inhibits tumor cell growth and invasion.	Anti-cancer drug
Irinotecan	Inhibits topoisomerase I, blocking DNA replication.	Anti-cancer drug
Lenalidomide	Modulates immune response, inhibits tumor growth.	Anti-cancer drug
BRD-K13994467	Disrupts tumor cell signaling, inhibiting growth.	Anti-cancer drug
BRD-K02251932	Inhibits tumor growth, requires further study.	Anti-cancer drug
AA-COCF3	Inhibits tumor cell activity.	Anti-cancer drug
SID 26681509	Disrupts tumor cell signaling and proliferation.	Anti-cancer drug
Bicalutamide	Anti-androgen, inhibits androgen receptor.	Hormonal therapy drug
Danazol	Modulates steroid pathways, used in hormone-dependent tumors.	Hormonal therapy drug
Oxymatrine	Antiviral, inhibits HBV, used for viral liver cancer.	Antiviral drug
Frentizole	General therapeutic use, mechanism unclear.	Other drugs
PF-477736	Inhibits kinase activity, potential anti-cancer effect.	Anti-cancer drug
Puromycin	Inhibits protein synthesis in tumor cells.	Antibacterial/Anti-cancer drug
Propranolol	Beta-blocker, modulates vascular effects in cancer.	Cardiovascular drug
Irinotecan	Inhibits topoisomerase I, blocking DNA replication.	Anti-cancer drug

FIGURE 8
Identification of potential therapeutic agents for high-risk HCC patients: **(A)** Spearman correlation analysis of drugs derived from CTRP. **(B)** Spearman correlation analysis of drugs derived from PRISM. **(C)** Analysis of differences AUC values for drugs derived from CTRP. **(D)** Analysis of differences in response (AUC values) for drugs derived from PRISM. **(E)** Screening and Mechanistic Classification of drugs. ***P<0.001.

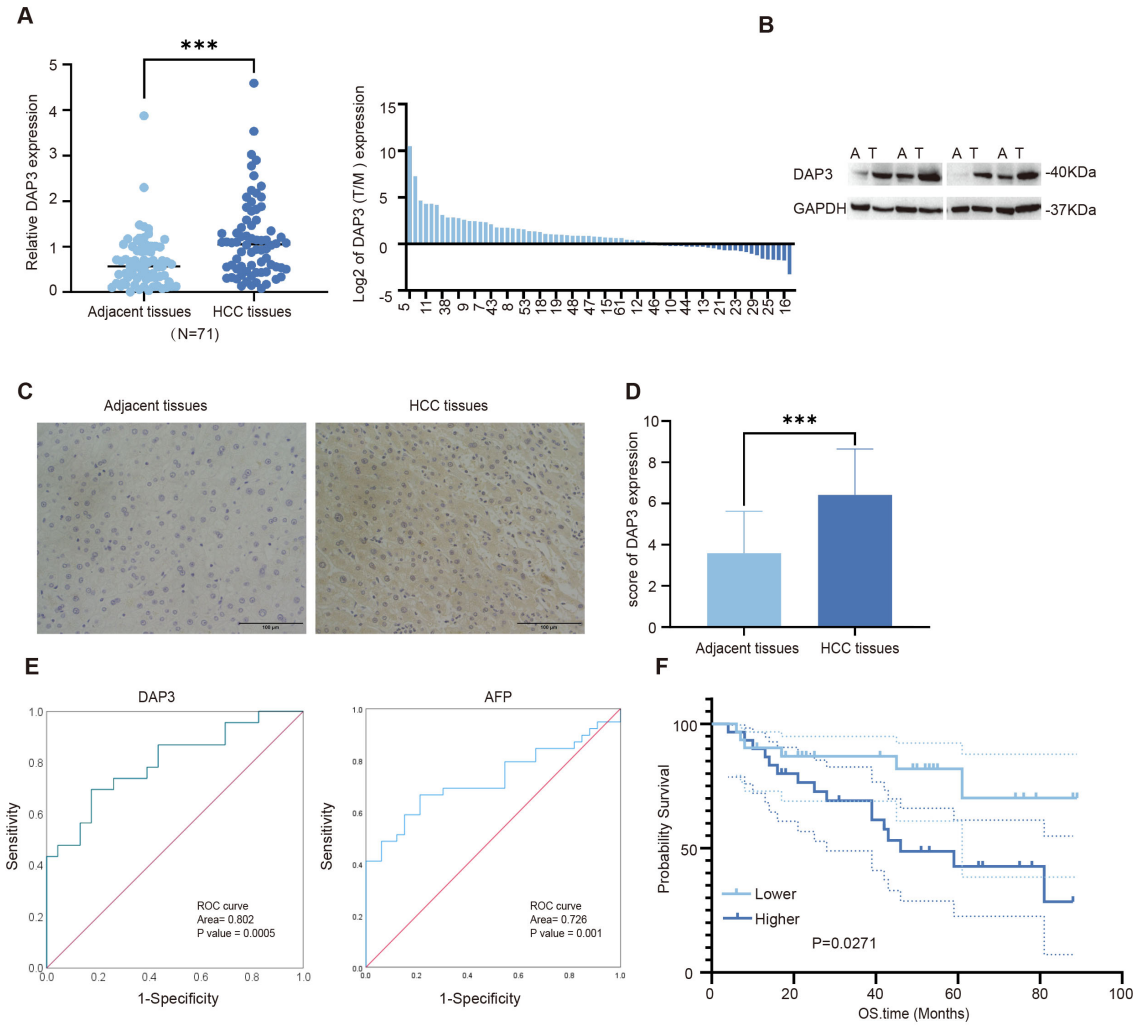

FIGURE 9
Increased DAP3 expression was associated with poor prognosis in HCC patients: **(A)** Relative DAP3 expression levels in HCC tissues as measured by qRT-PCR (n = 71). **(B)** DAP3 expression analyzed via Western blot in HCC tissues (n = 4). **(C)** Representative images of DAP3 expression in HCC tissues obtained through immunohistochemical staining (magnification: 40X; scale bar: 100 μm). **(D)** IHC scores for DAP3 expression. **(E)** ROC curve analysis of DAP3 expression and AFP value. **(F)** Overall survival (OS) time compared using Kaplan–Meier analysis. ***P<0.001.

outcomes. Clinically, high DAP3 expression was strongly associated with larger tumor size and elevated AFP levels, demonstrating good diagnostic value according to ROC analysis. Furthermore, survival analysis indicated that increased DAP3 expression was linked to poorer prognosis. Cox regression analysis identified DAP3 expression as a prognostic indicator for overall survival in HCC patients. *In vitro*, we performed functional experiments to examine the role of DAP3 in HCC progression. The upregulation of DAP3 expression was found to suppress the proliferation, migration, and invasion of HCC cells while promoting apoptosis. These findings underscored the strong association between elevated DAP3 expression and adverse outcomes in HCC patients, highlighting the potential significance of DAP3 in driving HCC progression.

Cancer is a multifaceted disease characterized by intricate reciprocal interactions between tumor cells and the immune system (30). The tumor microenvironment (TME) mainly consists of distinct immune cell populations in tumor islets and highly influences tumor growth, metastatic spread, and response to treatment (31, 32). Due to the poor prognosis following standard treatment, immunotherapy has been extensively investigated as an alternative treatment option (33). Cancer immunotherapies, particularly immune checkpoint blockade therapy, have fundamentally transformed cancer treatment by facilitating complete and sustained responses and have now emerged as a standard approach for a variety of malignancies (34). Regrettably, only a limited number of patients with specific cancer types respond to immunotherapy, possibly due to inadequate immune activation needed to detect tumor-specific antigens (35). Therefore, it is essential to identify additional potential therapeutic targets. Our initial exploration demonstrated that high DAP3 expression was closely associated with immune cell infiltration, immune evasion mechanisms, and gene expression patterns, especially impacting immunotherapy response and immune evasion, indicating that DAP3 plays a regulatory role in the tumor microenvironment and may serve as an important biomarker for immunotherapy in the clinic.

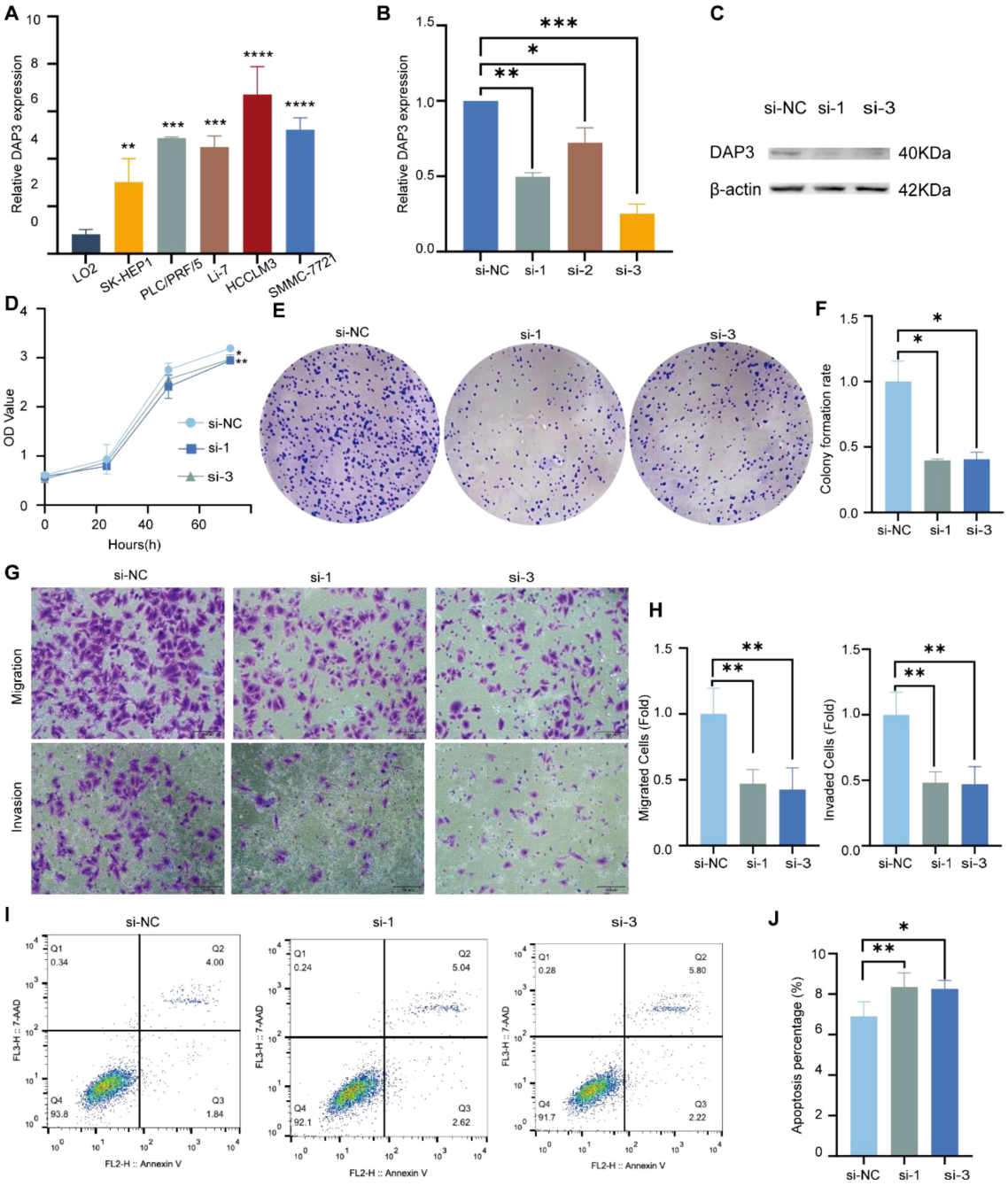

FIGURE 10
Knockdown of DAP3 inhibited the progression of HCC cells: **(A)** DAP3 expression levels in normal hepatocytes (LO2) compared to five HCC cell lines. **(B)** Knockdown efficiency in HCCLM3 cells confirmed by qRT-PCR. **(C)** Knockdown efficiency in HCCLM3 cells validated by Western blot. **(D)** CCK-8 assay results in DAP3-knockdown HCCLM3 cells. **(E)** Colony formation assay conducted in DAP3-knockdown HCCLM3 cells. **(F)** Number of colonies formed in DAP3-knockdown HCCLM3 cells. **(G)** Representative images from migration and invasion assays in DAP3-knockdown HCCLM3 cells. **(H)** Number of migrated or invaded cells in DAP3-knockdown HCCLM3 cells. **(I)** Apoptosis levels in DAP3-knockdown HCCLM3 cells. **(J)** Apoptotic rates in DAP3-knockdown HCCLM3 cells. *P<0.05,**P<0.01,***P<0.001,****P<0.0001.

Genetic mutations can disrupt normal cellular functions, including proliferation, differentiation, and apoptosis, ultimately leading to tumor formation (36). Different types of cancer are often associated with specific genetic mutations, which can influence cell behavior, treatment responsiveness, and immune recognition (37). In our study, we observed that high DAP3 expression was linked to increased genomic mutation rates, homologous recombination defects, and copy number variations. These findings revealed a potential role for DAP3 in driving genomic alterations within tumors.

Currently, high mortality and recurrence rates continue to pose significant challenges to the advancement of effective treatment options for this disease (38, 39). The prognosis for HCC patients remains poor, with a 5-year overall survival rate of only 12% (40).

10.3389/fimmu.2025.1528853

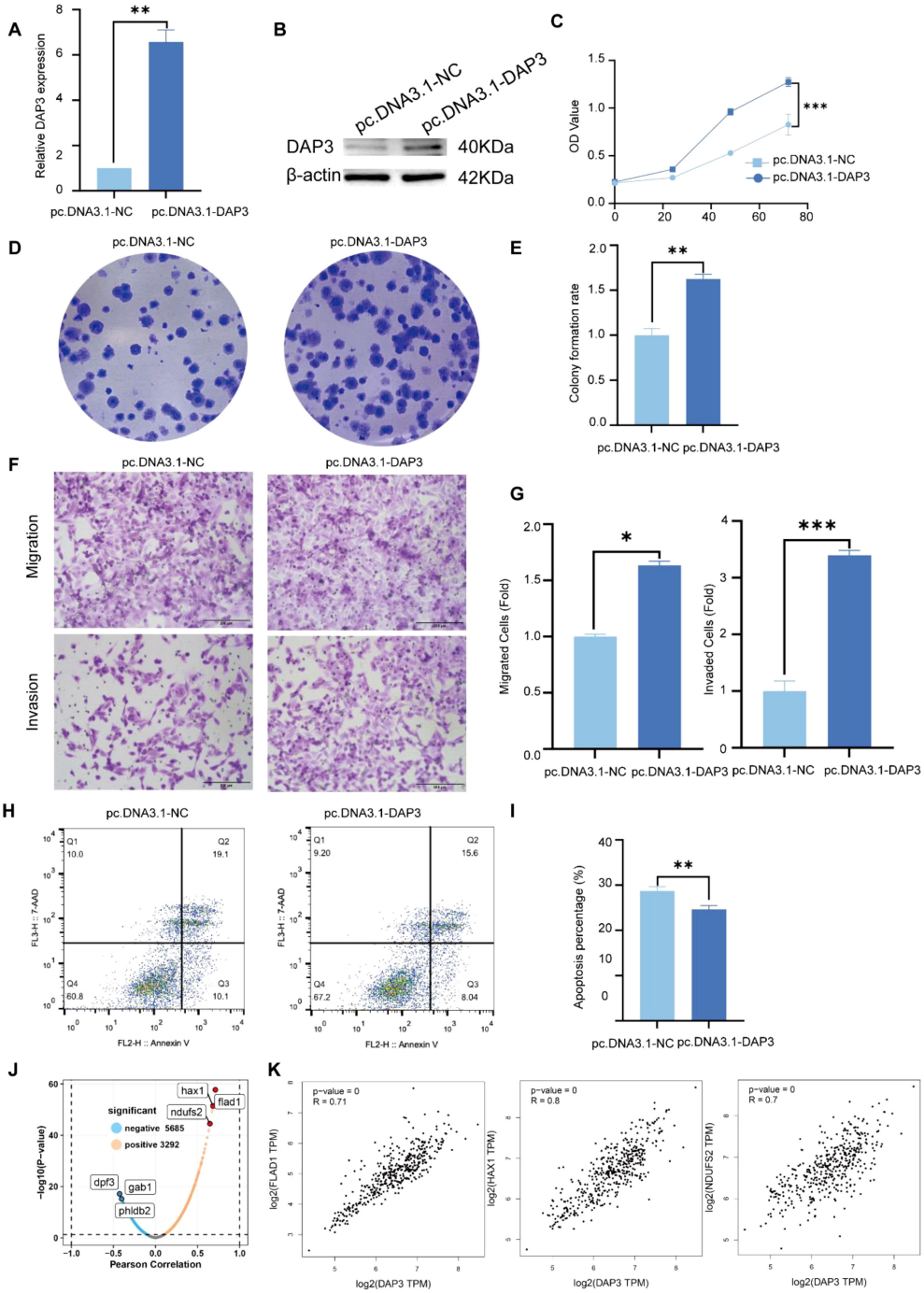

FIGURE 11
Overexpression of DAP3 promoted the progression of HCC cells: **(A)** Overexpression efficiency in SK-Hep1 cells confirmed by qRT-PCR. **(B)** Overexpression efficiency in SK-Hep1 cells validated by Western blot. **(C)** CCK-8 assay results in DAP3-overexpressing SK-Hep1 cells. **(D)** Colony formation assay conducted in DAP3-overexpressing SK-Hep1 cells. **(E)** Number of colonies formed in DAP3-overexpressing SK-Hep1 cells. **(F)** Representative images from migration and invasion assays in DAP3-overexpressing SK-Hep1 cells. **(G)** Number of migrated or invaded cells in DAP3-overexpressing SK-Hep1 cells. **(H)** Apoptosis levels in DAP3-overexpressing SK-Hep1 cells. **(I)** Apoptotic rates in DAP3-overexpressing SK-Hep1 cells. **(J)** Volcano plot shown the co-expressed protein with DAP3 in HCC. **(K)** Correlation analysis between DAP3, FLAD1, HAX1, and NDUFS2 based on GEPIA datasets. *P<0.05, **P<0.01, ***P<0.001.

There is an urgent need for novel prognostic predictors and the development of more robust prognostic models for HCC. We ultimately constructed a new prognostic model for HCC (41), and demonstrated that both the risk score and the nomogram were effective predictive tools that can accurately predict patient survival when combined with clinical characteristics. Moreover, to overcome drug resistance and improve the clinical outcomes of HCC patients, we identified potential chemotherapy drugs and found that these drugs had lower AUC values in the high-risk score group than in the low-risk score group and were negatively

TABLE 1 Correlation of DAP3 expression with clinicopathological characteristics in HCC patients.

Clinicopathological Characteristics	DAP3 expression		P value
	Low expression	High expression	
Age (years)			0.904
≥58	17 (48.6%)	18 (50.0%)	
<58	18 (51.4%)	18 (50.0%)	
Gender			0.945
Male	26 (74.3%)	27 (75.0%)	
Female	9 (25.7%)	9(25.0%)	
AFP (ng/mL)			0.044
≥40	14 (40.0%)	23 (63.9%)	
<40	21 (60.0%)	13 (36.1%)	
Tumor size (cm)			0.024
≥4	12 (34.3%)	22(61.1%)	
<4	23 (65.7%)	14 (38.9%)	
Tumor stage			0.561
I-II	15 (42.9%)	13 (36.1%)	
II-IV	20 (57.1%)	23 (63.9%)	
Vascular invasion			0.259
No	24 (68.6%)	20 (55.6%)	
Yes	11 (31.4%)	16 (44.4%)	

TNM stage, tumor node-metastasis stage; AFP, alpha fetoprotein; P-value ≤ 0.05 indicate statistical significance.

correlated with the risk score, indicating that chemotherapy drugs were more sensitive in the high-risk score group. Nevertheless, there are some limitations to the drug sensitivity findings; although the 20 candidate drugs exhibited increased drug sensitivity in patients with high-risk scores, the above analysis alone does not support the conclusion that these drugs have therapeutic effects on HCC.

In summary, DAP3 plays a regulatory role in both the tumor microenvironment and genomic alterations within tumors. Our findings confirmed that the risk score and nomogram model were effective predictive tools for HCC when combined with clinical characteristics. *In vitro* studies demonstrated that DAP3 could regulate proliferation, apoptosis, and metabolism in HCC cells. However, this study had several limitations. Although DAP3 shows promising potential as a biomarker and therapeutic target in liver cancer, the specific pathway for its clinical translation remains unclear. A larger sample size and more experimental validation would strengthen the conclusions and help establish more robust evidence for the role of DAP3 in liver cancer.

TABLE 2 Univariate and multivariate Cox regression analyses related to overall survival in patients with HCC.

Index	Univariable			Multivariable		
	P value	Hazard ratio	95% CI for Exp(B)	P value	Hazard ratio	95% CI for Exp(B)
DAP3	0.047	2.591	1.011-6.639	0.040	2.920	1.052-8.106
Gender	0.269	0.599	0.242-1.485			
Age	0.244	1.695	0.698-4.117			
TNM Stage	0.044	2.844	1.028-7.866	0.042	2.649	1.034-6.791
AFP	0.688	0.842	0.363-1.951			
Tumor size	0.511	1.328	0.570-3.094			

P-value ≤ 0.05 indicate statistical significance.

Conclusions

This study highlights DAP3 as a significant factor in cancer prognosis and immune regulation, offering insights that could inform future therapeutic strategies.

Data availability statement

The raw data supporting the conclusions of this article will be made available by the authors, without undue reservation.

Ethics statement

The studies involving humans were approved by Nantong Third People's Hospital. The studies were conducted in accordance with the local legislation and institutional requirements. The participants provided their written informed consent to participate in this study. Written informed consent was obtained from the individual(s) for the publication of any potentially identifiable images or data included in this article.

Author contributions

LY: Writing – original draft, Writing – review & editing, Data curation, Funding acquisition, Formal analysis. ZY: Writing – original draft, Writing – review & editing, Data curation, Investigation. QM: Writing – review & editing, Methodology. PZ: Writing – review & editing, Methodology. FX: Writing – review & editing, Conceptualization. LC: Writing – review & editing, Conceptualization, Funding acquisition.

Funding

The author(s) declare financial support was received for the research, authorship, and/or publication of this article. Health Commission of Jiangsu province (grant nos. LKM2023041), the Nantong Science and Technology Bureau (grant nos. MS2023080) and the Nantong Municipal Health Commission (grant nos. QN2022041).

Conflict of interest

The authors declare that the research was conducted in the absence of any commercial or financial relationships that could be construed as a potential conflict of interest.

Generative AI statement

The author(s) declare that no Generative AI was used in the creation of this manuscript.

Publisher's note

Supplementary material

The Supplementary Material for this article can be found online at: https://www.frontiersin.org/articles/10.3389/fimmu.2025.1528853/full#supplementary-material

SUPPLEMENTARY FIGURE 1
Correlation between DAP3 and immune-related functions in HCC: **(A)** The impact of DAP3 expression levels on Sorafenib treatment response. **(B)** ROC analysis of DAP3 expression and Sorafenib treatment response.

SUPPLEMENTARY FIGURE 2
A single-cell expression atlas and the identification of DAP3 in HCC by scRNA-seq: **(A)** Boxplot comparing CytoTRACE2 scores in the DAP3+ and DAP3– groups. **(B)** Correlation analysis between DAP3 expression levels and CytoTRACE2 scores. **(C)** UMAP plot illustrating the heterogeneity of CytoTRACE2 scores among different cell populations. **(D)** Volcano plot displaying differentially expressed genes between DAP3+ and DAP3– tumor cells. **(E)** Bubble plot showing the top enriched pathways. **(F)** Heatmap of metabolic pathway activity in DAP3+ and DAP3– groups across primary and relapsed tumor samples.

SUPPLEMENTARY FIGURE 3
Time-dependent ROC curve analysis to assess the predictive efficacy of the prognosis signature based on datasets.

References

1. Zhou Y, Li Y, Zhou T, Zheng J, Li S, Li HB. Dietary natural products for prevention and treatment of liver cancer. *Nutrients*. (2016) 8:156. doi: 10.3390/nu8030156

2. Li X, Ramadori P, Pfister D, Seehawer M, Zender L, Heikenwalder M. The immunological and metabolic landscape in primary and metastatic liver cancer. *Nat Rev Cancer*. (2021) 21:541–57. doi: 10.1038/s41568-021-00383-9

3. Li L, Wang H. Heterogeneity of liver cancer and personalized therapy. *Cancer Lett*. (2016) 379:191–7. doi: 10.1016/j.canlet.2015.07.018

4. Huang Z, Zhou JK, Peng Y, He W, Huang C. The role of long noncoding RNAs in hepatocellular carcinoma. *Mol Cancer*. (2020) 19:77. doi: 10.1186/s12943-020-01188-4

5. Johnson P, Zhou Q, Dao DY, Lo YMD. Circulating biomarkers in the diagnosis and management of hepatocellular carcinoma. *Nat Rev Gastroenterol Hepatol*. (2022) 19:670–81. doi: 10.1038/s41575-022-00620-y

6. Regula KM, Ens K, Kirshenbaum LA. Mitochondria-assisted cell suicide: a license to kill. *J Mol Cell Cardiol*. (2003) 35:559–67. doi: 10.1016/s0022-2828(03)00118-4

7. O'Brien TW, O'Brien BJ, Norman RA. Nuclear MRP genes and mitochondrial disease. *Gene*. (2005) 354:147–51. doi: 10.1016/j.gene.2005.03.026

8. Zhao JW, Zhao WY, Cui XH, Xing L, Shi JC, Yu L. The role of the mitochondrial ribosomal protein family in detecting hepatocellular carcinoma and predicting

prognosis, immune features, and drug sensitivity. *Clin Transl Oncol*. (2024) 26:496–514. doi: 10.1007/s12094-023-03269-4

9. Cavdar Koc E, Burkhart W, Blackburn K, Moseley A, Spremulli LL. The small subunit of the mammalian mitochondrial ribosome. Identification of the full complement of ribosomal proteins present. *J Biol Chem*. (2001) 276:19363–74. doi: 10.1074/jbc.M100727200

10. Cavdar Koc E, Ranasinghe A, Burkhart W, Blackburn K, Koc H, Moseley A, et al. A new face on apoptosis: death-associated protein 3 and PDCD9 are mitochondrial ribosomal proteins. *FEBS Lett*. (2001) 492:166–70. doi: 10.1016/s0014-5793(01)02250-5

11. Kim HR, Chae HJ, Thomas M, Miyazaki T, Monosov A, Monosov E, et al. Mammalian dap3 is an essential gene required for mitochondrial homeostasis *in vivo* and contributing to the extrinsic pathway for apoptosis. *FASEB J*. (2007) 21:188–96. doi: 10.1096/fj.06-6283com

12. Sui L, Ye L, Sanders AJ, Yang Y, Hao C, Hargest R, et al. Expression of death associated proteins DAP1 and DAP3 in human pancreatic cancer. *Anticancer Res*. (2021) 41:2357–62. doi: 10.21873/anticanres.15010

13. Mariani L, Beaudry C, McDonough WS, Hoelzinger DB, Kaczmarek E, Ponce F, et al. Death-associated protein 3 (Dap-3) is overexpressed in invasive glioblastoma cells *in vivo* and in glioma cell lines with induced motility phenotype in *vitro*. *Clin Cancer Res*. (2001) 7:2480–9.

14. Han J, An O, Hong H, Chan THM, Song Y, Shen H, et al. Suppression of adenosine-to-inosine (A-to-I) RNA editome by death associated protein 3 (DAP3) promotes cancer progression. *Sci Adv*. (2020) 6:eaba5136. doi: 10.1126/sciadv.aba5136

15. Jacques C, Fontaine JF, Franc B, Mirebeau-Prunier D, Triau S, Savagner F, et al. Death-associated protein 3 is overexpressed in human thyroid oncocytic tumours. *Br J Cancer*. (2009) 101:132–8. doi: 10.1038/sj.bjc.6605111

16. Jia Y, Li Z, Cheng X, Wu X, Pang F, Shi J, et al. Depletion of death-associated protein-3 induces chemoresistance in gastric cancer cells through the beta-catenin/LGR5/Bcl-2 axis. *J Investig Med*. (2019) 67:856–61. doi: 10.1136/jim-2018-000934

17. Sui L, Zeng J, Zhao H, Ye L, Martin TA, Sanders AJ, et al. Death associated protein−3 (DAP3) and DAP3 binding cell death enhancer−1 (DELE1) in human colorectal cancer, and their impacts on clinical outcome and chemoresistance. *Int J Oncol*. (2023) 62:7. doi: 10.3892/ijo.2022.5455

18. Wazir U, Jiang WG, Sharma AK, Mokbel K. The mRNA expression of DAP3 in human breast cancer: correlation with clinicopathological parameters. *Anticancer Res*. (2012) 32:671–4.

19. Tan S, Zhang X, Guo X, Pan G, Yan L, Ding Z, et al. DAP3 promotes mitochondrial activity and tumour progression in hepatocellular carcinoma by regulating MT-ND5 expression. *Cell Death Dis*. (2024) 15:540. doi: 10.1038/s41419-024-06912-2

20. Danilova L, Ho WJ, Zhu Q, Vithayathil T, De-Jesus-Acosta A, Azad NS, et al. Programmed cell death ligand-1 (PD-L1) and CD8 expression profiling identify an immunologic subtype of pancreatic ductal adenocarcinomas with favorable survival. *Cancer Immunol Res*. (2019) 7:886–95. doi: 10.1158/2326-6066.CIR-18-0822

21. Gyamfi J, Kim J, Choi J. Cancer as a metabolic disorder. *Int J Mol Sci*. (2022) 23:1155. doi: 10.3390/ijms23031155

22. Huang G, Liang M, Liu H, Huang J, Li P, Wang C, et al. CircRNA hsa_circRNA_104348 promotes hepatocellular carcinoma progression through modulating miR-187-3p/RTKN2 axis and activating Wnt/beta-catenin pathway. *Cell Death Dis*. (2020) 11:1065. doi: 10.1038/s41419-020-03276-1

23. Forner A, Llovet JM, Bruix J. Hepatocellular carcinoma. *Lancet*. (2012) 379:1245–55. doi: 10.1016/S0140-6736(11)61347-0

24. Broutier L, Mastrogiovanni G, Verstegen MM, Francies HE, Gavarro LM, Bradshaw CR, et al. Human primary liver cancer-derived organoid cultures for disease modeling and drug screening. *Nat Med*. (2017) 23:1424–35. doi: 10.1038/nm.4438

25. Zhou Z, Cao S, Chen C, Chen J, Xu X, Liu Y, et al. A novel nomogram for the preoperative prediction of edmondson-steiner grade III-IV in hepatocellular carcinoma patients. *J Hepatocell Carcinoma*. (2023) 10:1399–409. doi: 10.2147/JHC.S417878

26. Nsiah-Sefaa A, McKenzie M. Combined defects in oxidative phosphorylation and fatty acid beta-oxidation in mitochondrial disease. *Biosci Rep*. (2016) 36:e00313. doi: 10.1042/BSR20150295

27. Nisco A, Carvalho TMA, Tolomeo M, Di Molfetta D, Leone P, Galluccio M, et al. Increased demand for FAD synthesis in differentiated and stem pancreatic cancer cells is accomplished by modulating FLAD1 gene expression: the inhibitory effect of Chicago Sky Blue. *FEBS J*. (2023) 290:4679–94. doi: 10.1111/febs.16881

28. Fan Y, Murgia M, Linder MI, Mizoguchi Y, Wang C, Lyszkiewicz M, et al. HAX1-dependent control of mitochondrial proteostasis governs neutrophil granulocyte differentiation. *J Clin Invest*. (2022) 132:e153153. doi: 10.1172/JCI153153

29. Liu L, Qi L, Knifley T, Piecoro DW, Rychahou P, Liu J, et al. S100A4 alters metabolism and promotes invasion of lung cancer cells by up-regulating mitochondrial complex I protein NDUFS2. *J Biol Chem*. (2019) 294:7516–27. doi: 10.1074/jbc.RA118.004365

30. Zhu ZY, Tang N, Wang MF, Zhou JC, Wang JL, Ren HZ, et al. Comprehensive pan-cancer genomic analysis reveals PHF19 as a carcinogenic indicator related to immune infiltration and prognosis of hepatocellular carcinoma. *Front Immunol*. (2021) 12:781087. doi: 10.3389/fimmu.2021.781087

31. Xia L, Oyang L, Lin J, Tan S, Han Y, Wu N, et al. The cancer metabolic reprogramming and immune response. *Mol Cancer*. (2021) 20:28. doi: 10.1186/s12943-021-01316-8

32. Mao X, Xu J, Wang W, Liang C, Hua J, Liu J, et al. Crosstalk between cancer-associated fibroblasts and immune cells in the tumor microenvironment: new findings and future perspectives. *Mol Cancer*. (2021) 20:131. doi: 10.1186/s12943-021-01428-1

33. Long J, Wang A, Bai Y, Lin J, Yang X, Wang D, et al. Development and validation of a TP53-associated immune prognostic model for hepatocellular carcinoma. *EBioMedicine*. (2019) 42:363–74. doi: 10.1016/j.ebiom.2019.03.022

34. Rui R, Zhou L, He S. Cancer immunotherapies: advances and bottlenecks. *Front Immunol*. (2023) 14:1212476. doi: 10.3389/fimmu.2023.1212476

35. Lv M, Chen M, Zhang R, Zhang W, Wang C, Zhang Y, et al. Manganese is critical for antitumor immune responses via cGAS-STING and improves the efficacy of clinical immunotherapy. *Cell Res*. (2020) 30:966–79. doi: 10.1038/s41422-020-00395-4

36. Vogelstein B, Kinzler KW. Cancer genes and the pathways they control. *Nat Med*. (2004) 10:789–99. doi: 10.1038/nm1087

37. Stratton MR, Campbell PJ, Futreal PA. The cancer genome. *Nature*. (2009) 458:719–24. doi: 10.1038/nature07943

38. Llovet JM, De Baere T, Kulik L, Haber PK, Greten TF, Meyer T, et al. Locoregional therapies in the era of molecular and immune treatments for hepatocellular carcinoma. *Nat Rev Gastroenterol Hepatol*. (2021) 18:293–313. doi: 10.1038/s41575-020-00395-0

39. Berzigotti A, Reig M, Abraldes JG, Bosch J, Bruix J. Portal hypertension and the outcome of surgery for hepatocellular carcinoma in compensated cirrhosis: a systematic review and meta-analysis. *Hepatology*. (2015) 61:526–36. doi: 10.1002/hep.27431

40. Chen T, Huang H, Zhou Y, Geng L, Shen T, Yin S, et al. HJURP promotes hepatocellular carcinoma proliferation by destabilizing p21 via the MAPK/ERK1/2 and AKT/GSK3beta signaling pathways. *J Exp Clin Cancer Res*. (2018) 37:193. doi: 10.1186/s13046-018-0866-4

41. You JA, Gong Y, Wu Y, Jin L, Chi Q, Sun D. WGCNA, LASSO and SVM algorithm revealed RAC1 correlated M0 macrophage and the risk score to predict the survival of hepatocellular carcinoma patients. *Front Genet*. (2021) 12:730920. doi: 10.3389/fgene.2021.730920

frontiers | Frontiers in Molecular Biosciences

TYPE Original Research
PUBLISHED 11 April 2025
DOI 10.3389/fmolb.2025.1566293

OPEN ACCESS

EDITED BY
Matteo Becatti,
University of Firenze, Italy

REVIEWED BY
Hailin Tang,
Sun Yat-sen University Cancer Center (SYSUCC), China
Tang Tao,
Sun Yat-sen University Cancer Center (SYSUCC), China

*CORRESPONDENCE
Junjie Chen,
ntfycjj@ntu.edu.cn
Peng Ma,
5200234@ntu.edu.cn

†These authors have contributed equally to this work

RECEIVED 24 January 2025
ACCEPTED 31 March 2025
PUBLISHED 11 April 2025

CITATION
Li X, Li X, Ren Y, Wang L, Mao Z, Gao S, Ma P and Chen J (2025) HJURP modulates cell proliferation and chemoresistance via the MYC/TOP2A transcriptional axis in gastric cancer.
Front. Mol. Biosci. 12:1566293.
doi: 10.3389/fmolb.2025.1566293

HJURP modulates cell proliferation and chemoresistance via the MYC/TOP2A transcriptional axis in gastric cancer

Xu Li[1,2†], Xiwen Li[3†], Yanlin Ren[4†], Ling Wang[5], Zehao Mao[2], Shikun Gao[1,2], Peng Ma[1*] and Junjie Chen[2,6*]

[1]Department of Gastrointestinal Surgery, Affiliated Hospital of Nantong University, Medical School of Nantong University, Nantong, China, [2]Clinical Medical Research Center, Affiliated Hospital of Nantong University, Nantong, China, [3]Department of Central Laboratory, Kunshan Hospital of Chinese Medicine, Affiliated Hospital of Yangzhou University, Kunshan, China, [4]Department of Labor Hygiene and Occupational Disease Prevention and Control, Nantong Center for Disease Control and Prevention, Nantong, China, [5]Department of Hematology, Affiliated Hospital 2 of Nantong University, Nantong, China, [6]Nantong Key Laboratory of Gastrointestinal Oncology, Affiliated Hospital of Nantong University, Nantong, China

Background: The histone chaperone Holliday Junction Recognition Protein (HJURP) has been associated with multiple types of cancers, but its role in GC is not yet fully understood. Considering its functions in centromere stability and DNA repair, investigating HJURP's role in GC may offer novel therapeutic perspectives.

Methods: HJURP expression was examined in a dataset comprising TCGA-STAD samples and an internal group of GC patients, utilizing RNA sequencing and Western blot techniques. Functional experiments were carried out on the AGS and HGC-27 GC cell lines. The expression levels of HJURP, MYC, and Topoisomerase II alpha (TOP2A) were assessed via quantitative real-time PCR and Western blot. Proliferation rates of the cells were determined through EdU, CCK-8, and colony formation assays.

Results: Compared to adjacent normal tissues, HJURP expression was notably increased in GC tissues, a finding consistent across both the TCGA-STAD database and our internal patient group. Silencing HJURP markedly reduced GC cell growth and chemoresistance. Mechanistically, HJURP enhanced MYC stability, which in turn promoted TOP2A transcription. Rescue experiments confirmed that overexpression of TOP2A alters proliferation and chemoresistance of GC cells with HJURP knockdown, indicating the dependency of this axis on MYC activity.

Conclusion: Our study demonstrates that HJURP is critical for promoting GC proliferation and chemoresistance through the regulation of the MYC/TOP2A transcriptional network. Targeting HJURP might offer a novel therapeutic avenue for GC, necessitating further exploration of its clinical potential. This work

underscores the value of investigating histone chaperones as potential targets in cancer treatment.

KEYWORDS

gastric cancer, HJURP, MYC/TOP2A, proliferation, chemoresistance

1 Introduction

Gastric cancer (GC) is a particularly aggressive and deadly cancer that is difficult to detect early due to its vague symptoms, frequently leading to diagnosis at advanced stages and a 5-year survival rate of less than 20% (Chen et al., 2020; Siegel et al., 2024). The dietary habits, *Helicobacter pylori* infection and environmental factors contribute significantly to the incidence rates (Machlowska et al., 2020; Ou et al., 2024a). Despite advancements in surgical techniques, chemotherapy, and targeted therapies, the prognosis remains grim, particularly when the disease is not caught early. Furthermore, both inherent and acquired resistance to therapy are significant barriers to successful treatment (Lu and Zhang, 2022; He et al., 2024). Hence, there is an urgent requirement to develop innovative strategies and identify more effective early diagnostic markers to enhance the prognosis for GC patients.

The Holliday Junction Recognition Protein (HJURP, also referred to as hFLEG1) is a key centromeric protein involved in the incorporation and maintenance of the histone H3-like variant CENP-A at centromeres (Serafim et al., 2024). Across multiple carcinomas, HJURP has exhibited upregulation and a strong correlation with patient survival outcomes (Li et al., 2023; Jia et al., 2024). It has been identified as a prognostic biomarker and potential therapeutic target in cancers such as oral cancer (Tsevegjav et al., 2022) and clear cell renal cell carcinoma (Zhang F. et al., 2021). NFE2L1 mitigates ferroptosis by transcriptionally regulating HJURP, playing a role in the development of oral squamous cell carcinoma (Zhang et al., 2023). In ovarian cancer, HJURP inhibits cell proliferation by influencing CENP-A/CENP-N interactions (Zhang et al., 2022), while in prostate cancer, it enhances cell proliferation by increasing CDKN1A degradation through the GSK3β/JNK signaling pathway (Lai et al., 2021). A comprehensive analysis in hepatocellular carcinoma revealed that ASF1A and HJURP serve as a two-gene prognostic model due to their involvement in H3-H4 histone chaperone functions (Liu Y. et al., 2024). HJURP appears to play a crucial role in modulating chemoradiotherapy resistance in GC. In triple-negative breast cancer, it regulates chemoresistance via the YAP1/NDRG1 transcriptional axis (Mao et al., 2022). Moreover, HJURP aids in DNA repair by facilitating chromatin reorganization at double-strand break sites in astrocytoma (Serafim et al., 2024). Reducing HJURP levels disrupts clonogenic capacity and increases radiation-induced cell death in glioblastoma cells (Serafim et al., 2020). However, the expression patterns, functional roles, and prognostic implications of HJURP in GC remain largely unknown and warrant further investigation.

Topoisomerase II alpha (TOP2A), an enzyme critical for DNA replication and cell division, has attracted considerable attention in cancer research due to its pivotal role in tumor development and its potential as a therapeutic target (Uuskula-Reimand and Wilson, 2022; Liu et al., 2023; Zhang J. et al., 2025; Zou et al., 2025). This nuclear enzyme plays key roles in processes like chromosome condensation, chromatid segregation, and relieving torsional stress during DNA transcription and replication (Zhang et al., 2020). TOP2A facilitates these processes by temporarily breaking and rejoining double-stranded DNA, enabling the strands to pass through one another and modifying DNA topology. Two forms of this enzyme are believed to have arisen from a gene duplication event. The gene for the alpha form is situated on chromosome 17, whereas the gene for the beta form resides on chromosome 3. Research indicates that aberrant expression or amplification of TOP2A is common in various malignancies, including breast, lung, and GC, correlating with poor prognosis and resistance to chemotherapy (Li et al., 2022; Lee et al., 2023). Current studies are focused on elucidating the mechanisms underlying TOP2A's involvement in tumor progression and the development of resistance to treatment. Moreover, there is a growing interest in integrating TOP2A expression analysis into personalized medicine strategies, aiming to predict response to anthracycline-based chemotherapy, a treatment modality that targets TOP2A. Advances in genomics have facilitated the identification of co-amplified genes within the TOP2A amplicon, providing insights into potential synergistic targets for combinatorial therapy approaches (Mehraj et al., 2022). Despite these advances, challenges remain in translating these findings into clinical practice, necessitating further investigation into the complex interplay between TOP2A status and cancer biology.

This investigation found that HJURP is overexpressed in clinical samples of GC, with higher HJURP levels positively linked to cell cycle activity and DNA repair processes in GC. Knockdown of HJURP substantially suppressed cell growth and decreased chemoresistance in GC cells. The study also provided evidence that HJURP facilitates TOP2A transcription by improving MYC stability. Collectively, these findings suggest that HJURP may represent a potential therapeutic target for GC.

2 Material and methods

2.1 Patients and tissue samples

During the period from January to December 2023, six pairs of fresh GC tissues along with their matched adjacent normal tissues were collected from the Department of Gastrointestinal Surgery at the Affiliated Hospital of Nantong University. The tissues were stored in RNA later (ThermoFisher, catalog number AM7021). The main inclusion criteria were as follows:

1. Patients diagnosed with GC based on histopathological evaluation.

2. Patients without any concurrent malignant tumors or severe diseases affecting other organs.
3. Patients who had not received chemotherapy, radiotherapy, or immunotherapy prior to surgical intervention.
4. Patients with comprehensive clinical records.

Follow-up assessments were conducted both at the outpatient department and via telephone calls. The study was approved by the Human Research Ethics Committee of the Affiliated Hospital of Nantong University, and each participant provided signed informed consent (2023-K076-01).

2.2 Cell culture

The GC cell lines SNU-216 and MKN-45 were acquired from BeNa Culture Collection in Beijing, China. The AGS and HGC-27 GC cell lines were obtained from the National Collection of Authenticated Cell Cultures in Shanghai, China. Additionally, the BGC823 was gifted from Professor Q Guo, China Pharmaceutical University. All these cell lines were maintained in RPMI-1640 medium, which was enriched with 10% fetal bovine serum and antibiotics (100 U/mL penicillin and streptomycin). The fetal bovine serum was provided by Clark (Shanghai, China), while the antibiotics were supplied by Life Technologies (Shanghai, China). Cells were incubated at 37°C with 5% CO_2.

2.3 RNA extraction and quantitative real-time PCR (qRT-PCR)

Total RNA was isolated using the RNA isolater Total RNA Extraction Reagent (Vazyme, Nanjing, product code R401-01). The extracted RNA was then reverse-transcribed into cDNA using the HiScript III RT SuperMix for qPCR (+gDNA wiper) kit (Vazyme, Nanjing, product code R23-01). Quantitative real-time PCR (qRT-PCR) was conducted with the ChamQ Universal SYBR qPCR Master Mix (Vazyme, Nanjing, product codes Q711-02/03) on an Applied Biosystems QuantStudio 5 instrument (Thermo Fisher Scientific, United States). The primer sequences utilized in this study are as follows:

HJURP forward 5′-GATTCAAAAAGCGGTGAGGTCG-3′
HJURP reverse 5′-AGTCACACGTACATCCCTTCC-3′
TOP2A forward 5′-ACCATTGCAGCCTGTAAATGA-3′
TOP2A reverse 5′-GGGCGGAGCAAAATATGTTCC-3′
GAPDH forward 5′-CTTAGCACCCCTGGCCAAG-3′
GAPDH reverse: 5′- GATGTTCTGGAGAGCCCCG-3′

2.4 Western blot analysis

Western blot analysis was performed according to previously established methods (Hu et al., 2024; Wu et al., 2017; Ou et al., 2024b; Li et al., 2017). Protein extraction was conducted using Radioimmunoprecipitation Assay (RIPA) buffer from Epizyme (Shanghai, China). The protein concentration was measured using the Omni-Rapid™ Protein Quantitation Kit (Epizyme, Shanghai, China). The following antibodies were used: GAPDH (60004-1-Ig), HJURP (15283-1-AP), and TOP2A (66541-1-Ig) from Proteintech (Wuhan, China); Phospho-H2AX (bs-3185R) from Bioss (Beijing, China); and MYC (MAB3696) from R&D Systems (MN, United States).

2.5 Cell proliferation assays

The proliferative capacity of GC cells was assessed using 5-Ethynyl-2′-deoxyuridine (EdU) incorporation, Cell Counting Kit-8 (CCK-8), and colony formation assays. These assays were conducted following previously described protocols (Zhang Y. et al., 2021). To evaluate the chemosensitivity of GC cells, colony formation assays were specifically employed. In these sensitivity detection experiments, cells were seeded into 6-well plates and allowed to adhere for 24 h. Subsequently, they were treated with cisplatin (DDP, 1 μg/mL) for 2 h. Following this treatment, the conventional complete culture medium was replaced.

2.6 Bioinformatics analysis

The gene expression data for HJURP were obtained from the corrected The Cancer Genome Atlas (TCGA) dataset, specifically the RNA-seq data provided by the PanCanAtlas (https://www.cancer.gov/tcga). These data are sourced from the EBPlusPlusAdjustPANCAN_IlluminaHiSeq_RNASeqV2.geneExp.tsv file. To standardize the expression levels across different tumor types, the data were transformed into unitless Z-Score values. This transformation was performed using the formula $(x - \mu)/\sigma$, where:

- x represents the expression value of the gene in a given sample,
- μ is the mean expression value of that gene across all samples of the same tumor type, and
- σ denotes the standard deviation of the gene's expression across all samples of the same tumor type. Z-Score values less than −3 or greater than 3 are considered outliers and are removed from the dataset. Following outlier removal, only tumors with at least three corresponding normal samples are included in the analysis. Statistical differences in expression levels between tumor and normal tissues within the digestive system tumor datasets are compared using Wilcoxon Rank Sum Tests.

Paired differential gene expression analysis: (Same data as before) Using Wilcoxon Signed Rank Tests to compare the statistic difference of the expression level between the cancer/paracancer tissues in the TCGA dataset.

Gene Expression Omnibus (GEO) Data Analysis: The analysis workflow involves systematically downloading relevant GEO datasets and converting probe-level matrices into gene-level matrices, following the guidelines provided in the respective platform files for each dataset. For genes represented by multiple probes, the expression levels are averaged to ensure accurate representation. Next, the expression data are normalized to unitless Z-Score values for each tumor sample using the formula $(x - \mu)/\sigma$, where:

- x is the gene expression value,
- μ is the mean expression value across samples of the same tumor type, and
- σ is the standard deviation of expression within the same tumor type.

To assess statistical differences in expression between tumor and normal tissues within the dataset, Wilcoxon Rank Sum Tests are employed.

Receiver Operating Characteristic (ROC) Curve Analysis: The pROC package is utilized to conduct ROC analysis, which includes calculating the total area under the curve (AUC) and the 95% confidence interval, as well as plotting a smooth ROC curve. This analysis aims to evaluate the diagnostic performance of gene expression in distinguishing between the tumor disease group and the normal group.

Analysis of subtype: Tumor samples are divided into high/low expression groups according to the median value, the proportion of each subtype in each group is calculated, and Chi-square test is used to detect significance.

Gene set Variation Analysis (GSVA): The CancerSEA database sorted out the different functional states of 14 tumor cells. The z-score algorithm was proposed by Yuan et al. (2019). The activity of a given pathway was reflected by integrating the expression of characteristic genes, using R package GSVA in z-score parameter calculated the 14 functional state gene sets and obtained the combined z-score. We use the scale function to further standardize the score as the gene set score, and calculate the Pearson correlation between the gene and each gene set score (Hanzelmann et al., 2013).

2.7 Small interfering RNA (siRNA) and overexpression vector experiments

Small interfering RNAs (siRNAs) targeting HJURP and TOP2A were obtained from Tsingke Biotech (Beijing, China). Approximately 1 × 10^5 cells per well were seeded in 6-well plates and allowed to adhere for 24 h. Following this incubation period, HJURP/TOP2A siRNAs were transfected into the cells using Polyplus jetPRIME transfection reagent (Strasbourg, France) according to the manufacturer's protocol. Cells were harvested 48 h post-transfection for RNA and protein isolation, and knockdown efficiency was evaluated. For overexpression studies, the cDNA sequences of HJURP (NM_001282962.2) and TOP2A (NM_001067.4) were cloned into the pCMV3 vector provided by Nanjing Corues Biotech (Jiangsu, China). The resulting overexpression vectors were transfected into gastric cancer (GC) cells using Polyplus jetPRIME, following the manufacturer's instructions (Ou et al., 2024b). All experiments were conducted independently in triplicate to ensure reproducibility.

2.8 Statistical analysis

During the analysis of experimental data, we initially used Excel software for preliminary processing and analysis of the obtained data. Subsequently, to more professionally illustrate trends and distributions in the data, we utilized GraphPad Prism 10.0 (GraphPad Software, Inc., San Diego, CA, United States) for graph plotting.

For comparisons among multiple groups, one-way analysis of variance (One-way ANOVA) was performed, followed by *post hoc* tests to further investigate group differences. For comparisons between two groups, Student's t-test was utilized. Specifically, when comparing the means of two independent samples, an unpaired two-tailed Student's t-test was applied. All experimental data were obtained from at least three independent replicate experiments to ensure reliability and reproducibility.

Survival outcomes were assessed using Kaplan-Meier curves, with statistical significance evaluated via the log-rank test and Cox regression analysis (Gonzalez et al., 2024). Statistical significance or P values are denoted as follows: $^{*}p < 0.05$; $^{**}p < 0.01$; $^{***}p < 0.001$; $^{****}p < 0.0001$; ns indicates no statistical significance. Error bars in figures represent the mean ± standard deviation (SD).

3 Results

3.1 Elevated expression of HJURP in GC and its association with cell cycle and DNA repair

We initially analyzed the expression levels of HJURP across a pan-cancer cohort using RNA-seq data from TCGA. Compared to adjacent normal tissues, HJURP expression was significantly upregulated in nearly all types of cancer tissues, regardless of whether the samples were paired or unpaired (Figures 1A, B). Next, we evaluated HJURP expression in GC tissues and their paired adjacent normal tissues using 11 datasets from the GEO and TCGA-STAD databases (Figure 1C). The results confirmed a significant upregulation of HJURP in GC tissues, consistent with the findings from the TCGA analysis. Further analysis using TCGA-STAD data revealed that HJURP expression showed high diagnostic accuracy for GC. ROC curve analysis indicated an AUC value of 0.892, with a 95% confidence interval ranging from 0.851 to 0.931 (Figure 1D).

According to the 'Immune Landscape of Cancer' study, which conducted a large-scale immunogenomic analysis of over 10,000 tumor samples across 33 different cancer types in TCGA, six distinct immune subtypes were identified (Thorsson et al., 2018). Our analysis of GC data indicated that the C1 subtype (wound healing) was predominant in the high HJURP expression group, while the low HJURP expression group showed a significant increase in the proportion of the C3 subtype (inflammatory) (Figure 1E). To further explore the functional implications of HJURP expression, we performed GSVA. This analysis demonstrated that in GC, HJURP expression was positively correlated with scores related to cell cycle, DNA damage, DNA repair, and cell proliferation (Figure 1F). Both the immune subtype analysis and GSVA results suggest that HJURP expression is closely associated with cellular proliferative capacity.

10.3389/fmolb.2025.1566293

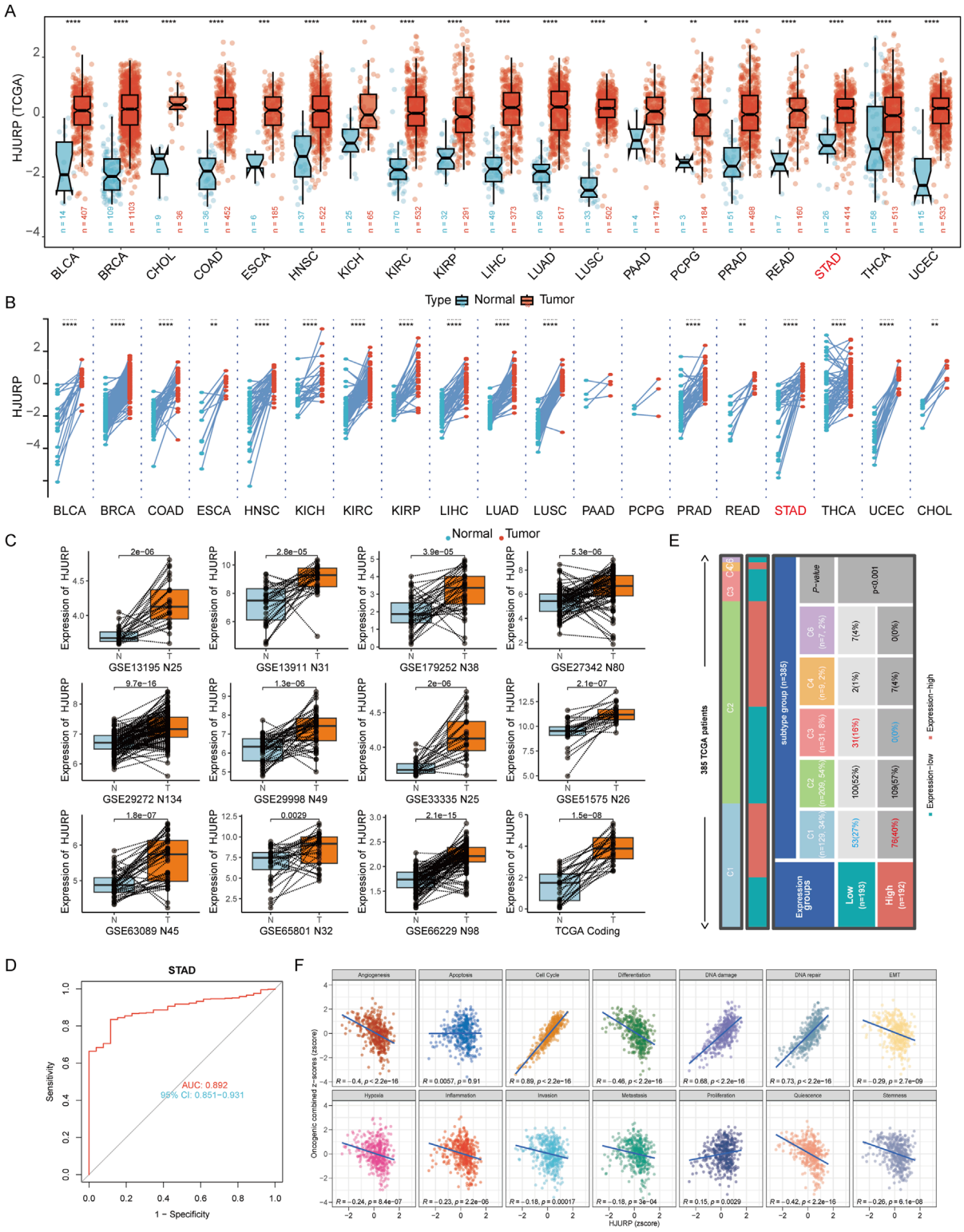

FIGURE 1
HJURP mRNA expression levels in GC. **(A, B)** Unpaired and paired analysis of HJURP mRNA expression level in normal tissues and cancers from TCGA databases. **(C)** HJURP mRNA expression level in normal and GC tissues from GEO database. **(D)** The ROC analysis of diagnostic accuracy for GC with HJURP expression in TCGA databases. **(E)** The identification of six distinct immune subtypes in GC patients. **(F)** GSVA showed the functional implications of HJURP expression in GC patients. *P < 0.05, **P < 0.01, ***P < 0.001, ****P < 0.0001. GC: gastric cancer, HJURP: Holliday Junction Recognition Protein, TCGA: The Cancer Genome Atlas, GEO: Gene Expression Omnibus, ROC: Receiver Operating Characteristic, GSVA: Gene set Variation Analysis.

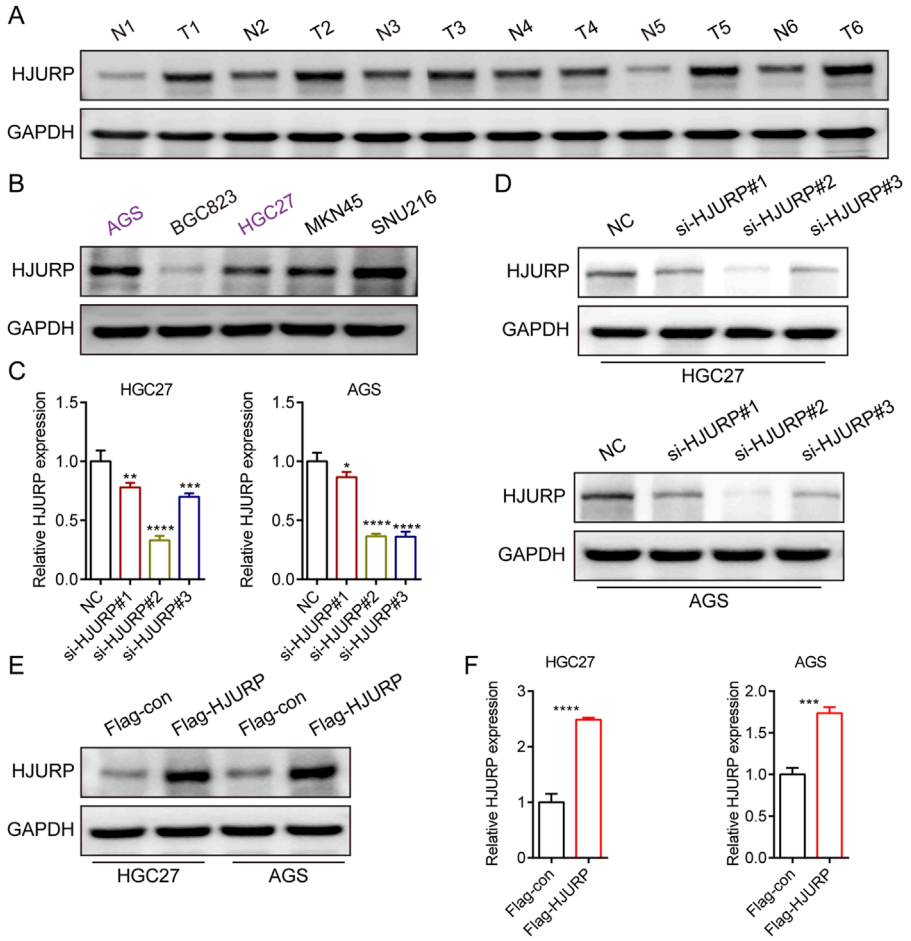

FIGURE 2
HJURP protein expression levels in GC cell lines and tissues. **(A)** Western blot showed the expression of HJURP in paired normal tissues and GC tissues. **(B)** Western blot showed the expression of HJURP in different GC cell lines. **(C, D)** HGC27 and AGS were transfected with NC siRNA or HJURP siRNA for 48 h and then cell samples were collected, and the levels of HJURP were determined by qRT-PCR and Western blot. **(E, F)** HGC27 and AGS were transfected with Flag-con or Flag-HJURP for 48 h and then cell samples were collected, and the levels of HJURP were determined by qRT-PCR and Western blot. *P < 0.05, **P < 0.01, ***P < 0.001, ****P < 0.0001. GC: gastric cancer, HJURP: Holliday Junction Recognition Protein.

3.2 Knockdown of HJURP reduces proliferation in GC cell lines

To evaluate the expression profile of HJURP in tissues, we analyzed the protein levels of HJURP in paired cancerous and adjacent non-tumor tissues from 6 GC patients. Our results revealed a significantly higher expression of HJURP in tumor tissues compared to their corresponding non-tumor tissues (Figure 2A). We screened multiple GC cell lines for HJURP expression levels and chose HGC27 and AGS cells, which displayed moderate expression levels of HJURP, for subsequent experiments (Figure 2B). Subsequently, to validate the knockdown and overexpression efficiency of si-HJURP and Flag-HJURP in these 2 GC cell lines, we performed Western blot and qRT-PCR analyses. The results indicated that among the tested siRNA sequences, si-HJURP#2 achieved the most potent silencing effect on HJURP when compared to the negative control (NC) (Figures 2C, D). Moreover, the overexpression vector Flag-HJURP was efficiently expressed in both HGC27 and AGS cells, as evidenced by increased protein and mRNA levels (Figures 2E, F).

To evaluate the role of HJURP in the growth of GC cells, we employed CCK-8 assays, colony formation assays, and EdU assays. The results demonstrated that the knockdown of HJURP using si-HJURP#2 significantly reduced the OD values in both HGC27 (Figure 3A) and AGS (Figure 3B) cell lines compared to the NC. Conversely, overexpression of HJURP using the Flag-HJURP plasmid led to a significant increase in OD values in both HGC27 (Figure 3C) and AGS (Figure 3D) cell lines compared to the Flag-con group. The EdU assay revealed a significant increase in the percentage of EdU-positive cells in both HGC27 (Figure 3E) and AGS (Figure 3F) cell lines upon HJURP overexpression. Moreover, the number of colonies formed by these cells was significantly decreased following HJURP knockdown (Figures 3G, H). These results indicated that HJURP positively regulates the proliferation of GC cells. Specifically, the reduction in HJURP expression led to decreased cell viability and proliferation, while increased HJURP

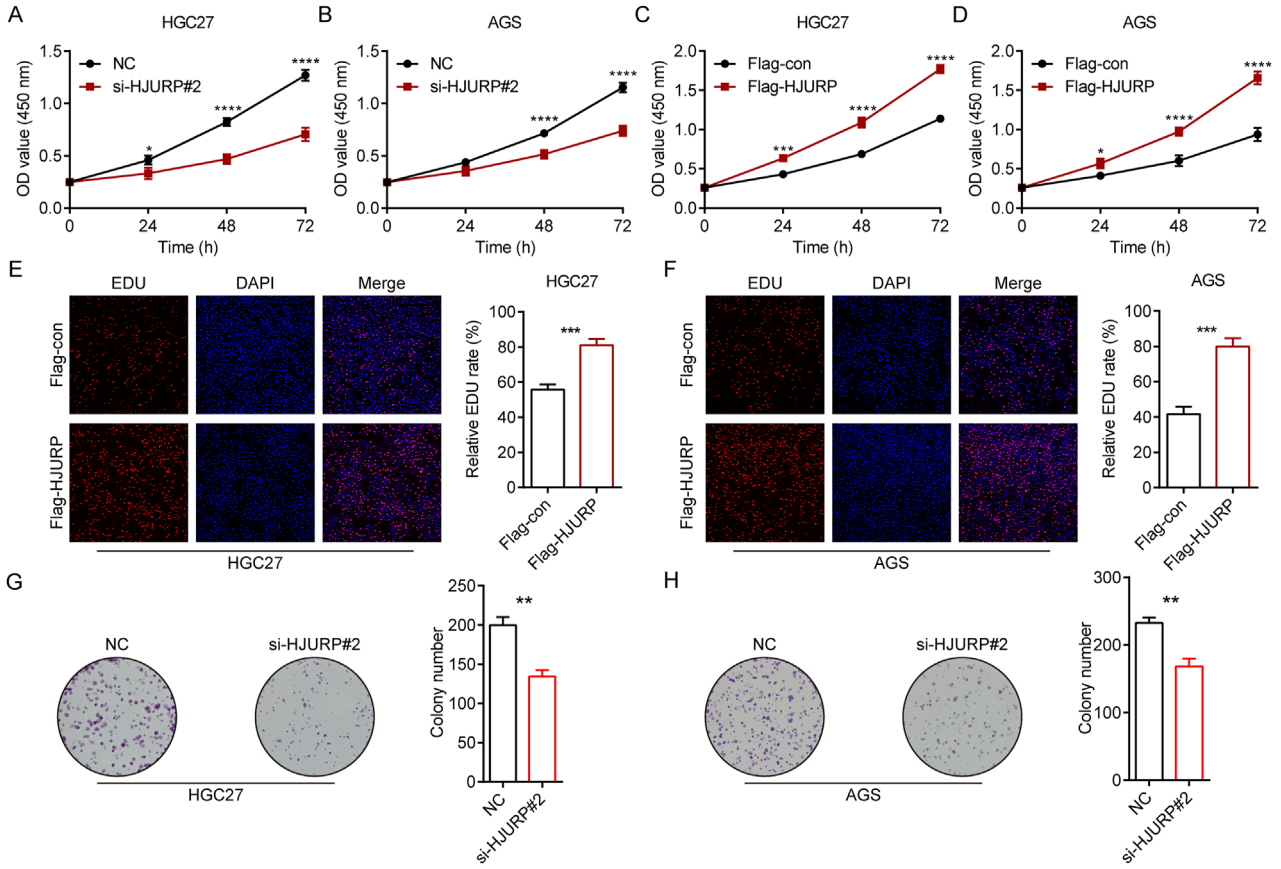

FIGURE 3
The effects of HJURP expression on the proliferation of GC cell lines. **(A)** CCK-8 assays were employed to evaluate the effect of HJURP knockdown on the proliferation of HGC27 GC cells. **(B)** CCK8 assays were employed to evaluate the effect of HJURP knockdown on the proliferation of AGS GC cells. **(C)** CCK8 assays were employed to evaluate the effect of HJURP overexpression on the proliferation of HGC27 GC cells. **(D)** CCK8 assays were employed to evaluate the effect of HJURP overexpression on the proliferation of AGS GC cells. **(E, F)** EdU assays were employed to evaluate the effect of HJURP overexpression on the proliferation of HGC27 and AGS GC cells. **(G, H)** Colony formation assays CCK8 assays were employed to evaluate the effect of HJURP knockdown on the proliferation of HGC27 and AGS GC cells. *P < 0.05, **P < 0.01, ***P < 0.001, ****P < 0.0001. GC: gastric cancer, HJURP: Holliday Junction Recognition Protein, CCK-8: Cell Counting Kit-8, EdU: 5-Ethynyl-2′-deoxyuridine.

expression enhanced these parameters, suggesting a critical role for HJURP in the growth and proliferation of GC cells.

3.3 HJURP overexpression enhances chemoresistance in GC cells

To investigate the impact of HJURP expression on GC patient survival, we analyzed data from the KM plotter database (http://www.kmplot.com/). Our findings indicated that while high versus low HJURP expression did not significantly affect overall survival (OS), it was negatively correlated with first progression survival (FP) in GC patients (Supplementary Figures S1A, B). We further stratified GC patients based on their treatment modalities into three groups: Surgery Only, Chemotherapy, and Other Adjuvant therapies. Notably, in the Chemotherapy group, higher HJURP expression was significantly associated with shorter OS and FP (Figures 4A, B, Supplementary Figures S1A, B). This observation aligns with our earlier finding that HJURP is positively correlated with DNA damage repair (Figure 1F), suggesting a potential link between HJURP expression and chemotherapeutic drug sensitivity.

To investigate the role of HJURP in chemoresistance, we conducted additional experiments. We transfected GC cells with the Flag-HJURP overexpression vector and then treated them with cisplatin (DDP). The results demonstrated that HJURP-overexpressing cells exhibited enhanced resistance to DDP compared to control cells, as evidenced by increased cell viability and reduced apoptosis rates (Figures 4C, D). Western blot results demonstrated that DDP-induced γ-H2AX protein expression, which serves as a marker for DNA damage, was markedly diminished in cells overexpressing HJURP (Figure 4E). This reduction in γ-H2AX levels implies a lower extent of DNA damage in HJURP-overexpressing cells. Collectively, these observations suggest that increased HJURP expression may contribute to chemoresistance in GC by promoting more efficient DNA damage repair. This finding underscores the significance of HJURP as a potential therapeutic target, especially in strategies aimed at enhancing chemosensitivity in GC treatment.

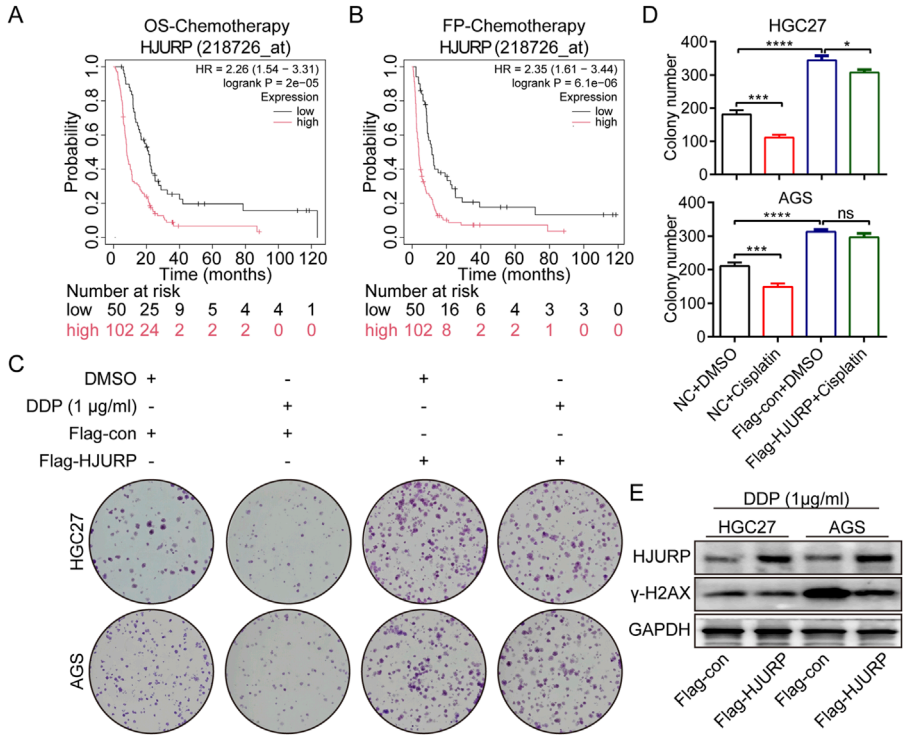

FIGURE 4
The effects of HJURP expression on the chemoresistance of GC cell lines. **(A)** The relationship between the expression of HJURP in Kaplan–Meier Plotter database and OS in GC patients. **(B)** The relationship between the expression of HJURP in Kaplan–Meier Plotter database and FP in GC patients. **(C, D)** Colony formation assays were employed to evaluate the effect of HJURP overexpression on the chemoresistance of HGC27 and AGS. **(E)** Western blot showed the γ-H2AX in HGC27 and AGS transfected with Flag-HJURP followed with DDP (1 μg/mL). *P < 0.05, ***P < 0.001, ****P < 0.0001. GC: gastric cancer, HJURP: Holliday Junction Recognition Protein, OS: overall survival, FP: first progression survival, DDP: cisplatin.

3.4 HJURP upregulates the mRNA levels of TOP2A

To reveal the complex mechanism by which HJURP induces GC cell progression, we embarked on an exploration using TCGA-STAD and GEO (GSE26253, GSE84433, GSE84437 and GSE183136) databases with sample sizes exceeding 100. Firstly, we extracted tumor samples from a specific dataset and divided them into two groups based on a cutoff value of 0.3: the top 30% of samples with the highest HJURP expression and the bottom 30% with the lowest HJURP expression. We performed differential expression analysis using the limma package. We visualized the top genes using a volcano plot or a waterfall plot (Figure 5A). Genes with an adjusted p-value <0.05 were considered significantly differentially expressed. We then identified the intersection of differentially expressed genes (DEGs) across five distinct datasets, yielding a list of 1,549 candidate genes (Figure 5B). To further understand the biological significance of these DEGs, we conducted Gene Ontology (GO) and Kyoto Encyclopedia of Genes and Genomes (KEGG) enrichment analyses. These analyses revealed significant enrichment in pathways related to chromatin stability, cell cycle regulation, and DNA damage repair (Figure 5C). Among the 1,549 DEGs, how does HJURP exert its regulatory functions? Hub genes play pivotal roles in biological processes, often acting as master regulators within pathways and serving as important therapeutic targets and research foci. Therefore, we analyzed these 1,549 genes using the STRING database to identify potential hub genes. By applying Maximal Clique Centrality (MCC) and Degree methods, our analysis identified TOP2A as a key hub gene, with significance in both methods (Figures 5D, E). Thus, we selected TOP2A for further exploration.

3.5 HJURP improves transcriptional activity of TOP2A in GC cells

Kaplan-Meier survival analysis revealed that among patients receiving chemotherapy, those with high TOP2A expression had significantly shorter overall survival (OS) and first progression (FP) times (Figures 6A, B). In GC cell lines, we conducted RT-qPCR and Western blot analyses following HJURP knockdown. The results showed a marked decrease in TOP2A mRNA and protein levels when HJURP was downregulated (Figures 6C, D). On the other hand, overexpression of HJURP led to a notable increase in TOP2A expression at both the mRNA and protein levels (Figures 6E, F). Cell rescue experiments confirmed that re-expression of TOP2A in HJURP-knockdown cells restored the diminished proliferative capacity (Figure 6G). Similarly, overexpression of HJURP in HGC27 cells markedly reduced cisplatin sensitivity, while simultaneous knockdown of TOP2A significantly enhanced cisplatin sensitivity

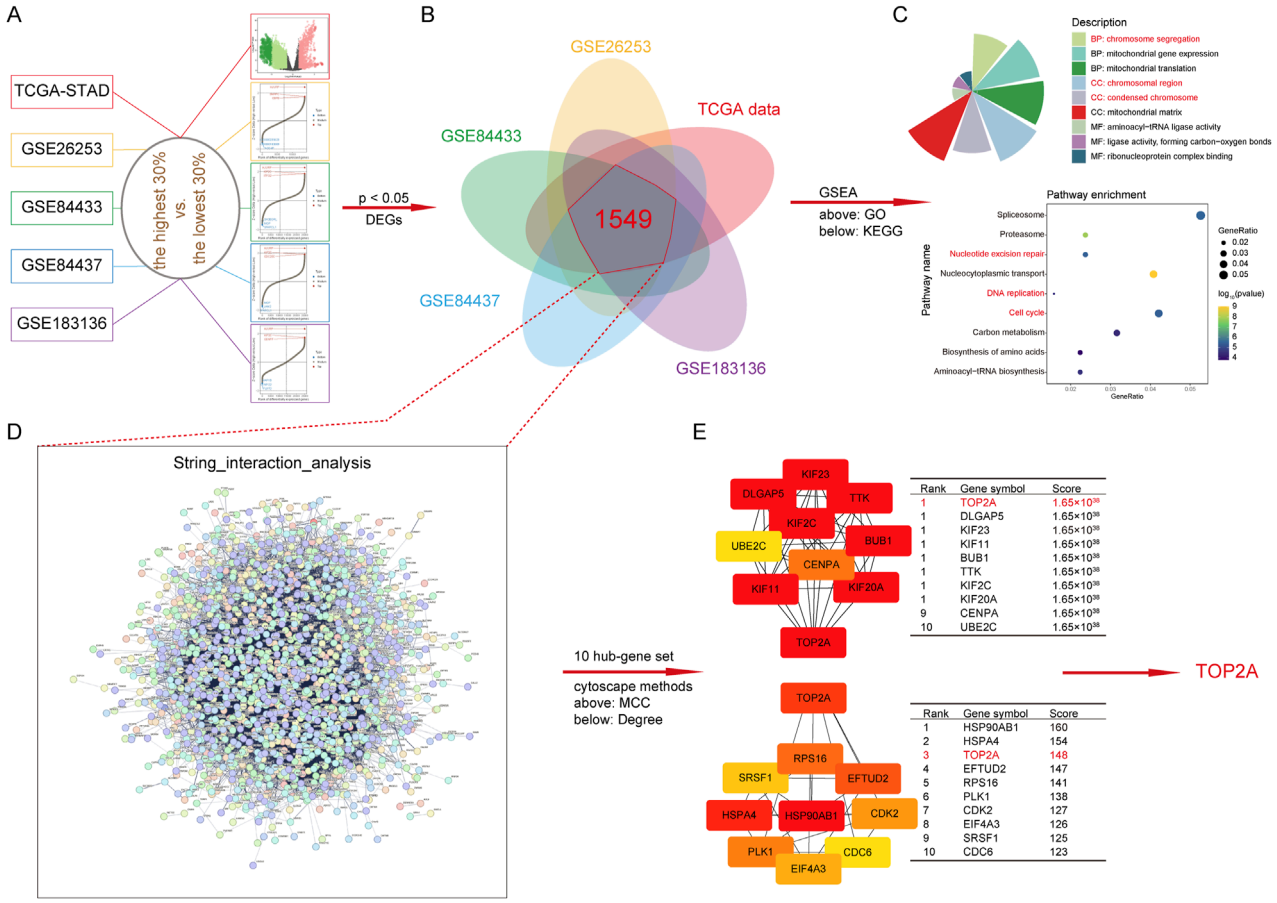

FIGURE 5
Functional enrichment analysis and downstream regulatory gene of HJURP. **(A)** Volcanic plot of HJURP differentially expressed genes (DEGs) in TCGA-STAD and GEO (GSE26253, GSE84433, GSE84437, and GSE183136) datasets. **(B)** The Venn diagram displays the intersection results of DEGs in TCGA-STAD and GEO (GSE26253, GSE84433, GSE84437, and GSE183136) datasets. **(C)** Chart of GO and Bubble plot of KEGG enrichment pathways based on DEGs. **(D)** The interaction analysis of DEGs using String dataset (cn.string-db.org/). **(E)** The determination of hub gene by Cytoscape (https://cytoscape.org/) with MCC and Degree methods. DEGs: differentially expressed genes, TCGA: The Cancer Genome Atlas, GEO: Gene Expression Omnibus, GO: Gene Ontology, KEGG: Kyoto Encyclopedia of Genes and Genomes, MCC: Maximal Clique Centrality, TOP2A: Topoisomerase II alpha.

(Figure 6H). These findings indicate that HJURP transcriptionally activates TOP2A (Figures 6C, E).

To further elucidate the transcription factors involved, bioinformatics predictions identified MYC, FLI1, MYBL2, and FOXM1 as potential regulators of TOP2A across multiple databases (Figure 7A). Given previous evidence that HJURP promotes malignant progression and mediates cisplatin sensitivity via MYC in serous ovarian cancer, we focused on MYC for further investigation (Dou et al., 2022). Consistent with prior research, altering HJURP expression in HGC27 and AGS cell lines led to notable changes in MYC protein levels, confirming the positive regulatory relationship between HJURP and MYC (Figure 6D). Further investigation demonstrated that knockdown of HJURP in AGS cells markedly reduced both mRNA and protein levels of MYC and TOP2A. Notably, overexpression of MYC via plasmid transfection exclusively restored the expression of MYC and TOP2A at transcriptional and translational levels, without affecting HJURP expression. Notably, when HJURP-targeting siRNA was co-transfected with the MYC-overexpressing plasmid, HJURP expression remained markedly suppressed, whereas the diminished expression of both MYC and TOP2A was partially rescued (Figures 7B, C). These findings strongly support a regulatory hierarchy in which HJURP modulates the transcriptional activity of MYC, thereby influencing downstream TOP2A expression. Subsequent analysis of TCGA data revealed significant positive correlations between the mRNA levels of TOP2A and HJURP, TOP2A and MYC, as well as MYC and HJURP (Figures 7D–F). Moreover, TCGA-STAD data indicated that both MYC and TOP2A were markedly upregulated in tumor tissues compared to adjacent normal tissues. These genes also showed high diagnostic accuracy for gastric cancer, as evidenced by their performance metrics (Figures 7G–J).

4 Discussion

Emerging evidence indicates that HJURP is frequently overexpressed in various types of cancer and plays a crucial oncogenic role in cancer progression (Dunleavy et al., 2009; Kato et al., 2007). Hypomethylation-driven overexpression of HJURP promotes the progression of hepatocellular carcinoma

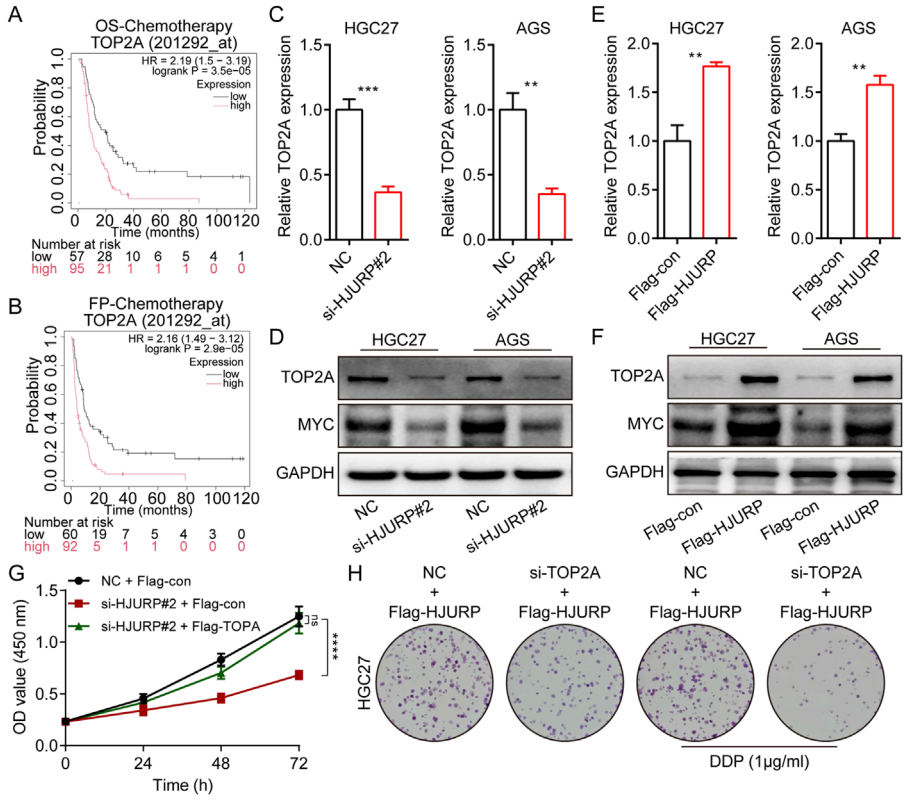

FIGURE 6
HJURP promotes proliferation and chemoresistance of GC cell by activating the TOP2A. **(A)** The relationship between the expression of TOP2A in Kaplan–Meier Plotter database and OS in GC patients. **(B)** The relationship between the expression of TOP2A in Kaplan–Meier Plotter database and FP in GC patients. **(C, D)** HGC27 and AGS were transfected with NC siRNA or HJURP siRNA for 48 h and then cell samples were collected, and the levels of TOP2A were determined by qRT-PCR and Western blot. **(E, F)** HGC27 and AGS were transfected with Flag-con or Flag-HJURP for 48 h and then cell samples were collected, and the levels of TOP2A were determined by qRT-PCR and Western blot. **(G)** CCK-8 assays were employed to evaluate the effect of HJURP knockdown with or without TOP2A overexpression on the proliferation of HGC27 GC cells. **(H)** Colony formation assays were employed to evaluate the effect of HJURP overexpression with or without TOP2A knockdown on the chemoresistance of HGC27 and AGS. **P < 0.01, ***P < 0.001, ****P < 0.0001. GC: gastric cancer, HJURP: Holliday Junction Recognition Protein, OS: overall survival, FP: first progression survival, DDP: cisplatin, TOP2A: Topoisomerase II alpha.

(HCC) and is associated with poor prognosis (Li et al., 2021). Specifically, HJURP enhances HCC proliferation by destabilizing p21 through the MAPK/ERK1/2 and AKT/GSK3β signaling pathways (Chen et al., 2018). In non-small cell lung cancer (NSCLC), knocking down HJURP inhibits cell proliferation, migration, and invasion by repressing Wnt/β-catenin signaling (Wei et al., 2019). Additionally, modulation of HJURP levels has been linked to glioblastoma cell survival (Valente et al., 2013). Despite these findings, the role of HJURP in GC remains incompletely understood. Consistent with the aforementioned studies, our research demonstrates that HJURP is upregulated in both GC cell lines and tissues, and its overexpression is associated with malignant characteristics. This suggests that HJURP may play a functional role in driving GC. Our study found that HJURP promotes GC growth and enhances chemotherapy resistance *in vitro*, providing further support for the hypothesis that HJURP is a functional driver of GC. These findings highlight the potential of HJURP as a therapeutic target and biomarker in GC treatment. Recent advances in liquid biopsies, circulating tumor DNA (ctDNA) testing, and methylation signatures have transformed cancer diagnosis and monitoring (Jahangiri, 2024; Ohyama et al., 2024; Gonzalez et al., 2024). These techniques are powerful tools for detecting genetic and epigenetic changes, and the applicability of the transcriptional regulatory networks involved in HJURP requires further investigation.

Numerous studies have provided evidence that growth and chemoradiotherapy resistance represent key processes in the development of malignant tumor (Joshi and Badgwell, 2021; Ouyang et al., 2022; Yang et al., 2024; Yu et al., 2023). Owing to the absence of typical early clinical symptoms and effective screening methods, the majority of GC patients are diagnosed at an advanced stage, resulting in poor prognoses (Smyth et al., 2020). As a result, chemoradiotherapy assumes a critical role in the management of advanced GC (Joshi and Badgwell, 2021; Leong et al., 2024; Zhang H. et al., 2025). However, primary or acquired resistance to therapy and the associated toxic side effects are major challenges that lead to treatment failure and a decline in quality of life, presenting significant hurdles during the course of treatment (Liu and Da, 2023). Previous research has established the involvement of HJURP in DNA repair and genomic stability. Recent studies have provided substantial evidence that HJURP and CENP-A play a crucial role in licensing homologous recombination (HR) during the G1 phase to repair Cas9-induced centromeric double-strand

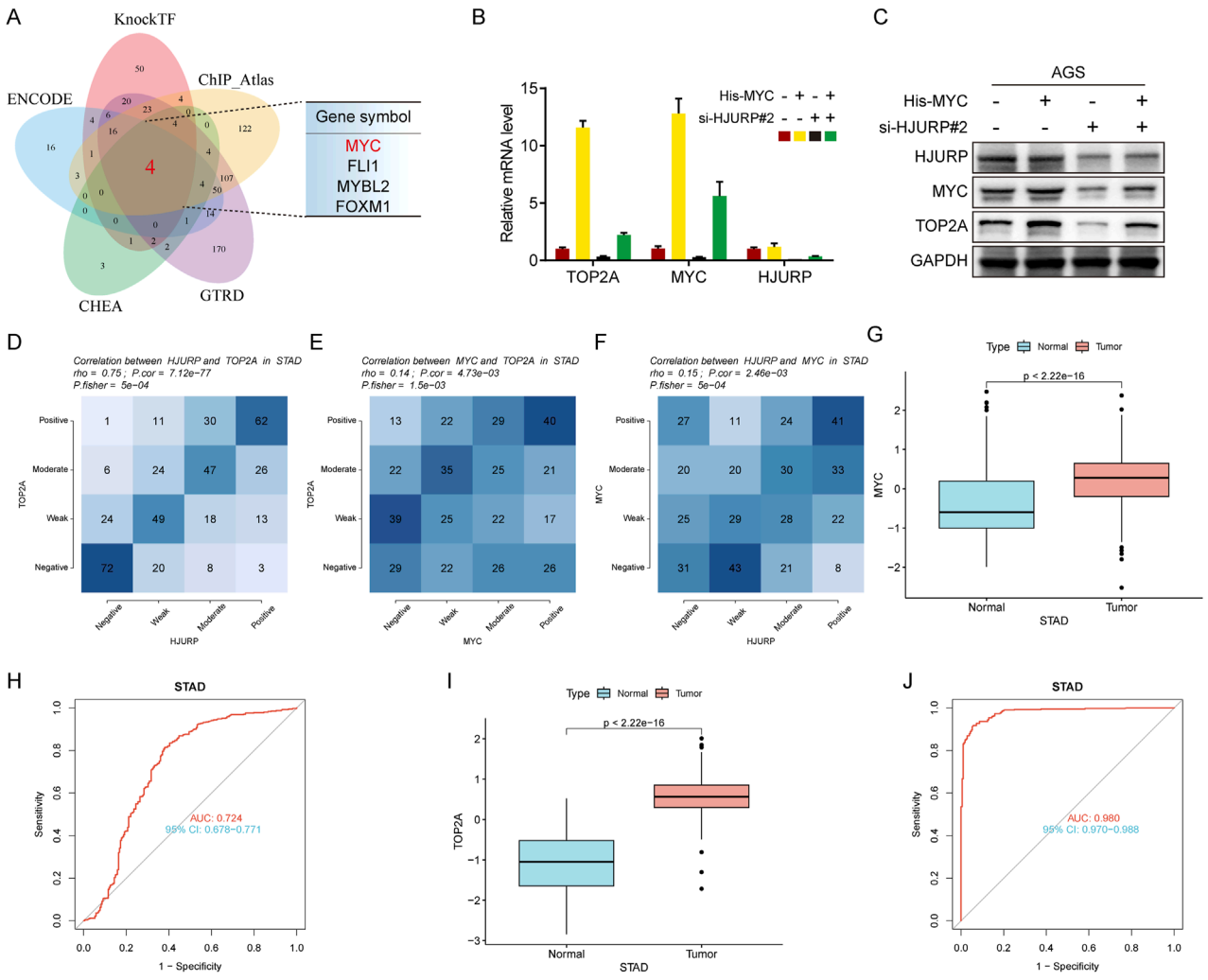

FIGURE 7
HJURP improves transcriptional activity of TOP2A via the promotion of MYC signaling. **(A)** The Venn diagram displays the potential transcription factors of TOP2A. **(B, C)** AGS were transfected with HJURP siRNA or His-MYC for 48 h and then cell samples were collected, and the levels of TOP2A, MYC and HJURP were determined by qRT-PCR and Western blot. **(D–F)** Genes are divided into 4 classes (Positive, Moderate, Weak, Negative) according to the expression level (visualized by contingency table heat map, and the depth of color represents the number of samples. The Pearson correlation of the two genes is calculated and Fisher's exact test is performed. **(G)** The difference of MYC expression in TCGA-STAD dataset. **(H)** The ROC analysis of diagnostic accuracy for GC with MYC expression in TCGA databases. **(I)** The difference of TOP2A expression in TCGA-STAD dataset. **(J)** The ROC analysis of diagnostic accuracy for GC with TOP2A expression in TCGA databases. TCGA: The Cancer Genome Atlas, HJURP: Holliday Junction Recognition Protein, TOP2A: Topoisomerase II alpha.

breaks (DSBs), even in the absence of sister chromatids (Jaramillo-Lambert et al., 2013). Misregulation of Scm3p/HJURP leads to chromosome instability in both *Saccharomyces cerevisiae* and human cells (Mishra et al., 2011). HJURP functions as a CENP-A chromatin assembly factor, sufficient to form a functional *de novo* kinetochore (Barnhart et al., 2011). The expression level of HJURP has been shown to have an independent prognostic impact and can predict sensitivity to radiotherapy in breast cancer (Hu et al., 2010). HJURP binds to CENP-A via a highly conserved N-terminal domain, facilitating its deposition at centromeres (Shuaib et al., 2010). It acts as a cell-cycle-dependent maintenance and deposition factor for CENP-A at centromeres (Dunleavy et al., 2009), mediating the centromere-specific assembly of CENP-A nucleosomes (Foltz et al., 2009). Prior studies have demonstrated that HJURP promotes tumor cell proliferation and chemoradiotherapy resistance by participating in cell cycle regulation and maintaining genomic stability. In our current study, we conducted bioinformatics analysis of TCGA and GEO datasets for gastric cancer (GC) to identify differentially expressed genes (DEGs). Among these genes, pathways related to the cell cycle and nucleotide excision repair were significantly enriched. Further analysis revealed that TOP2A is a hub gene within the regulatory network of HJURP. Mechanistically, we found that HJURP increases the transcription level of TOP2A in GC cells. The TCGA has been instrumental in identifying biomarkers and understanding the molecular landscape of cancers. Studies such as those on SCN3B in glioma (Liu H. et al., 2024), CDK2 in glioma (Liu and Weng, 2022), AIMP1 in head-neck squamous cell carcinoma (Li and Liu, 2022) and CNIH4 in head and neck

squamous cell carcinoma (Liu and Li, 2022) demonstrate the diverse applications of TCGA data in cancer research. However, TCGA studies are not without limitations. Technical and biological biases, such as those discussed in "Technical and Biological Biases in Bulk Transcriptomic Data Mining for Cancer Research" (Liu et al., 2025), can influence the reliability of findings. While TCGA provides a wealth of data for hypothesis generation, independent validation and multi-center studies are essential to address these biases and enhance the translational potential of TCGA discoveries.

TOP2A (DNA topoisomerase II alpha) is a critical enzyme that controls DNA supercoiling and is intimately involved in DNA replication, transcription, and chromatin remodeling (Nitiss, 2009; Zou et al., 2024; Lovejoy et al., 2025). Extensive research has highlighted the importance of TOP2A in cancer cell proliferation and its potential as a therapeutic target (Delgado et al., 2018). Overexpression of TOP2A is observed in multiple types of cancer, such as lung, breast, and liver cancer, and it is linked to tumor progression, chemoresistance, and resistance to radiotherapy (Sritharan and Sivalingam, 2021; Glisson and Ross, 1987; Chen et al., 2024; Jiang et al., 2024). Specifically, in the context of tumor cell proliferation, TOP2A is especially crucial during the S and G2/M phases of the cell cycle (Deng et al., 2023). During these phases, TOP2A mitigates the topological stress that occurs during DNA replication, ensuring smooth progression through the cell cycle and supporting efficient cell division. This makes it an attractive target for anticancer drugs, many of which inhibit TOP2A and induce DNA damage, leading to cell death. Research into the mechanisms of chemoresistance mediated by TOP2A has revealed that its overexpression can lead to decreased susceptibility to chemotherapeutic agents that target the enzyme (Zhu et al., 2021). For instance, in breast cancer, O-GlcNAcylation of TOP2A has been shown to enhance its catalytic activity, which in turn contributes to chemoresistance (Liu et al., 2023). This post-translational modification stabilizes the enzyme-DNA cleavage complex, reducing the effectiveness of drugs like doxorubicin. In terms of radiotherapy, TOP2A has been implicated in the development of radio-resistance in prostate cancer (Hansen et al., 2023). Moreover, TOP2A's role in non-small cell lung cancer (NSCLC) has been investigated in relation to immunotherapy and vasculogenic mimicry (Wu et al., 2023). Studies suggest that TOP2A may promote the expression of immune checkpoint molecules like PD-L1 and the formation of vasculogenic mimicry, which are associated with poor prognosis and resistance to therapy. The current landscape of research indicates that TOP2A is a multifaceted factor in tumorigenesis and treatment resistance. In agreement with this hypothesis, our research shows that HJURP overexpression boosts the transcriptional activity of TOP2A through the upregulation of MYC. This cascade of events leads to enhanced genomic stability, which facilitates GC cell proliferation and confers resistance to chemoradiotherapy.

MYC is a crucial transcription factor closely associated with various biological processes, including cell proliferation, metabolism, and apoptosis. There are reports indicating that excessive MYC induces DNA damage by increasing transcriptional stress (Vafa et al., 2002; Das et al., 2024). For instance, excessive MYC activity has been shown to trigger DNA damage responses, activating pathways such as p53, which attempts to halt cell cycle progression and initiate repair mechanisms. The activation of p53 in response to MYC-induced stress is a protective mechanism that attempts to mitigate the DNA damage caused by MYC's transcriptional activity (Das et al., 2024). However, our research results confirmed that HJURP reduces apoptosis and DNA damage and positively regulates MYC expression. Actually, studies have highlighted that MYC not only plays a significant role in tumor development but also exhibits a dual role in the induction of DNA damage. The dual effects of MYC have also been demonstrated in other types of cancer. In hepatocellular carcinoma (HCC), overexpression of MYC is closely related to cell cycle progression and apoptosis, and inhibition of MYC can significantly improve the sensitivity of HCC cells to chemotherapy (Papadopoulos et al., 2023). In addition, MYC also influences cell response to DNA damage by regulating gene expression related to DNA damage repair. Studies have found that there is a complex interaction between MYC and DNA damage repair network, which provides a new perspective for developing new cancer treatment strategies (Kaller et al., 2023). It is important to note that the relationship between MYC and DNA damage is complex and context-dependent. While previous studies have shown that excessive MYC can induce DNA damage through increased transcriptional stress, the role of MYC in our experimental system may be different due to the involvement of HJURP. HJURP might fine tune the function of MYC, and the level of MYC upregulated by HJURP may not reach the threshold that causes significant transcriptional stress and subsequent DNA damage. HJURP may interact with a series of proteins involved in DNA repair pathways (Serafim et al., 2024; Kato et al., 2007; Sousa et al., 2019). This interaction may enhance the cell's ability to repair DNA damage, even in the presence of increased MYC expression. The cells in our study may have a more efficient DNA repair mechanism, which can counteract the potential DNA - damaging effects of MYC. In conclusion, the dual role of MYC in DNA damage induction provides a new perspective for understanding the genesis and progression of tumors. MYC is not only a proto-oncogene that promotes cell proliferation, but also a key factor in maintaining genome stability. Future studies are needed to further explore the mechanisms of action of MYC in different cancer types in order to provide new targets and strategies for cancer treatment.

Collectively, our study revealed that HJURP strengthens TOP2A mRNA expression through enhancing the transcriptional activation ability of MYC. HJURP-MYC-TOP2A axis induces GC proliferation and chemoresistance. Therefore, the HJURP-MYC-TOP2A axis could serve as a potential target for the therapeutic of GC.

Data availability statement

The original contributions presented in the study are included in the article/Supplementary Material, further inquiries can be directed to the corresponding authors.

Ethics statement

The study was approved by the Human Research Ethics Committee of the Affiliated Hospital of Nantong University and each participant provided signed informed consent.

Author contributions

XuL: Data curation, Software, Validation, Writing – original draft. XiL: Methodology, Project administration, Software, Writing – original draft. YR: Data curation, Project administration, Visualization, Writing – original draft. LW: Funding acquisition, Resources, Writing – original draft. ZM: Data curation, Methodology, Validation, Writing – original draft. SG: Validation, Writing – review and editing. PM: Conceptualization, Methodology, Project administration, Writing – review and editing. JC: Conceptualization, Funding acquisition, Investigation, Supervision, Writing – review and editing.

Funding

The author(s) declare that financial support was received for the research and/or publication of this article. This work was supported by grants from the National Natural Science Foundation of China (No. 82203096), China Postdoctoral Science Foundation (No. 2022M711717), Nantong University clinical medicine special research fund (NTUB2023B77) and grants from Jiangsu Provincial Research Hospital (YJXYY202204-YSB27).

Conflict of interest

The authors declare that the research was conducted in the absence of any commercial or financial relationships that could be construed as a potential conflict of interest.

Generative AI statement

The authors declare that no Generative AI was used in the creation of this manuscript.

Publisher's note

Supplementary material

The Supplementary Material for this article can be found online at: https://www.frontiersin.org/articles/10.3389/fmolb.2025.1566293/full#supplementary-material

SUPPLEMENTARY FIGURE S1
The relationship between HJURP and the prognosis of STAD. **(A)** The relationship between the expression of HJURP in Kaplan–Meier Plotter database and OS in GC patients. **(B)** The relationship between the expression of HJURP in Kaplan–Meier Plotter database and FP in GC patients.

References

Barnhart, M. C., Kuich, P. H., Stellfox, M. E., Ward, J. A., Bassett, E. A., Black, B. E., et al. (2011). HJURP is a CENP-A chromatin assembly factor sufficient to form a functional *de novo* kinetochore. *J. Cell Biol.* 194, 229–243. doi:10.1083/jcb.201012017

Chen, J. J., Ren, Y. L., Shu, C. J., Zhang, Y., Chen, M. J., Xu, J., et al. (2020). JP3, an antiangiogenic peptide, inhibits growth and metastasis of gastric cancer through TRIM25/SP1/MMP2 axis. *J. Exp. Clin. Cancer Res. CR* 39, 118. doi:10.1186/s13046-020-01617-8

Chen, T., Huang, H., Zhou, Y., Geng, L., Shen, T., Yin, S., et al. (2018). HJURP promotes hepatocellular carcinoma proliferation by destabilizing p21 via the MAPK/ERK1/2 and AKT/GSK3β signaling pathways. *J. Exp. Clin. Cancer Res. CR* 37, 193. doi:10.1186/s13046-018-0866-4

Chen, Z., Vallega, K. A., Wang, D., Quan, Z., Fan, S., Wang, Q., et al. (2024). DNA topoisomerase II inhibition potentiates osimertinib's therapeutic efficacy in EGFR-mutant non-small cell lung cancer models. *J. Clin. Investigation* 134, e172716. doi:10.1172/JCI172716

Das, S. K., Karmakar, S., Venkatachalapathy, H., Jha, R. K., Batchelor, E., and Levens, D. (2024). Excessive MYC-topoisome activity triggers acute DNA damage, MYC degradation, and replacement by a p53-topoisome. *Mol. Cell* 84, 4059–4078.e10. doi:10.1016/j.molcel.2024.10.006

Delgado, J. L., Hsieh, C. M., Chan, N. L., and Hiasa, H. (2018). Topoisomerases as anticancer targets. *Biochem. J.* 475, 373–398. doi:10.1042/BCJ20160583

Deng, Z., Shen, D., Yu, M., Zhou, F., Shan, D., Fang, Y., et al. (2023). Pectolinarigenin inhibits bladder urothelial carcinoma cell proliferation by regulating DNA damage/autophagy pathways. *Cell Death Discov.* 9, 214. doi:10.1038/s41420-023-01508-9

Dou, Z., Qiu, C., Zhang, X., Yao, S., Zhao, C., Wang, Z., et al. (2022). HJURP promotes malignant progression and mediates sensitivity to cisplatin and WEE1-inhibitor in serous ovarian cancer. *Int. J. Biol. Sci.* 18, 1188–1210. doi:10.7150/ijbs.65589

Dunleavy, E. M., Roche, D., Tagami, H., Lacoste, N., Ray-Gallet, D., Nakamura, Y., et al. (2009). HJURP is a cell-cycle-dependent maintenance and deposition factor of CENP-A at centromeres. *Cell* 137, 485–497. doi:10.1016/j.cell.2009.02.040

Foltz, D. R., Jansen, L. E., Bailey, A. O., Yates, J. R., 3rd, Bassett, E. A., Wood, S., et al. (2009). Centromere-specific assembly of CENP-a nucleosomes is mediated by HJURP. *Cell* 137, 472–484. doi:10.1016/j.cell.2009.02.039

Glisson, B. S., and Ross, W. E. (1987). DNA topoisomerase II: a primer on the enzyme and its unique role as a multidrug target in cancer chemotherapy. *Pharmacol. Ther.* 32, 89–106. doi:10.1016/0163-7258(87)90054-4

Gonzalez, T., Nie, Q., Chaudhary, L. N., Basel, D., and Reddi, H. V. (2024). Methylation signatures as biomarkers for non-invasive early detection of breast cancer: a systematic review of the literature. *Cancer Genet.* 282-283, 1–8. doi:10.1016/j.cancergen.2023.12.003

Hansen, A. F., Hoiem, T. S., Selnaes, K. M., Bofin, A. M., Storkersen, O., Bertilsson, H., et al. (2023). Prediction of recurrence from metabolites and expression of TOP2A and EZH2 in prostate cancer patients treated with radiotherapy. *NMR Biomed.* 36, e4694. doi:10.1002/nbm.4694

Hanzelmann, S., Castelo, R., and Guinney, J. (2013). GSVA: gene set variation analysis for microarray and RNA-seq data. *BMC Bioinforma.* 14, 7. doi:10.1186/1471-2105-14-7

He, J., Li, M., Bao, J., Peng, Y., Xue, W., Chen, J., et al. (2024). β-Elemene promotes ferroptosis and reverses radioresistance in gastric cancer by inhibiting the OTUB1-GPX4 interaction. *Front. Pharmacol.* 15, 1469180. doi:10.3389/fphar.2024.1469180

Hu, Y., Zang, W., Feng, Y., Mao, Q., Chen, J., Zhu, Y., et al. (2024). mir-605-3p prevents liver premetastatic niche formation by inhibiting angiogenesis via decreasing exosomal nos3 release in gastric cancer. *Cancer Cell Int.* 24, 184. doi:10.1186/s12935-024-03359-5

Hu, Z., Huang, G., Sadanandam, A., Gu, S., Lenburg, M. E., Pai, M., et al. (2010). The expression level of HJURP has an independent prognostic impact and predicts the sensitivity to radiotherapy in breast cancer. *Breast Cancer Res. BCR* 12, R18. doi:10.1186/bcr2487

Jahangiri, L. (2024). Updates on liquid biopsies in neuroblastoma for treatment response, relapse and recurrence assessment. *Cancer Genet.* 288-289, 32–39. doi:10.1016/j.cancergen.2024.09.001

Jaramillo-Lambert, A., Hao, J., Xiao, H., Li, Y., Han, Z., and Zhu, W. (2013). Acidic nucleoplasmic DNA-binding protein (And-1) controls chromosome congression by

regulating the assembly of centromere protein A (CENP-A) at centromeres. *J. Biol. Chem.* 288, 1480–1488. doi:10.1074/jbc.M112.429266

Jia, Y., Chen, Y., Chen, M., He, M., Xu, S., Li, H., et al. (2024). Oncogenic HJURP enhancer promotes the aggressive behavior of triple-negative breast cancer in association with p53/E2F1/FOXM1-axis. *Cancer Lett.* 611, 217423. doi:10.1016/j.canlet.2024.217423

Jiang, J., Li, X., Zhang, C., Wang, J., and Li, J. (2024). Anti-cancer effects of Coix seed extract through KCTD9-mediated ubiquitination of TOP2A in lung adenocarcinoma. *Cell Div.* 19, 6. doi:10.1186/s13008-024-00112-2

Joshi, S. S., and Badgwell, B. D. (2021). Current treatment and recent progress in gastric cancer. *CA Cancer J. Clin.* 71, 264–279. doi:10.3322/caac.21657

Kaller, M., Shi, W., and Hermeking, H. (2023). c-MYC-Induced AP4 Attenuates DREAM-Mediated Repression by p53. *Cancers* 15, 1162. doi:10.3390/cancers15041162

Kato, T., Sato, N., Hayama, S., Yamabuki, T., Ito, T., Miyamoto, M., et al. (2007). Activation of Holliday junction recognizing protein involved in the chromosomal stability and immortality of cancer cells. *Cancer Res.* 67, 8544–8553. doi:10.1158/0008-5472.CAN-07-1307

Lai, W., Zhu, W., Xiao, C., Li, X., Wang, Y., Han, Y., et al. (2021). HJURP promotes proliferation in prostate cancer cells through increasing CDKN1A degradation via the GSK3β/JNK signaling pathway. *Cell Death Dis.* 12, 583. doi:10.1038/s41419-021-03870-x

Lee, S. B., Pan, J., Xiong, D., Palen, K., Johnson, B., Lubet, R. A., et al. (2023). Striking efficacy of a vaccine targeting TOP2A for triple-negative breast cancer immunoprevention. *NPJ Precis. Oncol.* 7, 108. doi:10.1038/s41698-023-00461-1

Leong, T., Smithers, B. M., Michael, M., Haustermans, K., Wong, R., Gebski, V., et al. (2024). Preoperative chemoradiotherapy for resectable gastric cancer. *N. Engl. J. Med.* 391, 1810–1821. doi:10.1056/NEJMoa2405195

Li, L., Yuan, Q., Chu, Y. M., Jiang, H. Y., Zhao, J. H., Su, Q., et al. (2023). Advances in holliday junction recognition protein (HJURP): structure, molecular functions, and roles in cancer. *Front. Cell Dev. Biol.* 11, 1106638. doi:10.3389/fcell.2023.1106638

Li, W., Wang, R., and Wang, W. (2022). Exploring the causality and pathogenesis of systemic lupus erythematosus in breast cancer based on Mendelian randomization and transcriptome data analyses. *Front. Immunol.* 13, 1029884. doi:10.3389/fimmu.2022.1029884

Li, X., Peng, B., Zhu, X., Wang, P., Xiong, Y., Liu, H., et al. (2017). Changes in related circular RNAs following ERβ knockdown and the relationship to rBMSC osteogenesis. *Biochem. Biophysical Res. Commun.* 493, 100–107. doi:10.1016/j.bbrc.2017.09.068

Li, Y., and Liu, H. (2022). Clinical powers of aminoacyl tRNA synthetase complex interacting multifunctional protein 1 (AIMP1) for head-neck squamous cell carcinoma. *Cancer Biomarkers Sect. A Dis. markers* 34, 359–374. doi:10.3233/CBM-210340

Li, Y., Yi, Q., Liao, X., Han, C., Zheng, L., Li, H., et al. (2021). Hypomethylation-driven overexpression of HJURP promotes progression of hepatocellular carcinoma and is associated with poor prognosis. *Biochem. Biophysical Res. Commun.* 566, 67–74. doi:10.1016/j.bbrc.2021.05.102

Liu, H., and Li, Y. (2022). Potential roles of Cornichon Family AMPA Receptor Auxiliary Protein 4 (CNIH4) in head and neck squamous cell carcinoma. *Cancer Biomarkers Sect. A Dis. Markers* 35, 439–450. doi:10.3233/CBM-220143

Liu, H., Li, Y., Karsidag, M., Tu, T., and Wang, P. (2025). Technical and biological biases in Bulk transcriptomic data mining for cancer research. *J. Cancer* 16, 34–43. doi:10.7150/jca.100922

Liu, H., and Weng, J. (2022). A comprehensive bioinformatic analysis of cyclin-dependent kinase 2 (CDK2) in glioma. *Gene* 822, 146325. doi:10.1016/j.gene.2022.146325

Liu, H., Weng, J., Huang, C. L., and Jackson, A. P. (2024). Is the voltage-gated sodium channel beta3 subunit (SCN3B) a biomarker for glioma? *Funct. Integr. Genomics* 24, 162. doi:10.1007/s10142-024-01443-7

Liu, Y., and Da, M. (2023). Wilms tumor 1 associated protein promotes epithelial mesenchymal transition of gastric cancer cells by accelerating TGF-beta and enhances chemoradiotherapy resistance. *J. Cancer Res. Clin. Oncol.* 149, 3977–3988. doi:10.1007/s00432-022-04320-7

Liu, Y., Liu, S., Jing, R., Li, C., Guo, Y., Cai, Z., et al. (2024). Identification of ASF1A and HJURP by global H3-H4 histone chaperone analysis as a prognostic two-gene model in hepatocellular carcinoma. *Sci. Rep.* 14, 7666. doi:10.1038/s41598-024-58368-1

Liu, Y., Yu, K., Zhang, K., Niu, M., Chen, Q., Liu, Y., et al. (2023). O-GlcNAcylation promotes topoisomerase IIα catalytic activity in breast cancer chemoresistance. *EMBO Rep.* 24, e56458. doi:10.15252/embr.202256458

Lovejoy, C. A., Wessel, S. R., Bhowmick, R., Hatoyama, Y., Kanemaki, M. T., Zhao, R., et al. (2025). SRBD1 facilitates chromosome segregation by promoting topoisomerase IIα localization to mitotic chromosomes. *Nat. Commun.* 16, 1675. doi:10.1038/s41467-025-56911-w

Lu, Y., and Zhang, X. (2022). Radiochemotherapy-induced DNA repair promotes the biogenesis of gastric cancer stem cells. *Stem Cell Res. Ther.* 13, 481. doi:10.1186/s13287-022-03165-8

Machlowska, J., Baj, J., Sitarz, M., Maciejewski, R., and Sitarz, R. (2020). Gastric cancer: epidemiology, risk factors, classification, genomic characteristics and treatment strategies. *Int. J. Mol. Sci.* 21, 4012. doi:10.3390/ijms21114012

Mao, M., Jia, Y., Chen, Y., Yang, J., Xu, L., Zhang, X., et al. (2022). HJURP regulates cell proliferation and chemo-resistance via YAP1/NDRG1 transcriptional axis in triple-negative breast cancer. *Cell Death Dis.* 13, 396. doi:10.1038/s41419-022-04833-6

Mehraj, U., Qayoom, H., Shafi, S., Farhana, P., Asdaq, S. M. B., and Mir, M. A. (2022). Cryptolepine targets TOP2A and inhibits tumor cell proliferation in breast cancer cells - an *in vitro* and *in silico* study. *Anti-Cancer Agents Med. Chem.* 22, 3025–3037. doi:10.2174/1871520622666220419135547

Mishra, P. K., Au, W. C., Choy, J. S., Kuich, P. H., Baker, R. E., Foltz, D. R., et al. (2011). Misregulation of Scm3p/HJURP causes chromosome instability in *Saccharomyces cerevisiae* and human cells. *PLoS Genet.* 7, e1002303. doi:10.1371/journal.pgen.1002303

Nitiss, J. L. (2009). Targeting DNA topoisomerase II in cancer chemotherapy. *Nat. Rev. Cancer* 9, 338–350. doi:10.1038/nrc2607

Ohyama, H., Hirotsu, Y., Amemiya, K., Mikata, R., Amano, H., Hirose, S., et al. (2024). Development of a molecular barcode detection system for pancreaticobiliary malignancies and comparison with next-generation sequencing. *Cancer Genet.* 280-281, 6–12. doi:10.1016/j.cancergen.2023.12.002

Ou, L., Hao, Y., Liu, H., Zhu, Z., Li, Q., Chen, Q., et al. (2024b). Chebulinic acid isolated from aqueous extracts of Terminalia chebula Retz inhibits *Helicobacter pylori* infection by potential binding to Cag A protein and regulating adhesion. *Front. Microbiol.* 15, 1416794. doi:10.3389/fmicb.2024.1416794

Ou, L., Liu, H., Peng, C., Zou, Y., Jia, J., Li, H., et al. (2024a). *Helicobacter pylori* infection facilitates cell migration and potentially impact clinical outcomes in gastric cancer. *Heliyon* 10, e37046. doi:10.1016/j.heliyon.2024.e37046

Ouyang, S., Li, H., Lou, L., Huang, Q., Zhang, Z., Mo, J., et al. (2022). Inhibition of STAT3-ferroptosis negative regulatory axis suppresses tumor growth and alleviates chemoresistance in gastric cancer. *Redox Biol.* 52, 102317. doi:10.1016/j.redox.2022.102317

Papadopoulos, D., Uhl, L., Ha, S. A., and Eilers, M. (2023). Beyond gene expression: how MYC relieves transcription stress. *Trends Cancer* 9, 805–816. doi:10.1016/j.trecan.2023.06.008

Serafim, R. B., Cardoso, C., Di Cristofaro, L. F. M., Pienna Soares, C., Araujo Silva, W., Jr., Espreafico, E. M., et al. (2020). HJURP knockdown disrupts clonogenic capacity and increases radiation-induced cell death of glioblastoma cells. *Cancer Gene Ther.* 27, 319–329. doi:10.1038/s41417-019-0103-0

Serafim, R. B., Cardoso, C., Storti, C. B., da Silva, P., Qi, H., Parasuram, R., et al. (2024). HJURP is recruited to double-strand break sites and facilitates DNA repair by promoting chromatin reorganization. *Oncogene* 43, 804–820. doi:10.1038/s41388-024-02937-1

Shuaib, M., Ouararhni, K., Dimitrov, S., and Hamiche, A. (2010). HJURP binds CENP-A via a highly conserved N-terminal domain and mediates its deposition at centromeres. *Proc. Natl. Acad. Sci. U. S. A.* 107, 1349–1354. doi:10.1073/pnas.0913709107

Siegel, R. L., Giaquinto, A. N., and Jemal, A. (2024). Cancer statistics, 2024. *CA Cancer J. Clin.* 74, 12–49. doi:10.3322/caac.21820

Smyth, E. C., Nilsson, M., Grabsch, H. I., van Grieken, N. C., and Lordick, F. (2020). Gastric cancer. *Lancet* 396, 635–648. doi:10.1016/S0140-6736(20)31288-5

Sousa, J. F., Serafim, R. B., Freitas, L. M., Fontana, C. R., and Valente, V. (2019). DNA repair genes in astrocytoma tumorigenesis, progression and therapy resistance. *Genet. Mol. Biol.* 43, e20190066. doi:10.1590/1678-4685-GMB-2019-0066

Sritharan, S., and Sivalingam, N. (2021). A comprehensive review on time-tested anticancer drug doxorubicin. *Life Sci.* 278, 119527. doi:10.1016/j.lfs.2021.119527

Thorsson, V., Gibbs, D. L., Brown, S. D., Wolf, D., Bortone, D. S., Ou Yang, T. H., et al. (2018). The immune landscape of cancer. *Immunity* 48, 812–830.e14. doi:10.1016/j.immuni.2018.03.023

Tsevegjav, B., Takano, A., Zhu, M., Yoshitake, Y., Shinohara, M., and Daigo, Y. (2022). Holliday junction recognition protein as a prognostic biomarker and therapeutic target for oral cancer. *Int. J. Oncol.* 60, 26. doi:10.3892/ijo.2022.5316

Uuskula-Reimand, L., and Wilson, M. D. (2022). Untangling the roles of TOP2A and TOP2B in transcription and cancer. *Sci. Adv.* 8, eadd4920. doi:10.1126/sciadv.add4920

Vafa, O., Wade, M., Kern, S., Beeche, M., Pandita, T. K., Hampton, G. M., et al. (2002). c-Myc can induce DNA damage, increase reactive oxygen species, and mitigate p53 function: a mechanism for oncogene-induced genetic instability. *Mol. Cell* 9, 1031–1044. doi:10.1016/s1097-2765(02)00520-8

Valente, V., Serafim, R. B., de Oliveira, L. C., Adorni, F. S., Torrieri, R., Tirapelli, D. P., et al. (2013). Modulation of HJURP (Holliday Junction-Recognizing Protein) levels is correlated with glioblastoma cells survival. *PLoS one* 8, e62200. doi:10.1371/journal.pone.0062200

Wei, Y., Ouyang, G. L., Yao, W. X., Zhu, Y. J., Li, X., Huang, L. X., et al. (2019). Knockdown of HJURP inhibits non-small cell lung cancer cell proliferation, migration, and invasion by repressing Wnt/β-catenin signaling. *Eur. Rev. Med. Pharmacol. Sci.* 23, 3847–3856. doi:10.26355/eurrev_201905_17812

Wu, J., Zhang, L., Li, W., Wang, L., Jia, Q., Shi, F., et al. (2023). The role of TOP2A in immunotherapy and vasculogenic mimicry in non-small cell lung cancer and its potential mechanism. *Sci. Rep.* 13, 10906. doi:10.1038/s41598-023-38117-6

Wu, Z., Ou, L., Wang, C., Yang, L., Wang, P., Liu, H., et al. (2017). Icaritin induces MC3T3-E1 subclone14 cell differentiation through estrogen receptor-mediated ERK1/2 and p38 signaling activation. *Biomed. Pharmacother.* 94, 1–9. doi:10.1016/j.biopha.2017.07.071

Yang, C., Deng, X., Tang, Y., Tang, H., and Xia, C. (2024). Natural products reverse cisplatin resistance in the hypoxic tumor microenvironment. *Cancer Lett.* 598, 217116. doi:10.1016/j.canlet.2024.217116

Yu, Z., Tang, H., Chen, S., Xie, Y., Shi, L., Xia, S., et al. (2023). Exosomal LOC85009 inhibits docetaxel resistance in lung adenocarcinoma through regulating ATG5-induced autophagy. *Drug Resist. Updat. Rev. Comment. Antimicrob. Anticancer Chemother.* 67, 100915. doi:10.1016/j.drup.2022.100915

Yuan, H., Yan, M., Zhang, G., Liu, W., Deng, C., Liao, G., et al. (2019). CancerSEA: a cancer single-cell state atlas. *Nucleic acids Res.* 47, D900–D908. doi:10.1093/nar/gky939

Zhang, M., Liang, C., Chen, Q., Yan, H., Xu, J., Zhao, H., et al. (2020). Histone H2A phosphorylation recruits topoisomerase IIα to centromeres to safeguard genomic stability. *EMBO J.* 39, e101863. doi:10.15252/embj.2019101863

Zhang, F., Yuan, D., Song, J., Chen, W., Wang, W., Zhu, G., et al. (2021). HJURP is a prognostic biomarker for clear cell renal cell carcinoma and is linked to immune infiltration. *Int. Immunopharmacol.* 99, 107899. doi:10.1016/j.intimp.2021.107899

Zhang, Y., Chen, J., Che, Z., Shu, C., Chen, D., Ding, K., et al. (2021). JP3 enhances the toxicity of cisplatin on drug-resistant gastric cancer cells while reducing the damage to normal cells. *J. Cancer* 12, 1894–1906. doi:10.7150/jca.50306

Zhang, Y., Zhang, W., Sun, L., Yue, Y., Shen, D., Tian, B., et al. (2022). HJURP inhibits proliferation of ovarian cancer cells by regulating CENP-A/CENP-N. *Bull. Du. Cancer* 109, 1007–1016. doi:10.1016/j.bulcan.2021.12.011

Zhang, M., Wang, Z., Yang, G., Han, L., and Wang, X. (2023). NFE2L1 restrains ferroptosis by transcriptionally regulating HJURP and participates in the progress of oral squamous cell carcinoma. *J. Bioenergetics Biomembr.* 55, 467–478. doi:10.1007/s10863-023-09987-2

Zhang, J., Yang, T., Wang, K., Pan, J., Qiu, J., Zheng, S., et al. (2025). Multi-omics analysis reveals the panoramic picture of TOP2A in pan-cancer. *Sci. Rep.* 15, 6046. doi:10.1038/s41598-025-85929-9

Zhang, H., Tang, H., Tu, W., and Peng, F. (2025). Regulatory role of non-coding RNAs in 5-Fluorouracil resistance in gastrointestinal cancers. *Cancer Drug Resist.* 8, 4. doi:10.20517/cdr.2024.167

Zhu, C., Zhang, L., Zhao, S., Dai, W., Xu, Y., Zhang, Y., et al. (2021). UPF1 promotes chemoresistance to oxaliplatin through regulation of TOP2A activity and maintenance of stemness in colorectal cancer. *Cell Death and Dis.* 12, 519. doi:10.1038/s41419-021-03798-2

Zou, J., Geng, R., Zhang, Z., Ji, X., Yin, Z., Wang, D., et al. (2025). Novel role of the SOX4/CSNK2A1 axis in regulating TOP2A phosphorylation in breast cancer progression. *FASEB J.* 39, e70315. doi:10.1096/fj.202401907RR

Zou, Y., Xu, L., Wang, W., Zhu, X., Lin, J., Li, H., et al. (2024). Muscone restores anoikis sensitivity in TMZ-resistant glioblastoma cells by suppressing TOP2A via the EGFR/Integrin β1/FAK signaling pathway. *Phytomedicine Int. J. phytotherapy Phytopharm.* 129, 155714. doi:10.1016/j.phymed.2024.155714

frontiers | Frontiers in Immunology

TYPE Original Research
PUBLISHED 11 April 2025
DOI 10.3389/fimmu.2025.1455095

OPEN ACCESS

EDITED BY
Matteo Becatti,
University of Firenze, Italy

REVIEWED BY
Eswari Dodagatta-Marri,
University of California, San Francisco, United States
Rongqiang Liu,
Renmin Hospital of Wuhan University, China
Giuseppe Bronte,
University of Ferrara, Italy

*CORRESPONDENCE
Liping Dai
lpdai@zzu.edu.cn
Jingjing Liu
jingliu@zzu.edu.cn

RECEIVED 26 June 2024
ACCEPTED 24 March 2025
PUBLISHED 11 April 2025

CITATION
Cao X, Li J, Liu S, Liu A, Zhang L, Chen F, Li Y, Ma H, Sun W, Ouyang S, Dai L and Liu J (2025) Plasma IgG and IgM autoantibodies to COPT1 as potential biomarkers for detection of non-small cell lung cancer.
Front. Immunol. 16:1455095.
doi: 10.3389/fimmu.2025.1455095

Plasma IgG and IgM autoantibodies to COPT1 as potential biomarkers for detection of non-small cell lung cancer

Xiaobin Cao[1,2], Jing Li[1], Siyu Liu[1,2], Aichen Liu[1], Lulu Zhang[1], Fengqi Chen[1], Yutong Li[1,2], Hanke Ma[1], Wenke Sun[1], Songyun Ouyang[3], Liping Dai[1]* and Jingjing Liu[1]*

[1]Henan Institute of Medical and Pharmaceutical Sciences & Henan Key Medical Laboratory of Tumor Molecular Biomarkers, Zhengzhou University, Zhengzhou, China, [2]Beijing Genomics Institution (BGI) College, Zhengzhou University, Zhengzhou, China, [3]Department of Respiratory and Sleep Medicine in the First Affiliated hospital, Zhengzhou University, Zhengzhou, China

Background: Early diagnosis of lung cancer is crucial for improving patient outcomes. Autoantibodies against tumor-associated antigens (TAAs) found in the plasma can serve as biomarkers for lung cancer detection. Copper transporter 1 (COPT1) is abnormally expressed in several cancers including lung cancer. The purpose of this study is to explore the significance of anti-COPT1 autoantibodies in the clinical diagnosis of non-small cell lung cancer (NSCLC).

Methods: The expression level of COPT1 in NSCLC and normal tissues was analyzed based on TCGA and the Human Protein Atlas (HPA) database. Through enzyme-linked immunosorbent assay (ELISA), the expression levels of anti-COPT1 autoantibodies in plasma samples from normal controls (NC), patients with benign pulmonary nodules (BPN), and patients with NSCLC were detected in the discovery (89 NC and 89 NSCLC) and verification (321 NC, 321 BPN and 321 NSCLC) groups. The ELISA results were verified by western blotting and indirect immunofluorescence experiments.

Results: Based on HPA and TCGA databases, the mRNA and protein levels of COPT1 were higher in NSCLC tissues than in normal tissues. The levels of anti-COPT1-IgG and anti-COPT1-IgM autoantibodies were significantly higher in patients with NSCLC ($P<0.05$). Anti-COPT1-IgG and anti-COPT1-IgM could discriminate NSCLC from NC with area under the curve (AUC) values of 0.733 (95% CI: 0.694-0.771) and 0.679 (95% CI: 0.638-0.720), respectively. Additionally, the combination of anti-COPT1-IgG, anti-COPT1-IgM, and carcinoembryonic antigen (CEA) could enhance the efficacy of NSCLC diagnosis from BPN with increased AUC values.

Conclusions: Our study indicated the potential significance of anti-COPT1-IgG and anti-COPT1-IgM autoantibodies as novel biomarkers for the detection of NSCLC. Furthermore, the combination of anti-COPT1-IgG and anti-COPT1-IgM improved the diagnostic value.

KEYWORDS

COPT1, autoantibody, non-small cell lung cancer, biomarkers, IgG, IgM

Introduction

In 2020, lung cancer was projected to account for 2.2 million new cases and 1.8 million deaths, making it the second most common cancer and the leading cause of cancer-related deaths (1). Approximately 85% of lung cancers are non-small cell lung cancer (NSCLC), including lung adenocarcinoma (LUAD) and lung squamous cell carcinoma (LUSC) (2). NSCLC is frequently diagnosed at an advanced stage, with a 5-year survival rate of 14%. Compared to the 5-year survival rate of 83% in patients with stage I NSCLC, early detection plays a crucial role in mitigating the high mortality rate associated with this lethal illness (3).

The early diagnosis of lung cancer is crucial for improving patient outcomes. Bronchoscopy and biopsies are the primary methods used to diagnose lung cancer. Despite being a minimally invasive technique, bronchoscopy may cause discomfort, especially when biopsy samples are obtained from suspected tissues, which can lead to complications. Therefore, monitoring the early development of lung cancer is essential to facilitate timely intervention and enhance the overall prognosis of the disease (4). Prior research has verified that autoantibodies against tumor-associated antigens (TAAs) found in the serum of cancer patients can serve as reliable cancer biomarkers (5, 6).

Autoantibodies are produced early in cancer development as a result of the humoral immune response, which is activated by abnormal expression of TAAs. Tumor-associated autoantibodies are promising candidates for the early detection and treatment of cancer. An increasing number of autoantibodies targeting TAAs have been identified, and their detection has been utilized in research and clinical analysis (7–9). The presence of autoantibodies in cancer patients reflects their increased immune reactivity and enhanced immune surveillance of cancer cells (10). In recent decades, the presence of circulating autoantibodies in the serum of cancer patients has opened up new possibilities for utilizing the immune system as a valuable source of cancer biomarkers (11). Several autoantibodies have been identified in lung cancer and are suggested as potential serum diagnostic markers (12). Among them, p53 autoantibodies in lung cancer have been widely studied, and their prevalence rate accounts for approximately 30% of all lung cancer patients (13). Relevant studies have shown that the production of autoantibodies precedes the appearance of symptoms and the diagnosis of NSCLC (14). Therefore, the detection and characterization of autoantibodies are likely to provide new insights into the complex biology of the humoral response in lung cancer and will have an important impact on the clinical management of lung cancer patients in the future.

Copper (Cu) transporter 1 (COPT1), a member of solute carrier family 31 (SLC31A1), is considered the key component of Cu absorption by mammalian cells and tissues (15). *COPT1* has recently been identified as a regulatory gene for copper, and high expression levels of COPT1 can lead to a types of cell death known as cuproptosis (16). The function of COPT1 in tumor progression has also been investigated. Blocking the COPT1-copper axis diminishes AKT signaling and reduces tumorigenesis (17). The COPT1-MEK-DNMT1-miR-124 feedback loop promotes pancreatic cancer progression (18). Moreover, COPT1 enhances chemoresistance by constraining CPT1A-mediated fatty acid oxidation process in ER-positive breast cancer (19). Expression levels of COPT1 have been shown to be elevated in breast invasive carcinoma, esophageal carcinoma, glioblastoma multiforme, and gastric adenocarcinoma compared with those in normal tissues (20). Li et al. found that COPT1 may be a promising biomarker for diagnosis and prognosis and a predictor of drug response in breast cancer (21). COPT1 has been identified as a TAA overexpressed in NSCLC patients, suggesting its potential as a biomarker for clinical diagnosis (20). TAAs exhibit significant limitations as biomarkers, including low expression in plasma and short circulation time. In contrast, autoantibodies against TAAs have the advantages of high stability, specificity and sensitivity. However, no relevant studies have investigated whether there is an autoantibody response to COPT1 in patients with NSCLC. The value of anti-COPT1 autoantibodies for in the detection of NSCLC has not yet been investigated.

In this study, we aimed to explore the expression levels of anti-COPT1 autoantibodies in the plasma of NSCLC patients, and their potential as biomarkers for the clinical diagnosis of NSCLC.

Materials and methods

Study design

The study design is illustrated in Figure 1. The plasma samples were divided into discovery and verification groups. First, the

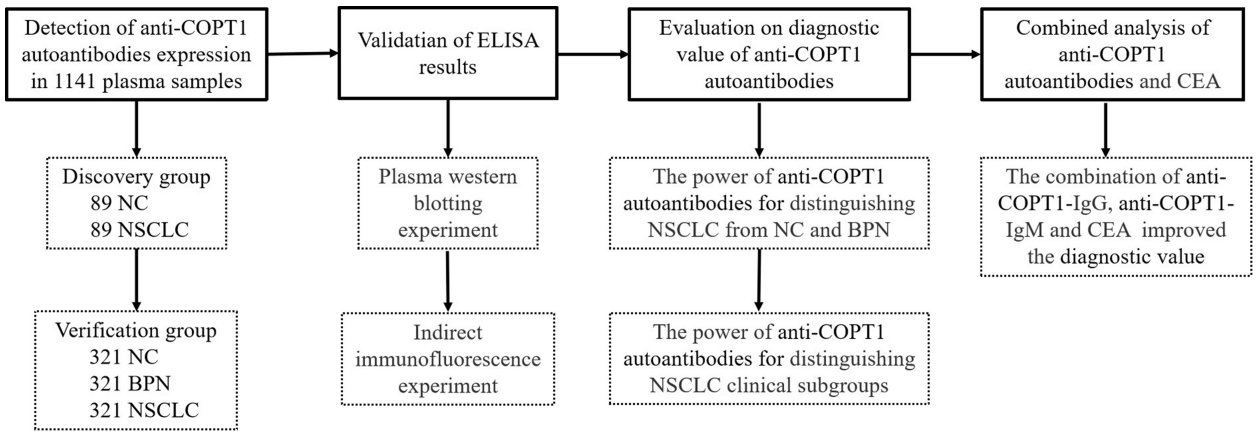

FIGURE 1
The overall study design. NSCLC, Non-small Cell Lung Cancer; NC, Normal Control; BPN, Benign Pulmonary Nodule; ELISA, Enzyme-linked Immunosorbent assay.

expression levels of anti-COPT1 autoantibodies were detected in both the discovery and verification groups using enzyme-linked immunosorbent assay (ELISA). Subsequently, western blotting and indirect immunofluorescence were performed to verify the experimental results of ELISA. Then, the diagnostic efficacy of anti-COPT1 autoantibodies in distinguishing NSCLC was analyzed. Finally, we evaluated the potential of anti-COPT1 autoantibodies in combination with carcinoembryonic antigen (CEA) as biomarkers for NSCLC detection.

Eligibility criteria

The samples were collected at the First Affiliated Hospital of Zhengzhou University (Zhengzhou, China). The sample cohort consisted of patients with NSCLC, patients with benign pulmonary nodules (BPN) and normal control controls (NC). There were 89 NSCLC and 89 NC in the discovery group, and 321 NSCLC, 321 BPN and 321 NC in the verification group. Among 321 NSCLC in the verification group, there were 174 early NSCLC and 89 advanced NSCLC. All patients involved in this study strictly complied with the diagnostic standards. NC individuals without any history of disease or tumors underwent physical examinations in the same hospital. The NSCLC, BPN and NC individuals were matched in a 1:1:1 ratio according to sex and age (± 5 years). This study was approved by the Ethics Committee of the First Affiliated Hospital of Zhengzhou University, and informed consent was obtained from all participants.

Sample collection

Blood samples were obtained using 5 ml vacuum blood collection tubes containing EDTA-K2 anticoagulant. Venous blood obtained from the elbow on an empty stomach was mixed with an anticoagulant by inverting the blood collection tube 5-8 times. Subsequently, the plasma was separated by centrifugation at 3000 r/min at 37°C for 5 min. The upper plasma was carefully extracted using a disposable straw and transferred to a 1.5 ml tube. Detailed information regarding sample numbers, clinical characteristics, and CEA expression level was noted before promptly storing the plasma samples in an ultra-low temperature freezer at -80°C. To prevent damage, the required samples were thawed in the refrigerator at 4°C prior to use, mitigating the need for repetitive freezing and thawing of the original tube.

Enzyme-linked immunosorbent assay

In this study, the expression of anti-COPT1 autoantibodies in the plasma with ELISA was detected using the recombinant COPT1 protein purchased from Cloud-Clone Corp (No.3AA85A2E08, Wuhan, China). The specific experimental procedure involved the coating of the recombinant COPT1 at a concentration of 0.125 μg/ml on a 96-well ELISA plate, followed by 1% BSA coating. After coating overnight, the plates were sealed at 37°C for 2 hours with 2% BSA solution. The blocking solution was discarded and the primary antibody was incubated at 37°C for 1 h. Finally, the secondary antibody was incubated at 37°C for 1 h. Plasma samples were diluted at a ratio of 1:100 to serve as the primary antibody. Goat anti-human IgG or IgM antibody labeled with horseradish peroxidase (HRP) was used as the secondary antibody. Anti-human IgG antibody was diluted at a ratio of 1:10000 and anti-human IgM antibody at a ratio of 1:5000. Each plate was equipped with two duplicate wells for quality control purposes and two blank controls to ensure consistency and precision of the optical density (OD) values obtained from all wells. Specific Binding Index (SBI) = (OD value of sample to be tested-OD value of blank hole)/(OD value of quality control sample-OD value of blank hole). The blood samples of 100 normal controls were fully and equally mixed for quality control which is used to eliminate the errors between enzyme-labeled plates and represent the general level of the population.

Western blotting

Western blotting was performed to confirm the expression of anti-COPT1 autoantibodies in plasma. The recombinant COPT1 protein was loaded onto a 10% SDS-PAGE gel at a total loading amount of 3 μg. Subsequently, the proteins were subjected to electrophoresis at 150 V for 60 min and transferred onto a PVDF membrane at 100 V for 90 min. After sealing for 2 h, the membrane was then cut into 10 strips of uniform size. Each strip was incubated with different primary antibodies. The mouse anti-COPT1 monoclonal antibody (67221-1-Ig, Proteintech, Wuhan, China) was diluted 1:1000 to serve as a positive control primary antibody for one strip. Nine different plasma samples (three LC, three BPN and three NSCLC) were diluted of 1:100 as the primary antibodies for the other nine strips, respectively. Finally, the secondary antibodies, goat anti-mouse and sheep anti-human IgG antibodies labeled with HRP, were utilized to detect specific protein bands indicative of presence of the anti-COPT1 autoantibodies.

Indirect immunofluorescence

To begin the experiment, A549 cells in logarithmic growth period were digested, centrifuged, and counted. The cell density was adjusted to 1×10^5 cells/ml. Subsequently, 20 μl of the diluted cell suspension was added to a cell slide, which was then placed into a 24-well plate. Once the cells adhered to the wall, 380 μl of complete culture medium was added to each well. Fixation was then performed using 4% paraformaldehyde for 20 min, followed by blocking with 0.5% BSA solution for 1 h. Next, the anti-COPT1 monoclonal antibody, one NSCLC and one NC plasma were served as primary antibodies, while goat anti-mouse IgG and sheep anti-human antibodies labeled with FITC were used as secondary antibodies. Finally, the fluorescence intensity of the cell slides incubated with different antibodies was observed using a fluorescence microscope.

Statistical analysis

Statistical analysis and visualization of experimental results were conducted using SPSS 21.0 and GraphPad 8.0. PASS 15.0 software was used to calculate the required sample size. Previous studies have showed that the diagnostic sensitivity of autoantibodies is approximately 10%-30%, and the specificity is 70%-80% (22). The allowable error δ is set to 0.05-0.1, and the confidence level is 1-α=0.95. The calculation formula is $n=(Z_\alpha/\delta)^2$ (1-*P*) *P*. According to PASS 15.0, the sample number for NSCLC was 86-333 and the sample number for BPN and NC was 66-333. The expression levels of anti-COPT1 autoantibodies in NSCLC, BPN and NC were compared using the Mann-Whitney U test.

Receiver operating characteristic (ROC) curve analysis was performed to evaluate the differential diagnostic value AUC, 95% confidence interval (95% CI), sensitivity, specificity, and Youden's index (YI) of anti-COPT1 autoantibodies for NSCLC and its various clinical features. AUC value was used to measure the diagnostic ability. AUC<0.5 shows no diagnostic ability. AUC>0.7 indicates certain diagnostic ability and AUC>0.8 indicates good diagnostic ability (23). The maximum YI is a comprehensive index of sensitivity and specificity that can help determine the best diagnostic threshold and compare the accuracy of different tests. Here, the maximum YI was used as the standard for the best threshold to identify true positives and avoid false positives.

Additionally, the positive rates of COPT1 autoantibodies in different clinical features of NSCLC patients were compared using the chi-square test. Pairwise comparisons between the two groups were further analyzed using the Wilcoxon test with Bonferroni adjustment. Logistic regression analysis was used to construct the combined models. The optimal cutoff value, which was utilized to determine the positive rate, was set at the SBI value with the largest YI. Statistical significance was determined when the AUC was greater than 0.5 and *P* was less than 0.05.

Results

COPT1 is highly expressed in patients with NSCLC

According to data from the Human Protein Atlas (HPA) online database, the protein level of COPT1 was higher in patients with NSCLC than in healthy individuals (Figure 2A). COPT1 was not expressed in normal lung vacuole cells but was moderately (2/6) or weakly (1/6) in LUAD, and moderately expressed (2/5) or weakly (1/5) expressed in LUSC by HPA database (Figure 2A). Furthermore, analyses of the TCGA and GTEx data revealed that the mRNA expression levels of COPT1 were elevated in patients with LUSC and LUAD ($P< 0.05$, Figure 2B). These findings collectively emphasized that the expression of COPT1 was significantly elevated in NSCLC patients compared with that in NC.

The expression level of anti-COPT1 autoantibodies was preliminarily detected in the discovery group

The expression levels of anti-COPT1-IgG and anti-COPT1-IgM in the plasma of the 89 NSCLC and 89 NC in the discovery group were detected by ELISA. The demographic information of the participants is presented in Table 1. ELISA results revealed that the patients with NSCLC exhibited significantly elevated levels of anti-COPT1-IgG and anti-COPT1-IgM compared with NC (Figures 3A, B). The AUCs of anti-COPT1-IgG and anti-COPT1-IgM autoantibodies for distinguishing NSCLC from NC were 0.885 (95% CI: 0.834-0.937, sensitivity=86.5%, specificity=82.0%) and 0.921 (95% CI: 0.883-0.958, sensitivity=88.8%, specificity=82.0%), respectively (Figures 3C, D). These results suggested that NSCLC patients have higher levels of anti-COPT1 autoantibodies expression.

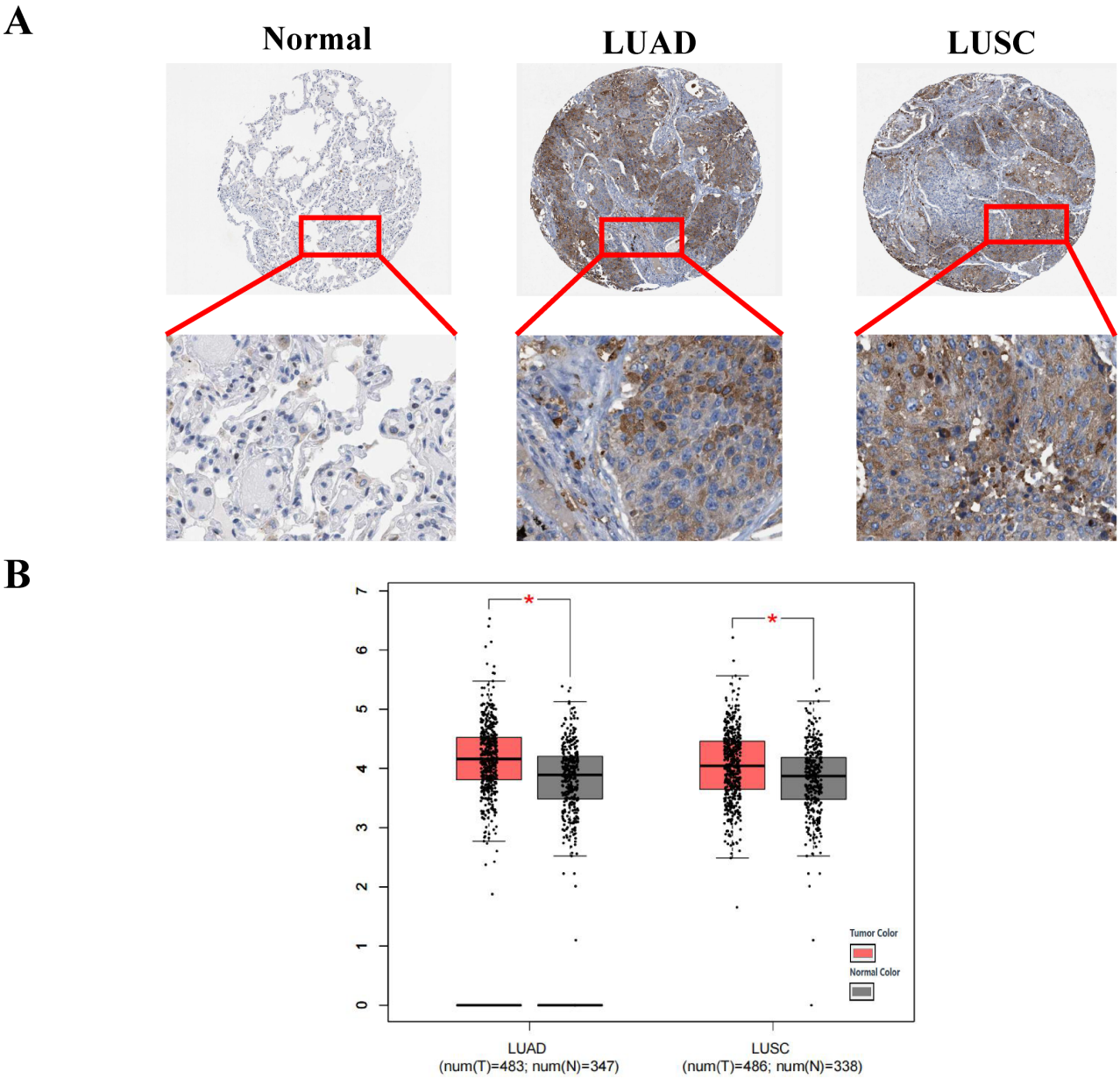

FIGURE 2
COPT1 was highly expressed in patients with non-small cell lung cancer. **(A)** IHC staining images of COPT1 from HPA database in normal tissues and NSCLC tissues. **(B)** The expression of COPT1 in normal tissues, LUAD and LUSC from TCGA and GTEx databases. HPA, The Human Protein Atlas; LUAD, Lung adenocarcinoma; LUSC, Lung squamous cell carcinoma; T, Tumor; N, Normal; *P<0.05.

The expression level of anti-COPT1 autoantibodies was verified in the verification group

The expression levels of anti-COPT1 autoantibodies in plasma were further detected in the verification group (321 NSCLC, 321 BPN and 321 NC) to validate previous findings and enhanced the robustness of the results (Table 2). The results showed that anti-COPT1-IgG and anti-COPT1-IgM levels were elevated in NSCLC patients compared with those in BPN and NC (Figures 4A, B).

The expression levels of anti-COPT1 autoantibodies in the plasma were confirmed by western blotting. Three plasma samples from NSCLC patients with high anti-COPT1 autoantibody expression levels, three plasma samples from BPN patients, and three plasma samples from NC were selected. To verify the ELISA results, a purchased monoclonal antibody of COPT1 was utilized as a positive control. The findings revealed that the NSCLC plasma with a high level of anti-COPT1 autoantibodies in ELISA also showed strong reactivity in western blotting analysis (Figure 4C). Western blotting results confirmed the occurrence of immunoreactivity to COPT1 in the plasma.

10.3389/fimmu.2025.1455095

TABLE 1 Clinical characteristics of NSCLC and NC in the discovery group.

Variables	NSCLC (n=89)	NC (n=89)	P
Age (year, %)			
≤55y	32(35.9)	36 (40.4)	>0.05
>55y	57(64.1)	53 (59.6)	
Mean ± SD	60 ± 10	58 ± 9	
Gender, n (%)			
Male	51(57.3)	49(55.0)	>0.05
Female	38(42.7)	40(45.0)	
Histology, n (%)			
LUAD	61(68.5)		
LUSC	16(17.9)		
Other NSCLC	12(13.6)		
Smoking, n (%)			
Yes	29(32.5)		
No Unknown	57(64.0) 3 (3.5)		
Drinking, n (%)			
Yes	13(14.5)		
No Unknown	73(82.0) 3 (3.5)		
Lymph node Metastasis, n (%)			
Yes	46(51.6)		
No	42(47.1)		
Unknown	1(1.3)		
Distant Metastasis, n (%)			
Yes	45(50.5)		
No	37(41.6)		
Unknown	7(7.9)		
Clinical stage, n (%)			
I	31(34.8)		
II	11(12.4)		
III	0(0)		
IV	47(52.8)		
Unknown	0(0)		

NSCLC, Non-small cell lung cancer; *NC*, Normal controls; *SD*, standard deviation.

Using IIF in A549 cells with high COPT1 expression (Supplementary Figure 1A), we detected the expression of anti-COPT1 autoantibodies in both NSCLC and NC to confirm the anti-COPT1 autoantibody response (Figures 4D–G). Our results confirmed the presence expression of anti-COPT1 autoantibodies in the plasma.

The diagnostic value of anti-COPT1 autoantibodies was evaluated as biomarkers to distinguish NSCLC from NC

The positive rates of anti-COPT1-IgG and anti-COPT1-IgM in NSCLC were higher than those in NC in the verification group (Figures 5A, B). When distinguishing NSCLC from NC, the AUC values of anti-COPT1-IgG and anti-COPT1-IgM were 0.733 (95% CI: 0.694-0.771, sensitivity=64.8%, specificity=70.4%) and 0.679 (95% CI: 0.638-0.720, sensitivity=81.9%, specificity=44.5%), respectively (Figures 5C, D). These results showed that anti-COPT1 autoantibodies can effectively distinguish NSCLC from NC.

Anti-COPT1 autoantibodies could distinguish LUSC and LUAD from NC

As LUSC and LUAD are the most common subtypes of NSCLC, we evaluated the diagnostic efficacy of anti-COPT1 autoantibodies in these two subtypes of NSCLC. The verification group comprised 227 patients with LUAD and 46 patients with LUSC. Both anti-COPT1-IgG and anti-COPT1-IgM autoantibodies exhibited higher expression levels in LUAD and LUSC than in NC. Interestingly, no statistically significant differences were observed in the expression levels of anti-COPT1-IgG and anti-COPT1-IgM autoantibodies between LUAD and LUSC (P>0.05) (Figures 6A, B). The AUC values for anti-COPT1-IgG autoantibodies in LUAD and LUSC were 0.726 (95% CI: 0.682-0.770) and 0.729 (95% CI: 0.651-0.807), respectively (Figures 6C, D). The AUC values of the anti-COPT1-IgM autoantibodies for distinguishing LUAD and LUSC from NC were 0.713 (95% CI: 0.670-0.755) and 0.668 (95% CI: 0.593-0.742), respectively (Figures 6E, F). Pairwise comparisons of different subgroups of LUAD stratified by age, gender, smoking and drinking status were performed (Supplementary Figure 2, Figures 6G, H). For individuals aged >55 years, the increased AUC values for anti-COPT1-IgG and anti-COPT1-IgM were 0.856 (95% CI: 0.812-0.901) and 0.778 (95% CI: 0.723-0.833), respectively. Therefore, anti-COPT1 autoantibodies can be used to distinguish LUAD and LUSC from NC.

Anti-COPT1 autoantibodies can distinguish NSCLC clinical subgroups from NC

To further study the expression level of anti-COPT1 autoantibodies in different clinical subgroups, NSCLC was divided according to clinical stage, lymph node metastasis, distant metastasis, smoking and drinking. There were no significant differences in the expression levels of anti-COPT1-IgG and anti-COPT1-IgM between the different subgroups (P>0.05) (Supplementary Figures 1B, C). In every subgroup, both anti-COPT1-IgG and anti-COPT1-IgM expression levels were higher in NSCLC (P<0.05) (Figures 7A, B). The AUC range for anti-COPT1-IgG in various clinical subgroups was 0.633-0.747 (Figure 7C, Supplementary Figure 3). There was no significant difference in the expression levels of anti-COPT1

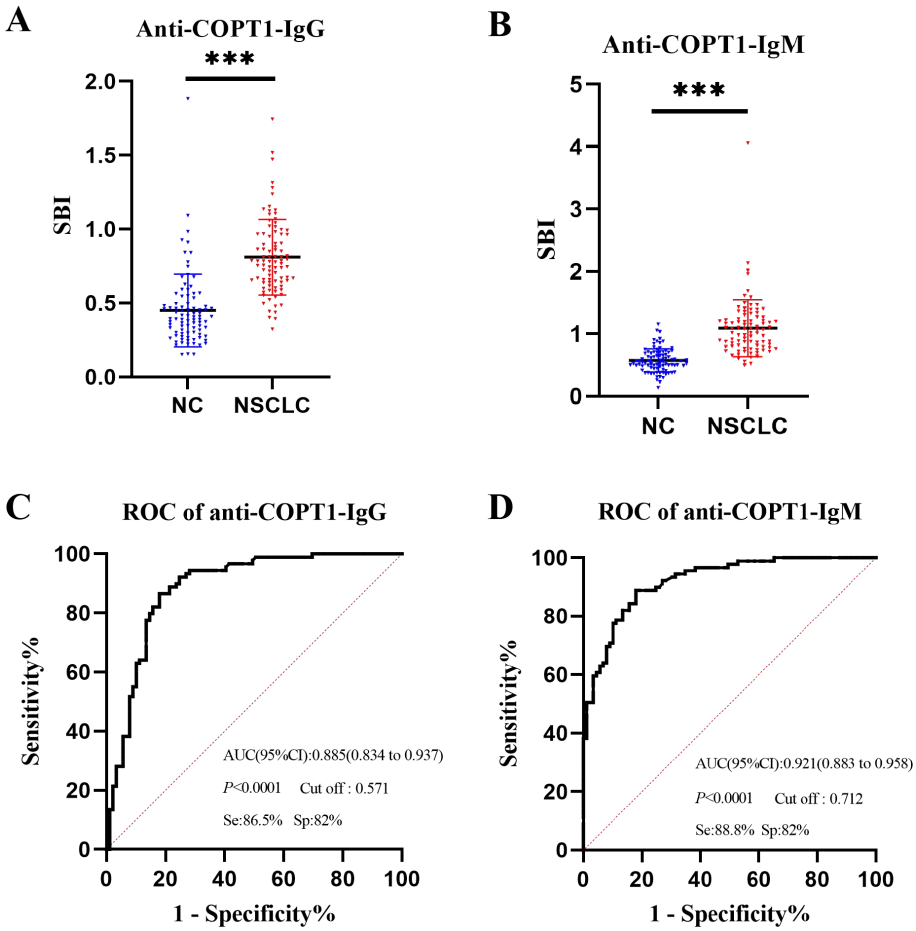

FIGURE 3
Expression level of anti-COPT1 autoantibodies in the discovery group. **(A, B)** Expression levels of anti-COPT1-IgG and anti-COPT1-IgM autoantibodies in 89 NSCLC patients and 89 normal controls, respectively. **(C, D)** ROC curve, AUC, specificity and sensitivity of anti-COPT1-IgG and anti-COPT1-IgM autoantibodies in 89 NSCLC patients and 89 NC, respectively. Se, Sensibility; Sp, Specificity. ***P<0.001.

autoantibodies between early and advanced NSCLC (Supplementary Figures 1B, C), indicating that the anti-COPT1 autoantibodies did not increase with tumor stage progression. The AUC value of anti-COPT1-IgG for the identification of early stage NSCLC from NC was 0.734 (95% CI: 0.686-0.781, sensitivity=63.8%, specificity=71.7%), which was higher than that for NSCLC with late stage (AUC=0.715, 95% CI: 0.649-0.782, sensitivity=38.2%, specificity=90.6%, Figure 7C, Supplementary Figures 3A, B). For the anti-COPT1-IgM autoantibody, the AUC range in different clinical subgroups was 0.683-0.701 (Figure 7D, Supplementary Figure 4). The anti-COPT1-IgM autoantibody could discriminate early NSCLC from NC, with an AUC of 0.683 (95% CI: 0.636-0.731, sensitivity=49.4%, specificity=77.9%) (Figure 7D, Supplementary Figure 4A). These results indicated the potential of anti-COPT1 autoantibodies as biomarkers for the detection of early NSCLC.

Pairwise comparisons of the different subgroups according to age and gender were performed. In the different subgroups, anti-COPT1 autoantibody levels were higher in NSCLC than in NC (Figures 7E–H). For female individuals, the AUC values of anti-COPT1-IgG and anti-COPT1-IgM autoantibodis for distinguishing NSCLC from NC were 0.801 (95% CI: 0.747-0.855, sensitivity=53.3%, specificity=94.1%) and 0.808 (95% CI: 0.755-0.861, sensitivity=64.8%, specificity=82.2%), respectively (Supplementary Figure 4). For individuals aged >55 years, the AUCs of anti-COPT1-IgG and anti-COPT1-IgM were 0.851 (95% CI: 0.810-0.891, sensitivity= 77.1%, specificity=74.2%) and 0.818 (95% CI: 0.773-0.864, sensitivity=95.5%, specificity=51.0%), respectively, which were higher than those for individuals aged ≤55 years (Supplementary Figures 3, 4). These expression of anti-COPT1 autoantibodies and the diagnostic accuracy were influenced by age and gender.

Anti-COPT1 autoantibodies can effectively distinguish NSCLC from BPN

The positive rates of anti-COPT1 autoantibodies in 321 NSCLC and 321 BPN were compared. The positive rates of anti-COPT1-IgG and anti-COPT1-IgM autoantibodies were higher in NSCLC than in BPN (Figures 8A, B) (P<0.05). The AUC values of anti-

10.3389/fimmu.2025.1455095

TABLE 2 Clinical characteristics of NSCLC, BPN and NC in the verification group.

Variables	NSCLC (n=321)	BPN (n=321)	NC (n=321)	P
Age (year, %)				
≤55y	164(51.1)	165(51.4)	170(53.0)	>0.05
>55y	157(48.9)	156(48.6)	151(47.0)	
Mean ± SD	56 ± 11	55 ± 12	56 ± 11	
Gender, n (%)				
Male	199(62.0)	200(62.3)	204(63.5)	>0.05
Female	122(38.0)	121(37.7)	117(36.5)	
Histology, n (%)				
LUAD	227(70.7)			
LUSC	46(14.3)			
Other NSCLC	48(15.0)			
Smoking, n (%)				
Yes	114(35.5)	42(13.1)		
No Unknown	207(64.5) 0(0)	267(83.1) 12(3.8)		
Drinking, n (%)				
Yes	85(26.5)	86(26.8)		
No Unknown	236(73.5) 0(0)	233(72.6) 2(0.6)		
Lymph node Metastasis, n (%)				
Yes	97(30.2)			
No	185(57.6)			
Unknown	39(12.2)			
Distant Metastasis, n (%)				
Yes	40(12.5)			
No	228(71.0)			
Unknown	53(16.5)			
Clinical stage, n (%)				
I	158(49.2)			
II	16(5.0)			
III	53(16.5)			
IV	36(11.2)			
Unknown	58(18.1)			

NSCLC, Non-small cell lung cancer; *BPN*, Benign pulmonary nodules; *NC*, Normal controls; *SD*, standard deviation.

COPT1-IgG and anti-COPT1-IgM were 0.648 (95% CI: 0.605-0.690, sensitivity=77.9%, specificity=48.9%) and 0.571 (95% CI: 0.526-0.615, sensitivity=84.7%, specificity=31.2%), respectively (Figures 8C, D). The results indicated that anti-COPT1-IgG and anti-COPT1-IgM autoantibodies could distinguish NSCLC from BPN.

Anti-COPT1 autoantibodies can distinguish NSCLC clinical subgroups from BPN

The expression of anti-COPT1-IgG autoantibodies in different clinical subgroups except for the NSCLC subgroup with distant metastasis, was higher than that in BPN (Figure 9A). The

10.3389/fimmu.2025.1455095

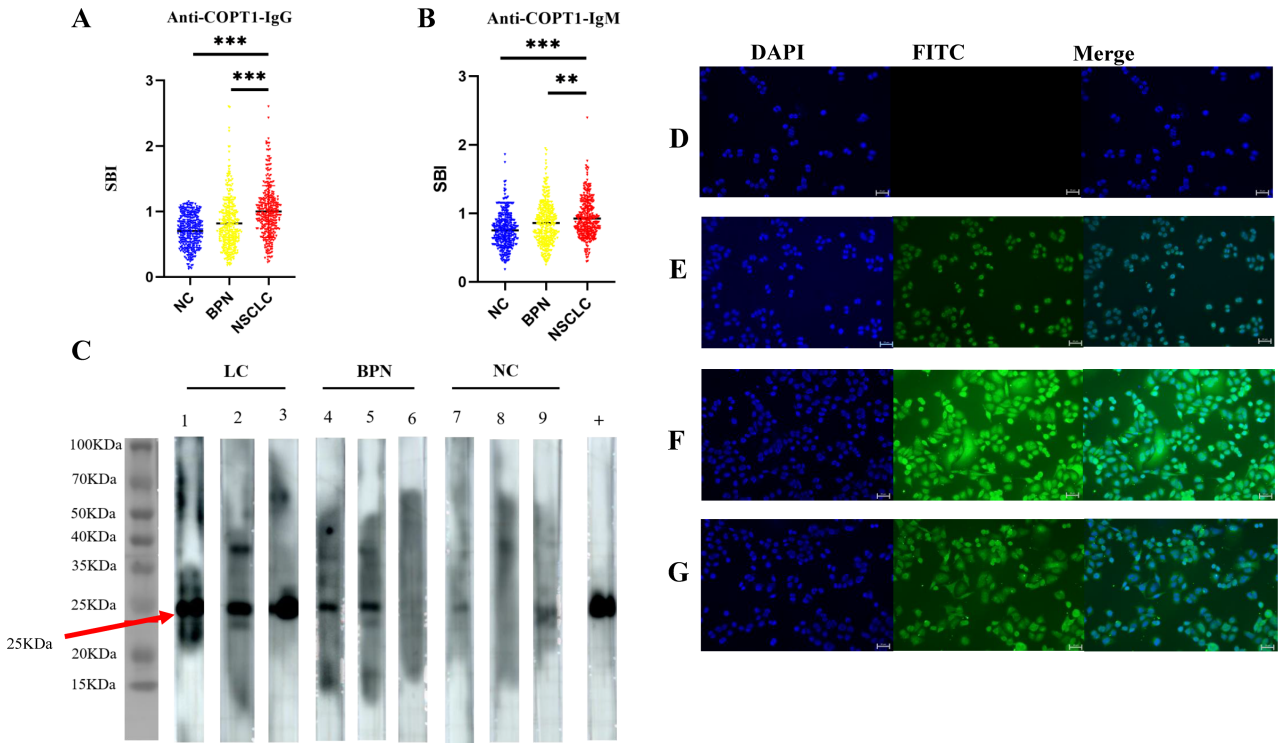

FIGURE 4
Validation of anti-COPT1 autoantibodies expression in the verification group. **(A, B)** The expression of anti-COPT1-IgG and anti-COPT1-IgM autoantibodies in 321 NSCLC, 321 BPN and 321 NC were detected by ELISA. **(C)** The expression of anti-COPT1 autoantibodies in the plasma samples of 3 NSCLC, 3 BPN and 3 NC was detected by western blotting. Lane +, The anti-COPT1 monoclonal antibody used as the positive control. **(D–G)**, Indirect immunofluorescence detection of anti-COPT1 autoantibodies in the plasma samples of NSCLC and NC. **(D)** The blank control, PBS a s primary antibody incubation; **(E)** The positive control, an anti-COPT1 monoclonal antibody as primary antibody; **(F)** The plasma of NSCLC as primary antibody; **(G)** NC plasma as primary antibody. ***P*<0.01; ****P*<0.001.

expression level of anti-COPT1-IgM autoantibody in NSCLC patients with a history of drinking and smoking was not statistically different from that in BPN (*P*>0.05) (Figure 9B). The AUC of the different subgroups was obtained (Figures 9C, D). The AUC value of anti-COPT1-IgG in NSCLC with different clinical features ranged from 0.566 to 0.661 (Figure 9C), while the AUC value of anti-COPT1-IgM in NSCLC with different clinical features ranged from 0.524 to 0.598 (Figure 9D). Anti-COPT1-IgG and anti-COPT1-IgM autoantibodies discriminated early NSCLC from BPN, with AUC values of 0.649 and 0.574, respectively (Figures 9C, D).

Pairwise comparisons of the subgroups stratified by age, gender, smoking status and drinking status were performed. In females, anti-COPT1 autoantibody levels were higher in NSCLC than in BPN (Figures 9E, F). The AUC values of anti-COPT1-IgG and anti-COPT1-IgM to distinguish NSCLC from BPN in females was 0.720 (95% CI: 0.655-0.784, sensitivity=60.7%, specificity=74.4%) and 0.682 (95% CI: 0.615-0.749, sensitivity=86.9%, specificity=47.1%), respectively (Supplementary Figures 4A, B). For individuals aged >55 years, the AUC values of anti-COPT1-IgG and anti-COPT1-IgM were 0.745 (95% CI: 0.690-0.800, sensitivity=94.3%, specificity=50.0%) and 0.713 (95% CI: 0.656-0.770, sensitivity=82.2%, specificity=55.8%), respectively (Figures 9G, H, Supplementary Figures 4C, D). Stratified by smoking and drinking status, the anti-COPT1-IgG levels were higher in NSCLC without smoking and drinking history, and the AUC values for the subgroups increased (Figures 9I–L, Supplementary Figures 4E–H). Anti-COPT1-IgG autoantibody had a higher diagnostic value (AUC=0.707, 95% CI: 0.659-0.756, sensitivity=79.7%, specificity=53.6%) for distinguishing NSCLC without drinking history from BPN (Supplementary Figure 4E).

Combination of anti-COPT1-IgG and anti-COPT1-IgM improved the diagnostic value

In the verification group, samples with expression information for the traditional tumor marker CEA were selected for multiplex biomarker assays. The combined diagnostic value of anti-COPT1-IgG, anti-COPT1-IgM and CEA in 226 NC, 150 NSCLC and 105 BPN were analyzed to examined the additional information on NSCLC diagnosis. The results indicated that the combined diagnosis of anti-COPT1-IgG and anti-COPT1-IgM autoantibodies can improve the diagnostic value (AUC=0.784, 95% CI: 0.736-0.833) for distinguishing NSCLC from NC (Figure 10A). The accuracy of biomarker testing was increased by the combinational analysis (Table 3). However, combined diagnosis with CEA did not significantly improve the diagnostic value (Figure 10A). The combination of anti-COPT1-IgG, anti-COPT1-IgM, and CEA

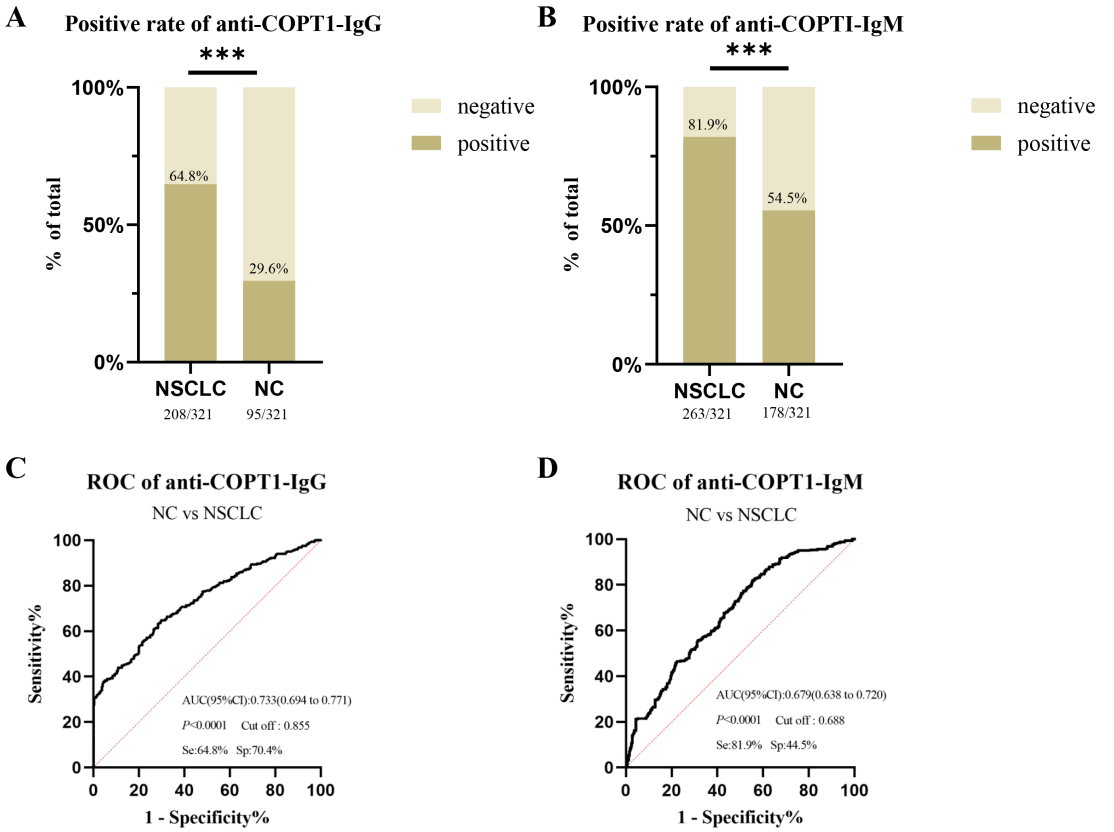

FIGURE 5
The diagnostic value of anti-COPT1 autoantibodies. **(A, B)** the positive rates of anti-COPT1-IgG and anti-COPT1-IgM autoantibodies in NSCLC and NC, respectively. **(C, D)** ROC curve, AUC, sensitivity and specificity of anti-COPT1-IgG and anti-COPT1-IgM autoantibodies in 321 NSCLC and 321 NC, respectively. Se, Sensibility; Sp, Specificity. ***P<0.001.

enhanced the efficacy of NSCLC diagnosis from BPN, and the AUC value increased up to 0.670 (95% CI: 0.603-0.737) (Figure 10B, Table 4). Moreover, the combination models improved the diagnostic value for distinguishing early NSCLC from NC and BPN, with the AUC values increasing up to 0.771 (95%CI: 0.703-0.883, sensitivity=63.2%, specificity=82.3%) and 0.624 (95% CI: 0.541-0.706, sensitivity=81.6%, specificity=43.3%), respectively (Figures 10C, D, Table 4). Finally, we performed the combined analysis to distinguish LUAD from BPN (Figures 10E, F). The results showed that this combination can improve the diagnostic ability of LUAD (AUC=0.657, 95% CI: 0.548-0.702), especially for early LUAD (AUC=0.627, 95% CI: 0.540-0.715).

Discussion

In this study, we identified anti-COPT1 autoantibodies as novel tumor-associated autoantibody biomarkers for NSCLC detection. Our study showed that the expression levels of anti-COPT1-IgG and anti-COPT1-IgM in NSCLC were significantly higher than those in BPN and NC. Anti-COPT1-IgG and anti-COPT1-IgM autoantibodies can effectively distinguish NSCLC from NC with AUC values of 0.733 and 0.679 respectively, and distinguish NSCLC from BPN with AUC value of 0.648 and 0.571 respectively. The combined diagnosis of anti-COPT1-IgG and anti-COPT1-IgM improved the diagnostic value for distinguishing NSCLC from NC, and the AUC values increased to 0.784. When distinguishing NSCLC from BPN, the combined diagnosis of anti-COPT1-IgG, anti-COPT1-IgM and CEA enhanced the accuracy of NSCLC detection with AUC of 0.670.

Over the past decade, tissue and blood biomarkers have been identified for NSCLC detection and treatment decisions (24, 25). Plasma-based assays offer numerous advantages over tissue-based assays owing due to their non-invasive nature, rapidity, and ease of repeatability over time. There are various tissue and blood-based assays for biomarker detection, each with its own strengths and limitations (4). Various TAAs have been identified in almost all types of cancers. Many antigens found in blood have been evaluated as potential biomarkers of lung cancer. The most studied biomarkers include CYFRA21-1, CEA, neuron Specific Enolase (NSE), and squamous cell carcinoma antigen (SCC-Ag). CEA is a cell surface glycoprotein produced during fetal development that plays a crucial role in cell adhesion. Elevated CEA levels have been linked to various cancers, such as lung, colorectal, and thyroid cancers (26). Increased serum CEA levels are frequently observed in NSCLC patients, particularly those with adenocarcinoma (27, 28). However, the diagnostic value of CEA alone for lung cancer is limited due to its low sensitivity and specificity (29, 30). Tumor-

10.3389/fimmu.2025.1455095

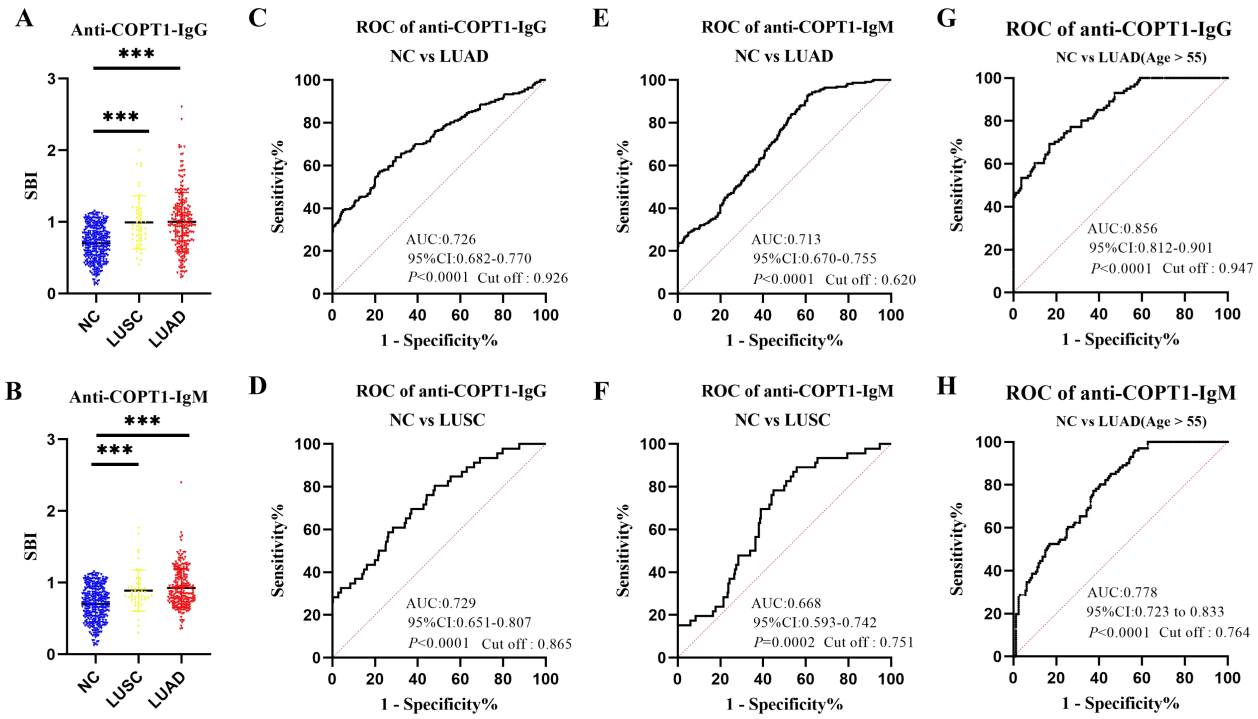

FIGURE 6
Anti-COPT1 autoantibodies can distinguish LUAD and LUSC from NC. **(A, B)** The expression of anti-COPT1-IgG and anti-COPT1-IgM in LUSC, LUAD and NC, respectively. **(C, D)** ROC curve analysis of anti-COPT1-IgG autoantibody to distinguish LUAD and LUSC patients from NC, respectively. **(E, F)** ROC curve analysis of anti-COPT1-IgM autoantibody to distinguish LUAD and LUSC patients from NC, respectively. **(G, H)** ROC curve analysis of anti-COPT1-IgG and anti-COPT1-IgM autoantibody to distinguish LUAD with age>55 from NC, respectively. ***P<0.001.

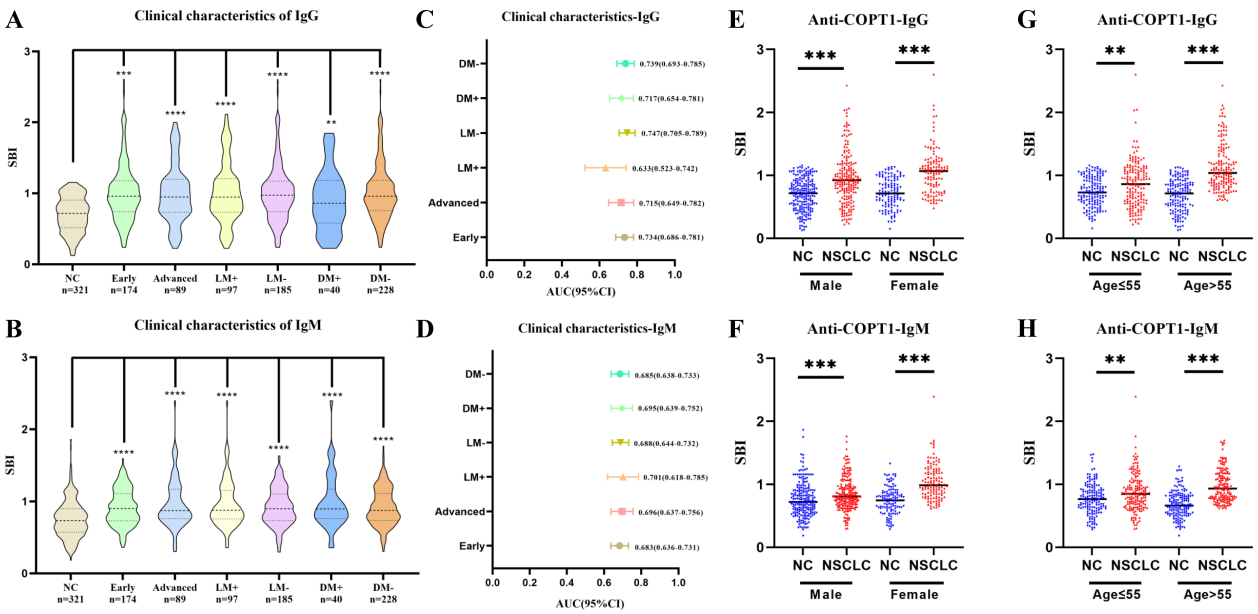

FIGURE 7
Expression of anti-COPT1 in different clinical subgroups and NC. **(A, B)** Expression of anti-COPT1-IgG and anti-COPT1-IgM autoantibodies in different clinical subgroups, respectively. **(C, D)** AUC and 95% CI of anti-COPT1 autoantibodies in different clinical subgroups to distinguish NSCLC with different clinical features from NC. **(E–H)** The expression of anti-COPT1-IgG and anti-COPT1-IgM autoantibodies stratified by age and gender. Early, Patients with early NSCLC (clinical stage I&II); Advanced, Patients with advanced NSCLC (clinical stage III&IV); LM+, Lymph node metastasis positive; LM-, Lymph node metastasis negative; DM+, Distant metastasis positive; DM-, Distant metastasis negative; **P<0.01, ***P<0.001, ****P<0.0001.

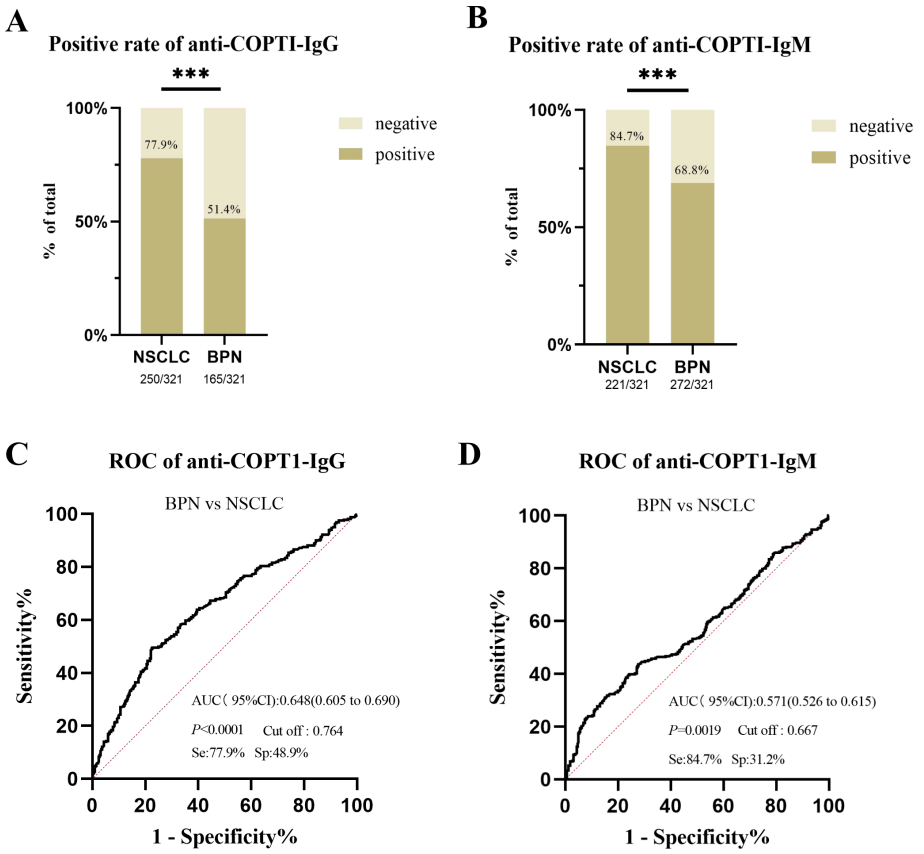

FIGURE 8
Anti-COPT1 autoantibodies can effectively distinguish NSCLC from BPN. **(A, B)** The positive rates of anti-COPT1-IgG and anti-COPT1-IgM in NSCLC and BPN, respectively. **(C, D)** ROC curve analysis of anti-COPT1 autoantibodies to distinguish NSCLC from BPN. Se, Sensibility; Sp, Specificity. ***P<0.001.

associated autoantibodies are antibodies produced by the immune response against various TAAs, such as overexpressed antigens, mutated proteins, or post-translationally modified proteins (31). Some autoantibodies have high potential as biomarkers due to their sensitivity and specificity (32).

As commonly understood, copper is a crucial cofactor for all organisms, including the human body (16). When copper concentrations exceed the normal threshold, it becomes toxic and causes cell death, known as cuproptosis (33). Abnormal regulation of some cuproptosis-related genes has been shown to play an important role in the occurrence and progression of cancers (34–36). Zhang et al. (37), comprehensively examined the carcinogenicity of COPT1 in various cancer types, and demonstrated that COPT1 may be an effective biomarker for cancer prognosis. COPT1 expression correlated with the expression of PD-L1 and the infiltration of immune cell infiltration, indicating its potential significance in tumor treatment (38, 39). In addition, some studies found that COPT1 is a potential copper death-related gene in breast cancer, which is significantly upregulated, and has great potential for predicting the prognosis, diagnosis and drug sensitivity of breast cancer (21). Based on TIMER and HPA databases, the expression level of COPT1 was higher in NSCLC and correlated with various infiltrated immune cells (Supplementary Figure 5). COPT1 mutations were identified in multiple tumors, including lung cancer with a mutation rate of 1.5% (40). High expression of COPT1 and COPT1 mutations may trigger strong immune responses to COPT1 autoantibodies. In addition, COPT1 expression was positively correlated with infiltrated $CD4^+$ T, $CD8^+$ T, and B cells. These results suggest that COPT1 is a TAA and induced the increase of anti-COPT1 autoantibodies in NSCLC patients. However, elevated COPT1 expression were reported in various tumors, indicating that anti-COPT1 autoantibodies may be induced in other tumors. The clinical value of anti-COPT1 autoantibodies for the detection of other cancers and their specificity for NSCLC should be elucidated in future studies.

Autoantibodies play a significant role in the diagnosis and prognosis of lung cancer. Certain autoantibodies exhibit promising diagnostic capabilities, and studies have indicated that serum autoantibodies targeting GAGE7, MAGEA1, CAGE, and p53 can aid in the diagnosis of lung cancer. Immunoglobulin G (IgG) and immunoglobulin M (IgM) autoantibodies are important components produced by humoral immune reactions and secreted into the blood. Many studies have shown that cancer patients can produce humoral immune responses and then produce autoantibodies at an early stage before cancer diagnosis (41). Therefore, IgM and IgG autoantibodies, as the first and second

10.3389/fimmu.2025.1455095

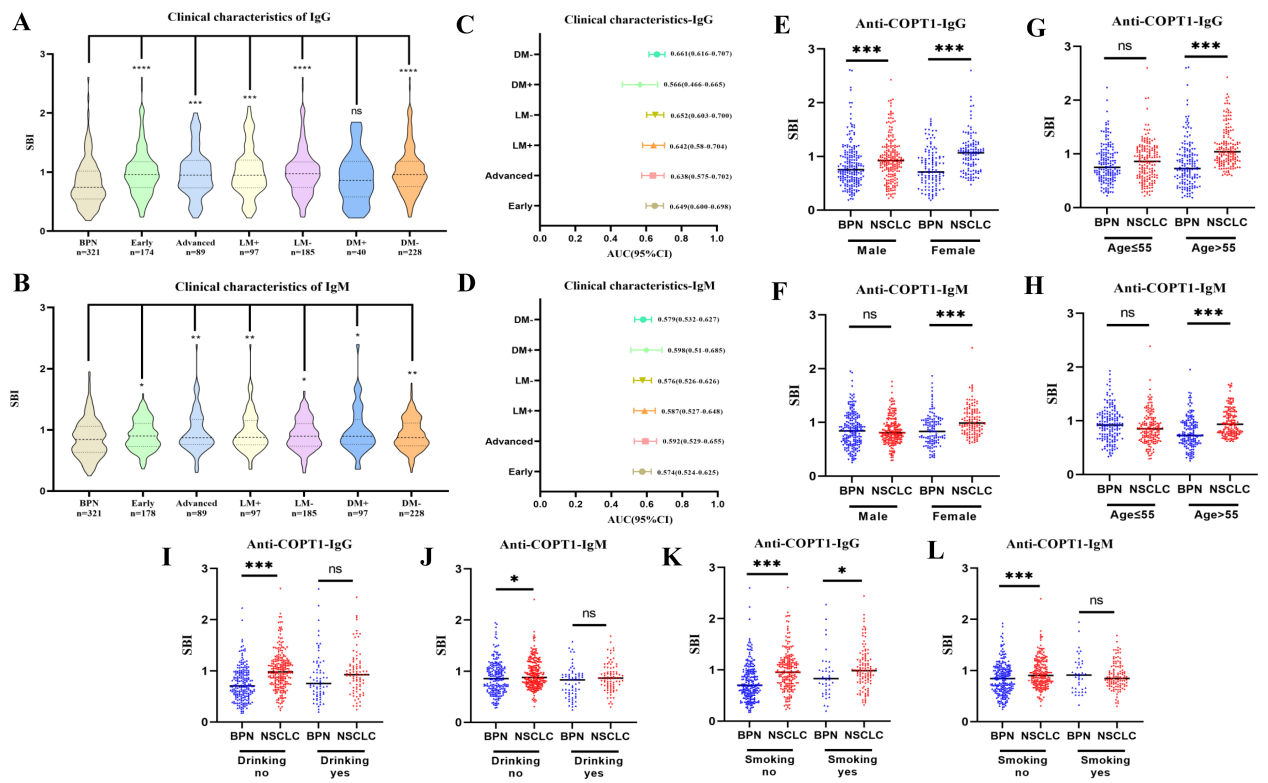

FIGURE 9
Expression of anti-COPT1 in different clinical subgroups and BPN. **(A, B)** Analysis of the expression of anti-COPT1 autoantibodies in different clinical subgroups and BPN, respectively. **(C, D)** AUC value and 95% CI of anti-COPT1 autoantibodies to distinguish NSCLC with different clinical characteristics from BPN. **(E–L)** The expression of anti-COPT1-IgG and anti-COPT1-IgM autoantibodies stratified by age, gender, smoking and drinking status. Early, Patients with early NSCLC (clinical stage I&II); Advanced, Patients with advanced NSCLC (clinical stage III&IV); LM+, Lymph node metastasis positive; LM-, Lymph node metastasis negative; DM+, Distant metastasis positive; DM-, Distant metastasis negative; Smoking yes/no, Individuals with or without smoking history; Drinking yes/no, Individuals with or without drinking history. *P<0.05, **P<0.01, ***P<0.001.

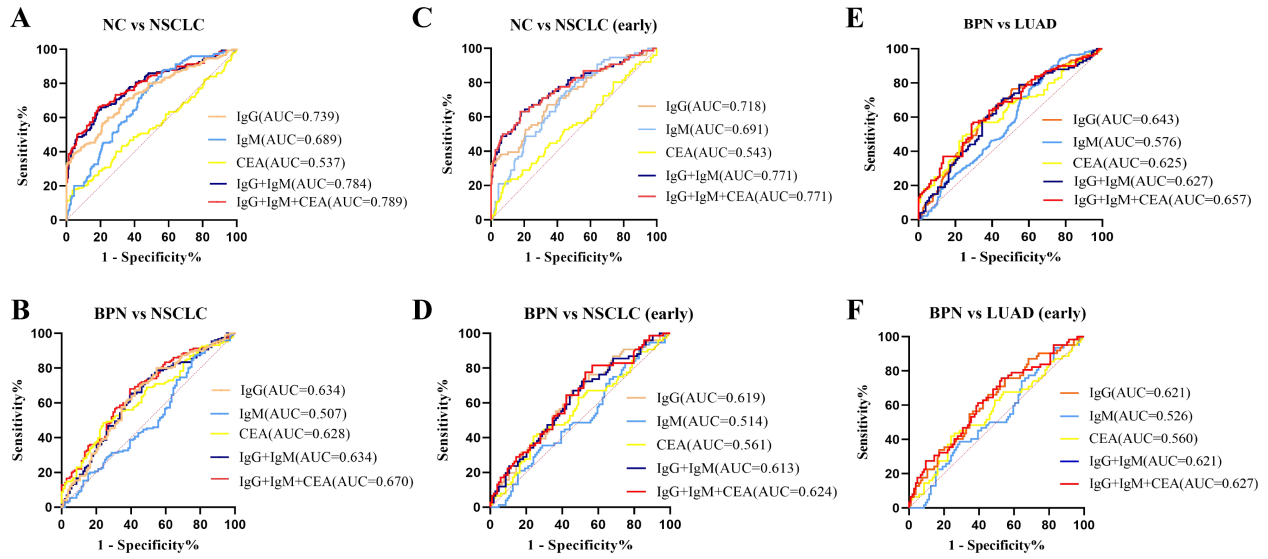

FIGURE 10
Combined diagnosis of anti-COPT1 autoantibodies and CEA to evaluate the diagnostic value. **(A)** Combined diagnosis of anti-COPT1 autoantibodies and CEA to distinguish NSCLC from NC. **(B)** Combined diagnosis of anti-COPT1 autoantibodies and CEA to distinguish NSCLC from BPN. **(C)** Combined diagnosis of anti-COPT1 autoantibodies and CEA to distinguish early NSCLC from NC. **(D)** Combined diagnosis of anti-COPT1 autoantibodies and CEA to distinguish early NSCLC from BPN. **(E)** Combined diagnosis of anti-COPT1 autoantibodies and CEA to distinguish LUAD from BPN. **(F)** Combined diagnosis of anti-COPT1 autoantibodies and CEA to distinguish early LUAD from BPN. IgG, Anti-COPT1-IgG autoantibody; IgM, Anti-COPT1-IgM autoantibody.

TABLE 3 Diagnostic efficacy of anti-COPT1 autoantibodies combined with CEA in NSCLC vs NC.

		AUC	95% CI	Se (%)	Sp (%)	AR (%)
NC vs NSCLC	IgG	0.739	0.686-0.791	70.0	65.9	56.7
	IgM	0.689	0.636-0.742	87.3	43.8	61.2
	CEA	0.537	0.476-0.599	17.3	96.5	64.9
	IgG+IgM	0.784	0.736-0.833	64.0	81.9	74.7
	IgG+IgM+CEA	0.789	0.740-0.838	66.0	81.4	75.0
NC vs NSCLC (Early)	IgG	0.718	0.648-0.788	67.1	65.9	66.2
	IgM	0.691	0.625-0.757	75.0	54.9	59.9
	CEA	0.543	0.465-0.622	22.4	91.2	70.8
	IgG+IgM	0.771	0.703-0.838	63.2	81.9	77.1
	IgG+IgM+CEA	0.771	0.703-0.838	63.2	82.3	77.5

Se, Sensitivity; Sp, Specificity; AR, Agreement rate; CI, Confidence interval; IgG, Anti-COPT1-IgG autoantibody; IgM, Anti-COPT1-IgM autoantibody.

reaction products of humoral immunity, have great potential as early diagnostic indicators of cancer (42). Currently, research on screening autoantibody biomarkers for the diagnosis and treatment of lung cancer primarily forced on IgG autoantibodies (43–45). However, IgM autoantibodies, as the first antibodies produced by immune response, may be more suitable for screening indicators for early cancer diagnosis (46). A study shows that (36), IgM autoantibodies are crucial for the immune surveillance against malignant epithelial cells. In this study, the levels of both anti-COPT1-IgG and anti-COPT1-IgM autoantibodies in NSCLC, BPN and NC were detected by ELISA, and combined with the traditional tumor marker CEA to evaluate the diagnostic value. The expression of anti-COPT1 autoantibodies were higher in NSCLC. Anti-COPT1-IgG and anti-COPT1-IgM autoantibodies were demonstrated to be preferable biomarkers for NSCLC detection. Anti-COPT1-IgG performed a higher power for NSCLC detection than anti-COPT1-IgM. Moreover, the combined detection of anti-COPT1 autoantibodies and CEA in patient plasma improved the accuracy of NSCLC diagnosis.

Our study demonstrated that anti-COPT1 autoantibodies have the potential to enhance the early detection of NSCLC, thereby improving patient outcomes. However, limitations such as the small sample size and reliance on a single sample source need to be addressed. Large-sample, multicenter studies are warranted to further validate these findings. Sensitivity and specificity are basic statistical principles for assessing the performance of diagnostic tests. In the present study, the sensitivity and specificity were not particularly high. Population diversity including age, gender and ethnicity may affect the generalizability of the findings. Thus, it now seems to be premature to define anti-COPT1 autoantibodies combined with CEA as cancer screening or early stage cancer biomarkers for clinical application. Further validation studies involving large-scale, well-defined cohorts with diverse populations and comprehensive clinical data are warranted to confirm the diagnostic potential of anti-COPT1 autoantibodies. Additionally, comprehensive combination analysis integrating anti-COPT1 autoantibodies with other conventional tumor markers (e.g., AFP, CA199, CA125) are recommended to enhance their clinical utility and diagnostic accuracy. Retrospective or prospective studies should conducted to verify its usefulness for cancer diagnosis and prognosis in the future study.

Furthermore, to enhance the translational potential of anti-COPT1 autoantibodies for NSCLC detection, the functional studies should be performed to investigate the mechanism of action of anti-COPT1 autoantibodies in NSCLC progression.

In summary, this is the first study to report anti-COPT1 autoantibodies in NSCLC. Anti-COPT1 autoantibodies were highly expressed in NSCLC and could distinguish NSCLC from NC and BPN. Both IgG and IgM autoantibodies against COPT1 present the diagnostic value for the patients with NSCLC at early

TABLE 4 Diagnostic efficacy of anti-COPT1 autoantibodies combined with CEA in NSCLC vs BPN.

		AUC	95%CI	Sp (%)	Sp (%)	AR (%)
BPN vs NSCLC	IgG	0.634	0.564-0.705	80.0	45.2	47.2
	IgM	0.507	0.433-0.581	87.3	23.1	61.0
	CEA	0.628	0.559-0.697	48.6	76.0	58.7
	IgG+IgM	0.634	0.564-0.705	80.0	45.2	65.7
	IgG+IgM+CEA	0.670	0.603-0.737	52.7	75.5	61.8
BPN vs NSCLC (Early)	IgG	0.619	0.537-0.701	67.1	54.8	59.4
	IgM	0.514	0.429-0.599	92.1	16.3	48.3
	CEA	0.561	0.475-0.647	48.6	76.0	60.5
	IgG+IgM	0.613	0.531-0.696	72.4	49.0	58.9
	IgG+IgM+CEA	0.624	0.541-0.706	81.6	43.3	59.4

Se, Sensitivity; Sp, Specificity; AR, agreement rate; CI, Confidence interval; IgG, Anti-COPT1-IgG autoantibody; IgM, Anti-COPT1-IgM autoantibody.

stage. The combination of anti-COPT1 autoantibodies and CEA had contributed to the further improvements in the early diagnosis for NSCLC. Our study indicated that anti-COPT1 autoantibodies can be used as potential novel plasma biomarkers for detecting NSCLC.

Data availability statement

The raw data supporting the conclusions of this article will be made available by the authors, without undue reservation.

Ethics statement

The studies involving humans were approved by The Ethics Committee at First Affiliated Hospital of Zhengzhou University. The studies were conducted in accordance with the local legislation and institutional requirements. The participants provided their written informed consent to participate in this study. Written informed consent was obtained from the individual(s) for the publication of any potentially identifiable images or data included in this article.

Author contributions

XC: Data curation, Methodology, Writing – original draft. JL: Data curation, Formal analysis, Writing – review & editing. SL: Data curation, Formal analysis, Writing – review & editing. AL: Data curation, Formal analysis, Writing – review & editing. LZ: Data curation, Formal analysis, Writing – review & editing. FC: Data curation, Writing – review & editing. YL: Data curation, Writing – review & editing. HM: Data curation, Writing – review & editing. WS: Data curation, Writing – review & editing. SO: Writing – review & editing, Resources. LD: Resources, Writing – review & editing, Validation. JJL: Validation, Writing – review & editing, Funding acquisition, Project administration.

Funding

The author(s) declare that financial support was received for the research and/or publication of this article. This work was supported by the Key Scientific and Technological Project of Henan Province (No. 242102310208) and Project of Basic Research Fund of Henan Institute of Medical and Pharmacological Sciences (Grant No. 2023BP0202, 2023BP0204).

Acknowledgments

The authors thank Henan Key Laboratory for Pharmacology of Liver Diseases for the continuous support, where most experiments were performed.

Conflict of interest

The authors declare that the research was conducted in the absence of any commercial or financial relationships that could be construed as a potential conflict of interest.

Publisher's note

Supplementary material

The Supplementary Material for this article can be found online at: https://www.frontiersin.org/articles/10.3389/fimmu.2025.1455095/full#supplementary-material

References

1. Sung H, Ferlay J, Siegel RL, Laversanne M, Soerjomataram I, Jemal A, et al. Global cancer statistics 2020: GLOBOCAN estimates of incidence and mortality worldwide for 36 cancers in 185 countries. *CA Cancer J Clin*. (2021) 71:209–49. doi: 10.3322/caac.21660

2. Molina JR, Yang P, Cassivi SD, Schild SE, Adjei AA. Non-small cell lung cancer: epidemiology, risk factors, treatment, and survivorship. *Mayo Clin Proc*. (2008) 83:584–94. doi: 10.1016/S0025-6196(11)60735-0

3. Jemal A, Siegel R, Ward E, Hao Y, Xu J, Murray T, et al. Cancer statistics, 2008. *CA Cancer J Clin*. (2008) 58:71–96. doi: 10.3322/CA.2007.0010

4. Nooreldeen R, Bach H. Current and future development in lung cancer diagnosis. *Int J Mol Sci*. (2021) 22(16):8661. doi: 10.3390/ijms22168661

5. Wang T, Liu M, Zheng SJ, Bian DD, Zhang JY, Yao J, et al. Tumor-associated autoantibodies are useful biomarkers in immunodiagnosis of α-fetoprotein-negative hepatocellular carcinoma. *World J Gastroenterol*. (2017) 23:3496–504. doi: 10.3748/wjg.v23.i19.3496

6. Huangfu M, Xu S, Li S, Sun B, Lee K-H, Liu L, et al. A panel of autoantibodies as potential early diagnostic serum biomarkers in patients with cervical cancer. *Tumor Biol*. (2016) 37:8709–14. doi: 10.1007/s13277-015-4472-1

7. Pierpont TM, Limper CB, Richards KL. Past, present, and future of rituximab-the world's first oncology monoclonal antibody therapy. *Front Oncol*. (2018) 8:163. doi: 10.3389/fonc.2018.00163

8. Ma J, Mo Y, Tang M, Shen J, Qi Y, Zhao W, et al. Bispecific antibodies: from research to clinical application. *Front Immunol*. (2021) 12:626616. doi: 10.3389/fimmu.2021.626616

9. Jiang D, Zhang X, Liu M, Wang Y, Wang T, Pei L, et al. Discovering panel of autoantibodies for early detection of lung cancer based on focused protein array. *Front Immunol*. (2021) 12:658922. doi: 10.3389/fimmu.2021.658922

10. Kaae J, Wohlfahrt J, Boyd HA, Wulf HC, Biggar RJ, Melbye M. The impact of autoimmune diseases on the incidence and prognosis of cutaneous Malignant melanoma. *Cancer Epidemiol Biomarkers Prev*. (2007) 16:1840–4. doi: 10.1158/1055-9965.EPI-07-0459

11. Finke C, Bartels F, Lütt A, Prüss H, Harms L. High prevalence of neuronal surface autoantibodies associated with cognitive deficits in cancer patients. *J Neurology*. (2017) 264:1968–77. doi: 10.1007/s00415-017-8582-0

12. Solassol J, Maudelonde T, Mange A, Pujol JL. Clinical relevance of autoantibody detection in lung cancer. *J Thorac Oncol*. (2011) 6:955–62. doi: 10.1097/JTO.0b013e318215a0a4

13. Soussi T. p53 Antibodies in the sera of patients with various types of cancer: a review. *Cancer Res*. (2000) 60:1777–88. doi: 10.1016/S0016-5085(98)70360-9

14. Qiu J, Choi G, Li L, Wang H, Pitteri SJ, Pereira-Faca SR, et al. Occurrence of autoantibodies to annexin I, 14-3-3 theta and LAMR1 in prediagnostic lung cancer sera. *J Clin Oncol*. (2008) 26:5060–6. doi: 10.1200/JCO.2008.16.2388

15. Lutsenko S. Dynamic and cell-specific transport networks for intracellular copper ions. *J Cell Sci*. (2021) 134(21):jcs240523. doi: 10.1242/jcs.240523

16. Tsvetkov P, Coy S, Petrova B, Dreishpoon M, Verma A, Abdusamad M, et al. Copper induces cell death by targeting lipoylated TCA cycle proteins. *Science*. (2022) 375:1254–61. doi: 10.1126/science.abf0529

17. Guo J, Cheng J, Zheng N, Zhang X, Dai X, Zhang L, et al. Copper promotes tumorigenesis by activating the PDK1-AKT oncogenic pathway in a copper transporter 1 dependent manner. *Adv Sci (Weinh)*. (2021) 8:e2004303. doi: 10.1002/advs.202004303

18. Jin J, Ma M, Yan B, Qiu B, Lu S, Yang L, et al. A SLC31A1-MEK-DNMT1-miR-124 feedback loop contributes to pancreatic cancer progression. *Genes Dis*. (2023) 10:654–6. doi: 10.1016/j.gendis.2022.05.033

19. Li X, Ge J, Wan M, Feng T, Li X, Zhang H, et al. SLC31A1 promotes chemoresistance through inducing CPT1A-mediated fatty acid oxidation in ER-positive breast cancer. *Neoplasia*. (2025) 61:101125. doi: 10.1016/j.neo.2025.101125

20. Kong F-S, Ren C-Y, Jia R, Zhou Y, Chen J-H, Ma Y. Systematic pan-cancer analysis identifies SLC31A1 as a biomarker in multiple tumor types. *BMC Med Genomics*. (2023) 16:61. doi: 10.1186/s12920-023-01489-9

21. Li X, Ma Z, Mei L. Cuproptosis-related gene SLC31A1 is a potential predictor for diagnosis, prognosis and therapeutic response of breast cancer. *Am J Cancer Res*. (2022) 12:3561–80. doi: 10.1242/jcs.240523

22. Tan EM, Zhang J. Autoantibodies to tumor-associated antigens: reporters from the immune system. *Immunol Rev*. (2008) 222:328–40. doi: 10.1111/j.1600-065X.2008.00611.x

23. Webbe J, Allin B, Knight M, Modi N, Gale C. How to reach agreement: the impact of different analytical approaches to Delphi process results in core outcomes set development. *Trials*. (2023) 24:345. doi: 10.1186/s13063-023-07285-1

24. Wang J, Zou ZH, Xia HL, He JX, Zhong NS, Tao AL. Strengths and weaknesses of immunotherapy for advanced non-small-cell lung cancer: a meta-analysis of 12 randomized controlled trials. *PLoS One*. (2012) 7:e32695. doi: 10.1371/journal.pone.0032695

25. Morgensztern D, Campo MJ, Dahlberg SE, Doebele RC, Garon E, Gerber DE, et al. Molecularly targeted therapies in non-small-cell lung cancer annual update 2014. *J Thorac Oncol*. (2015) 10:S1–63. doi: 10.1097/JTO.0000000000000405

26. Grunnet M, Sorensen JB. Carcinoembryonic antigen (CEA) as tumor marker in lung cancer. *Lung Cancer*. (2012) 76:138–43. doi: 10.1016/j.lungcan.2011.11.012

27. Molina R, Augé JM, Bosch X, Escudero JM, Viñolas N, Marrades R, et al. Usefulness of serum tumor markers, including progastrin-releasing peptide, in patients with lung cancer: correlation with histology. *Tumour Biol*. (2009) 30:121–9. doi: 10.1159/000224628

28. Cedrés S, Nuñez I, Longo M, Martinez P, Checa E, Torrejón D, et al. Serum tumor markers CEA, CYFRA21-1, and CA-125 are associated with worse prognosis in advanced non-small-cell lung cancer (NSCLC). *Clin Lung Cancer*. (2011) 12(3):172–9. doi: 10.1016/j.cllc.2011.03.019

29. Pastor A, Menéndez R, Cremades MJ, Pastor V, Llopis R, Aznar J. Diagnostic value of SCC, CEA and CYFRA 21.1 in lung cancer: a Bayesian analysis. *Eur Respir J*. (1997) 10:603–9. doi: 10.1183/09031936.97.10030603

30. Okamura K, Takayama K, Izumi M, Harada T, Furuyama K, Nakanishi Y. Diagnostic value of CEA and CYFRA 21-1 tumor markers in primary lung cancer. *Lung Cancer*. (2013) 80:45–9. doi: 10.1016/j.lungcan.2013.01.002

31. Olsen NJ, Choi MY, Fritzler MJ. Emerging technologies in autoantibody testing for rheumatic diseases. *Arthritis Res Ther*. (2017) 19:172. doi: 10.1186/s13075-017-1380-3

32. Endres D, Werden R, Schweizer T, Schröter N, Schiele MA, Nickel K, et al. Novel neuronal autoantibodies in huntington's disease. *Biol Psychiatry*. (2022) 91:e21–e3. doi: 10.1016/j.biopsych.2020.12.032

33. Jiang Y, Huo Z, Qi X, Zuo T, Wu Z. Copper-induced tumor cell death mechanisms and antitumor theragnostic applications of copper complexes. *Nanomedicine (Lond)*. (2022) 17:303–24. doi: 10.2217/nnm-2021-0374

34. Wu G, Peng H, Tang M, Yang M, Wang J, Hu Y, et al. ZNF711 down-regulation promotes CISPLATIN resistance in epithelial ovarian cancer via interacting with JHDM2A and suppressing SLC31A1 expression. *EBioMedicine*. (2021) 71:103558. doi: 10.1016/j.ebiom.2021.103558

35. Zhang S, Guan X, Liu W, Zhu Z, Jin H, Zhu Y, et al. YTHDF1 alleviates sepsis by upregulating WWP1 to induce NLRP3 ubiquitination and inhibit caspase-1-dependent pyroptosis. *Cell Death Discovery*. (2022) 8:244. doi: 10.1038/s41420-022-00872-2

36. Brändlein S, Pohle T, Ruoff N, Wozniak E, Müller-Hermelink HK, Vollmers HP. Natural IgM antibodies and immunosurveillance mechanisms against epithelial cancer cells in humans. *Cancer Res*. (2003) 63:7995–8005.

37. Zhang P, Yang H, Zhu K, Chang C, Lv W, Li R, et al. SLC31A1 identifying a novel biomarker with potential prognostic and immunotherapeutic potential in pan-cancer. *Biomedicines*. (2023) 11(11):2884. doi: 10.3390/biomedicines11112884

38. Voli F, Valli E, Lerra L, Kimpton K, Saletta F, Giorgi FM, et al. Intratumoral copper modulates PD-L1 expression and influences tumor immune evasion. *Cancer Res*. (2020) 80:4129–44. doi: 10.1158/0008-5472.CAN-20-0471

39. Li L, Li L, Sun Q. High expression of cuproptosis-related SLC31A1 gene in relation to unfavorable outcome and deregulated immune cell infiltration in breast cancer: an analysis based on public databases. *BMC Bioinf*. (2022) 23:350. doi: 10.1186/s12859-022-04894-6

40. Qi Y, Yao Q, Li X, Li X, Zhang W, Qu P. Cuproptosis-related gene SLC31A1: prognosis values and potential biological functions in cancer. *Sci Rep*. (2023) 13:17790. doi: 10.1038/s41598-023-44681-8

41. Dai L, Li J, Tsay JJ, Yie TA, Munger JS, Pass H, et al. Identification of autoantibodies to ECH1 and HNRNPA2B1 as potential biomarkers in the early detection of lung cancer. *Oncoimmunology*. (2017) 6:e1310359. doi: 10.1080/2162402X.2017.1310359

42. Pilyugin M, Descloux P, André PA, Laszlo V, Dome B, Hegedus B, et al. BARD1 serum autoantibodies for the detection of lung cancer. *PLoS One*. (2017) 12:e0182356. doi: 10.1371/journal.pone.0182356

43. Li P, Shi JX, Dai LP, Chai YR, Zhang HF, Kankonde M, et al. Serum anti-MDM2 and anti-c-Myc autoantibodies as biomarkers in the early detection of lung cancer. *Oncoimmunology*. (2016) 5:e1138200. doi: 10.1080/2162402X.2016.1138200

44. Jia J, Wang W, Meng W, Ding M, Ma S, Wang X. Development of a multiplex autoantibody test for detection of lung cancer. *PLoS One*. (2014) 9:e95444. doi: 10.1371/journal.pone.0095444

45. Pei L, Liu H, Ouyang S, Zhao C, Liu M, Wang T, et al. Discovering novel lung cancer associated antigens and the utilization of their autoantibodies in detection of lung cancer. *Immunobiology*. (2020) 225:151891. doi: 10.1016/j.imbio.2019.11.026

46. Zhang X, Li J, Wang Y, Liu M, Liu F, Zhang X, et al. A diagnostic model with igM autoantibodies and carcinoembryonic antigen for early detection of lung adenocarcinoma. *Front Immunol*. (2021) 12:728853. doi: 10.3389/fimmu.2021.728853

frontiers | Frontiers in Oncology

TYPE Review
PUBLISHED 16 April 2025
DOI 10.3389/fonc.2025.1532924

OPEN ACCESS

EDITED BY
Giuseppe Bronte,
University of Ferrara, Italy

REVIEWED BY
Federica Rubbino,
Humanitas Research Hospital, Italy
Tamer A. Addissouky,
University of Menoufia, Egypt

*CORRESPONDENCE
Yonghuan Mao
maoyonghuan@163.com
Ji Miao
njglyymj@126.com
Qiang Li
liqnanjing@163.com

†These authors have contributed equally to this work

RECEIVED 22 November 2024
ACCEPTED 27 March 2025
PUBLISHED 16 April 2025

CITATION
Zhang J, Zhu H, Liu W, Miao J, Mao Y and Li Q (2025) Prognostic and predictive molecular biomarkers in colorectal cancer. *Front. Oncol.* 15:1532924. doi: 10.3389/fonc.2025.1532924

Prognostic and predictive molecular biomarkers in colorectal cancer

Jianzhi Zhang[1,2†], Hao Zhu[3†], Wentao Liu[4], Ji Miao[1,2*], Yonghuan Mao[1,2*] and Qiang Li[1,2*]

[1]Department of General Surgery, Affiliated Drum Tower Hospital, Nanjing University Medical School, Nanjing, China, [2]Department of General Surgery, Nanjing Drum Tower Hospital Clinical College of Nanjing Medical University, Nanjing, China, [3]Department of General Surgery, Affiliated Drum Tower Hospital, Nanjing University of Chinese Medicine, Nanjing, China, [4]Department of General Surgery, Affiliated Drum Tower Hospital, JiangSu University, Nanjing, China

Precision medicine has brought revolutionary changes to the diagnosis and treatment of cancer patients, and is currently a hot and challenging research topic. Currently, the treatment regimens for most colorectal cancer (CRC) patients are mainly determined by several biomakers, including Microsatellite Instability (MSI), RAS, and BRAF. However, the roles of promising biomarkers such as HER-2, consensus molecular subtypes (CMS), and circulating tumor DNA (ctDNA) in CRC are not yet fully clear. Therefore, it is urgent to explore the potential of these emerging biomarkers in the diagnosis and treatment of CRC patients. In this paper, we discuss recent advances in CRC biomarkers, especially clinical data, and focus on the roles of biomarkers in prognosis, prediction, treatment strategies, and the intrinsic connections with clinical pathological features, hoping to promote better precision medicine for colorectal cancer.

KEYWORDS

colorectal cancer, biomarkers, circulating tumor DNA, non-coding RNA, POLE/POLD1, RET

1 Introduction

Colorectal cancer (CRC) ranks third in global incidence and second in mortality, its epidemiological trajectory showing an alarming upward trend worldwide (1). Although existing screening strategies have moderately reduced mortality rates, the majority of patients are still diagnosed at advanced stages, underscoring an urgent need for transformative approaches in CRC management. The quest for biomarkers with enhanced specificity and clinical utility has therefore become a critical frontier in oncology research by influencing three key areas: early detection accuracy, dynamic monitoring capabilities, and precision therapeutics development. The biomarker revolution in CRC has entered a pivotal phase. Traditional molecular markers such as BRAF and KRAS mutations are widely used in the diagnosis and treatment of colorectal cancer patients (2). However, compared to the revolutionary changes brought by immunotherapy to other cancers (3), the benefits of CRC patients from these biomarker-based treatments are limited, with only 3.8% of mCRC patients with MSI subtypes benefiting

from corresponding treatments—a therapeutic gap that highlights the imperative for next-generation biomarker discovery (4). In recent years, with the development of next-generation sequencing, bioinformatics analysis, liquid biopsy, and other technologies, research on biomarkers has entered a new stage: For instance, circulating tumor DNA (ctDNA) has transcended the limitations of tissue biopsies through real-time genomic monitoring, playing a pivotal role in early detection and recurrence monitoring of colorectal cancer patients. Meanwhile, non-coding RNAs (ncRNAs) have unveiled a previously hidden regulatory cosmos, fundamentally reshaping our understanding of CRC pathogenesis. Additionally, RET fusion genes have emerged as targetable oncogenic drivers, demonstrating significant associations with sensitivity to targeted therapies.

n this comprehensive review, we systematically summarize the most recent advancements in biomarker research and critically evaluate their potential for translation into tangible clinical benefits. Our analysis provides an integrative framework that effectively bridges the gap between molecular discovery and clinical implementation, offering valuable insights for both researchers and clinicians in the field of precision medicine.

2 Her-2

HER2 is a protein tyrosine kinase receptor encoded on chromosome 17q12, also known as EGFR-2/ErbB-2/CD340. It belongs to the epidermal growth factor receptor (ERBB) family. It has been reported that approximately 7% of CRC patients exhibit alterations of HER2, especially in tumors with wild-type RAS and BRAF. However, the role and impact of HER2 in advanced CRC have not been fully explicit.

2.1 The correlation with pathological features

Tumors overexpressing HER-2 are more commonly found in the left colon or rectum, with an increasing incidence from the right colon to the left colon and then to the rectum (5) (Figure 1). The overexpression of HER-2 is significantly associated with higher tumor mutational burden (TMB), higher AJCC staging, and lymph node metastasis (6). Of course, HER-2 also has intrinsic correlations with other biomarkers. For example, point mutations in HER2 are positively correlated with MSI-H tumors, but MSI-H was not found in cases of HER-2 amplification (7). There is also evidence suggesting that the typical molecular subtype (CMS2) is enriched in HER-2 positive tumors, accompanied by changes in epithelial differentiation, WNT, and MYC signaling.

2.2 Prognostic value

Currently, the prognostic significance of HER-2 in advanced CRC remains controversial. Compared to HER-2 wild-type tumors, HER-2 amplification in CRC is associated with increased invasiveness and poorer prognosis (6). A retrospective analysis of the PETACC-8 trial (n = 1795) found that HER-2 amplification and mutation were associated with shorter disease-free survival (DFS)

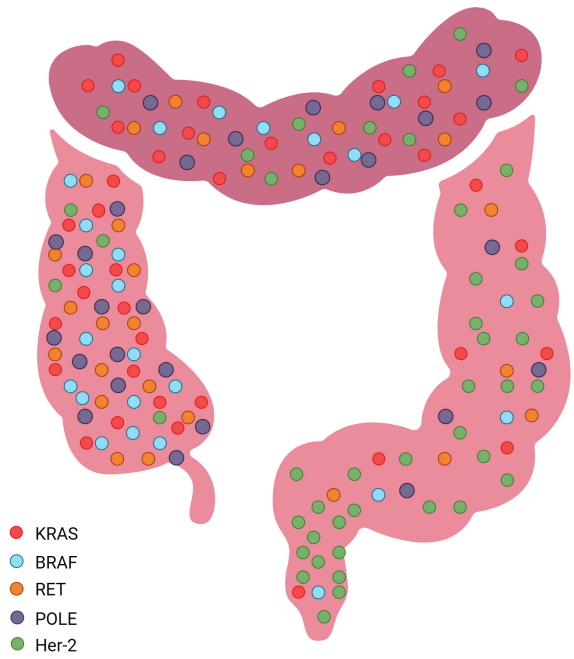

FIGURE 1
Common sites of molecular markers in the Colorectum.

(95% confidence interval [CI] 1.02-2.36, P = 0.04) and worse overall survival (OS) (95% CI 0.99-2.5, P = 0.05) Even after adjusting for other prognostic factors such as RAS mutations, grading, tumor location, pT and pN status, bowel obstruction or perforation, lymphatic or venous invasion, the prognostic impact still persisted (8). A study in 2021 supported this view: analysis of 370 mCRC patients found that HER2-positive patients had significantly worse OS compared to patients with low HER-2 expression, indicating potential prognostic value of HER-2 expression in mCRC (9). In contrast, data from the German Rectal Cancer Study Group showed that in 264 rectal cancer patients, HER-2 positivity was associated with better disease-free survival (DFS) and cancer-specific survival (10). However, in a meta-analysis, Richman SD did not find a statistically significant association between HER-2 expression and OS (11). These discrepancies may stem from multiple factors: 1.Anatomical heterogeneity – HER-2's prognostic impact appears context-dependent, with left-sided colon cancers showing different patterns from rectal tumors; 2.Molecular subtype variations – CMS2-enriched HER-2+ tumors may exhibit distinct biological behaviors; 3.Technical variability in HER-2 assessment methods across studies. The low HER-2 alteration frequency in CRC further complicates conclusive interpretation. This context-dependent prognostic role necessitates standardized molecular subtyping in future studies.

2.3 Predictive value

HER-2 alterations have been established as predictive biomarkers of resistance to anti-EGFR therapies, mediating therapeutic escape through two distinct mechanisms: HER-2 gene amplification or heregulin (HRG)-induced HER-3 receptor activation. These pathways converge to constitutively activate downstream ERK1/2 signaling, thereby sustaining oncogenic survival cascades that drive anti-EGFR resistance. However, emerging evidence suggests context-dependent predictive utility: 1. In wild-type KRAS/NRAS/BRAF/PI3KCA populations, HER-2 amplification strongly correlates with shorter response duration to EGFR inhibitors (12, 13). 2.we found that colorectal cancer patients with HER-2 amplification have a shorter duration of response to EGFR monoclonal antibody therapy and worse prognosis compared to those with wild-type RAS/BRAF, approaching even those with RAS or BRAF mutations 3. Recent antibody-drug conjugate (ADC) trials demonstrate HER-2's positive predictive value for targeted therapies like T-DXd (14). This duality – serving as both resistance marker and therapeutic target – underscores the need for dynamic biomarker assessment throughout treatment courses.

2.4 Treatment strategies

Current therapeutic strategies targeting HER-2 include monoclonal antibodies, antibody-drug conjugates (ADCs), and tyrosine kinase inhibitors (TKIs). Although some clinical trial results appear promising, none of these therapies have yet received regulatory approval for metastatic colorectal cancer (mCRC). As previously discussed, HER-2 amplification/mutations mediate resistance to anti-EGFR antibodies, while combination therapy with anti-HER2 and anti-EGFR agents demonstrates synergistic growth inhibition (13). Clinical investigations of pertuzumab-trastuzumab combination therapy in pretreated HER-2-amplified mCRC reveal significant clinical benefit in RAS wild-type HER-2-positive patients, whereas those with RAS mutations show limited therapeutic response (15). Notably, recent progress in TKI development includes pyrotinib—an irreversible dual HER-2/EGFR inhibitor—demonstrating potent antitumor activity when combined with trastuzumab (16). Among ADCs, trastuzumab emtansine (T-DM1) and trastuzumab deruxtecan (T-DXd) have undergone clinical evaluation. Phase II studies of pertuzumab-T-DM1 combination therapy in RAS/RAF wild-type ERBB2-positive mCRC patients demonstrate encouraging efficacy profiles (17).

3 BRAF

BRAF is a key serine/threonine protein kinase in the MAPK pathway, including V600 mutations (Class I) and non-V600 mutations. Among them, the Class I BRAF V600E mutation is the most common, accounting for approximately 95%, and exhibits kinase activity 700 times higher than normal BRAF (18). Patients with this type of mutation generally have a poorer prognosis, are typically located in the right colon, more common in females and elderly patients, and are associated with mucinous adenocarcinoma and poorer tumor differentiation (19). At the molecular level, the co-occurrence rate of BRAFV600E mutation and MSI is relatively high, with approximately 52% of MSI tumors having BRAF mutations, while 55% of BRAF mutation tumors exhibit MSI (20).

3.1 Prognostic value

Compared to BRAF wild-type CRC patients, patients with BRAF mutations generally have a poorer survival rate. MSI-H tumors carrying BRAF mutations exhibit better OS and lower invasiveness compared to Microsatellite Stability (MSS) tumors with BRAF mutations, suggesting that MSI-H tumors may help mitigate the adverse prognostic impact of BRAF mutations. However, the reported results regarding the prognostic differences among BRAF subtypes are mixed. Patients with BRAF Class I and II mutations generally have a poorer prognosis compared to Class III mutations. On the other hand, another study found that patients with Class II and III mutations seemed to have better survival outcomes (18, 21). Given the dismal prognosis of BRAF V600E-mutant metastatic CRC (mCRC), identifying early efficacy biomarkers post-first-line chemotherapy is critical. Early tumor shrinkage (ETS) and depth of response (DpR) serve as quantifiable metrics for initial treatment assessment. At the 2024 Japanese Society of Medical Oncology (JSMO) conference, clinical data validated these parameters as prognostic surrogates in BRAF V600E-mutant mCRC patients undergoing first-line chemotherapy (22).

3.2 Treatment strategies

3.2.1 Chemotherapy combined with anti-VEGFR antibodies

The first-line treatment choice for mCRC patients is dual (FOLFIRI/FOLFOX/CAPOX) or triple (FOLFOXIRI) chemotherapy combined with bevacizumab (anti-VEGFR antibody) (23). Subsequent studies have shown that triple chemotherapy increases toxicity compared to dual chemotherapy regimens, with almost no difference in actual efficacy (24). However, patients with right-sided CRC do benefit from triple chemotherapy regimens (25). Currently, the ESMO clinical practice guidelines recommend dual chemotherapy + bevacizumab for MSS-type BRAF V600E-mutated CRC patients, with triple chemotherapy + bevacizumab being reserved for special circumstances (such as tumors located on the right side).

3.2.2 BRAF inhibitors

Previous studies have indicated that BRAF inhibitors alone do not achieve satisfactory outcomes, as they can lead to feedback activation of EGFR and reactivation of the MAPK pathway. Therefore, the combination of the BRAF inhibitor encorafenib with the anti-EGFR antibody cetuximab is considered the optimal choice for second-line treatment in MSS-type BRAF-mutated mCRC patients (23). Recently, a study added nivolumab to the above regimen and investigated the outcomes of combination therapy. The current results show that combination therapy is more effective and well-tolerated by patients (26).

3.2.3 Immunotherapy

About 70% of BRAF mutation tumors belong to CMS1 type, suggesting that MSI-H mCRC patients with BRAF mutations may benefit from immunotherapy (27). KEYNOTE-177 and CHECKMATE 142 evaluated the efficacy of pembrolizumab and nivolumab monotherapy in BRAF-mutant MSI-H mCRC patients, respectively. The results showed that immunotherapy was more effective than traditional therapy (28, 29). CheckMate-142 also evaluated the efficacy of ipilimumab + nivolumab combination therapy, and the results showed that the combination therapy was more effective than nivolumab alone (30). In addition, when relatlimab was used in combination with PD-1 blockade, it significantly slowed CRC tumor formation in mice (31). Therefore, we speculate that anti-LAG-3 monoclonal antibodies may enhance the efficacy of immune checkpoint inhibitors (ICIs) in CRC patients.

4 KRAS

The RAS protein family, classified as small GTPases, comprisesHRAS, NRAS, and KRAS, which are among the most commonly mutated genes in human cancers. In colorectal cancer, KRAS mutations are the most common (43%), followed by NRAS (9%) and HRAS (1%).

Kirsten rat sarcoma viral (KRAS), also known as the P21 gene, is a commonly mutated gene in cancer. In KRAS mutations, 97% (to be verified) involve mutations in the 12th or 13th amino acid residues, with the most common being G12D, G12V, and G13D mutations. KRAS mutations are more common in the right colon and are associated with advanced disease stage, poorly differentiated tumors, distant metastasis, and poorer survival rates. They are also more common in females and younger patients (32). Additionally, KRAS mutations are associated with shorter time to recurrence (TTR), recurrence-free survival (SAR), and OS in patients with non-microsatellite instability (MSI) tumors (33).

4.1 Prognostic value

KRAS mutations are closely associated with the occurrence and development of CRC, with studies indicating that patients with KRAS-mutant CRC generally have a worse prognosis compared to those with wild-type KRAS. Prognostic heterogeneity exists across mutation subtypes: One study showed that mutations in codon 12 were significantly correlated with both OS and Disease-free survival (DFS), particularly G12D and G12V mutations (34). Meanwhile, G12C mutations may represent a poorer prognosis, while the prognosis for patients with G12D mutations may fall between wild-type and G12C mutations (35). The prognostic significance of mutations in codon 13 remains controversial (34). A study based on the double-blind, controlled, phase 3 RECURSE trial and using two independent datasets demonstrated that codon-specific KRAS mutations could predict the clinical benefits of patients with mCRC receiving chemotherapy with trifluridine/tipiracil (FTD/TPI): patients with KRASG12 mutations did not benefit significantly from FTD/TPI chemotherapy in terms of OS, whereas KRASG13 mutations represented a poorer prognosis and had better efficacy with FTD/TPI (36). Rare variants (e.g., G12F, G13C) remain understudied, with limited data on their clinical implications.

4.2 Predictive value

KRAS mutations are also considered predictive markers for poor response to chemotherapy combined with anti-EGFR treatment: this is because when KRAS mutates, it remains in a constitutively active state by continuously binding to GTP, thereby bypassing the activating effect of EGFR ligands. However, not all KRAS mutations confer resistance to anti-EGFR treatment. Previous studies have shown that colorectal cancer patients with G13D mutations benefit from first-line chemotherapy plus cetuximab, but their progression-free survival (PFS), OS, and response rates(RR) are still lower than those of patients with wild-type KRAS tumors (37). Currently, the combination of bevacizumab (anti-VEGFR) with chemotherapy is considered the best first-line treatment for patients with KRAS-mutant mCRC (38).

4.3 Treatment strategies

4.3.1 Direct inhibition

Currently, directly inhibiting the KRAS gene is highly challenging for several reasons. Firstly, due to the exceptionally

high affinity of KRAS for GTP and GDP, developing a competitive small molecule inhibitor is extremely difficult. Secondly, KRAS has a broad range of functions, and inhibiting KRAS may lead to significant toxicity. Moreover, designing a drug that selectively inhibits mutated KRAS without affecting normal KRAS is not straightforward. Presently, two KRASG12C inhibitor: Adagrasib and Sotorasib, have shown significant efficacy in non-small cell lung cancer, but their efficacy in CRC remains limited (39, 40). However, when used in combination with other drugs, such as adagrasib combined with cetuximab (response rate 43%, disease control rate 100%), the efficacy is remarkably improved (41). Similarly, sotorasib in combination with panitumumab also has a beneficial effect on improving patient prognosis (42). Studies have also evaluated the effects of KRASG12C inhibitors combined with anti-PD-L1 therapy and found that the combination leads to a further increase in the number of CD3+ T cells and CD8+ T cells in patients, offering a promising therapeutic approach (43).

4.3.2 Nucleotide exchange inhibitors

Recently, researchers have discovered BAY-293, which is an inhibitor that disrupts the binding of SOS1 protein to KRAS. Meanwhile, BI-3406 is a more effective and selective SOS1 inhibitor that only inhibits SOS1 without affecting SOS2 (44). SHP2 inhibitors, similar to SOS1 inhibitors, can prevent the loading of GTP on RAS. Currently, SHP2 inhibitors are in the early stages of clinical trials, such as rmmc-4630 and TNO155, with TNO155 found to enhance the efficacy against KRASG12C-mutant CRC when used in combination with KRASG12C covalent inhibitors (45). Both types of inhibitors can suppress tumor growth, and experiments targeting these inhibitors are currently underway.

4.3.3 Inhibiting KRAS-related signaling pathways

Inhibiting the KRAS-related signaling pathway is another approach for treating patients with KRAS-mutant CRC. RAF is a direct downstream effector of KRAS, and selective inhibition of RAF may have limited therapeutic efficacy due to feedback loops or RAF dimerization activating MEK (46). Therefore, the therapeutic effect of selective RAF inhibition is limited. Researchers have utilized pan-RAF inhibitors that block RAF dimer-dependent signaling, such as belvarafenib, which has shown promising anti-tumor activity (47). In addition, MEK inhibitors such as Selumetinib, Trametinib, cobimetinib, have demonstrated good efficacy, but MEK inhibitors may have significant toxicity issues that need to be addressed, and simultaneous inhibition of RAF and MEK may be a better treatment option. Furthermore, inhibiting ERK1/2 may overcome the limitations of upstream RAF or MEK inhibitors, and LY3214996 (an ERK1/2 inhibitor) has shown promising anti-tumor activity in preclinical studies and acceptable safety in trials, further supporting its efficacy as monotherapy or in combination therapy (48, 49). Inhibiting the PI3K-AKT-mTOR pathway is another effective approach: the triple combination of PI3K inhibitor alpelisib + encorafenib (a BRAF inhibitor) + cetuximab (anti-EGFR monoclonal antibody) has shown encouraging results in mCRC patients (50). It is worth noting that most mTOR inhibitors have poor efficacy as monotherapy (51).

Inhibiting one pathway can lead to compensatory activation of another pathway, so simultaneously inhibiting MAPK/PI3K is a promising strategy. Given compensatory pathway activation during single-target inhibition, concurrent MAPK/PI3K blockade emerges as a rational strategy. While preclinical models support PI3K/MEK inhibitor synergy against KRAS-mutant tumors (52). However, in recent clinical trials, the tolerability and activity of these inhibitor combinations have not been satisfactory (53).

Other emerging therapeutic approaches, such as targeting tumor metabolism processes, KRAS-targeted siRNA, anti-RAS vaccines, offer hope for inhibiting tumor growth and providing a potential treatment option for KRAS-mutant colorectal cancer. However, their clinical efficacy remains to be further validated.

5 MSI

Microsatellite Instability (MSI) refers to a type of repetitive DNA sequences present in the human genome. Due to the high-frequency repeats of these sequences, errors are prone to occur during replication, and cells rely on DNA mismatch repair proteins (MMR) to correct these errors. However, when MMR function is deficient (dMMR), replication errors in microsatellites cannot be corrected, leading to the accumulation of sequence length or composition changes, resulting in microsatellite instability (MSI). Based on the detection of loci, MSI is classified into MSS, MSI-L, and MSI-H. Previous studies have shown that MSI-L has no significant biological differences compared to MSS tumors, so MSI-L is often grouped with MSS in clinical practice.

5.1 The correlation with pathological features

dMMR/MSI-H CRCs are more commonly found on the right side, mostly presenting as mucinous adenocarcinomas, and are closely associated with poorly differentiated tumors (54). Researchers have observed an increased occurrence of BRAF mutations in advanced dMMR/MSI-H CRC tumors. In fact, preclinical data suggests that the BRAF V600E mutation can promote the dMMR/MSI-H phenotype by activating the MAPK pathway. Additionally, influenced by the tumor microenvironment (TME), approximately 70% of dMMR/MSI-H CRCs cluster within the CMS1 subtype (55).

5.2 Prognostic value

dMMR/MSI-H is more commonly observed in the early stages of tumors, which may be due to the high tumor mutational burden (TMB) in early-stage colorectal cancer generating abundant neoantigens, activating CD8+ T cell infiltration, forming an immunogenic microenvironment that inhibits tumor progression. However, when tumors metastasize, dMMR/MSI-H becomes a negative prognostic factor, which may be related to the confounding effect of BRAF mutations: in advanced MSI-H CRC, the BRAF V600E

mutation rate reaches up to 20%, suggesting that this prognostic difference may be driven by BRAF mutations rather than MSI itself.

5.3 Treatment strategies

Although colorectal cancer patients with MSI-H generally exhibit favorable responses to ICIs such as anti-PD-1, PD-L1, or CTLA-4 antibodies (56), emerging evidence has revealed critical modifying factors: 1. Spatial heterogeneity: Ascites-associated peritoneal metastases significantly diminish ICI efficacy, likely resulting from the interplay between malignant ascites and an immunosuppressive tumor microenvironment (57); 2. Microbiome interference: The use of broad-spectrum antibiotics (ATBs) negatively impacts ICI therapeutic efficacy, potentially due to their disruption of the gut microbiota and consequent adverse effects on immune function (58), Conversely, leveraging gut microbiota to enhance immunotherapy shows promise; for instance, Fusobacterium nucleatum has been shown to potentiate the anti-tumor effects of PD-L1 blockade in colorectal cancer (59). These findings challenge the paradigm of MSI-H as a standalone predictive biomarker and underscore the necessity of adopting a composite biomarker strategy.

6 MSS

Microsatellite Stable (MSS) refers to a phenotype in colorectal cancer (CRC) where microsatellite sequences maintain stable length and composition during replication, with its pathogenesis being closely associated with proficient mismatch repair (pMMR) functionality. Unlike MSI-H/dMMR-type CRC, MSS/pMMR tumors exhibit low tumor mutational burden (TMB) and reduced immune cell infiltration within the tumor microenvironment (TME), typically manifesting as a 'cold tumor' phenotype. These characteristics result in poor response to immune checkpoint inhibitor monotherapy (60).

6.1 The correlation with pathological features

MSS-type CRC accounts for about 85% to 90% of all colorectal cancers, mostly found in the left half of the colon and rectum, and the histology is predominantly adenocarcinoma with a high degree of differentiation. Notably, the immune microenvironment of MSS-type CRC is dominated by suppressive immune cells (e.g., T regulatory cells, M2-type macrophages), and the expression level of PD-L1 is generally low, leading to active immune escape mechanisms (61).

6.2 Prognostic value

The prognosis of MSS-type CRC is strongly correlated with tumor stage and tumor microenvironment (TME) characteristics. While early-stage MSS patients demonstrate comparable survival outcomes to MSI-H cases, advanced-stage MSS patients exhibit significantly poorer survival rates than their MSI-H counterparts, potentially attributable to chemotherapy resistance and immunosuppressive TME. Recent studies have identified tumor-infiltrating lymphocyte (TIL) density as a critical prognostic biomarker in MSS CRC: Compared with MSI-TIL-H subtypes, MSS-TIL-H patients maintain microsatellite stability yet paradoxically demonstrate superior survival advantages. Specifically, MSS-TIL-H patients show significantly improved overall survival (HR = 0.53) and disease-free survival (HR = 0.52) compared to MSS-TIL-L subgroups (62). This finding highlights that elevated TIL infiltration confers substantial survival benefits even within the MSS context.

6.3 Treatment strategies

Modulating the immune microenvironment of MSS colorectal cancer to convert 'cold tumors' into 'hot tumors' has become particularly crucial in refractory MSS-type CRC, especially for advanced metastatic patients. Current clinical strategies to enhance immunotherapy efficacy in CRC primarily focus on two approaches: 1. Combination Therapies: ①Immune-targeted combinations: Emerging evidence suggests fruquintinib (a VEGFR inhibitor) combined with PD-1 inhibitors represents a promising therapeutic option for refractory MSS metastatic CRC (mCRC), demonstrating tolerable toxicity. Notably, incorporation of local therapies in patients with liver metastases may significantly extend overall survival (OS) (63). ②Dual immunotherapy: Early-phase trials indicate that botensilimab (BOT, a multifunctional CTLA-4 inhibitor) combined with balstilimab (BAL, a PD-1 blocker) achieves durable responses and prolonged OS across all subgroups while maintaining a favorable safety profile (64); 2. Biomarker-driven Strategies:Identification of predictive molecular biomarkers for immunotherapy response in MSS CRC, including previously discussed tumor-infiltrating lymphocytes (TILs), POLE/POLD mutations, and tumor mutational burden (TMB). These biomarkers may enable patient stratification to optimize therapeutic outcomes.

7 CMS

The Consensus Molecular Subtypes (CMS) is a widely used molecular classification method in colorectal cancer, which divides tumors into four subgroups (CMS1-4) based on mRNA gene expression patterns:CMS1 (MSI immune subtype): Associated with MSI, dDNA mismatch repair, BRAF V600E mutation, hypermutation (Abnormally accelerated gene mutation rates, often in immune cells to rapidly generate antibody variants), CIMP, and primarily observed in females. These tumors have higher histopathological grades and poorer survival rates after recurrence.CMS2 (Canonical subtype): Characterized by chromosomal instability, immune desert (Tumor regions with minimal immune cell presence), TP53 mutation, and upregulation of the EGFR pathway. Tumors in this subtype are typically located on the left side.CMS3 (Metabolic subtype): Typically characterized by abnormalities in metabolic pathways, KRAS mutation, and lower levels of CIMP and CIN.CMS4

(Mesenchymal subtype): Characterized by upregulation of EMT and SCNA, chromosomal instability, and constitutive activation of VEGFR and TGF-β pathways. CMS4 tumors are primarily associated with advanced stages (III and IV).CMS1 and CMS4 are associated with immune infiltration and considered "hot" tumors, while CMS2 and CMS3 are the opposite, characterized as "cold" tumors in terms of immune response.

7.1 Prognostic value

7.1.1 Local

The PETACC-3 study found that compared to other subtypes, CMS4 subtype has a significantly worse prognosis, and the same conclusion was drawn after adjusting for KRAS, BRAF, and MSI status (65). This may be related to the higher expression levels of monocytes, lymphocytes, and inflammatory and immune suppressive characteristic factors in the CMS4 subtype.

7.1.2 Metastasis

If the tumor metastasizes distantly, CMS1 exhibits the worst prognosis in terms of OS and PFS compared to other subtypes, consistent with its higher BRAF V600E mutation rate and the negative prognostic impact of MSI (66). CMS2 generally has a better prognosis, while the prognosis of CMS3 and CMS4 falls between the two (66).

7.2 Predictive value

7.2.1 Chemotherapy

Research indicates that CRC patients with the CMS3 subtype only benefit from chemotherapy in stage III ($p = 0.001$), while patients with the CMS2 subtype (stage II and III) show improved survival rates after receiving adjuvant chemotherapy ($p = 0.02$ and $p < 0.001$) (67). However, CMS1/CMS4 subtypes show no survival advantage from adjuvant chemotherapy (68).

7.2.2 Targeted therapy

The FIRE-3 trial included 514 mCRC patients who were randomly assigned to receive first-line treatment with FOLFIRI plus bevacizumab or cetuximab. The results revealed a better prognosis for CMS2 (29 months), while CMS4 (24.8 months) and CMS3 (18.6 months) had intermediate prognoses. CMS1 subgroup showed the shortest survival, with only 15.9 months (69). Consistent conclusions were drawn by the CALGB/SWOG 80405 trial, which also found that compared to FOLFIRI plus cetuximab, bevacizumab treatment was more effective for CMS1 tumors. This is consistent with their characteristics: CMS1 is more commonly associated with BRAF mutations or RAS mutations, which lead to resistance to anti-EGFR therapy, making patients more responsive to bevacizumab. Conversely, a completely opposite scenario was observed in the CMS2 subtype, which may be because CMS2 is more common in left-sided tumors, where anti-EGFR drugs are more effective (70).

CMS3 tumors can also benefit from treatment with bevacizumab plus capecitabine, with significant improvements in both PFS and OS (71). In CMS4, patients receiving bevacizumab plus FOLFIRI often experience better PFS and OS compared to chemotherapy alone. However, when bevacizumab is replaced with capecitabine, patients show better prognosis (71).

A recent study from Panama included 296 RAS wild-type mCRC patients and evaluated the efficacy of panitumumab (Pmab) plus fluorouracil/leucovorin (FU/FA) in various CMS types. The results showed beneficial outcomes with Pmab + FU/FA in CMS2/4 tumors, while no efficacy was observed in CMS1/3 tumors (72).

7.2.3 Immune therapy

Given the characteristics of CMS1 subtype, (ICIs) may be an effective approach for treating patients with this subtype. A study presented at ASCO GI 2022 demonstrated that combining Nivolumab with standard treatment in CMS1 and CMS3 subtypes could potentially yield clinical benefits (73).

8 Circulating tumor DNA

The small fragments of DNA released into the bloodstream after cell apoptosis or necrosis are called circulating free DNA (cfDNA), among which DNA released by tumor cells is referred to as circulating tumor DNA (ctDNA). Liquid biopsy utilizes peripheral blood extraction for ctDNA analysis, enabling real-time monitoring of tumor evolution. This approach provides three key advantages over conventional biopsies:1. Minimally invasive procedure; 2. Flexible temporal sampling; 3. Simplified specimen storage (Figure 2). Currently, ctDNA serves as a powerful biomarker closely associated with patient prognosis and can predict recurrence in CRC patients. Additionally, ctDNA detection can provide relevant molecular profiles (such as RAS/RAF/HER), replacing tissue sequencing to guide subsequent treatment.

8.1 Prognostic value

In 2019, literature reported on the prognostic role of ctDNA in stage I-III CRC patients. The study included 125 patients and collected a total of 829 plasma samples. The findings revealed that patients positive for ctDNA, whether postoperative or post-ACT (adjuvant chemotherapy), were associated with a high risk of recurrence. Moreover, patients negative for ctDNA had a significantly better prognosis compared to ctDNA-positive patients, with ctDNA proving to be a more valuable prognostic indicator than radiological parameters (74). Gong Chen and colleagues confirmed this conclusion, demonstrating that even after adjusting for known clinical and pathological risk factors, ctDNA positivity remained the most important independent predictor of disease-free survival in stage II-III colorectal cancer patients (75). It's worth noting that only postoperative ctDNA minimal residual disease (MRD) can predict the prognosis of postoperative CRC patients, even identifying those at high risk of recurrence, while preoperative ctDNA testing cannot predict patient prognosis (76). Another study, which merged patient data from three studies and had a follow-up period exceeding 5 years,

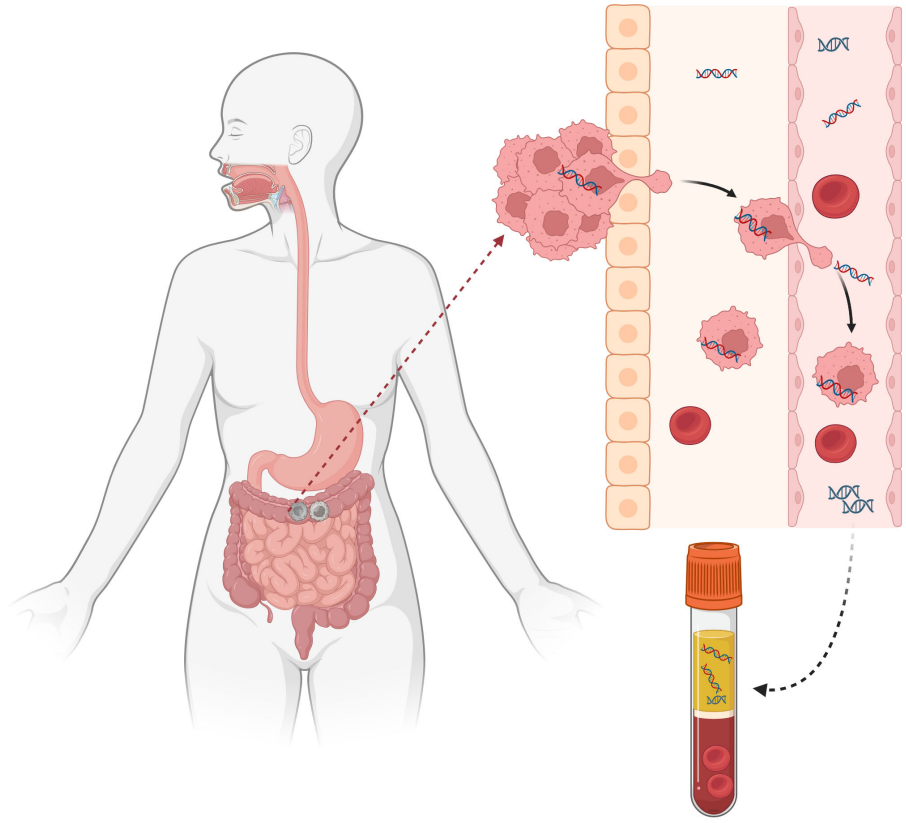

FIGURE 2
Liquid biopsy.

confirmed the prognostic value of ctDNA. It found that ctDNA had higher predictive accuracy for recurrence-free survival (RFS) compared to individual clinical and pathological risk factors. When combined with all clinical variables, ctDNA significantly improved the accuracy of recurrence prediction (77).

8.2 Predictive value

ctDNA serves not only as a prognostic marker in colorectal cancer (CRC) but recent research suggests it may also function as a predictive biomarker for treatment response. A study on IDEA-France's post hoc analysis revealed that irrespective of clinical high-risk factors, stage III CRC patients positive for ctDNA had better outcomes with a 6-month chemotherapy regimen compared to 3 months (78). To evaluate whether a ctDNA-guided approach could reduce adjuvant chemotherapy use without compromising recurrence risk, researchers, led by Jeanne, randomly allocated 441 stage II colon cancer patients in a 2:1 ratio based on ctDNA and clinical-pathological characteristics to guide treatment decisions. The results showed that ctDNA-negative patients maintained high 2-year disease-free survival (DFS) without adjuvant chemotherapy. Additionally, although the proportion of patients receiving adjuvant chemotherapy was lower in the ctDNA-guided group, it did not affect survival, and the efficacy was non-inferior to the standard management (79).

A study based on the phase III PARADIGM trial explored the predictive value of ctDNA negativity for RAS wild-type mCRC patients regarding panitumumab selection (no predefined resistant gene mutations detected). Findings suggest that ctDNA-guided molecular selection (rather than primary tumor location) identifies patients likely to benefit from first-line panitumumab-chemotherapy combinations (80). A recent study found that ctDNA may predict treatment choice for gastrointestinal stromal tumors (GISTs) treated with either ripretinib or sunitinib. Analysis of KIT exon mutations in peripheral blood ctDNA showed better efficacy with sunitinib in patients with KIT exon 11 + 13/14 mutations, while patients with KIT exon 11 + 17/18 mutations had better progression-free survival (PFS) with ripretinib (81).

Furthermore, ctDNA also has the ability to predict the emergence of acquired resistance, being more convenient and sensitive than traditional tumor biopsies. For example, ctDNA exhibits higher sensitivity to acquired RAS mutations, allowing us to exploit this advantage to circumvent acquired resistance to anti-EGFR therapy. The NCT04776655 trial is a prospective randomized phase III study based on ctDNA aimed at evaluating the optimal monoclonal antibody therapy in mCRC patients with RAS/BRAF wild-type and liquid biopsy RAS mutations. In addition to anti-EGFR drugs, ctDNA has been validated to have predictive value in targeted therapies such as anti-HER-2, anti-BRAF/EGFR, and KRASG12C-directed therapies (2, 82, 83). On the other hand, (ICIs), as emerging treatments in recent

years, are also closely associated with ctDNA. The ARETHUSA clinical trial treated pMMR, RAS-mutated mCRC patients with temozolomide (TMZ). Analysis of ctDNA showed that TMZ treatment resulted in MMR deficiency, increased TMB, increased sensitivity to immune therapy, and ctDNA can accurately measure blood TMB (bTMB) and predict the efficacy of pembrolizumab, similar to previous Canadian study results. Thus, ctDNA can be considered a marker for assessing TMZ efficacy (84).

9 Non-coding RNA

Non-coding RNAs (ncRNAs) comprise >90% of the human transcriptome despite lacking protein-coding capacity. These molecules critically regulate protein biosynthesis, cellular homeostasis, and transcriptional networks. Mounting evidence implicates ncRNAs—particularly microRNAs (miRNAs), long noncoding RNAs (lncRNAs), and circular RNAs (circRNAs)—in colorectal carcinogenesis and progression.

Mechanistically, ncRNAs modulate colorectal cancer phenotypes via STAT3 pathway regulation and epithelial-mesenchymal transition (EMT) modulation. Their dysregulated expression patterns have emerged as multifunctional biomarkers for prognosis prediction, therapy response assessment, and drug resistance targeting in colorectal cancer.

9.1 MicroRNA

MicroRNAs (miRNAs) are non-coding, single-stranded short RNA sequences that regulate gene expression and influence biological behaviors such as cell proliferation, differentiation, and apoptosis. Both low and high expression of miRNAs can potentially impact the initiation, progression, and prognosis of tumors. Certain miRNAs have been demonstrated to be associated with the clinical and pathological characteristics of colorectal cancer (CRC) patients. For instance, compared to healthy individuals and benign adenomas, miR-874 is downregulated in CRC patients, and its downregulation is associated with advanced tumor stage, lymph node metastasis, and distant metastasis, serving as an independent prognostic factor for CRC (85). Wang et al., through ROC curve analysis, found that miR-377-3p and miR-381-3p can serve as diagnostic biomarkers for early-stage CRC (86). Additionally, the combination of miRNA and CEA for CRC diagnosis has been shown to improve diagnostic accuracy, such as the combination of miR-150-5p and CEA (87).

The miRNA/STAT3 axis regulates CRC tumors by influencing EMT, thereby affecting patient prognosis. For example, upregulation of miR-34a, miR-200b, miR-27a, and miR-330 can decrease the proliferation and invasion capacity of CRC tumor cells (88, 89). However, miR-22 serves as a crucial regulatory factor; it downregulates MAX to inhibit EMT and consequently suppresses the expression of NLRP3, leading to reduced invasive and metastatic abilities of CRC (90). On the contrary, the high expression of certain miRNAs can promote EMT and thus facilitate the progression and metastasis of CRC (such as miR-645) (91).

Furthermore, miRNAs have good predictive value for chemotherapy resistance in CRC patients. In recent years, it has been discovered that overexpression of HIF-1α under hypoxia can intervene in patients' resistance to oxaliplatin by reducing the level of miR-338-3p in the blood (92). In 2021, Chinese scholars found that upregulation of miR-208b can target PDCD4, enhancing patients' resistance to oxaliplatin (93).

9.2 Long non-coding RNA

Long non-coding RNAs (lncRNAs) are relatively stable and can participate in tumor progression through various pathways, including competitive inhibition with miRNAs, regulation of tumor cell stemness, influence on RNA-binding proteins, and intervention in cell autophagy. Therefore, they can serve as biomarkers for diagnosis, prognosis, and prediction in CRC.

9.2.1 The correlation with pathological features and prognostic value

Compared to healthy individuals, many CRC patients exhibit significantly elevated levels of serum lncRNAs, which are often associated with poorer prognosis. One representative example is Colorectal Cancer Associated Transcript (CCAT), whose overexpression has been shown to correlate with increased tumor invasiveness and lymph node metastasis. RPPH1 is another lncRNA confirmed to be associated with clinical pathological features, with its high expression in tumor tissues correlating with later stage and poorer prognosis, both of which can serve as diagnostic and prognostic markers. Other lncRNAs found to be associated with TNM staging include GLCC1, which, when combined with TNM staging, can more accurately analyze CRC prognosis.

9.2.2 Predictive value

LncRNAs can promote or inhibit EMT, thereby affecting the occurrence and development of CRC and patient prognosis. Some lncRNAs can induce EMT and promote colorectal cancer invasion and metastasis by regulating miRNAs. For example, lncRNA CASC21 (94) and lncRNA XIST (95) can downregulate their target miRNAs. Therefore, targeting the lncRNA/EMT axis holds promise as a new therapeutic approach for treating CRC patients. Additionally, lncRNAs have predictive value for treatment selection. For instance, MIR100HG, UCA1, CRART16, SLCO4A1AS1, and TTN-AS1, whose high expression can enhance patient sensitivity to cetuximab and panitumumab (96). In 2022, Qiu et al. combined H&E images with deep learning and found significant differences in mRNA, miRNA, and lncRNA between MSI-H and MSI-L/MSS patient groups (97). Also in the same year, a study found that LINC00963 is highly expressed in CRC patients and is associated with increased response to MSI-H and immunotherapy (98). LncRNAs are also associated with genes related to KRAS mutations. Additionally, lncRNAs interact with KRAS-mutant pathways: An Iranian cohort study identified 12 prognosis-linked lncRNAs (including SSTR5-AS1 and RASSF8-AS1) that modulate Rap1/RAS signaling networks (99).

9.3 Circular RNA

Circular RNAs (circRNAs) are a type of RNA with a more stable covalently closed-loop structure, which functions include acting as miRNA sponges, interacting with mRNA, regulating transcription, and protein translation. Currently, there are various methods for detecting circRNAs, such as reverse transcription quantitative polymerase chain reaction (RT-qPCR), droplet digital PCR (ddPCR), microarray analysis, RNA sequencing (RNA-seq), Northern blotting, fluorescence in situ hybridization (FISH), NanoString technology, and more. Increasing evidence suggests that circRNAs play a crucial role in the pathological and physiological functions (such as proliferation, migration, etc.) and drug resistance of tumor cells.

9.3.1 Prognostic value

There are significant differences in circRNA expression between normal tissues and colorectal cancer tissues. For example, circHERC4 is upregulated in colorectal cancer tissues and positively correlated with advanced tumor stage (100). Conversely, circPLCE1 is downregulated in colorectal cancer tissues and associated with poorer prognosis and advanced clinical stage (101). In a study involving 1430 colorectal cancer patients, it was found that the differential expression of circRNAs in cancer tissues is often associated with tumor size, differentiation, TNM staging, invasiveness, lymph node, and distant metastasis. Patients with low circRNA expression tend to have better prognosis and longer survival, while the opposite is true for those with high expression (102). These findings confirm the significant potential of circRNAs as diagnostic and prognostic markers. Additionally, some circRNAs have been found to effectively predict the resistance to colorectal cancer treatment, such as circ_0000236 (103) and circ-ZEB1 (104), which are associated with chemotherapy resistance in CRC. circLHFPL2 and circIFNGR2 are significantly associated with resistance to cetuximab and MEK inhibitors (105, 106).

9.3.2 Predictive value

CircRNAs associated with tumor cells may become new therapeutic targets. Animal experiments have shown that short hairpin RNAs (shRNAs) targeting circMETTL3 can inhibit tumor growth and metastasis (107). Many other animal experiments have confirmed this viewpoint, indicating that targeting cancer-related shRNAs or small interfering RNAs (siRNAs) may inhibit the occurrence and development of colorectal cancer and become a potential treatment method (107, 108). Recent research suggests that CTLA4 in combination with some shRNAs (sh-circQSOX1) can effectively reduce the resistance of colorectal cancer immunotherapy (109). Additionally, targeting circRNA with antisense oligonucleotides (ASOs) can reduce the invasion and metastasis of CRC (110). Innovative treatment strategies include using engineered exogenous circRNAs (cloning circRNA into a virus and transfecting CRC cells) as molecular sponges for oncogenic miRNAs to inhibit tumor growth (111) and developing new circRNA vaccines (such as recently discovered SARS-CoV-2 circRNA vaccines) (112).

10 POLE/POLD1 mutation

POLE and POLD1 are genes that encode the catalytic subunits of DNA polymerase ε and DNA polymerase δ, respectively. Pathogenic variants (PVs) within their exonuclease domain (ED) can lead to loss of cell proofreading function and the generation of numerous neoantigens, resulting in a better response to immunotherapy. However, not all mutations located within the exonuclease domain are meaningful. Currently, common and pathogenic hotspot mutations include P286R, V411L, S297F, A456P, and S459F. In recent years, researchers have discovered some mutations that are pathogenic despite not being located within the exonuclease domain, such as POLE V1368M (113).

10.1 The correlation with pathological features

Earlier studies analyzing 6517 CRC patients found that POLE somatic mutations are more common in males, right-sided colon cancer, and early-stage patients, and are associated with a favorable prognosis (114). However, in recent years, Hu et al. discovered for the first time that different regions may significantly influence the primary sites of POLE-driven mutations: in the Asian population, POLE-driven mutations are more likely to occur in the left colon (left vs. right: 77.78% vs. 11.11%), while non-Asian patients are more likely to occur in the right colon (115).

10.2 The relationship with MSI

Similar to MSI-H tumors, tumors with POLE/POLD1 mutations generally exhibit high tumor mutation burden (TMB). However, the mutations in the latter generally exceed 100 mut/Mb, also known as hypermutation. Moreover, most colorectal cancers with POLE/POLD1 mutations exhibit a microsatellite stable (MSS) phenotype. Compared to patients with POLE wild-type or non-exonuclease domain mutations (POLE non-EDMs), patients with POLE EDMs have a higher frequency of MSI-H (115). However, there is still some controversy regarding the sequence of occurrence of MSI-H and POLE/POLD1 mutations in tumors. The current mainstream view seems to favor POLE mutations as the driving factor of dMMR/MSI-H (116). However, some scholars hold the opposite view, suggesting that dMMR can significantly increase TMB in tumors by affecting POLE function (117). More research is still needed to confirm the exact order of occurrence of the two.

10.3 Predictive value and treatment strategies

POLE/POLD1 has been recognized as a biomarker for CRC therapy. In a retrospective study, patients with pathogenic POLE/POLD1 mutations who received PD-1/PD-L1 monotherapy or combination therapy with CTLA-4 inhibitors showed significantly higher clinical benefit rates and improved survival outcomes compared to patients with benign mutations (113). Another study involving over 2500 patients found that 75% of tumors with

pathogenic POLE/POLD1 mutations responded well to ICI therapy, either achieving remission or showing significant improvement in prognosis post-immunotherapy Functional landscapes of pole and pold1 mutations in checkpoint blockade-dependent antitumor immunity. In a survival analysis of stage II CRC patients, those carrying POLE ED mutations had excellent prognosis regardless of MSI status. Thus, POLE/POLD1 mutations can be considered as a biomarker independent of MSI-H/dMMR (118).

Considering the rarity of this mutation, there are still relatively few prospective clinical studies ongoing. Currently, a phase II clinical trial (NCT03810339) is underway, investigating the use of toripalimab in the treatment of advanced solid tumors with POLE/POLD1 mutations, with the hope of reaching conclusions soon.

11 RET fusions

RET is an oncogene that encodes a transmembrane receptor with a tyrosine kinase domain. Recent findings have linked RET to intestinal motility function, with its signaling persisting in the adult intestine. It can stimulate intestinal motility by limiting the release of PYY from enteroendocrine cells, and this mechanism primarily occurs in adult males (119, 120). Activation of RET can initiate downstream signaling pathways such as RAS/MAPK, PI3K/AKT, JAK–STAT, or JNK, leading to excessive cell proliferation and promoting tumorigenesis. RET activation mechanisms include mutations and fusions, each with distinct clinical and pathological features. Here, we focus on the clinical significance of RET fusions in CRC.

RET fusions are not common in colorectal cancer, accounting for less than 1%, but research on this mechanism is relatively abundant. In colorectal cancer, NCOA4-RET is the most common fusion variant, accounting for approximately 46%. RET fusion is associated with older age, right-sided colon location, RAS/BRAF wild-type, MSI-H, and worse prognosis, while also exhibiting a higher median TMB. Therefore, it can be identified as a distinct molecular subgroup of colorectal cancer (121). The 2024 V1 version of the colorectal cancer NCCN guidelines includes RET fusion genes as recommended biomarkers for testing. Therefore, testing for RET fusion genes in these "advantaged populations" can help determine the prognosis of mCRC patients and seek treatment opportunities. A multicenter, phase 1/2, basket study published in Nature Medicine included 45 patients with RET gene fusions (including 10 patients with colorectal cancer) and found significant anti-tumor activity of Selpercatinib in patients with RET fusion-positive advanced colorectal cancer. In addition to RET fusion (especially NCOA4), TMB, and TP53 mutation status may influence the efficacy of selpercatinib (122).

12 Conclusion

Currently, KRAS, BRAF, and MSI status play a crucial role in predicting resistance in CRC patients. Therefore, routine testing for these genes is necessary in CRC patients to determine subsequent treatment plans. Among these, MSI status has the highest relevance, as even advanced MSI CRC patients have a high chance of long-term survival after immunotherapy (29). Research on HER-2 in colorectal cancer is becoming increasingly profound, and its strong predictive ability is recognized. However, few drugs targeting HER-2 have been approved for use in colorectal cancer, making the development of anti-HER-2 drugs a current priority (123).

In recent years, new biomarkers have emerged, such as inflammation-related indicators like the lymphocyte-to-monocyte ratio (LMR), which not only predicts overall survival in colorectal cancer patients but also shows better predictive value than some conventional biomarkers like neutrophil-to-lymphocyte ratio (NLR), platelet-to-lymphocyte ratio (PLR), and modified Glasgow Prognostic Score (mGPS) (124). Intestinal microbiota such as Fusobacterium nucleatum has also been identified as a predictive biomarker for colorectal cancer (125). The emergence of consensus molecular subtypes can further divide CRC patients into different subgroups, providing better guidance for patient treatment and enabling more precise personalized treatment by doctors.

Furthermore, new biomarker detection methods are rapidly evolving, such as liquid biopsy, a minimally invasive method that can detect components of cancer tissue origin in the blood, allowing real-time monitoring of tumor dynamics. The detection of ctDNA and non-coding RNA may play important roles in predicting recurrence, monitoring metastasis, and guiding treatment. However, due to issues such as low molecular content from tumor sources and low mutation signal intensity, as well as the frequency of monitoring still under debate, their clinical application is not yet widespread. Recently, new research results similar to ctDNA were published in NEJM: blood cfDNA (sensitivity for colorectal cancer was 83%, for precancerous lesions was 13%) and a second-generation multi-target fecal DNA detection method (sensitivity for colorectal cancer was 93.9%, for precancerous lesions was 43.4%). The achievements of these two major studies signify significant progress in colorectal cancer detection technology and methods (126, 127). Other emerging biomarkers such as POLE/POLD1 and RET, though still in early validation phases, have expanded stratification and therapeutic approaches for colorectal cancer patients. Therefore, it may currently be necessary to integrate multiple biomarkers to design a novel predictive model that enhances and refines risk stratification in colorectal cancer and guides personalized treatment strategies. However, the critical challenge lies in integrating these biomarkers into clinical decision-making frameworks. Current evidence supporting their clinical utility remains limited, and more multicenter studies are required to assess the feasibility and safety of clinical translation for these biomarkers.

Considering that we are in the era of personalized medicine, focusing on biomarker detection and development, gaining a deeper understanding of potential mechanisms of treatment resistance, and developing new treatment targets are the major trends in future colorectal cancer research.

Author contributions

JZ: Writing – original draft. HZ: Writing – review & editing. WL: Writing – review & editing. JM: Conceptualization, Writing – review & editing. YM: Conceptualization, Writing – original draft, Writing – review & editing. QL: Conceptualization, Writing – original draft, Writing – review & editing.

Funding

The author(s) declare that financial support was received for the research and/or publication of this article. This work was supported by Nanjing Drum Tower Hospital Clinical Research Special Fund (HB3340202201, Q Li).

Conflict of interest

The authors declare that the research was conducted in the absence of any commercial or financial relationships that could be construed as a potential conflict of interest.

Generative AI statement

The author(s) declare that no Generative AI was used in the creation of this manuscript.

Publisher's note

All claims expressed in this article are solely those of the authors and do not necessarily represent those of their affiliated organizations, or those of the publisher, the editors and the reviewers. Any product that may be evaluated in this article, or claim that may be made by its manufacturer, is not guaranteed or endorsed by the publisher.

References

1. Siegel RL, Miller KD, Wagle NS, Jemal A. Cancer statistics, 2023. *CA Cancer J Clin*. (2023) 73:17–48. doi: 10.3322/caac.21763

2. Yaeger R, Weiss J, Pelster MS, Spira AI, Barve M, Ou SI, et al. Adagrasib with or without cetuximab in colorectal cancer with mutated kras G12c. *N Engl J Med*. (2023) 388:44–54. doi: 10.1056/NEJMoa2212419

3. Kraehenbuehl L, Weng CH, Eghbali S, Wolchok JD, Merghoub T. Enhancing immunotherapy in cancer by targeting emerging immunomodulatory pathways. *Nat Rev Clin Oncol*. (2022) 19:37–50. doi: 10.1038/s41571-021-00552-7

4. Akagi K, Oki E, Taniguchi H, Nakatani K, Aoki D, Kuwata T, et al. Real-world data on microsatellite instability status in various unresectable or metastatic solid tumors. *Cancer Sci*. (2021) 112:1105 – 13. doi: 10.1111/cas.v112.3

5. Raghav K, Loree JM, Morris JS, Overman MJ, Yu R, Meric-Bernstam F, et al. Validation of her2 amplification as a predictive biomarker for anti-epidermal growth factor receptor antibody therapy in metastatic colorectal cancer. *JCO Precis Oncol*. (2019) 3:1–13. doi: 10.1200/po.18.00226

6. Ingold Heppner B, Behrens HM, Balschun K, Haag J, Krüger S, Becker T, et al. Her2/neu testing in primary colorectal carcinoma. *Br J Cancer*. (2014) 111:1977–84. doi: 10.1038/bjc.2014.483

7. Qiu MZ, He CY, Yang XH, Yang LQ, Lin JZ, Zhou DL, et al. Relationship of her2 alteration and microsatellite instability status in colorectal adenocarcinoma. *Oncologist*. (2021) 26:e1161–e70. doi: 10.1002/onco.13786

8. Laurent-Puig P, Balogoun R, Cayre A, Malicot KL, Tabernero JM, Mini E, et al. Erbb2 alterations a new prognostic biomarker in stage iii colon cancer from a folfox based adjuvant trial (Petacc8). *Ann Oncol*. (2016) 27(Supplement 6):vi149–vi206. doi: 10.1093/annonc/mdw370.08

9. Yagisawa M, Sawada K, Nakamura Y, Fujii S, Yuki S, Komatsu Y, et al. Prognostic value and molecular landscape of her2 low-expressing metastatic colorectal cancer. *Clin Colorectal Cancer*. (2021) 20:113–20.e1. doi: 10.1016/j.clcc.2020.11.002

10. Conradi LC, Styczen H, Sprenger T, Wolff HA, Rödel C, Nietert M, et al. Frequency of her-2 positivity in rectal cancer and prognosis. *Am J Surg Pathol*. (2013) 37:522–31. doi: 10.1097/PAS.0b013e318272ff4d

11. Richman SD, Southward K, Chambers P, Cross D, Barrett J, Hemmings G, et al. Her2 overexpression and amplification as a potential therapeutic target in colorectal cancer: analysis of 3256 patients enrolled in the quasar, focus and piccolo colorectal cancer trials. *J Pathol*. (2016) 238:562–70. doi: 10.1002/path.4679

12. Raghav KPS, Guthrie KA, Tan B Jr., Denlinger CS, Fakih M, Overman MJ, et al. Trastuzumab plus pertuzumab versus cetuximab plus irinotecan in patients with ras/braf wild-type, her2-positive, metastatic colorectal cancer (S1613): A randomized phase ii trial. *J Clin Oncol*. (2025) JCO-24-01710. doi: 10.1200/jco-24-01710

13. Sawada K, Nakamura Y, Yamanaka T, Kuboki Y, Yamaguchi D, Yuki S, et al. Prognostic and predictive value of her2 amplification in patients with metastatic colorectal cancer. *Clin Colorectal Cancer*. (2018) 17:198–205. doi: 10.1016/j.clcc.2018.05.006

14. Yoshino T, Di Bartolomeo M, Raghav K, Masuishi T, Loupakis F, Kawakami H, et al. Final results of destiny-crc01 investigating trastuzumab deruxtecan in patients with her2-expressing metastatic colorectal cancer. *Nat Commun*. (2023) 14:3332. doi: 10.1038/s41467-023-38032-4

15. Meric-Bernstam F, Hurwitz H, Raghav KPS, McWilliams RR, Fakih M, VanderWalde A, et al. Pertuzumab plus trastuzumab for her2-amplified metastatic colorectal cancer (Mypathway): an updated report from a multicentre, open-label, phase 2a, multiple basket study. *Lancet Oncol*. (2019) 20:518–30. doi: 10.1016/s1470-2045(18)30904-5

16. Fu X, Ying J, Yang L, Fang W, Han W, Hu H, et al. Dual targeted therapy with pyrotinib and trastuzumab for her2-positive advanced colorectal cancer: A phase 2 trial. *Cancer Sci*. (2023) 114:1067–74. doi: 10.1111/cas.15660

17. Sartore-Bianchi A, Lonardi S, Martino C, Fenocchio E, Tosi F, Ghezzi S, et al. Pertuzumab and trastuzumab emtansine in patients with her2-amplified metastatic colorectal cancer: the phase ii heracles-B trial. *ESMO Open*. (2020) 5:e000911. doi: 10.1136/esmoopen-2020-000911

18. Sahin IH, Klostergaard J. Braf mutations as actionable targets: A paradigm shift in the management of colorectal cancer and novel avenues. *JCO Oncol Pract*. (2021) 17:723–30. doi: 10.1200/op.21.00160

19. Martinelli E, Cremolini C, Mazard T, Vidal J, Virchow I, Tougeron D, et al. Real-world first-line treatment of patients with braf(V600e)-mutant metastatic colorectal cancer: the capstan crc study. *ESMO Open*. (2022) 7:100603. doi: 10.1016/j.esmoop.2022.100603

20. Grassi E, Corbelli J, Papiani G, Barbera MA, Gazzaneo F, Tamberi S. Current therapeutic strategies in braf-mutant metastatic colorectal cancer. *Front Oncol*. (2021) 11:601722. doi: 10.3389/fonc.2021.601722

21. Jones JC, Renfro LA, Al-Shamsi HO, Schrock AB, Rankin A, Zhang BY, et al. (Non-V600) braf mutations define a clinically distinct molecular subtype of metastatic colorectal cancer. *J Clin Oncol*. (2017) 35:2624–30. doi: 10.1200/jco.2016.71.4394

22. Udagawa S, Osumi H, Ooki A, Wakatsuki T, Fukuoka S, Yoshino K, et al. Impact of early tumor shrinkage and depth of response in patients with braf V600e-mutant metastatic colorectal cancer. *J Clin Oncol*. (2024) 42:142. doi: 10.1200/JCO.2024.42.3_suppl.142

23. Cervantes A, Adam R, Roselló S, Arnold D, Normanno N, Taïeb J, et al. Metastatic colorectal cancer: esmo clinical practice guideline for diagnosis, treatment and follow-up. *Ann Oncol*. (2023) 34:10–32. doi: 10.1016/j.annonc.2022.10.003

24. Cremolini C, Antoniotti C, Stein A, Bendell J, Gruenberger T, Rossini D, et al. Individual patient data meta-analysis of folfoxiri plus bevacizumab versus doublets plus bevacizumab as initial therapy of unresectable metastatic colorectal cancer. *J Clin Oncol*. (2020) 38:3314–24. doi: 10.1200/jco.20.01225

25. Moretto R, Elliott A, Rossini D, Intini R, Conca V, Pietrantonio F, et al. Benefit from upfront folfoxiri and bevacizumab in brafv600e-mutated metastatic colorectal cancer patients: does primary tumour location matter? *Br J Cancer*. (2022) 127:957–67. doi: 10.1038/s41416-022-01852-0

26. Morris VK, Parseghian CM, Escano M, Johnson B, Raghav KPS, Dasari A, et al. Phase I/ii trial of encorafenib, cetuximab, and nivolumab in patients with microsatellite stable, brafv600e metastatic colorectal cancer. *J Clin Oncol*. (2022) 40:12. doi: 10.1200/JCO.2022.40.4_suppl.012

27. Ros J, Rodríguez-Castells M, Saoudi N, Baraibar I, Salva F, Tabernero J, et al. Treatment of braf-V600e mutant metastatic colorectal cancer: new insights and biomarkers. *Expert Rev Anticancer Ther*. (2023) 23:797–806. doi: 10.1080/14737140.2023.2236794

28. Overman MJ, McDermott R, Leach JL, Lonardi S, Lenz HJ, Morse MA, et al. Nivolumab in patients with metastatic DNA mismatch repair-deficient or microsatellite instability-high colorectal cancer (Checkmate 142): an open-label, multicentre, phase 2 study. *Lancet Oncol*. (2017) 18:1182–91. doi: 10.1016/s1470-2045(17)30422-9

29. Diaz LA Jr., Shiu KK, Kim TW, Jensen BV, Jensen LH, Punt C, et al. Pembrolizumab versus chemotherapy for microsatellite instability-high or mismatch repair-deficient metastatic colorectal cancer (Keynote-177): final analysis of a randomised, open-label, phase 3 study. *Lancet Oncol*. (2022) 23:659–70. doi: 10.1016/s1470-2045(22)00197-8

30. André T, Lonardi S, Wong KYM, Lenz HJ, Gelsomino F, Aglietta M, et al. Nivolumab plus low-dose ipilimumab in previously treated patients with microsatellite instability-high/mismatch repair-deficient metastatic colorectal cancer: 4-year follow-up from checkmate 142. *Ann Oncol*. (2022) 33:1052–60. doi: 10.1016/j.annonc.2022.06.008

31. Yu X, Huang X, Chen X, Liu J, Wu C, Pu Q, et al. Characterization of a novel anti-human lymphocyte activation gene 3 (Lag-3) antibody for cancer immunotherapy. *MAbs*. (2019) 11:1139–48. doi: 10.1080/19420862.2019.1629239

32. Dienstmann R, Mason MJ, Sinicrope FA, Phipps AI, Tejpar S, Nesbakken A, et al. Prediction of overall survival in stage ii and iii colon cancer beyond tnm system: A retrospective, pooled biomarker study. *Ann Oncol*. (2017) 28:1023–31. doi: 10.1093/annonc/mdx052

33. Taieb J, Le Malicot K, Shi Q, Penault-Llorca FM, Bouché O, Tabernero JM, et al. Prognostic value of braf and kras mutations in msi and mss stage iii colon cancer. *J Of Natl Cancer Institute*. (2017) 109:djw272. doi: 10.1093/jnci/djw272

34. Li W, Liu Y, Cai S, Yang C, Lin Z, Zhou L, et al. Not all mutations of kras predict poor prognosis in patients with colorectal cancer. *Int J Clin Exp Pathol*. (2019) 12:957–67.

35. Van Cutsem E, Cervantes A, Adam R, Sobrero A, Van Krieken JH, Aderka D, et al. Esmo consensus guidelines for the management of patients with metastatic colorectal cancer. *Ann Oncol*. (2016) 27:1386–422. doi: 10.1093/annonc/mdw235

36. van de Haar J, Ma X, Ooft SN, van der Helm PW, Hoes LR, Mainardi S, et al. Codon-specific kras mutations predict survival benefit of trifluridine/tipiracil in metastatic colorectal cancer. *Nat Med*. (2023) 29:605–14. doi: 10.1038/s41591-023-02240-8

37. De Roock W, Jonker DJ, Di Nicolantonio F, Sartore-Bianchi A, Tu D, Siena S, et al. Association of kras P.G13d mutation with outcome in patients with chemotherapy-refractory metastatic colorectal cancer treated with cetuximab. *Jama*. (2010) 304:1812–20. doi: 10.1001/jama.2010.1535

38. You XH, Jiang YH, Fang Z, Sun F, Li Y, Wang W, et al. Chemotherapy plus bevacizumab as an optimal first-line therapeutic treatment for patients with right-sided metastatic colon cancer: A meta-analysis of first-line clinical trials. *ESMO Open*. (2020) 5:e000605. doi: 10.1136/esmoopen-2019-000605

39. Hong DS, Fakih MG, Strickler JH, Desai J, Durm GA, Shapiro GI, et al. Kras (G12c) inhibition with sotorasib in advanced solid tumors. *N Engl J Med*. (2020) 383:1207–17. doi: 10.1056/NEJMoa1917239

40. Riely G, Ou S-HI, Rybkin II, Spira AI, Papadopoulos KP, Sabari JK, et al. 99o_Prkrystal-1: activity and preliminary pharmacodynamic (Pd) analysis of adagrasib (Mrtx849) in patients (Pts) with advanced non–small cell lung cancer (Nsclc) harboring krasg12c mutation. *J Thorac Oncol*. (2021) 16:S751–S752. doi: 10.1016/S1556-0864(21)01941-9

41. Weiss J, Yaeger RD, Johnson ML, Spira A, Klempner SJ, Barve MA, et al. Lba6 krystal-1: adagrasib (Mrtx849) as monotherapy or combined with cetuximab (Cetux) in patients (Pts) with colorectal cancer (Crc) harboring a krasg12c mutation. *Ann Oncol*. (2021) 32:S1294. doi: 10.1016/j.annonc.2021.08.2093

42. Fakih MG, Falchook GS, Hong DS, Yaeger R, Chan E, Mather O, et al. 434p codebreak 101 subprotocol H: phase ib study evaluating combination of sotorasib (Soto), a krasg12c inhibitor, and panitumumab (Pmab), an egfr inhibitor, in advanced kras P.G12c-mutated colorectal cancer (Crc). *Ann Oncol*. (2021) 32:S551. doi: 10.1016/j.annonc.2021.08.955

43. Canon J, Rex K, Saiki AY, Mohr C, Cooke K, Bagal D, et al. The clinical kras (G12c) inhibitor amg 510 drives anti-tumour immunity. *Nature*. (2019) 575:217–23. doi: 10.1038/s41586-019-1694-1

44. Hofmann MH, Gmachl M, Ramharter J, Savarese F, Gerlach D, Marszalek JR, et al. Bi-3406, a potent and selective sos1-kras interaction inhibitor, is effective in kras-driven cancers through combined mek inhibition. *Cancer Discovery*. (2021) 11:142–57. doi: 10.1158/2159-8290.Cd-20-0142

45. Liu C, Lu H, Wang H, Loo A, Zhang X, Yang G, et al. Combinations with allosteric shp2 inhibitor tno155 to block receptor tyrosine kinase signaling. *Clin Cancer Res*. (2021) 27:342–54. doi: 10.1158/1078-0432.Ccr-20-2718

46. Degirmenci U, Wang M, Hu J. Targeting aberrant ras/raf/mek/erk signaling for cancer therapy. *Cells*. (2020) 9:198. doi: 10.3390/cells9010198

47. Kim TW, Lee J, Shin SJ, Kim J-S, Kim YJ, Han HS, et al. Belvarafenib, a novel pan-raf inhibitor, in solid tumor patients harboring braf, kras, or nras mutations: phase I study. *J Clin Oncol*. (2019) 37:3000. doi: 10.1200/JCO.2019.37.15_suppl.3000

48. Pant S, Bendell JC, Sullivan RJ, Shapiro G, Millward M, Mi G, et al. A phase I dose escalation (De) study of erk inhibitor, ly3214996, in advanced (Adv) cancer (Ca) patients (Pts). *J Clin Oncol*. (2019) 37:3001. doi: 10.1200/JCO.2019.37.15_suppl.3001

49. Bhagwat SV, McMillen WT, Cai S, Zhao B, Whitesell M, Shen W, et al. Erk inhibitor ly3214996 targets erk pathway-driven cancers: A therapeutic approach toward precision medicine. *Mol Cancer Ther*. (2020) 19:325–36. doi: 10.1158/1535-7163.Mct-19-0183

50. van Geel R, Tabernero JM, Élez E, Bendell JC, Spreafico A, Schuler M, et al. A phase ib dose-escalation study of encorafenib and cetuximab with or without alpelisib in metastatic braf-mutant colorectal cancer. *Cancer Discovery*. (2017) 7 6:610–9. doi: 10.1158/2159-8290.CD-16-0795

51. Samalin E, Fouchardière C, Thézenas S, Boige V, Senellart H, Guimbaud R, et al. Sorafenib plus irinotecan combination in patients with ras-mutated metastatic colorectal cancer refractory to standard combined chemotherapies: A multicenter, randomized phase 2 trial (Nexiri-2/prodige 27). *Clin Colorectal Cancer*. (2020) 19:301–10.e1. doi: 10.1016/j.clcc.2020.04.008

52. Hoeflich KP, Merchant M, Orr C, Chan J, Den Otter D, Berry L, et al. Intermittent administration of mek inhibitor gdc-0973 plus pi3k inhibitor gdc-0941 triggers robust apoptosis and tumor growth inhibition. *Cancer Res*. (2012) 72:210–9. doi: 10.1158/0008-5472.Can-11-1515

53. Ramanathan RK, Von Hoff DD, Eskens F, Blumenschein G Jr., Richards D, Genvresse I, et al. Phase ib trial of the pi3k inhibitor copanlisib combined with the allosteric mek inhibitor refametinib in patients with advanced cancer. *Target Oncol*. (2020) 15:163–74. doi: 10.1007/s11523-020-00714-0

54. Ward R, Meagher A, Tomlinson I, O'Connor T, Norrie M, Wu R, et al. Microsatellite instability and the clinicopathological features of sporadic colorectal cancer. *Gut*. (2001) 48:821–9. doi: 10.1136/gut.48.6.821

55. Guinney J, Dienstmann R, Wang X, de Reyniès A, Schlicker A, Soneson C, et al. The consensus molecular subtypes of colorectal cancer. *Nat Med*. (2015) 21:1350–6. doi: 10.1038/nm.3967

56. Le DT, Durham JN, Smith KN, Wang H, Bartlett BR, Aulakh LK, et al. Mismatch repair deficiency predicts response of solid tumors to pd-1 blockade. *Science*. (2017) 357:409–13. doi: 10.1126/science.aan6733

57. Fucà G, Cohen R, Lonardi S, Shitara K, Elez ME, Fakih M, et al. Ascites and resistance to immune checkpoint inhibition in dmmr/msi-H metastatic colorectal and gastric cancers. *J Immunother Cancer*. (2022) 10:e004001. doi: 10.1136/jitc-2021-004001

58. Elkrief A, Derosa L, Kroemer G, Zitvogel L, Routy B. The negative impact of antibiotics on outcomes in cancer patients treated with immunotherapy: A new independent prognostic factor? *Ann Oncol*. (2019) 30:1572–9. doi: 10.1093/annonc/mdz206

59. Gao Y, Bi D, Xie R, Li M, Guo J, Liu H, et al. Fusobacterium nucleatum enhances the efficacy of pd-L1 blockade in colorectal cancer. *Signal Transduct Target Ther*. (2021) 6:398. doi: 10.1038/s41392-021-00795-x

60. Guven DC, Kavgaci G, Erul E, Syed MP, Magge T, Saeed A, et al. The efficacy of immune checkpoint inhibitors in microsatellite stable colorectal cancer: A systematic review. *Oncologist*. (2024) 29:e580–600. doi: 10.1093/oncolo/oyae013

61. Lin KX, Istl AC, Quan D, Skaro A, Tang E, Zheng X. Pd-1 and pd-L1 inhibitors in cold colorectal cancer: challenges and strategies. *Cancer Immunol Immunother*. (2023) 72:3875–93. doi: 10.1007/s00262-023-03520-5

62. Wankhede D, Yuan T, Kloor M, Halama N, Brenner H, Hoffmeister M. Clinical significance of combined tumour-infiltrating lymphocytes and microsatellite instability status in colorectal cancer: A systematic review and network meta-analysis. *Lancet Gastroenterol Hepatol*. (2024) 9:609–19. doi: 10.1016/s2468-1253(24)00091-8

63. Yang X, Zhou H, Liu Z, Yin X, Guo G, Zeng Y, et al. P-145 efficacy, safety, and predictors of fruquintinib plus pd-1 in refractory mss metastatic colorectal cancer in a real-world setting. *Ann Oncol*. (2023) 34:S66. doi: 10.1016/j.annonc.2023.04.201

64. Bullock A, Fakih M, Gordon M, Tsimberidou A, El-Khoueiry A, Wilky B, et al. Lba-4 results from an expanded phase 1 trial of botensilimab (Bot), a multifunctional anti-ctla-4, plus balstilimab (Bal; anti-pd-1) for metastatic heavily pretreated microsatellite stable colorectal cancer (Mss crc). *Ann Oncol*. (2023) 34:S178–S9. doi: 10.1016/j.annonc.2023.04.014

65. Taieb J, Gallois C. Adjuvant chemotherapy for stage iii colon cancer. *Cancers (Basel)*. (2020) 12:2679. doi: 10.3390/cancers12092679

66. Sveen A, Kopetz S, Lothe RA. Biomarker-guided therapy for colorectal cancer: strength in complexity. *Nat Rev Clin Oncol*. (2020) 17:11–32. doi: 10.1038/s41571-019-0241-1

67. Purcell RV, Schmeier S, Lau YC, Pearson JF, Frizelle FA. Molecular subtyping improves prognostication of stage 2 colorectal cancer. *BMC Cancer*. (2019) 19:1155. doi: 10.1186/s12885-019-6327-4

68. Dunne PD, O'Reilly PG, Coleman HG, Gray RT, Longley DB, Johnston PG, et al. Stratified analysis reveals chemokine-like factor (Cklf) as a potential prognostic marker in the msi-immune consensus molecular subtype cms1 of colorectal cancer. *Oncotarget*. (2016) 7:36632–44. doi: 10.18632/oncotarget.9126

69. Stintzing S, Wirapati P, Lenz HJ, Neureiter D, Fischer von Weikersthal L, Decker T, et al. Consensus molecular subgroups (Cms) of colorectal cancer (Crc) and first-line efficacy of folfiri plus cetuximab or bevacizumab in the fire3 (Aio krk-0306) trial. *Ann Oncol*. (2019) 30:1796–803. doi: 10.1093/annonc/mdz387

70. Lenz HJ, Ou FS, Venook AP, Hochster HS, Niedzwiecki D, Goldberg RM, et al. Impact of consensus molecular subtype on survival in patients with metastatic colorectal cancer: results from calgb/swog 80405 (Alliance). *J Clin Oncol*. (2019) 37:1876–85. doi: 10.1200/jco.18.02258

71. Mooi JK, Wirapati P, Asher R, Lee CK, Savas P, Price TJ, et al. The prognostic impact of consensus molecular subtypes (Cms) and its predictive effects for bevacizumab benefit in metastatic colorectal cancer: molecular analysis of the agitg max clinical trial. *Ann Oncol*. (2018) 29:2240–6. doi: 10.1093/annonc/mdy410

72. Stahler A, Hoppe B, Na IK, Keilholz L, Müller L, Karthaus M, et al. Consensus molecular subtypes as biomarkers of fluorouracil and folinic acid maintenance therapy with or without panitumumab in ras wild-type metastatic colorectal cancer (Panama, aio krk 0212). *J Clin Oncol*. (2023) 41:2975–87. doi: 10.1200/jco.22.02582

73. Lenz H-J, Parikh AR, Spigel DR, Cohn AL, Yoshino T, Kochenderfer MD, et al. Nivolumab (Nivo) + 5-fluorouracil/leucovorin/oxaliplatin (Mfolfox6)/bevacizumab (Bev) versus mfolfox6/bev for first-line (1l) treatment of metastatic colorectal cancer (Mcrc): phase 2 results from checkmate 9x8. *J Clin Oncol*. (2022) 40:8. doi: 10.1200/JCO.2022.40.4_suppl.008

74. Reinert T, Henriksen TV, Christensen E, Sharma S, Salari R, Sethi H, et al. Analysis of plasma cell-free DNA by ultradeep sequencing in patients with stages I to iii colorectal cancer. *JAMA Oncol*. (2019) 5:1124–31. doi: 10.1001/jamaoncol.2019.0528

75. Chen G, Peng J, Xiao Q, Wu HX, Wu X, Wang F, et al. Postoperative circulating tumor DNA as markers of recurrence risk in stages ii to iii colorectal cancer. *J Hematol Oncol*. (2021) 14:80. doi: 10.1186/s13045-021-01089-z

76. Yukami H, Nakamura Y, Mishima S, Ando K, Bando H, Watanabe J, et al. Circulating tumor DNA (Ctdna) dynamics in patients with colorectal cancer (Crc) with molecular residual disease: updated analysis from galaxy study in the circulate-Japan. *J Clin Oncol*. (2024) 42:6. doi: 10.1200/JCO.2024.42.3_suppl.6

77. Tie J, Cohen JD, Lo SN, Wang Y, Li L, Christie M, et al. Prognostic significance of postsurgery circulating tumor DNA in nonmetastatic colorectal cancer: individual patient pooled analysis of three cohort studies. *Int J Cancer*. (2021) 148:1014–26. doi: 10.1002/ijc.33312

78. Taieb J, Taly V, Henriques J, Bourreau C, Mineur L, Bennouna J, et al. Prognostic value and relation with adjuvant treatment duration of ctdna in stage iii colon cancer: A *post hoc* analysis of the prodige-gercor idea-France trial. *Clin Cancer Res*. (2021) 27:5638–46. doi: 10.1158/1078-0432.Ccr-21-0271

79. Tie J, Cohen JD, Lahouel K, Lo SN, Wang Y, Kosmider S, et al. Circulating tumor DNA analysis guiding adjuvant therapy in stage ii colon cancer. *N Engl J Med*. (2022) 386:2261–72. doi: 10.1056/NEJMoa2200075

80. Shitara K, Muro K, Watanabe J, Yamazaki K, Ohori H, Shiozawa M, et al. Baseline ctdna gene alterations as a biomarker of survival after panitumumab and chemotherapy in metastatic colorectal cancer. *Nat Med*. (2024) 30:730–9. doi: 10.1038/s41591-023-02791-w

81. Heinrich MC, Jones RL, George S, Gelderblom H, Schöffski P, von Mehren M, et al. Ripretinib versus sunitinib in gastrointestinal stromal tumor: ctdna biomarker analysis of the phase 3 intrigue trial. *Nat Med*. (2024) 30:498–506. doi: 10.1038/s41591-023-02734-5

82. Tan L, Tran B, Tie J, Markman B, Ananda S, Tebbutt NC, et al. A phase ib/ii trial of combined braf and egfr inhibition in braf V600e positive metastatic colorectal cancer and other cancers: the evict (Erlotinib and vemurafenib in combination trial) study. *Clin Cancer Res*. (2023) 29:1017–30. doi: 10.1158/1078-0432.Ccr-22-3094

83. Nakamura Y, Okamoto W, Kato T, Esaki T, Kato K, Komatsu Y, et al. Circulating tumor DNA-guided treatment with pertuzumab plus trastuzumab for her2-amplified metastatic colorectal cancer: A phase 2 trial. *Nat Med*. (2021) 27:1899–903. doi: 10.1038/s41591-021-01553-w

84. Crisafulli G, Sartore-Bianchi A, Lazzari L, Pietrantonio F, Amatu A, Macagno M, et al. Temozolomide treatment alters mismatch repair and boosts mutational burden in tumor and blood of colorectal cancer patients. *Cancer Discovery*. (2022) 12:1656–75. doi: 10.1158/2159-8290.Cd-21-1434

85. Zhang N, Zhang PP, Huang JJ, Wang ZY, Zhang ZH, Yuan JZ, et al. Reduced serum exosomal mir-874 expression predicts poor prognosis in colorectal cancer. *Eur Rev Med Pharmacol Sci*. (2020) 24:664–72. doi: 10.26355/eurrev_202001_20043

86. Wang L, Song X, Yu M, Niu L, Zhao Y, Tang Y, et al. Serum exosomal mir-377-3p and mir-381-3p as diagnostic biomarkers in colorectal cancer. *Future Oncol*. (2022) 18:793–805. doi: 10.2217/fon-2021-1130

87. Zhang Y, Wang S, Lai Q, Fang Y, Wu C, Liu Y, et al. Cancer-associated fibroblasts-derived exosomal mir-17-5p promotes colorectal cancer aggressive phenotype by initiating a runx3/myc/tgf-β1 positive feedback loop. *Cancer Lett*. (2020) 491:22–35. doi: 10.1016/j.canlet.2020.07.023

88. Mansoori B, Mohammadi A, Naghizadeh S, Gjerstorff M, Shanehbandi D, Shirjang S, et al. Mir-330 suppresses emt and induces apoptosis by downregulating hmga2 in human colorectal cancer. *J Cell Physiol*. (2020) 235:920–31. doi: 10.1002/jcp.29007

89. Shi X, Kaller M, Rokavec M, Kirchner T, Horst D, Hermeking H. Characterization of a P53/mir-34a/csf1r/stat3 feedback loop in colorectal cancer. *Cell Mol Gastroenterol Hepatol*. (2020) 10:391–418. doi: 10.1016/j.jcmgh.2020.04.002

90. Xia S, Wang X, Wu Y, Zhou T, Tian H, Liu Z, et al. Mir-22 suppresses emt by mediating metabolic reprogramming in colorectal cancer through targeting myc-associated factor X. *Dis Markers*. (2022) 2022:7843565. doi: 10.1155/2022/7843565

91. Li S, Hou X, Wu C, Han L, Li Q, Wang J, et al. Mir-645 promotes invasiveness, metastasis and tumor growth in colorectal cancer by targeting efna5. *BioMed Pharmacother*. (2020) 125:109889. doi: 10.1016/j.biopha.2020.109889

92. Xu K, Zhan Y, Yuan Z, Qiu Y, Wang H, Fan G, et al. Hypoxia induces drug resistance in colorectal cancer through the hif-1α/mir-338-5p/il-6 feedback loop. *Mol Ther*. (2019) 27:1810–24. doi: 10.1016/j.ymthe.2019.05.017

93. Ning T, Li J, He Y, Zhang H, Wang X, Deng T, et al. Exosomal mir-208b related with oxaliplatin resistance promotes treg expansion in colorectal cancer. *Mol Ther*. (2021) 29:2723–36. doi: 10.1016/j.ymthe.2021.04.028

94. Zhang C EJ, Yu E. Lncrna casc21 induces hgh1 to mediate colorectal cancer cell proliferation, migration, emt and stemness. *RNA Biol*. (2021) 18:369–81. doi: 10.1080/15476286.2021.1950464

95. Zeng ZL, Lu JH, Wang Y, Sheng H, Wang YN, Chen ZH, et al. The lncrna xist/mir-125b-2-3p axis modulates cell proliferation and chemotherapeutic sensitivity via targeting wee1 in colorectal cancer. *Cancer Med*. (2021) 10:2423–41. doi: 10.1002/cam4.3777

96. Wei S, Hu W, Feng J, Geng Y. Promotion or remission: A role of noncoding rnas in colorectal cancer resistance to anti-egfr therapy. *Cell Commun Signal*. (2022) 20:150. doi: 10.1186/s12964-022-00960-x

97. Qiu W, Yang J, Wang B, Yang M, Tian G, Wang P, et al. Evaluating the microsatellite instability of colorectal cancer based on multimodal deep learning integrating histopathological and molecular data. *Front Oncol*. (2022) 12:925079. doi: 10.3389/fonc.2022.925079

98. Li T, Liu W, Wang C, Wang M, Hui W, Lu J, et al. Multidimension analysis of the prognostic value, immune regulatory function, and cerna network of ly6e in individuals with colorectal cancer. *J Immunol Res*. (2022) 2022:5164265. doi: 10.1155/2022/5164265

99. Saliani M, Jalal R, Javadmanesh A. Differential expression analysis of genes and long non-coding rnas associated with kras mutation in colorectal cancer cells. *Sci Rep*. (2022) 12:7965. doi: 10.1038/s41598-022-11697-5

100. He J, Chu Z, Lai W, Lan Q, Zeng Y, Lu D, et al. Circular rna circherc4 as a novel oncogenic driver to promote tumor metastasis via the mir-556-5p/ctbp2/E-cadherin axis in colorectal cancer. *J Hematol Oncol*. (2021) 14:194. doi: 10.1186/s13045-021-01210-2

101. Liang ZX, Liu HS, Xiong L, Yang X, Wang FW, Zeng ZW, et al. A novel nf-κb regulator encoded by circplce1 inhibits colorectal carcinoma progression by promoting rps3 ubiquitin-dependent degradation. *Mol Cancer*. (2021) 20:103. doi: 10.1186/s12943-021-01404-9

102. Li C, He X, Zhang L, Li L, Zhao W. A pair-wise meta-analysis highlights circular rnas as potential biomarkers for colorectal cancer. *BMC Cancer*. (2019) 19:957. doi: 10.1186/s12885-019-6136-9

103. Cheng PQ, Liu YJ, Zhang SA, Lu L, Zhou WJ, Hu D, et al. Rna-seq profiling of circular rnas in human colorectal cancer 5-fluorouracil resistance and potential biomarkers. *World J Gastrointest Oncol*. (2022) 14:678–89. doi: 10.4251/wjgo.v14.i3.678

104. Chen H, Zhang J, Yang L, Li Y, Wang Z, Ye C. Circ-zeb1 regulates epithelial-mesenchymal transition and chemotherapy resistance of colorectal cancer through acting on mir-200c-5p. *Transl Oncol*. (2023) 28:101604. doi: 10.1016/j.tranon.2022.101604

105. Chong X, Chen J, Zheng N, Zhou Z, Hai Y, Chen S, et al. Pik3ca mutations-mediated downregulation of circlhfpl2 inhibits colorectal cancer progression via upregulating pten. *Mol Cancer*. (2022) 21:118. doi: 10.1186/s12943-022-01531-x

106. Zhang Q, Zheng Y, Liu J, Tang X, Wang Y, Li X, et al. Circifngr2 enhances proliferation and migration of crc and induces cetuximab resistance by indirectly targeting kras via sponging to mir-30b. *Cell Death Dis*. (2023) 14:24. doi: 10.1038/s41419-022-05536-8

107. Zhang F, Su T, Xiao M. Runx3-regulated circrna mettl3 inhibits colorectal cancer proliferation and metastasis via mir-107/per3 axis. *Cell Death Dis*. (2022) 13:550. doi: 10.1038/s41419-022-04750-8

108. Fu Z, Zhang P, Zhang R, Zhang B, Xiang S, Zhang Y, et al. Novel hypoxia-induced hif1α-circtdrd3-positive feedback loop promotes the growth and metastasis of colorectal cancer. *Oncogene*. (2023) 42:238–52. doi: 10.1038/s41388-022-02548-8

109. Liu Z, Zheng N, Li J, Li C, Zheng D, Jiang X, et al. N6-methyladenosine-modified circular rna qsox1 promotes colorectal cancer resistance to anti-ctla-4 therapy through induction of intratumoral regulatory T cells. *Drug Resist Update*. (2022) 65:100886. doi: 10.1016/j.drup.2022.100886

110. Han K, Wang FW, Cao CH, Ling H, Chen JW, Chen RX, et al. Circlonp2 enhances colorectal carcinoma invasion and metastasis through modulating the maturation and exosomal dissemination of microrna-17. *Mol Cancer*. (2020) 19:60. doi: 10.1186/s12943-020-01184-8

111. Yang KD, Wang Y, Zhang F, Luo BH, Feng DY, Zeng ZJ. Circn4bp2l2 promotes colorectal cancer growth and metastasis through regulation of the mir-340-5p/cxcr4 axis. *Lab Invest*. (2022) 102:38–47. doi: 10.1038/s41374-021-00632-3

112. Qu L, Yi Z, Shen Y, Lin L, Chen F, Xu Y, et al. Circular rna vaccines against sars-cov-2 and emerging variants. *Cell*. (2022) 185:1728–44.e16. doi: 10.1016/j.cell.2022.03.044

113. Garmezy B, Gheeya J, Lin HY, Huang Y, Kim T, Jiang X, et al. Clinical and molecular characterization of pole mutations as predictive biomarkers of response to immune checkpoint inhibitors in advanced cancers. *JCO Precis Oncol*. (2022) 6:e2100267. doi: 10.1200/po.21.00267

114. Domingo E, Freeman-Mills L, Rayner E, Glaire M, Briggs S, Vermeulen L, et al. Somatic pole proofreading domain mutation, immune response, and prognosis in colorectal cancer: A retrospective, pooled biomarker study. *Lancet Gastroenterol Hepatol*. (2016) 1:207–16. doi: 10.1016/s2468-1253(16)30014-0

115. Hu H, Cai W, Wu D, Hu W, Dong Wang L, Mao J, et al. Ultra-mutated colorectal cancer patients with pole driver mutations exhibit distinct clinical patterns. *Cancer Med*. (2021) 10:135–42. doi: 10.1002/cam4.3579

116. Haradhvala NJ, Kim J, Maruvka YE, Polak P, Rosebrock D, Livitz D, et al. Distinct mutational signatures characterize concurrent loss of polymerase proofreading and mismatch repair. *Nat Commun*. (2018) 9:1746. doi: 10.1038/s41467-018-04002-4

117. Hwang HS, Kim D, Choi J. Distinct mutational profile and immune microenvironment in microsatellite-unstable and pole-mutated tumors. *J Immunother Cancer*. (2021) 9:e002797. doi: 10.1136/jitc-2021-002797

118. He J, Ouyang W, Zhao W, Shao L, Li B, Liu B, et al. Distinctive genomic characteristics in pole/pold1-mutant cancers can potentially predict beneficial clinical outcomes in patients who receive immune checkpoint inhibitor. *Ann Transl Med*. (2021) 9:129. doi: 10.21037/atm-20-7553

119. Shepherd A, Feinstein L, Sabel S, Rastelli D, Mezhibovsky E, Matthews L, et al. Ret signaling persists in the adult intestine and stimulates motility by limiting pyy release from enteroendocrine cells. *Gastroenterology*. (2024) 166:437–49. doi: 10.1053/j.gastro.2023.11.020

120. Ray K. Ret signalling controls gut motility. *Nat Rev Gastroenterol Hepatol*. (2024) 21:71. doi: 10.1038/s41575-023-00882-0

121. Nagasaka M, Brazel D, Baca Y, Xiu J, Al-Hallak MN, Kim C, et al. Pan-tumor survey of ret fusions as detected by next-generation rna sequencing identified ret fusion positive colorectal carcinoma as a unique molecular subset. *Transl Oncol*. (2023) 36:101744. doi: 10.1016/j.tranon.2023.101744

122. Duke ES, Bradford D, Marcovitz M, Amatya AK, Mishra-Kalyani PS, Nguyen E, et al. Fda approval summary: selpercatinib for the treatment of advanced ret fusion-positive solid tumors. *Clin Cancer Res*. (2023) 29:3573–8. doi: 10.1158/1078-0432.Ccr-23-0459

123. Strickler JH, Yoshino T, Graham RP, Siena S, Bekaii-Saab T. Diagnosis and treatment of erbb2-positive metastatic colorectal cancer: A review. *JAMA Oncol*. (2022) 8:760–9. doi: 10.1001/jamaoncol.2021.8196

124. Chan JC, Chan DL, Diakos CI, Engel A, Pavlakis N, Gill A, et al. The lymphocyte-to-monocyte ratio is a superior predictor of overall survival in comparison to established biomarkers of resectable colorectal cancer. *Ann Surg*. (2017) 265:539–46. doi: 10.1097/sla.0000000000001743

125. Rubinstein MR, Baik JE, Lagana SM, Han RP, Raab WJ, Sahoo D, et al. Fusobacterium nucleatum promotes colorectal cancer by inducing wnt/β-catenin modulator annexin A1. *EMBO Rep*. (2019) 20:e47638. doi: 10.15252/embr.201847638

126. Chung DC, Gray DM 2nd, Singh H, Issaka RB, Raymond VM, Eagle C, et al. A cell-free DNA blood-based test for colorectal cancer screening. *N Engl J Med*. (2024) 390:973–83. doi: 10.1056/NEJMoa2304714

127. Imperiale TF, Porter K, Zella J, Gagrat ZD, Olson MC, Statz S, et al. Next-generation multitarget stool DNA test for colorectal cancer screening. *N Engl J Med*. (2024) 390:984–93. doi: 10.1056/NEJMoa2310336

frontiers | Frontiers in Molecular Biosciences

TYPE Brief Research Report
PUBLISHED 16 May 2025
DOI 10.3389/fmolb.2025.1556736

OPEN ACCESS

EDITED BY
Matteo Becatti,
University of Firenze, Italy

REVIEWED BY
Sheng Xia,
Jiangsu University, China
Vito D'Agnano,
University of Campania Luigi Vanvitelli, Italy

*CORRESPONDENCE
Hao Chen,
chenhao6938@163.com
Mingjie Kuang,
doctorkmj@tmu.edu.cn
Wei Chong,
chongwei.good@163.com,
chongwei@sdfmu.edu.cn

†These authors share first authorship

RECEIVED 07 January 2025
ACCEPTED 22 April 2025
PUBLISHED 16 May 2025

CITATION
Chen H, Zhong Y, Feng R, Zhu X, Xu K, Kuang M and Chong W (2025) Clinical and molecular implications of cGAS/STING signaling in checkpoint inhibitor immunotherapy.
Front. Mol. Biosci. 12:1556736.
doi: 10.3389/fmolb.2025.1556736

Clinical and molecular implications of cGAS/STING signaling in checkpoint inhibitor immunotherapy

Hao Chen[1*†], Yang Zhong[1,2†], Rongjie Feng[3†], Xingyu Zhu[4], Kang Xu[4], Mingjie Kuang[3*] and Wei Chong[4*]

[1]Clinical Research Center of Shandong University, Clinical Epidemiology Unit, School of Public Health, Cheeloo College of Medicine, Qilu Hospital of Shandong University, Jinan, Shandong, China, [2]Department of Epidemiology and Health Statistics, School of Public Health, Cheeloo College of Medicine, Shandong University, Jinan, Shandong, China, [3]Department of Orthopedics, Shandong Provincial Hospital Affiliated to Shandong First Medical University, Jinan, Shandong, China, [4]Department of Gastrointestinal Surgery, Shandong Provincial Hospital Affiliated to Shandong First Medical University, Key Laboratory of Engineering of Shandong Province, Jinan, Shandong, China

Recent studies reported that cytoplasmic dsDNA-induced activation of cyclic GMP-AMP synthase (cGAS)/stimulator of interferon genes (STING) signaling has tremendous potential for antitumor immunity by inducing the production of type I Interferon (IFN), resulting in activation of both innate and adaptive immunity. However, the potential role of STING signaling in modulating immunological checkpoint inhibitor (CPI) therapeutic efficacy remains unexplored. In this research, we employed the single-sample gene set enrichment analysis (ssGSEA) algorithm to calculate the enrichment score of STING signaling across 15 immunotherapy cohorts, including melanoma, lung, stomach, urothelial, and renal cancer. Logistic and Cox regression models were utilized to investigate the association between STING signaling and checkpoint inhibitor therapeutic response. Furthermore, we evaluated the tumor immunogenicity of STING1 molecule expression in the Cancer Genome Atlas (TCGA) pan-cancer datasets. STING signaling was associated with improved immune response in the Mariathasan2018_PD-L1, Gide2019_combined, Jung2019_PD-1/L1, and Gide2019_PD-1 datasets and with prolonged overall survival in the Gide2019_PD-1, Nathanson2017_post, Jung2019_PD-1/L1, and Mariathasan2018_PD-L1 datasets. However, the Braun_2020_PD-1 cohort exhibited worse prognosis outcomes in the high STING signaling subgroup. Our study extended the molecular knowledge of STING signaling activation in regulating the antitumor immune response and provided clinical clues about the combination treatments of STING agonists and CPIs for improving tumor therapeutic efficacy.

KEYWORDS

cGAS/STING, checkpoint inhibitors therapy, tumor immunogenomics, predictive marker, CPI

Introduction

Checkpoint inhibitor (CPI) therapies, including antibodies targeting programmed cell death protein 1 (PD-1), programmed death-ligand 1 (PD-L1), or cytotoxic T-lymphocyte-associated protein 4 (CTLA4), have demonstrated astounding clinical efficacy in treating advanced cancers (Galon and Bruni, 2019). Analyses of clinical datasets have identified several positive predictive markers for CPI, including high levels of tumor mutation burden (TMB), PD-L1 overexpression, ARNT2 low expression, and T lymphocyte infiltration, among others (Litchfield et al., 2021). Recent studies reported that cytosolic DNA-sensing cyclic GMP-AMP synthase (cGAS)/stimulator of interferon genes (STING) signaling (referred to as STING signaling) has tremendous potential for antitumor immunity by inducing the production of type I Interferon (IFN) and chemokines and resulting in activation of both innate and adaptive immunity (Kwon and Bakhoum, 2020). However, the comprehensive evaluation of the STING signaling activities in pan-cancer and their potential role in modulating CPI therapeutic efficacy remains unexplored. In this study, we investigated the clinical implications of STING signaling in response to CPI treatment in 15 immunotherapy datasets across melanoma, lung, urothelial, stomach, and renal cancers and evaluated the tumor immunogenicity of STING1 expression among The Cancer Genome Atlas (TCGA) pan-cancer datasets.

Method

We collated transcriptomic data for more than 900 CPI-treated patients and utilized standardized bioinformatics workflows and clinical outcome criteria to identify the role of cGAS/STING signaling in CPI sensitization (Supplementary Table S1). We validated the reliability of the ssGSEA-derived STING signaling score using integrated transcriptomic and phosphoproteomic datasets. The cGAS/STING-related gene set was curated from MSigDB V7.1 (REACTOME subset) and a literature review (Hopfner and Hornung, 2020) (Supplementary Table S2). The relative activity of STING signaling among individual CPI-treated tumors was quantified by using a single-sample GSEA (ssGSEA) algorithm with the GSVA package (Hanzelmann et al., 2013), which calculated separate enrichment scores for each pairing of a sample and a curated gene set. We also utilized two independent datasets (Gillette et al., 2020; Chen et al., 2020) with integrated transcriptomic and phosphoproteomic data to validate the reliability of enrichment scores on evaluation of STING signaling activities (Supplementary Method). A uniform clinical endpoint of response was defined across all the 15 CPI datasets derived from 11 independent studies based on the radiological response as per the RECIST criteria, with "CR/PR" being classified as a responder and "SD/PD," as well as any "NE" cases, being classed as a non-responder. Logistic regression model and survival analyses were utilized to uncover the association between STING signaling and therapeutic response.

Abbreviations: AA, Age acceleration; IBS, Irritable bowel syndrome; CI, Confidence interval; FEV1, Forced expiratory volume in one second; KDM-BA, Klemera–Doubal method biological age; SD, Standard deviation; SE, Standard error.

Results

Clinical implications of STING signaling in CPI immunotherapy

The constructed STING signaling scoring scheme exhibited a promising correlation with the phosphorylation level of STING1, IRF3, and TBK1 in integrated transcriptomic and phosphoproteomic datasets (Supplementary Figures S1A–C). The ROC curve analysis also validated the predictive value of the established STING signaling scoring model (Supplementary Figures S1D, E). Furthermore, we adopted the model to explore the association of STING signaling with immunotherapy benefit and found that an improved immune response in the Mariathasan2018_PD-L1, Kim2018_PD-1, Gide2019_combined, Jung2019_PD-1/L1, and Gide2019_PD-1 datasets (logistic regression model, $P < 0.05$) and marginal significance in Riaz2017_progPD-1 ($P = 0.083$) (Figure 1A). Multivariate analysis indicated the association remained statistically significant in the Mariathasan2018_PD-L1, Gide2019_combined, Jung2019_PD-1/L1, and Gide2019_PD-1 datasets after considering age, gender, site, or stage (Supplementary Figures S2A–F). Although the association in the Kim2018_PD-1 dataset was not significant after multivariate adjustment, the STING signaling activities were significantly upregulated in Epstein–Barr virus (EBV)-positive, Microsatellite instability-high (MSI-H), and immune signature subtype (Supplementary Figures S3A–C). We also performed the survival analyses and noticed that STING signaling scores were significantly associated with prolonged overall survival in the Gide2019_PD-1, Nathanson2017_post, Jung2019_PD-1/L1, and Mariathasan2018_PD-L1 datasets (univariate Cox model, HR < 1, $P < 0.05$, Figure 1B). However, the STING signaling activity was inversely correlated with overall survival in the Braun2020_PD-1 dataset (HR, 1.047 [95% CI, 1.002 to 1.093], $P = 0.039$). Braun et al. demonstrated that numerous chromosomal alterations, rather than conventional genomic markers like TMB and $CD8^+$ T cell infiltration, were associated with clinical responses or resistance to PD-1 blockade in advanced renal cell carcinoma. Leveraging these insights, we investigated these biomarkers and determined that STING signaling activity was inversely associated with the favorable PBRM1 mutation and purity and positively correlated with unfavorable chromosomal losses at 9q34.3 and 9q21.3 and ERV2282 overexpression (Supplementary Figures S3D–H). These findings further elucidate the unfavorable association between STING signaling activity and overall survival as observed in the Braun2020_PD-1 dataset.

We divided the four aforementioned datasets into low versus high expression subgroups based on the median STING signaling level. Prognosis analysis with the Kaplan–Meier model showed the comparable survival outcomes (log-rank test, $P < 0.05$; Figure 1C). Additionally, we explored the association between immune-related molecular characteristics and STING signaling score using the Mariathasan2018_PD-L1 and Jung2019_PD-1/L1 datasets, which provided sufficient sample size and molecular variables. Notably,

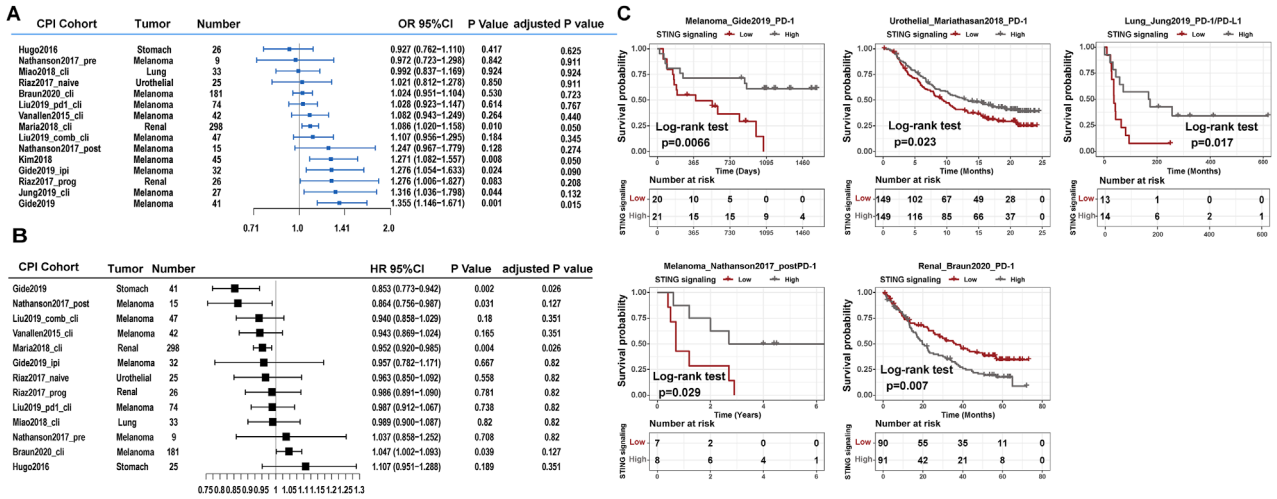

FIGURE 1
Clinical implications of STING signaling in CPI therapy. Forest plot representation of the association between the identified STING signaling and clinical response among 15 CPI datasets. **(A)** Logistic regression model estimated clinical immune response with STING signaling. **(B)** The Cox model estimated patients' overall survival with STING signaling. The length of the horizontal line represented the 95% confidence interval for each subgroup. **(C)** Kaplan–Meier curves for overall survival of STING activity subtypes in CPI immunotherapy cohorts of the Gide2019_PD-1, Mariathasan2018_PD-L1, Jung2019_PD-1/L1, Nathanson2017_postPD-1, and Braun2020_PD-1 datasets.

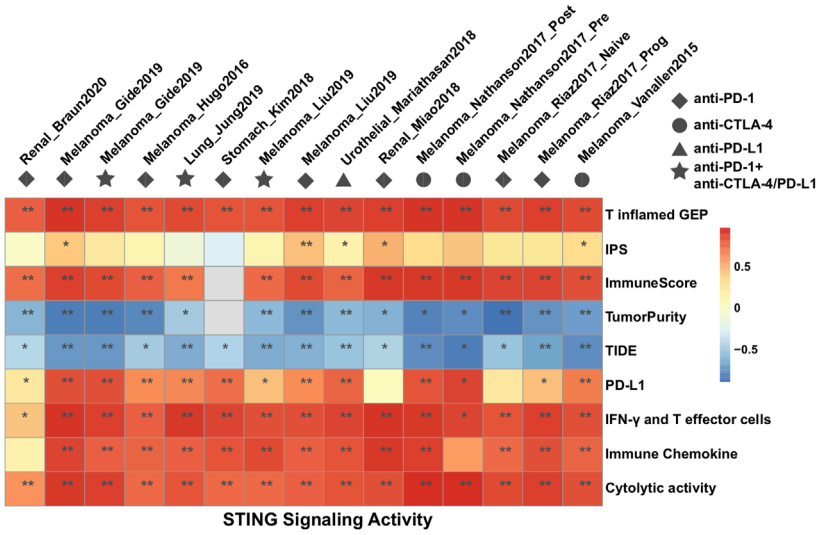

FIGURE 2
Heat maps showing the Spearman rank correlation coefficient between the identified STING signaling and predictors of immune response to CPI treatment among 15 datasets.

the STING signaling activities were significantly upregulated in the immune-inflamed phenotype and higher neoantigen burden subgroups in Mariathasan2018_PD-L1 (Kruskal–Wallis test, $P < 0.05$; Supplementary Figures S4A, B) and were also significantly correlated with global methylation and aneuploidy levels in the Jung2019_PD-1/L1 dataset (Pearson correlation, $P < 0.05$, Supplementary Figures S4C, D).

Association between STING signaling activities and identified predictors of immune response to CPI

We further investigated the correlation of STING signaling activities with various transcriptomic signatures that had been proposed for predicting immune response to CPI therapy,

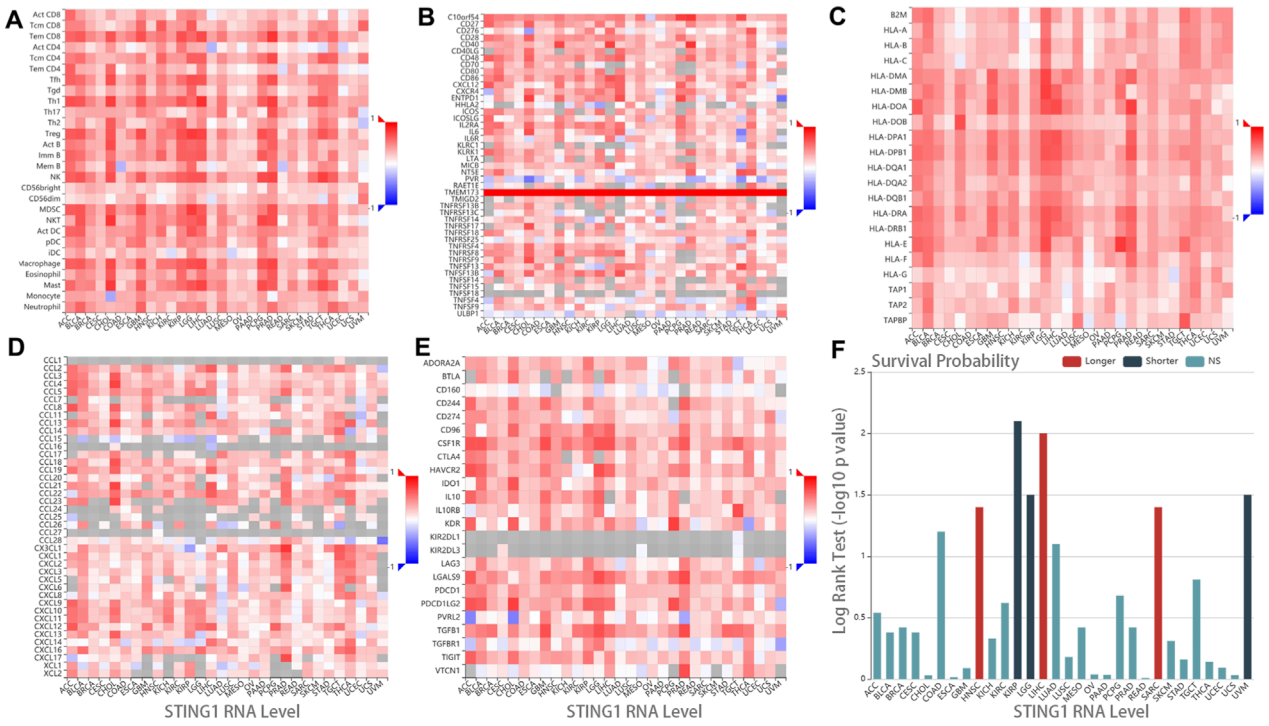

FIGURE 3
Molecular implications of STING1 expression in immunomodulation and prognosis. **(A–E)** Spearman's correlation of STING1 RNA expression with immunogenomic features within the TCGA pan-cancer dataset, including **(A)** TILs, **(B)** immunostimulators, **(C)** MHCs, **(D)** chemokines, and **(E)** immunoinhibitors. **(F)** Associations between STING1 expression and overall survival across human cancers in the TCGA dataset. The red and dark-blue bars represent the STING1 expression significantly associated with longer and shorter survival, respectively. NS indicates not significant.

including PD-L1, T inflamed-Gene expression profile (GEP), Immunophenoscore (IPS), ImmuneScore, Tumor Immune Dysfunction and Exclusion (TIDE), Interferon-γ (IFN-γ), and T effector cells, cytolytic activity, and immune chemokines (Supplementary Table S3). In most of the CPI datasets, T inflamed-GEP, ImmuneScore, TumorPurity, TIDE, IFN-γ, and T effector cells, and immune chemokines were strongly correlated with STING signaling activities, while the IPS signature was scarcely statistically significant (Spearman correlation; Figure 2). These findings suggested that STING signaling has a similar statistical significance to previously hypothesized predictors of CPI efficacy, and a prospective immunotherapy cohort and *in vivo* and *in vitro* experiments were required to validate the molecular mechanism of STING signaling on immune regulation.

Tumor immunogenicity of STING1 in pan-cancer

The tumor microenvironment (TME) has been associated with immune infiltration and response to immunotherapy across multiple cancer types (Fridman et al., 2017). Given the central role of STING1 (TMEM173) in STING signaling, we further investigated the correlation between STING1 RNA expression and key immunogenomic features, including tumor-infiltrating lymphocyte (TIL), immunoregulatory factors, major histocompatibility complex (MHC), and chemokines, across the TCGA pan-cancer datasets. The heatmap showed that STING1 was positively correlated with the abundance of multiple lymphocytes within solid tumors, such as activated $CD8^+$ T cells, $CD4^+$ T cells, dendritic cells (DC), macrophages, and natural killer (NK) cells (Figure 3A). Meanwhile, immunostimulators and MHC molecules were strongly associated with STING1 expression in a majority of cancer types (Figures 3B, C), suggesting that the activated STING signaling enforced tumor-antigen presentation and cross-primed $CD8^+$ T cells for antitumor immunity (Zhang et al., 2020). In addition, STING1 was positively correlated with most inflammatory chemokines and checkpoint molecules (Figures 3D, E), further indicating combination treatment of STING1 agonists and CPIs can synergistically improve cancer biotherapeutic efficacy (Wang et al., 2020). We also investigated the association between STING1 expression and patient prognosis, as well as its differential expression in tumor versus normal tissues, using the TCGA pan-cancer dataset. We found that high STING1 expression was associated with worse survival outcomes in kidney renal papillary cell carcinoma (KIRP) and lower-grade glioma (LGG) (Figure 3F), suggesting that STING1 overexpression may serve as an unfavorable indicator of prognosis and CPI efficacy in renal carcinoma. Furthermore, STING1 expression was differentially regulated across various tumor types, with significantly higher levels observed in tumor tissues than paired normal tissues in kidney renal clear cell carcinoma (KIRC), pancreatic adenocarcinoma (PAAD), and thymoma (THYM), while lower expression was noted in KIRP, lung squamous cell carcinoma (LUSC), prostate

adenocarcinoma (PRAD), uterine corpus endometrial carcinoma (UCEC), etc. (Supplementary Figure S5).

In summary, a comprehensive assessment of the STING signaling in CPI treatment will contribute to enhancing our understanding of innate immunity in CPI efficacy and guide the precision immunotherapy (Chen et al., 2022). In the upcoming era of combination or bispecific antibody immunotherapy (Zhang et al., 2023), our study extends the molecular knowledge of STING signaling activation in regulating the tumor immunogenicity and provides the clinical clues of the combination treatment of STING agonists and CPIs for improving tumor therapeutic efficacy. Further investigation in a prospective randomized clinical trial is warranted.

Discussion

A comprehensive assessment of STING signaling in CPI treatment contributes to understanding innate immunity in CPI efficacy and guides precision immunotherapy. In the emerging era of combination or bispecific antibody immunotherapy, our study extends knowledge of STING signaling activation in regulating tumor immunogenicity. The findings suggest that combining STING agonists with CPIs may enhance the therapeutic efficacy. However, further investigation in prospective randomized clinical trials is warranted to validate these findings.

Recent advances in STING agonists for cancer immunotherapy are promising. Several, including TAK-676 (a CDN analog) and SNX281 (a non-CDN agonist), are in Phase I/II trials (Wang et al., 2020). Engineered bacteria like SYNB1891 are also being tested for direct, localized delivery of STING agonists, reducing side effects (Samson and Ablasser, 2022). Additionally, STING agonists combined with immune checkpoint inhibitors, such as ADU-S100 with spartalizumab, show promising results, advancing optimal treatment strategies (Chong et al., 2024; Hines et al., 2023).

However, several limitations must be considered. First, the study relies primarily on retrospective data from multiple immunotherapy cohorts, which can be subject to biases such as selection and recall bias, affecting the generalizability of the results. Second, the inclusion of different tumor types (e.g., melanoma, lung cancer, and urothelial carcinoma) introduces heterogeneity, making it difficult to draw universal conclusions regarding STING signaling efficacy across all cancer types. Additionally, the observed variability in the association between STING signaling and therapeutic response may be influenced by factors such as tumor microenvironment differences or genetic heterogeneity. The use of bioinformatics tools, like the ssGSEA algorithm, while valuable, is dependent on the quality and completeness of the data, and the results may not fully capture the complexities of the cGAS/STING pathway *in vivo*. Finally, while significant associations were found, prospective randomized clinical trials are needed to validate these findings, suggesting that the current results should be considered preliminary.

Data availability statement

The original contributions presented in the study are included in the article/Supplementary Material; further inquiries can be directed to the corresponding authors.

Author contributions

HC: Project administration, Resources, Writing – original draft. YZ: Writing – original draft. RF: Writing – original draft. XZ: Writing – review and editing. KX: Writing – review and editing. MK: Writing – review and editing. WC: Conceptualization, Data curation, Formal Analysis, Funding acquisition, Writing – review and editing.

Funding

The author(s) declare that financial support was received for the research and/or publication of this article. This work was supported by the National Natural Science Foundation of China, Award number: 82103322.

Conflict of interest

The authors declare that the research was conducted in the absence of any commercial or financial relationships that could be construed as a potential conflict of interest.

Generative AI statement

The author(s) declare that no Generative AI was used in the creation of this manuscript.

Publisher's note

Supplementary material

The Supplementary Material for this article can be found online at: https://www.frontiersin.org/articles/10.3389/fmolb.2025.1556736/full#supplementary-material

References

Chen, H., Zhang, T., Zhang, Y., Wu, H., Fang, Z., Liu, Y., et al.(2022). Deciphering the tumor microenvironment cell-infiltrating landscape reveals microenvironment subtypes and therapeutic potentials for nonsquamous NSCLC. *JCI Insight* 7(12), e152815. doi:10.1172/jci.insight.152815

Chen, Y. J., Roumeliotis, T. I., Chang, Y. H., Chen, C. T., Han, C. L., Lin, M. H., et al. (2020). Proteogenomics of non-smoking lung cancer in East Asia delineates molecular signatures of pathogenesis and progression. *Cell* 182 (1), 226–244.e17. doi:10.1016/j.cell.2020.06.012

Chong, W., Ren, H., Chen, H., Xu, K., Zhu, X., Liu, Y., et al. (2024). Clinical features and molecular landscape of cuproptosis signature-related molecular subtype in gastric cancer. *Imeta* 3 (3), e190. doi:10.1002/imt2.190

Fridman, W. H., Zitvogel, L., Sautes-Fridman, C., and Kroemer, G. (2017). The immune contexture in cancer prognosis and treatment. *Nat. Rev. Clin. Oncol.* 14 (12), 717–734. doi:10.1038/nrclinonc.2017.101

Galon, J., and Bruni, D. (2019). Approaches to treat immune hot, altered and cold tumours with combination immunotherapies. *Nat. Rev. Drug Discov.* 18 (3), 197–218. doi:10.1038/s41573-018-0007-y

Gillette, M. A., Satpathy, S., Cao, S., Dhanasekaran, S. M., Vasaikar, S. V., Krug, K., et al. (2020). Proteogenomic characterization reveals therapeutic vulnerabilities in lung adenocarcinoma. *Cell* 182 (1), 200–225.e35. doi:10.1016/j.cell.2020.06.013

Hanzelmann, S., Castelo, R., and Guinney, J. (2013). GSVA: gene set variation analysis for microarray and RNA-seq data. *BMC Bioinf* 14, 7. doi:10.1186/1471-2105-14-7

Hines, J. B., Kacew, A. J., and Sweis, R. F. (2023). The development of STING agonists and emerging results as a cancer immunotherapy. *Curr. Oncol. Rep.* 25 (3), 189–199. doi:10.1007/s11912-023-01361-0

Hopfner, K. P., and Hornung, V. (2020). Molecular mechanisms and cellular functions of cGAS-STING signalling. *Nat. Rev. Mol. Cell Biol.* 21 (9), 501–521. doi:10.1038/s41580-020-0244-x

Kwon, J., and Bakhoum, S. F. (2020). The cytosolic DNA-sensing cGAS–STING pathway in cancer. *Cancer Discov.* 10 (1), 26–39. doi:10.1158/2159-8290.CD-19-0761

Litchfield, K., Reading, J. L., Puttick, C., Thakkar, K., Abbosh, C., Bentham, R., et al. (2021). Meta-analysis of tumor- and T cell-intrinsic mechanisms of sensitization to checkpoint inhibition. *Cell* 184 (3), 596–614.e14. doi:10.1016/j.cell.2021.01.002

Samson, N., and Ablasser, A. (2022). The cGAS–STING pathway and cancer. *Nat. Cancer* 3 (12), 1452–1463. doi:10.1038/s43018-022-00468-w

Wang, Y., Luo, J., Alu, A., Han, X., Wei, Y., and Wei, X. (2020). cGAS-STING pathway in cancer biotherapy. *Mol. Cancer* 19 (1), 136. doi:10.1186/s12943-020-01247-w

Zhang, T., Lin, Y., and Gao, Q. (2023). Bispecific antibodies targeting immunomodulatory checkpoints for cancer therapy. *Cancer Biol. Med.* 20 (3), 181–195. doi:10.20892/j.issn.2095-3941.2023.0002

Zhang, X., Bai, X. C., and Chen, Z. J. (2020). Structures and mechanisms in the cGAS-STING innate immunity pathway. *Immunity* 53 (1), 43–53. doi:10.1016/j.immuni.2020.05.013

frontiers | Frontiers in Molecular Biosciences

TYPE Original Research
PUBLISHED 21 November 2025
DOI 10.3389/fmolb.2025.1654426

OPEN ACCESS

EDITED BY
Giuseppe Bronte,
University of Ferrara, Italy

REVIEWED BY
Paula Dobosz,
Poznan University of Medical Sciences, Poland
Pawel Zielinski,
Poznan University of Medical Sciences,
Poznan, Poland

*CORRESPONDENCE
Hang Fai Kwok,
hfkwok@um.edu.mo
Hui Zou,
zouhui@hunnu.edu.cn
Liqing Hu,
huliqing@hunnu.edu.cn

†These authors have contributed equally to this work and share first authorship

RECEIVED 26 June 2025
REVISED 22 October 2025
ACCEPTED 29 October 2025
PUBLISHED 21 November 2025

CITATION
Li J, Zhang J, Zhang X, Cao C, Zhou T, Liu F, Hu L, Kwok HF and Zou H (2025) Prognostic model for lung adenocarcinoma based on experimental drug-resistant cell lines and clinical patients.
Front. Mol. Biosci. 12:1654426.
doi: 10.3389/fmolb.2025.1654426

Prognostic model for lung adenocarcinoma based on experimental drug-resistant cell lines and clinical patients

Junnan Li[1†], Jiasheng Zhang[2†], Xinyang Zhang[1], Chengwu Cao[1], Tianjie Zhou[1], Fengxian Liu[1], Liqing Hu[1]*, Hang Fai Kwok[2,3,4]* and Hui Zou[1]*

[1]Key Laboratory of Study and Discovery of Small Targeted Molecules of Hunan Province, School of Pharmacy, Health Science Center, Hunan Normal University, Changsha, China, [2]Department of Biomedical Sciences, Faculty of Health Sciences, University of Macau, Avenida de Universidade, Taipa, Macao SAR, China, [3]Cancer Centre, Faculty of Health Sciences, University of Macau, Avenida de Universidade, Taipa, Macao SAR, China, [4]MoE Frontiers Science Center for Precision Oncology, University of Macau, Avenida de Universidade, Taipa, Macao SAR, China

Objective: Despite advances in EGFR-TKIs for lung adenocarcinoma (LUAD), resistance remains a major hurdle. This study aimed to develop a prognostic model integrating immune microenvironment features and *in vitro* resistance mechanisms to predict outcomes and guide therapy.
Materials and methods: erlotinib-, gefitinib-, and osimertinib-resistant HCC827 cell lines were established by exposing them to increasing EGFR-TKIs concentrations. RNA-sequencing was conducted on non-resistant HCC827 and erlotinib/gefitinibresistant cell lines. From the erlotinib-resistant, gefitinib-resistant cell lines and The Cancer Genome Atlas Program-Lung adenocarcinoma (TCGA-LUAD) data, a prognostic risk score model was constructed via Least Absolute Shrinkage and Selection Operator-Cox Proportional Hazards Model (LASSO-COX). Furthermore, immune infiltration was assessed using Gene Set Variation Analysis (GSVA), and single-cell RNA-seq (GSE241934) resolved expression patterns in EGFR-mutant vs. wild-type tumors. *In vitro* validation included RT-PCR in Osimertinib resistant (OR)-HCC827 cells.
Results: A 3-gene (*PPP1R3G, CREG2, LYPD3*) RiskScore were developed. The RiskScore predicted poor survival and resistance across all EGFR-TKI generations, with osimertinib-resistant HCC827 cells showing significant upregulation of signature genes. High-risk patients exhibited immune-suppressive microenvironments (enriched regulatory T cells, depleted mast cells) and distinct scRNA-seq profiles. A nomogram (C-index = 0.7) integrated RiskScore with clinical factors for personalized prognosis.
Conclusion: This model bridges *in vitro* resistance mechanisms with clinical immune landscapes, offering a tool to stratify patients for EGFR-TKIs, immunotherapies, or combinatorial strategies.

KEYWORDS

lung cancer, prognosis prediction, EGFR-TKIs resistance, immune microenvironment, single cell RNA-seq (scRNA-seq)

Highlights

- Novel prognostic model: A robust RiskScore model for lung adenocarcinoma (LUAD) was developed using three resistance-associated genes (*PPP1R3G*, *CREG2,* and *LYPD3)*, validated across erlotinib-, gefitinib-, and osimertinib-resistant cell lines and clinical cohorts.
- Immune microenvironment insights: The RiskScore stratifies LUAD patients into distinct immune profiles, with high-risk groups showing elevated regulatory T cells and activated $CD4^+$ T cells, suggesting potential resistance to immunotherapies. Single-cell RNA-seq (scRNA-seq) revealed differential gene expression in EGFR-mutant tumors, linking immune evasion to resistance mechanisms.
- Clinical implications: The model stratifies patients into high-risk groups who may be more prone to developing EGFR-TKI resistance, supported by *in vitro* data showing overexpression of the signature genes in osimertinib-resistant cells, which lends preliminary support to its potential clinical relevance.
- Integrated tool: A nomogram combining RiskScore and clinical factors predicts survival and resistance risk, offering a actionable framework for personalized therapy selection.

1 Introduction

Lung cancer is still a significant contributor to cancer-related mortality over the world (Siegel et al., 2021). Lung adenocarcinoma, a subtype of non-small cell lung cancer (NSCLC), represents the predominant histological type of lung cancer in humans (Tan et al., 2015). According to World Health Organization (WHO) statistics, adenocarcinoma constitutes roughly 40% of all lung cancer diagnoses. (Yang et al., 2019). Notably, it is the most prevalent lung cancer subtype among non-smokers and is disproportionately common in women as well as in younger individuals (Li et al., 2022). Although the identification of EGFR mutations and the advancement of EGFR tyrosine kinase inhibitors (EGFR-TKIs) have enhanced patient outcomes, the emergence of drug resistance impedes the effectiveness and long-term success of such treatments, presenting a significant challenge in the management of lung adenocarcinoma (Du et al., 2021; Hrustanovic et al., 2013). In light of this, researchers continue to conduct innovative studies aimed at improving the therapeutic efficacy, survival rates, and prognostic outcomes for individuals with lung adenocarcinoma.

Recent research has progressively elucidated the mechanisms underlying resistance to EGFR tyrosine kinase inhibitors (EGFR-TKIs) and established a strong correlation between this resistance and the clinical outcomes of cancer patients following EGFR-TKI therapy (Hayakawa et al., 2013; Kobayashi et al., 2005).After conducting the RNA-sequencing and detecting the differentially expressed genes among erlotinib-resistant cell line, gefitinib-resistant cell line and TCGA-LUAD patients, a prognostic prediction model based on three differentially expressed genes (*PPP1R3G, CREG2, LYPD3*) was established. Besides, the immune landscape of these three genes in LUAD were explored by immune cell infiltration analysis. This prognostic prediction model has been validated in the Gene Expression Omnibus (GEO) database and has the potential to accurately forecast the outcomes for patients with lung adenocarcinoma (LUAD).

Considering all the above facts, this work aims at developing a prognostic prediction model, based on drug resistant genes, so as to provide prognosis information, stratify patients into different risk group, and guide personalized treatment.

Abbreviations: LUAD, Lung Adenocarcinoma; scRNA-seq, single-cell RNA sequencing; EGFR-TKI, Epidermal Growth Factor Receptor–Tyrosine Kinase Inhibitor; MTT, 3-(4,5-dimethylthiazol-2-yl)-2,5-diphenyltetrazolium bromide; TCGA-LUAD, The Cancer Genome Atlas Program-Lung Adenocarcinoma; GSVA, Gene Set Variation Analysis; rms, Regression Modeling Strategies; GEO, Gene Expression Omnibus; OR, Osimertinib resistant; EDR, erlotinib drug resistant; GDR, gefitinib drug resistant; LASSO-COX, Least Absolute Shrinkage and Selection Operator- Cox Proportional Hazards Model.

2 Materials and methods

2.1 Establishment of erlotinib-resistant cells and gefitinib-resistant cells

The HCC827 cell line was obtained from the Shanghai Institute for Biological Sciences, which is affiliated with the Chinese Academy of Sciences. These cells were maintained in RPMI-1640 medium, supplemented with 10% fetal bovine serum provided by Gibco™ and sourced from Grand Island, New York. To establish erlotinib-resistant and gefitinib-resistant derivatives of the HCC827 cell line, the parental cells were incrementally exposed to increasing concentrations of either erlotinib or gefitinib. The dosing regimen commenced at 100 nM and culminated at 10 μM (Ikeda et al., 2011; Yamamoto et al., 2010). During the development of the corresponding EGFR-TKI resistance, the medium and drug were replaced twice per week. Subsequent experiments were conducted on these adapted cell lines. HCC827 Osimertinib resistant cell line was kindly given by Prof. Kim Tam from University of Macao.

2.2 The 3-(4,5-dimethylthiazol-2-yl)-2,5-diphenyltetrazolium bromide (MTT) assay

MTT reagent (Sigma, Catalog Number: M2128) was used to conducted and evaluate the effectiveness of various treatments. Initially, the EGFR-TKIs resistant cells were plated into a 96-well plate at a density of 5,000 cells per well and allowed to incubate for 24 h. After exposure to PBS or drug treatments for an additional 24 h period, 10 μL of the MTT reagent were introduced into each well, and the cells were incubated for a further 2–4 h. The media were subsequently removed, and 100 μL of dimethyl sulfoxide (DMSO) were added to each well to dissolve the resultant formazan crystals. The optical density (OD) of the wells was then measured at a wavelength of 570 nm using a Thermo Scientific Microplate Reader (Multiskan Spectrum) to quantify the response to treatment. For each treatment condition, we included triplicates (n = 3) in the 96-well plate format, and the entire experiment was repeated three times. IC_{50}, or half maximal inhibitory concentration, is a key measure in pharmacology and drug development. IC_{50} is the concentration of a substance (usually a drug or inhibitor) required

to inhibit a specific biological or biochemical function by 50%. It's commonly used to assess the potency of a compound—the lower the IC_{50} value, the more potent the inhibitor.

2.3 mRNA extraction and RNA-sequencing

To conduct mRNA extraction and subsequent RNA sequencing, total RNA was isolated utilizing a RNeasy Kit (catalog number 74136, Qiagen, Germany). Complementary DNA (cDNA) libraries were then created using the NEBNext® Ultra™ Directional RNA Library Prep Kit for Illumina® (catalog number E7760, New England Biolabs, Ipswich, MA, USA). These cDNA libraries underwent sequencing on an Illumina Hi-Seq platform (Illumina, San Diego, CA). The initial RNA-sequencing data were assessed with FastQC for quality control. The RNA-sequencing (including data QC, mapping, quantification and differential analysis) for erlotinib drug resistant (EDR) cell line, gefitinib drug resistant (GDR) cell line and HCC827 was conducted by the leading provider of genomic services and solutions company Novogene Co., Ltd. (https://www.novogene.com/amea-en/).

High-quality RNA-sequencing reads from each library were aligned and mapped to the reference genome using STAR v2.6.1day software (developed by the Cold Spring Harbor Laboratory). Total mapping rates of all samples are all larger than 95%.

Genes with expression levels that exhibited a change of more than 2-fold ($|\log2FoldChange| > 1$) and an adjusted p-value (FDR) < 0.05 in the paired samples were considered as upregulated or downregulated. For functional annotation and interpretation of the transcriptome profiles, differentially expressed genes were analyzed through Gene Ontology (GO) analysis. This was performed using the web-based tool DAVID v6.8 (The Database for Annotation, Visualization, and Integrated Discovery, supported by the National Institute of Allergy and Infectious Diseases, part of the NIH). R version 4.3.1 was used for the comparative analysis of RNA-sequencing. Differential expression genes (DEGs) analysis of LUAD in TCGA was performed by R package Deseq2 and raw count was used as input. DEGs analysis between two risk group in GEO data was conducted by R package "Limma". Fragments per kilobase of transcript per million mapped reads (FPKM) was used for survival anlysis and gene expression in cross-sample comparison.

2.4 Data acquisition

The transcriptome profiles along with the corresponding clinical data for 50 normal and 504 lung adenocarcinoma (LUAD) samples were downloaded from The Cancer Genome Atlas (TCGA) database (https://portal.gdc.cancer.gov/). The RNA expression data and clinical information were download and accessed by the project name TCGA-LUAD and Experimental Strategy RNA-Seq. In addition, the microarray data and related clinical details for 11 normal and 57 LUAD samples were obtained from the Gene Expression Omnibus (GEO) under accession number GSE116959, using platform GPL17077 (https://www.ncbi.nlm.nih.gov/geo/query/acc.cgi?acc=GSE116959). Also, we retrieved microarray data for 442 LUAD samples from the GEO dataset with accession number GSE72094, which is based on platform GPL15048, accessed on the 27 May 2024 through the GEO website (https://www.ncbi.nlm.nih.gov/geo/query/acc.cgi?acc=GSE72094). The single-cell RNA sequencing (scRNA-seq) data GSE241934 (https://www.ncbi.nlm.nih.gov/geo/query/acc.cgi?acc=GSE241934, download in 27 March 2025) comprises of 11 resected tumors from earlystage EGFR-mutant patients as well as 34 tumors which were all confirmed wildtype lung adenocarcinoma (LUAD) or adenosquamous carcinoma (AdSqC). Candidate genes were analyzed in LUAD patients harboring EGFR mutation in (L858R, exon 19 deletions [Exon19del], and exon 20 insertions [Exon20ins]), compared with LUAD patients with wild type EGFR. R package "Seurat" V5 was used to filter and process scRNA-seq data. R package 'singleR' was conducted for cell cluster annotation, which is a commonly used computational framework for the annotation of scRNA-seq by reference to bulk transcriptomes (Xin et al., 2024; Aran et al., 2019). TCGA-LUAD cohort was used as training dataset and the other three independent dataset GSE 116959, GSE72094 and GSE241934 were used as validation datasets, to delineate mutation-specific transcriptional signatures.

2.5 GO and KEGG functional enrichment analyses

Functional enrichment analyses using Gene Ontology (GO) and Kyoto Encyclopedia of Genes and Genomes (KEGG) were performed to investigate the biological processes associated with differentially expressed genes. This analysis was conducted utilizing R statistical software packages, including "clusterProfiler," "org.Hs.e.g.,.db," "enrichplot," "ggplot2," and "GOplot." The GO analysis provided insights into three main categories: cellular component (CC), biological process (BP), and molecular function (MF).

2.6 LASSO-COX dimension reduction analysis

The LASSO-COX dimension reduction method was utilized to analyze data, employing the "glmnet" (Lasso and Elastic-Net Regularized Generalized Linear Models) and "survival" packages within the R programming environment. Lambda is regularization parameter, controlling the amount of shrinkage. We used Cox regression model with the LASSO to achieve shrinkage and variable selection simultaneously. Ten-fold cross validation was used to determine the optimal value of λ. This method divided the TCGA-LUAD RNA-sequencing data into 10 subsets (folds). For each fold, the model was trained on k-1 folds and validate it on the remaining fold and the performance metric like partial likelihood deviation was recorded in a range of λ value. Then the partial likelihood deviation was averaged across all folds for each λ. In the training process, a subset of variables was identified by shrinking the coefficients of less important variables into zero. We selected λ.min for our final model. We note that the more parsimonious λ.1se criterion resulted in a null model (zero genes). Given that the 3-gene signature at λ.min was highly predictive and successfully validated externally, we proceeded with this model to identify a biologically and clinically relevant signature.The optimal λ value lambda.min (λ.min) for our research was identified as the one that corresponded

to the lowest partial likelihood deviance and minimum mean cross-validated error. Ultimately, based on the optical optimalλ (λ.min = 0.09785), we identified three genes of interest along with their respective coefficient: *PPP1R3G* (0.07797704), *CREG2* (0.04387373) and *LYPD3* (0.02302433). The risk score for each patient was derived using the following formula:

$$\begin{aligned}\text{risk score} = &(\text{expression of } PPP1R3G \times \text{coefficient for } PPP1R3G)\\ &+ (\text{expression of } CREG2 \times \text{coefficient for } CREG2)\\ &+ (\text{expression of } LYPD3 \times \text{coefficient for } LYPD3)\end{aligned}$$

In this formula, "expression of gene" refers to the gene's expression level, and "coefficient for gene" is its coefficient corresponding λ.min.

2.7 Nomogram construction and time-dependent AUC

A nomogram analysis was developed within the training cohort using the Regression Modeling Strategies (rms) package in R. This nomogram is bifurcated, with the upper section serving as a scoring guide and the lower section as a predictive tool. The nomogram enables the precise prediction of the 1-, 2-, 3-, 5-, and 10-year survival for patients with LUAD, based on the cumulative points of each contributing factor. The accuracy of the nomogram in predicting overall survival (OS) was validated in the validation group. Calibration curves and C-Index values were employed to assess and quantify the precision of these survival predictions. Time-dependent AUC was calculated using the "timeROC" R package at 1, 2, and 3-year time points. Bootstrap C-index with 1000 resamples was performed using the "boot" package.

2.8 Immune cell infiltration analysis

We utilized Gene Set Variation Analysis (GSVA) to analyze the immune microenvironment within LUAD tumors (Li, 2017). This technique enables the identification of 28 distinct immune cell populations, such as seven subtypes of T cells, plasma cells, naive and memory B cells (Charoentong et al., 2017). We depicted the variations in immune cell composition between high-RiskScore and low-RiskScore groups through bar plots. The GSVA generates normalized scores ranging from 0–1, representing the abundance of the immune cell population. In subsequent analyses aimed at identifying differences in immune cell infiltration levels between these two groups, only samples with a p-value of less than 0.05 were taken into account (Systematic RNA, 2009).

2.9 Statistical analysis

Statistical analyses were conducted utilizing R (https://www.r-project.org/, v3.5.0), available at R Project, SPSS software version 25.0 from IBM, headquartered in Chicago, IL, and GraphPad Prism version 8.0, which is a product of La Jolla, CA. The prognostic significance was assessed through Kaplan-Meier survival analysis and COX proportional hazards modeling. Gene Set Enrichment Analysis (GSEA) was conducted using the GSEA package accessible through the Broad Institute's website at GSEA (http://software.broadinstitute.org/gsea/index.jsp), while Gene Ontology (GO) and KEGG (Kyoto Encyclopedia of Genes and Genomes) analysis was carried out using the clusterProfiler package. A p-value of less than 0.05 was set as the threshold for statistical significance across all methods.

3 Results

3.1 Differential expressed genes (DEGs) among EGFR-TKIs resistant cells and LUAD patients

To simulate the clinical development of drug resistance and enhance the potency of EGFR-TKIs therapies, we developed EGFR-TKIs-resistant HCC827 cell lines. This was achieved by culturing the cells in increasing doses of erlotinib and gefitinib, resulting in the HCC827 EDR (erlotinib-resistant cell line) and HCC827 GDR (gefitinib-resistant cell line), respectively. As shown in Figure 1A, HCC827 EDR cells were less sensitive to erlotinib treatment alone than parental HCC827 cells. Additionally, the IC50 value for erlotinib was significantly higher in the HCC827 EDR cells (54.8 ± 1.87 uM) than parental HCC827 cells (0.033 ± 0.015 uM) (Figure 1C). The phenomenon also be observed with the HCC827 GDR cells (Figures 1B,C). These results collectively indicate that we have successfully established EGFR-TKI-resistant cell lines, which will serve as valuable models for further investigation.

Following the development of drug-resistant cell lines, RNA-sequencing was per-formed for the parental HCC827 cells, HCC827 EDR cells and HCC827 GDR cells. We then conducted a comparative analysis of the RNA sequencing data between the parental HCC827 cells and each of the resistant cell lines—HCC827 EDR and HCC827 GDR—to discern the genes that were differentially expressed. Using a threshold of FDR<0.05 and $|\log2FC| > 1$ (2 fold change),the volcano plot analysis of HCC827 GDR cells uncovered 3264 differentially expressed genes (DEGs), with 2099 genes upregulated and 1165 genes downregulated (Figure 1D). Meanwhile, the HCC827 EDR cells exhibited a different pattern, with 415 genes upregulated and 514 genes downregulated (Figure 1E). To dissect and pinpoint the central genes associated with resistance to EGFR-TKIs and the prognostic indicators of lung cancer, a Venn diagram analysis was employed. This method was utilized to identify genes that were co-regulated across both the experimentally derived drug-resistant lung cancer cells and samples from clinical patients. The Venn diagram analysis demonstrated a shared upregulation of 414 genes in both the HCC827 GDR cells and tumor tissues from lung adenocarcinoma (LUAD) patients (Figure 1F). Additionally, it revealed that 104 genes were commonly upregulated in the HCC827 EDR cells and LUAD tumor tissues (Figure 1G). Only 24 genes were found to be concurrently upregulated in both drug-resistant cells and LUAD tumor tissues, as depicted in Figure 1H. Additionally, Gene Ontology (GO) and Kyoto Encyclopedia of Genes and Genomes (KEGG) analyses were performed on the total 494 upregulated genes in drug-resistant cells and LUAD tumor tissues. These analyses indicated an enrichment of genes associated with amino acid biosynthesis and metabolism,

10.3389/fmolb.2025.1654426

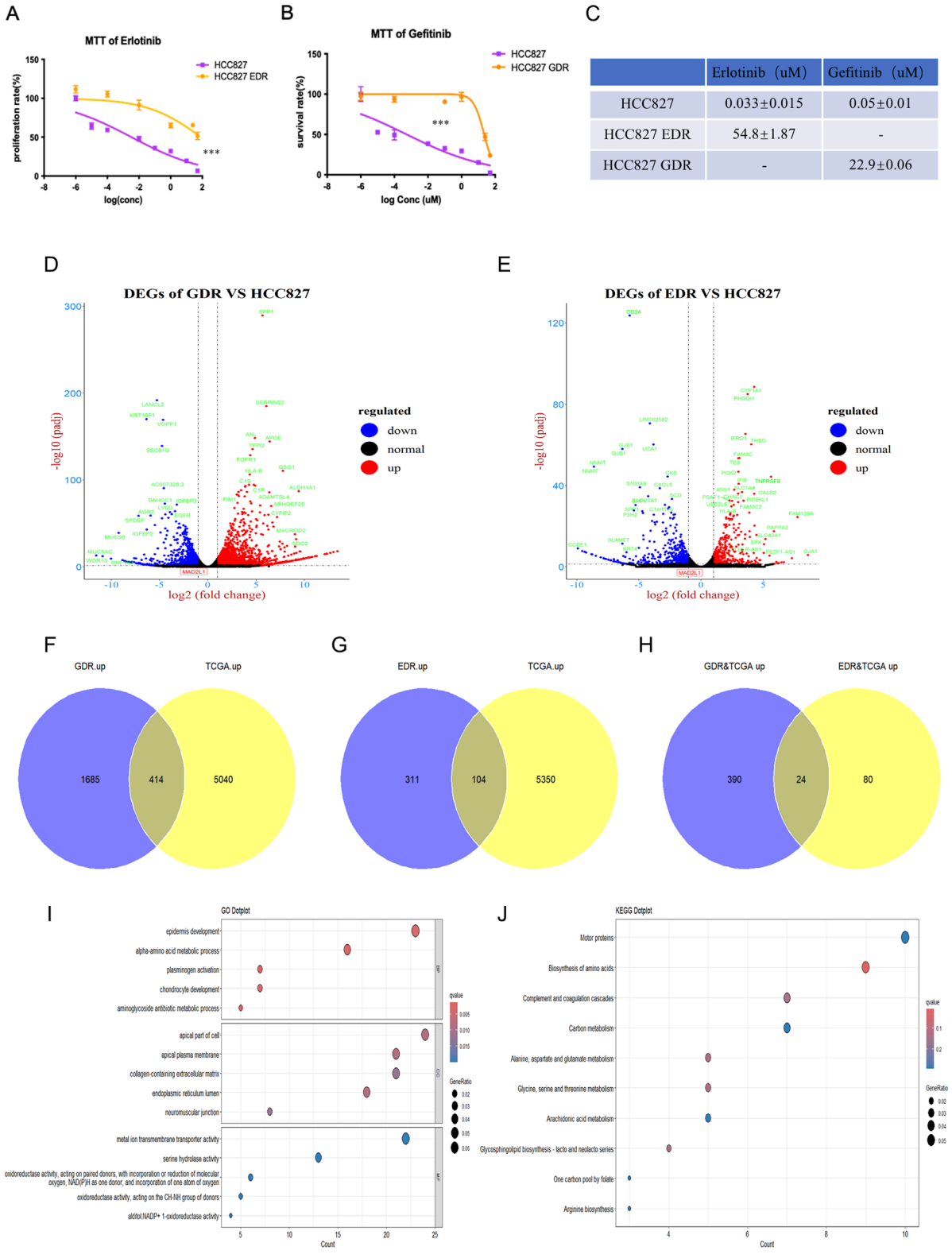

	Erlotinib（uM）	Gefitinib（uM）
HCC827	0.033±0.015	0.05±0.01
HCC827 EDR	54.8±1.87	-
HCC827 GDR	-	22.9±0.06

FIGURE 1
Establishment of erlotinib and gefitinib resistance cell line. **(A–C)** The IC50 of erlotinib and gefitinib were detected in erlotinib-resistant cell line, gefitinib-resistant cell line and paternal HCC827 cell line via MTT, respectively.***P < 0.001, by Student's t-test. **(D,E)** Differential expression genes were detected via RNA-sequencing in gefitinib-resistant cell line and erlotinib-resistant cell line. **(F–H)** Venn plot showed the overlap of upregulated genes between gefitinib/erlotinib resistant cell line and LUAD patients' tissues in TCGA. **(I,J)** GO and KEGG analyses revealed the enriched pathways among the upregulated differentially expressed genes in GDR&TCGA and EDR&TCGA.

which may play a role in tumor progression and the development of acquired drug resistance, as illustrated in Figures 1I,J.

3.2 Model construction based on the (DEGs) among EGFR-TKIs resistant cells and LUAD patients

To establish a prognostic model for LUAD patients, LASSO-COX dimension reduction analysis was conducted based on those 494 DEGs. The cross-validation plot shows the deviance across log(λ) values. The left dashed line indicates λ.min, which selected a 3-gene signature. The right dashed line indicates λ.1se, which resulted in a null model (zero genes) (Figures 2A,B). Finally, three candidate genes (*PPP1R3G*, *CREG2* and *LYPD3*) and their corresponding lambda values were used to calculate the RiskScore for each patient. All three of these were newly identified biomarkers for lung cancer and EGFR-TKIs resistance. The median RiskScore (0.19182) of the training database was set as the cutoff value.

To explore the prognostic prediction value of *PPP1R3G*, *CREG2* and *LYPD3* in LUAD patients, we conducted Kaplan-Meier analyses based on the TCGA and GEO databases respectively. Patients with higher expression of *PPP1R3G*, *CREG2* and *LYPD3* all had significantly shorter overall survival compared with those with lower expression in the TCGA database (Figures 2C–E). In addition, the survival rate of *PPP1R3G*, *CREG2* and *LYPD3* was verified in the GEO database (Figures 2F–H). Besides, the individual gene expression analyses of *PPP1R3G*, *CREG2*, and *LYPD3* indicated that the expression levels of all three genes were significantly elevated in lung tumor tissues as compared to normal tissues. This overexpression was consistently observed in both the training and validation datasets (Figures 3A–F). To validate the translational relevance of our signature, we investigated the protein expression of our three genes using the CPTAC-LUAD proteomic dataset. This analysis revealed that the protein levels of both LYPD3 and PPP1R3G were significantly elevated in lung adenocarcinoma tissues compared to matched normal adjacent tissues ($p < 0.05$ for both; Reference to the supplementary S1A,B). The protein for CREG2 was not detected in this cohort. These results demonstrate that the prognostic signal from our transcriptomic signature is reflected in actual protein abundance changes for the majority of its components in patient tumors, strengthening its biological and clinical relevance.

These findings collectively indicate that the expression levels of *PPP1R3G*, *CREG2*, and *LYPD3* are strong prognostic indicators for LUAD patients, suggesting their potential utility in predicting outcomes of EGFR-TKI treated patients and guiding personalized treatment decisions.

3.3 Relationship between RiskScores of the prognostic signature and clinical-pathologic characteristics

In order to figure out the relationship between RiskScores and clinical-pathologic characteristics, the correlation between the RiskScore and various clinical and pathological factors was further examined. It was found that the RiskScore was significantly higher in tumor tissues compared to normal tissues in both TCGA and GEO patient cohorts (Figures 3G,H). In addition, the RiskScore exhibited a moderate, albeit slight, increase in patients with more advanced tumor stages, as observed in both the training and validation databases (Figures 3I,J). Nonetheless, in both the training and validation datasets, no association was observed between the RiskScore and factors such as gender, age and race. These findings suggest that the RiskScore is primarily associated with tumor biology rather than demographic factors, highlighting its potential as a valuable biomarker for predicting LUAD prognosis and guiding personalized treatment strategies.

3.4 Relationship between RiskScore and patients' survival

Then, patients were further categorized into distinct RiskScore groups and demon-strated comparable profiles in terms of clinical and pathological traits, mirroring the patterns observed in the training dataset (Figures 4A,B). However, no significant different in terms of clinical and pathological traits between the high-RiskScore group and low-RiskScore group.

Subsequently, Kaplan-Meier analyses were performed taking into account the RiskScore. The prognostic models exhibited enhanced predictive accuracy for overall survival and progression-free survival across both the training and validation datasets (Figures 4C,D). These results indicate that the RiskScore is a powerful predictor of clinical outcomes in LUAD.

3.5 The RiskScore is closely related to cell division and DNA metabolism

In an effort to uncover the biological functions and pathways that correlate with the RiskScore, a series of analytical methods were employed. Initially, genes with the strongest ties to the RiskScore were identified. We conducted a comparative analysis of the differentially expressed genes between the high-RiskScore group and low-RiskScore group, and the volcano plot analysis uncovered 731 differentially expressed genes (DEGs), with 405 genes upregulated and 326 genes downregulated (Figure 5A).

Subsequently, Gene Ontology (GO) and Kyoto Encyclopedia of Genes and Genomes (KEGG) were utilized to conduct a functional enrichment analysis on this refined set of genes. Additionally, Gene Set Enrichment Analysis (GSEA) was applied to further elucidate the biological significance behind the RiskScore. The GO analysis showed that the RiskScore was closely related to the connective tissue development and serine-type peptidase activity (Figure 5B). The KEGG analysis showed that the RiskScore was closely related to the protein digestion and absorption signaling pathway (Figure 5C). Furthermore, the close association of the RiskScore with key biofunctions and signaling pathways—such as cytoskeleton organization, late endosome function, skin and epi-dermal development—was corroborated through GSEA analysis of data from the TCGA databases (Figures 5D–G). GSEA revealed significant upregulation of pathways associated with cytoskeleton organization, epidermal development, and skin development. In contrast, the late endosome pathway exhibited significant downregulation. The similar finding could also be observed in the validation datasets (Figures 6A–G).

10.3389/fmolb.2025.1654426

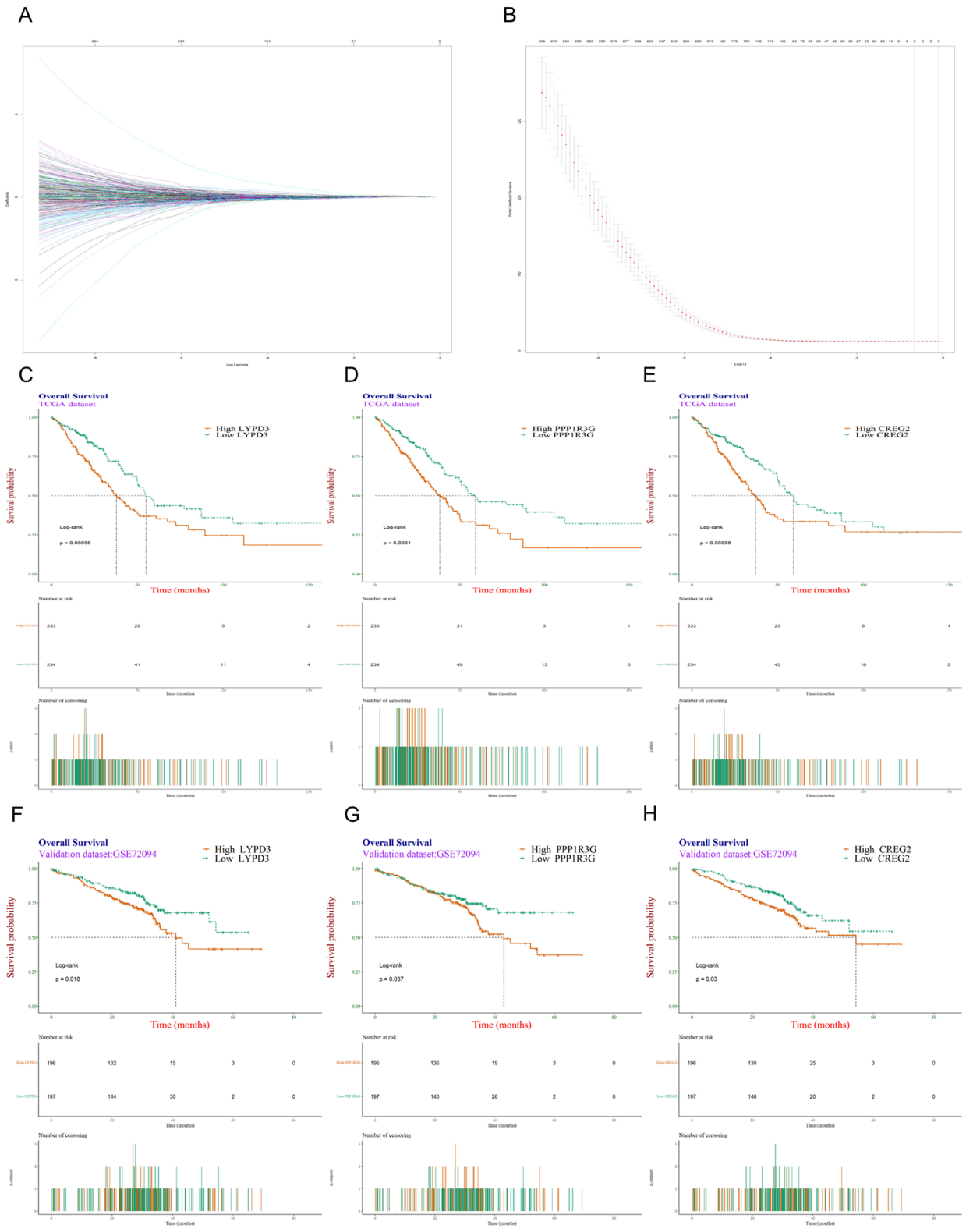

FIGURE 2
Screening and validation of genes most associated with resistance to EGFR-TKIs. **(A)** Trace plot of coeffecient fit by LASSO-Cox: each curve corresponding to a variable; **(B)** Cross-validation curve for the LASSO-Cox regression model. The left dashed line indicates λ.min, and right dashed line indicates λ.1se; **(C–E)** Kaplan-Meier survival analysis was conducted on the TCGA dataset to evaluate the influence of three individual genes, LYPD3, PPP1R3G, and CREG2, on patients' overall survival. **(F–H)** The KM survival analysis was validated in another independent dataset GSE72094.

10.3389/fmolb.2025.1654426

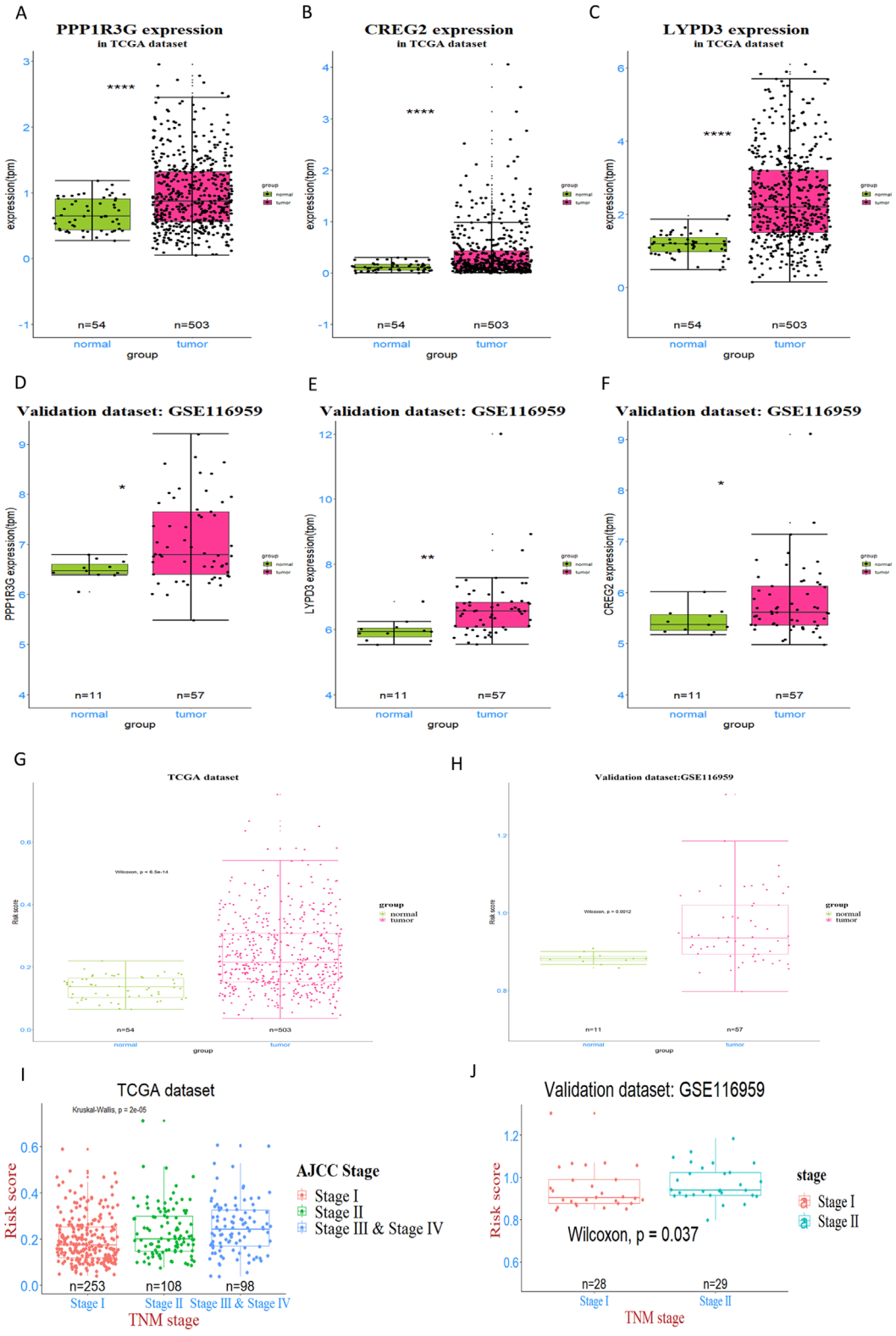

FIGURE 3
Expression analysis and validation of three prognostic genes in LUAD patients. **(A–C)** The expression levels of three genes—PPP1R3G, CREG2, and LYPD3—were detected and compared between tumor tissues and normal tissues in TCGA dataset. **(D–F)** This pattern was further validated in GSE116959 dataset. **(G, H)** the RiskScore, derived from the expression of the genes PPP1R3G, CREG2, and LYPD3, was assessed and compared between tumor and normal tissues in both the training and validation datasets **(I, J)** The Kruskal–Wallis test was applied to identify overall differences in risk scores across various tumor stages, while the Wilcoxon test was used for pairwise comparisons to pinpoint specific stage-related disparities.

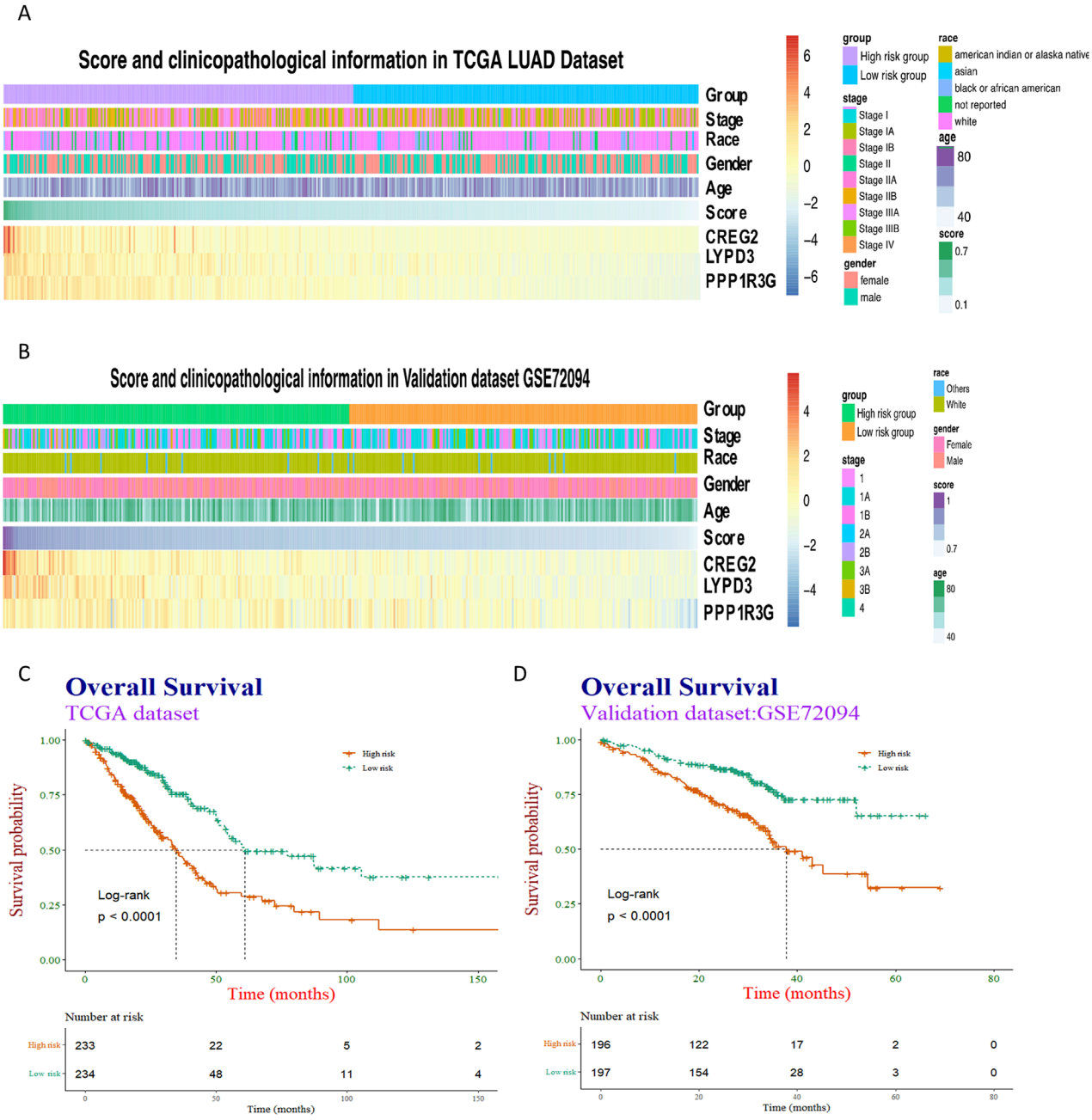

FIGURE 4
Heatmap visualization and survival analysis of clinical-pathological factors and gene expression in cancer cohorts. **(A,B)** Clinical-pathological factors and the expression of three representative genes—PPP1R3G, CREG2, and LYPD3—were visualized in heatmaps arranged by descending risk score, both in the training dataset and the validation dataset. **(C,D)** The association between the risk score and patients' overall survival was then examined using Kaplan-Meier survival curves, with separate analyses conducted for the training and validation cohorts.

3.6 Association analysis of RiskScore with tumor immune microenvironment characteristics and EGFR mutation status

In addition, the presence of immune cells within tumors significantly influences both neoplastic progression and the effectiveness of therapies designed to combat cancer. Herein, we conducted an analysis to determine the extent of immune cell infiltration in both TCGA database and GEO database. Our findings indicated that in the high RiskScore group, there was an increase in the infiltration of regulatory T cell, Memory B cell and activated CD4 T cell. Conversely, in the low RiskScore group, a higher level of infiltration was observed for mast cell and eosinophil with these differences being statistically significant ($p < 0.05$) (Figure 5H). The similar finding could also be observed in the validation GEO database, strongly suggesting that high-RiskScore patients may exhibit reduced responsiveness to immunotherapies due to their immunosuppressive microenvironment (Figure 6H). However, the

10.3389/fmolb.2025.1654426

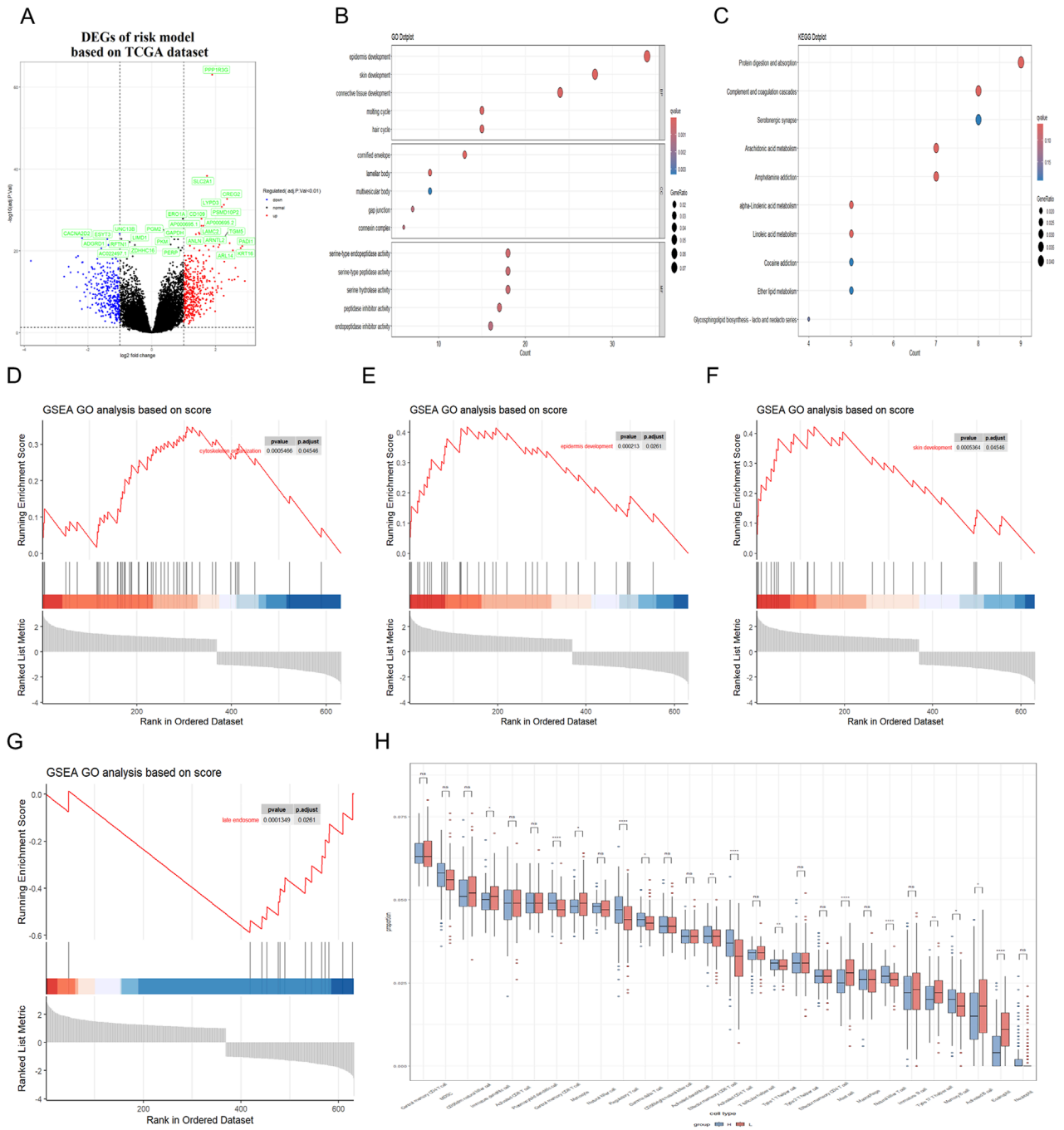

FIGURE 5
Correlation between RiskScore and biological functions in training dataset. **(A)** Volcano plot was utilized to illustrate the differentially expressed genes (DEGs) between the high-risk and low-risk groups in the TCGA dataset. **(B,C)** GO and KEGG analyses were conducted to identify the enriched signaling pathways associated with these DEGs. **(D–G)** GSEA revealed significant upregulation of pathways related to cytoskeleton organization, cell cycle processes, epidermal and skin development; Besides, the late endosome pathway was found to be significantly downregulated. **(H)** Immune cell infiltration analysis was conducted to demonstrate a close association between DEGs and various immune cells.

tumor immune microenvironment is an intricate system, and it is premature to categorically determine whether the presence of immune cell infiltration is beneficial or harmful to patients. The multifaceted nature of these cells within the tumor microenvironment necessitates further investigation to elucidate their precise roles. Various studies are essential to clarify the implications of these immune cells on patient outcomes. These results suggest that the high RiskScore group and low RiskScore group possess distinct immune profiles and exhibit varied reactions to immunotherapeutic interventions that target distinct immune checkpoints.

Moreover, we conducted single-cell RNA sequencing (scRNA-seq) analysis of GSE241934 dataset to reveal distinct expression

10.3389/fmolb.2025.1654426

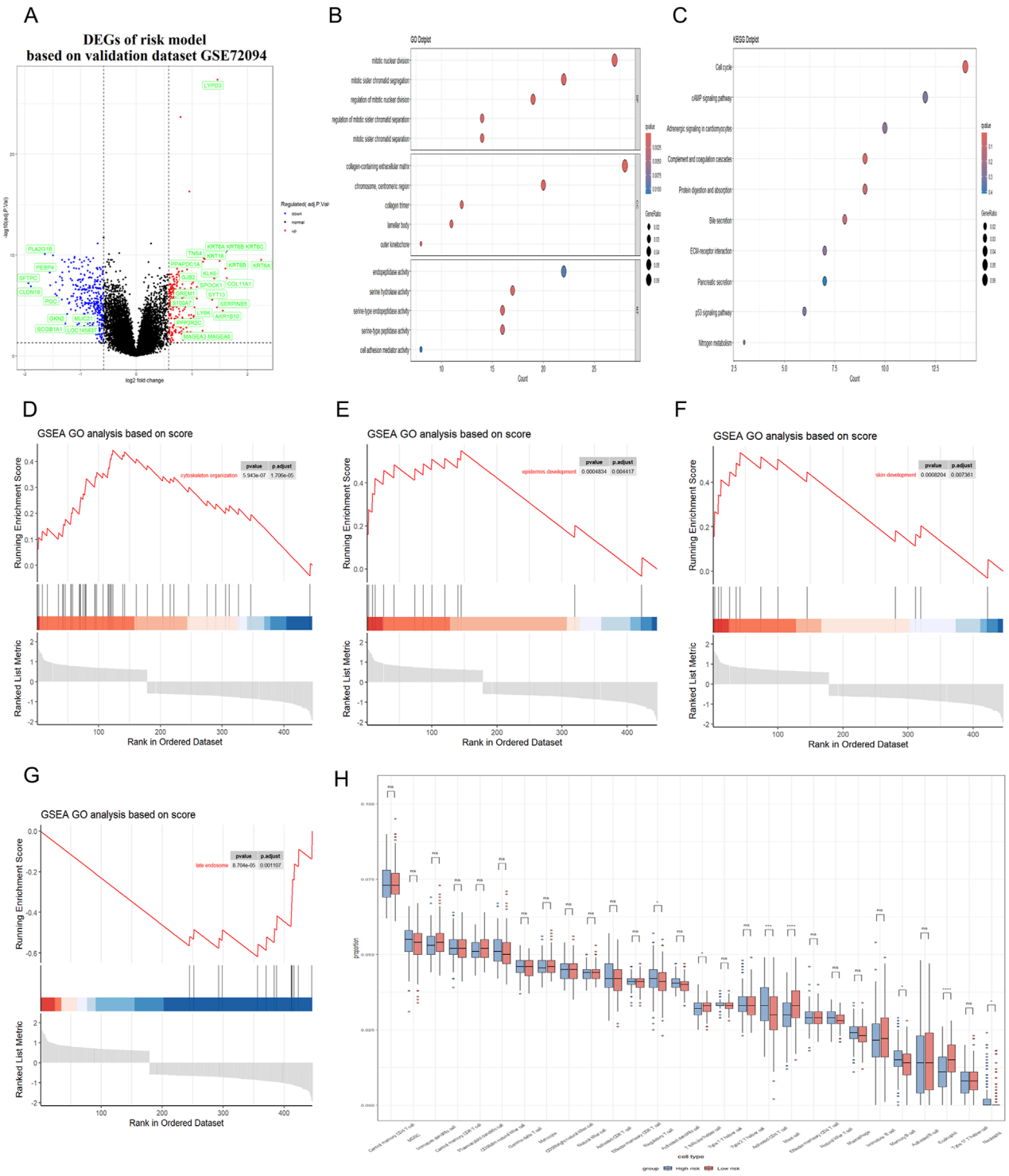

FIGURE 6
Correlation between RiskScore and biological functions in validation dataset. **(A)** Volcano plot was utilized to illustrate the differentially expressed genes (DEGs) between the high-risk and low-risk groups in the GEO dataset. **(B,C)** GO and KEGG analyses were conducted to identify the enriched signaling pathways associated with these DEGs. **(D–G)** GSEA revealed significant upregulation of pathways related to cytoskeleton organization, cell cycle processes, epidermal and skin development; Besides, the late endosome pathway was found to be significantly downregulated. **(H)** Immune cell infiltration analysis was conducted to demonstrate a close association between DEGs and various immune cells.

patterns of *LYPD3*, *PPP1R3G*, and *CREG2* between EGFR-mutant and wild-type LUAD patients. We note that this cohort consists of LUAD patients who received neoadjuvant immunochemotherapy, a potential confounder for gene expression. With this important caveat, we observed that these three genes exhibited significant downregulation in tumor cells from EGFR-mutant patients

(L858R/Exon19del/Exon20ins) compared with non-mutant counterparts (Figures 7A–F), though we cannot rule out that this expression pattern was influenced by the prior therapy. This observation appears paradoxical to our cell line model where these genes were upregulated in acquired resistance. However, this discrepancy may reflect fundamental differences in resistance mechanisms and could be explained by several hypothesis: 1. We speculate that the cell line model simulates acquired resistance through progressive drug selection, whereas clinical samples in GSE241934 represent intrinsic resistance or early treatment-naive mutations. 2. Alternatively, the clinical cohort received neoadjuvant immunochemotherapy, which may induce immunomodulatory changes that suppress these genes' expression. These findings collectively suggest that these genes are closely associated with acquired resistance (as shown *in vitro*). Their expression patterns in clinical settings may be influenced by additional layers of tumor heterogeneity, treatment interventions, and immune system interactions that require further investigation. To address the potential confounding effect of neoadjuvant immunochemotherapy in the single-cell cohort (GSE241934), we investigated the relationship between our 3-gene signature and treatment response. We found no significant difference in the signature risk score between patients who achieved a Major Pathological Response (MPR) and those who did not ($p = 0.46$; Reference to supplementary S2A). This indicates that the signature is not a direct predictor of response to this regimen. Despite this, the signature retained its power to stratify patients by overall survival, suggesting it captures fundamental aspects of tumor biology and intrinsic aggressiveness that are independent of the response to immunochemotherapy.

3.7 The individualized prediction model showed robust predictive accuracy

To enhance the practicality of the prognostic prediction model in clinical settings, a personalized prediction model was developed. A personalized model for predicting Progression-Free Survival (PFS) was developed, incorporating a set of independent predictive factors. These included the RiskScore, gender and pathologic stage. Figure 8A illustrates that the individualized prediction model can be used to estimate the tumor recurrence probability for Lung Adenocarcinoma (LUAD) patients at various time points, including 1-, 3-, 5-, and 10-year post-treatment. The calibration curve, which compares the nomogram predictions with actual outcomes, demonstrates a good match in both the training and validation datasets, as depicted in Figures 8B,C, suggesting high predictive accuracy. Furthermore, to quantify the precision of the model's predictive accuracy, we computed the C-index with a 95% confidence interval via 1000 bootstrap resamples. The prognostic performance of the 3-gene signature was consistent across both the training and external validation cohorts. In the training set, the model achieved a C-index of 0.643 (95% CI: 0.594–0.687), which was closely replicated in the independent validation set with a C-index of 0.612 (95% CI: 0.556–0.671). Similarly, time-dependent AUC values ranged between 0.62 and 0.67 in both cohorts at key time points (Figures 8D,E). These results indicate that the signature provides a modest but stable and generalizable level of discriminative ability.The C-index of this nomogram model was 0.7, which is higher than any other prediction model (Figure 8F). These findings collectively underscore the potent predictive capability of our developed model. To evaluate the potential of the RiskScore as a predictive biomarker, we assessed its association with clinical response to therapy. In the GSE241934 cohort of patients treated with neoadjuvant immunochemotherapy, we found no significant difference in the RiskScore between patients who achieved a Major Pathological Response (MPR) and those who did not ($p = 0.46$; supplementary S2A). This indicates that the RiskScore is not predictive of response to this treatment regimen. Its validated utility remains its significant association with overall survival, establishing it as a prognostic biomarker.

3.8 Validation of the prognostic model in osimertinib-resistant cell lines

To further validate the reliability of our prognostic model, we extended our analysis to third-generation EGFR-TKI (osimertinib)-resistant cell lines. Specifically, we established an osimertinib-resistant HCC827 cell line (OR-HCC827) by progressively exposing parental HCC827 cells to increasing concentrations of osimertinib. Consistent with our observations in erlotinib- and gefitinib-resistant models, the OR-HCC827 cells exhibited significantly higher IC50 values compared to the parental HCC827 cells (Figure 9A), confirming the successful development of osimertinib resistance.

Subsequently, RT-PCR analysis revealed that the expression levels of *LYPD3*, *PPP1R3G*, and *CREG2* were markedly upregulated in OR-HCC827 cells relative to the parental line (Figures 9B–D). These findings corroborate the robustness of our prognostic signature across multiple generations of EGFR-TKIs. The consistent overexpression of these biomarkers in osimertinib-resistant cells further supports their potential utility in stratifying high-risk LUAD patients.

4 Discussion

The discovery of EGFR-activating mutations in a subset of lung cancer patients led to the use of EGFR tyrosine kinase inhibitors (EGFR-TKIs) to treat non-small cell lung cancer (NSCLC) with these specific mutations (Kobayashi et al., 2005; Bean et al., 2007; Ninomiya et al., 2018). While EGFR-TKIs have significantly improved outcomes for these patients, resistance to these drugs is a common issue. Furthermore, lung adenocarcinoma (LUAD) is characterized by a poor prognosis and a lack of effective screening techniques, contributing to a low rate of successful clinical treatment (Lee et al., 2020; Altintas and Tothill, 2013). Consequently, there is a pressing need to develop innovative biomarkers that can accurately predict the prognosis of LUAD after EGFR-TKIs treatments.

In the current study, we embarked on a multifaceted approach to tackle the challenge of acquired resistance to EGFR-TKIs in LUAD. Initially, we developed EGFR-TKIs resistant cell lines and this *in vitro* model provided a valuable platform for identifying genes that are crucial in the resistance mechanism. The discovery of 494 co-upregulated genes in resistant cells and LUAD patient samples represents a significant step forward in understanding the molecular underpinnings of resistance. Through bioinformatics analysis, we

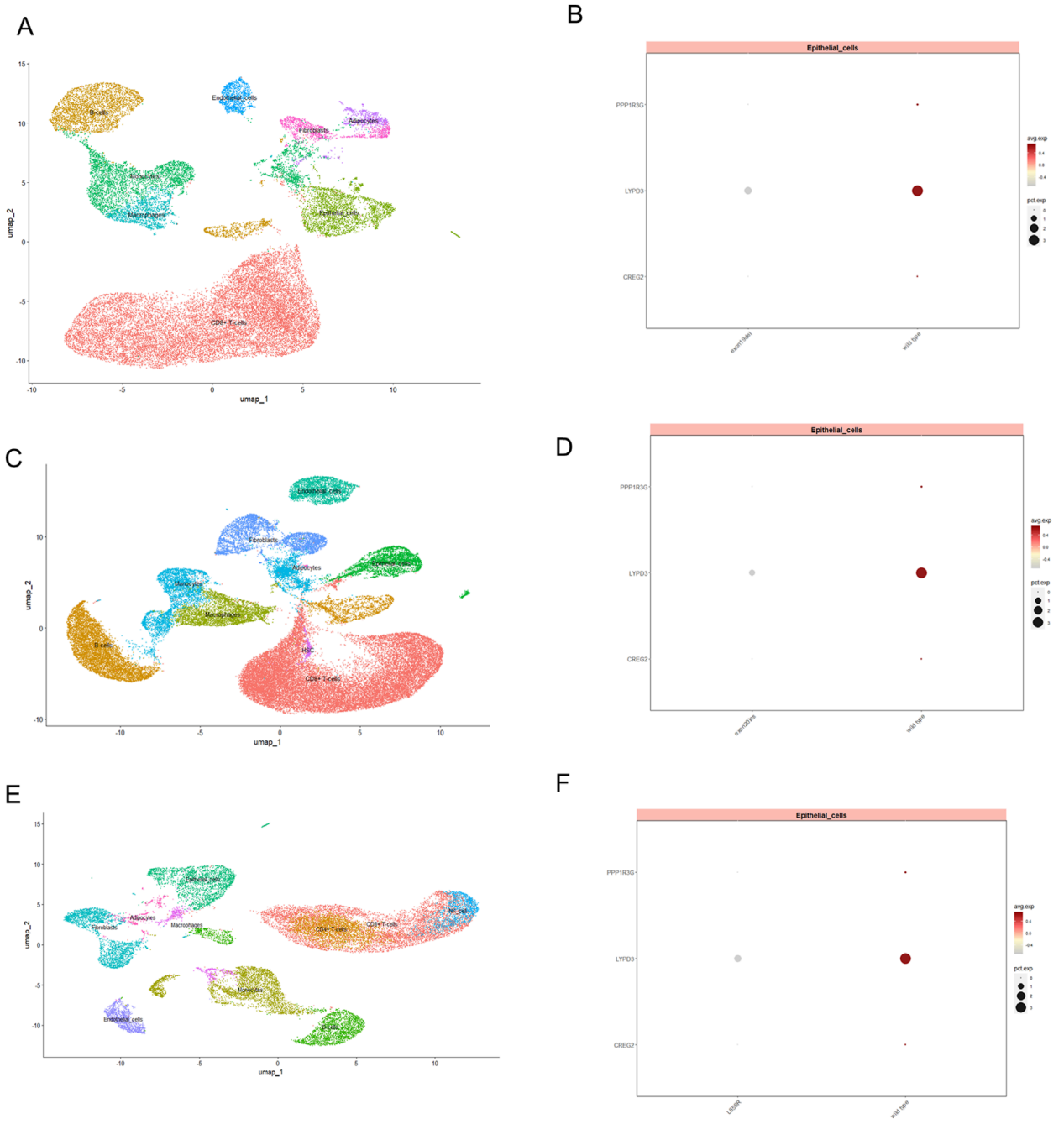

FIGURE 7
The expression of three model genes in EGFR-TKI resistant LUAD patients revealed by single cell transcriptomics profiling. UMAP visualization of single-cell RNA-seq data, illustrating the distribution of distinct cellular populations in tumor tissue from LUAD patients with exon19del **(A)**, exon20ins **(C)** and L858R **(E)**. Each cluster represents a transcriptionally distinct cell type, with epithelial cells prominently marked. Dot plot displaying the expression levels of PPP1R3G, LYPD3, and CREG2 in epithelial cell subsets between wild type and patients with exon19del **(B)**, exon20ins **(D)** and L858R **(F)** mutation. Dot size indicates the proportion of cells expressing each gene, while color intensity reflects the average expression level.

identified pathways related to amino acid biosynthesis and metabolism as being central to the resistant phenotype. Amino acid metabolism is intricately linked to drug resistance in cancer cells, where certain amino acids, such as glutamine and serine, can fuel metabolic pathways that neutralize drug effects or promote repair mechanisms, leading to decreased treatment efficacy. These results have facilitated the identification of potential resistance-related markers and have led to the development of a prognostic model that shows promise in guiding clinical treatment strategies. Then, the LASSO-COX method for dimensionality reduction was employed to pinpoint an optimal set of prognostic indicators. This analysis led to the discovery of a 3-gene signature—comprising *PPP1R3G*, *CREG2*, and *LYPD3*—that is characteristic of the resistant lung cancer cells. We acknowledge that the LASSO λ.1se criterion, which favors maximum parsimony, did not

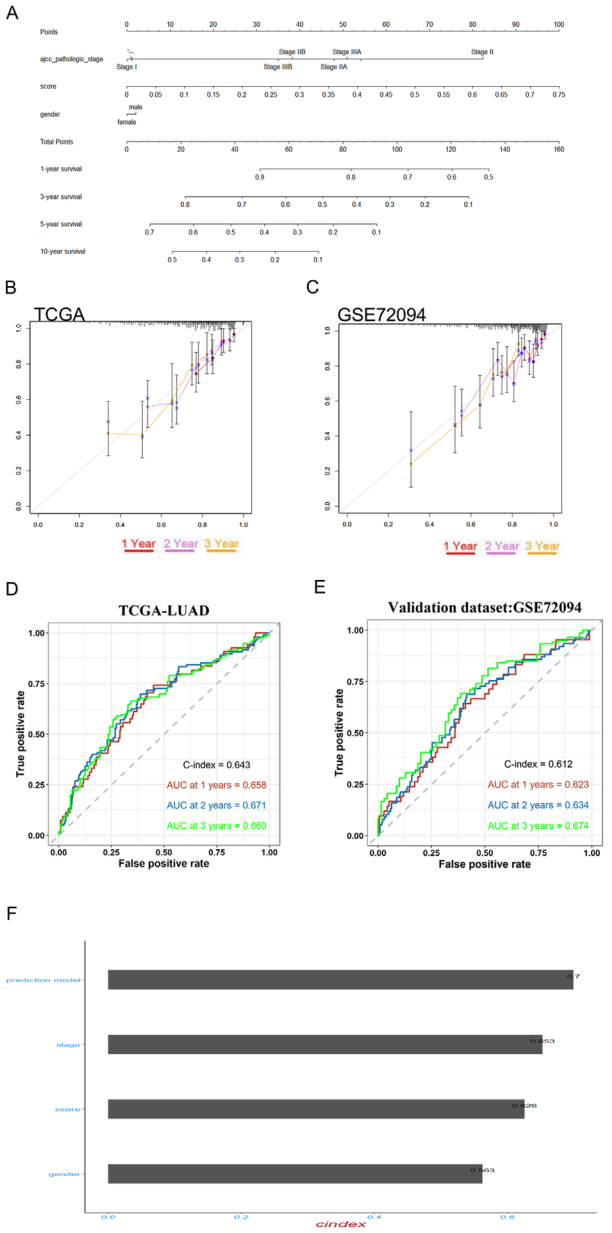

FIGURE 8
Prognostic model validation and personalized prediction of LUAD patient survival post-EGFR-TKI treatment. **(A)** The nomogram accurately predicted the 1-, 3-, 5-, and 10-year overall survival (OS) times for lung adenocarcinoma (LUAD) patients following treatment with gefitinib and erlotinib. **(B,C)** Calibration plots were employed to assess the concordance between the predicted and actual OS rates at 1-, 2-, and 3-year intervals for both the training and validation datasets, demonstrating the model's reliability. **(D,E)** time-dependent ROC and bootstrap C-index analyses of the 3-gene signature in TCGA-LUAD and external validation cohort GSE72094 **(F)** The predictive efficacy of the personalized prognostic model, along with the individual risk score and clinical prognostic factors for LUAD patients' OS, was evaluated using the concordance index (C-Index).

select any genes, indicating the challenge of deriving a highly stable signature from this gene set. However, the external validation of our λ.min-derived 3-gene signature confirms its robust prognostic value, suggesting these genes capture a meaningful biological signal related to prognosis in lung adenocarcinoma.

Researchers have identified several genes associated with cancer progression and treatment resistance. *PPP1R3G*, encoding a regulatory subunit of protein phosphatase 1 (PP1), plays a role in cellular processes like cell division and signal transduction (Shi et al., 2023; Zhuo et al., 2021). Its dysregulation may contribute to cancer therapy resistance by helping cancer cells evade drug effects. *CREG2*, involved in cellular respiration and energy metabolism, has potential indirect effects on cancer development. The CREG2 gene is implicated in Lung Adenocarcinoma (LUAD), where its high expression is linked to poor prognosis and advanced tumor stages. CREG2's role in cancer is complex, with some studies suggesting it may have a pro-cancer effect by influencing stromal cells and proliferation, while other research has identified it as a potential prognostic biomarker that could help in predicting patient outcomes and guiding personalized treatment strategies. (Kunita et al., 2002; Min et al., 2025; Hao et al., 2025). *LYPD3*, encoding a lysozyme-like protein, is implicated in immune response and cell differentiation (Gruet et al., 2020; Wang et al., 2017). It may modulate immune cell activity against tumors, with its expression linked to distinct immune profiles and responses to immunotherapy in different risk groups (Xin et al., 2024; Hu et al., 2020). While *LYPD3's* role in cancer is becoming more defined, additional studies are needed to confirm its involvement in cancer development or progression.

Then, a novel RiskScore-based nomogram was constructed to predict the prognosis and resistance of LUAD following curative resection. The nomogram, incorporating the RiskScore, patient age, gender and pathologic stage successfully identify patients at high risk of acquired resistance. The nomogram serves as a visual aid for clinicians to estimate the risk of acquired resistance and tailor treatment strategies accordingly, thereby enhancing the precision of patient care. Additionally, the successful validation in OR-HCC827 cells (Figures 9B–D) confirms these genes' potential role in resistance mechanisms spanning all generations of EGFR-TKIs. Our study successfully derives and validates a 3-gene prognostic signature for lung adenocarcinoma, rooted in the biology of experimentally-defined drug resistance. The model demonstrated consistent and statistically significant performance in both the discovery and external validation cohorts, with C-indices consistently around 0.65. While the discriminative accuracy is modest, this level of consistency strongly argues against overfitting and confirms that the signature captures a real and reproducible biological signal relevant to patient outcomes. It is important to note that such compact transcriptomic signatures often explain a portion of the prognostic variance; their clinical utility may ultimately lie in being integrated with established clinical variables like stage or performance status to build more powerful composite models. The independent validation of LYPD3 and PPP1R3G protein overexpression in LUAD tumors via the CPTAC database provides crucial support for our findings. It moves our signature beyond a transcriptomic correlation to a finding with direct implications for the tumor's functional proteomic state. The absence of CREG2 data in this resource highlights a limitation but does not diminish the collective evidence supporting the signature's biological plausibility.

Additionally, we also examined the relationship between RiskScore and both Tumor Immune Microenvironment (TME) characteristics and EGFR mutation status. Our immune infiltration analyses revealed that high-RiskScore tumors exhibit an immunosuppressive profile characterized by elevated regulatory T cells (Tregs) and activated

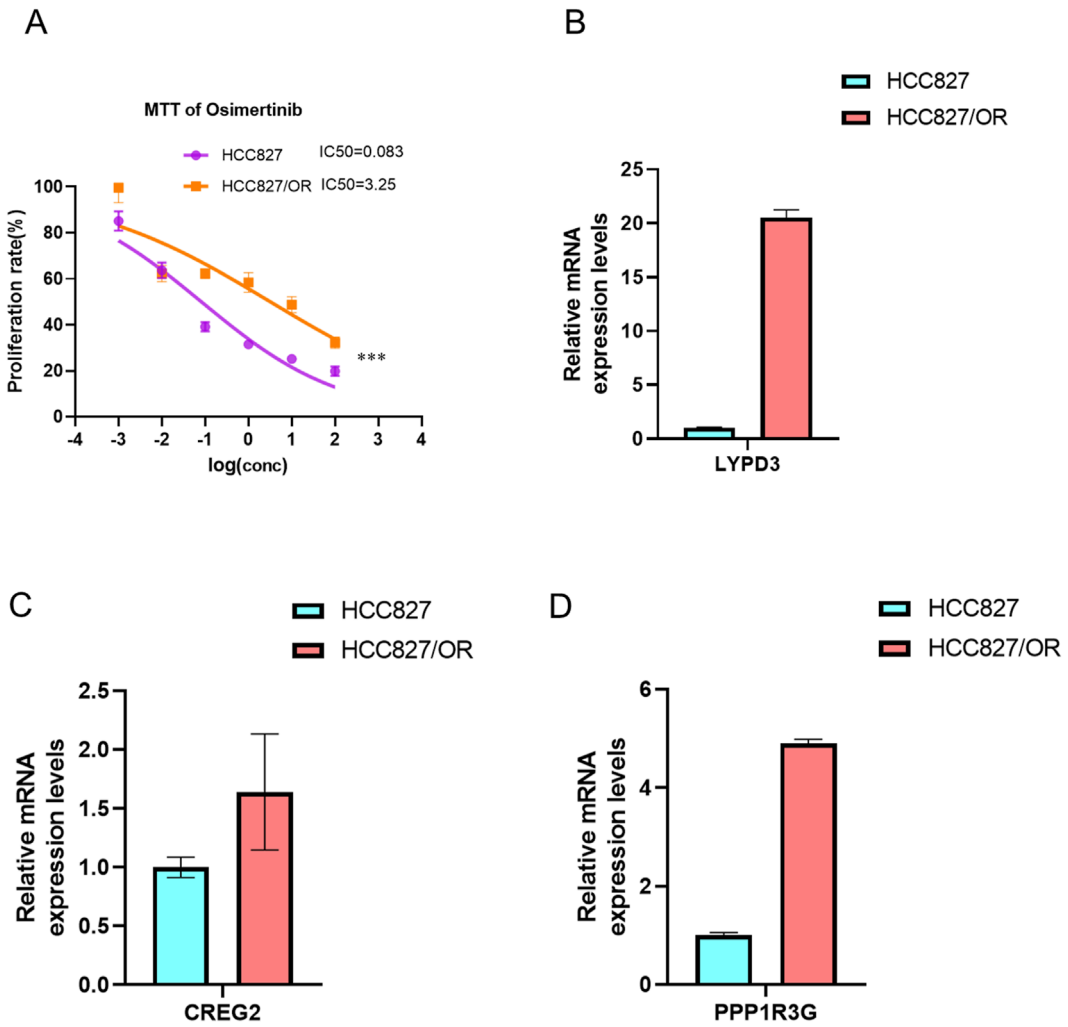

FIGURE 9
Establishment of Osimertinib resistance cell line. The IC50 of Osimertinib were detected in osimertinib-resistant cell line and paternal HCC827 cell line via MTT,***P < 0.001, by Student's t-test. **(A)** The bar graph showed the expression of three drug resistant associated genes LYPD3 **(B)**, CREG2 **(C)** and PPP1R3G **(D)** between osimertinib-resistant cell line and paternal HCC827 cell line, detected by RT-PCR.

CD4$^+$ T cells, alongside depletion of mast cells and eosinophils (Figures 5H, 6H). This specific immune contexture may explain the observed correlation with poor immunotherapy response, as Tregs are known to suppress anti-tumor immunity while mast cells/eosinophils often associate with favorable outcomes. Interestingly, Our single-cell RNA-seq analysis of clinical samples (GSE241934) revealed an intriguing paradox: these genes were paradoxically downregulated in EGFR-mutant tumors compared to the upregulation observed in resistant cell lines (Figures 7A–F). This divergence likely reflects fundamental biological differences between *in vitro* models and clinical samples. *In vitro* models capture acquired resistance through direct drug selection pressure, where these genes may confer survival advantages. However, clinical samples represent a more complex ecosystem, as the patients in the GSE241934 dataset underwent neoadjuvant immunochemotherapy, introducing additional variables that differentiate them from *in vitro* models. A key finding from our single-cell validation was that the prognostic power of our signature persisted in a cohort uniformly treated with neoadjuvant immunochemotherapy. Crucially, a sensitivity analysis revealed that the signature score was not associated with MPR status. This dissociation is highly informative: it suggests that the aggressive biology captured by our drug resistance-derived signature operates through mechanisms distinct from those determining immediate response to immunochemotherapy. It may instead reflect a tumor's inherent capacity for long-term progression, immune evasion, or relapse, explaining its stable prognostic value across different clinical contexts. A limitation of our study is the use of a single-cell cohort where all patients received neoadjuvant therapy. However, our analysis showing no link between the signature and MPR status strengthens our confidence that the prognostic signal is genuine and not merely a reflection of treatment response. Our study clarifies the clinical applicability of the 3-gene signature. While the genes were identified in a model of drug resistance, the integrated RiskScore functions primarily as a prognostic, not a predictive, biomarker. This is evidenced by our finding that the score did not predict pathological response to neoadjuvant immunochemotherapy in a

clinical cohort. This distinction is critical: our signature identifies a patient subgroup with aggressive tumor biology and poor survival outcomes, but it does not appear to determine initial response to this specific therapy. Consequently, this signature could be used to stratify high-risk patients who may require more intensive monitoring or alternative therapeutic strategies, rather than to guide the selection of initial immunochemotherapy.

5 Conclusion

This research bridges the gap between *in vitro* EGFR-TKI resistance and clinical outcomes in LUAD. We established a RiskScore model using *PPP1R3G*, *CREG2*, and *LYPD3*, validated its predictive accuracy for survival across multiple EGFR-TKIs, and linked it to specific immune microenvironmental characteristics. The identification of distinct immune profiles and the development of a combined nomogram underscore the model's potential to guide personalized therapy selection, including combination strategies. Despite the need for further experimental confirmation, this work offers a promising tool for improving risk stratification for LUAD patients facing the challenge of EGFR-TKI resistance.

Data availability statement

The data presented in the study are deposited in the Figshare repository, accession link: https://doi.org/10.6084/m9.figshare.28579784.v1

Ethics statement

Ethical approval was not required for the studies on humans in accordance with the local legislation and institutional requirements because only commercially available established cell lines were used. Ethical approval was not required for the studies on animals in accordance with the local legislation and institutional requirements because only commercially available established cell lines were used.

Author contributions

JL: Conceptualization, Formal Analysis, Writing – review and editing, Writing – original draft. JZ: Formal Analysis, Methodology, Writing – review and editing, Software, Writing – original draft. XZ: Writing – review and editing. CC: Writing – review and editing. TZ: Writing – review and editing. FL: Writing – review and editing. LH: Resources, Writing – original draft, Writing – review and editing, Supervision, Validation. HK: Supervision, Writing – original draft, Funding acquisition, Writing – review and editing. HZ: Writing – original draft, Resources, Funding acquisition, Supervision, Writing – review and editing.

Funding

The author(s) declare that financial support was received for the research and/or publication of this article. This study was supported by the Hunan Provincial Natural Science Foundation (grant no. 2024JJ6326), Natural Science Foundation of Changsha (grant no. kq2208176), the Hunan Normal University undergraduates innovative experiment project, entrepreneurship program (2024267), the Science and Technology Development Fund of Macau S.A.R. (FDCT) (File no. 0027/2022/A1), the University of Macau (UM) — Dr Stanley Ho Medical Development Foundation "Set Sail for New Horizons, Create the Future" Grant 2024 (File no. SHMDF-VSEP/2024/002), and the UM Multi-Year Research Grant General Research Grant (File no. MYRG-GRG-2025-0067-FHS). Jiasheng Zhang was in receipt of a PhD Assistantship from the Faculty of Health Sciences, UM.

Acknowledgements

We would like to thank all the staff in the Genomics and Bioinformatics Core at the Faculty of Health Sciences, University of Macau for technical support. We thank Professor Kin Yip TAM from Faculty of Health Sciences for kindly providing the HCC827 cell line used in this study.

Conflict of interest

The authors declare that the research was conducted in the absence of any commercial or financial relationships that could be construed as a potential conflict of interest.

The author(s) declared that they were an editorial board member of Frontiers, at the time of submission. This had no impact on the peer review process and the final decision.

Generative AI statement

The author(s) declare that no Generative AI was used in the creation of this manuscript.

Any alternative text (alt text) provided alongside figures in this article has been generated by Frontiers with the support of artificial intelligence and reasonable efforts have been made to ensure accuracy, including review by the authors wherever possible. If you identify any issues, please contact us.

Publisher's note

Supplementary material

The Supplementary Material for this article can be found online at: https://www.frontiersin.org/articles/10.3389/fmolb.2025.1654426/full#supplementary-material

References

Altintas, Z., and Tothill, I. (2013). Biomarkers and biosensors for the early diagnosis of lung cancer. *Sensors Actuators B-Chemical* 188, 988–998. doi:10.1016/j.snb.2013.07.078

Aran, D., Looney, A. P., Liu, L., Wu, E., Fong, V., Hsu, A., et al. (2019). Reference-based analysis of lung single-cell sequencing reveals a transitional profibrotic macrophage. *Nat. Immunol.* 20 (2), 163–172. doi:10.1038/s41590-018-0276-y

Bean, J., Brennan, C., Shih, J. Y., Riely, G., Viale, A., Wang, L., et al. (2007). MET amplification occurs with or without T790M mutations in EGFR mutant lung tumors with acquired resistance to gefitinib or erlotinib. *Proc. Natl. Acad. Sci. U. S. A.* 104 (52), 20932–20937. doi:10.1073/pnas.0710370104

Charoentong, P., Finotello, F., Angelova, M., Mayer, C., Efremova, M., Rieder, D., et al. (2017). Pan-cancer immunogenomic analyses reveal genotype-immunophenotype relationships and predictors of response to checkpoint blockade. *Cell Rep.* 18 (1), 248–262. doi:10.1016/j.celrep.2016.12.019

Du, X., Yang, B., An, Q., Assaraf, Y. G., Cao, X., and Xia, J. (2021). Acquired resistance to third-generation EGFR-TKIs and emerging next-generation EGFR inhibitors. *Innovation* 2 (2), 100103. doi:10.1016/j.xinn.2021.100103

Gruet, M., Cotton, D., Coveney, C., Boocock, D. J., Wagner, S., Komorowski, L., et al. (2020). β2-Adrenergic signalling promotes cell migration by upregulating expression of the metastasis-associated molecule LYPD3. *Biology-Basel* 9 (2), 39. doi:10.3390/biology9020039

Hao, Y., Wang, X., Ni, Z., Ma, Y., Wang, J., and Su, W. (2025). Analysis of ferritinophagy-related genes associated with the prognosis and regulatory mechanisms in non-small cell lung cancer. *Front. Med. (Lausanne)* 12, 1480169. doi:10.3389/fmed.2025.1480169

Hayakawa, H., Ichihara, E., Ohashi, K., Ninomiya, T., Yasugi, M., Takata, S., et al. (2013). Lower gefitinib dose led to earlier resistance acquisition before emergence of T790M mutation in epidermal growth factor receptor-mutated lung cancer model. *Cancer Sci.* 104 (11), 1440–1446. doi:10.1111/cas.12284

Hrustanovic, G., Lee, B. J., and Bivona, T. G. (2013). Mechanisms of resistance to EGFR targeted therapies. *Cancer Biol. and Ther.* 14 (4), 304–314. doi:10.4161/cbt.23627

Hu, P., Huang, Y., Gao, Y., Yan, H., Li, X., Zhang, J., et al. (2020). Elevated expression of LYPD3 is associated with lung adenocarcinoma carcinogenesis and poor prognosis. *DNA Cell Biol.* 39 (4), 522–532. doi:10.1089/dna.2019.5116

Ikeda, R., Vermeulen, L. C., Lau, E., Jiang, Z., Kavanaugh, S. M., Yamada, K., et al. (2011). Isolation and characterization of erlotinib-resistant human non-small cell lung cancer A549 cells. *Oncol. Lett.* 2 (1), 91–94. doi:10.3892/ol.2010.198

Kobayashi, S., Boggon, T. J., Dayaram, T., Jänne, P. A., Kocher, O., Meyerson, M., et al. (2005). EGFR mutation and resistance of non-small-cell lung cancer to gefitinib. *N. Engl. J. Med.* 352 (8), 786–792. doi:10.1056/NEJMoa044238

Kunita, R., Otomo, A., and Ikeda, J. E. (2002). Identification and characterization of novel members of the CREG family, putative secreted glycoproteins expressed specifically in brain. *Genomics* 80 (5), 456–460. doi:10.1006/geno.2002.6857

Lee, P., Goldman, J., and Donington, J. S. (2020). Lung cancer: advances in diagnosis and management. *Seminars Respir. Crit. Care Med.* 41 (3), 333–334. doi:10.1055/s-0040-1709995

Li, G. (2017). Molecular and clinical characterization of TIM-3 in glioma through 1,024 samples. Oncoimmunology. *BMC Bioinforma.* 6 (8), 7.

Li, F., Niu, Y., Zhao, W., Yan, C., and Qi, Y. (2022). Construction and validation of a prognostic model for lung adenocarcinoma based on endoplasmic reticulum stress-related genes. *Sci. Rep.* 12 (1), 19857. doi:10.1038/s41598-022-23852-z

Min, S., Pan, L., Zhang, X., Chen, H., Qiu, L., Wang, X., et al. (2025). Integration of single cell and bulk transcriptomes identifies T cell stress subtypes in LUAD. *Discov. Onc* 16, 1360. doi:10.1007/s12672-025-03170-2

Ninomiya, K., Ohashi, K., Makimoto, G., Tomida, S., Higo, H., Kayatani, H., et al. (2018). MET or NRAS amplification is an acquired resistance mechanism to the third-generation EGFR inhibitor naquotinib. *Sci. Rep.* 8, 1955. doi:10.1038/s41598-018-20326-z

Shi, H., Kong, R., Miao, X., Gou, L., Yin, X., Ding, Y., et al. (2023). Decreased PPP1R3G in pre-eclampsia impairs human trophoblast invasion and migration *via* Akt/MMP-9 signaling pathway. *Exp. Biol. Med. (Maywood)* 248 (16), 1373–1382. doi:10.1177/15353702231182214

Siegel, R. L., Miller, K. D., Fuchs, H. E., and Jemal, A. (2021). Cancer statistics, 2021. *Ca-a Cancer J. Clin.* 71 (1), 7–33. doi:10.3322/caac.21654

Systematic RNA (2009). Systematic RNA interference reveals that reveals that Oncog. KRAS-driven cancers require TBK1. *Nat*. 462 (7269): 108–112.

Tan, C. S., Gilligan, D., and Pacey, S. (2015). Treatment approaches for EGFR-inhibitor-resistant patients with non-small-cell lung cancer. *Lancet Oncol.* 16 (9), E447–E459. doi:10.1016/S1470-2045(15)00246-6

Wang, L., Hirohashi, Y., Ogawa, T., Shen, M., Takeda, R., Murai, A., et al. (2017). LY6/PLAUR domain containing 3 has a role in the maintenance of colorectal cancer stem-like cells. *Biochem. Biophysical Res. Commun.* 486 (2), 232–238. doi:10.1016/j.bbrc.2017.02.112

Xin, T., Zheng, C., Li, G. Z., Xu, X., Zhang, J., Jia, C., et al. (2024). Comprehensive analysis of exosome gene LYPD3 and prognosis/immune cell infiltration in lung cancer. *Transl. Cancer Res.* 13 (3), 1394–1405. doi:10.21037/tcr-23-1557

Yamamoto, C., Basaki, Y., Kawahara, A., Nakashima, K., Kage, M., Izumi, H., et al. (2010). Loss of PTEN expression by blocking nuclear translocation of EGR1 in gefitinib-resistant lung cancer cells harboring epidermal growth factor receptor–activating mutations. *Cancer Res.* 70 (21), 8715–8725. doi:10.1158/0008-5472.CAN-10-0043

Yang, B., Guo, L., Lu, G., Shan, W., Duan, L., and Duan, S. (2019). Radiomic signature: a non-invasive biomarker for discriminating invasive and non-invasive cases of lung adenocarcinoma. *Cancer Manag. Res.* 11, 7825–7834. doi:10.2147/CMAR.S217887

Zhuo, X., Chen, L., Lai, Z., Liu, J., Li, S., Hu, A., et al. (2021). Protein phosphatase 1 regulatory subunit 3G (PPP1R3G) correlates with poor prognosis and immune infiltration in lung adenocarcinoma. *Bioengineered* 12 (1), 8336–8346. doi:10.1080/21655979.2021.1985817

Frontiers in
Molecular Biosciences

Explores biological processes in living organisms on a molecular scale

Focuses on the molecular mechanisms underpinning and regulating biological processes in organisms across all branches of life.

Discover the latest Research Topics

See more →

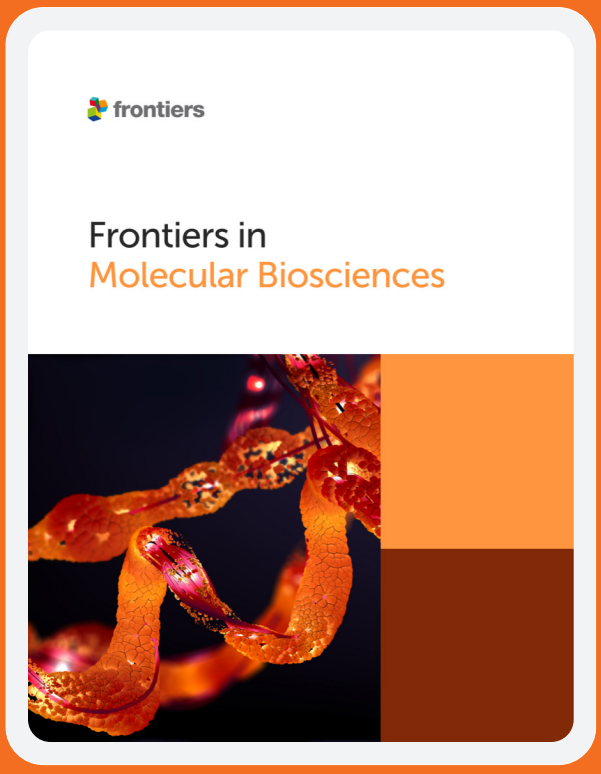

Frontiers

Avenue du Tribunal-Fédéral 34
1005 Lausanne, Switzerland
frontiersin.org

Contact us

+41 (0)21 510 17 00
frontiersin.org/about/contact